CHALMERS

Moment distribution and cumulative plastic rotation in reinforced concrete slabs subjected to concentrated forces

A study based on 3D non-linear finite element analyses

Master of Science Thesis in the Master's Programme Structural Engineering and Building Technology

ANDREAS LINDELÖF
BJÖRN WALHELM

Moment distribution and cumulative plastic rotation in reinforced concrete slabs subjected to concentrated forces

A study based on 3D non-linear finite element analyses

Master of Science Thesis in the Master's Programme Structural Engineering and Building Technology

ANDREAS LINDELÖF & BJÖRN WALHELM

Moment distribution and cumulative plastic rotation in reinforced concrete slabs subjected to concentrated forces

A study based on 3D non-linear finite element analyses

Master of Science Thesis in the Master's Programme Structural Engineering and Building Technology

ANDREAS LINDELÖF
BJÖRN WALHELM

Cover:
Illustration of the two main studied aspects in this Thesis; moment distribution and cumulative plastic rotation in slabs, where the latter arise from moving cyclic load.

Moment distribution and cumulative plastic rotation in reinforced concrete slabs subjected to concentrated forces

A study based on 3D non-linear finite element analyses

Master of Science Thesis in the Master's Programme Structural Engineering and Building Technology

ANDREAS LINDELÖF & BJÖRN WALHELM

Department of Civil and Environmental Engineering
Division of Structural Engineering
Concrete structures
Chalmers University of Technology

ABSTRACT

The use of 3D finite element (FE) analysis has increased substantially in recent years for design of reinforced concrete slabs. A common problem in this type of analysis is the occurrence of unrealistic force concentrations, caused by concentrated forces or supports. These concentrations may not be as critical in reality due to the non-linear response of reinforced concrete and introducing methods for estimating this more favourable force distribution is therefore of interest. Recently, guidelines of how to treat this problem have been presented in the literature.

The aim of this Thesis was to examine how force concentrations in linear elastic FE analysis can be redistributed to better simulate the real behaviour of a structure. Focus was directed towards moment distribution in the serviceability limit state, where different scenarios which may appear in real structures were examined. An objective was also to evaluate the recommendations given by the present guidelines.

The main instrument for the studies conducted in this Thesis was non-linear FE analysis. A beam grillage model, in liaison with multi-linear moment-curvature relations that defined the material response, was utilized. However, difficulties arose regarding the choice of the torsional stiffness and how it should be implemented in such an analysis. A parametric study demonstrated that the behaviour of a beam grillage model is highly dependant on the torsional stiffness adopted. However, even with conservatively chosen values of the torsional stiffness, the recommendations given in the literature were still shown to be conservative.

The aim of this Thesis was also to study how cyclic loading influences the development of plastic rotation in reinforced concrete slabs. The objective was to study how the plastic rotation accumulates and develops with an increased number of load cycles, different load combinations and varying load magnitudes.

The studies showed that the structures in this Thesis adapted to the moving forces and thus the influence of the forces decreased as the number of load cycles increased. Further, the analyses of moving forces demonstrated that such repetitive load combination yields significantly more damage to a structure than static forces of the same magnitudes. A superposition approach was finally proposed for estimating future development of plastic rotations, caused by moving concentrated forces.

Key words: Non-linear 3D FE analysis, reinforced concrete slabs, concentrated forces, moment distribution, cumulative plastic rotation, beam grillage model

Momentfördelning och ackumulerande plastisk rotation i armerade betongplattor utsatta för koncentrerade laster

En studie baserad på 3D icke-linjära finita elementanalyser

Examensarbete inom mastersprogrammet Structural Engineering and Building Technology

ANDREAS LINDELÖF & BJÖRN WALHELM

Institutionen för bygg- och miljöteknik
Avdelningen för konstruktionsteknik
Betongbyggnad
Chalmers tekniska högskola

SAMMANFATTNING

Användningen av tredimensionella finita elementanalyser (FE-analyser) har ökat kraftigt under de senaste åren. Ett vanligt problem vid dessa typer av analyser är förekomsten av orealistiskt stora koncentrationer av påkänningar från koncentrerade laster eller stöd. Dessa koncentrationer är inte nödvändigtvis kritiska för verkliga konstruktioner på grund av det olinjära verkningssätt som armerad betong uppvisar. Det är således av intresse att studera och introducera metoder som tar hänsyn till den verkliga konstruktionens mer fördelaktiga spridning av påkänningar. Riktlinjer för hur dessa frågeställningar ska behandlas har nyligen presenterats i litteraturen.

Syftet med detta examensarbete var att studera hur kraftkoncentrationer i linjärelastiska FE-analyser kan omfördelas för att bättre simulera en konstruktions verkliga beteende. Fokus har riktats mot momentfördelning i bruksgränstillstånd där olika scenarier som kan förekomma i verkliga konstruktioner studerades. Avsikten var att utvärdera de aktuella rekommendationer som presenterats i litteraturen.

Verktyget för de studier som genomförts i detta examensarbete var ickelinjära FE-analyser där multilinjära moment-krökningssamband definierade materialresponsen i balkrostmodeller. Svårigheter påträffades emellertid gällande valet av vridstyvhet och hur den ska behandlas i vald modell. En parameterstudie visade att beteendet, till hög grad, styrs av vridstyvheten. Fastän en låg vridstyvhet valdes, visades det att de rekommendationer, givna i litteraturen, är konservativa.

Syftet var också att studera inverkan av rörlig cyklisk belastning och hur den påverkar utvecklingen av plastisk rotation i armerade betongplattor. Avsikten var att studera hur plastisk rotation ackumuleras och utvecklas för ett ökande antal lastcykler, olika lastkombinationer och varierande laststorlekar.

Genomförda studier visade att undersökta konstruktioner anpassades till den skada som de cykliska lasterna gav upphov till samt att lasternas inverkan på skadeutvecklingen minskade då antalet lastcykler ökade. Analyser påvisade också att cykliska laster ger upphov till betydligt större skada än motsvarande statiska laster. En metod baserad på superposition introducerades i detta examensarbete för estimering av framtida utveckling av plastisk rotation, orsakad av rörlig cyklisk belastning.

Nyckelord: 3D finit elementanalys, armerade betongplattor, koncentrerade laster, momentfördelning, ackumulerad plastisk rotation, balkrostmodell

Contents

Preface

This Master's Thesis focuses on the moment distribution, force redistribution and the cumulative development of plastic rotation in reinforced concrete slabs, directed towards an application on bridge structures. The work of the Thesis was performed during 2014, from January to June, at Reinertsen Sverige AB as a final part of the master's programme *Structural Engineering and Building Technology* at *Chalmers University of Technology,* Sweden. The Thesis was written in collaboration with the Department of Civil and Environmental Engineering, Division of Structural Engineering, Concrete Structures at Chalmers University of Technology.

We would especially like to show our gratitude to our supervisor, Adjunct Professor Morgan Johansson, Reinertsen Sverige AB, for his excellent guidance and insightful comments throughout the work of this Thesis. We would also like to thank our examiner, Associate Professor Mario Plos, Chalmers, for his guidance.

Göteborg, 2014

Andreas Lindelöf & Björn Walhelm

Notations

Roman upper case letters

A	Area
A_s	Area of reinforcement
E	Young's modulus
E_c	Young's modulus for concrete
E_I	Young's modulus for uncracked state
E_s	Young's modulus for steel
F	External force
F_c	Force in concrete
F_s	Force in steel
$F_{s.I}$	Force in steel in state I
G	Shear modulus
GC	Gravity centre
I	Moment of inertia
I_I	Moment of inertia in state I
I_{II}	Moment of inertia in state II
K_v	Torsional stiffness
L	Length
L_c	Characteristic span width
M	Moment
M_{cr}	Cracking moment
M_y	Moment at yielding
M_u	Ultimate moment
M_{pl}	Plastic moment
M_{el}	Elastic moment
Q	Axle load
R	Reaction force
R	Resultant force
T	Torsional moment
V	Shear force
V_{Ed}	Design value of shear

Roman lower case letters

a	Distance
b	Width of cross-section
b	Width of concentrated force
c	Concrete cover
d	Effective depth of cross-section
d	Distance between concentrated forces
f_{cc}	Concrete compressive strength
f_{ct}	Concrete tensile strength
f_{ctm}	Mean value of concrete tensile strength
f_t	Steel strength in tension
f_y	Yield stress of reinforcing steel
h	Height of cross-section
h	Slab thickness
k_λ	Modification factor for rotation capacity
l	Length
l_{pl}	Development length of a plastic region
m	Moment per unit width
m_{cr}	Cracking moment per unit width
m_{rd}	Ultimate moment capacity per unit width
m_{xy}	Torsional moment per unit width
n	Number of load cycles
n_u	Number of load cycles to failure
q	Distributed load
u	Displacement
r	Radius of curvature
t	Thickness of the surfacing
w	Distribution width
w_{eff}	Effective distribution width
x	Coordinate
x	Height of compression zone
x_u	Height of compression zone in the ultimate state
x_0	Distance between maximum and zero moment
y	Coordinate
y_{cs}	Distance from the centre of the load to the critical cross-section

z	Distance from gravity centre
z	Coordinate

Greek lower case letters

α	Ratio between stiffness in two direction
α_s	Ratio between Young's Modulus for reinforcement and concrete
α_R	Stress block factor
α_q	Adjustment factor
α_Q	Adjustment factor
β	Constant depending on width to height ratio of a rectangular cross-section
β_R	Stress block factor
β_Q	Adjustment factor
γ	Ratio
δ	Ratio between average and maximum moment
ε	Strain
ε_c	Concrete strain
ε_{cc}	Concrete compression strain
$\varepsilon_{c.cr}$	Concrete strain at cracking
ε_{cu}	Ultimate concrete strain
ε_s	Steel strain
ε_y	Yield strain
ε_{su}	Ultimate steel strain
ε_{el}	Elastic strain
ε_{pl}	Plastic strain
θ	Angle
θ_{pl}	Plastic rotation
$\theta_{pl.d}$	Design value of plastic rotation
θ_{rd}	Plastic rotation capacity
λ	Shear slenderness
μ	Factor
v	Poisson's ratio
σ	Stress
σ_c	Concrete stress
$\sigma_{c.I}$	Concrete stress in state I
$\sigma_{c.II}$	Concrete stress in state II

σ_{ct} Concrete tensile stress

σ_s Steel stress

$\sigma_{s.I}$ Steel stress in state I

$\sigma_{s.II}$ Steel stress in state II

φ Angle of twist

χ Curvature

χ_{cr} Curvature at cracking

χ_y Curvature at yielding

χ_u Ultimate curvature

χ_{el} Elastic curvature

χ_{pl} Plastic curvature

1 Introduction

This chapter covers the background, scope, method and limitations of this Thesis. Further, the outline of the report is presented.

1.1 Background

Structural engineers have in the past used traditional design tools such as analytical two-dimensional (2D) analysis for the design of reinforced concrete bridge deck slabs. However, with increased computational power and software development, the use of three-dimensional (3D) finite element (FE) analysis has increased substantially in recent years. The advantage of such analyses is the possibility for a more accurate approximation of the structural response. The introduction of FE analysis has, however, introduced problems that were not present in traditional 2D analysis. A common problem in linear elastic FE analysis is unrealistic force concentrations caused by concentrated forces or supports, such as columns. These force concentrations may not be as critical in reality due to the non-linear behaviour of reinforced concrete. In reality, a redistribution of forces will take place which can be a result of cracking of concrete and yielding of reinforcement. Hence, in a real structure, there will normally be a considerably more favourable force distribution than what is obtained from a linear elastic FE analysis.

It is possible to create a more realistic approximation of the structural behaviour with the help of a more advanced FE model that takes the non-linear behaviour of reinforced concrete into account. This will however require an iterative and thus more time-consuming procedure which may not be feasible for design of an ordinary civil engineering structure. It is therefore important to understand how force concentrations obtained from linear elastic analysis should be distributed in the design process. Guidelines have recently been presented in Pacoste *et al.* (2012) on how to treat this problem. These recommendations are however believed to be conservative and a literature study performed by Pacoste *et al.* show that a very small amount of studies within the field have been documented. A too conservative method yields unnecessary use of materials together with economic and environmental losses which motivates further studies within the field.

This project is a continuation of a previous Master Thesis on the subject, Lim (2013). That Thesis was mostly directed towards the ultimate limit state and studied the plastic rotation in a cantilever slab exposed to concentrated forces. Lim gave recommendations for further studies within the area where one such recommendation was to study the effect of moving load; in order to study in what way it might affect the total need of plastic rotation. A moving load can for instance be a traffic load on a bridge structure.

1.2 Aim and objectives

The aim of this Thesis was to examine how the force concentrations in linear elastic finite element analyses can be redistributed to better imitate the real behaviour of a reinforced concrete slab. Focus was directed toward moment distribution in the serviceability limit state (SLS). One objective was to improve understanding of how cracking and varying stiffness in different directions would influence the moment

distribution in the slab. For example, varying stiffness can be a product of different reinforcement amounts in two main directions, or a product of different normal stresses in those directions. In addition, the response of a single and two adjacent concentrated forces were studied. Another objective was to evaluate the recommendations in Pacoste *et al.* (2012).

The aim was also to study in which way a moving load would affect the total plastic rotation in a reinforced concrete slab. The objective was to study how the plastic rotation accumulates with the number of load cycles, load combinations and varying load magnitudes.

1.3 Method

Tools for this project were linear and non-linear FE analyses. A large number of case studies were of interest which motivated the choice of a numerically stable and relatively simple analysing tool. It was therefore chosen to utilize a beam grillage model, where multi-linear moment-curvature relations can be used as input. The use of beam grillage models is a relatively common approach to analyse different types of structures assuming a linear elastic response, while the method is uncommon for non-linear analysis. However, the method is believed to yield a satisfactory approximation of the non-linear behaviour of reinforced concrete for the studies conducted in this Thesis. The finite element software used was the student version of ADINA (2012).

In this Thesis, simple structures were examined and the knowledge gained from these was aimed to enable understanding of more complex structures. Two different types of structures were chosen, a cantilever slab and a simply supported one-way slab.

For studies related to moment distribution in SLS, a number of cases were studied which were intended to represent scenarios which may appear in a reinforced concrete bridge. Examples of such cases are varying reinforcement amounts in different directions and the effect of normal stresses in the slab. Multi-linear moment-curvature relations were constructed to approximate the non-linear behaviour of reinforced concrete and the solutions were compared with the isotropic and orthotropic linear elastic solutions.

For studies related to cumulative plastic rotation, bilinear moment-curvature relations were used as input, where the second branch of the relation was intended to represent yielding of reinforcement. A value of the plastic rotation capacity was calculated and concentrated forces were modelled such that they moved across the slab along a chosen path. The slab was then exposed to several load cycles until it reached its calculated rotation capacity. Several cases were studied including varying load magnitudes and varying distance between two concentrated forces.

1.4 Limitations

Due to the limited time of this Master's Thesis, only a small selection of structures and different load combinations were examined. Focus was directed toward bending action in the slab; hence shear forces and displacements were not discussed. In this Thesis, the effect of creep and shrinkage was not taken into account, which may have a significant effect. Further, all analyses in this Thesis are static and do not take into account the dynamic response. No tests of real structures have been performed in

order to verify the FE models, but they are assumed to describe the reality to a satisfactory extent.

1.5 Outline of the report

The first part, Chapter 2, states basic background theory of reinforced concrete. The material response of plain concrete and reinforcing steel is discussed and expanded to how a moment-curvature relation for a reinforced concrete beam can be simplified. Further, reinforced concrete slabs are categorised and torsional forces in slabs are discussed.

In Chapter 3, finite element models for slabs are discussed, which include shell element models and beam grillage models. The recommendations for moment redistribution for linear elastic FE analyses given in Pacoste *et al.* (2012) are presented. Further, traffic load models stated in Eurocode are presented.

Chapter 4 and 5 treats moment distribution in SLS for a cantilever slab and a simply supported one-way slab, respectively. The methodology used when constructing the moment-curvature relations is explained and the results from the analyses performed are presented. In Chapter 4, the influence of the torsional stiffness of the beam elements in the beam grillage model is discussed.

Chapter 6 and 7 treats cumulative plastic rotation for a cantilever slab and a simply supported one-way slab, respectively. The bilinear moment-curvature relations used as input are presented and a plastic rotational capacity is calculated. Further, the results from the analyses performed are presented.

The results from Chapter 4 to 7 are discussed in Chapter 8, where observations and comparisons are made.

Finally, concluding remarks and recommendations for further studies are presented in Chapter 9.

2 Structural response of reinforced concrete

This chapter covers the material response of reinforcing steel and concrete. The material response of these two materials is also expanded to structural response of reinforced concrete beams and slabs. The different states of concrete from first loading to failure and the development of plastic rotation and the plastic rotation capacity of a cross-section is also treated in this chapter.

2.1 Material response

Concrete is a complex material with a wide range of stress-strain relationships depending on the concrete strength class. Since concrete is a brittle material, it will crack for relatively low stresses in the magnitude of 2-4 MPa, while the strength in compression is considerably higher. Common structural concrete have an axial compressive strength in the range of 20-50 MPa. A typical stress-strain relation for axially loaded plain concrete is illustrated in Figure 2.1a. For characteristic strength values of concrete, the reader is referred to Eurocode 2, CEN (2004).

Reinforcing steel has a pronounced linear elastic behaviour up to a certain stress where the steel starts to yield. When the yield stress f_y is reached, the reinforcing steel will develop plastic deformations. Reinforcing steel of grade B or C exhibits a pronounced strain hardening effect when the steel is loaded beyond the yield stress. The stress-strain relationship for typical hot-rolled reinforcing steel (class B and C) are shown in Figure 2.1b. For characteristic strength values of reinforcing steel the reader is referred to Eurocode 2.
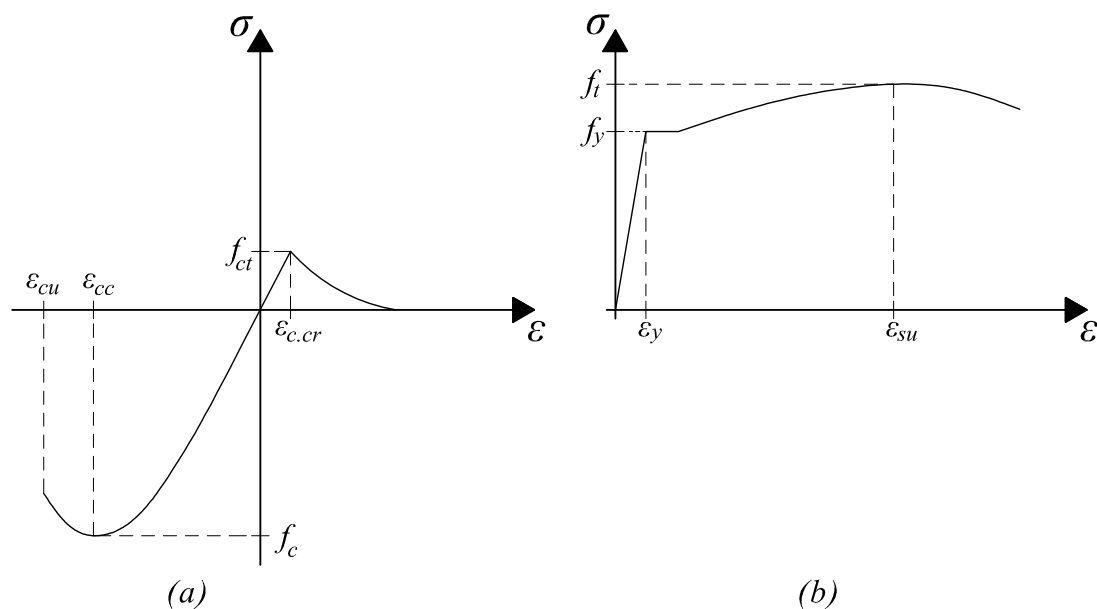
Figure 2.1   Typical stress-strain relationship for: (a) plain concrete (b) hot-rolled reinforcing steel of class B or C in tension.

When unloaded, both steel and concrete will have unloading curves as shown in Figure 2.2. If a second load cycle is initiated the load will follow a similar path to the original stress-strain curve. The dashed line in the figure represents an approximation for both steel and concrete where the unloading and reloading follows the same curve.
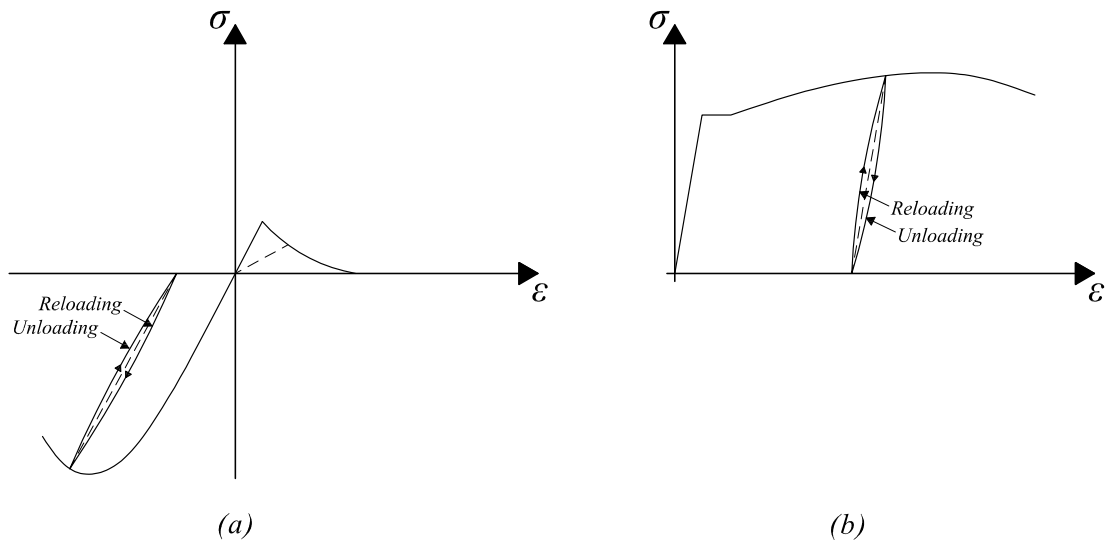
Figure 2.2   Typical unloading and reloading behaviour for: (a) concrete, and (b) hot-rolled reinforcing steel of class B or C in tension.

2.2 Structural response of beams

This section will, as an introduction of the structural response of reinforced concrete, cover the response of reinforced concrete beams since it is the most comprehensive structure to analyse in a simplified way. The theories presented in this section can be expanded to more complex structures, such as slabs.

2.2.1 Introduction to local and global response

The nature of reinforced concrete is a highly non-linear behaviour as shown in Section 2.1. The structural response of a reinforced concrete member is influenced by the structural response of the two constituent materials and the interaction between them. The most pronounced non-linear behaviour is derived from cracking of concrete and yielding of reinforcement.

The response of a reinforced concrete member can be divided into local and global response. The local response is the structural response of the cross-section in a single section of the beam and is determined by the relationship between the moment and the average curvature in that particular section. The sum of all local responses yields the overall behaviour of the beam i.e. the global response. The curvature χ of a cross-section is the inclination of the local deformation, i.e. strain ε, shown in Figure 2.3 and Equation (2-1).
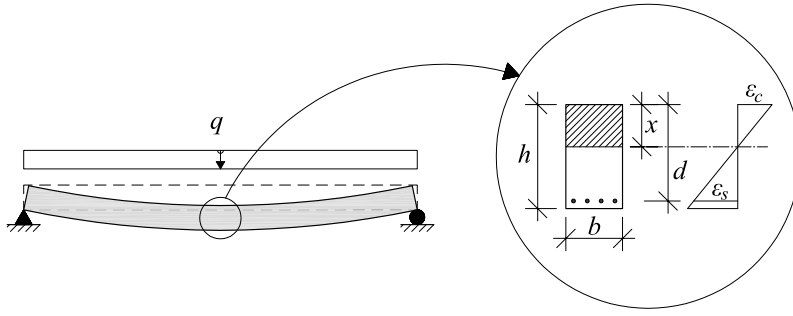
Figure 2.3   Relation between deformation and curvature.

$$\chi = \frac{1}{r} = \frac{\varepsilon_s - \varepsilon_c}{d}$$

<div align="right">(2-1)</div>

Where: χ = curvature

r = radius of curvature

ε_c = concrete strain

ε_s = reinforcement strain

d = effective depth of the cross-section

When loaded until failure, the beam illustrated in Figure 2.3 will go through three stages; State I (uncracked state), State II (cracked state) and State III (ultimate state) according to Eurocode 2, CEN (2004). If the applied moment and the corresponding curvature are plotted, the three states mentioned above are clearly visible as can be seen in Figure 2.4.
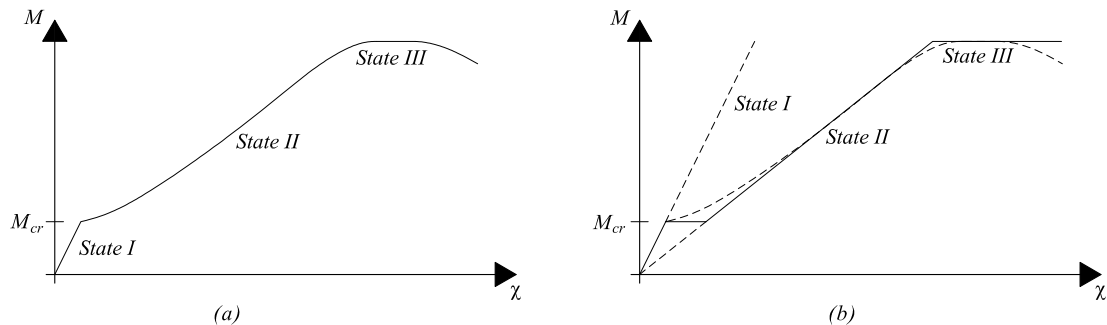
Figure 2.4   Response of a reinforced concrete member subjected to bending illustrated (a) the moment-curvature relation and (b) a simplified model for a combination of State I, II and III.

2.2.2   Uncracked state (State I)

The uncracked state (State I) is characterised by a linear behaviour of the cross-section. The curvature of the cross-section increases linearly with the applied bending moment, which is also reflected by the global response. It is generally assumed that the reinforcement have a small impact on the behaviour of the cross-section in the uncracked state. This is an assumption which underestimates the stiffness of the uncracked section since the stiffness can be increased by more than 20 % when the reinforcement is included, depending on the reinforcement amount, according to Engström (2011).
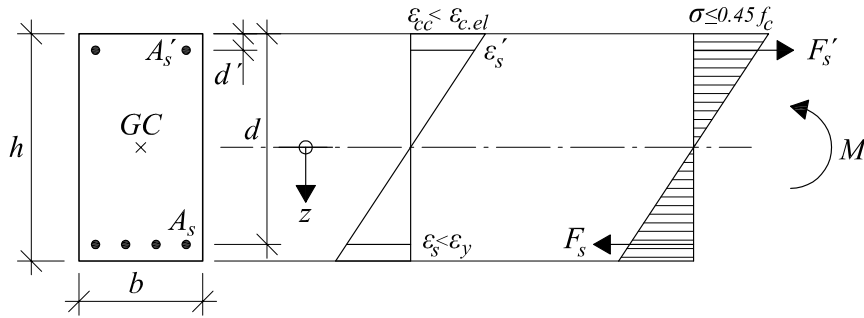
Figure 2.5   Internal forces, stresses and strains for a reinforced concrete cross-section in State I.

In order to evaluate the uncracked reinforced concrete section, illustrated in Figure 2.5, α_s is introduced as a factor between the stiffness of the reinforcement and the concrete, using the latter as the reference stiffness:

$$\alpha_s = \frac{E_s}{E_c} \tag{2-2}$$

Where: α_s = stiffness factor

E_s = Young's modulus for reinforcing steel

E_c = Young's modulus for concrete

The concrete stresses are calculated as:

$$\sigma_{c.I}(z) = \frac{M}{I_I} \cdot z \tag{2-3}$$

Where: $\sigma_{c.I}$ = concrete stress at the level z

M = bending moment at the considered section

z = distance from the gravity centre, see Figure 2.5

I_I = moment of inertia for a State I cross-section

The steel stress is calculated according to Equation (2-4) and can be calculated as a resulting force according to Equation (2-5).

$$\sigma_{s.I} = \alpha_s \sigma_{c.I}(z_s) \tag{2-4}$$

$$F_{s.I} = \sigma_{s.I} A_s \tag{2-5}$$

Where: $\sigma_{s.I}$ = steel stress in State I

z_s = distance from the gravity centre to the reinforcement

$F_{s.I}$ = resultant steel force in State I

A_s = reinforcement area

The moment-curvature relation for a State I model can be calculated according to Equation (2-6) and is shown in Figure 2.6.

$$\chi_{cr} = \frac{M_{cr}}{E_I I_I}$$

(2-6)

Where: χ_{cr} = curvature at cracking in State I

M_{cr} = moment corresponding to cracking of the cross-section

E_I = Young's modulus in State I
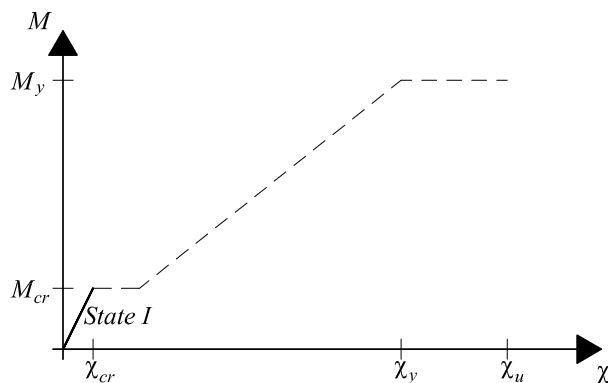
Figure 2.6   Moment-curvature relation for a State I model.

2.2.3 Cracked state (State II)

The cracked state (State II) is initiated when the concrete cracks. This will be the case when the stress in the outermost fibre of the cross-section reaches the tensile strength of the concrete f_{ct}. The local response of the reinforced concrete section in a State II model is, just as in a State I model, characterised by a linear behaviour.

The stiffness of a cracked reinforced concrete section is less than for an uncracked section. The effect of this can be seen in Figure 2.4 where the inclination of the line in the moment-curvature diagram is decreased when Stage II is initiated. There is a horizontal leap from State I to State II at the cracking moment. This is because the State II model assumes all local cross-sections of the global structure to be fully cracked, this is however not the case in a real structure.

As in the State II model, the stiffness in a real structure decreases when the concrete cracks. However, the decrease in stiffness does not occur immediately at the cracking moment M_{cr} due to a phenomenon called tension stiffening. As can be seen in Figure 2.7, there are still uncracked sections between the cracks that occur at the cracking moment. These uncracked sections are still in State I and will therefore contribute to the global stiffness positively. As a result, the State II model overestimates the overall deformations. When the moment is increased, the number of fully cracked sections will increase and thus approaching the assumption of a fully cracked member. The effect of tension stiffening can be incorporated in a simplified model as can be seen in Figure 2.7b.
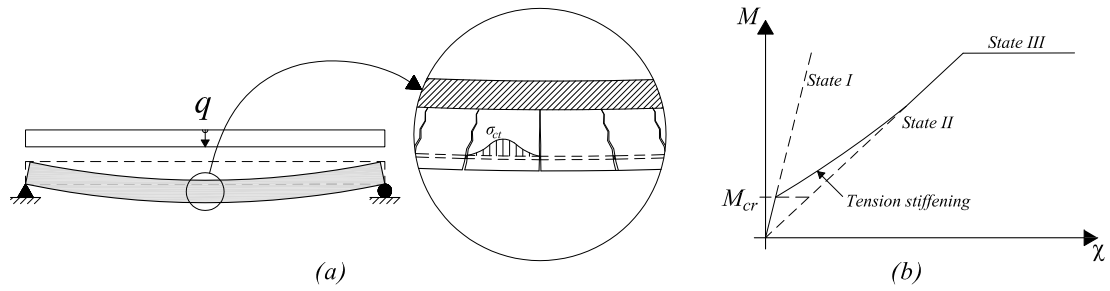
Figure 2.7   Influence of tension stiffening: (a) beam in state II (b) a simplified model including tension stiffening.

The State II model contains limitations related to steel stress and concrete compressive stresses. The model is limited to steel stresses up to yielding f_y and compressive stresses up to 50 % of the concrete compressive strength f_c according to Engström (2011). If this is the case, it is preferable to analyse the reinforced concrete section with a State III model that allows a non-linear material response of concrete independently of the response of the reinforcement.
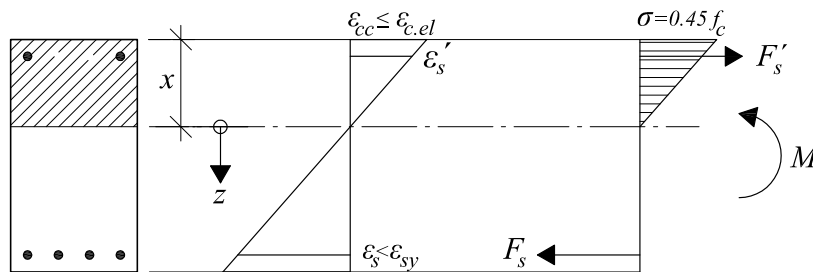
Figure 2.8   Internal forces, stresses and strains for a reinforced concrete cross-section in State II.

The concrete stresses in State II are calculated in a similar manner as for the State I model:

$$\sigma_{c.II}(z) = \frac{M}{I_{II}} \cdot z \tag{2-7}$$

Where: $\sigma_{c.II}$ = concrete stress at the level z in State II

   I_{II} = moment of inertia for a State II cross-section

The steel stress is calculated according to Equation (2-8) and can be calculated as a resulting force according to Equation (2-9).

$$\sigma_{s.II} = \alpha_s \sigma_{c.II}(z_s) \tag{2-8}$$

$$F_{s.II} = \sigma_{s.II} A_s \tag{2-9}$$

Where: $\sigma_{s.II}$ = steel stress in State II

   $F_{s.II}$ = resultant steel force in State II

The moment-curvature relation for a State II model can be calculated according to Equation (2-10) and is shown in Figure 2.9.

$$\chi_y = \frac{\varepsilon_{cc}}{x_y} \tag{2-10}$$

Where: χ_y = curvature at reinforcement yielding in State II

x_y = height of the compressive zone related to the moment at which the reinforcement starts to yield

ε_{cc} = concrete strain
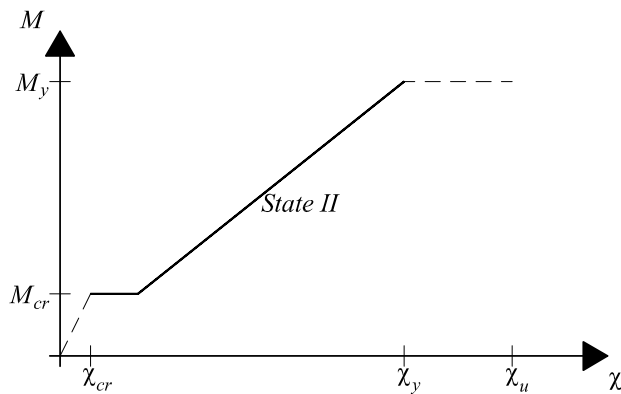
Figure 2.9   Moment-curvature relation for a State II model.

2.2.4 Ultimate state (State III)

The ultimate state (State III) is initiated when the reinforcement starts to yield or when the concrete stress reaches its compressive strength. The capacity of the cross-section can be increased due to a decreased height of the compression zone, or due to the positive effect of strain hardening of the tensile reinforcement. The ultimate capacity of the cross-section is assumed to be reached when the tensile reinforcement is torn off or the concrete is crushed.
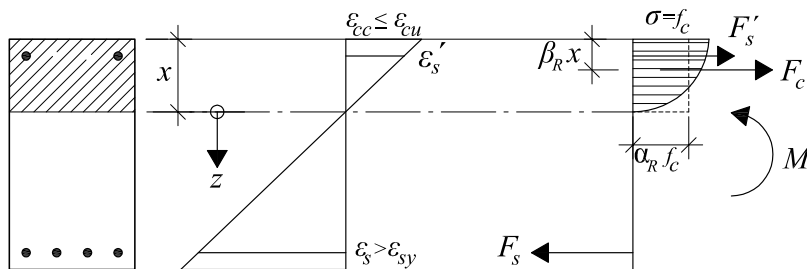
Figure 2.10 Internal forces, stresses and strains for a reinforced concrete cross-section in State III.

The concrete stresses in State III are calculated according to Equation (2-11) as a resultant force of the non-linear stress profile shown in Figure 2.10.

$$F_c = \alpha_R f_c b x \tag{2-11}$$

Where: F_c = resultant concrete force for State III concrete

α_R = stress block factor

f_c = concrete compressive strength

b = width of the cross-section

x = height of the compressive zone, see Figure 2.10

The values of the stress block factors, α_R and β_R, varies as a function of the concrete compressive strain ε_{cc}. The values of the stress block factors for the ultimate compressive strain ε_{cu} for normal strength concrete (C12/16-C50/60) are stated in Equation (2-12) and (2-13). For stress block factors for concrete compressive strains other than the ultimate compressive strain, the reader is referred to Engström (2011).

$$\alpha_R = 0.810 \tag{2-12}$$

$$\beta_R = 0.416 \tag{2-13}$$

The reinforcing steel is assumed to be yielding in the State III model and the steel stress is therefore replaced by the yield stress f_y according to:

$$F_s = f_y A_s \tag{2-14}$$

Where: F_s = resultant steel force

f_y = steel yield stress

The moment-curvature relation for a State III model can be calculated according to Equation (2-15) and is shown in Figure 2.11.
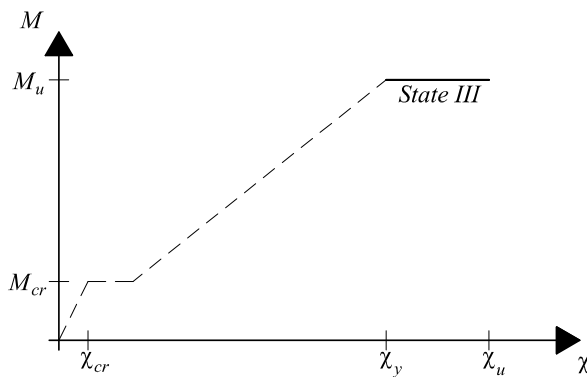
Figure 2.11 Moment-curvature relation for a State III model.

$$\chi_u = \frac{\varepsilon_{cu}}{x_u} \tag{2-15}$$

Where: χ_u = ultimate curvature in State III

x_u = height of the ultimate compressive zone

ε_{cu} = ultimate concrete strain

Note that the plastic curvature will propagate over a plastic region. This is covered in Section 2.2.6.

2.2.5 Simplified non-linear behaviour

The non-linear moment-curvature relationship for reinforced concrete shown in Figure 2.4 can be simplified to multiple linear curves as shown in Section 2.2.1 to 2.2.4. These curves can be used as input data for finite element analysis in order to model the non-linear behaviour of reinforced concrete. Figure 2.12 illustrates how these curves can be combined in order to capture this behaviour from first loading, to cracking of the concrete, yielding of the reinforcement and finally failure of the structure.
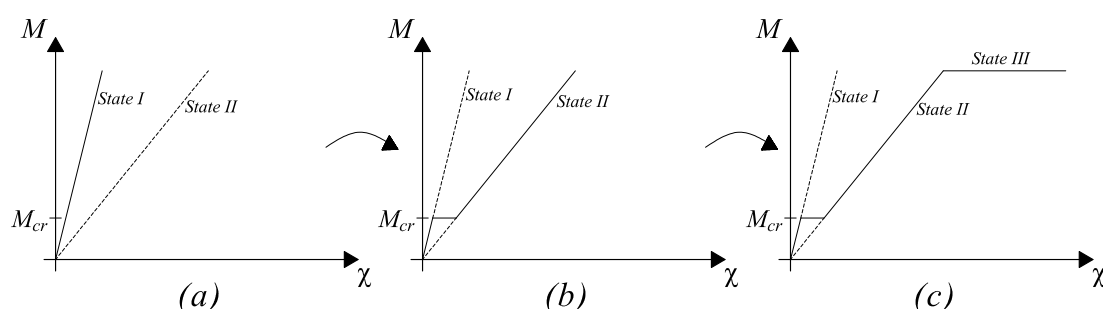
Figure 2.12   Linear, trilinear and quadlinear models used for reinforced concrete in a: (a) State I, (b) State II and (c) State III model.

2.2.6 Plastic rotation capacity

The reason for a collapse of a reinforced concrete member can either be derived from local or global failure. In order to develop a global failure, the structure needs to have sufficient plastic rotation capacity. If the structure does not have sufficient plastic rotation capacity, local failure, such as crushing of concrete or reinforcement rip off will take place and cause a global collapse.

In the yield line theory, plastic hinges are assumed to be concentrated to singular points with no propagation along the member in the global structural analysis model, Engström (2011). The response of the structure is assumed to behave linear elastically between the plastic hinges that are formed. The plastic hinges are considered as single or double, depending on where in a member it forms, see Figure 2.13. Single plastic hinges can be formed in fixed ends, such as cantilever supports while double plastic hinges can be formed in the span of a beam or over an inner support of a continuous structure.
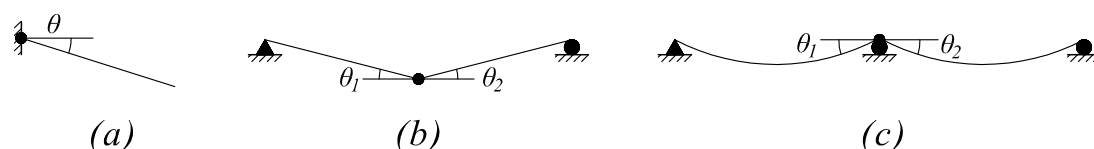
Figure 2.13   Single and double plastic hinges formed in: (a) a cantilever support, (b) the span of a simply supported beam, and (c) the mid-support of a continuous beam.

In a real structure, the plastic hinges will propagate over a certain length l_{pl} where the tensile steel strain exceeds the yield strain, see Figure 2.14.
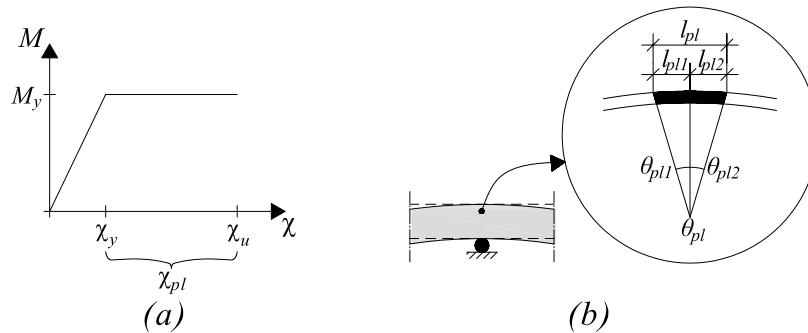
Figure 2.14 (a) moment-curvature relationship for elastic-plastic and plastic case and (b) plastic rotation development length over an inner support.

In case of a double plastic hinge, the total length of the plastic region is the sum of the lengths l_{pl1} and l_{pl2} and the total plastic rotation is in accordance the sum of the plastic rotation θ_{pl1} and θ_{pl2}, see Figure 2.14b. The plastic rotation can be obtained by integrating the plastic curvature over the propagation length of the plastic region l_{pl}, see Figure 2.14 and the following equations:

$$\theta_{pl} = \int_{x_1}^{x_2} \chi_{pl}\,dx \tag{2-16}$$

Where:

$$\chi_{pl} = \chi - \chi_y \tag{2-17}$$

$$l_{pl} = x_1 - x_2 \tag{2-18}$$

Where: θ_{pl} = plastic rotation

χ_{pl} = plastic curvature

χ = curvature

χ_y = yield curvature

l_{pl} = propagation length of a plastic region

x_1 = section x_1

x_2 = section x_2

Eurocode 2, CEN (2004), provides a simplified approach in order to estimate the plastic rotation capacity of a reinforced concrete cross-section. This simplified approach is based on the plastic rotation capacity as a function of the x_u/d ratio. Values of the plastic rotation capacity are presented in a diagram in Eurocode 2. Since no explicit values are stated in Eurocode 2, an interpretation of the diagram is presented in Figure 2.15, and the interpreted values are stated in Table 2.1. This diagram is valid for reinforced concrete sections with a shear slenderness $\lambda=3$, and concrete strength classes with an upper limit of C90/105 and reinforcement steel of ductility class B and C. For concrete strength classes C55/67 to C80/95, linear interpolation should be used. The diagram yields conservative values of the plastic rotation capacity and the positive effect of any transverse reinforcement is neglected.

Reinforcement class A is not recommended if plastic rotation is demanded and is therefore omitted in this section. For cross-sections with a shear slenderness $\lambda \neq 3$, the values from Figure 2.15 should be multiplied by a factor k_λ according to Equation (2-19).
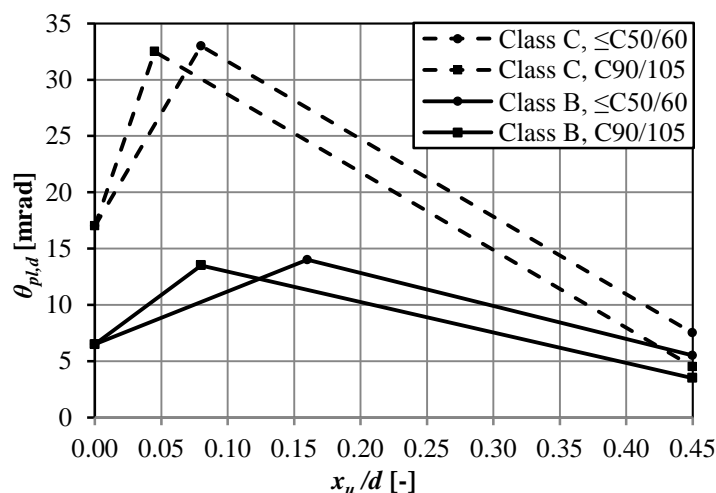
Figure 2.15 Diagram representing the correlation between maximum allowable plastic rotation, $\theta_{pl,d}$ and x_u/d ratio for concrete sections of different concrete strengths with reinforcement class B and C. This diagram is valid for sections with a shear slenderness $\lambda=3$.

Table 2.1 Interpreted values from Eurocode 2 of the maximum allowable plastic rotation $\theta_{pl,d}$ and x_u/d ratio for concrete sections of different concrete strengths with reinforcement class B and C

Concrete strength class	$\theta_{pl,d}$ ($x_u/d = 0$) [mrad]	$\theta_{pl,d,\mathrm{max}}$		$\theta_{pl,d}$ ($x_u/d = 0.45$) [mrad]
		$\theta_{pl,d}$ [mrad]	x_u / d [m]	
Class C, $\leq$ C50/60	17.0	33.0	0.080	7.50
Class C, $\leq$ C90/105	17.0	32.5	0.045	4.50
Class B, $\leq$ C50/60	6.50	13.5	0.160	5.50
Class B, $\leq$ C90/105	6.50	13.0	0.080	3.00

The plastic rotation capacity increases with increasing x_u/d ratio for small values of x_u/d up to a certain break point. The reason for this behaviour is that for small values of x_u/d, the plastic rotation capacity is limited by the ultimate steel strain ε_{su}. For higher values of x_u/d, i.e. after the breaking point, the rotation capacity is limited by the ultimate concrete strain ε_{cu}.

According to Eurocode 2, CEN (2004), for shear slenderness values other than $\lambda=3$, the plastic rotation capacity θ_{rd} can be calculated as:

$$\theta_{rd} = k_\lambda \theta_{pl,d} \tag{2-19}$$

Where:

$$k_\lambda = \sqrt{\frac{\lambda}{3}} \tag{2-20}$$

$$\lambda = \frac{x_0}{d} \tag{2-21}$$

Where: θ_{rd} = plastic rotation capacity

$\theta_{pl,d}$ = plastic rotation capacity according to Figure 2.15

k_λ = modification factor

λ = shear slenderness

x_0 = distance between the considered maximum moment section and the adjacent zero moment section after plastic redistribution, see Figure 2.16

d = effective depth of the considered cross-section
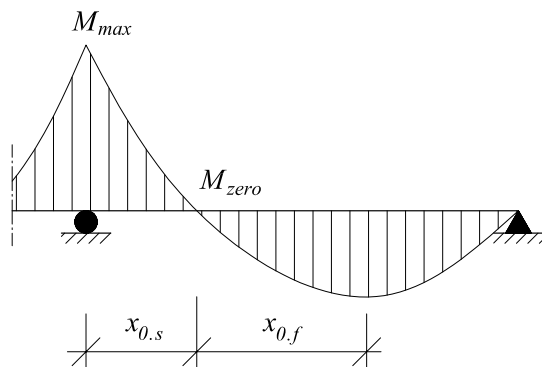
Figure 2.16 Example of distance between maximum and zero moment x_0 and effective depth of the considered cross-section d, after plastic redistribution.

In order to simplify Equation (2-21), Eurocode 2 provides a possibility to estimate the shear slenderness λ based on the design forces and effective depth of the considered cross-section as:

$$\lambda = \frac{M_{Ed}}{V_{Ed} d} \tag{2-22}$$

Where: M_{Ed} = design value of bending moment

V_{Ed} = design value of shear force

2.3 Structural response of slabs

This section covers the definition and categorisation of slabs, presented in Eurocode 2, CEN (2004), that are used in this Thesis. Furthermore, the influence of torsional forces in slabs and how these can be treated in analyses is covered.

2.3.1 Definition and categorisation

The structural response of a slab is different to that of a beam. The difference can be derived from the transverse action that needs to be considered in a slab due to a high width to height ratio. According to Eurocode 2, there is a strict difference in definition between a beam and a slab that is specifically related to the relationship between the width and the height of the cross-section. A slab is, by this definition, a structural member with a width to height ratio, no smaller than 5. Furthermore, Eurocode 2 distinguishes between two types of slabs; one-way and two-way spanning slabs where the first of the two is defined as:

"A slab subjected to dominantly uniformly distributed loads may be considered to be one-way spanning if either:

- *it possesses two free (unsupported) and sensibly parallel edges, or*
- *it is the central part of a sensibly regular slab supported on four edges with a ratio of the longer to shorter span greater than 2."*

Since the definition presented in Eurocode 2 does not cover all possible cases, Pacoste *et al.* (2012) defined a third category of slabs, predominantly one-way supported slabs. The practical application of this third type is slab bridges where the slabs often are supported by a combination of line supports (abutments) and point supports (intermediate columns). The columns are arranged in such a way that the span is significantly larger in one direction compared to the other, see Figure 2.17.
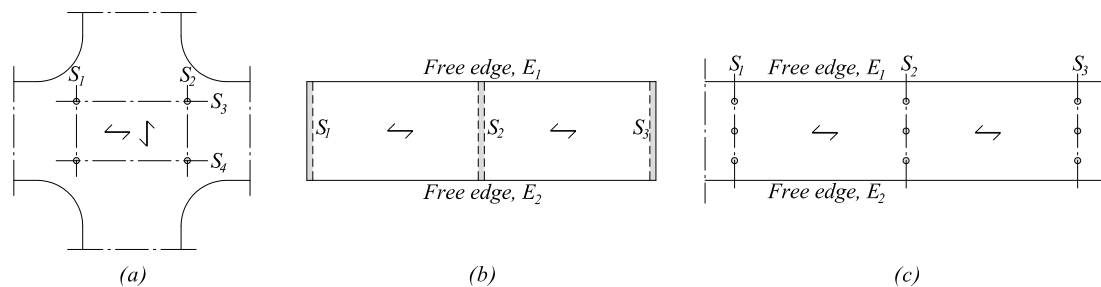
Figure 2.17   Examples of bridge structures that can be interpreted as: (a) two-way spanning slabs, (b) one-way spanning slabs and (c) predominantly one-way spanning slabs, proposed by Pacoste et al. (2012).

The cantilever slab is also a frequently used structure in the bridge design community. The difference between the type of slabs mentioned above and the cantilever slab is that in the latter case, the loads are mainly carried in the transversal direction of the bridge to the main load carrying structure.

Cantilever slabs can be observed in a vast range of structures. The most common cantilever slab in buildings is the cantilevered balcony. In the bridge design community, cantilever slabs are mainly found in composite bridges or concrete beam bridges, see Figure 2.18.
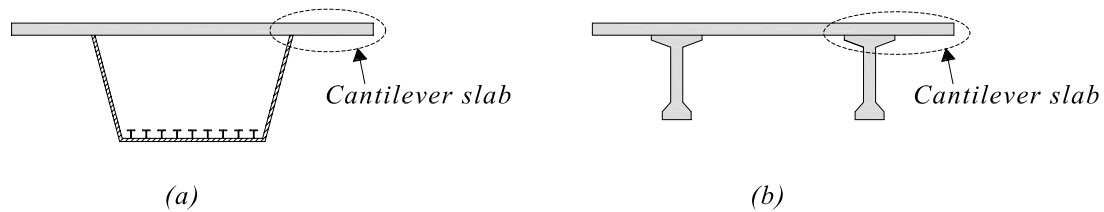
Figure 2.18 Cantilever slab in: (a) composite bridges and (b) concrete beam bridges.

2.3.2 Torsional forces

The torsional stiffness has a significant influence on the structural behaviour and thus the displacements of slabs. Torsion is particularly important for slabs which are subjected to concentrated forces. However, there is little knowledge of the torsional stiffness in slabs, especially in the cracked state (State II). In the ultimate limit state (State III), the torsional stiffness is usually omitted and the slab is considered to carry the load only in the directions of the reinforcement which is sufficient to fulfil equilibrium. However, in the service state, when there is a need to estimate the actual moments experienced by the slab, the torsional stiffness has a significant role.

For members where the load is predominantly carried by bending, a relation between uncracked and cracked stiffness in the range of 3-5 is reasonable. Since the stiffness range is highly dependent on the reinforcement amount and the position of the bars, the stiffness relation might therefore be outside of the above stated interval. However, when torsion has a predominant role, this relation is no longer valid. Torsional moments lead to a greater loss of stiffness in the cracked state than that of bending. According to tests performed on a reinforced concrete slab in Lopes *et al.* (2014), the torsional stiffness in a cracked state is about 1/17-1/15 of the stiffness in the elastic state. BBK (2004) states that when calculating deformations caused by torsion in reinforced concrete beams, the torsional stiffness should be reduced with a factor 0.3 of the elastic stiffness. This applies if flexural cracks are present and a factor 0.1 should be used if shear or torsional cracks are present.

If a beam grillage model is used for non-linear analysis, it is important to characterize the torsional stiffness of the beams in order to receive a representative behaviour. It was discussed in Lopes *et al*. that in numerical simulation, the torsional stiffness adopted in the stiffness matrix of the finite element, greatly influence the slabs deformation in both linear and non-linear analysis. However, it is complicated and cumbersome to relate the torsional moment with angle of twist for beam elements in the grillage model, particularly in the post-cracking state. The problem originates both from the fact that bundled beams that are not attached to each other longitudinally behave very differently from a solid section with the same total width, and that there is little knowledge of the torsional stiffness in the cracked state.

3 FE-modelling and traffic load application

This chapter covers background theory of possible ways to model slabs with the finite element method. This chapter also covers load models on bridge structures provided by Eurocode 1, CEN (2003), and the actual loads that can occur on real bridge structures. As a final part of this chapter, current recommendations by Pacoste *et al.* (2012) on how to redistribute moments from concentrated forces in different types of slabs are covered.

3.1 Finite element models for slabs

In this Thesis, slabs are analysed using finite element models. The finite element software used is the student version of ADINA (2012). Several approaches to model reinforced concrete slabs exist. For instance, different types of elements can be utilized which approximates the structural behaviour in different ways. In this Thesis, the beam grillage model was chosen for non-linear analysis. In addition, linear elastic shell element models were used for an early verification. However, fundamental differences between the shell element model and the beam grillage model exist and these will therefore not yield the same results even for matching input data. One of these fundamental differences is how torsional moments are treated. The two different types of models are illustrated in Figure 3.1.
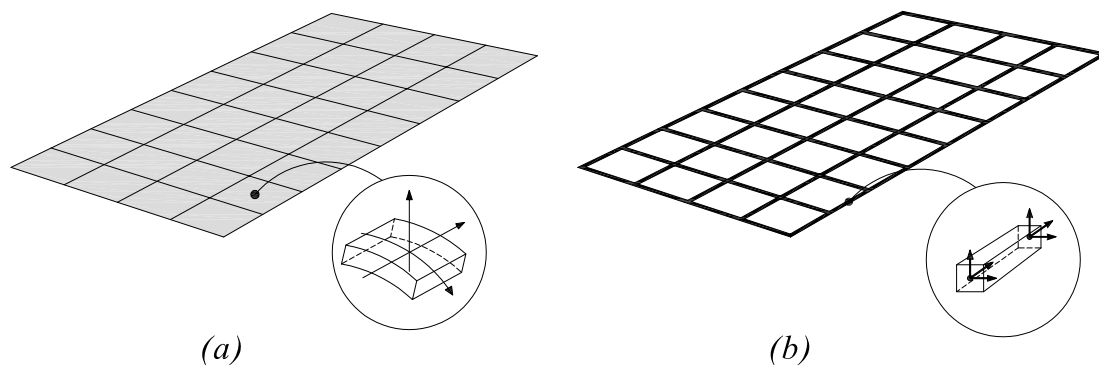
Figure 3.1   (a) Shell element model, (b) Beam grillage model

3.1.1 Shell element models

In the early stages of ordinary reinforcement moment design, there is no knowledge of the stiffness proportions in different directions of a slab. It can therefore be necessary to start with a linear elastic isotropic model to acquire approximate reinforcement amounts. The shell element model offers a simple way to model the behaviour of a slab and the approach is widely used in both the bridge and building design community. However, since the moment distribution is governed by stiffness, this type of analysis will not yield the actual moment distribution experienced by the slab since the behaviour is changed when reinforcement amounts are chosen. It is however possible with shell elements, when reinforcement amounts are chosen, to perform a second iteration with different stiffness in different directions corresponding to the chosen reinforcement amount and layout. This can be made by manipulating the Young's modulus in different directions.

A result of linear finite element analysis using shell elements is that unrealistic concentrations of cross-sectional moments and shear forces occur. According to Pacoste *et al.* (2012), there are mainly two simplifications of the reality that creates these unrealistic force concentrations. The first of these two is geometrical simplifications such as simplification of connections, supports and loads, which is common in finite element analysis in order to save computation power and time. When a support, or a concentrated force, is applied to a single node, a singularity is introduced in the system and thus the solution. The second simplification is an approximation of the mechanical properties of the chosen materials. It is often assumed that reinforced concrete is an isotropic material and behaves linear elastically. However, reinforced concrete shows a high degree of non-linear behaviour due to cracking and crushing of concrete and yielding of reinforcement.

When a 3D linear elastic analysis is made for reinforcement design, calculated sectional forces contain both bending and torsional moments, see Figure 3.2.
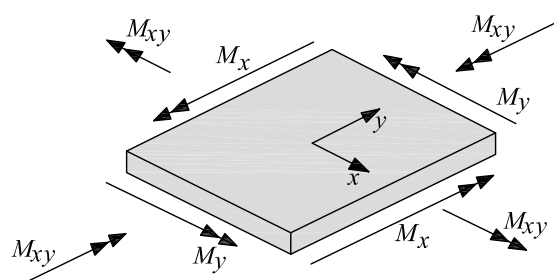
Figure 3.2   Bending and torsional moments acting on a shell element.

In reality, it is most common for the reinforcement to be arranged in grids with reinforcement bars perpendicular to each other. This means that torsional moments cannot be resisted effectively by the reinforcement. For simplicity, it is recommended to transform the torsional moments into bending moments in the two main directions:

$$m_{rx,pos(neg)} = m_x \pm \mu \left| m_{xy} \right| \tag{3-1}$$

$$m_{ry,pos(neg)} = m_y \pm \frac{1}{\mu} \left| m_{xy} \right| \tag{3-2}$$

Where: m_{rx} = design reinforcement moment in *x*-direction

m_{ry} = design reinforcement moment in *y*-direction

m_x = bending moment in *x*-direction from the linear solution

m_y = bending moment in *y*-direction from the linear solution

m_{xy} = torsional moment from the linear solution

μ = factor that can be chosen with respect to practical considerations, usually close to 1.0 or equal to 1.0

The indices *pos* and *neg* in the equations above refer to bottom and top reinforcement, where for positive bending moments, a positive contribution from the torsional moment should be added, and vice versa.

For analyses including shell elements in this Thesis, four-node isoparametric shell elements were used. The element formulation used in ADINA is based on two main assumptions, ADINA (2012):

- A line normal to the midsurface of the element that is originally straight remains straight during deformations.
- The stress in the direction normal to the midsurface of the structure is zero.

Newton-Cotes integration method is used over the thickness of the shell elements with 7 integration points, while Gauss integration method is used over the width of the elements with two integration points in both directions.

3.1.2 Beam grillage models

In order to model the non-linear behaviour of reinforced concrete slabs, the Thesis utilizes a method offered in ADINA where non-linear moment-curvature relations are used as input for beam elements which are used in a beam grillage model. The method offers a simplified approach to model the non-linear response due to cracking and yielding of reinforcement. Each section can be in different states regarding the reinforced concrete response, see Figure 3.3. Each beam element can be given an individual moment-curvature relation input, which yields the possibility to model different behaviour in different directions.
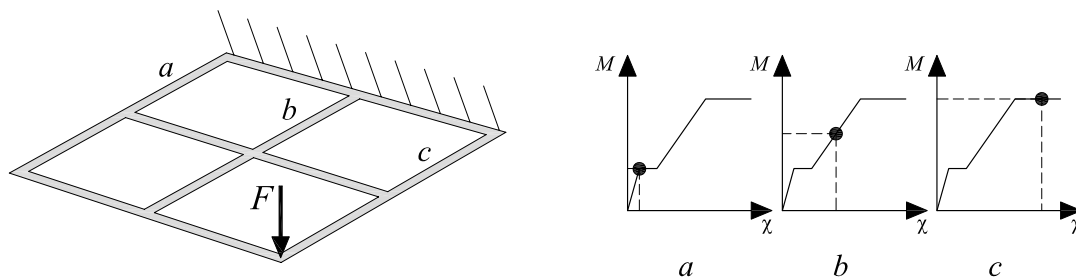
Figure 3.3   Beam grillage model where different sections are in different states and therefore in different levels in their corresponding moment-curvature relationship.

The relevant inputs needed for this approach are the moment-curvature relations around three axes. The three axes are illustrated in Figure 3.4 and are in ADINA denoted *s*, *t* and *r*. The moment-curvature input for axes *s* and *t* correspond to flexural bending while the input for *r*-direction corresponds to torsion and the input is therefore named *torsional moment versus angle of twist*. The bending stiffness around the *t*-axis will not affect the structural behaviour of a slab to a significant extent and the input data for this parameter is therefore omitted in this section. Hence, when moment-curvature input is further discussed in this Thesis, it is referred to bending around the *s*-axis.
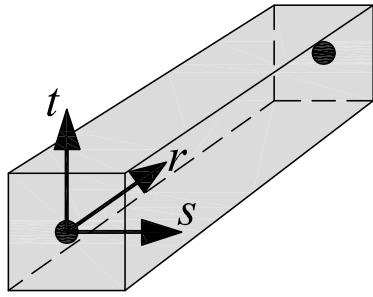
Figure 3.4   Local coordinate system for a beam element in ADINA.

The use of a beam grillage models is believed to be an acceptable approximation of the structural response for the analyses made in this Thesis. Even though more refined models exist, where concrete and reinforcement is modelled separately, the beam grillage model has the advantage of being more numerically stable.

The torsional behaviour of a beam, and thus also a beam grillage model, is different from the torsional behaviour of a plate element, see Figure 3.5. It can therefore be difficult to approximate the torsional stiffness that should be used as input for the beam grillage model.
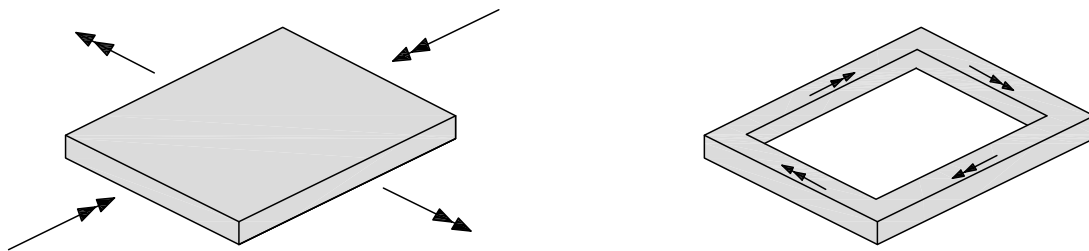
Figure 3.5   Principle torsional moments for a shell element and a beam grillage section.

As described in Lim (2013), the results obtained from the beam grillage model for the linear elastic case were highly dependent on the density of the chosen mesh. The torsional stiffness is highly dependent on the cross-sectional geometry, especially the width of the cross-section, see Equation (3-3). Therefore, the torsional stiffness changes with the mesh density as the cross-sectional width is chosen equal to the spacing between the beams. With a coarser mesh, wider cross-sections of the beams are obtained and therefore a significant increase of the torsional stiffness. It can therefore be concluded that, in comparison to shell elements, an increased mesh density does not lead to convergence.

$$K_v = \beta h b^3 \tag{3-3}$$

Where: K_v = torsional stiffness of a rectangular cross-section.

   β = constant depending on the height to width ratio of the cross-section

   h = height of a rectangular cross-section

   b = width of a rectangular cross-section

CHALMERS, *Civil and Environmental Engineering*, Master's Thesis 2014:73

For analysis involving beam elements in this Thesis, two-node elements were used. The element is initially straight and is based on assumptions of a Hermitian beam which neglects the effect of transverse shear deformations.

3.2 Traffic loads on bridges

There are numerous load models and load application types defined in standards that are used in different parts of the world. This section focuses on the two most commonly used vertical load models for vehicles (LM1 and LM2) presented in Eurocode 1, CEN (2003). For additional applications and limitations for the two load models, the reader is referred to Eurocode 1. Horizontal forces, such as breaking and acceleration forces, are not covered in this Thesis and are therefore omitted in this section.

3.2.1 Load model 1

Load model 1 (LM1) is presented in Eurocode 1 and is described as:

"Concentrated and distributed loads, which cover most of the effects of the traffic of lorries and cars. This model should be used for general and local verifications"

Load model 1 consists of two partial systems. The first system consists of double-axle concentrated loads where the load on each axle is defined as:

$$\alpha_Q \cdot Q_k \tag{3-4}$$

where α_Q is an adjustment factor which can be found in Eurocode 1. The load from each axle pair is assumed to be distributed to two identical wheels, each consisting of the concentrated load:

$$0.5 \cdot \alpha_Q \cdot Q_k \tag{3-5}$$

where the contact surface of each wheel is a square with a side of 0.4 m. The second system consists of uniformly distributed loads that only should be applied in the unfavourable parts of the structure with a load according to:

$$\alpha_q \cdot q_k \tag{3-6}$$

where α_q is an adjustment factor. The characteristic load values include the influence of dynamic amplification and are presented in Table 3.1.

Table 3.1   Characteristic loads values valid for load model 1 Eurocode 1.

Location	Axle loads Q_{ik} [kN]	Distributed loads q_{ik} [kN/m^2]
Lane Number 1	300	9
Lane Number 2	200	2.5

Lane Number 3	100	2.5
Other lanes	0	2.5
Remaining area	0	2.5

Load model 1 is illustrated in Figure 3.6 where each lane has a width of 3 m.
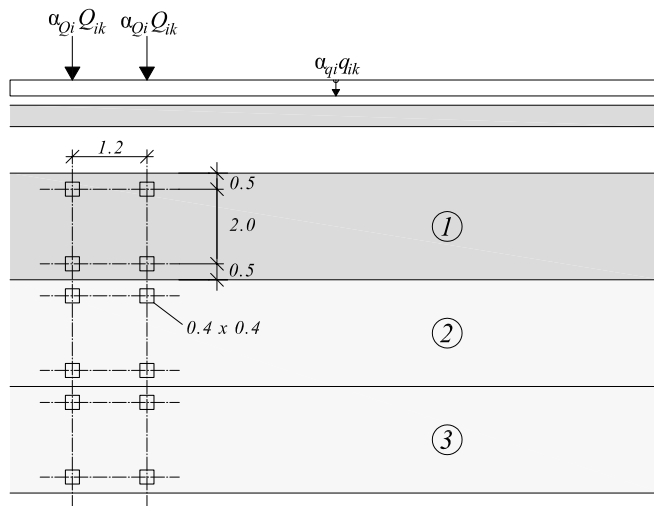
Figure 3.6   Geometrical application for load model 1 (LM1), Eurocode 1.

3.2.2 Load model 2

Load model 2 (LM2), in comparison to load model 1, only consist of one single axle load which can be applied at any location on the carriageway. The value of each axle load is defined as:

$$\beta_Q \cdot Q_{ak} \tag{3-7}$$

where $Q_{ak} = 400$ kN which includes the influence of dynamic amplification and β_Q is an adjustment factor. The load from the axle pair is assumed to be distributed to two identical wheels, each consisting of the concentrated load:

$$0.5 \cdot \beta_Q \cdot Q_{ak} \tag{3-8}$$

The contact surface for each wheel should be modelled as a rectangle of sides 0.35 and 0.6 m, see Figure 3.7.
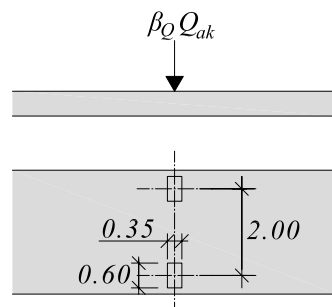
Figure 3.7   Geometrical application for load model 2 (LM2), Eurocode 1

CHALMERS, *Civil and Environmental Engineering*, Master's Thesis 2014:73

3.3 Measured traffic loads on bridges

A crucial part of ensuring a long service life of a bridge structure is to measure the actual load levels that it is subjected to. A common approach to obtain this data today is to utilize the Weigh-in-Motion (WIM) technique, Zhou *el al.* (2014). WIM is a device that is designed to capture and record axle weights and gross vehicle weights as vehicles passes over a predefined measurement site. This technique is capable of measuring vehicles travelling at normal speed and is therefore comprehensive for measuring the loads acting on a bridge structure.

It is stated in Eurocode 1, CEN (2003) that bridge structures should be able to resist the characteristic value for a 1000-year return period. This means that the probability of the occurrence of one such load should be less than 5 % in a time period of 50 years. Since it is impossible to collect data for such time periods, smaller samples of measurements and various extrapolation methods are used.

The load models presented in Eurocode 1 are based on WIM data collected in 1986 at a WIM station on the heavy trafficked A6 motorway in Auxerre, France. The data obtained from this two week period of measurements were used for calibrating the characteristic values presented in Eurocode 1, Zhou *el al*. In a study conducted by Zhou *et al.* the data from 1986 was compared with WIM data from a comparable bridge, a bridge located on the A9 motorway in St Jean de Vedas, France. It was shown from these results that the mean flow (vehicles per hour) had more than doubled since 1986. The traffic composition showed that five-axle trucks and thus the heavy traffic had a large increase during that time period. It was concluded that the load models provided by Eurocode 1 still yields satisfying safety margin but it has been reduced since the writing of the code due to changed regulations on weights and dimensions of vehicles.

From what have been found in the literature study conducted in this Thesis, no WIM results have given indications of higher total applied loads than what is predicted by the load models provided by Eurocode 1. Siegert *et al.* (2008) studied the deflections in the mid-span of a bridge during a 256 days period in 2004 and 2005. From the obtained data, estimated values, based on a 1000 year return period, were presented and compared with LM1, presented in Eurocode. The deflections from an LM1 model yielded deflections 42 % greater than what was estimated by the study and the load model was therefore considered as conservative in that isolated case.

Severe load events have, however, been observed which may cause local damages. An extreme value was found in a study conducted by Treacy & Brühwiler (2013) which was assumed to be derived from a special permission vehicle. This assumption was based on the fact that the value was obtained on a Sunday when such loads usually are permitted due to lesser traffic and safety reasons. It was also assumed by Nowak (1993) that extremely heavy loaded trucks purposefully avoids routs with known WIM stations and the data obtained for the severe loads might therefore be underestimated. This indicates that loads of magnitudes higher than expected might arise on a bridge structure during its service life.

3.4 Redistribution of reinforcement moments

The moment distribution in a slab is more complex to predict compared to that of a beam because of the transverse action. It is however necessary to make a reasonable estimation of the moment distribution, both in the service state and the ultimate limit state. The different states vary both in magnitude and shape of the moment distribution due to the non-linear behaviour of concrete. In recent years, 3D finite element analysis has become more frequently used for design of reinforced concrete bridges. However, in linear elastic 3D analysis, some problems occur that was not present in traditional 2D design. One such problem is how to treat force concentrations which, for example, can be caused by concentrated loading or concentrated supports, such as columns. Recently, guidelines on how to treat this problem have been presented by Pacoste *et al.* (2012). These recommendations are given as widths under which the total bending moment can be assumed to be distributed, with a constant moment distribution over the width. These recommended widths are based on old regulations such as Bro (2004) and BBK 04 (2004).

In this section, an example of a traditional approach is presented for better understanding of how this situation was treated in old regulations. Further, the recommendations in Pacoste *et al*. for FE analysis are presented.

3.4.1 Traditional approach

In the bridge design community, 2D analysis has been the main tool for design of reinforced concrete bridge decks up until recent years. Demands and requirements of structures are normally stated in norms, which also treated moment distribution widths for concentred loading to some extent. For example, the old code B7 (1968), included recommendations on moment distribution widths for concentrated loading on slabs. For slabs supported along two parallel edges, the total moment in the ultimate limit state was recommended to be distributed with a constant value within a width calculated in Equation (3-9), see Figure 3.8 for notations.

$$w = \min\left(\frac{3}{4}l, 2.5\text{m}\right) + b + t \qquad (3\text{-}9)$$

Where: w = distribution width

l = the characteristic span length

b = width of the concentrated force

t = height of fill material
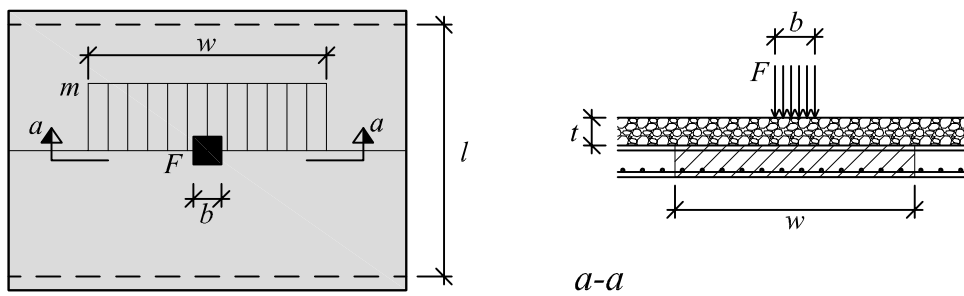
Figure 3.8   Moment distribution width for slabs supported along two parallel edges.

Together with the recommendation for distribution width, demands were also made on the transverse reinforcement. B7 also included recommendations for cantilever slabs, designed with edge beams. The expressions take the stiffness of the edge beam and the stiffness along the support into account, see Equation (3-10). For notations see Figure 3.9.

$$w = \frac{2}{n} \tag{3-10}$$

Where:

$$n = \sqrt[4]{\frac{c}{4EI_1}} \tag{3-11}$$

Where:

$$c = \frac{3EI_2}{a^3} \tag{3-12}$$

Where: E = Young's modulus for concrete

I_1 = moment of inertia of the edge beam and an additional part of the slab from the edge beam to the applied load

I_2 = moment of inertia along the support, per unit width

a = distance from support to applied load
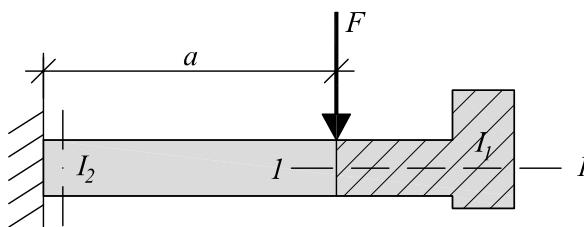
Figure 3.9   Notations for a cantilever slab structure with an edge beam.

3.4.2 Recommendations from Pacoste *et al.* for FE analysis

The recommendations, restrictions and limitations presented in this section can be generally applied for slabs. There is however additional limitations and recommendations for each individual type of slab presented in Figure 2.17. Simply supported one-way slabs are treated in Section 3.4.2.1 and 3.4.2.2, cantilever slabs are treated in Section 3.4.2.3, while two-way and predominantly one-way spans are omitted in this Thesis. For information on the latter two types of slabs, the reader is referred to Pacoste *et al.* (2012). The following recommendations for moment distribution widths at a support are given by Pacoste *et al*:

$$w = \min\left(3h, \frac{l}{10}\right) \qquad \text{for } \frac{x_u}{d} = 0.45 \text{ (0.35 for concrete grades} \geq \text{C55/67)} \qquad (3\text{-}13)$$

$$w = \min\left(5h, \frac{l}{5}\right) \qquad \text{for } \frac{x_u}{d} = 0.30 \text{ (0.23 for concrete grades} \geq \text{C55/67)} \qquad (3\text{-}14)$$

$$w = \frac{l}{4} \qquad \text{for } \frac{x_u}{d} = 0.25 \text{ (0.15 for concrete grades} \geq \text{C55/67)} \qquad (3\text{-}15)$$

$$w = \frac{l}{2} \qquad \text{for } \frac{x_u}{d} = 0.15 \text{ (0.10 for concrete grades} \geq \text{C55/67)} \qquad (3\text{-}16)$$

$$w = \min\left(5h, \frac{l}{5}\right) \qquad \text{for } \frac{x_u}{d} = 0.0 \qquad (3\text{-}17)$$

Where: h = height of the cross-section

x_u = depth of the neutral axis in ultimate limit state after redistribution

d = effective depth at the critical cross-section

l = characteristic span length

For ductility values between the limits stated above, linear interpolation can be used in order to obtain values of the corresponding distribution width *w*. Independent of the requirements of ductility; the distribution width should be chosen according to:

$$w \geq w_{\min} = 2h + a \qquad (3\text{-}18)$$

Where *a* is the dimension of the support in the considered direction. When using Equation (3-13) to (3-17), additional limitations for columns with drop panels apply. These types of supports are not covered in this Thesis but for more information on the subject, the reader is referred to Pacoste *et al.* (2012). There is however an additional restriction to the above stated equations on the ratio between the average and maximum reinforcement moment:

$$\delta = \frac{m_{rx,av}}{m_{rx,\max}} \geq 0.6 \qquad (3\text{-}19)$$

Where $m_{rx,av}$ and $m_{rx,max}$ can be determined based on Figure 3.10a and Equation (3-20) if the distribution width exceeds the distance between the points of zero moments and Figure 3.10b and Equation (3-21) if the distribution width is smaller than the distance between the points of zero moments.
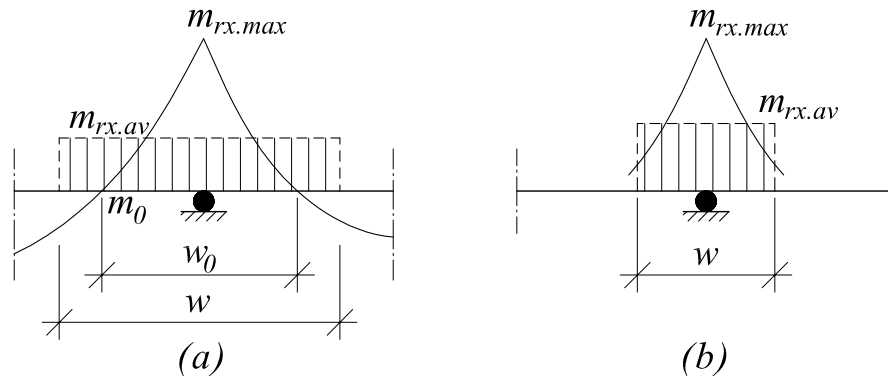
Figure 3.10 *Definition of the average value of reinforcement moment distribution where: (a) the distribution width is greater than the distance between the points of zero moment and (b) the distribution width is less than the distance between the points of zero moment.*

The average moment after distribution $m_{rx,av}$ in Figure 3.10a and Figure 3.10b can be obtained using Equation (3-20) and (3-21), respectively.

$$m_{rx,av} = \frac{1}{w} \int_0^{w_0} m_{rx} dy \tag{3-20}$$

$$m_{rx,av} = \frac{1}{w} \int_0^{w} m_{rx} dy \tag{3-21}$$

3.4.2.1 Distribution widths for one-way slabs in ULS

The recommendations and restrictions on how to determine the distribution width for simply supported one-way slabs are treated in this section. These are applied in addition to those stated for slabs in Section 3.4.2. The distribution width for the moment is divided into longitudinal and transversal direction. The characteristic span length in the longitudinal direction is defined by Equation (3-22) and by Equation (3-23) in the transverse direction and illustrated in Figure 3.11. In addition to the general restrictions defined in Equation (3-13) to (3-17), the distribution width in the transverse direction is limited to Equation (3-24).

$$l = L_y \tag{3-22}$$

$$l = B_x \tag{3-23}$$

$$w_x \leq \frac{L_y}{2} \tag{3-24}$$
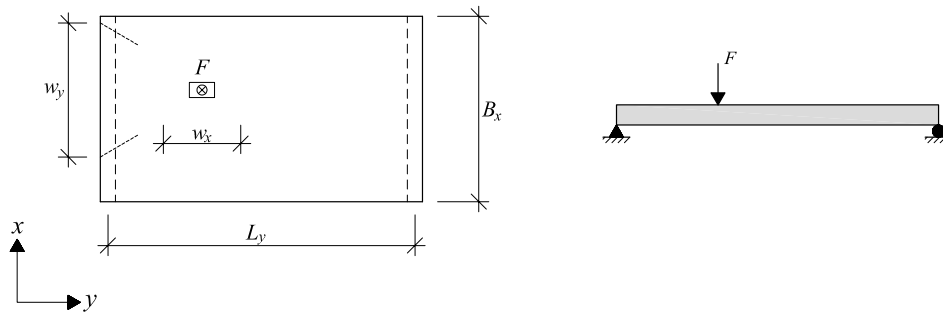
Figure 3.11   Distribution widths for a simply supported one-way slab in longitudinal and transversal direction.

3.4.2.2   Distribution widths for one-way slabs in SLS

According to Pacoste *et al.* (2012), there are very few recommendations in the literature on how to choose an appropriate distribution width for moments in the serviceability limit state. The reason for this is the difficulty of determining the behaviour of the reinforced concrete immediately after the slab starts to crack.

The distribution of the reinforcement should reflect the assumed behaviour of the slabs in working conditions which leads to a concentration of reinforcement over columns. Pacoste *et al.* recommends that 50 % of the total amount of the top reinforcement should be concentrated to a strip over the column with the width, *w*:

$$w = \frac{l_1}{8} + \frac{l_2}{8} \tag{3-25}$$

where l_1 and l_2 are the distances between the column and the adjacent columns in the direction perpendicular to the reinforcement which is illustrated in Figure 3.12. This approach generally leads to a larger reinforcement concentration in the column strip than what is obtained by linear elastic analysis.
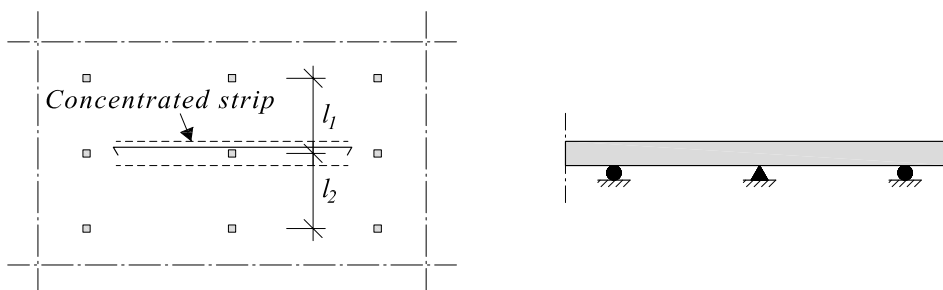
Figure 3.12   Illustration of Equation (3-25).

The recommendation is to adapt a more conservative approach when choosing moment distribution widths in SLS in comparison to the ULS. Due to this reason, Pacoste *et al.* recommends the distribution width to be restricted to the equation below, which is a combination of Equation (3-13) and (3-14).

$$\min\left(3h, \frac{l}{10}\right) \leq w \leq \min\left(5h, \frac{l}{5}\right) \tag{3-26}$$

3.4.2.3 Distribution widths for cantilever slabs

The recommendations given by Pacoste *et al.* are the result of a literature study, mainly based on recommendations from Swedish handbooks such as BBK 04 (2004) and also Davidson (2003). These recommendations are originally based on the work and tests performed by Hedman and Losberg (1976). According to Pacoste *et al*, these recommendations are not believed to be as conservative as the recommendations for moment and shear distribution widths for simply supported slabs.

The simplest case of moment distribution in a cantilever slab is for one concentrated static force. The load is transferred to the support over a distribution width due to the effect of plastic redistribution. For one concentrated force, see Figure 3.13a, the width *w* over which the moment is distributed in the ultimate limit state is defined as:

$$w = \min \begin{cases} 7d + b + t \\ 10d + 1.3 y_{cs} \end{cases}$$ (3-27)

Where: x_u = depth of the neutral axis in ultimate limit state after redistribution
d = effective depth at the critical cross-section
h = height of the cantilever at the critical cross-section
b = width of the load
t = thickness of the surfacing
y_{cs} = distance from the centre of the load to the critical cross-section

The above stated distribution width *w* applies for the following limits of the x_u/d ratio:

$$0.15 \le \frac{x_u}{d} \le 0.25 \text{ for concrete classes } C12/15 \text{ to } C50/60$$ (3-28)

$$0.10 \le \frac{x_u}{d} \le 0.15 \text{ for concrete classes } C55/67 \text{ and greater}$$ (3-29)

For values outside the above stated limits, the distribution width w_y should be defined as the distribution width for the serviceability limit state:

$$w_y = 2h + b + t$$ (3-30)
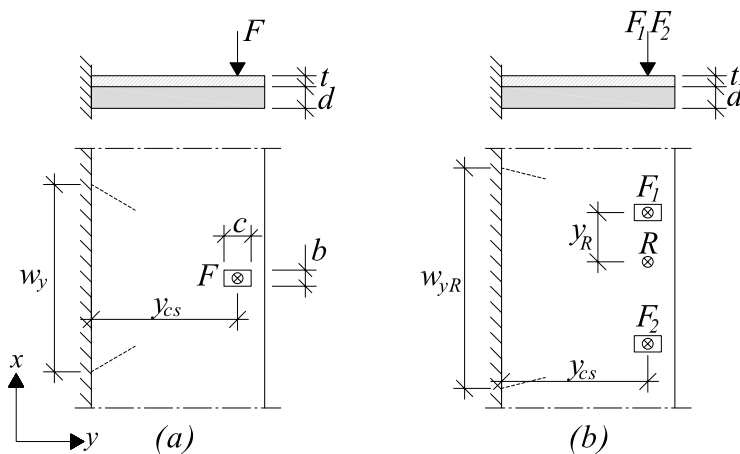
Figure 3.13 Moment distribution widths for: (a) one concentrated force and (b) two or several concentrated forces.

For the case of two or several concentrated forces, a similar distribution width as for one concentrated force can be used. If the distance between the concentrated forces is such that the distribution widths do not overlap, Equation (3-27) can be used for each individual load. If on the other hand, the distribution widths from the concentrated forces overlap, the combined distribution width w_{yR} should be used:

$$w_{yR} = 2y_R + w_y \tag{3-31}$$

Where:

$$y_R = \min\begin{cases} y_1 \\ y_n \end{cases} \tag{3-32}$$

Here, y_R is the minimum distance between the outer concentrated forces and the resultant force R, for a geometrical interpretation see Figure 3.14.
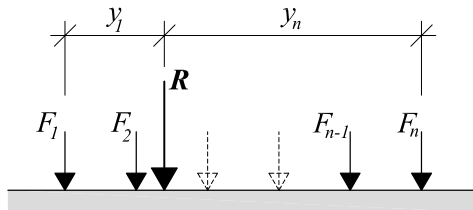
Figure 3.14   Geometrical interpretation of Equation (3-32).

4 Moment distribution in SLS – Cantilever slab

In this Thesis, simple structures were examined and the knowledge gained from these is aimed to enable understanding of more complex structures. The aim of Chapter 4 and 5 was to increase the understanding of moment distribution in slabs which are subjected to concentrated forces in the service limit state. The shear force distribution is not discussed in this Thesis, but is shown in Appendix I for the interested reader. In this chapter, a cantilever slab was analysed. First, the response of a single concentrated force was studied in Section 4.2. This study was then expanded to the response of two concentrated forces which is covered in Section 4.3. The methodology was then repeated for a new structure, a simply supported one-way slab in Chapter 5.

The cantilever slab was 8 m long and had a free edge and a fixed edge along the length. The slab was 1.6 m wide, had a thickness of 0.2 m and is illustrated in Figure 4.1. A coordinate system was chosen so that the *x*-axis was along the length of the slab, and y-direction was along the width of the slab.
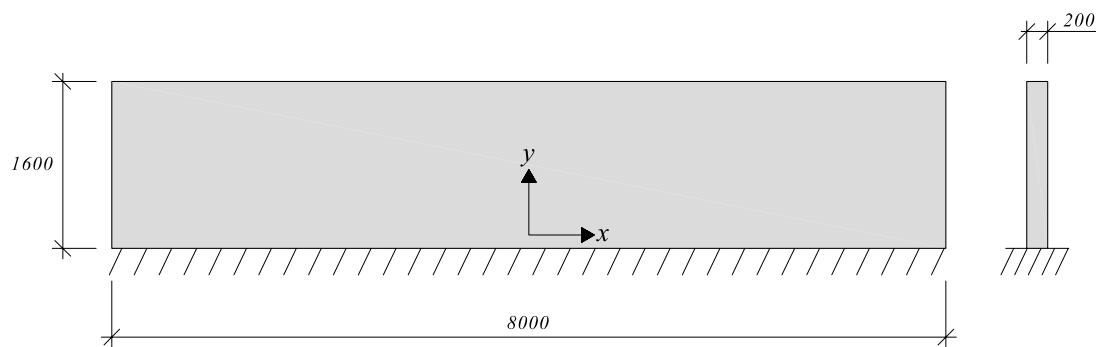
Figure 4.1   Geometry and dimensions of the studied cantilever slab.

4.1 Methodology

This section covers the methodology used for the studies related to moment distribution in the service state and thus also applies to Chapter 5.

4.1.1 Moment-curvature relations

In this study, the aim was to gather reasonable estimates of the moment distribution in slabs and gather more knowledge around important factors which can influence the distribution. Such factors can be varying stiffness in different directions due to varying reinforcement amounts or normal stresses. A stiffness factor *α* was therefore introduced as:

$$\alpha = \frac{E_x}{E_y} \tag{4-1}$$

Where E_x and E_y was the stiffness in the *x*- and *y*-direction, respectively. Also, in an effort to include parts of the non-linear behaviour of reinforced concrete, analyses involving trilinear moment-curvature relations were performed. The moment-

curvature relations were used as input in beam grillage models and were intended to imitate the behaviour before yielding in a small reinforced concrete section, see Figure 4.2.
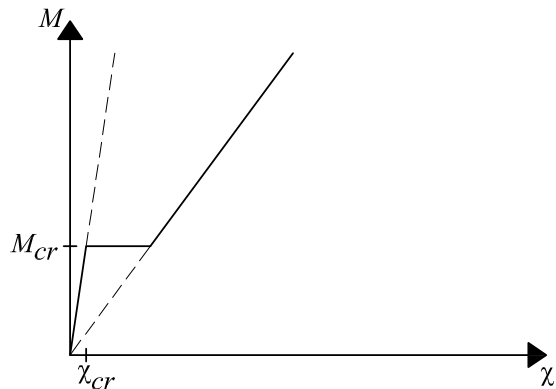
Figure 4.2   Trilinear moment-curvature relation.

This study was directed towards serviceability limit state and no yielding was therefore allowed in the model. The shape of the real moment-curvature relationship for a small section in a slab is case specific, and will depend on several factors including slab thickness and reinforcement amounts. Also, the stiffness of reinforced concrete is significantly influenced by normal stresses. Therefore, the study was divided into three parts, representing different scenarios. The three scenarios were intended to represent different regions of a bridge, where the cantilevering part of the structure is subjected to global forces. For example, the upper flange of a bridge cross-section will be in compression for a positive global moment, have no bending stresses where the moment is zero, and be in tension for a negative global moment, see Figure 4.3.
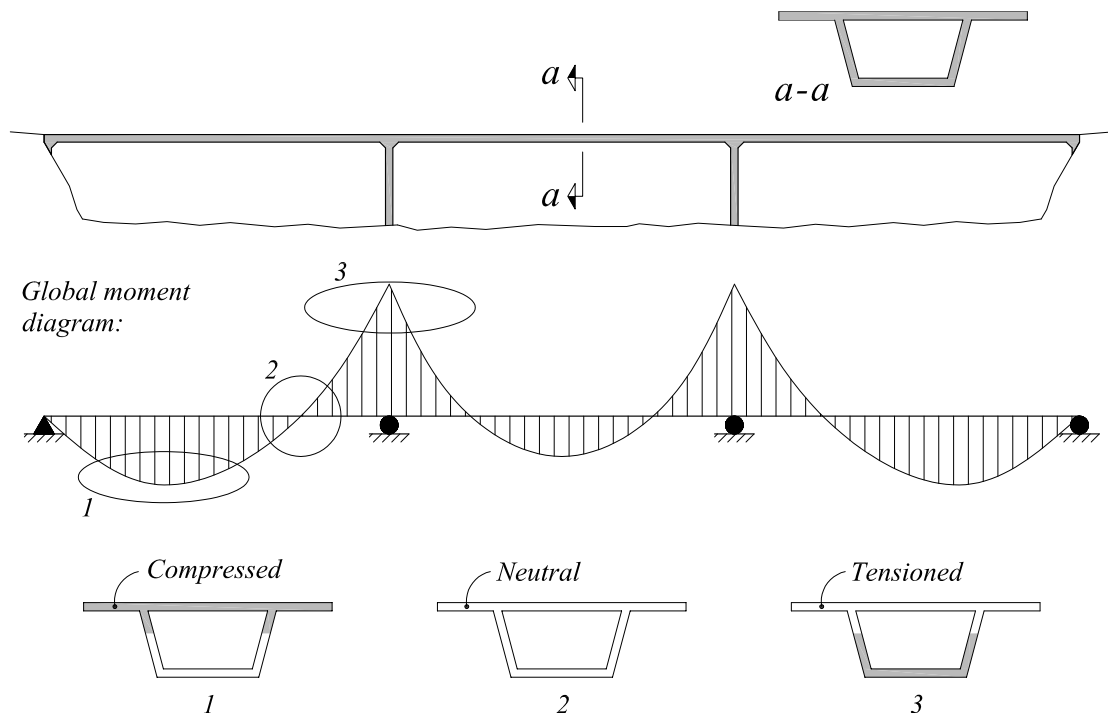
Figure 4.3   The three studied scenarios, dividing the cantilever in the categories Uncracked (compressed), Neutral and Cracked (tensioned).

The names of the scenario imply on the state and corresponding stiffness in the *x*-direction.

The three chosen scenarios were:

1. "Uncracked" (U), where the slab was assumed to be compressed in *x*-direction, i.e. have the stiffness of uncracked concrete. In *y*-direction, the slab was assumed to be uncracked at the starting point but able to crack as the force was applied, i.e. have a trilinear moment-curvature relation.

2. "Neutral" (N), where the slab was assumed to be loaded only by the concentrated force, i.e. have no significant normal stresses in the *x*-direction due to the global response. The slab was modelled with trilinear moment-curvature relations in both directions.

3. "Cracked" (C), where the slab was assumed to be under tension in *x*-direction, i.e. already in a cracked state when the concentrated force was applied, while it had a trilinear moment-curvature relation in *y*-direction.

In addition, a variety of stiffness proportions and values of the cracking moment were chosen. The magnitude of the applied load influence the behaviour since it decides in which state the structure is in, for example if the structure experience a small or large effect from tension stiffening. In order to have better control over the effect from tension stiffening, it was decided that the cracking moment would be determined from a factor of the maximum moment obtained from the corresponding orthotropic linear solution. Two different levels of cracking moments were chosen, namely one half and one third of the maximum linear moment:

$$M_{cr} = \frac{M_{max.linear}(E_x = \alpha E_y)}{2} \tag{4-2}$$

$$M_{cr} = \frac{M_{max.linear}(E_x = \alpha E_y)}{3} \tag{4-3}$$

The lower branch of the trilinear moment-curvature relation in Figure 4.2 represents an uncracked concrete section and the curvature χ_{cr} at the cracking moment M_{cr} was calculated analytically as:

$$\chi_{cr} = \frac{M_{cr}}{E_c I_I} \tag{4-4}$$

Where: E_c = 33 GPa

         I_c = moment of inertia for one uncracked beam used in the beam grillage model

In a linear case, for example with the use of linear elastic shell elements, it is possible to utilize a simple variation of stiffness proportions by modifying the modulus of elasticity in different directions. If one direction is kept constant while the other direction is given a fictitious modulus of elasticity, it would mean that for high values of the stiffness factor α, the stiffness would be greater than the stiffness in the uncracked state. When using trilinear moment-curvature input, with an analytically computed stiffness in the uncracked state, it is thus no longer possible to utilize the same kind of methodology. The upper branch of the moment-curvature relation represented cracked reinforced concrete sections. A range of inclinations were chosen to represent different reinforcement amounts.

For the case "Uncracked", the stiffness proportions can be large since uncracked concrete has a larger stiffness compared to when it is in the cracked state. Therefore a variety of the stiffness factor α, from 1 to 10 was studied, where 10 was the stiffness that corresponded to a stiffness that was 10 times softer than in the uncracked state, see Table 4.1. The table present the methodology used when constructing the input data, however, the exact input data used is stated in Appendix C. Note that, since two levels of cracking moment were chosen, each case of stiffness proportion yielded two solutions.

For the case "Neutral", the stiffness range was lower since the proportions imply on a cracked state, which was why only a variety of the stiffness factor α, from 0.5 to 2 was studied. A reinforcement ratio of 0.5 % was used as reference and the corresponding stiffness was calculated analytically as:

$$A_s = 0.005 \cdot b \cdot h \tag{4-5}$$

$$\text{Find x :} \quad \frac{b \cdot x^2}{2} = \frac{E_s}{E_c} \cdot A_s \cdot (d - x) \tag{4-6}$$

$$I_{II} = \frac{b \cdot x^3}{3} + \frac{E_s}{E_c} \cdot A_s \cdot (d - x)^2 \tag{4-7}$$

$$\chi_{0.5\%} = \frac{M_1}{E_c \cdot I_{II}} \tag{4-8}$$

Where: x = height of the compression zone with a triangular stress block
      I_{II} = the moment of inertia for a transformed concrete section

The calculated value was used for the upper branch in the moment-curvature relation and was used in both directions for the case $E_x=E_y$, see Table 3.2. For calculated values, see Appendix C.

For the case "Cracked", the same moment-curvature relations used in "Neutral" were utilized but with a linear relation corresponding to a cracked state in x-direction, since the slab was considered cracked before the concentrated load was applied, see Table 4.3.

Table 4.1   Moment-curvature relations for the case Uncracked.

Global region:
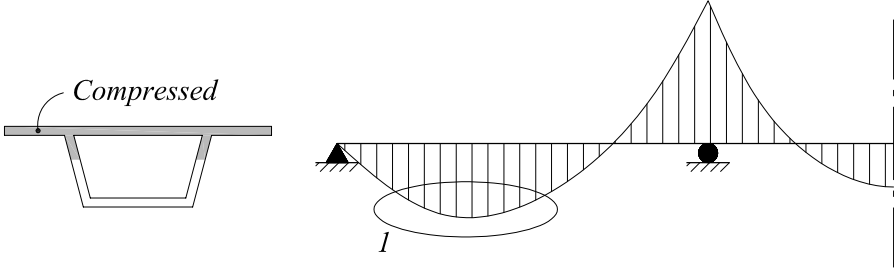
	Moment-curvature relations used in x-direction	Moment-curvature relations used in y-direction
$E_x = 2E_y$		
$E_x = 5E_y$		
$E_x = 10E_y$		
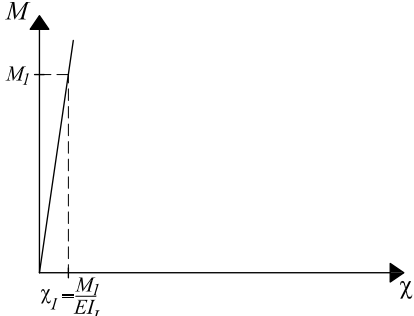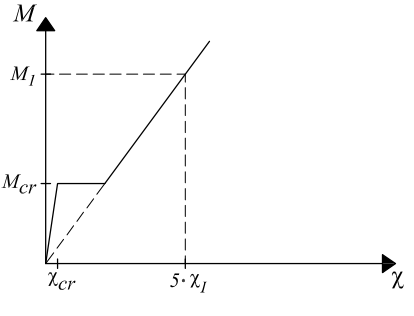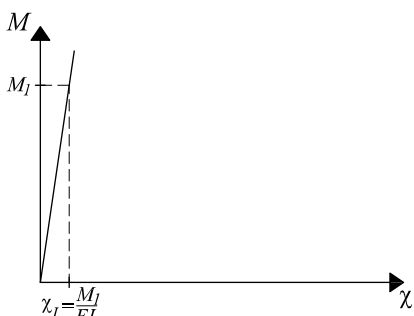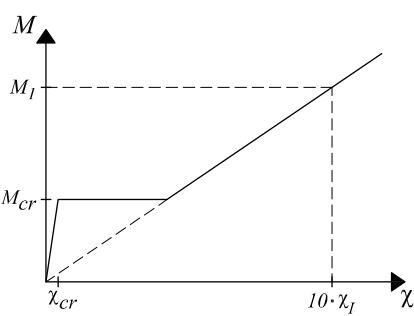
Table 4.2   Moment-curvature relations for the case Neutral.
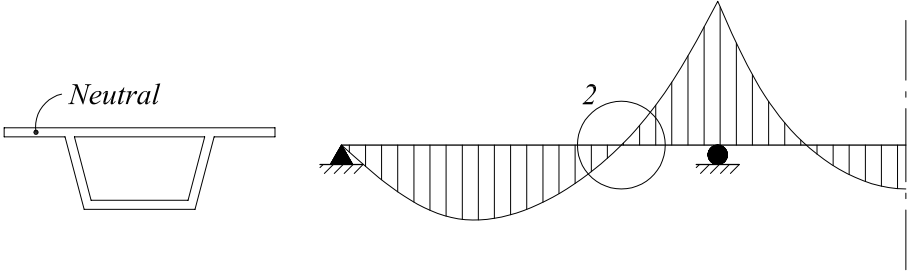
Global region:		
	Moment-curvature relations used in x-direction	Moment-curvature relations used in y-direction
$E_x = 0.5E_y$		
$E_x = E_y$		
$E_x = 2E_y$		

CHALMERS, *Civil and Environmental Engineering*, Master's Thesis 2014:73
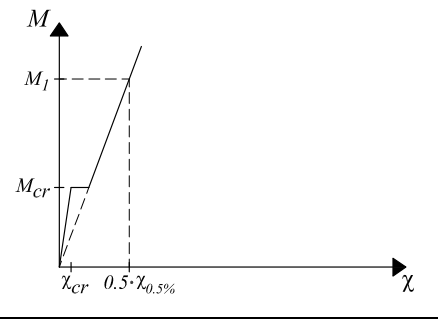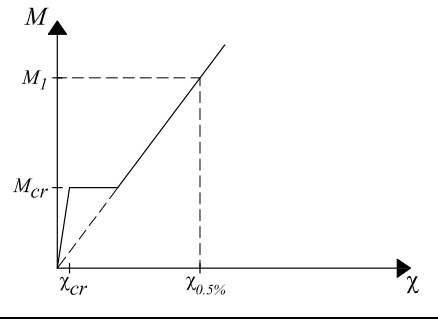
Table 4.3   Moment-curvature relations for the case Cracked.

Global region:

	Moment-curvature relations used in x-direction	Moment-curvature relations used in y-direction
$E_x = 0.5E_y$	M, M_1, $2 \cdot \chi_{0.5\%}$, χ	M, M_1, M_{cr}, χ_{cr}, $\chi_{0.5\%}$, χ
$E_x = E_y$	M, M_1, $\chi_{0.5\%}$, χ	M, M_1, M_{cr}, χ_{cr}, $\chi_{0.5\%}$, χ
$E_x = 2E_y$	M, M_1, $0.5 \cdot \chi_{0.5\%}$, χ	M, M_1, M_{cr}, χ_{cr}, $\chi_{0.5\%}$, χ

Due to numerical stability reasons, a slight inclination was chosen for the second branch of the trilinear relations, such that $M_2 = 1.05 M_{cr}$. Where M_2 is the moment at the intersection between the second and third line. Tests showed that this inclination did not affect the results to a significant extent.

4.1.2 Finite element model

The finite element software used was the student version of ADINA (2012). Due to a restraint in the student version, which only allows a maximum of 900 nodes, the slab was modelled with a symmetry boundary condition, dividing the model to a length of 4 m. The moment distribution along the fixed edge was of interest in this study and is presented along the length of 4 m. The coordinate $x = 0$ refer to the centre of the fixed edge. The modelled part of the slab is presented in Figure 4.4.
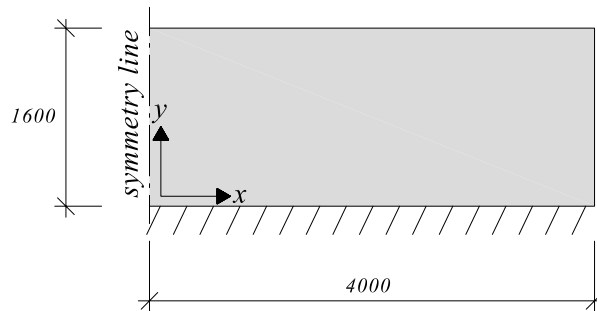
Figure 4.4   Modelled part of the slab.

For the majority of analyses, beam grillage models where moment-curvature relations are used as input were utilized. However, shell element models were used for early verification of the linear elastic beam grillage models. For the shell element model, it was concluded that a mesh size of 0.2 m gave satisfying results in terms of convergence, see Appendix A. In the linear elastic case, where the concrete was assumed to be uncracked, it was concluded that the grillage model with a beam width of 0.2 m yielded results that were similar to the results from a shell element model, which is why the width of 0.2 m was chosen, see Appendix A. The choice of 0.2 m width was also made in Lim (2013). For further information about the shell and beam element type and properties, see Section 3.1.

The concentrated force was modelled as a point load to a single node for both the shell element model and the beam grillage model. Since the moment along the fixed support was of interest, which is a certain distance from the applied load, it was concluded that this approximation was acceptable. The boundary condition along the fixed edge was modelled as fixed in all translations and rotations. The symmetry boundary condition was modelled as a fixed rotation around the *y*-axis and a fixed translation in the *x*-direction. Beams that were placed in the symmetry lines were modelled as beams with half the cross-sectional width.

The Poisson's ratio was chosen to 0. The iteration method for the non-linear analysis was chosen to the full Newton method in ADINA and the iteration tolerance type was set to energy.

4.1.3 Torsional stiffness

When modelling the structure in a cracked state, difficulties arise regarding which torsional stiffness of the beam elements that should be used. In Lim (2013), an elastic (uncracked) torsional stiffness was used throughout the Thesis. It was however discovered that the torsional stiffness dominates the behaviour of the structure. A parametric study was performed with varying values of the torsional stiffness, see Appendix B. The structure studied was the cantilever slab presented in this section and a variety of the torsional stiffness was chosen which included 1, 1/8, 1/16 and 0 of the elastic (uncracked) torsional stiffness of a concrete beam with a width and height of 0.2 m. It was shown that, for a linear elastic isotropic case with a concentrated force of 200 kN, the maximum moment was in the range between 75 and 113 kNm/m, see Figure 4.5a. The influence of the torsional stiffness on the plastic rotation was also studied. Both bilinear and trilinear moment-curvature relations were used in the study, which showed that the plastic rotation significantly increases as the torsional stiffness decreases, see Figure 4.5b. The case with zero torsional stiffness became too unstable and the analysis was aborted. For more detailed information of the study, see Appendix B.
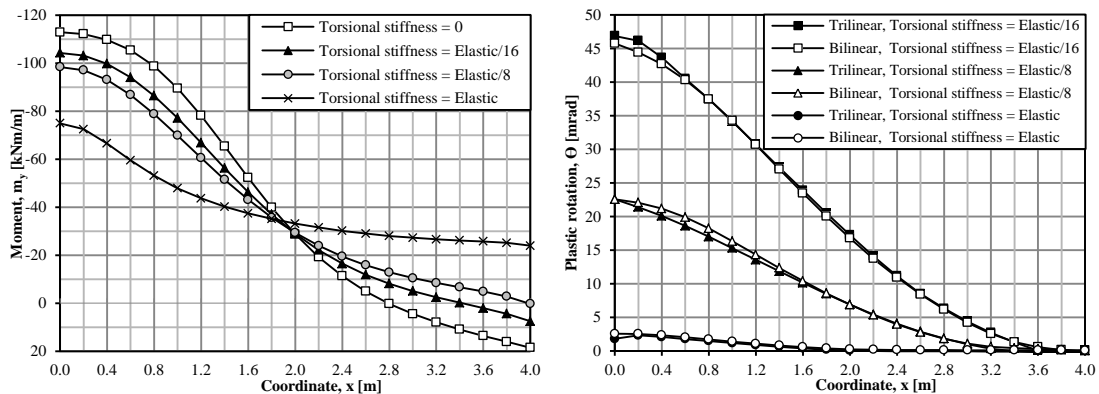
Figure 4.5   Results from the parametric study of the torsional stiffness: a) moment distribution for an isotropic linear case, b) plastic rotation for an isotropic bilinear and trilinear case.

According to tests presented in Lopes (2014), the torsional stiffness of a slab in a cracked state is about 1/17-1/15 of the stiffness in the elastic state. Based in this, the torsional stiffness of the beam elements throughout this Thesis was chosen to a linear relation of 1/16 of the elastic stiffness of a concrete beam with a width and height of 0.2 m. The relation was kept constant independent on stiffness proportions. As stated in Section 3.1, it should however be noted that the torsional stiffness of a plate is different from the torsional stiffness of a beam grillage model, which further complicates the choice of torsional stiffness. However, the choice was believed to be conservative.

The torsional stiffness for a beam element is defined by a torsional moment verses angle of twist per unit length relation. Since a linear relation of 1/16 of the elastic stiffness was chosen, the model was unable to accurately describe parts that were uncracked in the structure. A better approximation would have been to connect the torsional stiffness to the bending moment such that when the element was uncracked in bending, an elastic uncracked torsional stiffness would be active. This was however not possible in ADINA and was believed to make the choice of torsional stiffness even more conservative.

The relation between torsional moment and angle of twist for a beam is defined as:

$$\varphi = \frac{T}{GK_v}$$ (4-1)

Where: φ = angle of twist per unit length
        T = torsional moment
        G = shear modulus
        K_v = torsion constant, see Equation (3-3)

For a linear relation, ADINA requires two points in the torsional moment versus angle of twist diagram to be defined and interpolates linearly between those two points. Since one point was defined in the origin, only one point needed to be calculated. A reference torsional moment of 10 kNm was chosen and the corresponding angle of twist which was 16 times weaker than the torsional stiffness of uncracked concrete became:

$$G = \frac{E_c}{2(1-v)} = \frac{33 \cdot 10^9}{2(1-0)} = 16.5 \, \text{GPa}$$ (4-2)

$$K_v = \beta \cdot h \cdot b^3 = 0.141 \cdot 0.2 \cdot 0.2^3 = 2.26 \cdot 10^{-4} \, \text{m}^4$$ (4-3)

$$\varphi = \frac{T}{GK_v} = \frac{10'000}{16.5 \cdot 10^9 \cdot 2.26 \cdot 10^{-4}} \cdot 16 = 0.043 \, \frac{1}{\text{m}}$$ (4-4)

Where: E_c = modulus of elasticity
        v = poisons ratio, chosen to 0
        β = constant depending on the height to width ratio of the cross-section, equal to 0.141 for a section with equal width and height

It should be noted that by reducing the torsional stiffness of the beam elements, the results will not match the results obtained by a shell element model, even for a linear elastic case.

4.2 Response of a single concentrated force

The first case of interest was the response of a single concentrated force. The study is then in Section 4.3 expanded to the response of two concentrated forces. The model was analysed for a static concentrated force with a magnitude of 200 kN, see Figure 4.6.
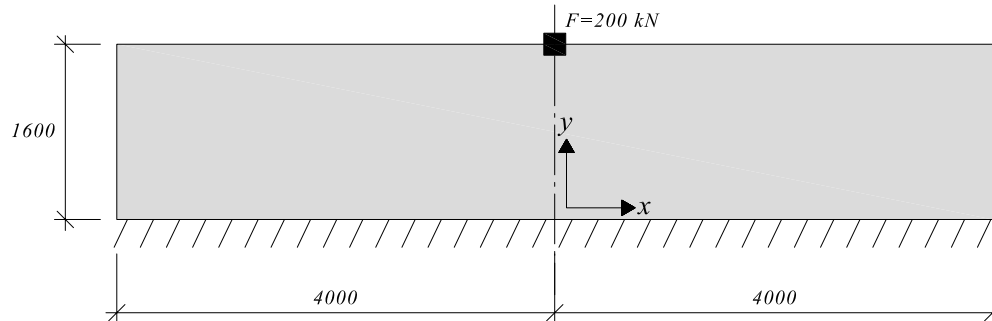
Figure 4.6   Location and magnitude of the applied concentrated force.

4.2.1 Linear elastic orthotropic case

In the start of ordinary design, there is no knowledge of the stiffness proportions in different directions of a slab. It is therefore necessary to start with a linear elastic isotropic model to acquire needed reinforcement amounts. However, since the moment distribution is governed by stiffness, this type of analysis will not yield the actual moment distribution experienced by the slab. It was therefore of interest to investigate how the design values are influenced by changes in stiffness in different directions.

The slab was analysed using a linear elastic model to acquire values to which a more refined model could be compared. In addition, a range of stiffness proportions was used as input to later investigate how well a simple linear elastic orthotropic model can describe the moment distribution when the reinforcement amounts are known. The analysis was based on a beam grillage model where moment-curvature relations were used as input for the beam elements. In the isotropic case, $E_x = E_y$, the beams were given an uncracked stiffness in both directions and the relation between curvature and moment was calculated analytically as:

$$\chi = \frac{M}{E_c I_I} \tag{4-5}$$

Where: E_c = 33 GPa

I_I = moment of inertia for the gross concrete section of one beam element

For the orthotropic cases, the curvature in the y-direction was kept constant while the stiffness in the x-direction varied with the stiffness factor α. The torsional stiffness of the beam elements was, as previously stated in Section 4.1.3, 1/16 of the elastic uncracked stiffness. The results from the analysis are shown in Figure 4.7.
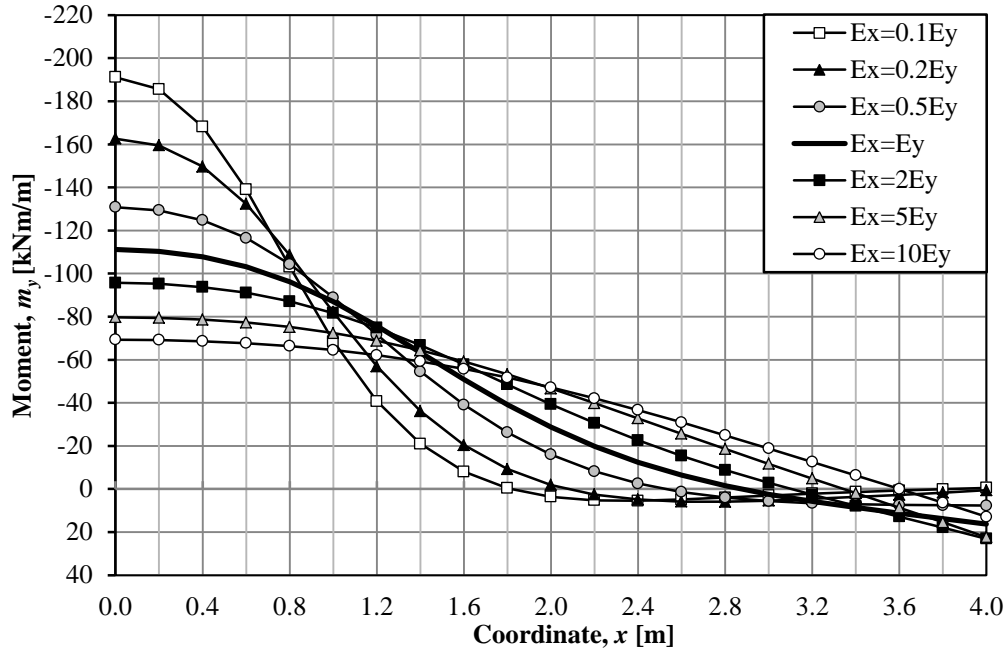
Figure 4.7   Linear elastic orthotropic moment distribution.

4.2.2 Trilinear elastic orthotropic case

Following the methodology presented in Section 4.1, the cantilever slab was analysed with multilinear moment-curvature input. As stated in Section 4.1.1, the magnitude of the cracking moment was a factor 1/2 and 1/3 of the maximum moment measured in the corresponding orthotropic linear elastic solution, presented in Figure 4.7. This means that for each stiffness proportion there were two magnitudes of the cracking moment.

The results from the analysis are presented in Figure 4.8 to Figure 4.10. The distributions with equal stiffness factor α are plotted against each other together with both the isotropic and their corresponding orthotropic linear solutions, which are the same solutions as presented in Figure 4.7. The influence from uncracked concrete sections, i.e. the effect of tension stiffening, can then be observed. The linear solution, $M_{cr}=M_{lin}/3$ and $M_{cr}=M_{lin}/2$ can be seen as no, small and large effect of tension stiffening, respectively.

For exact input data, see Appendix C. The results are discussed in Section 4.2.3.

a) $E_x = 2E_y$
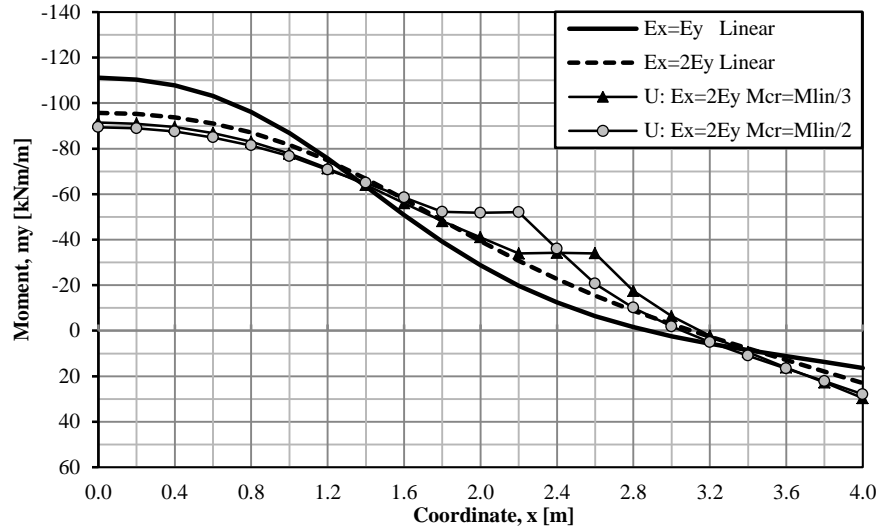
b) $E_x = 5E_y$
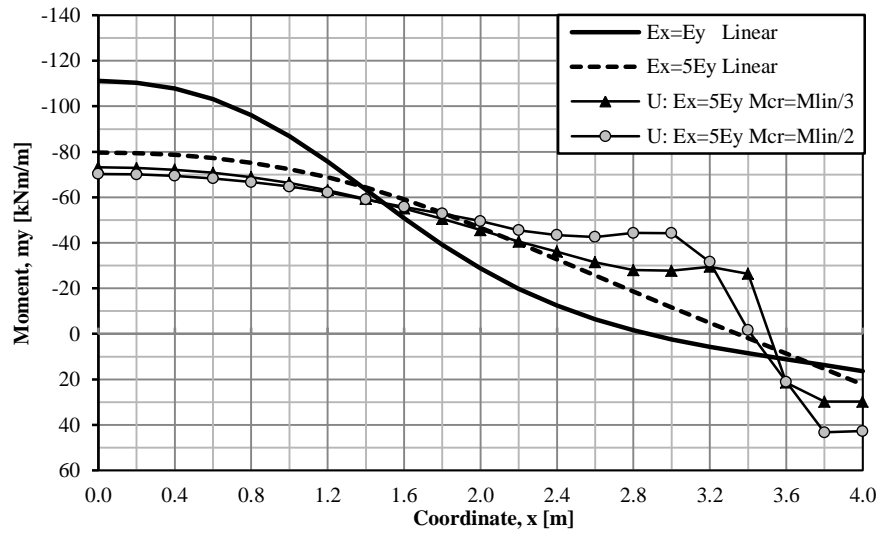
c) $E_x = 10E_y$
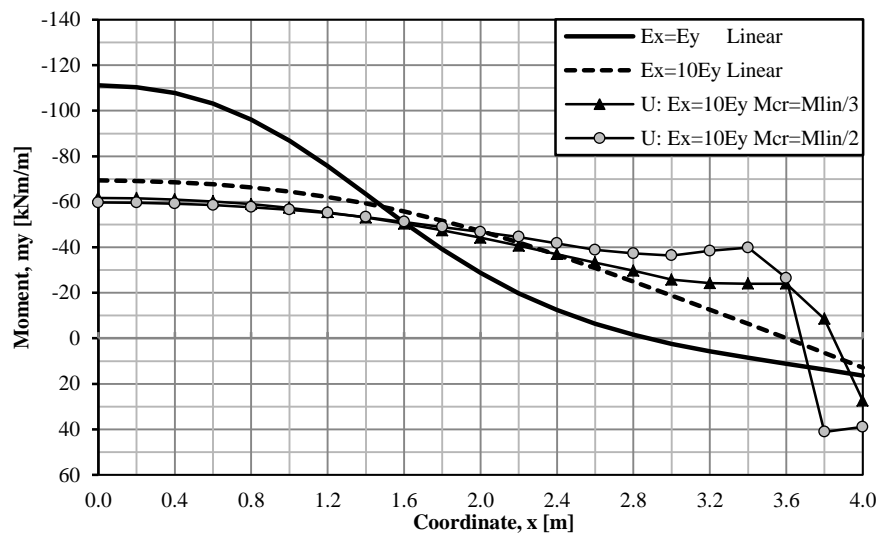
Figure 4.8   Moment distributions from the case Uncracked with varying magnitude of the cracking moment.
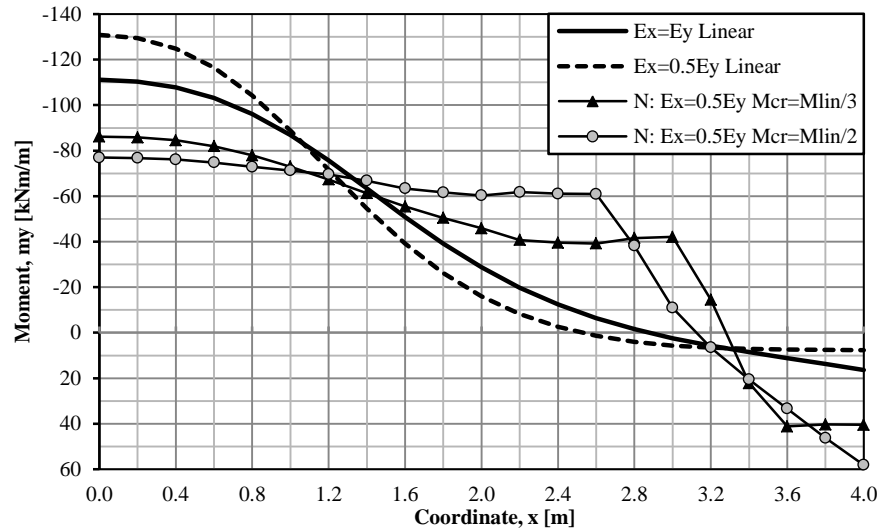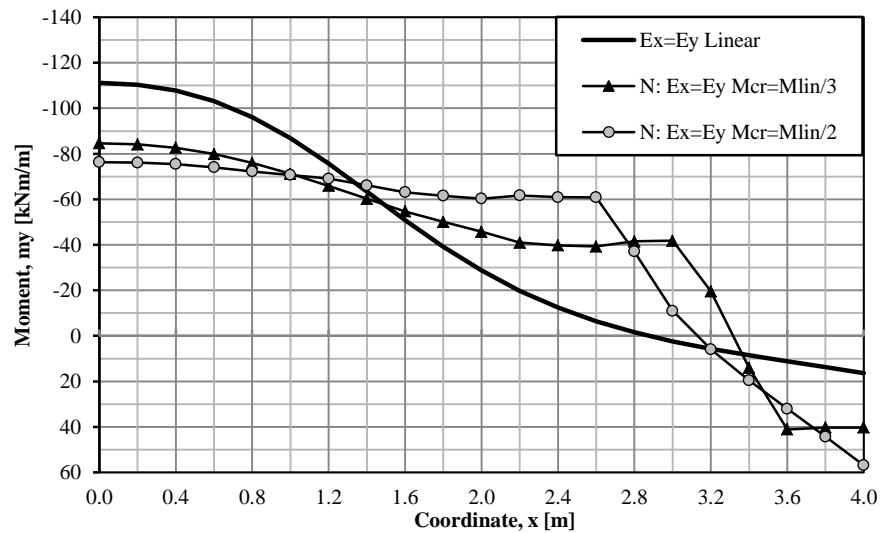
a) $E_x = 0.5E_y$
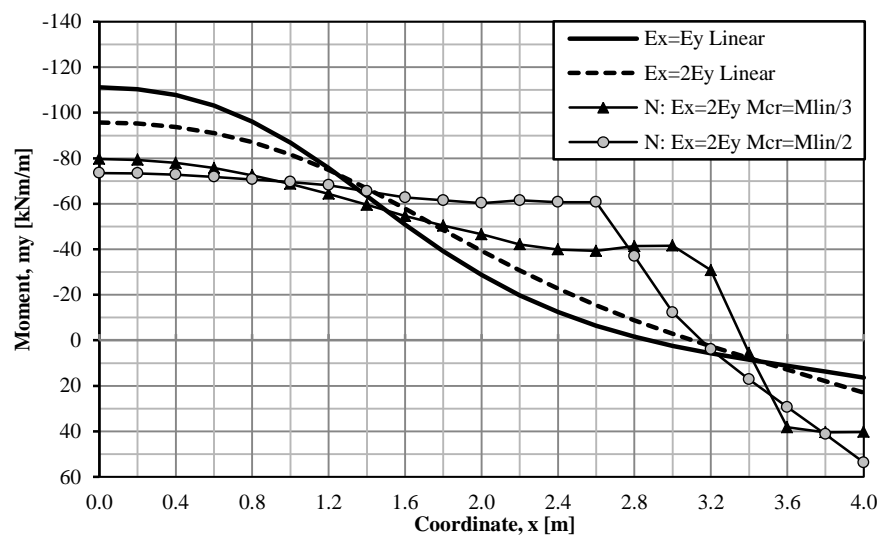
b) $E_x = E_y$

c) $E_x = 2E_y$

*Figure 4.9   Moment distributions from the case Neutral with varying magnitude of
the cracking moment.*

CHALMERS, *Civil and Environmental Engineering*, Master's Thesis 2014:73

a) $E_x = 0.5E_y$
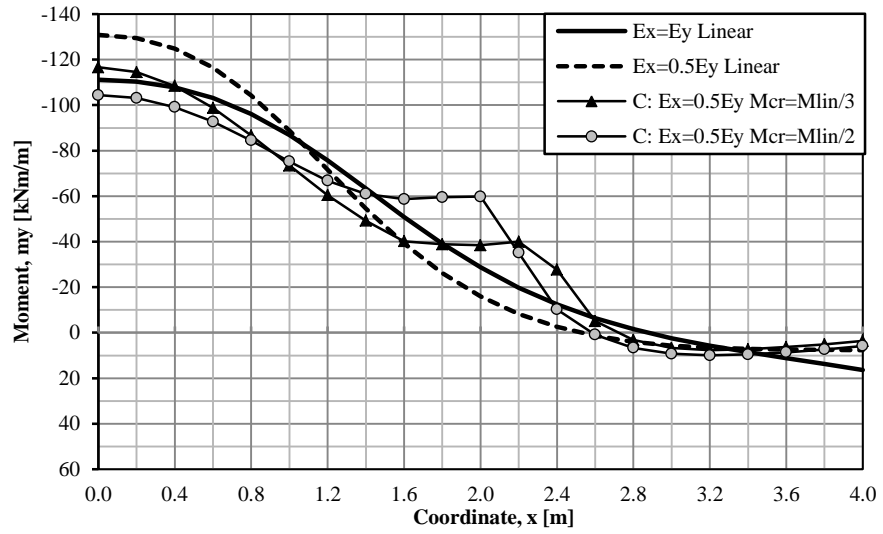
b) $E_x = E_y$
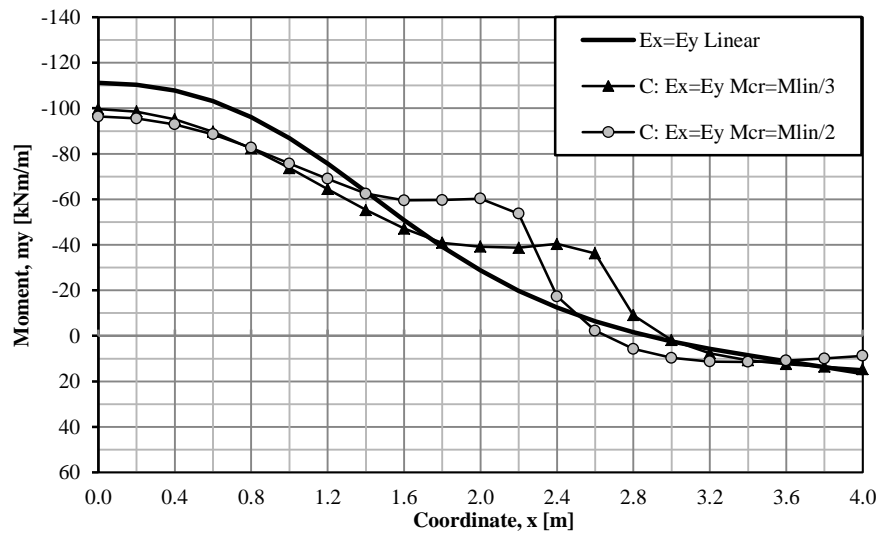
c) $E_x = 2E_y$
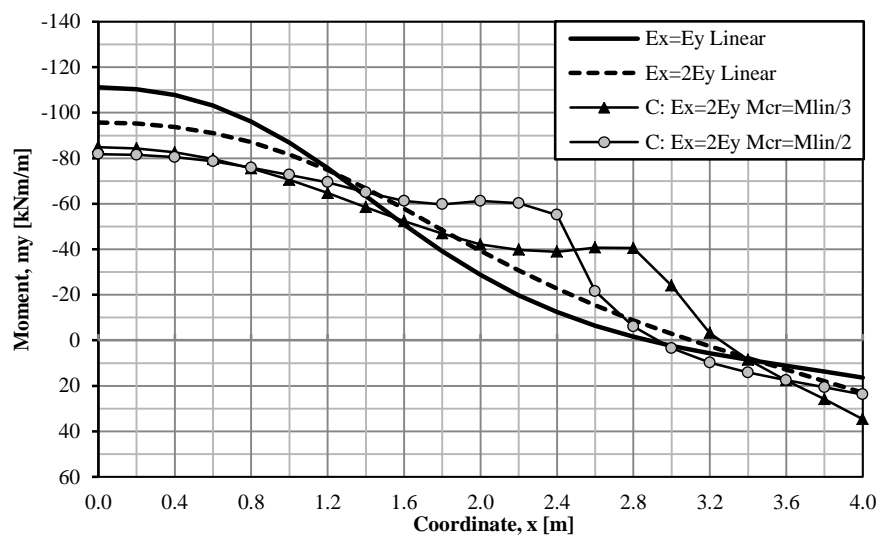
Figure 4.10   Moment distributions from the case Cracked with varying magnitude of the cracking moment.

4.2.3 Discussion

The maximum moment was found at the centre of the slab where the concentrated force was applied. It should be noted that no self-weight was applied, which means that the concentrated force was acting on the model exclusively.

In the results from the case Uncracked, shown in Figure 4.8, it is clearly visible that a lower maximum moment was obtained as the stiffness in the x-direction increased. The orthotropic linear solution and the trilinear solutions are fairly similar, but the trilinear solutions show a marginally lower maximum moment. This is due to the fact that some elements still were in the uncracked state and therefore attracted additional moment, close to the edge of the slab. However, there seems to be an insignificant difference between the two levels of cracking moment.

The cracking moment is clearly visible throughout the results as a plateau, similar to what would be expected from a bilinear moment-curvature input where yielding takes place. However, as the curvature further increases, the beam element reaches the upper branch in the trilinear moment-curvature relation and adopts the stiffness of state II. In the case Uncracked, it is the stiffness in y-direction which was varied and the plateau is situated on a level of 1/3 and 1/2 of the maximum moment of the orthotropic linear solution. However, in the case Neutral, it was the stiffness in x-direction which was varied which means that the plateau was situated on the same level for all different stiffness proportions, since it is the moment in y-direction which is presented.

The orthotropic linear solution is no longer close to the trilinear solutions for the case Neutral. The trilinear solutions are very similar independent on stiffness proportions; i.e. the stiffness in x-direction seems to have a very low influence. It should be noted that the uncracked stiffness was equal for all cases, which could mean that the uncracked stiffness in x-direction dominates the behaviour.

In the case Cracked, the linear orthotropic solution was again close to the trilinear solutions. As in the case Neutral, the plateau is situated on the same level for all stiffness proportions since the moment-curvature input in the y-direction was the same. However, contrary to the case Neutral, the trilinear solutions are not similar between the different stiffness proportions. The two levels of cracking moment do however still seem to have a low influence.

A positive moment was observed close to the edge of the slab, and was believed to be a phenomenon owing to the use of a beam grillage model. The beams positioned in the x-direction are deflected downwards due to the applied load. However, the beams in the y-direction acted as spring supports which pushed the edges of the beams in the x-direction upwards, creating a positive moment, see Figure 4.11.
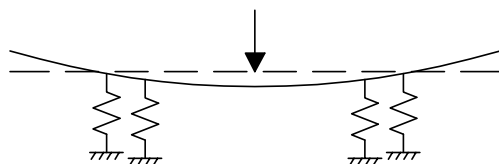
Figure 4.11   Illustration of how the positive moment occurs.

The effect was believed to be strongest in the trilinear solution because the beams were still in an uncracked stiffness, due to the low moment close to the edges, making the springs in Figure 4.11 stiffer.

4.3 Response of two concentrated forces

In the case of two static concentrated forces, the examined slab was exposed to two forces acting along the free edge of the slab. The two forces were of equal magnitude and were positioned with a mutual distance of 1.2 m, see Figure 4.12. The chosen distance between the loads originates from the traffic load model described in Section 3.2.
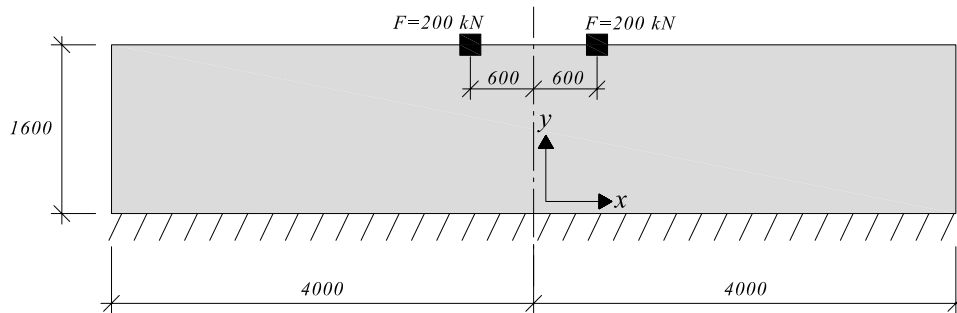
Figure 4.12   Geometry and position of loading.

4.3.1 Linear elastic orthotropic case

The linear elastic orthotropic analysis presented in Section 4.2.1 was also performed here, and the results are presented in Figure 4.13.
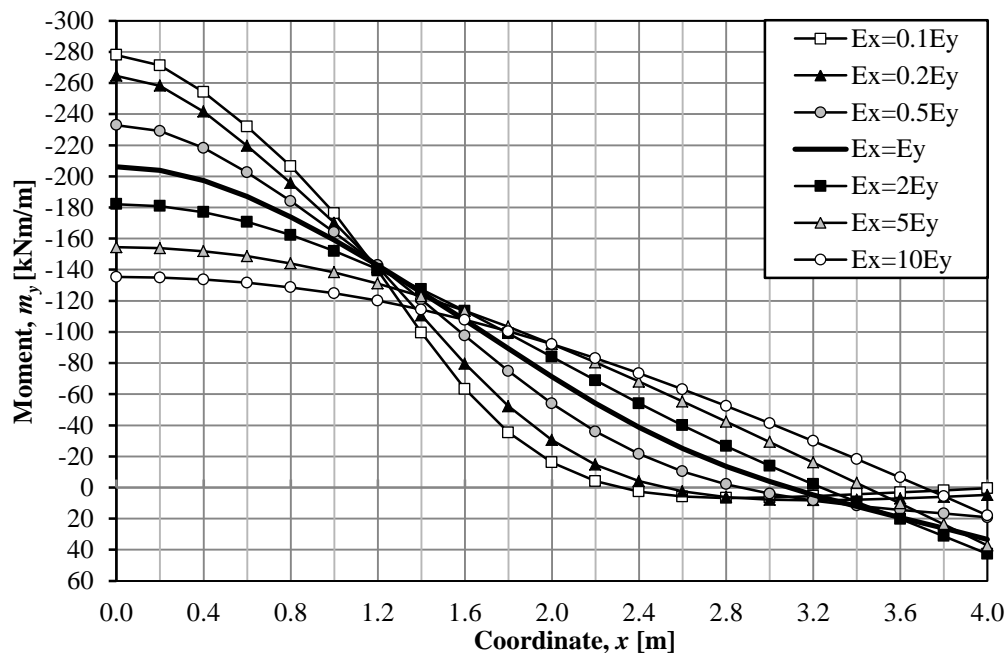
Figure 4.13   Linear elastic orthotropic moment distribution.

4.3.2 Trilinear elastic orthotropic case

The multilinear analysis presented in Section 4.2.2 was also performed here, and the results are presented in Figure 4.14 to Figure 4.16. For exact input data, see Appendix C. The results are discussed in Section 4.3.3.

a) $E_x = 2E_y$
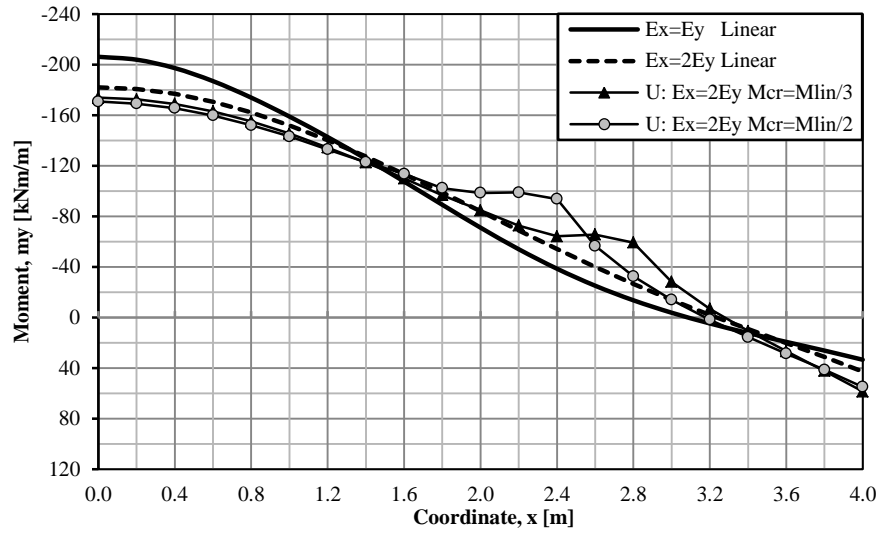
b) $E_x = 5E_y$
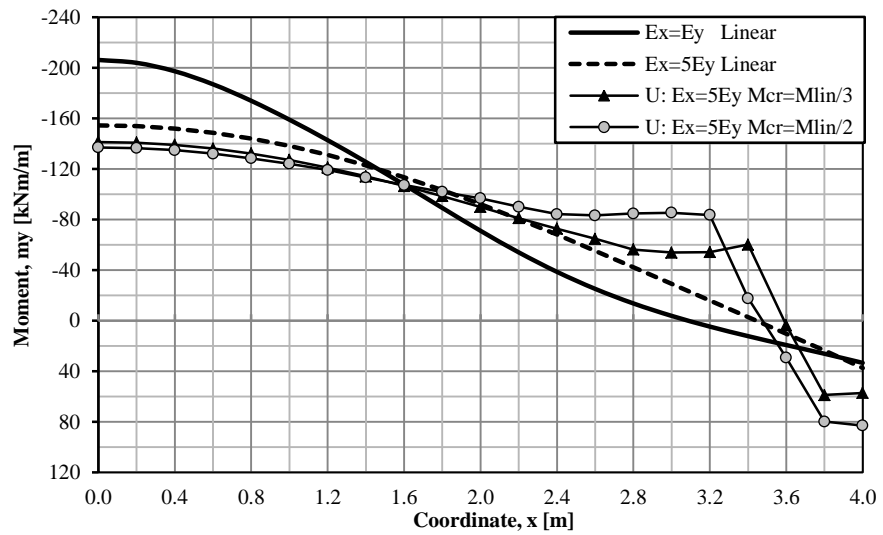
c) $E_x = 10E_y$
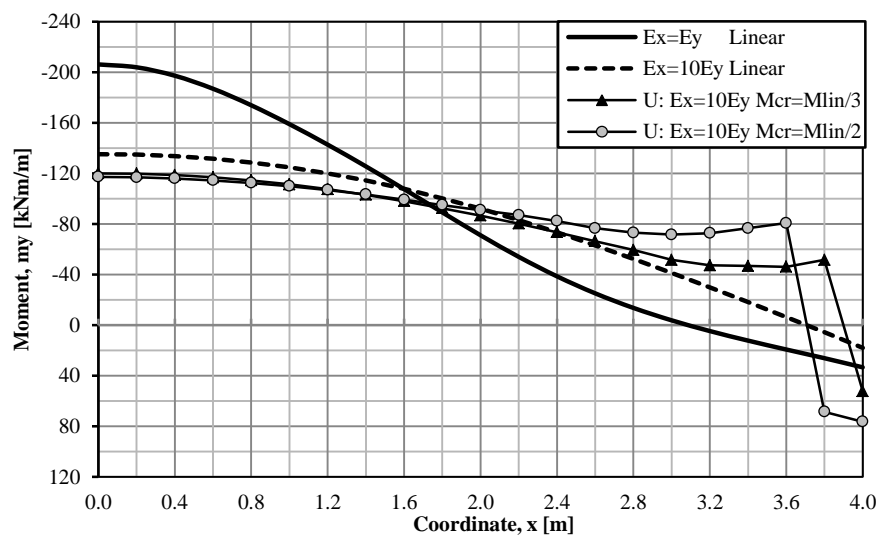
Figure 4.14   Moment distributions from the case Uncracked with varying magnitude of the cracking moment.

CHALMERS, *Civil and Environmental Engineering*, Master's Thesis 2014:73
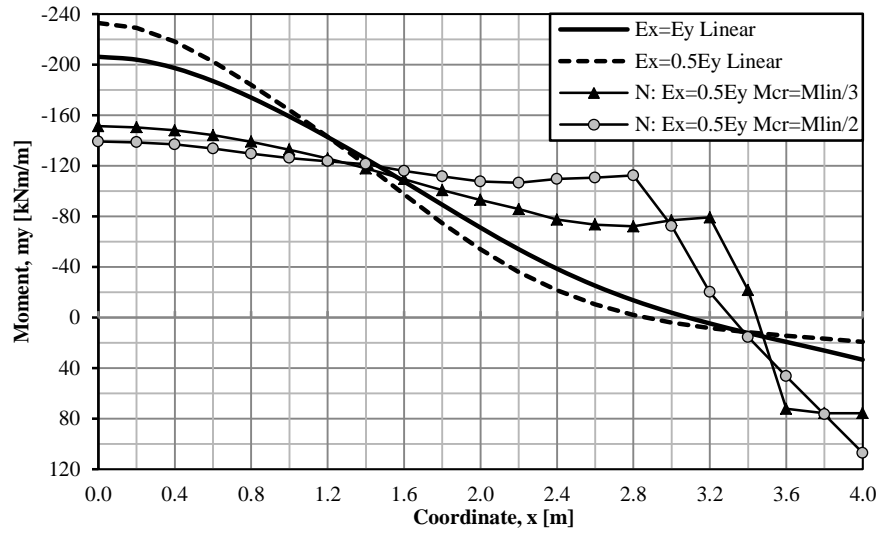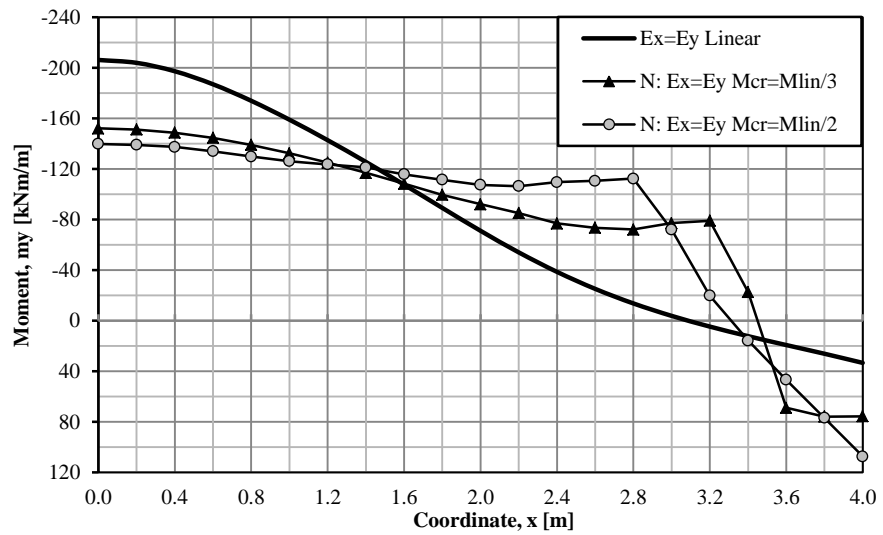
a) $E_x = 0.5E_y$
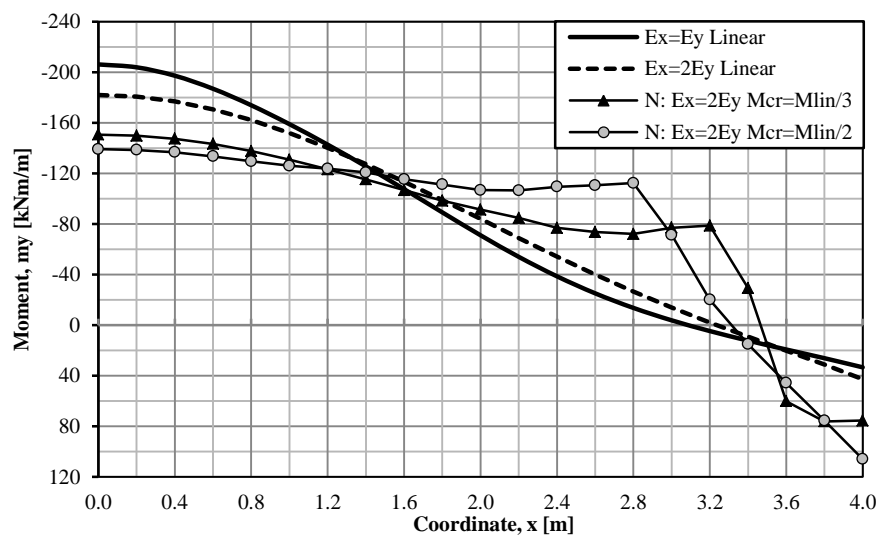
b) $E_x = E_y$

c) $E_x = 2E_y$

Figure 4.15   Moment distributions from the case Neutral with varying magnitude of the cracking moment.

a) $E_x = 0.5E_y$
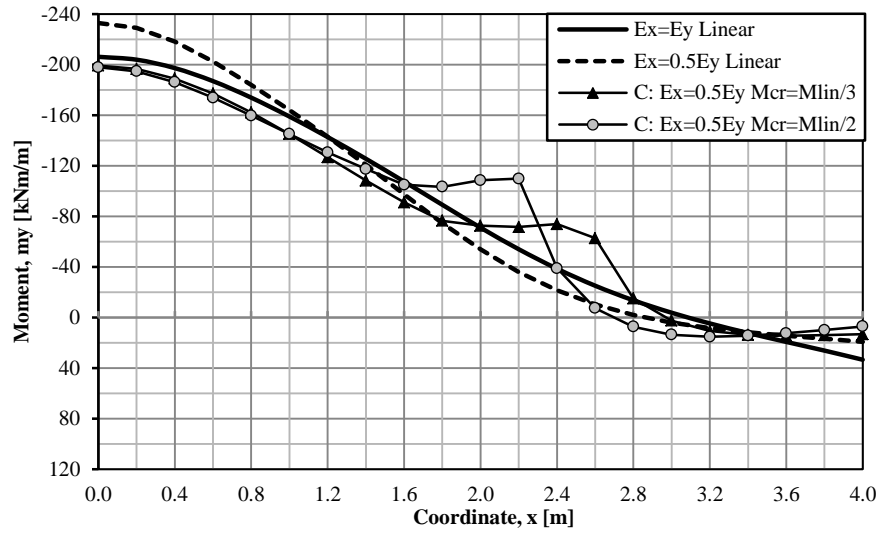
b) $E_x = E_y$
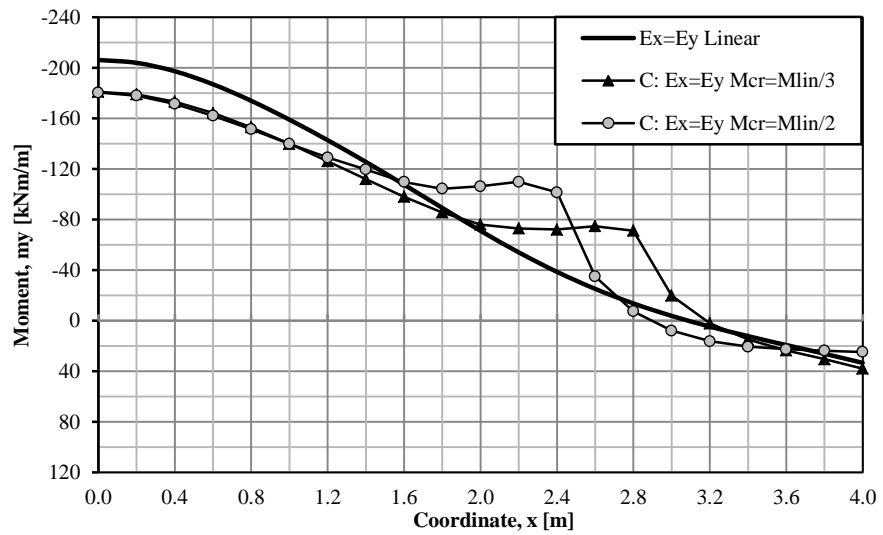
c) $E_x = 2E_y$
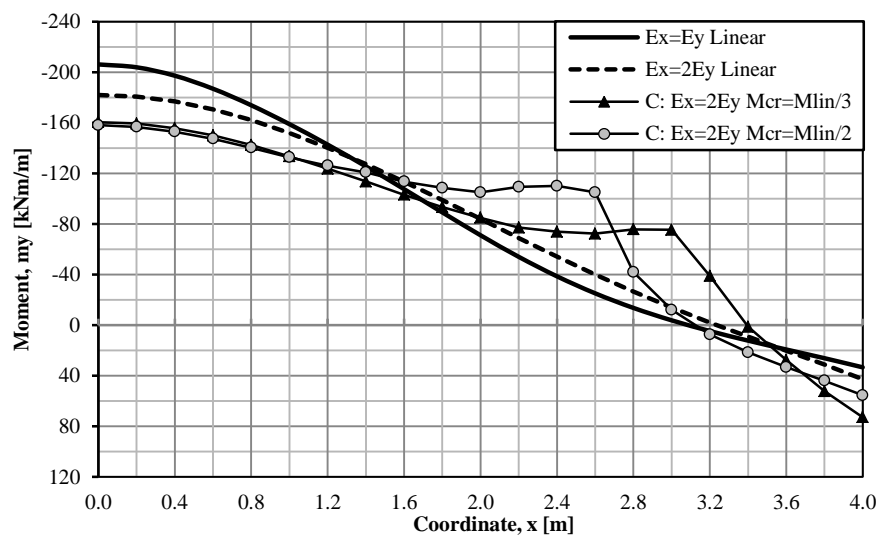
Figure 4.16   Moment distributions from the case Cracked with varying magnitude of the cracking moment.

CHALMERS, *Civil and Environmental Engineering*, Master's Thesis 2014:73

4.3.3 Discussion

In general, the same observations made in Section 4.2.3 also apply here. As for the single concentrated force, the linear orthotropic solution describes the trilinear solutions fairly well for the cases Uncracked and Cracked, while it differs from the trilinear solutions for the case Neutral.

The maximum moment was still found at the centre of the slab, which means that the spacing between the loads were small enough to have a substantial overlapping effect. The isotropic linear solution was slightly lower than the isotropic linear solution for a single point load multiplied by 2, which is reasonable since there was a certain distance between the loads.

The linear results were also compared by means of superposition. For example, for the linear isotropic case, the moment for a single concentrated force at the position $x = 0.6$ m was:

$$m_{1F} \ (x = 0.6) = 103 \ \text{kNm/m} \tag{4-6}$$

Since both of the loads in the case with two concentrated forces were acting a distance of 0.6 m from the centre of the slab, the moment measured at $x = 0$ should be twice as large:

$$2 \cdot m_{1F} \ (x = 0.6) = 2 \cdot 103 = 206 \ \text{kNm/m} \tag{4-7}$$

The actual moment measured in the case for two concentrated forces at $x = 0$ was:

$$m_{2F} \ (x = 0) = 206 \ \text{kNm/m} \tag{4-8}$$

This means that, for the isotropic linear case, the structure was long enough for superposition of the results.

5 Moment distribution in SLS – Simply supported slab

In the previous chapter, the cantilever slab was examined. The same types of analyses were expanded to a new structure, a simply supported one-way slab. The comparison between the cantilever slab and the simply supported slab were believed to be interesting because of the, in some ways similar and in other ways different, structural behaviour. For example, when exploiting a symmetry condition for the simply supported structure, the forces acting on the two structures are mirrored, see Figure 5.1.

Cantilever:
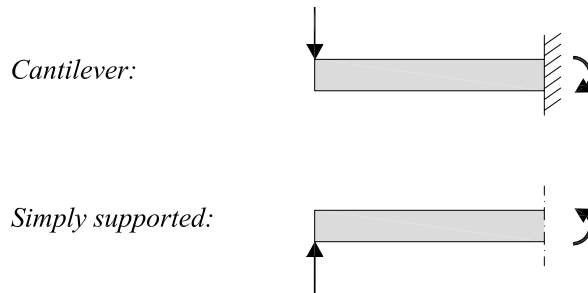
Simply supported:

Figure 5.1   Similarities between a cantilever and a simply supported one-way structure.

The examined slab was similarly to the cantilever slab 8 m long, but had a width of 3.2 m. It was simply supported along the length of the slab, see Figure 5.2. The moment distribution in the middle of the slab, along the length, was of primary interest in this case. The shear force distribution is not discussed in this Thesis, but is shown in Appendix I for the interested reader. A coordinate system was chosen such that the *x*-axis runs along the length of the slab, while the *y*-axis runs along the width.
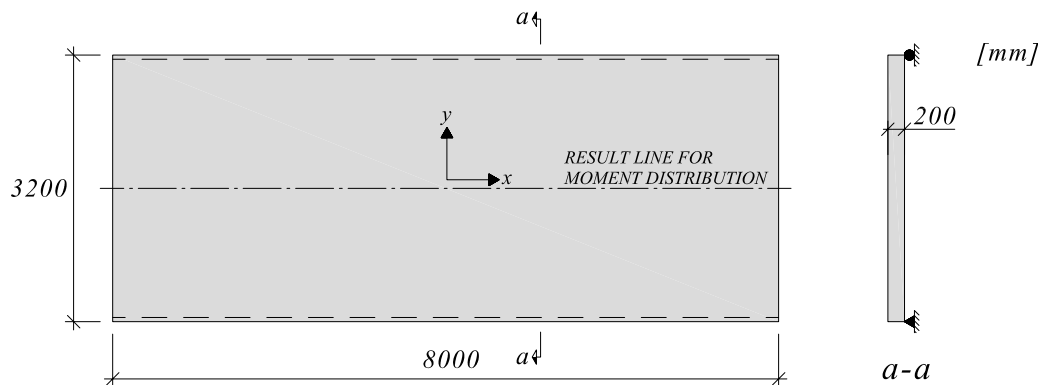
Figure 5.2   Geometry and dimensions of the studied one-way slab.

As for the cantilever slab, analyses where trilinear moment-curvature relations were used as input were conducted to investigate the influence of uncracked concrete sections in the slab. This study was directed towards serviceability limit state and no yielding was therefore allowed in the model. The methodology presented in Section 4.1 was also applied here. See Table 4.1 to Table 4.3 for descriptions of the moment-curvature relations used in this study. For exact moment-curvature input data, see Appendix C.

5.1 Finite element model

In general, the choices described in Section 4.1.2 also apply here. However, some specific choices were made for the simply supported slab which is described in this section.

The slab was modelled with symmetry boundary conditions, dividing the model to a length of 4 m and a width of 1.6 m. The moment distribution along the centre of the slab was of interest in this study and is therefore presented along the length of 4 m. The coordinate $x = 0$ refer to the centre of the slab. The modelled part of the slab is presented in Figure 5.3.
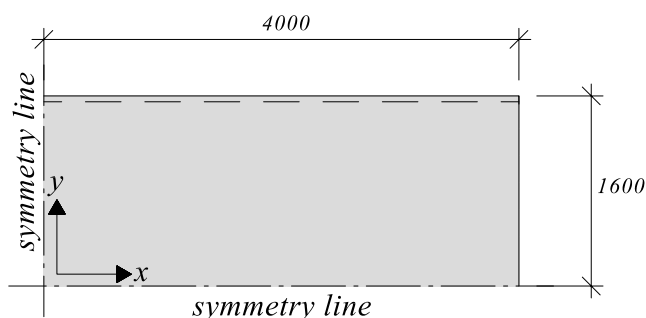
Figure 5.3   Layout of the modelled slab with symmetry conditions.

As for the cantilever slab, shell element models were used for early verification. It was concluded that shell element mesh sizes of 0.2 m gave satisfying results in terms of convergence, see Appendix A. As for the cantilever slab, it was found that for the linear elastic case where the concrete was assumed to be uncracked, beam widths of 0.2 m in the beam grillage model gave similar results as the shell element model. Based on this, the spacing between beams in the grillage model was chosen to 0.2 m.

Since the moment distribution along the centreline was of interest, the point load was positioned in the line where the moment was measured. Contrary to the cantilever slab where the moment was measured a certain distance from the point load, attention had to be directed to how the point load was modelled in order to obtain reasonable results. It was therefore chosen to spread the concentrated force over an area of 0.4 x 0.4 m^2. However, since it is not possible to model pressure loads on beam elements, it was decided that the load should be divided into smaller point loads acting on the intersection points within the chosen area, see Figure 5.4a. Note that the nodal forces were divided in such a way that the proportion of each point load represented the sum of an equivalent pressure load. In the modelled part of the slab, one quarter of the load was modelled for the case with one concentrated force, see Figure 5.4b. For the case with two concentrated forces, half of the load was modelled, see Figure 5.4c.
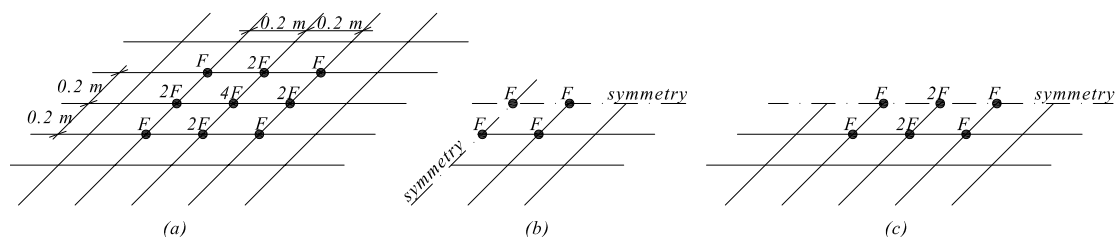
Figure 5.4   Force application on the beam grillage model.

5.2 Response of a single concentrated force

In the case of a single static concentrated force, the examined slab was exposed to a force acting in the centre of the slab, see Figure 5.5.
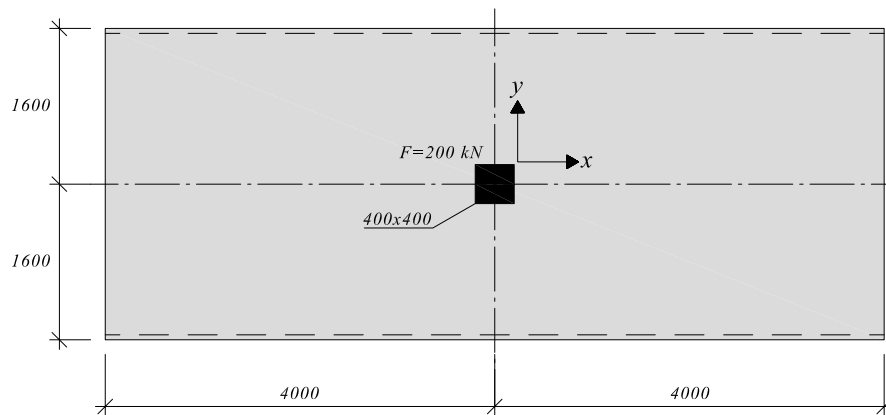
Figure 5.5   Position of loading on the modelled part of the slab.

5.2.1 Linear elastic orthotropic case

The linear elastic orthotropic analysis presented in Section 4.2.1 was also performed here, and the results are presented in Figure 5.6.
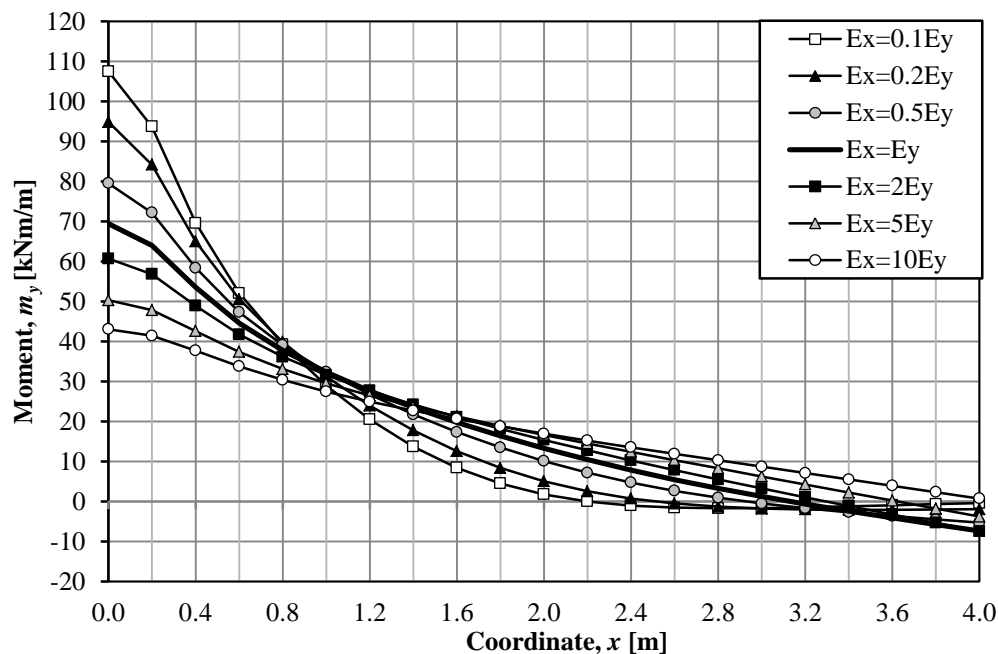
Figure 5.6   Linear elastic orthotropic moment distribution.

5.2.2 Trilinear elastic orthotropic case

The multilinear analysis presented in Section 4.2.2 was also performed here, and the results are presented in Figure 5.7 to Figure 5.9. For exact input data, see Appendix C. The results are discussed in Section 5.2.3.

a) $E_x = 2E_y$
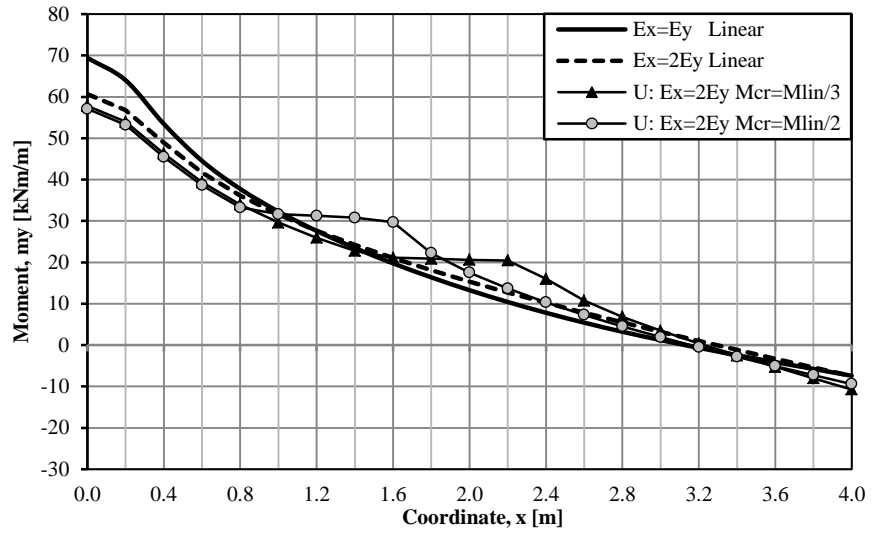
b) $E_x = 5E_y$
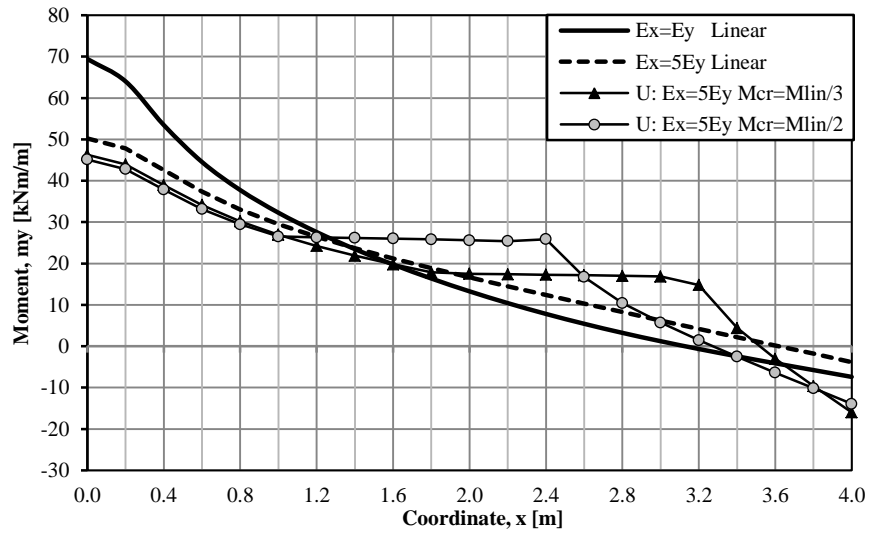
c) $E_x = 10E_y$
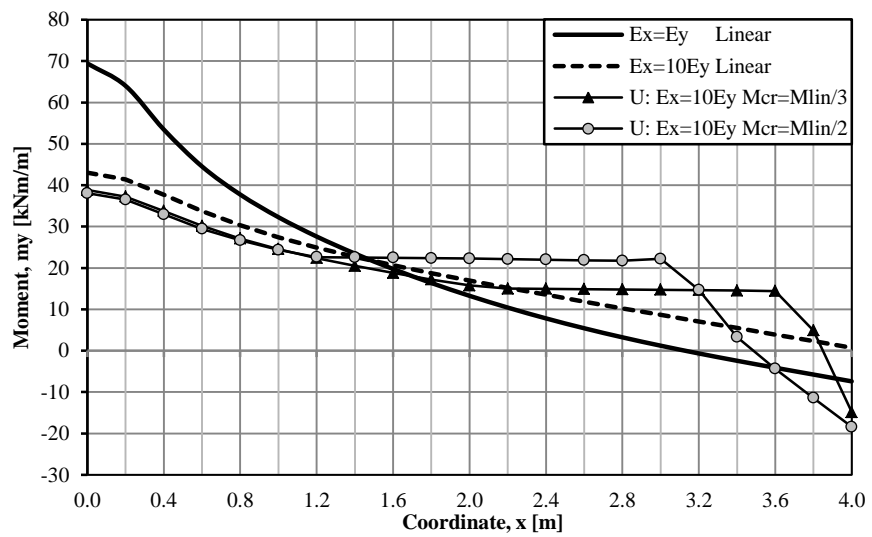
Figure 5.7   Moment distributions from the case Uncracked with varying magnitude of the cracking moment.
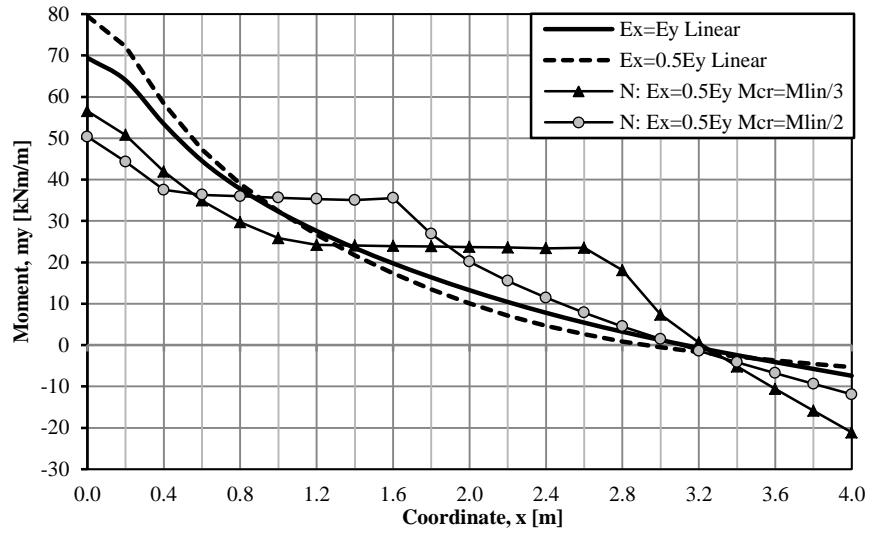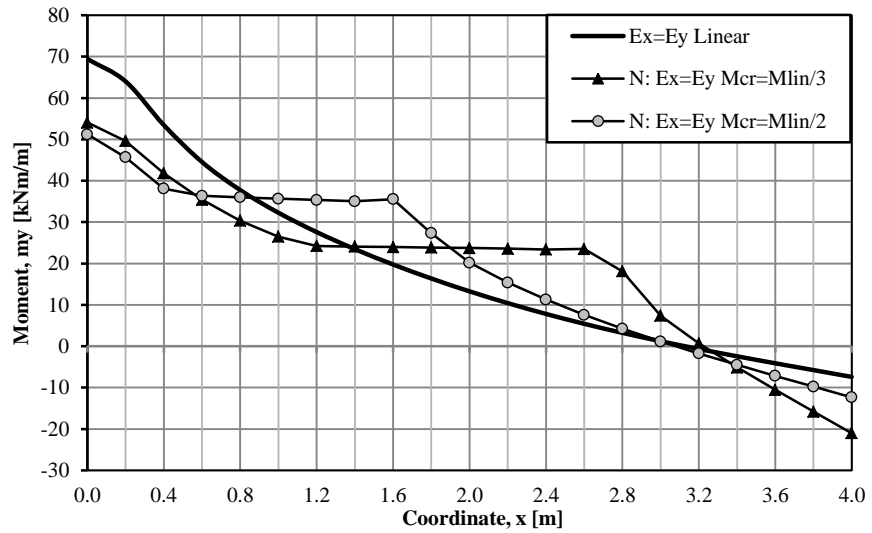
a) $E_x = 0.5E_y$
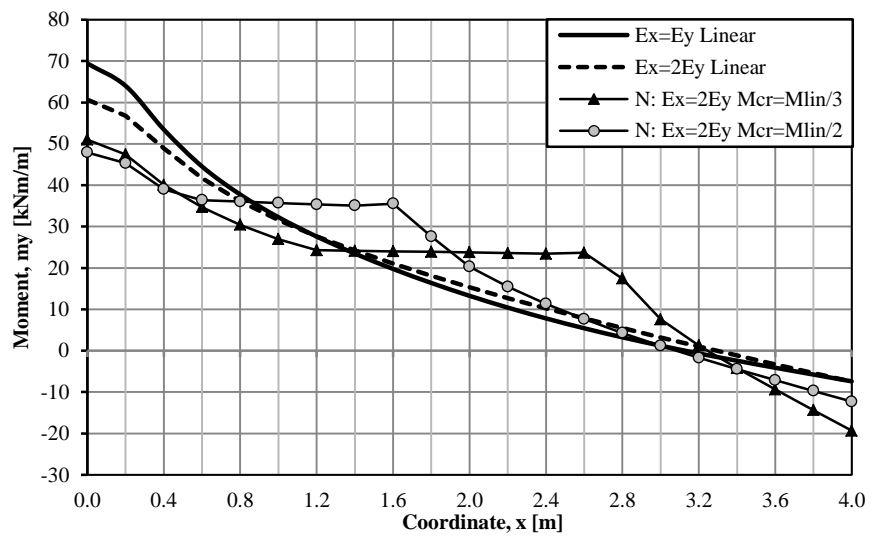
b) $E_x = E_y$

c) $E_x = 2E_y$

Figure 5.8   *Moment distributions from the case Neutral with varying magnitude of the cracking moment.*

a) $E_x = 0.5E_y$
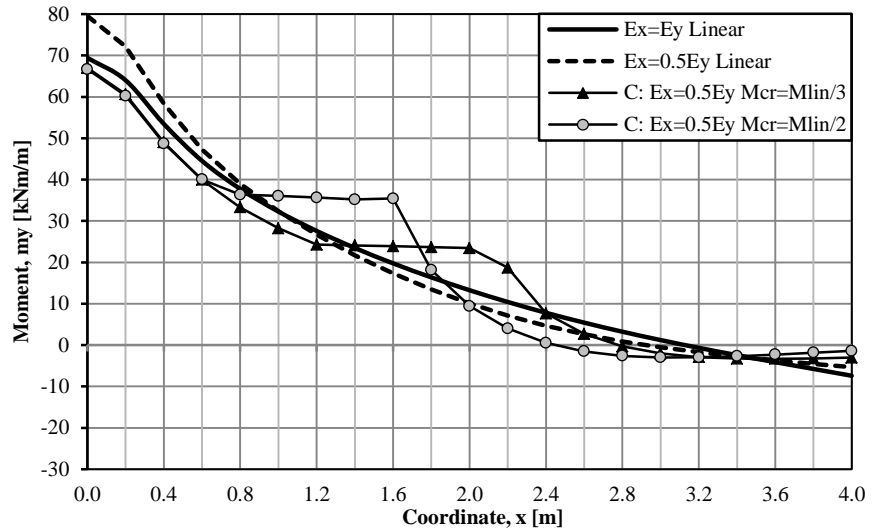
b) $E_x = E_y$
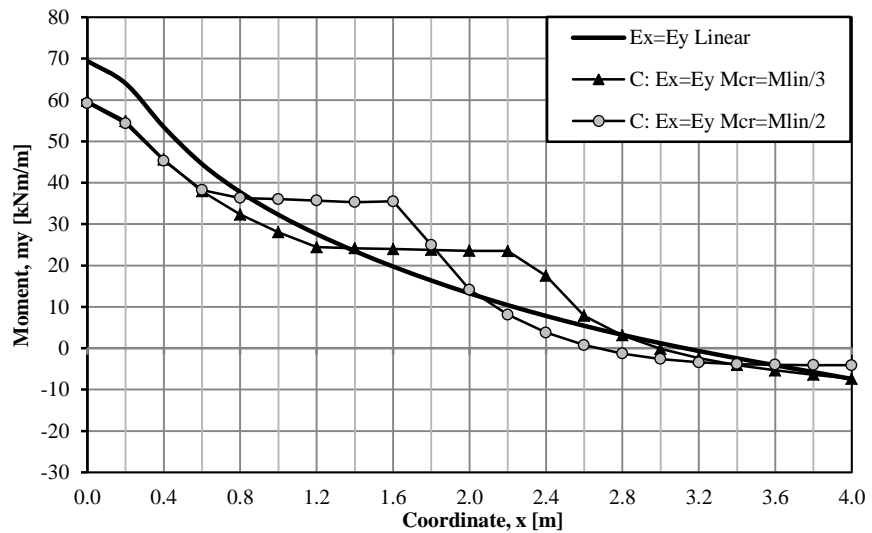
c) $E_x = 2E_y$
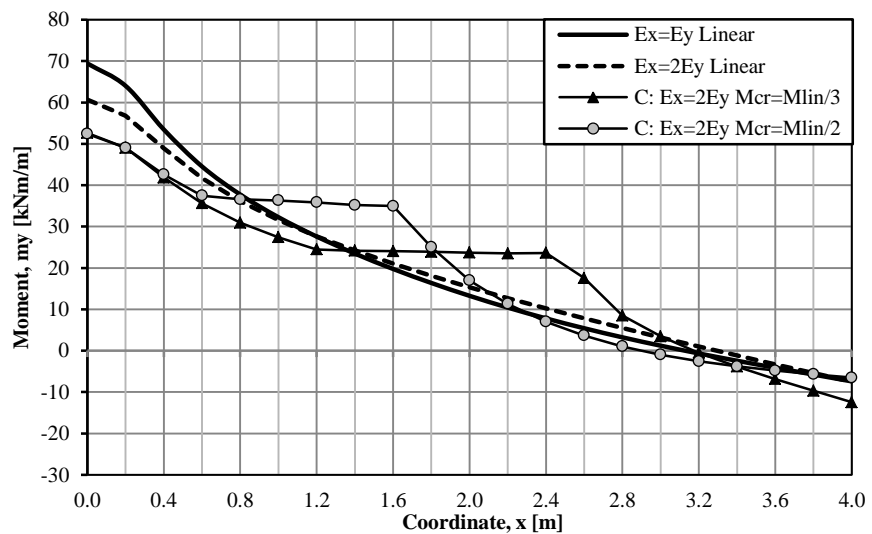
Figure 5.9   Moment distributions from the case Cracked with varying magnitude of the cracking moment.

CHALMERS, *Civil and Environmental Engineering*, Master's Thesis 2014:73

5.2.3 Discussion

The results follow the same pattern as for the cantilever slab in Section 4.2.2 and 4.3.2. The orthotropic linear solution describes the trilinear solutions fairly well for the cases Uncracked and Cracked, while the trilinear solutions differ from the orthotropic linear solution for the case Neutral.

The curves are not as smooth, close to the applied load, in comparison to the cantilever slab. This is due to the fact that the moment was measured directly under the point load, while for the cantilever slab, the moment was measured a certain distance from the load.

The trilinear solutions for the case Neutral are again very similar, independent on stiffness proportion. The low influence from the variety of stiffness in the x-direction can be explained by the dominating behavior from uncracked concrete sections which had equal stiffness. It would mean that most of the beams in x-direction still were in an uncracked state. To investigate this behavior further, different load levels were chosen for the case Neutral with a level of the cracking moment $M_{cr}=M_{lin}/3$ and the resulting moment distributions are presented in Figure 5.10. Moment distributions with equal cracking moment, but varying stiffness proportions, are plotted together for the load levels 100, 200 and 400 kN.
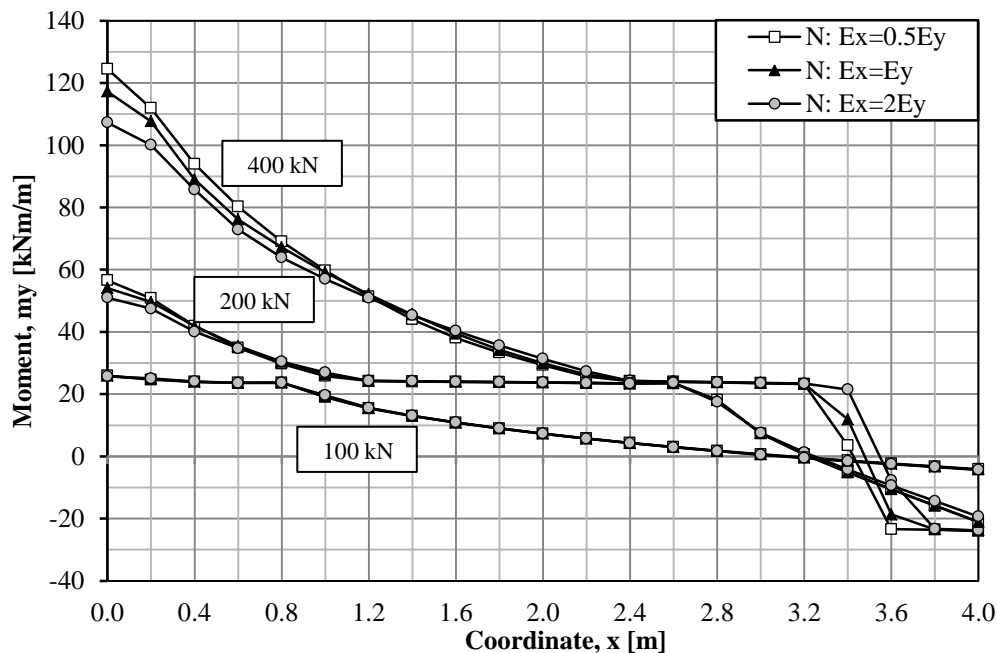
Figure 5.10   Moment distributions from the case Neutral, with the cracking moment $M_{cr}=M_{lin}/3$ and varying stiffness proportions.

It is observed that, for larger forces, the solutions became more dependent on the stiffness proportions which were believed to be an effect of decreasing tension stiffening.

The trilinear solutions from each stiffness proportion in the case Cracked were very similar, independent on the level of the cracking moment.

5.3 Response of two concentrated forces

In the case of two static concentrated forces, the examined slab was exposed to two forces acting along the centreline of the slab. The two forces were of equal magnitude and were positioned with a mutual distance of 1.2 m, see Figure 5.11. The chosen distance between the loads originates from the traffic load model described in Section 3.2.
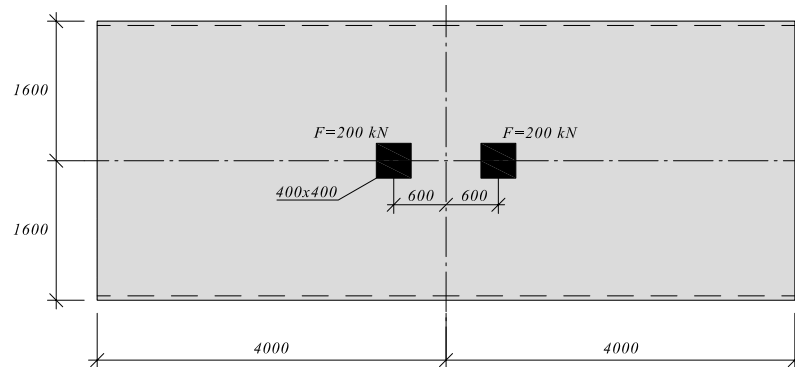
Figure 5.11   Geometry and position of loading.

5.3.1 Linear elastic orthotropic case

The linear elastic orthotropic analysis presented in Section 4.2.1 was also performed here, and the results are presented in Figure 5.12.
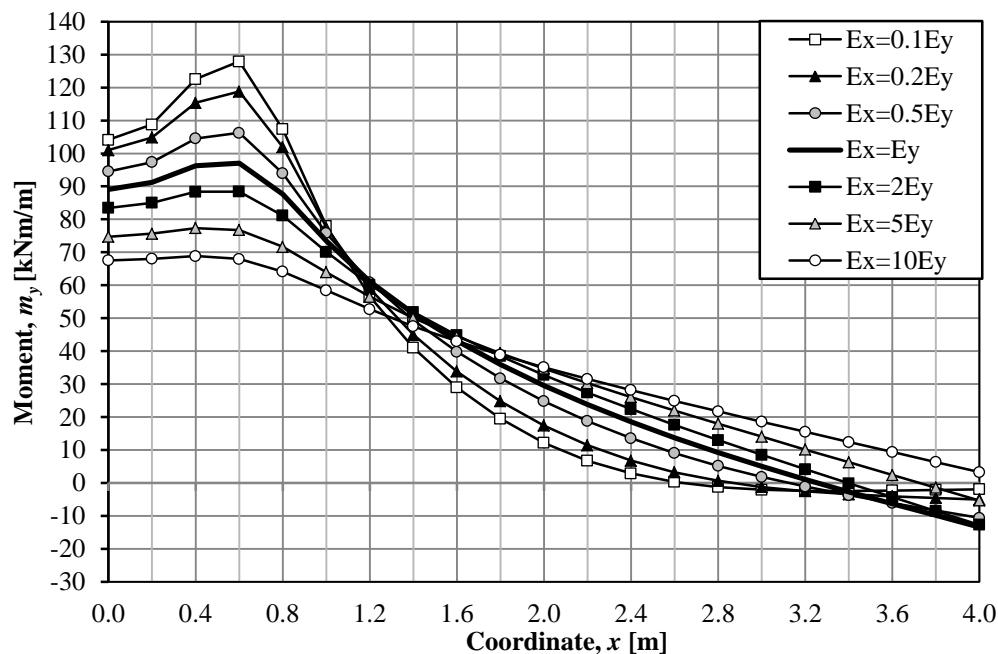
Figure 5.12   Linear elastic orthotropic moment distribution.

5.3.2 Trilinear elastic orthotropic case

The multilinear analysis presented in Section 4.2.2 was also performed here, and the results are presented in Figure 5.13 to Figure 5.15. For exact input data, see Appendix C. The results are discussed in Section 5.3.3.

a) $E_x = 2E_y$
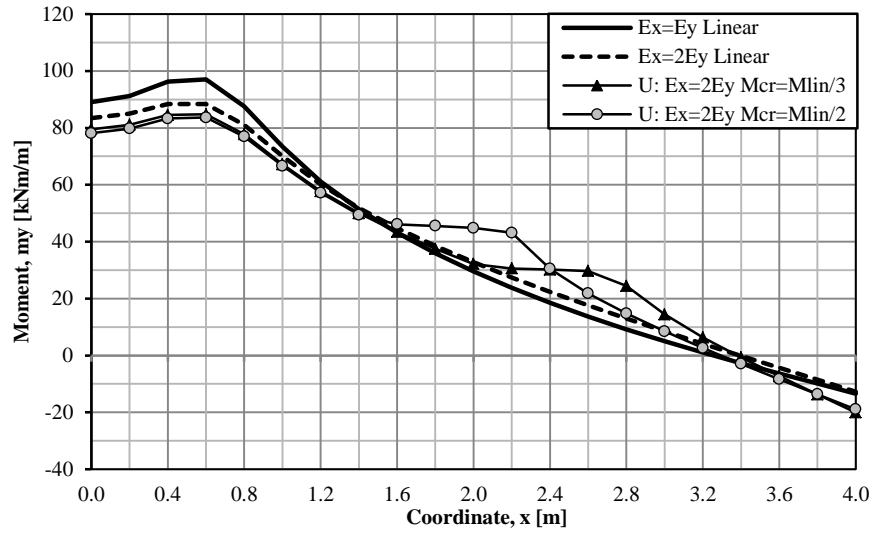
b) $E_x = 5E_y$
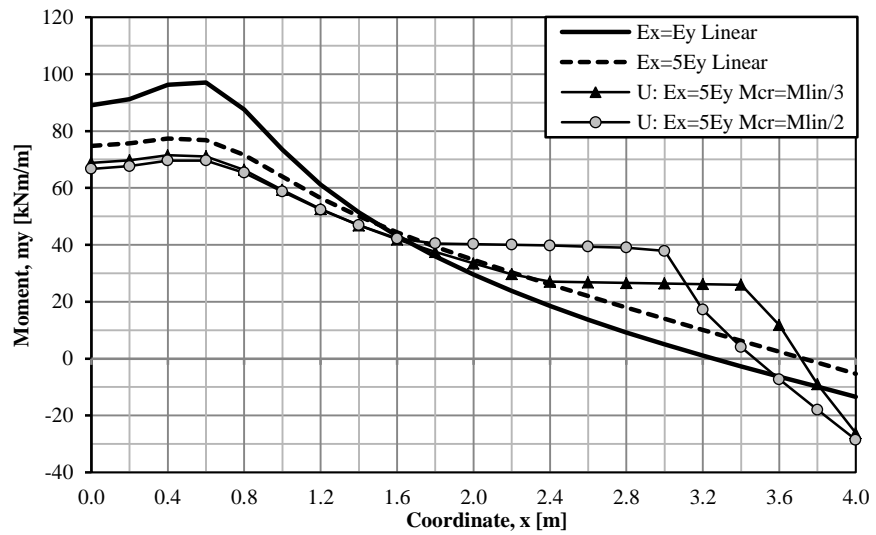
c) $E_x = 10E_y$
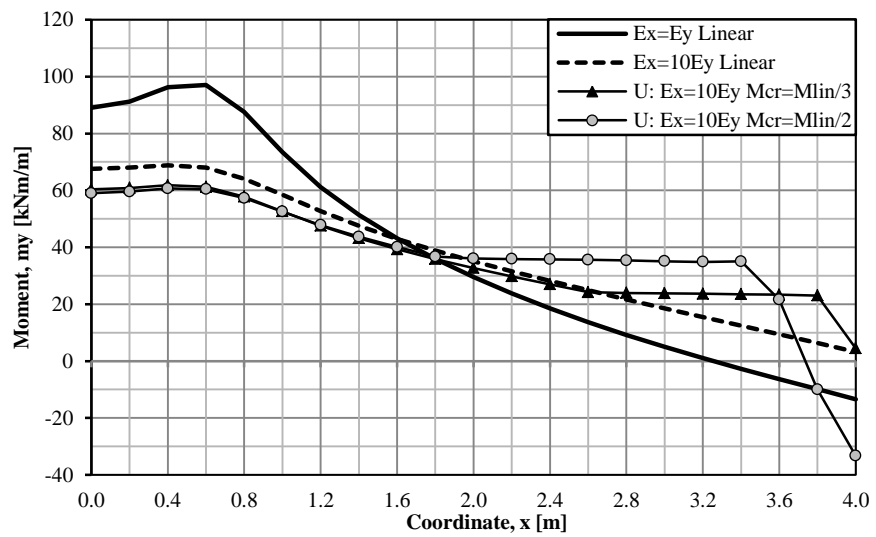
Figure 5.13 Moment distributions from the case Uncracked with varying magnitude of the cracking moment.
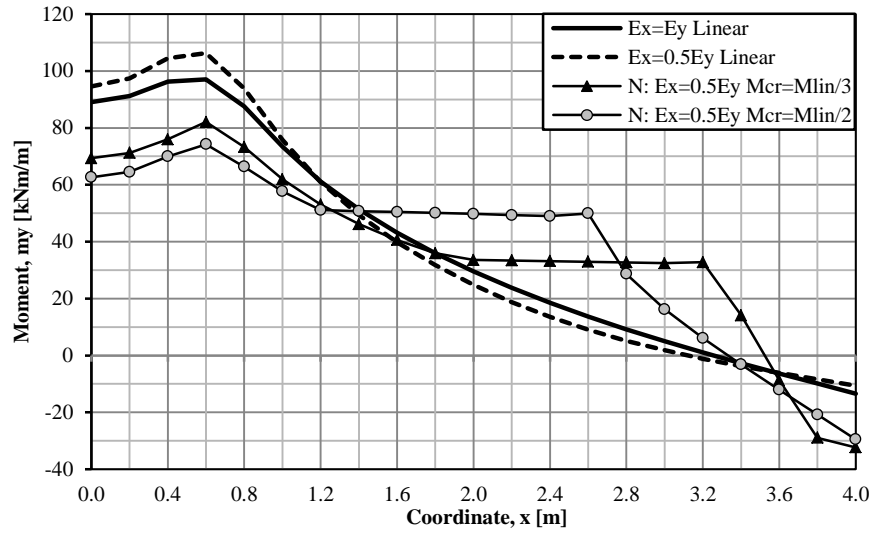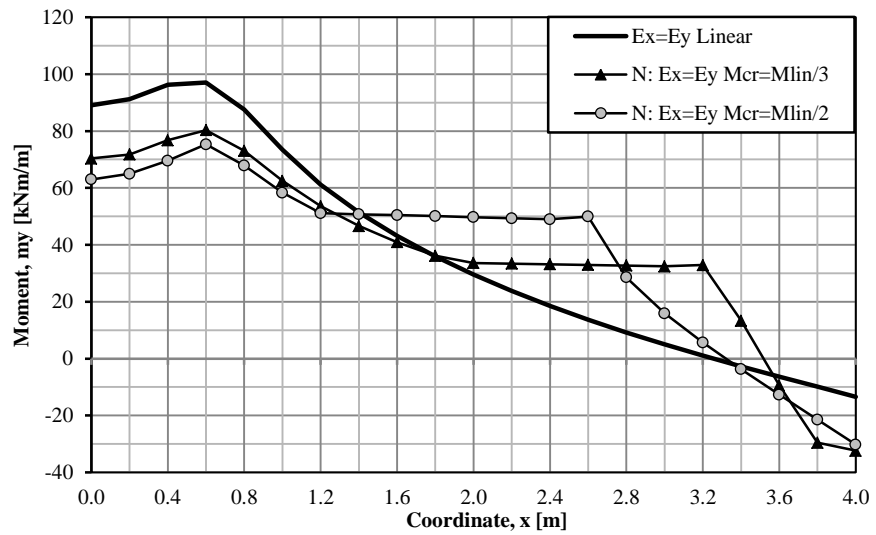
a) $E_x = 0.5E_y$
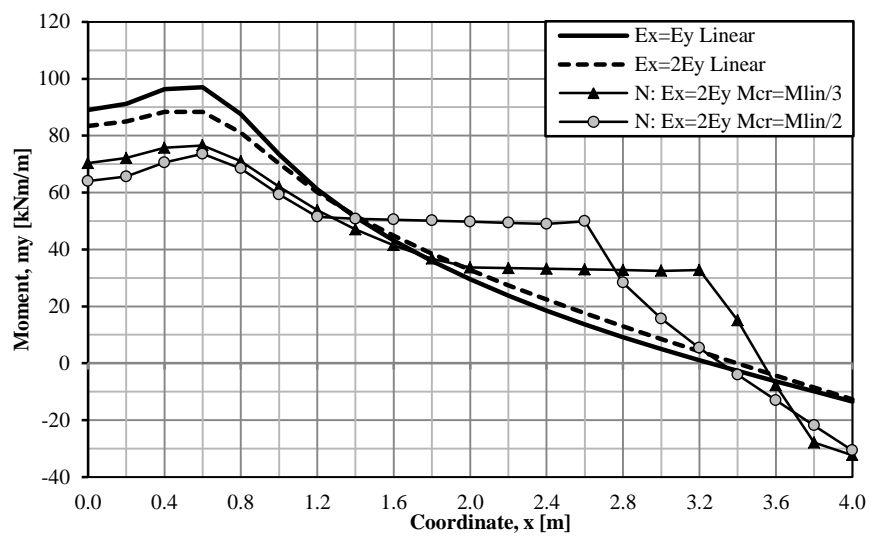
b) $E_x = E_y$

c) $E_x = 2E_y$

Figure 5.14 Moment distributions from the case Neutral with varying magnitude of the cracking moment.

CHALMERS, *Civil and Environmental Engineering*, Master's Thesis 2014:73

a) $E_x = 0.5E_y$
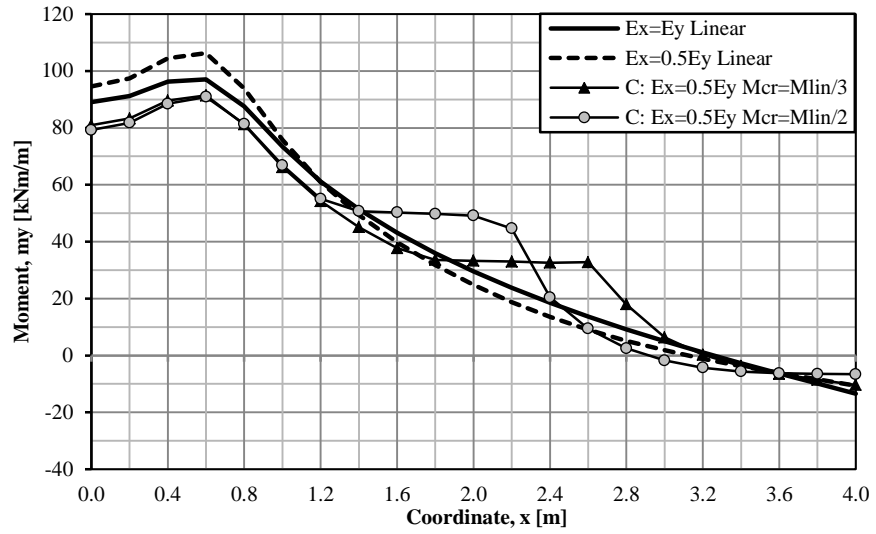
b) $E_x = E_y$
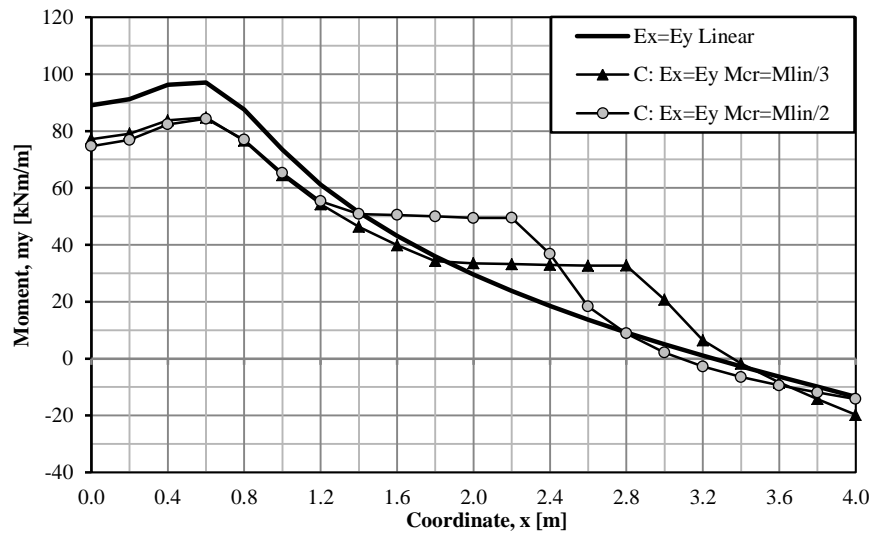
c) $E_x = 2E_y$
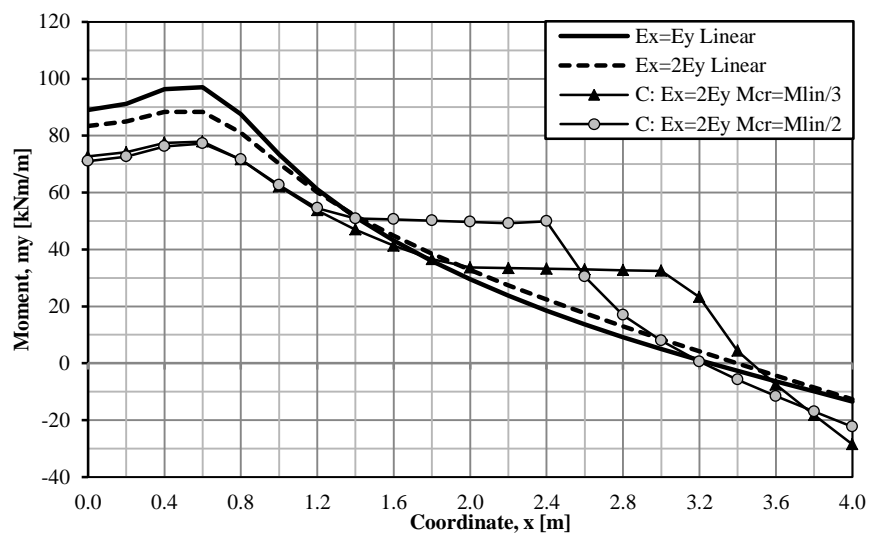
Figure 5.15   Moment distributions from the case Cracked with varying magnitude of the cracking moment.

5.3.3 Discussion

In general, the results follow the same pattern as in Section 4.2.3, 4.3.3 and 5.2.3. However, contrary to the cantilever slab in the case with two concentrated forces, the maximum moment was not found in the slab centre. This is most likely due to the fact that, contrary to the cantilever slab, the moment was measured directly under the concentrated force.

As described in Section 4.3.3, the linear results can be compared between a single and two concentrated forces by means of superposition. Here, the measured moment for a single concentrated force at the position $x = 0.6$ m was:

$$m_{1F} \; (x = 0.6) = 44.5 \text{ kNm/m} \tag{5-1}$$

Since both of the loads in the case with two concentrated forces were acting a distance of 0.6 m from the centre of the slab, the moment measured at $x = 0$ should be twice as large:

$$2 \cdot m_{1F} \; (x = 0.6) = 2 \cdot 44.5 = 89 \text{ kNm/m} \tag{5-2}$$

The actual moment measured in the case for two concentrated forces at $x = 0$ was:

$$m_{2F} \; (x = 0) = 89 \text{ kNm/m} \tag{5-3}$$

This means that, for the isotropic linear case, the structure was long enough for superposition of the results.

6 Cumulative plastic rotation – Cantilever slab

As mentioned in Chapter 4, simple structures were in this Thesis examined and the knowledge gained from these are intended to enable understanding of more complex structures. The aim of Chapter 6 and 7 was to increase the understanding of development of accumulated damage in long slabs which are subjected to moving concentrated forces at, below or above magnitudes predicted by the serviceability limit state, SLS. The response of static forces was first studied for comparison purposes and as reference results. The response of a single moving concentrated force was thereafter studied and then expanded to two moving concentrated forces. The forces were applied with constant and varying magnitudes in different orders. The distance d between the two moving concentrated forces was altered in order to cover a broader spectrum of possible load combinations. The same methodology was repeated for a simply supported one-way slab, presented in Chapter 7.

The cantilever slab studied in Chapter 4 was for these analyses modelled without a symmetry boundary since such a boundary could not reflect the moving forces of interest in this Thesis. When the cantilever slab from Chapter 4 was modelled without symmetry boundary conditions, numerical problems occurred. These numerical problems were obtained due to disturbances of the slab in the vicinity of the free edges. Since the scope of this analysis was to investigate how plastic rotation in a long cantilever slab develops, the previous dimensions were altered. The new slab width was set to 12 m while other geometrical parameters were kept constant.
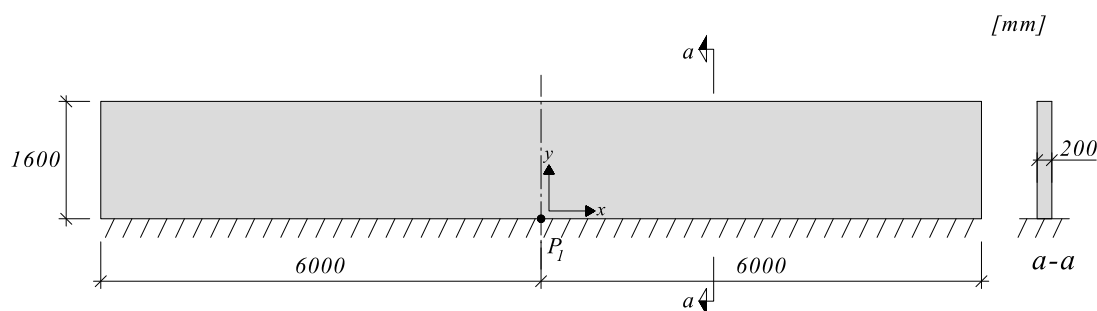
Figure 6.1   Geometry and dimensions of the studied cantilever slab

6.1 Methodology

This section covers the methodology used for the studies related to the development of plastic rotation and thus also applies for Chapter 7. The background and the practical application of these studies, the moment-curvature relations, the finite element model and the influence of the torsional stiffness are also treated in this section.

6.1.1 Background

The aim of this study was to gather reasonable estimates of the development of plastic rotation in long slabs and to gather knowledge around important factors which can influence the development. This study was directed towards load magnitudes that causes plastic rotation in bridge structures but is also applicable for structures subjected to similar forces. This Thesis defined two likely situations where plastic rotation may occur which are presented below.

The first of the two situations were observed in Chapter 4, where moments higher than predicted by a simplified linear elastic analysis occurred when a more refined analysis was conducted. This difference was derived from the orthotropic stiffness which was a result from varying reinforcement amounts in different directions. This behaviour was observed for the linear elastic orthotropic case in Figure 4.7 and is also illustrated here in Figure 6.2.
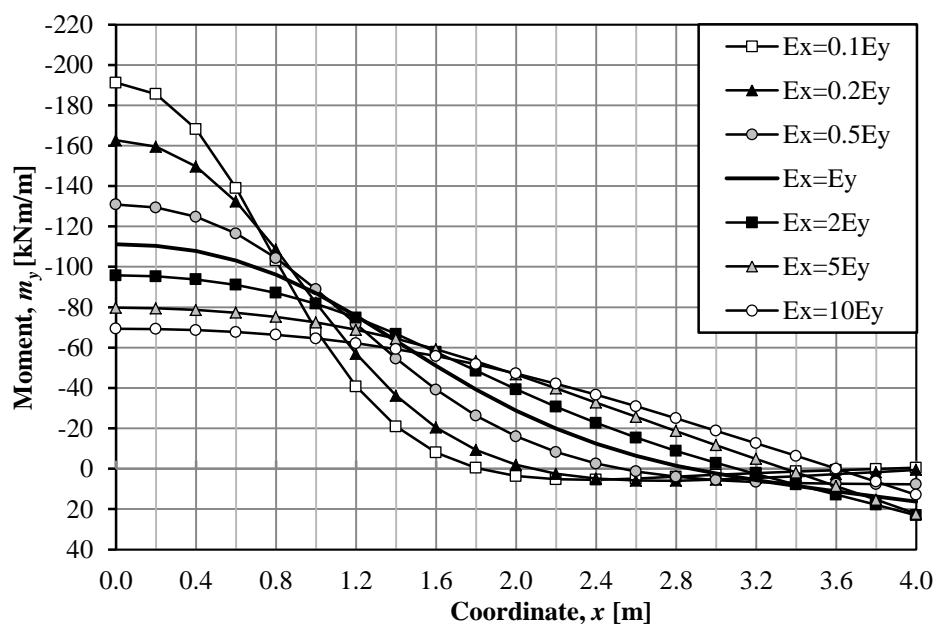
Figure 6.2   Linear elastic orthotropic moment distribution.

As can be seen in Figure 6.2, there was a significant difference in maximum moment between the isotropic (solid line) and the orthotropic solutions where an orthotropic case yielded the highest moment. This means that a bridge structure, designed according to a simplified linear elastic model, can be subjected to moments higher than the design values and thus initiate plastic rotation.

The second situation when loads causes plastic rotation was here defined as forces of magnitudes above what is predicted by the serviceability limit state (SLS) but below those defined by the ultimate limit state (ULS), see Figure 6.3.
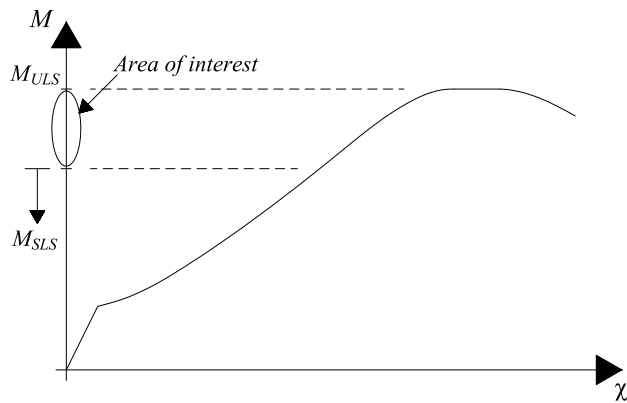
Figure 6.3   Area of interest for the analyses in this section.

Bridge structures should not be exposed to these load levels but due to heavy transportation, such as authorized industrial transportation and uncontrolled highly loaded vehicles, these load levels may still be exceeded. When these load levels are exceeded, a permanent damage arises in the structure which will continue to grow each time the serviceability limit state load is exceeded. For additional information about these load situations, the reader is referred to Section 3.3

The analyses in this section were conducted for a large number of load cycles n where each load cycle represents a crossing of a vehicle below, at, or above the serviceability limit state load that causes plastic rotation.
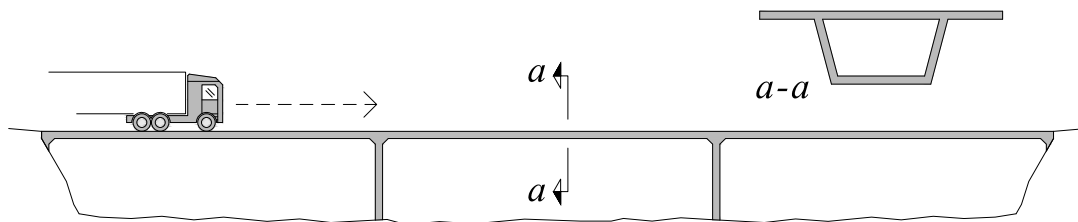
Figure 6.4   Practical interpretation of the load model used in this section.

6.1.2 Moment-curvature relations

The non-linear behaviour of reinforced concrete, used in Chapter 4, was here simplified to a bilinear behaviour. The trilinear moment-curvature relation used in Chapter 4 could not be implemented in a plastic analysis due to restrictions in the FE software ADINA. A simplified moment-curvature relation was therefore used in these analyses and the reader is referred to Appendix C for additional information. The moment-curvature relation used as input for the beam grillage models was intended to simulate a simplified behaviour of the reinforced concrete structure, see Figure 6.5.
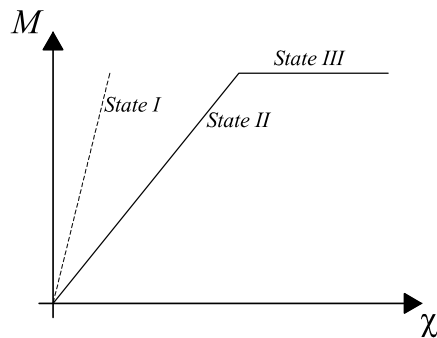
Figure 6.5   Bilinear plastic moment-curvature relation.

As can be seen in Figure 6.5, the elastic section of the moment-curvature relation was based on a state II model, i.e. the cracked stiffness of a small reinforced concrete section. The background for this choice can be derived from the restrictions in the ADINA software and are treated separately in Appendix C.

Due to the limited timeframe of this Thesis, the analyses was only conducted on an isotropic structure with a stiffness factor $\alpha = 1$ according to Equation (6-1). The same moment-curvature relations were therefore utilized in both *x*- and *y*-direction.

$$\alpha = \frac{E_x}{E_y} \tag{6-1}$$

The bilinear plastic moment-curvature relation for the slab was based on the elastic response of an isotropic, cracked cantilever slab subjected to a concentrated force of 200 kN at the centre of the primary free edge. This was the elastic moment-curvature relation used for the cracked case in Chapter 4 for the cantilever structure in SLS. The elastic part of the moment-curvature relation and the corresponding moment distribution in the fixed support is illustrated in Figure 6.6.
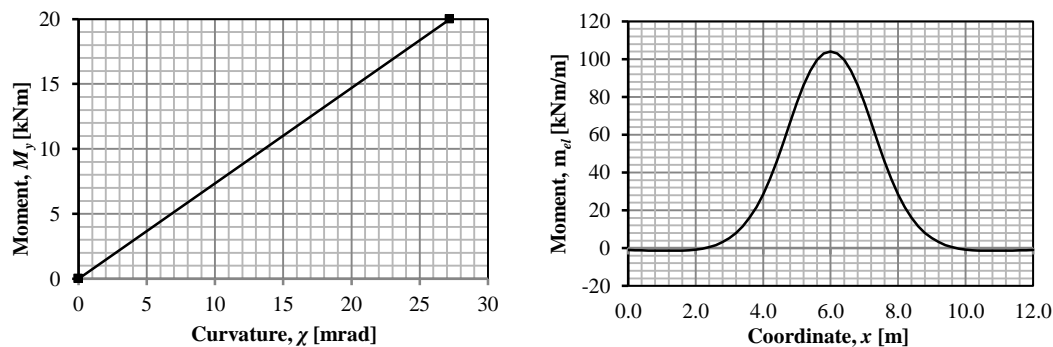
Figure 6.6   Elastic moment-curvature relation and the corresponding moment distribution in the fixed support.

The plastic moment M_{pl} was chosen to 60 % of the maximum elastic moment M_{el}:

$$M_{pl} = 0.6 \cdot M_{el} \qquad (6\text{-}2)$$

The choice of the plastic moment was based on a recommendation by Pacoste *et al.* (2012) where the following limits for redistribution of reinforcement moments were proposed:

$$0.6 \cdot M_{elastic} \leq M_{plastic} \leq M_{elastic} \qquad (6\text{-}3)$$

Failure of the cantilever slab was defined as the plastic rotation capacity θ_{rd} for a cross-section with a reinforcement amount of 0.5 %:

$$\theta_{rd} = 23.44 \text{ mrad} \qquad (6\text{-}4)$$

For additional and a more profound description on the modelling choices, the construction of the plastic moment and the design of the plastic rotation capacity, the reader is referred to Appendix C.

To summarize; the bilinear plastic moment-curvature relation used in this section was based on:

- The elastic response of an isotropic, cracked cross-section
- The plastic moment M_{pl}, based on the elastic response of the structure
- The plastic rotation capacity θ_{rd} of the cross-section

Since the beam grillage model was designed with beams of the half cross-sectional width in the boundaries, which is covered in Section 6.1.3, the plastic moment was set to half of that in the rest of the beams in the beam grillage model. These two moment-curvature relations used as input for the FE model are illustrated in Figure 6.7.
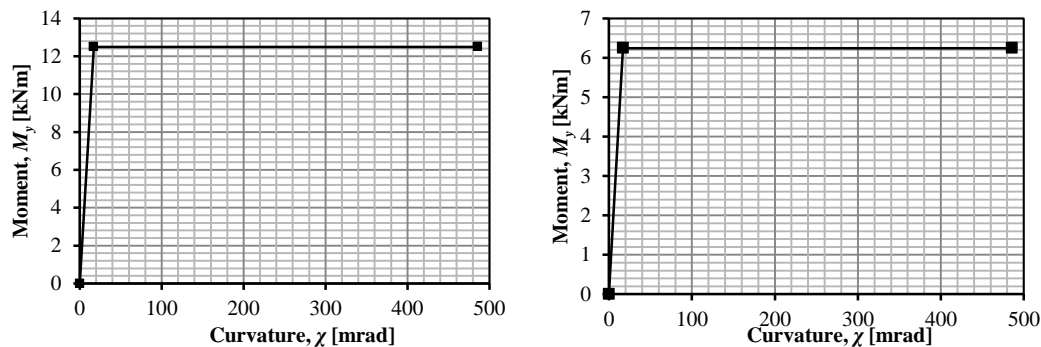
Figure 6.7   Bilinear plastic moment-curvatures used for the analyses in this section.

6.1.3 Finite element model

As mentioned in the introduction of Chapter 6, the cantilever structure experienced numerical problems due to disturbances at the boundaries. The cantilever slab was therefore extended to 12 m and the moving concentrated forces was set to operate within a length of 4.8 m, concentrated to the centre of the slab. The numerical problems were in this way avoided and the model used for these analyses is illustrated in Figure 6.8.
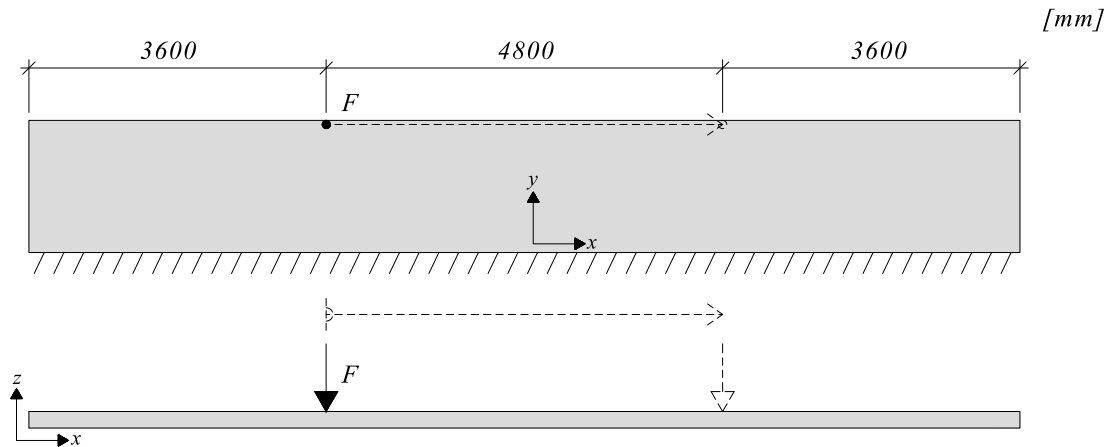
Figure 6.8   Geometry and dimensions of the studied cantilever slab, here subjected to a single moving concentrated force.

As in the analyses of moment distribution in Chapter 4 and 5, the finite element software used was the student version of ADINA (2012). The plastic rotation and the development of plastic rotation in the centre of the fixed support were of interest in this study and are therefore presented in this section in the result point P1, illustrated in Figure 6.1. When the development of the plastic rotation along the fixed support is illustrated in this section, the coordinate $x = 0$ refer to the centre of the fixed support (due to the symmetry behaviour of the structure).

For the beam grillage model, it was concluded that a beam width of 0.2 m yielded satisfactory results. The mesh was however orthotropic with an increased mesh density at the fixed support, where the element length was set to 0.05 m which is further discussed in Appendix C. This mesh density was also chosen for similar studies in Lim (2013).

The moving concentrated forces were modelled as point loads, applied to single nodes. Since the plastic rotation at the fixed support was of interest, which was a certain distance from the applied forces, it was concluded that this approximation was acceptable. The boundary condition at the fixed support was modelled as fixed in all translations and rotations. The beams in the beam grillage model that were placed in the boundaries (the fixed support and the free edges) were modelled as beams with half the cross-sectional width.

The FE model was designed as static, i.e. without considering any dynamic effects of the structure or of the load application. This modelling choice was believed to yield results on the unsafe side. The dynamic amplification of the applied forces is however included in the characteristic load values provided by Eurocode 1 (2003) which was presented in Section 3.2. Since the aim of this section was to study the development of plastic rotation in a bridge structure, it was reasonable to treat the problem as static since it is the most common approach in the bridge design community and recommended by Eurocode 1.

The Poisson's ratio was chosen to 0. The iteration method for the non-linear analysis was chosen to the full Newton method in ADINA and the iteration tolerance type was set to energy.

Since the behaviour of a long slab was of interest in this analysis, the plastic rotation θ_{pl} was only measured at the centre of the fixed support in the result point P_1 which

CHALMERS, *Civil and Environmental Engineering*, Master's Thesis 2014:73

can be seen in Figure 6.1. The plastic rotation was measured after each completed load cycle *n*.

The plastic rotation was calculated using an approximate approach from the deflection in the second and third node, u_2 and u_3. The angle α, i.e. the plastic rotation, was calculated from the triangle created by the deflected nodes, which can be seen in Figure 6.9
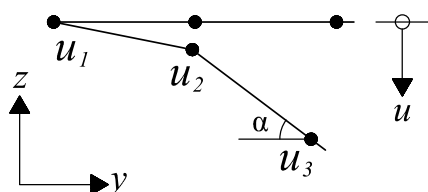
Figure 6.9   The approximate approach for calculating the plastic rotation θ_{pl} in the centre of the fixed support in the cantilever slab.

The angle α and thus the plastic rotation θ_{pl}, was calculated from the deflection from the second and third node due to how the ADINA software treats the plastic curvature in the FE model. ADINA provides the plastic curvature χ_{pl} in five integrations points, uniformly distributed over each element. The plastic rotation is obtained if the area A_1 and A_2, which are illustrated in Figure 6.10, is calculated. This is one of the options that ADINA provides in order to obtain the plastic rotation. The FE program distributes the plastic curvature to the two nodes of the element and thus gives contributions to the plastic curvature to those nodes. In order to capture the plastic rotation for the complete element, the difference in deflection has to be calculated using the second and third node, as described above.
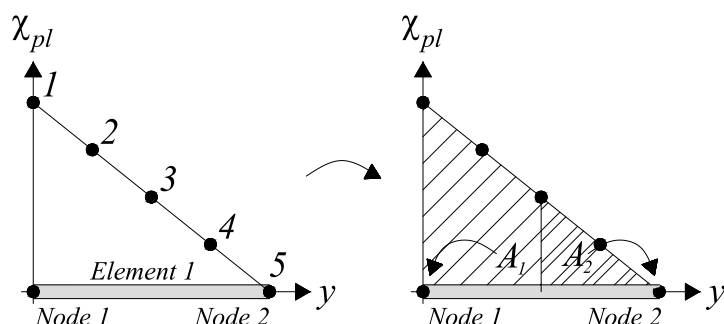
Figure 6.10 Illustration of how ADINA treats the plastic curvature and how it is distributed to the two nodes of the element.

The angle α was dependent on the mesh density since a finer mesh provides a better approximation. The orthotropic mesh density described above yielded satisfactory results and an increase of the mesh density did not influence the results significantly.

As described above, ADINA provides an option for obtaining the plastic curvature in the integration points for each element. If the plastic curvature is summarized over the element length, the plastic rotation is obtained. This option provided by ADINA is, however rather cumbersome when exporting the obtained data for analysis. The influence of the approximation stated above was small and the option provided by ADINA was therefore rejected. The reader is referred to Appendix D for the study and the influence of the approximation of determining the plastic rotation in the cantilever structure

6.1.4 Torsional stiffness

It was concluded in Section 4.1.3 that the torsional stiffness dominates the behaviour of the structures in this Thesis when subjected to concentrated static forces. It was also concluded that difficulties arose regarding how to model the torsional stiffness in the cracked state (state II). Lim (2013) assumed that the torsional stiffness of a beam in the beam grillage model had a constant value of the torsional stiffness independently of the state of the reinforced concrete. A parametric study was also here performed in order to evaluate the influence of the torsional stiffness on moving concentrated forces. The structure studied was the cantilever slab presented in this section where the torsional stiffness was set according to the values presented in Section 4.1.3. As in the case of a single static concentrated force, the plastic rotation significantly increases as the torsional stiffness decreases, see Figure 6.11. The case of an elastic torsional stiffness yielded no plastic rotation and the case with zero torsional stiffness became too unstable and the analysis was aborted. For more detailed information of the study the reader is referred to Appendix B.
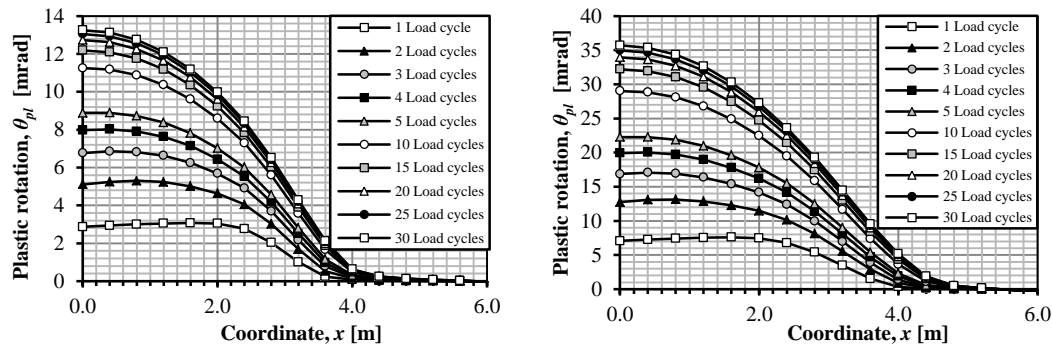
Figure 6.11   Plastic rotation development for a moving concentrated force of 150 kN. Torsional stiffness of 1/8 and 1/16 of the elastic stiffness to the left and right, respectively.

Based on the work done by Lopes (2014) and what is presented and treated in Section 4.1.3 the torsional stiffness of the beam elements throughout the Thesis was chosen to a linear relation of 1/16 of the elastic stiffness of a concrete beam with a width and height of 0.2 m. As stated in Section 4.1.3, it should however be noted that the torsional stiffness of a plate is different from the torsional stiffness of a beam grillage model which further complicates the choice of torsional stiffness. As in Section 4.1.3 the choice of torsional stiffness is believed to be conservative.

As described in Section 4.1.3, the torsional stiffness of a beam element is defined by a torsional moment versus the angle of twist per unit length. Since a linear relation of 1/16 of the elastic stiffness was chosen, the model does not accurately describe parts that are uncracked in the structure. The whole structure was however assumed to be fully cracked due to the restrictions in the ADINA software which yielded even more conservative results. For the definition and more detailed information of the torsional stiffness, the reader is referred to Section 4.1.3.

6.2 Response of a single and two static forces

The response and the development of plastic rotation for a single and two static forces of varying magnitudes are treated in this section. The aim of this section was to study how the cantilever structure behaves under static forces so that the development of plastic rotation caused by moving concentrated forces can be compared and evaluated. This evaluation is treated in Section 6.6.2.

The cantilever slab was subjected to single forces F of the following magnitudes:

$$F = \begin{bmatrix} 115 \, 120 \, 125 \, ... \, 205 \, 210 \, 215 \end{bmatrix} \text{kN} \qquad (6\text{-}5)$$

The forces that were applied on the slab had a range of 115 kN, where no plastic rotation occurred, and 215 kN which was the force of the smallest magnitude to cause failure due to plastic rotation θ_{pl}. The forces were applied in the centre of the primary free edge which can be seen in Figure 6.12.
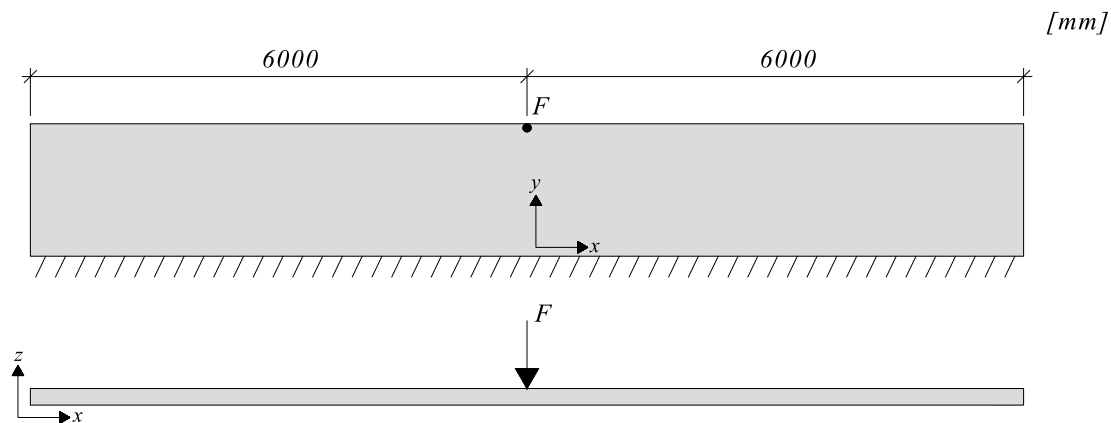
Figure 6.12   Geometry and dimensions of the studied cantilever slab subjected to a single static concentrated force.

The slab was also subjected to two concentrated forces F_1 and F_2 that varied according to the following magnitudes:

$$F_1 = F_2 = \begin{bmatrix} 65 \, 70 \, 75 \, ... \, 125 \, 130 \, 135 \end{bmatrix} \text{kN} \qquad (6\text{-}6)$$

The distance between the two forces was altered according to:

$$d = \begin{bmatrix} 1.2 \, 1.6 \, 2.0 \end{bmatrix} \text{m} \qquad (6\text{-}7)$$

The forces that were applied on the slab had a range of 65 kN, where no plastic rotation occurred for $d = 1.2$ m, and 135 kN which was the force of the smallest magnitude to cause failure due to plastic rotation for $d = 2.0$ m. The forces were also here applied in the centre of the primary free edge which can be seen in Figure 6.13.
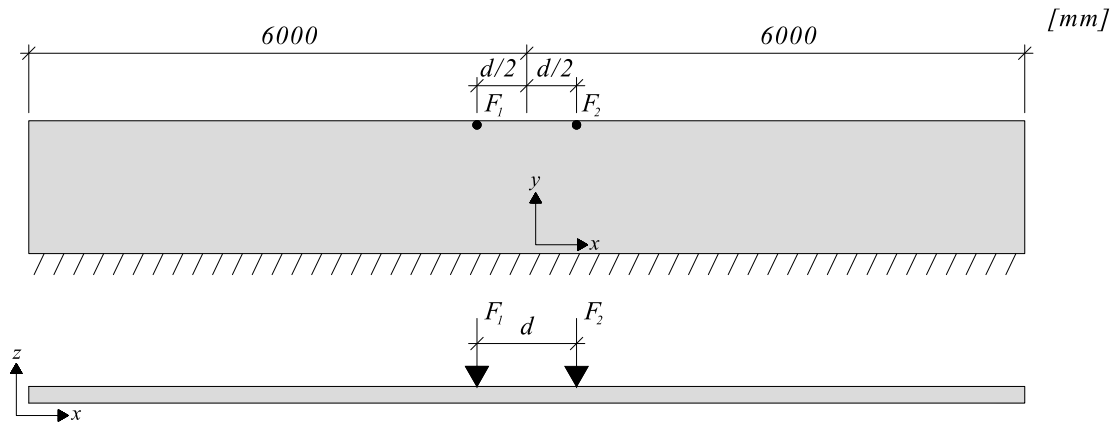
Figure 6.13 Geometry and dimensions of the studied cantilever slab subjected to a pair of static concentrated forces.

The results from the analyses are shown in Figure 6.14 where it is clearly shown that it was advantageous for the cantilever structure with an increased distance between the two concentrated forces. In order to compare the pair of static forces to a single static force, the total applied force F_{tot} was defined according to:

$$F_{tot} = F_1 + F_2 \qquad \qquad (6\text{-}8)$$
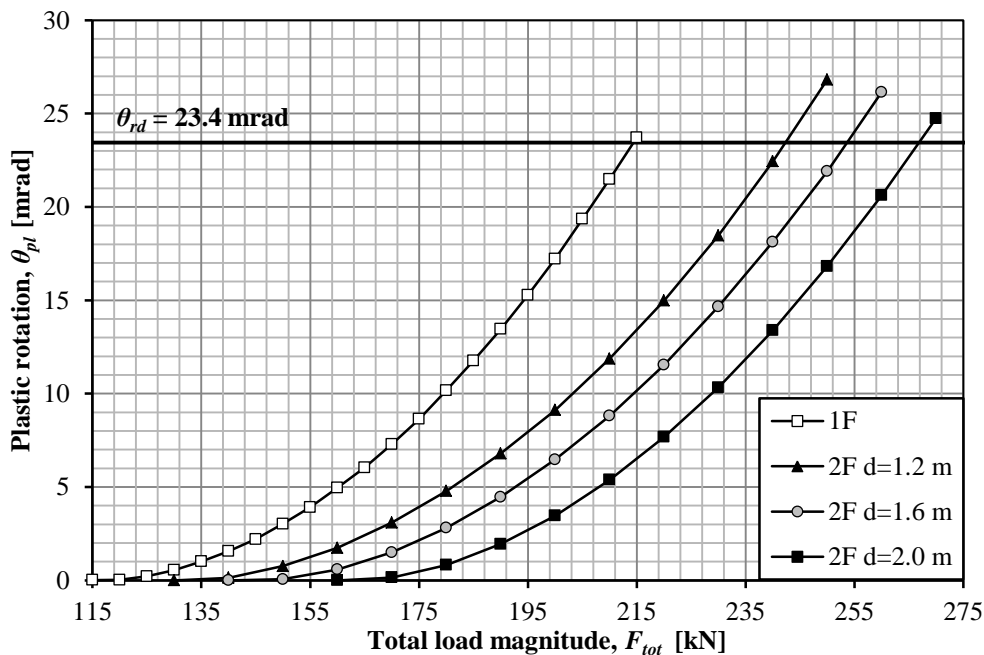
Figure 6.14 Plastic rotation at the centre of the cantilever slab for different magnitudes of static forces.

As a validation of the model, the cantilever structure was subjected to a single static force of 180 kN that were applied over ten load cycles (applied and removed ten times). A static force should in theory cause a plastic rotation that does not develop when the number of load applications increases. As can be seen in Figure 6.15, there is a slight development during the first load cycles but the model was after that stabilized and no further disturbances occurred.
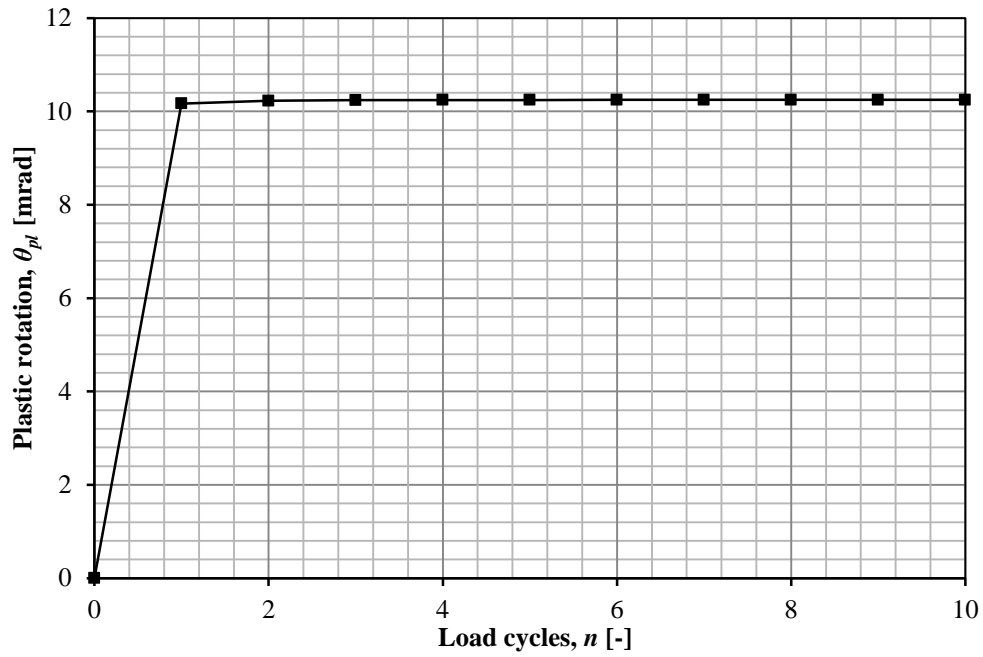
Figure 6.15   Plastic rotation at the centre of the cantilever slab for a static force F=180 kN during ten load cycles.

6.3 Response of a single moving force

The response and the development of accumulated damage, i.e. plastic rotation, for a single moving concentrated force of constant and varying magnitudes is treated in this section. A comparison between the different load combinations and how a traditional superposition approach corresponds to the behaviour of the slab from the conducted analyses is also treated in this section.
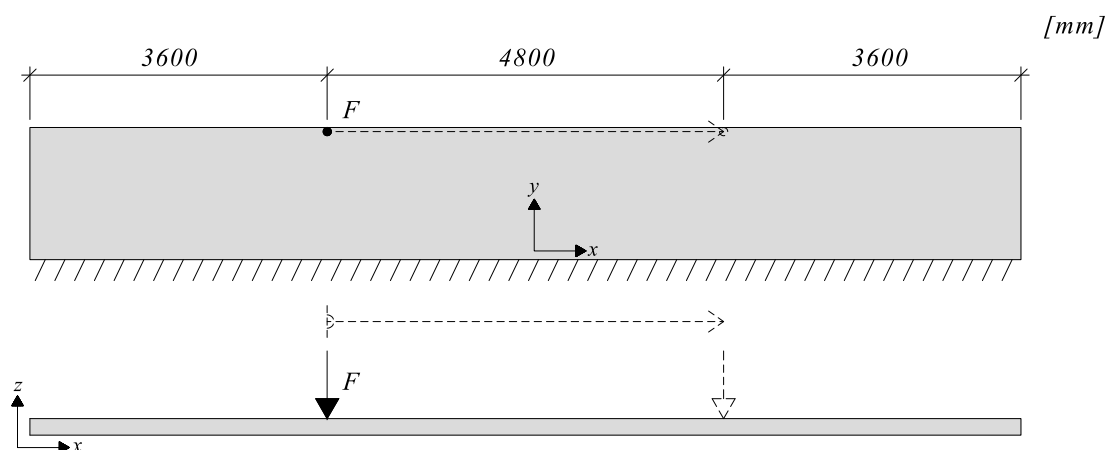
Figure 6.16 Geometry and dimensions of the studied cantilever slab subjected to a single moving concentrated force.

6.3.1 Load magnitudes – Constant

The slab in Figure 6.16 was exposed to a range of a moving concentrated forces *F* of different magnitudes:

$$F = \begin{bmatrix} 115 & 120 & 125 & ... & 175 & 180 & 185 \end{bmatrix} \text{kN} \tag{6-9}$$

The forces that were applied on the slab had a range of 115 kN, where no plastic rotation occurred, and 185 kN where failure occurred during the first load cycle. As can be seen in Figure 6.17, a high load magnitude led to failure in a small number of load cycles while a low load magnitude led to failure with a higher number of load cycles. This behaviour corresponded to the expected behaviour of the structure.

The cantilever slab was subjected to up to 150 load cycles *n* for each load magnitude *F*.

Forces with a magnitude ranging from 165 kN to 185 kN reached failure in two or less load cycles, which is shown in Figure 6.18 for scale purposes.
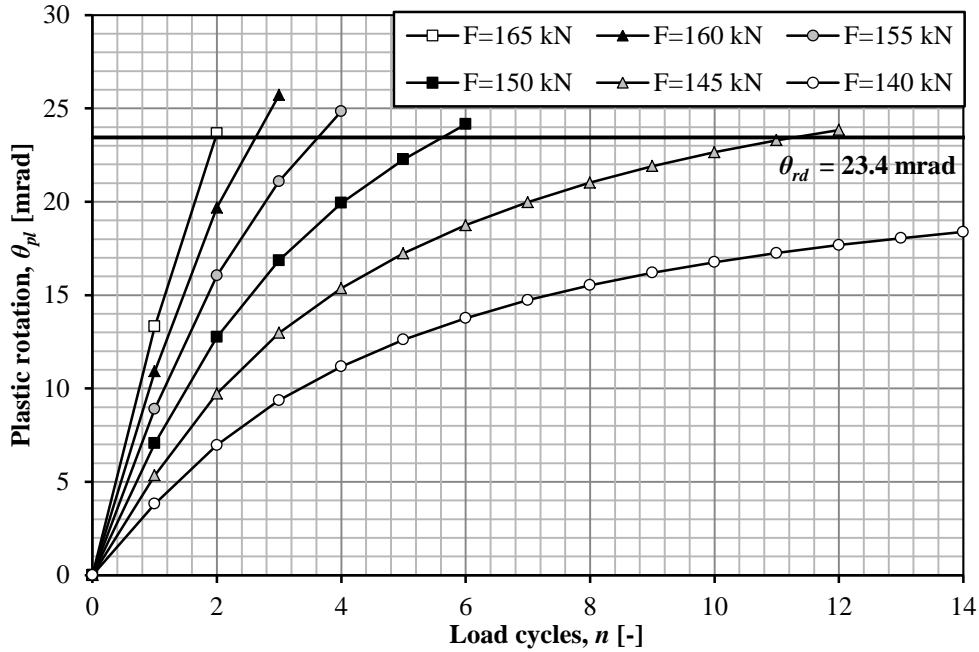
Figure 6.17   Plastic rotation for different magnitudes of moving concentrated forces.
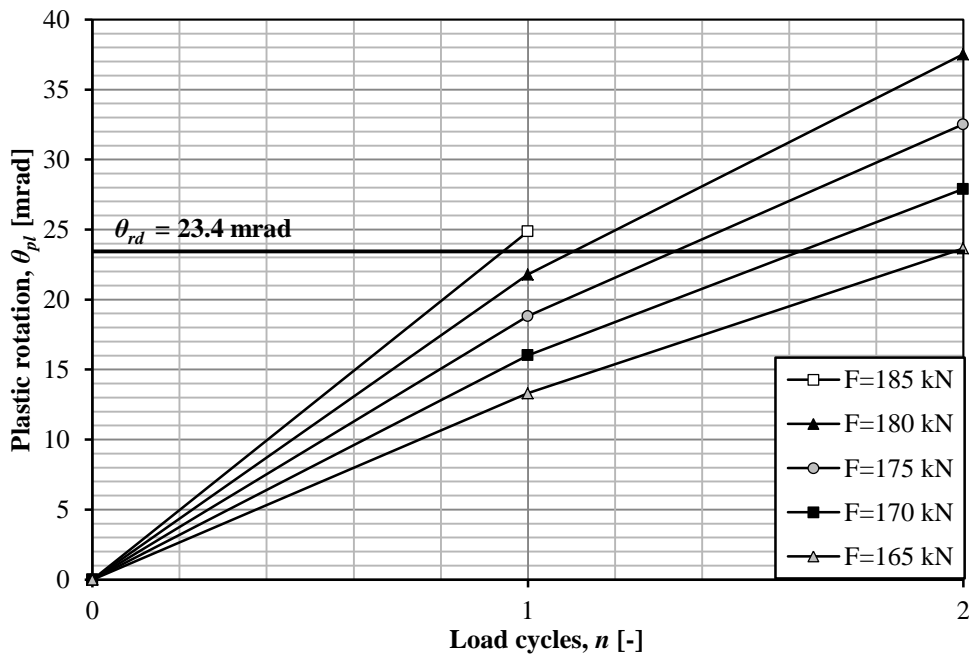
Figure 6.18   Plastic rotation for different magnitudes of moving concentrated forces.

It is clear that the magnitude of the applied force F have a substantial influence on the number of load cycles the cantilever slab can sustain before the occurrence of failure due to plastic rotation. The number of load cycles to failure n_u for different magnitudes of the applied forces is shown in Figure 6.19.
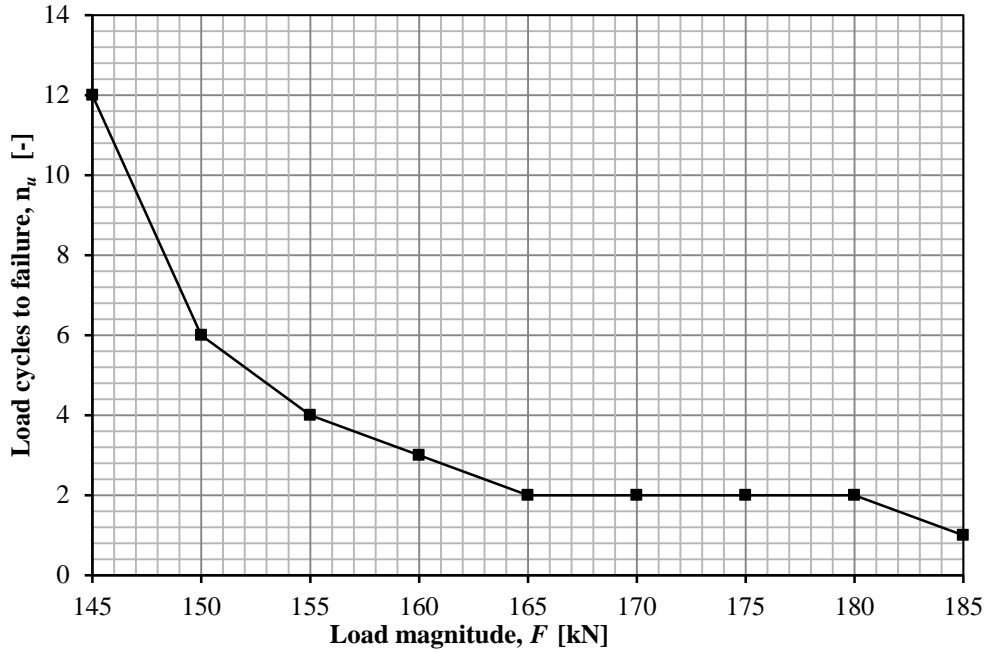
Figure 6.19 Number of load cycles to failure for different magnitudes of moving concentrated forces.

For a certain load level, plastic rotation was obtained during the early load cycles while an increased number of load cycles approached a stable value of the plastic rotation. The plastic rotation approached a stable state where the occurrence of failure was unlikely to occur within a number of load cycles that could be analysed in this Thesis. Due to this reason, a critical force F_{crit} was defined in this Thesis as the force F that causes failure of the cantilever slab at 150 load cycles:

$$\theta_{pl}(F_{crit}) = \theta_{rd} \tag{6-10}$$
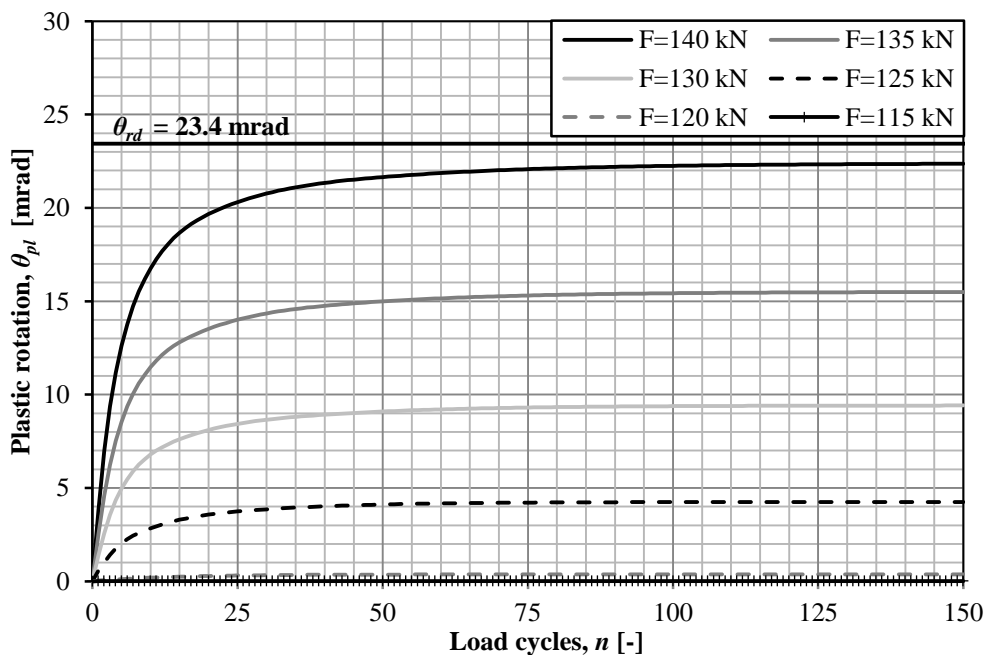
Figure 6.20 Plastic rotation for different magnitudes of moving concentrated forces.

CHALMERS, *Civil and Environmental Engineering*, Master's Thesis 2014:73

The critical force was in the case a single moving concentrated force somewhere between 140 kN and 145 kN. It can, from Figure 6.20 and the critical force, be concluded that forces that causes a relative high degree of plastic rotation can be acceptable for the studied structure. It is relatively safe to assume that a force $F \leq 140$ kN does not reach failure due to the asymptotic behaviour.

The reason for the phenomenon shown in Figure 6.20 can be derived from how the cantilever slab behaves when the yield moment is marginally exceeded.
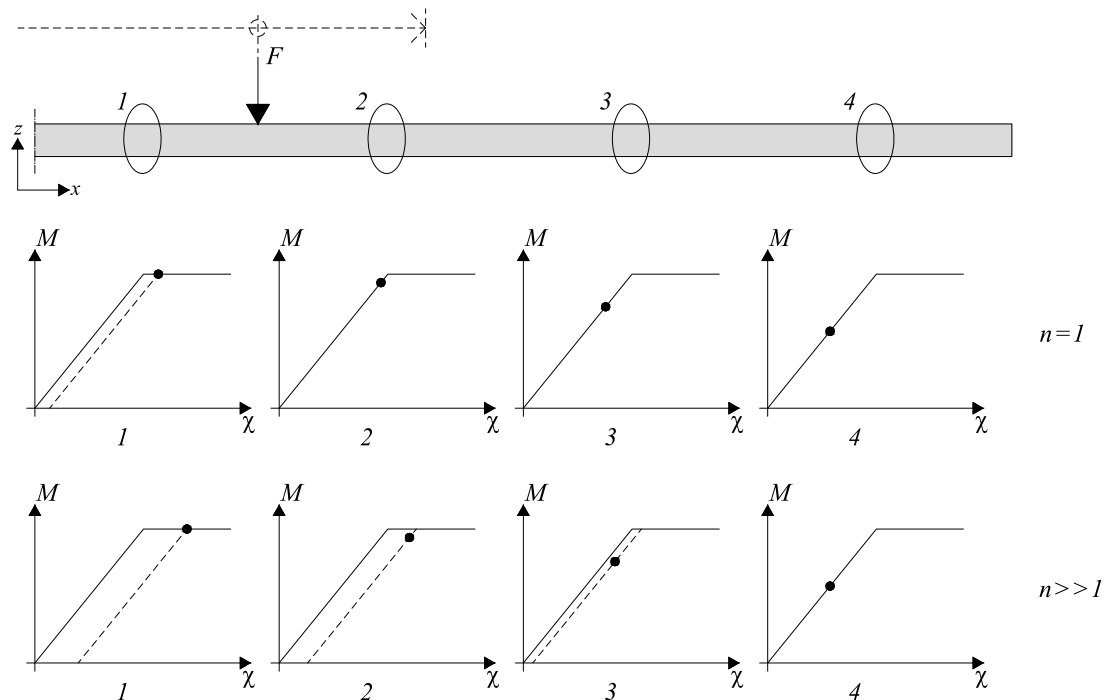
Figure 6.21   Development of the plastic rotation θ_{pl} over time in the cantilever slab after one and several load cycles.

During the first load cycle, the load requires plastic rotation in the slab in the most critical section, which in this analysis was located at the centre of the fixed support. As the first element started to yield, no additional load was taken in this element which led to a redistribution of forces to the elements in the immediate vicinity. As the number of load cycles increased, an increased number of elements reached yielding. The redistribution of forces from the elements in the plastic state led to a point where the slab approximately behaved linear elastically due to the fact that the number of active elements approached a stable state. It should here, however, be noted that the slab was not linear elastic but merely exhibited such behaviour. This hypothesis is illustrated in Figure 6.21 where half of the studied cantilever slab is illustrated with corresponding moment-curvature relations. The dots on the moment-curvature relations illustrates where in this relation each section of the structure was located. This illustrates how the plastic rotation developed in the cantilever structure and the reason for the linear elastic behaviour that was obtained after a large number of load cycles.

The hypothesis illustrated in Figure 6.21 was studied for a moving concentrated force with a magnitude of 135 kN for an increasing number of load cycles. As can be seen in Figure 6.20, the development of plastic rotation in the centre of the cantilever slab for a moving concentrated force of 135 kN was decreased with an increased number of load cycles. The plastic rotation along the fixed boundary is therefore shown in

Figure 6.22 where it is clearly visible that the cantilever slab approached a linear elastic behaviour as the number of load cycles increased.

It can be seen that the plastic rotation did not reach its maximum in the centre of the slab during the first four load cycles. The reason for this behaviour was believed to be derived from the fact that the slab was completely undamaged before the first load cycle. The plastic rotation development of the slab in Figure 6.22 is illustrated on the half of the slab where the moving force was removed, i.e. not the half that was subjected to the force first. This means that the moving force accumulated plastic rotation as it passed over the structure. When the structure accumulated enough damage (after five load cycles for this particular force magnitude), the maximum plastic rotation was located in the centre of the fixed support where it continued to grow.
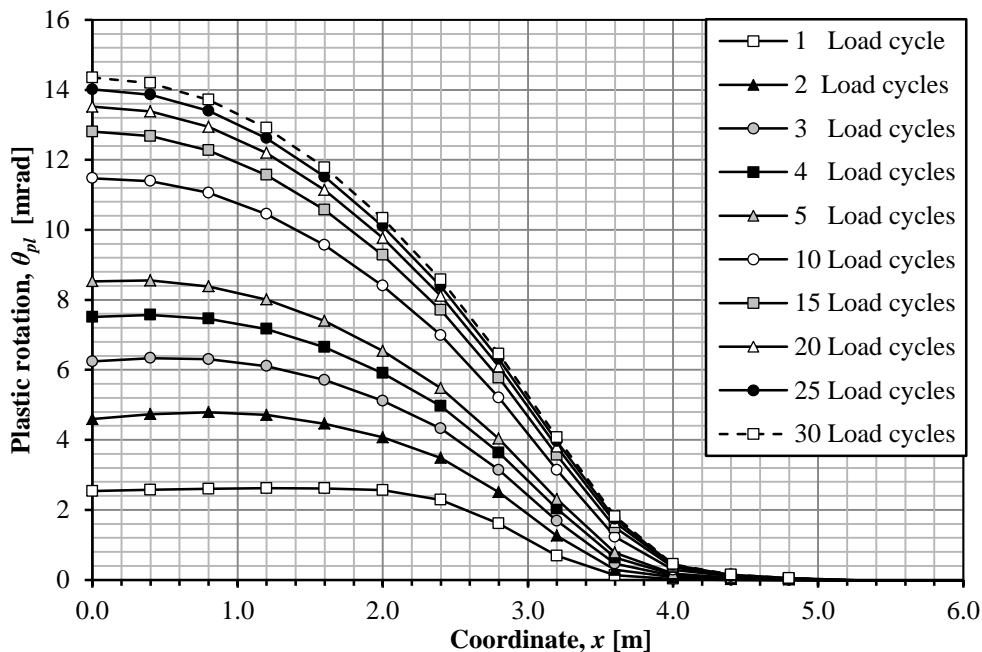
Figure 6.22   Development of plastic rotation θ_{pl} along the fixed support for a load magnitude of 135 kN.

The phenomenon described above would not occur if the load were applied over the total length of the cantilever slab. In such a case, the plastic rotation would increase near the free edges since there would be insufficient elements in order to redistribute forces efficiently. This is also what caused the numerical problems that were mentioned in the beginning of this section. These results are however valid for a long cantilever structure without secondary free edges which are the most common cantilever structure in the bridge design community.

6.3.2 Load magnitudes – Varying

The analyses for the constant load magnitudes for a single moving concentrated force illustrated how the plastic rotation develops in the cantilever structure. The load combination where a bridge structure was subjected to a constant force above the serviceability limit state must be considered as an extreme case. If a bridge structure is subjected to such loads, they are likely to be of different magnitudes and applied for varying number of load cycles. In order to study how the cantilever structure behaves

under such circumstances, it was subjected to two different load combinations, LC_A and LC_B.

The first load combination, LC_A, was defined as a combination of one force of such magnitude that it caused significant plastic rotation combined with a force of inferior magnitude. The larger of the two forces was applied once and the inferior force was applied several times. The forces were applied in such order that the larger force was applied before or after the inferior forces, not in between.

In order to reflect these two load application orders, the load combination was divided into two subcategories, LC_{A1}, and LC_{A2}. Load combination LC_{A1} was defined according to Equation (6-11) and is illustrated in Figure 6.23.

$$F_{1,n=1} > F_{2,n=5} \tag{6-11}$$
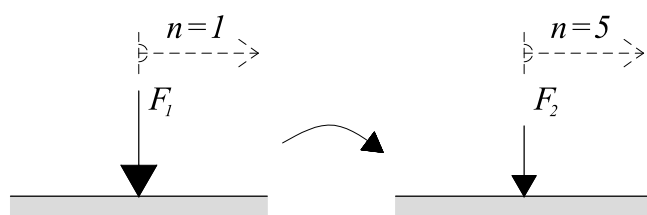
Figure 6.23   Load combination A₁, LC_{A1}

Load combination LC_{A2} was defined according to Equation (6-12) and is illustrated in Figure 6.24.

$$F_{1,n=5} < F_{2,n=1} \tag{6-12}$$
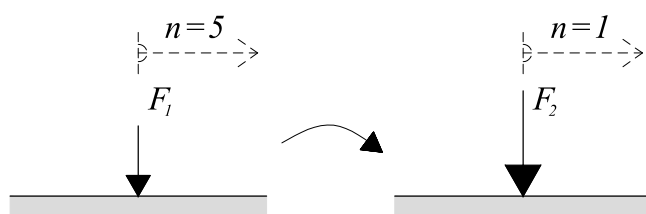
Figure 6.24   Load combination A₂, LC_{A2}

The magnitude of the larger force was set to 165 kN since it caused failure after two load cycles. The magnitude of the inferior force was set to a range of 120 kN to 145 kN. 120 kN was the lower limit since it was the force of the smallest magnitude to cause plastic rotation and 145 kN was the force of the smallest magnitude to cause failure within 150 load cycles. A force magnitude of 145 kN was also the smallest force to cause failure after five load cycles in combination with the larger force. This force magnitude was therefore of interest since that timeframe was evaluated.

As can be seen in Figure 6.25, the development of plastic rotation depends on the load history.
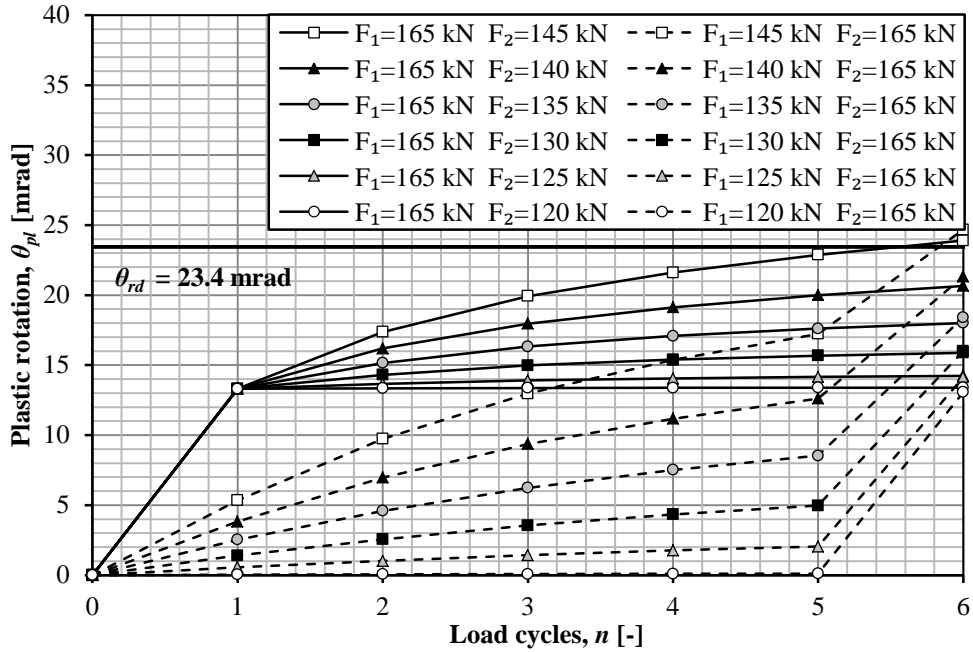
Figure 6.25 Plastic rotation for varying magnitudes of moving concentrated forces for six load cycles.

It is clear from Figure 6.25 that there is a small, but noticeable, difference in plastic rotation after six load cycles between the two different load combinations. The plastic rotation was measured after six load cycles and the difference between the two load combinations was calculated using Equation (6-13). The difference is shown in Figure 6.26.
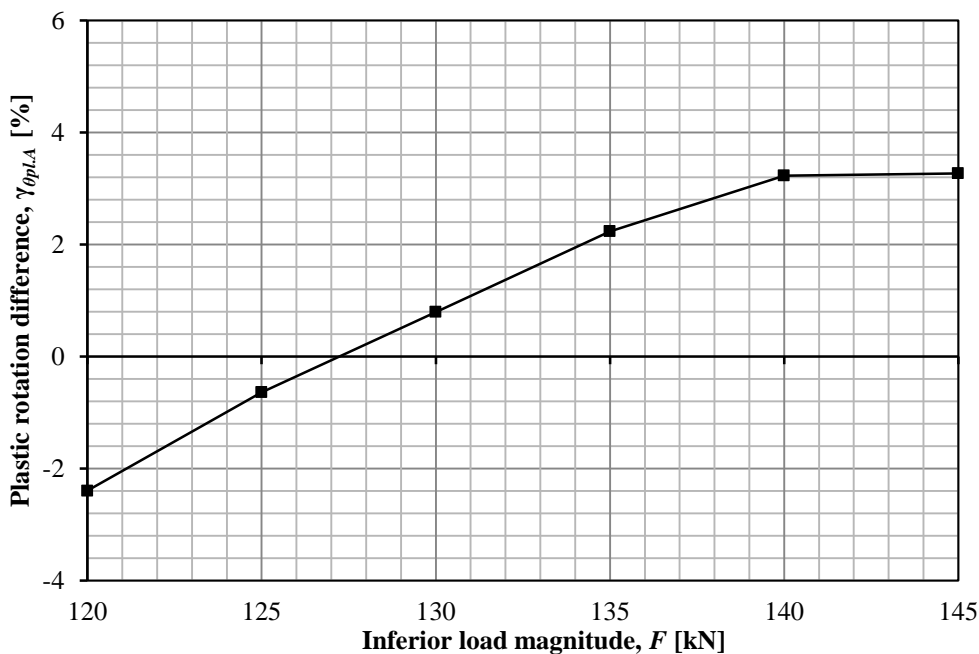
Figure 6.26 Difference in plastic rotation $\gamma_{\theta pl.A}$ between load combination A_1 and A_2, shown in percent for different magnitudes of the inferior forces.

$$\gamma_{\theta pl.A} = \frac{\theta_{pl.A2} - \theta_{pl.A1}}{\theta_{pl.A1}} \tag{6-13}$$

The values used in Equation (6-13) are tabulated in Appendix H for the interested reader.

The second load combination, LC_B consisted of two constant loads of two different magnitudes, but applied in three steps. In this analysis the load F_1 was applied two times, first with three load cycles and then with two load cycles. In between these load applications, a load of greater magnitude F_2 was applied once.

$$F_1 = F_{1,n=3} = F_{2,n=2} \tag{6-14}$$

$$F_2 = F_{2,n=1} > F_1 \tag{6-15}$$
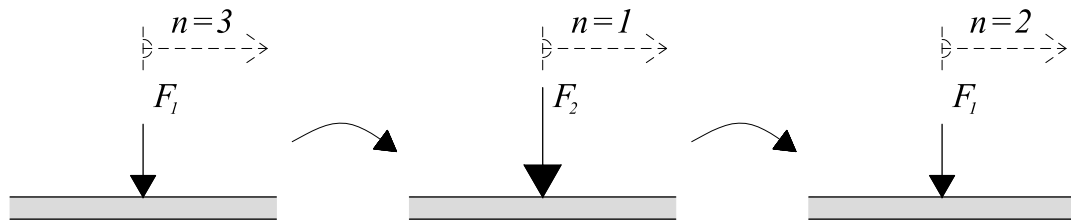
Figure 6.27   Load combination B, LC_B

The magnitudes of the larger and the smaller forces were the same as in the case of the first load combination, LC_A and were based on the same background. It can be seen in Figure 6.28 that the behaviour of the slab approached the behaviour for the case of a single moving concentrated force of 165 kN, which is reasonable.
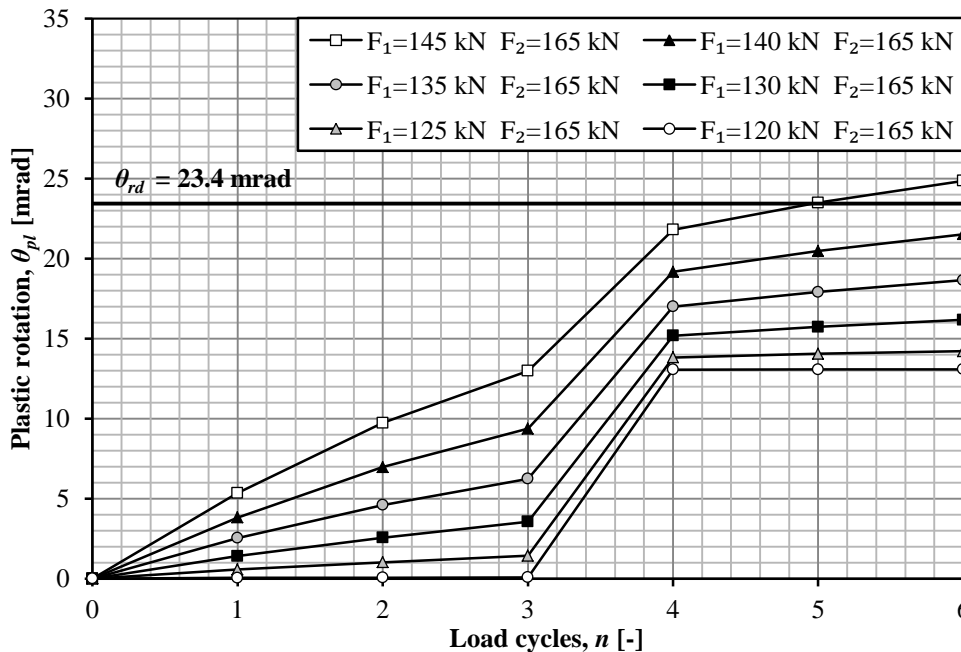
Figure 6.28   Plastic rotation for varying magnitudes of moving concentrated forces.

This load combination was believed to reflect a likely load combination principle on a real bridge structure. This is due to the fact that the highest applied force on the

structure is not as likely to occur as a force of lower magnitude. Therefore it is also reasonable to assume that the highest applied force is not likely to occur as the first or last load to exceed the serviceability limit state, as assumed in load combination A. The most likely load combination would be a range of smaller forces in combination with one or a few forces of high magnitudes. However, such a load combination was not investigated since it was beyond the timeframe of this Thesis.

6.3.3 Comparison

In order to determine which of the studied load combinations in Section 6.3.2 is the most critical in terms of plastic rotation, these load combinations is compared in Figure 6.29.
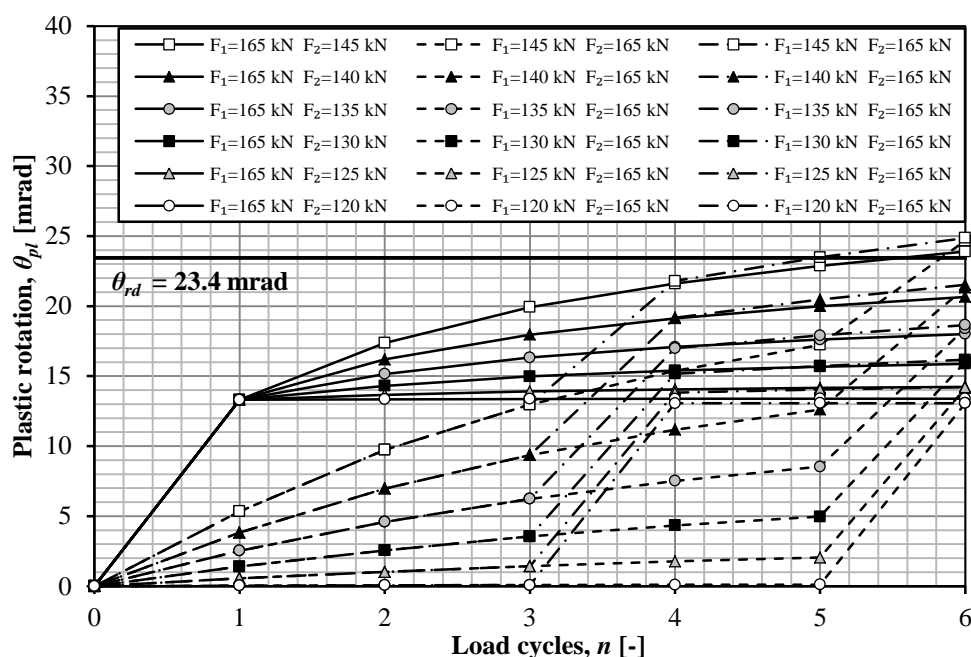
Figure 6.29 Plastic rotation for varying magnitudes of moving concentrated forces for six load cycles.

It is clear from Figure 6.29 that there is a small, but noticeable, difference in plastic rotation after six load cycles between the three different load combinations. The plastic rotation was measured for load combination LC_{A1}, LC_{A2} and LC_B after six load cycles and the difference between the load combinations was calculated using Equation (6-16) and (6-17) for LC_{A2} and LC_B, respectively. The difference is shown in Figure 6.30.

$$\gamma_{\theta pl.A} = \frac{\theta_{pl.A2} - \theta_{pl.A1}}{\theta_{pl.A1}} \tag{6-16}$$

$$\gamma_{\theta pl.B} = \frac{\theta_{pl.B} - \theta_{pl.A1}}{\theta_{pl.A1}} \tag{6-17}$$

The values used in Equation (6-16) and (6-17) are tabulated in Appendix H for the interested reader.
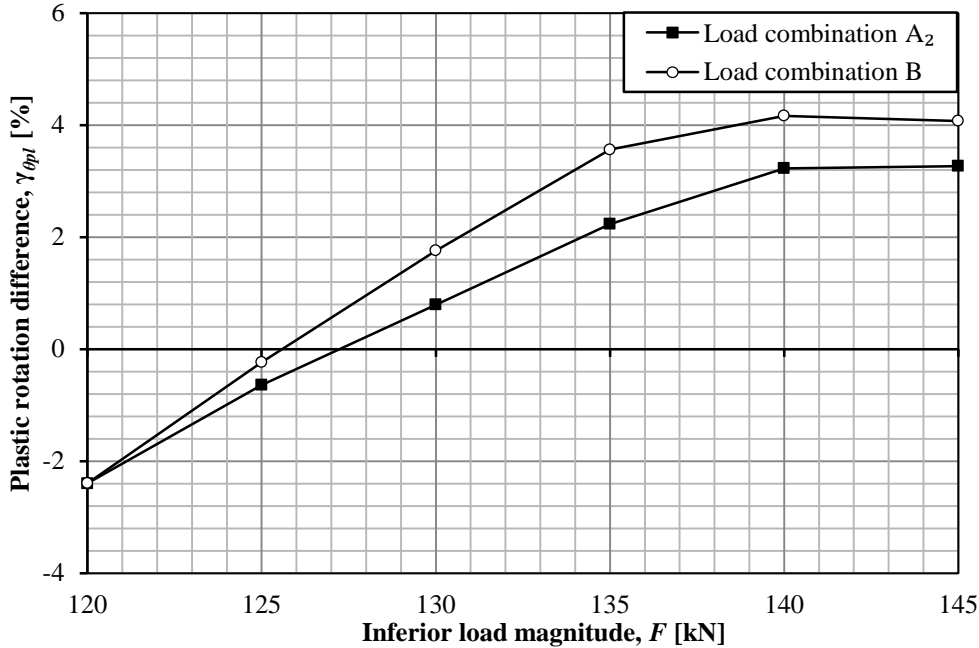
Figure 6.30 Difference in plastic rotation $\gamma_{\theta pl}$ between load combination A_1 and load combination A_2 and B, shown in percent for different magnitudes of the inferior forces.

It can be seen in Figure 6.30 that load combination LC_B results in the highest plastic rotation of the slab after six load cycles for inferior forces of a magnitude greater than 125 kN. For inferior forces of a magnitude below this value, load combination LC_{A1} results in the highest plastic rotation of the slab after six load cycles. These results indicate that the most likely load combination of the structure, LC_B, for the majority of the investigated forces is also the one to cause the highest plastic rotation.

The result also indicates that a force of great magnitude causes more damage if it is applied after a number of forces above the serviceability limit state. It also indicates that the force of greater magnitude causes even more damage if it is applied after fewer forces above the serviceability limit state than stated above. This means that the greater force causes more damage if it is applied after a permanent damage has been initiated, but the influence of the force diminishes as the permanent damage of the slab increases.

It should however be noted that the difference between the two load combinations is small and the results should therefore be treated with care.

6.3.4 Traditional Superposition approach

It has been shown in the previous sections that the development of plastic rotation is dependent on the load history, which indicates that a superposition method is not recommended. The error of a traditional superposition approach is here evaluated for the two load combinations LC_A and LC_B examined in Section 6.3.2

The results from the superposition approach were obtained by merging results from Section 6.3.1 where all the loads were applied on an unloaded cantilever slab. Two or more loads series were merged and thus the behaviour of each load series was captured. The theory of the superposition approach is illustrated in Figure 6.31.
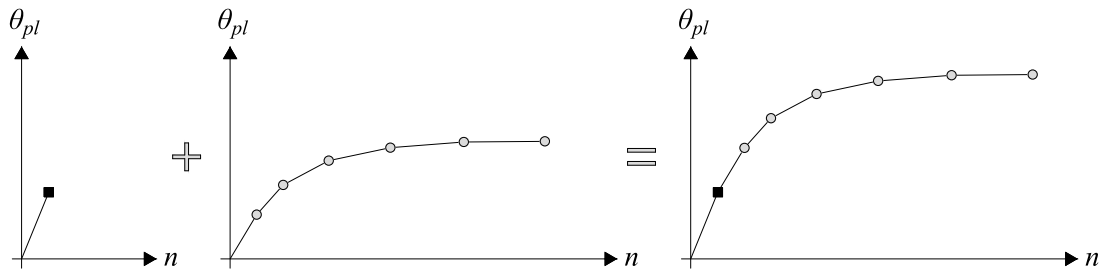
Figure 6.31   The superposition approach used in this Thesis.

The whole load model was applied according to the superposition approach and not each load cycle. Such a superposition approach would not have accounted for the decreasing effect that the applied forces have on the plastic rotation as the number of load cycles increases and thus resulted in a linear development of the plastic rotation. Such an approach is illustrated in Figure 6.32.
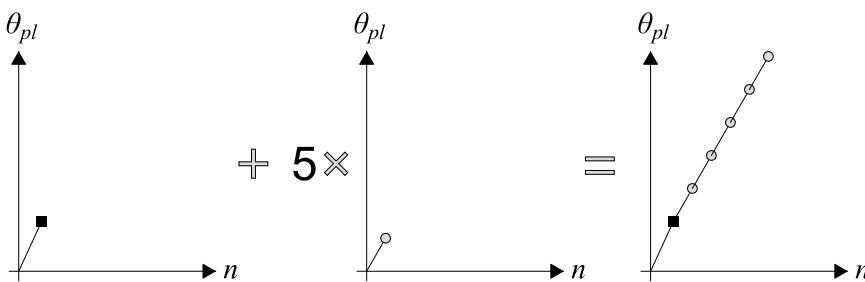
Figure 6.32   A superposition approach omitted in this Thesis.

The development of plastic rotation for LC_{A1}, which is shown in Figure 6.23 is extended to 20 load cycles and is shown in Figure 6.33. The results for the different load magnitudes from Section 6.3.1 were used in order to obtain a plastic rotation development based on a superposition method. This is shown in Figure 6.34.
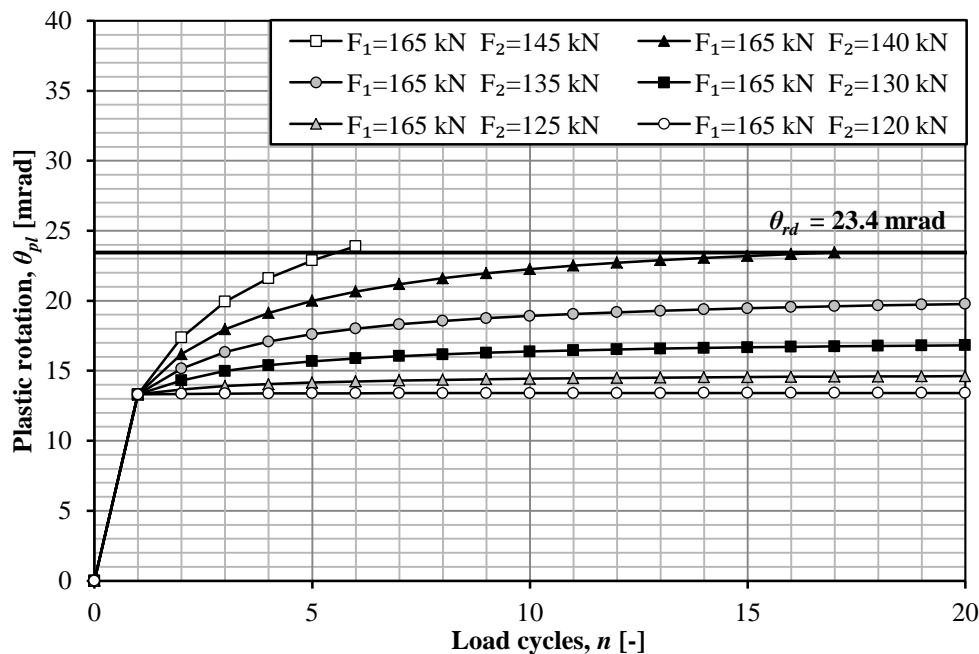
Figure 6.33   Plastic rotation for varying magnitudes of moving concentrated forces.
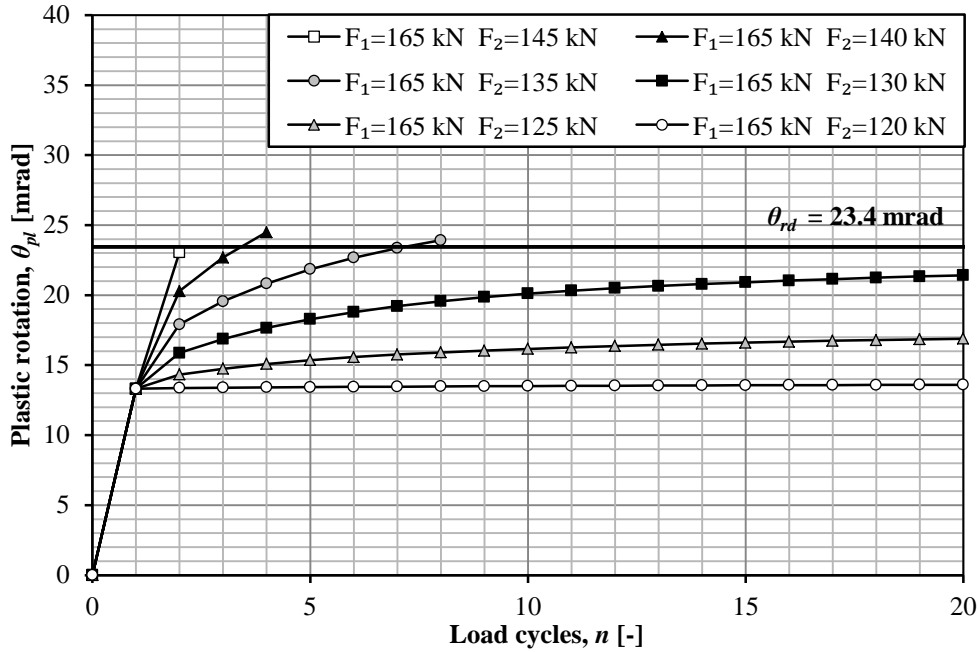
Figure 6.34 Plastic rotation for varying magnitudes of moving concentrated forces, based on the superposition approach.

It is clear from Figure 6.33 and Figure 6.34 that there is a significant difference between the results from the analyses and the results from a superposition approach. The plastic rotation was measured after six load cycles and the difference between the analyses and the superposition approach was calculated using Equation (6-18). The difference is shown in Figure 6.35.
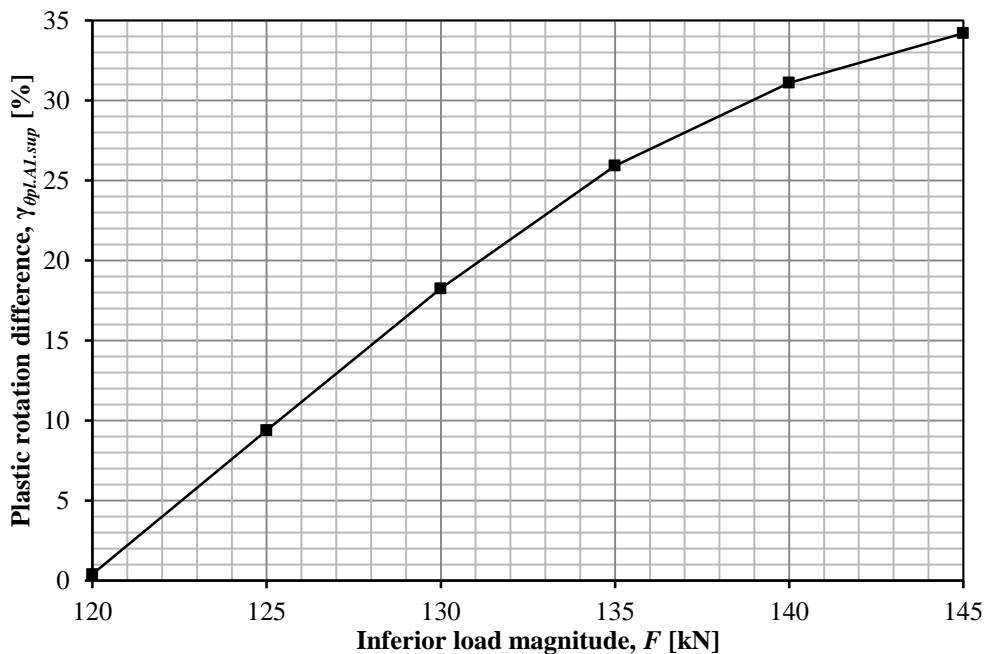
Figure 6.35 Difference in plastic rotation $\gamma_{A1.sup}$ for load combination A_1 between results from analyses and results from a superposition approach, shown in percent for different magnitudes of the inferior forces.

$$\gamma_{\theta pl.A1.\sup} = \frac{\theta_{pl.A1.\sup} - \theta_{pl.A1.ana}}{\theta_{pl.A1.ana}} \tag{6-18}$$

The values used in Equation (6-18) are tabulated in Appendix H.

The development of plastic rotation for LC_B, which was illustrated in Figure 6.28, is also shown in Figure 6.36 for comparison purposes. The plastic rotation development based on the superposition method is shown in Figure 6.37. The same superposition approach that was used for load combination LC_{A1} was also used in this case.
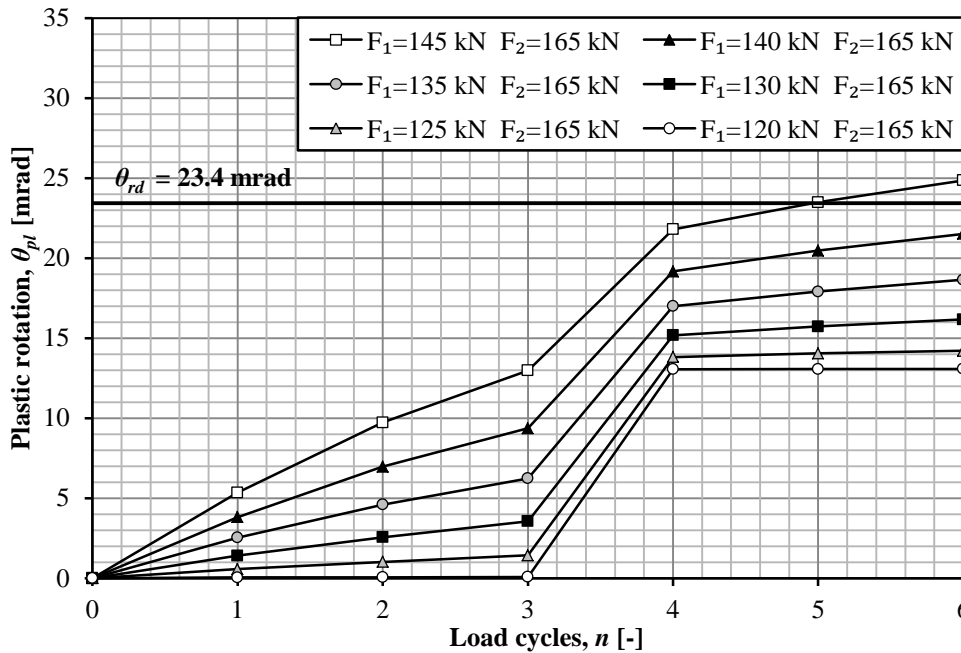
Figure 6.36   Plastic rotation for varying magnitudes of moving concentrated forces.
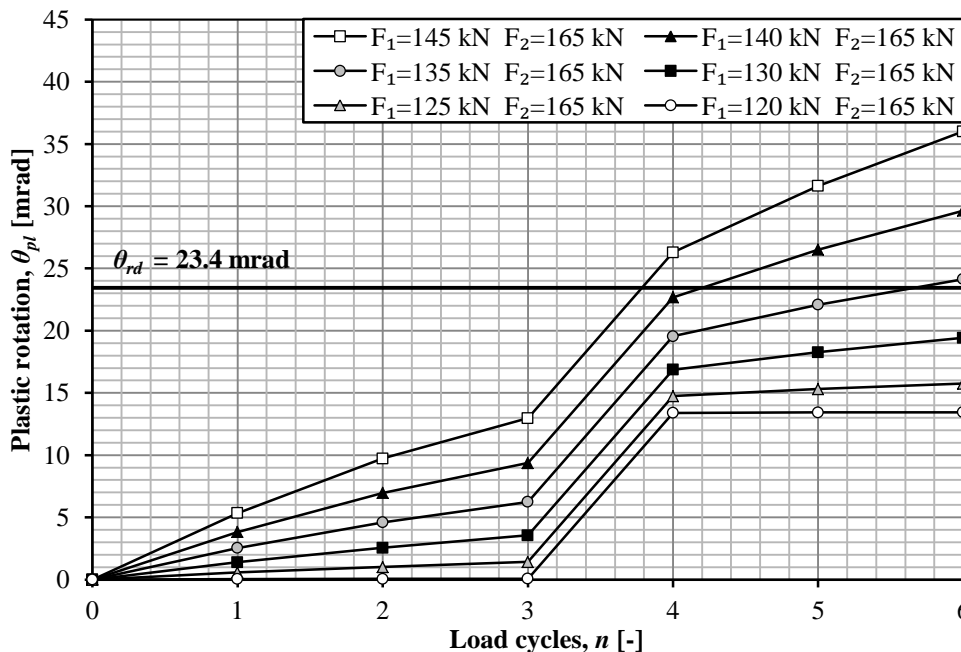
Figure 6.37   Plastic rotation for varying magnitudes of moving concentrated forces, based on a traditional superposition approach.

CHALMERS, *Civil and Environmental Engineering*, Master's Thesis 2014:73

It is also from this load combination clear that there is a significant difference between the result from the analyses and the results from a superposition approach. The plastic rotation was also here measured after six load cycles and the difference between the analyses and the superposition approach was calculated using Equation (6-19). The difference is shown in Figure 6.38.

$$\gamma_{\theta pl.B.\text{sup}} = \frac{\theta_{pl.B.\text{sup}} - \theta_{pl.B.ana}}{\theta_{pl.B.ana}}$$

(6-19)

The values used in Equation (6-19) are tabulated in Appendix H for the interested reader.
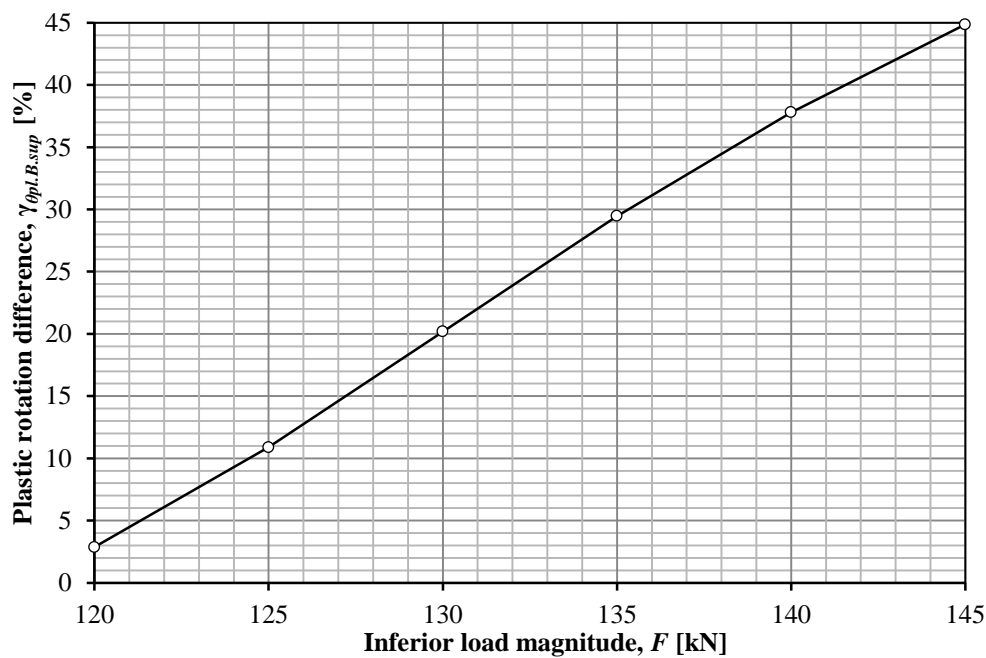
Figure 6.38 Difference in plastic rotation $\gamma_{\theta pl.B.sup}$ for load combination B between results from analyses and results from a superposition approach, shown in percent for different magnitudes of the inferior forces.

If Figure 6.35 and Figure 6.38 are combined, the difference in percentage between the analyses and the superposition approach for load combination LC_A and LC_B can be shown in Figure 6.39.
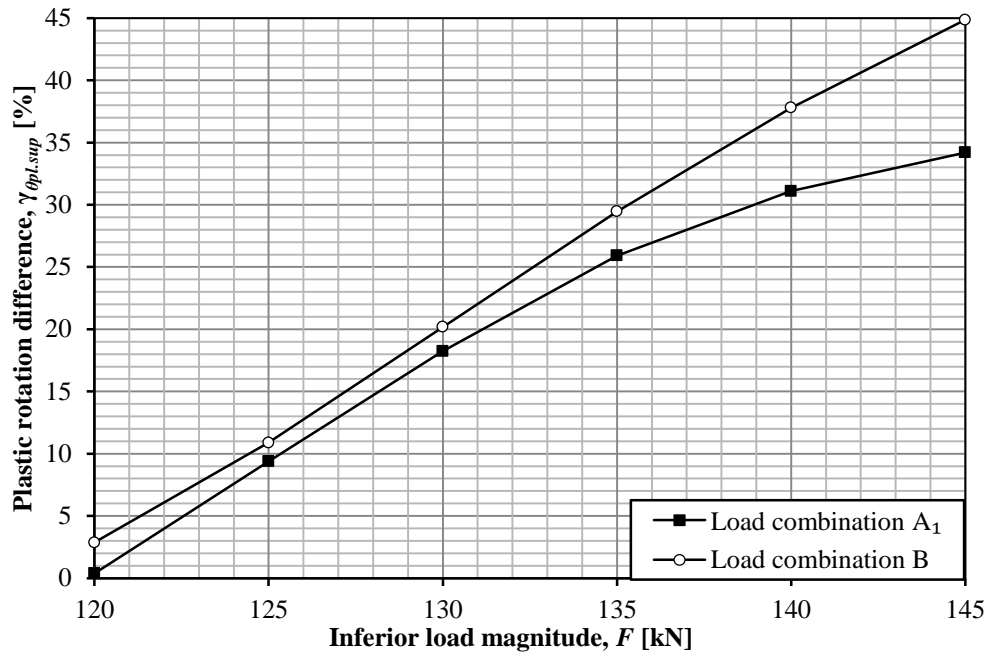
Figure 6.39 Difference in plastic rotation $\gamma_{\theta pl.sup}$ for load combination A_1 and B between results from an analysis and results from a superposition approach shown in percent for different magnitudes of the inferior forces.

It is clear that the superposition approach overestimates the plastic rotation in the structure for both load combination LC_A and LC_B. This behaviour was expected since the adaptation of the slab due to repeated loading is not fully captured by the traditional superposition approach. The difference in plastic rotation between the analyses and the superposition approach is greater for load combination LC_B than LC_A. The reason for this difference can be derived from the fact that the plastic rotation from each load is overestimated and load combination B consists of three separate loads instead of two separate loads which is the case for load combination A.

6.4 Response of two moving forces – Equal magnitudes

The slab in this analysis was modelled with the same geometry and moment-curvature relations as the slab in Section 6.3.
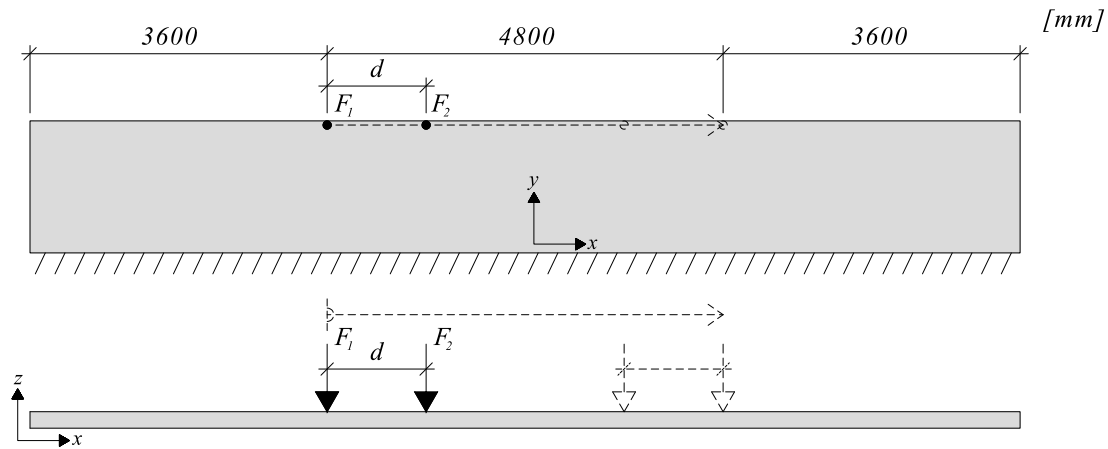
Figure 6.40 Geometry and dimensions of the studied cantilever slab for two concentrated forces of equal magnitudes.

The modelling choices and moment-curvature relation from the analysis of a single moving concentrated force was also used in this analysis. The reason for this approach was to enable a comparison between the effects of subjecting a cantilever slab to one or two concentrated forces. In addition, this approach also enables a comparison of the effects of the distance d between a pair of concentrated forces and the influence of varying load levels within a pair of concentrated forces.

The sum of the loads applied on the slab in this analysis differed between the distances between the pair of concentrated forces. An increased distance resulted in a decreased plastic rotation and additional force was therefore applied to study the behaviour of the structure. The distance between the forces was altered according to Equation (6-20) and the influence of this parameter is treated in separate sections.

$$d = \begin{bmatrix} 1.2 & 1.6 & 2.0 \end{bmatrix} \text{m}$$ (6-20)

6.4.1 Constant distance, $d = 1.2$ m

In the case of a constant distance of $d = 1.2$ m, the applied forces F_1 and F_2 varied according to the following magnitudes:

$$F_1 = F_2 = \begin{bmatrix} 65 & 70 & 75 \dots 100 & 105 & 110 \end{bmatrix} \text{kN}$$ (6-21)

The forces F_1 and F_2 that were applied on the slab ranged from 65 kN to 110 kN based on the same background as stated in Section 6.3.1. The total applied load F_{tot} of the forces F_1 and F_2 is defined in Equation (6-22):

$$F_{tot} = F_1 + F_2$$ (6-22)

As in the case of a single moving concentrated force, the analyses were conducted with 150 load cycles n for each pair of concentrated forces if failure of the cantilever

slab did not occur within this range. The plastic rotation in the centre of the slab for different magnitudes of forces is shown in Figure 6.41.
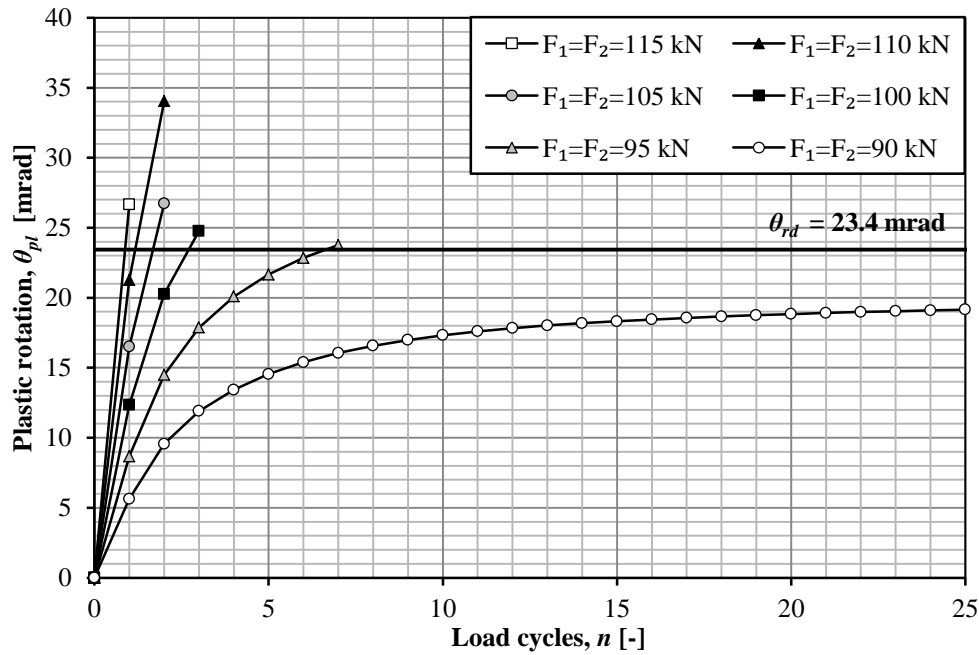
Figure 6.41 Plastic rotation for different magnitudes of a pair of moving concentrated forces.

As in the case of a single moving concentrated force, the magnitude of the total force F_{tot} have a big influence on the number of load cycles the cantilever slab can sustain before the occurrence of failure due to plastic rotation. The number of load cycles to failure n_u for different magnitudes of the applied forces is shown in Figure 6.42.
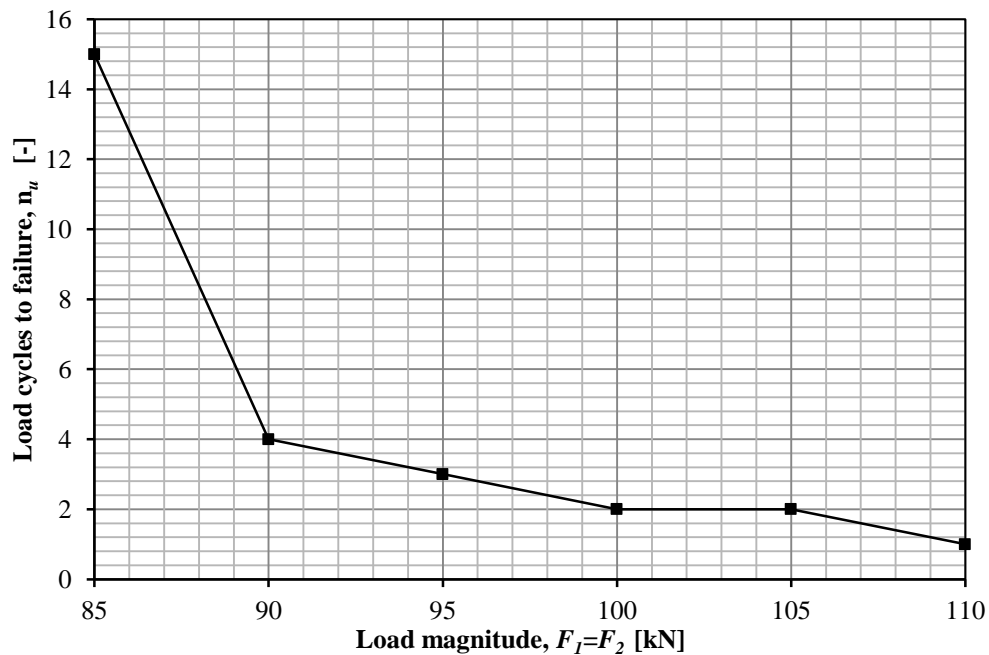
Figure 6.42 Number of loading cycles to failure for different magnitudes of a pair of moving concentrated forces for d = 1.2 m.

As in the case of a single moving concentrated force, the plastic rotation approached a stable value where the occurrence of failure was unlikely to occur within the number of load cycles studied in this Thesis. This was the case when the total force was below the critical force F_{crit} which in this case was somewhere between 80 kN and 85 kN. The reason for this phenomenon is described in Section 6.3.1.
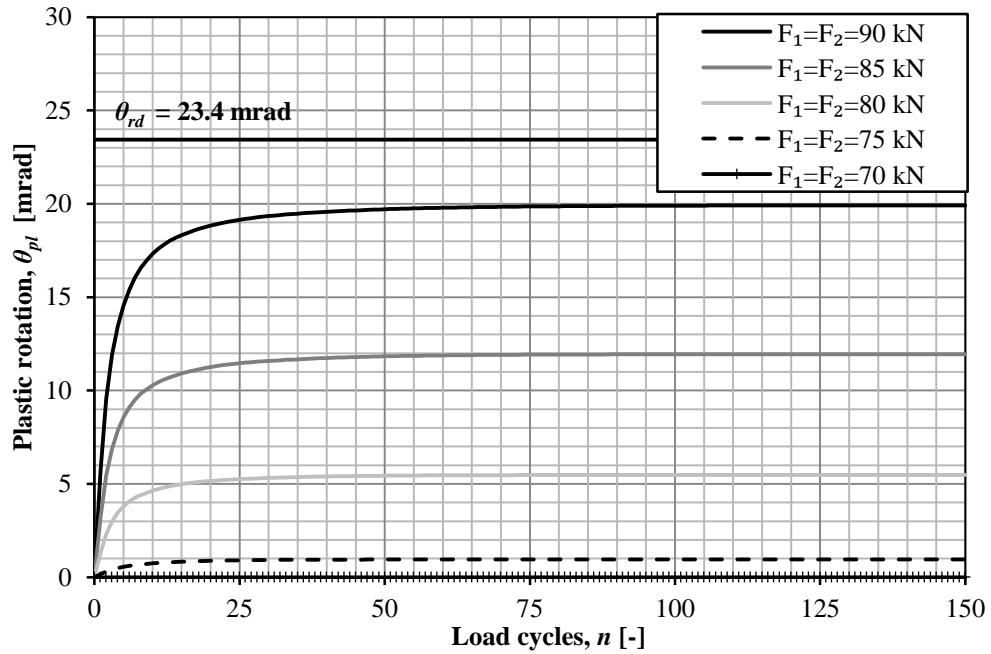
Figure 6.43   Plastic rotation for different magnitudes of a pair of moving concentrated forces.

6.4.2 Constant distance, $d = 1.6$ m

In the case of a constant distance of $d = 1.6$ m, the applied forces F_1 and F_2 varied between the following magnitudes:

$$F_1 = F_2 = \begin{bmatrix} 70 \ 75 \ 80 \dots 105 \ 110 \ 115 \end{bmatrix} \text{kN} \qquad (6\text{-}23)$$

The plastic rotation in the centre of the slab for different magnitudes of forces is shown in Figure 6.44.
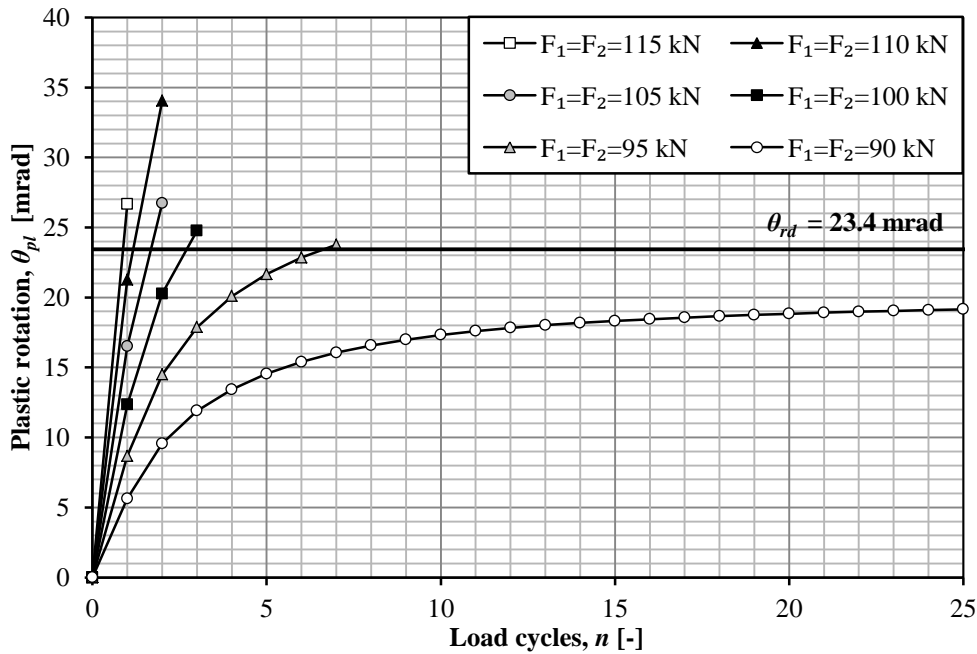
Figure 6.44 Plastic rotation for different magnitudes of a pair of moving concentrated forces.
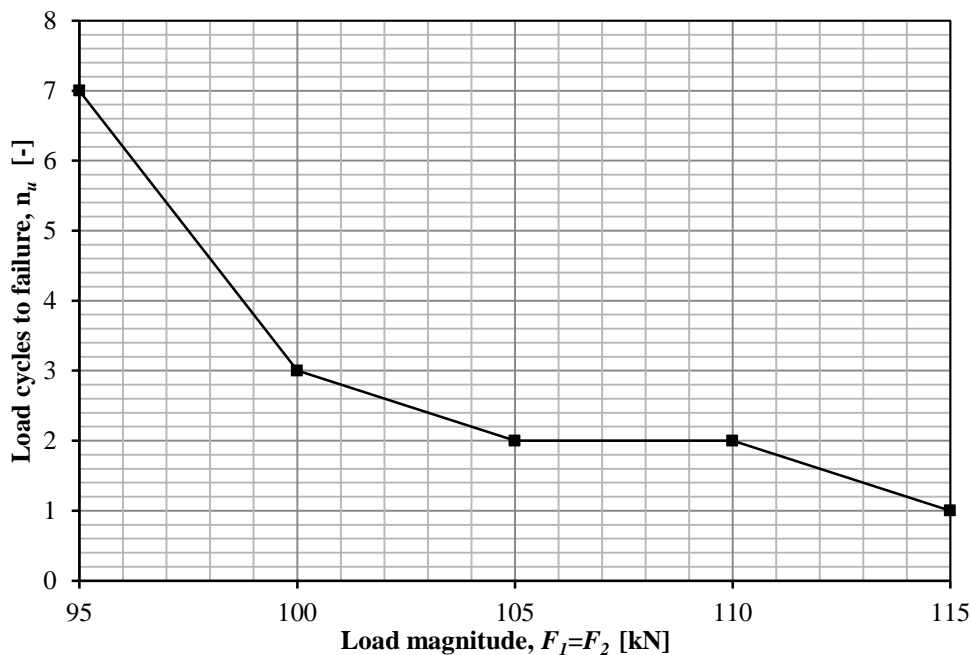
Figure 6.45 Number of load cycles to failure for different magnitudes of a pair of moving concentrated forces with for d = 1.6 m.

The critical force F_{crit} was in this case somewhere between 90 kN and 95 kN.
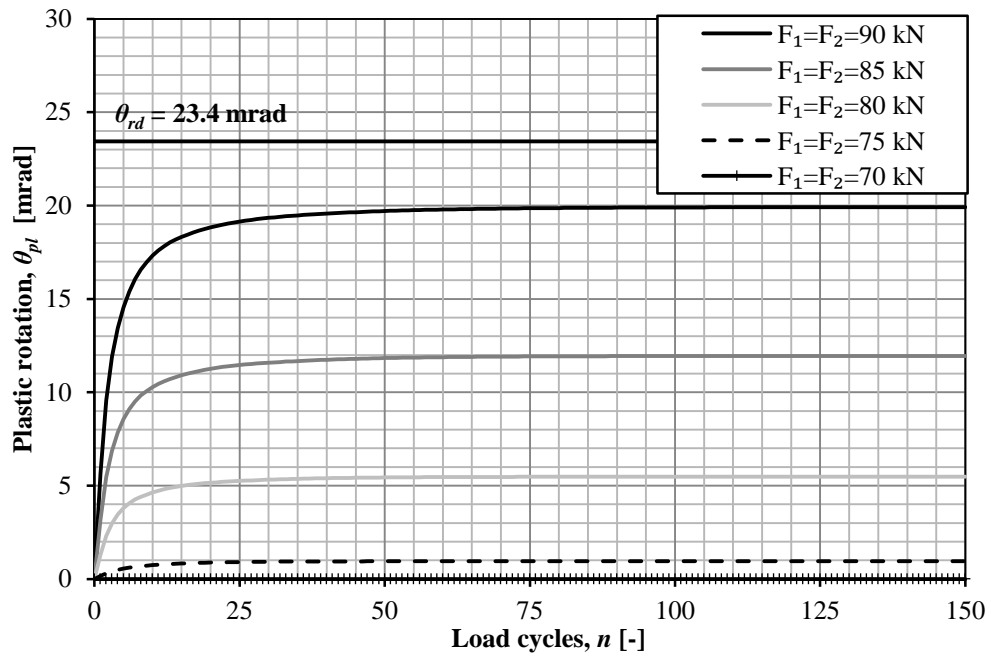
Figure 6.46 Plastic rotation for different magnitudes of a pair of moving concentrated forces.

6.4.3 Constant distance, $d = 2.0$ m

In the case of a constant distance of $d = 2.0$ m, the applied forces F_1 and F_2 varied between the following magnitudes:

$$F_1 = F_2 = [80\ 85\ 90\ ...\ 110\ 115\ 120]\ \text{kN} \tag{6-24}$$

The plastic rotation in the centre of the slab for different magnitudes of forces is shown in Figure 6.47.
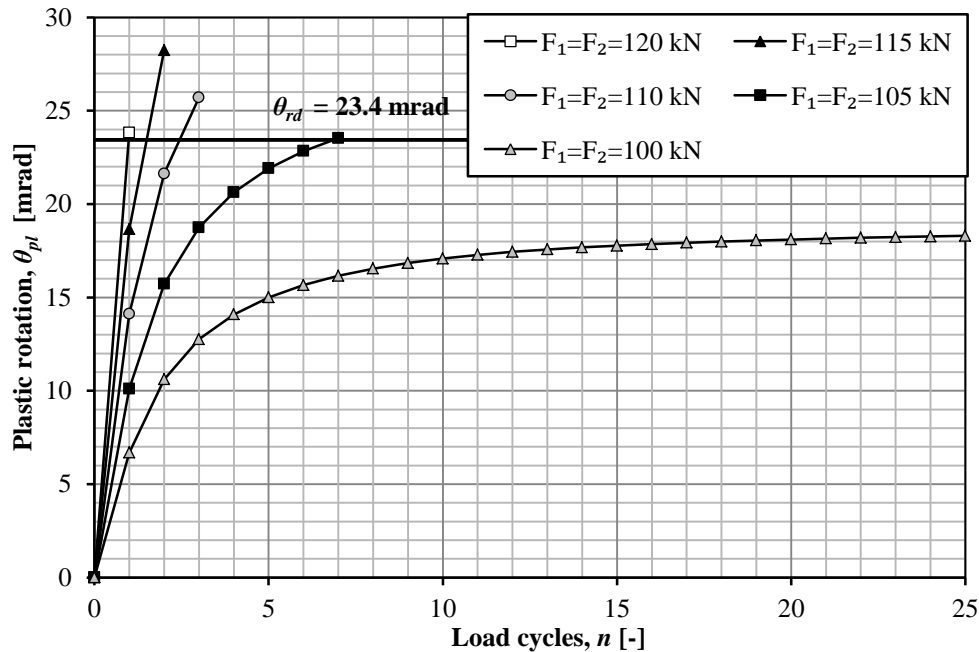
Figure 6.47   Plastic rotation for different magnitudes of a pair of moving concentrated forces.
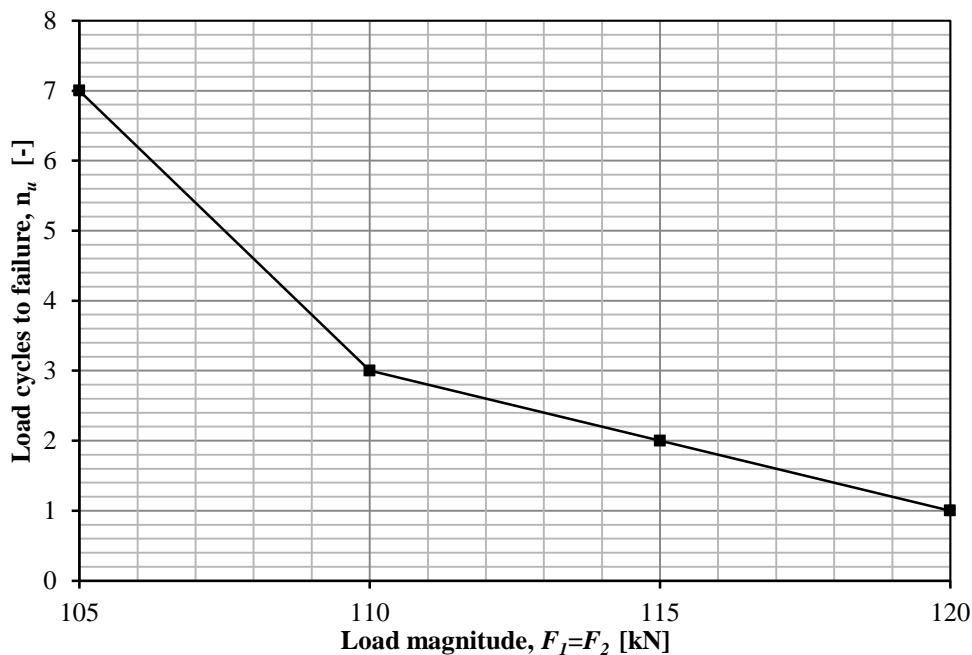
Figure 6.48   Number of load cycles to failure for different magnitudes of a pair of moving concentrated forces with for d = 2.0 m.

The critical force F_{crit} was in this case somewhere between 100 kN and 105 kN.
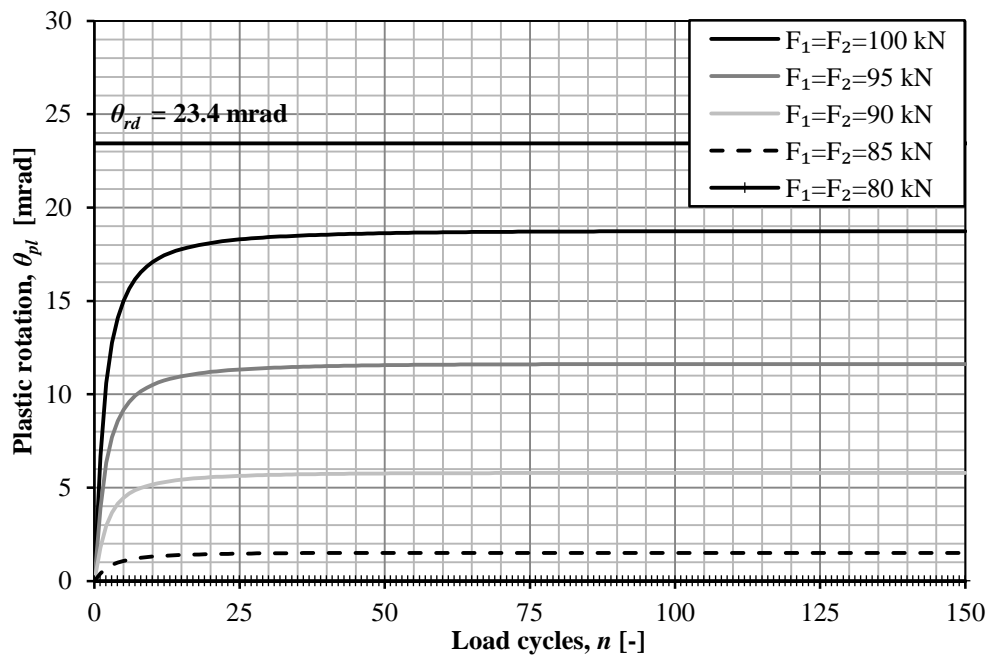
Figure 6.49 Plastic rotation for different magnitudes of a pair of moving concentrated forces.

6.4.4 Comparison

In order to compare the plastic rotation caused by the different loads and load magnitudes, the number of load cycles to cause failure n_u was compared with the total load magnitude F_{tot} from Equation (6-22) for the different loads applied on the cantilever slab. This behaviour is shown in Figure 6.50.
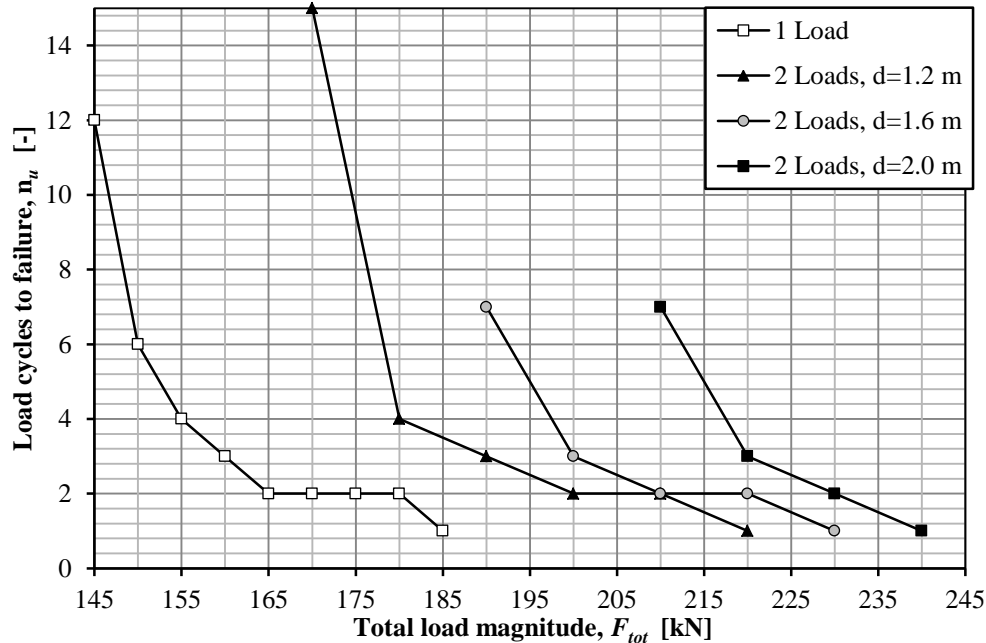
Figure 6.50 Number of load cycles to failure for different loads and load magnitudes.

It is clearly shown in Figure 6.50 that it is advantageous for the cantilever slab, from the perspective of plastic rotation, with an increased distance between a pair of moving concentrated forces. It is also clearly shown that the case of two concentrated forces is advantageous in comparison to the case of one moving concentrated force with the same load magnitude. As the concentrated force was separated into two forces and the distance between those two increased, the total load magnitude and number of load cycles to failure increased. This behaviour corresponds to what was expected.

In order to compare the number of load cycles to cause failure for the different loads and load magnitudes, a load magnitude factor $\gamma_{\theta plu.F}$ was defined. This factor is related to the largest single moving concentrated force not cause any plastic rotation to the slab F_{el}. The relative load magnitude factor was defined as:

$$\gamma_{\theta plu.F} = \frac{F_{tot}(n_u)}{F_{el}} \qquad (6-25)$$

Where F_{tot} = the total applied force

F_{el} = the force of the greatest magnitude not to cause any plastic rotation for a single moving concentrated force, in this case 115 kN

n_u = the number of load cycles to failure for each applied force

It is possible, from this relation, to predict the vulnerability of the slab, i.e. how much a moving concentrated force can be increased in magnitude before failure due to plastic rotation occurs. This relation is shown in Figure 6.51 with the same configuration as observed in Figure 6.50.
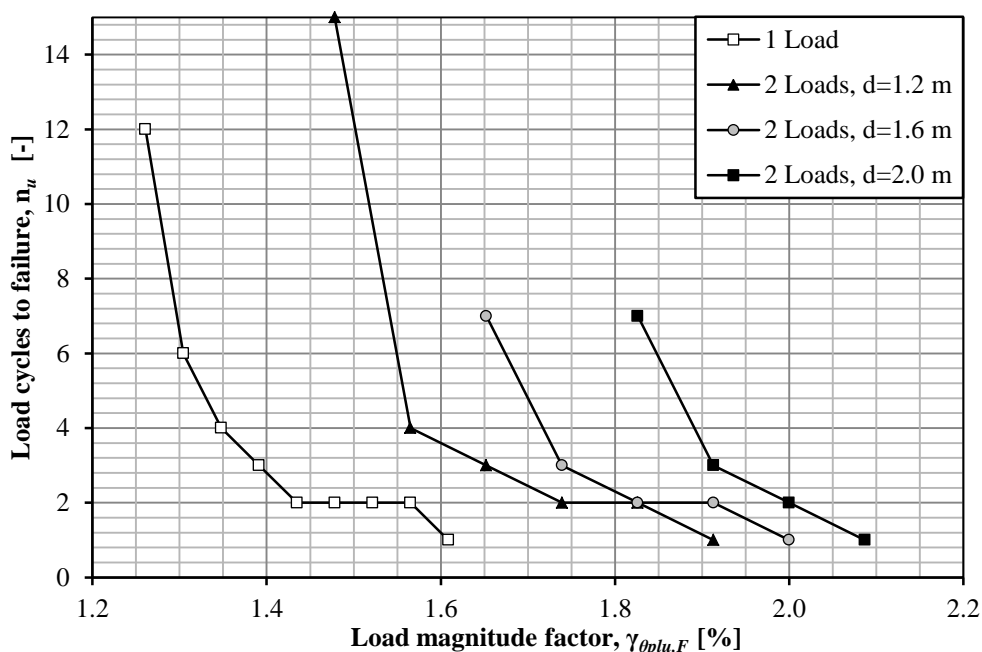
Figure 6.51 *Number of load cycles to failure for a load magnitude factor* $\gamma_{\theta plu.F}$ *related to the load* F_{el}.

It can be seen in Figure 6.51 that the moving concentrated force of the highest magnitude not to cause any plastic rotation in the structure, could be increased by 26 % before failure of the cantilever slab occurred within 150 load cycles. If the total force was separated into two concentrated forces with a distance of 1.2 m instead, the total load could be increased by 47 % before failure of the cantilever slab occurred within 150 load cycles. An increase of the distance between the two concentrated forces generates an increase in total load magnitude before failure occurs. From the behaviour observed in Figure 6.51, it is reasonable to assume that there is a distance *d* between the pair of moving forces such that the cantilever structure experiences the force pair as two independent forces. This behaviour was studied in the following section.

6.4.5 Influence of distance, *d*

It was clearly shown in the previous section that it is advantageous for the cantilever structure with an increased distance between the pair of moving concentrated forces. In order to evaluate how the distance influences the plastic rotation of the structure, the distance was increased with the same increments as in the previous sections, up to a distance *d* = 4.8 m:

$$d = \begin{bmatrix} 1.2 \ 1.6 \ 2.0 \ 2.4 \ 2.8 \ 3.2 \ 3.6 \ 4.0 \ 4.4 \ 4.8 \end{bmatrix} m \tag{6-26}$$

The same type of analyses as presented in the previous sections was conducted for all presented distances. All distances was analysed for force magnitudes not to cause any

plastic rotation to force magnitudes where failure occurred during the first load cycle. The results from these analyses are presented in Appendix F and are summarized in this section.

The number of load cycles to cause failure n_u was compared with the total load magnitude F_{tot} (defined in Section 6.4.1) which can be seen in Figure 6.52. A load magnitude factor $\gamma_{\theta plu.F}$ was used, as in Section 6.4.4, in order to evaluate the influence of d on the total force that can be applied on the slab. This can be seen in Figure 6.53.
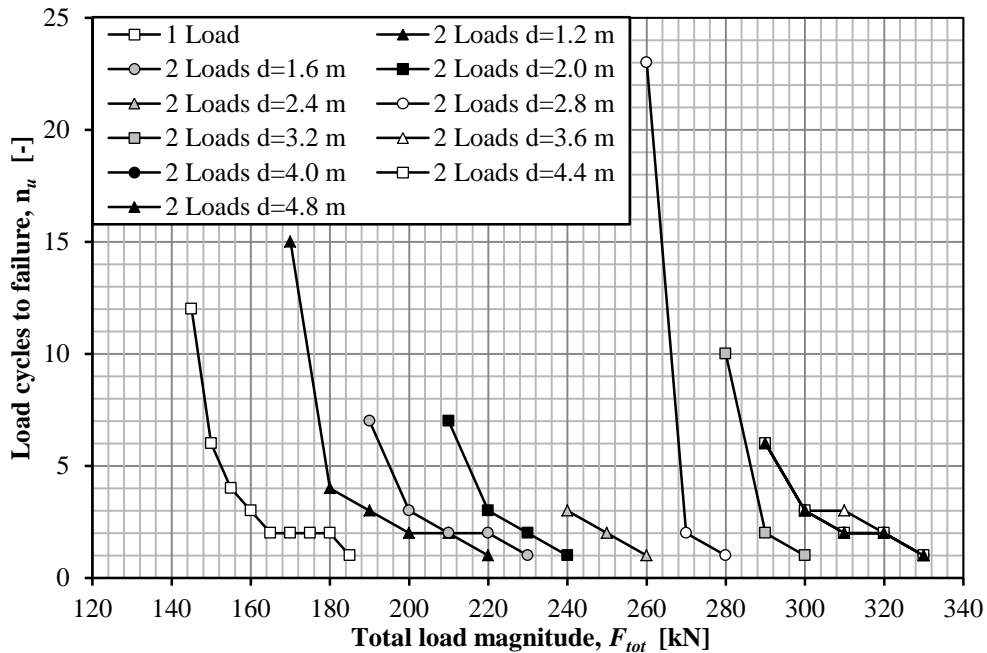
Figure 6.52 Number of load cycles to failure for different loads and load magnitudes.
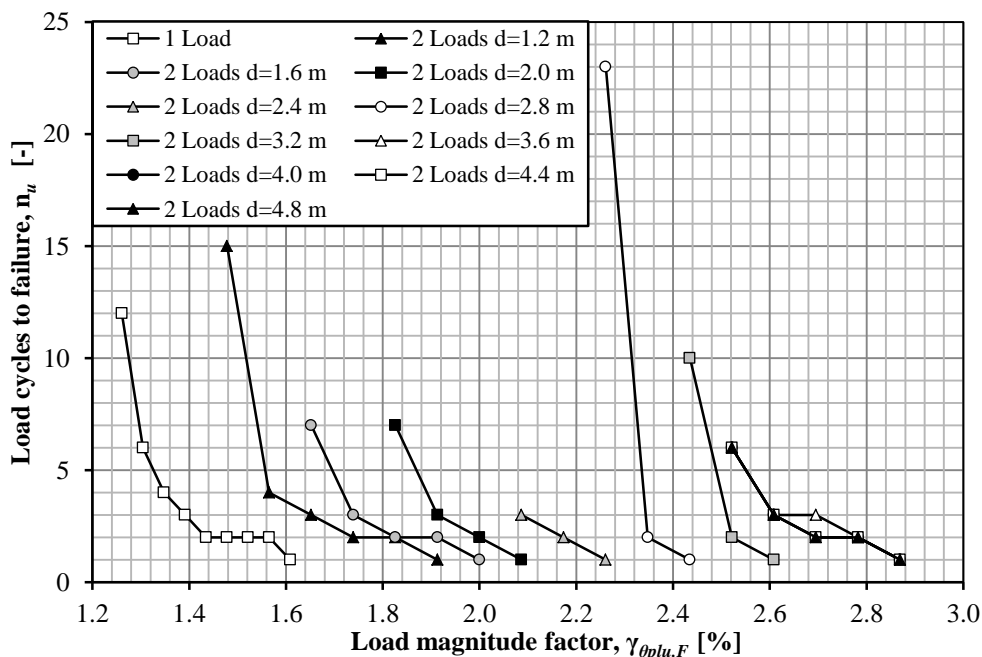
Figure 6.53 Number of load cycles to failure for a load magnitude factor $\gamma_{\theta plu.F}$ related to the load F_{el}.

CHALMERS, *Civil and Environmental Engineering*, Master's Thesis 2014:73

It can be seen in Figure 6.53 which value of the total load magnitude that causes failure after one load cycle for each distance. The other extreme case is the largest total load magnitude not to cause any plastic rotation to the structure. These extreme values and the development of plastic rotation are presented in Appendix F and shown in Figure 6.54 below.
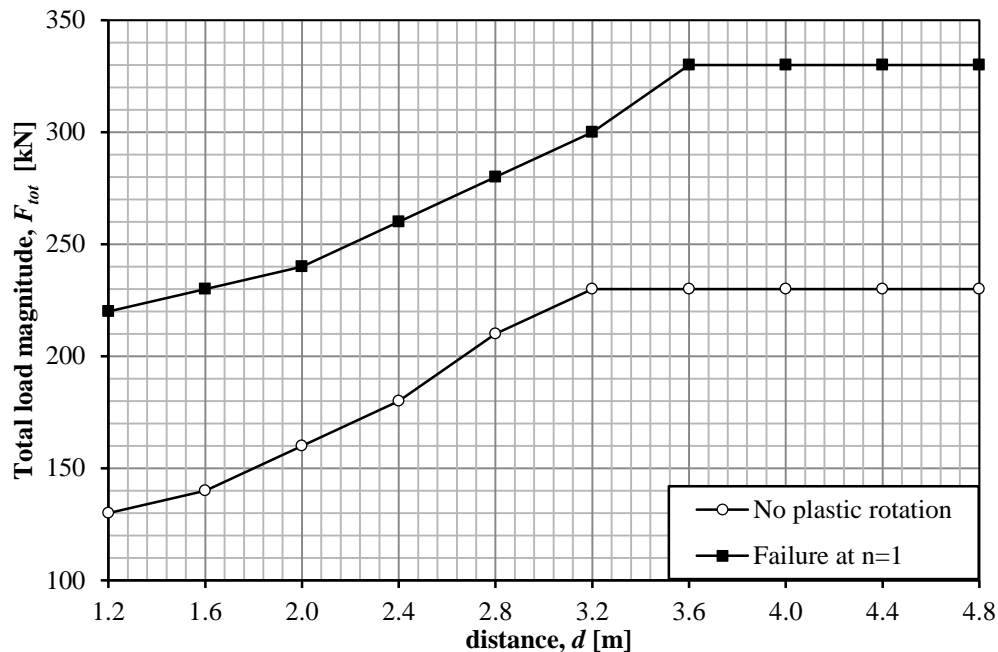
Figure 6.54   Relation between total load magnitude F_{tot} and distance d for forces not to cause any plastic rotation and failure after one load cycle.

As predicted in Section 6.4.4, when the distance reached a certain value, the two forces started to behave like two independent forces. When the distance was increased above 3.2 m, the total applied force not to cause any plastic rotation remained constant. The total force F_{tot} was in this case 230 kN which yielded that each individual force had a magnitude of 115 kN. The magnitude was in this case the same ($F = 115$ kN) as F_{el}, which was the greatest magnitude of a single moving concentrated force not to cause any plastic rotation to the structure. This means that the distance exceeded a critical value d_{crit} where the cantilever structure experienced the pair of concentrated forces as two individual forces. It also means that one of the forces did not amplify the plastic rotation development of the other force for this magnitude.

If the distance was increased above 3.6 m, the total applied force to cause failure due to plastic rotation after one load cycle remained constant. The total force was in this case 330 kN which yielded that each individual force had a magnitude of 165 kN. The magnitude was in this case the same ($F = 165$ kN) as the force of the lowest magnitude to cause failure for a single moving concentrated force after *two* load cycles. This means that the cantilever slab experienced two load cycles for each individual load cycle for a pair of moving concentrated forces with a distance greater than 3.6 m. If the distance was increased to 4.8 m, which corresponded to the total length of the force application, the plastic rotation development corresponded exactly to what was obtained from a single moving concentrated force.

As can be seen in Figure 6.54, there is a discrepancy between the load magnitudes and the corresponding distances when the cantilever slab experienced the force pair as two

independent forces. The reason for this behaviour was believed to be the derived from the moment distribution that is a result from the plastic behaviour of the slab. When the slab was completely elastic, a distance of 3.2 m between the forces was sufficient for the slab to experience the force pair as two individual forces. When the slab was partly plastic, the distance between the forces was increased to 3.6 m before the slab experienced the two forces as two independent forces. This means that the redistribution of forces in the cantilever structure is disadvantageous with respect to the development of plastic rotation caused by several concentrated forces.

6.5 Response of two moving forces – Different magnitudes

The slab shown in Figure 6.40 was in these analyses subjected to a number of forces of different magnitudes in order to investigate the influence of such load combinations. In order to investigate the influence of varying load magnitudes within the pair of moving concentrated forces, the total applied force F_{tot} was set to:

$$F_{tot} = F_1 + F_2 = 170 \text{ kN} \tag{6-27}$$

Where:

$$F_1 \neq F_2 \tag{6-28}$$

$$F_1 = \begin{bmatrix} 10 \ 20 \ 30 \ 40 \ 50 \ 60 \ 70 \ 80 \end{bmatrix} \text{kN} \tag{6-29}$$

$$F_2 = \begin{bmatrix} 160 \ 150 \ 140 \ 130 \ 120 \ 110 \ 100 \ 90 \end{bmatrix} \text{kN} \tag{6-30}$$

Where F_1 was the second force of the force pair to load the slab which can be seen in Figure 6.40 and Figure 6.55. The magnitude of the force F_2 was, for this load application order, always greater than the force F_1 according to Equation (6-31) and Figure 6.55.

$$F_1 < F_2 \tag{6-31}$$
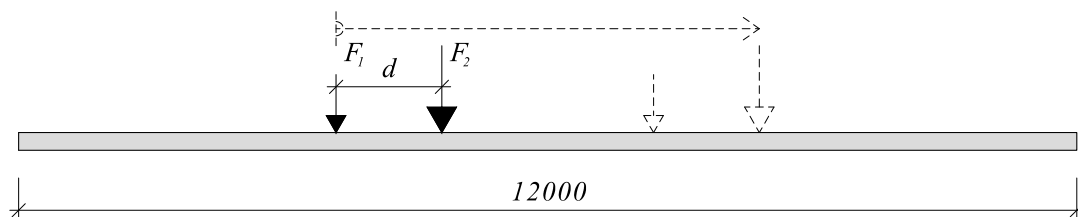
Figure 6.55   The first load application order LAO₁ of the studied cantilever slab.

The plastic rotation caused by the applied force pair was not significantly influenced by the load application order, i.e. if the values of F_2 were set to the values of F_1 and vice versa. The study on how the development of plastic rotation was influenced by the load application order is presented in Appendix E and the analyses in this section follow the first load application order LAO_1 which is stated in Equation (6-27) to (6-31).

6.5.1 Constant distance, d = [1.2 1.6 2.0] m

The distance d between the force pair applied on the cantilever slab was kept from the previous analyses in Section 6.4 and the results from the analyses are shown in Figure 6.56 to Figure 6.58:
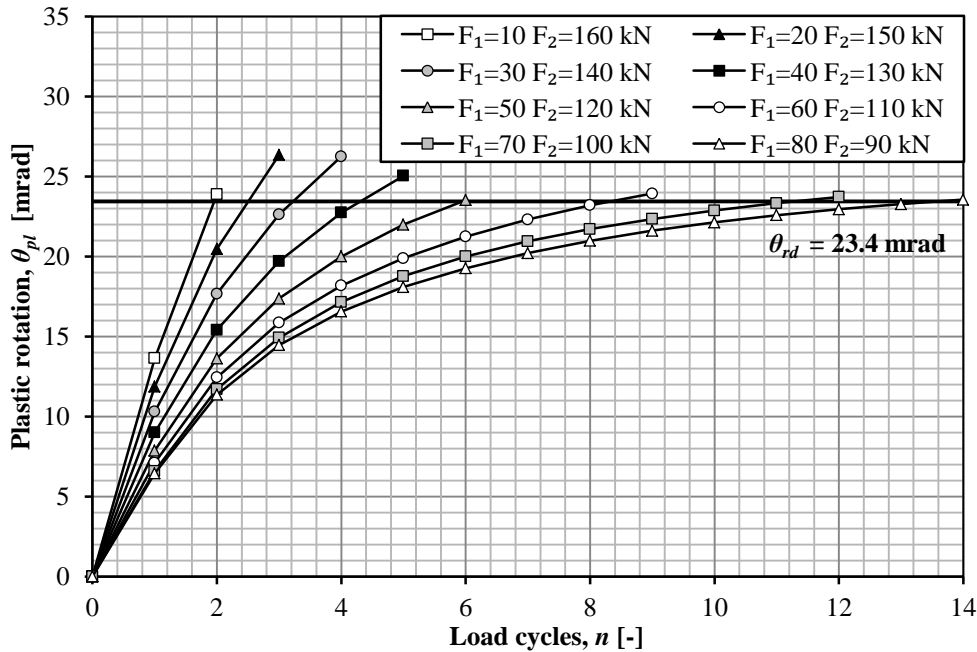
Figure 6.56   Plastic rotation for different load combinations of a pair of moving concentrated forces of varying magnitudes for d = 1.2 m.
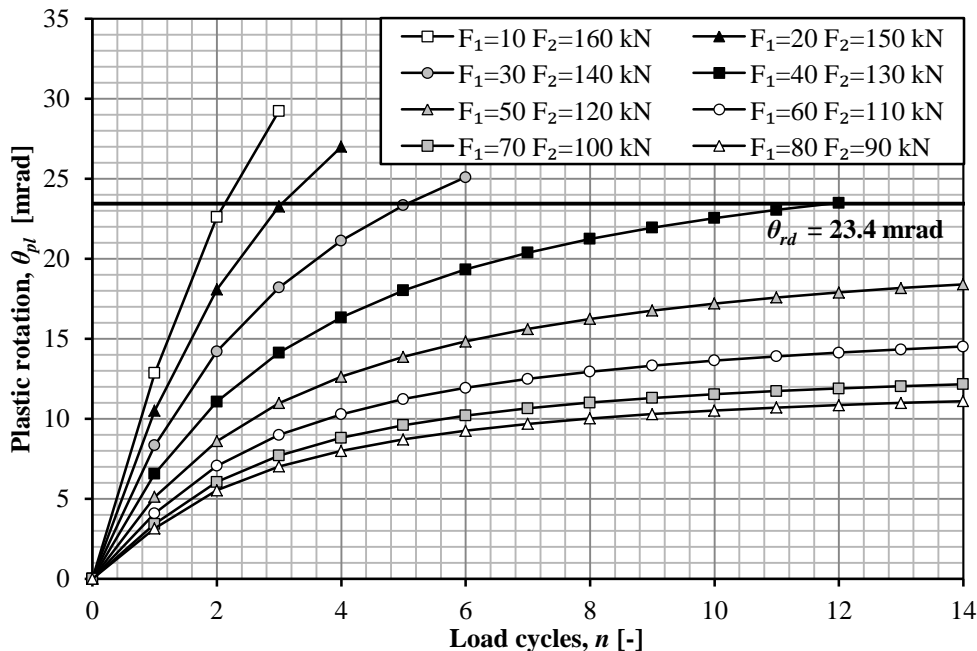
Figure 6.57   Plastic rotation for different load combinations of a pair of moving concentrated forces of varying magnitudes for d = 1.6 m.
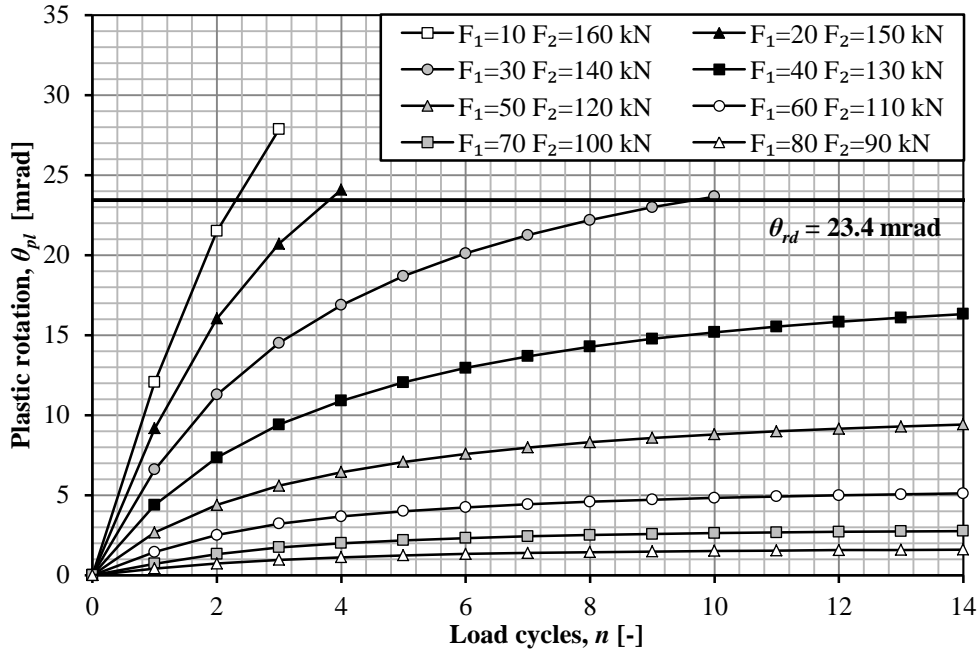
Figure 6.58   Plastic rotation for different load combinations of a pair of moving concentrated forces of varying magnitudes for d = 2.0 m.

As expected, and as observed in Section 6.4 it was advantageous for the cantilever structure with an increased distance between the moving concentrated forces. It is also clear that it was advantageous for the cantilever structure with a more evenly distributed force application, i.e. when the two forces approached a mean value.

From Figure 6.56 to Figure 6.58, it can be seen that:

- For the distance $d = 1.2$ m, all investigated load combinations led to failure within 14 load cycles or less.
- For the distance $d = 1.6$ m, four of the investigated load combinations led to failure within 14 load cycles or less.
- For the distance $d = 2.0$ m, three of the investigated load combinations led to failure within 14 load cycles or less.

It can be seen in Figure 6.58 that the force pairs with more equal distribution approached a state where no plastic rotation occurred for the investigated loads. A further increase of the distance between the moving concentrated forces would likely yield a significant decrease in the number of load combinations to cause failure due to plastic rotation.

How the plastic rotation developed in the centre of the slab during the first 10 load cycles for $d = 1.2$ m is shown in Figure 6.59. It can be seen that the development of plastic rotation decreased when the forces approached a mean value and that it approached a stable state when the number of load cycles increased. This corresponds to what was observed in Figure 6.56 to Figure 6.58.
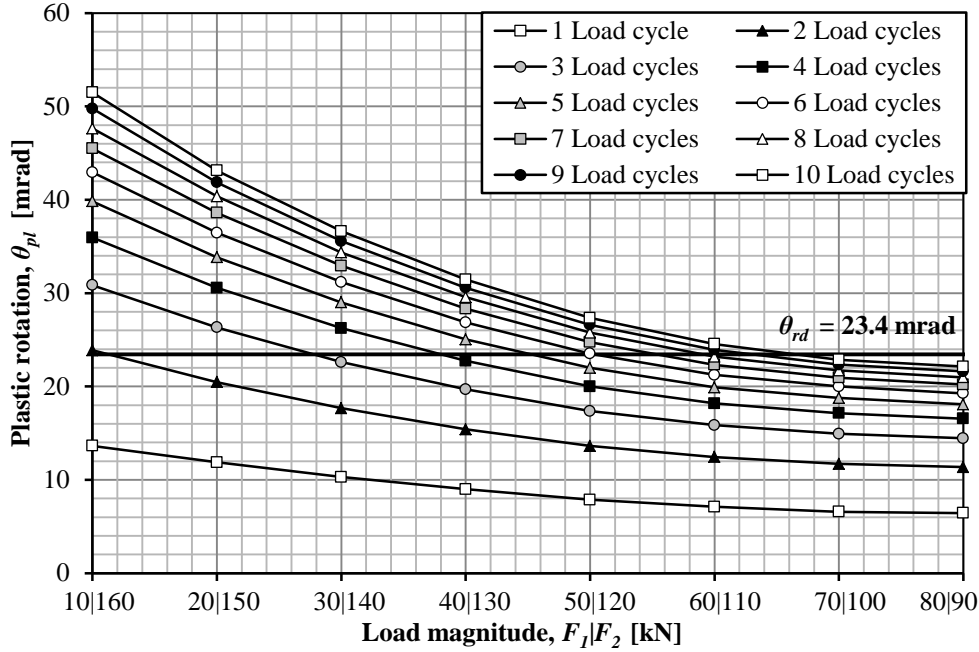
Figure 6.59 Development of plastic rotation for different load combinations of a pair of moving concentrated forces of varying magnitudes for d = 1.2 m.

It can be seen in Figure 6.59 that the load combinations with a large difference in force magnitudes between the two forces led to failure after only a few load cycles. The plastic rotation for these loads greatly exceeded the plastic rotation capacity for the cross-section but is presented in this figure in order to evaluate how the accumulated damage developed in the centre of the cantilever structure. It can be seen that the accumulated damage caused by the forces of more equal magnitudes approached a stable state more rapidly that the force pair with a larger difference in magnitude between the two forces. This can also be observed in Figure 6.56 where the distance between the curves decreases as the forces approaches a mean value.

6.5.2 Comparison

In order to determine how the plastic rotation was influenced by the distance d between the moving concentrated forces of varying magnitudes, the different analyses are compared below. The plastic rotation obtained from the analyses with $d = 1.6$ m and $d = 2.0$ m was compared to the plastic rotation with $d = 1.2$ m according to Equation (6-32) and (6-33) and is shown in Figure 6.60 and Figure 6.61.

$$\gamma_{\theta pl.1.6m} = \frac{\theta_{pl.1.6m} - \theta_{pl.1.2m}}{\theta_{pl.1.2m}} \tag{6-32}$$

$$\gamma_{\theta pl.2.0m} = \frac{\theta_{pl.2.0m} - \theta_{pl.1.2m}}{\theta_{pl.1.2m}} \tag{6-33}$$

The plastic rotation difference $\gamma_{\theta pl}$ was calculated for each load cycle n and each distance d and is shown for the first 15 load cycles in the figures below.
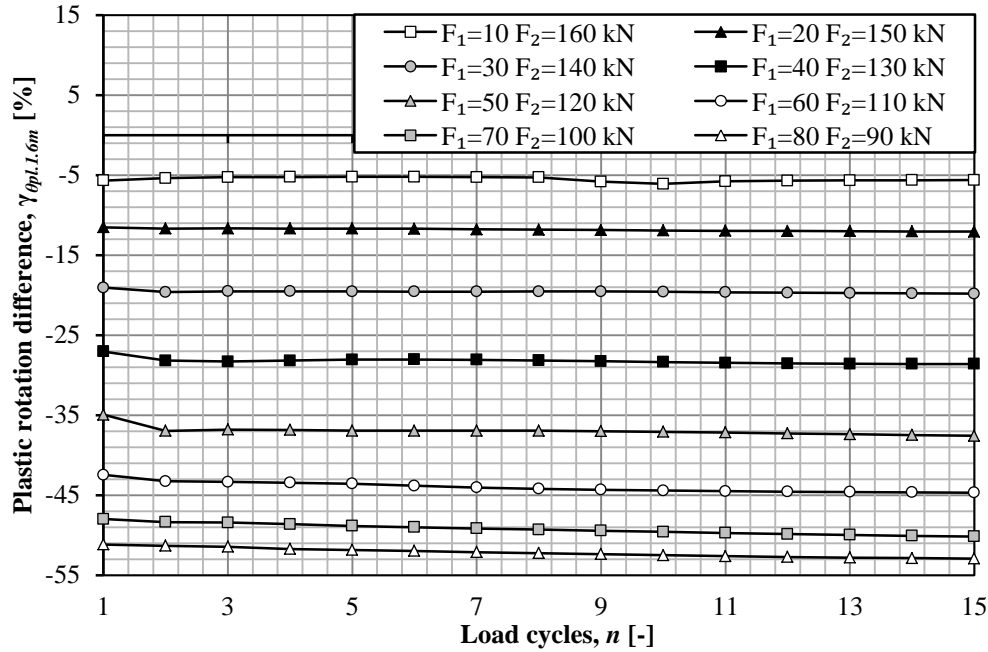
Figure 6.60   Difference in plastic rotation $\gamma_{\theta pl.1.6m}$ for different load combinations between d = 1.2 and d = 1.6 m.
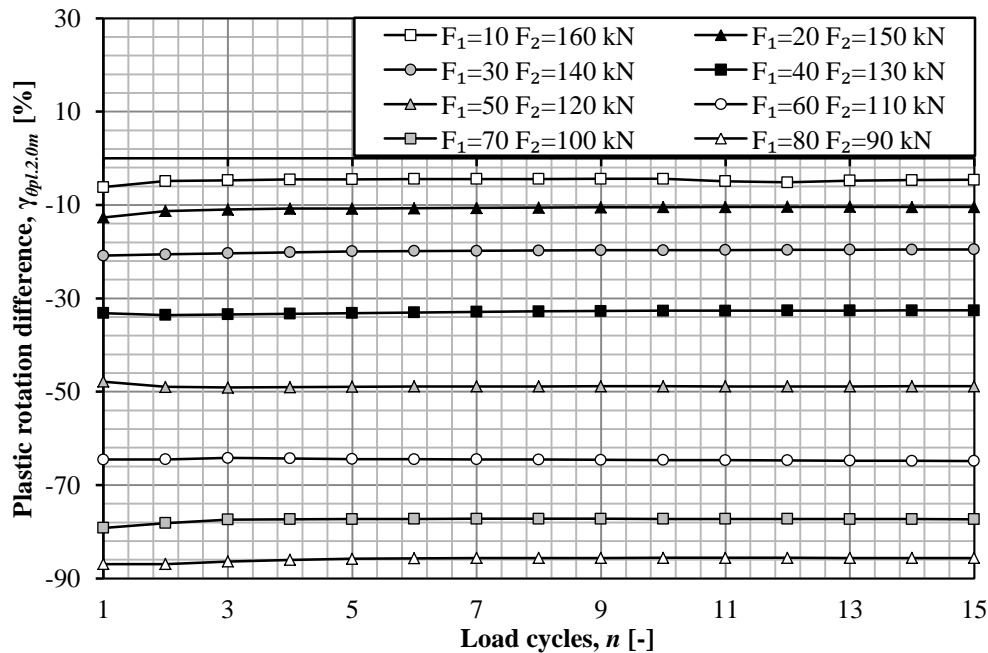
Figure 6.61   Difference in plastic rotation $\gamma_{\theta pl.2.0m}$ for different load combinations between d = 1.2 m and d = 2.0 m.

It is clear from Figure 6.60 and Figure 6.61 that it was, as in the case of a force pair of equal magnitudes, advantageous for the cantilever structure with an increased distance between the forces. It is also clear that the difference in plastic rotation was almost constant for each separate load combination and distance which means that the difference is independent from the number of load cycles. Due to this fact, it was convenient to measure the mean difference in plastic rotation which is presented below:

$$\bar{\gamma}_{\theta pl.1.6m} = \frac{\bar{\theta}_{pl.1.6m} - \bar{\theta}_{pl.1.2m}}{\bar{\theta}_{pl.1.2m}} \qquad (6\text{-}34)$$

$$\bar{\gamma}_{\theta pl.2.0m} = \frac{\bar{\theta}_{pl.2.0m} - \bar{\theta}_{pl.1.2m}}{\bar{\theta}_{pl.1.2m}} \qquad (6\text{-}35)$$

Where the mean plastic rotation for the two cases was calculated according to:

$$\bar{\theta}_{pl.1.6m} = \frac{\sum_{0}^{n} \theta_{pl.1.6m}}{n} \qquad (6\text{-}36)$$

$$\bar{\theta}_{pl.2.0m} = \frac{\sum_{0}^{n} \theta_{pl.2.0m}}{n} \qquad (6\text{-}37)$$

Where $n = 150$, which was the total number of load cycles in the conducted analyses. The results from these calculations are shown in Figure 6.62. The values derived from Equation (6-34) and (6-35) are tabulated in Appendix H for the interested reader.
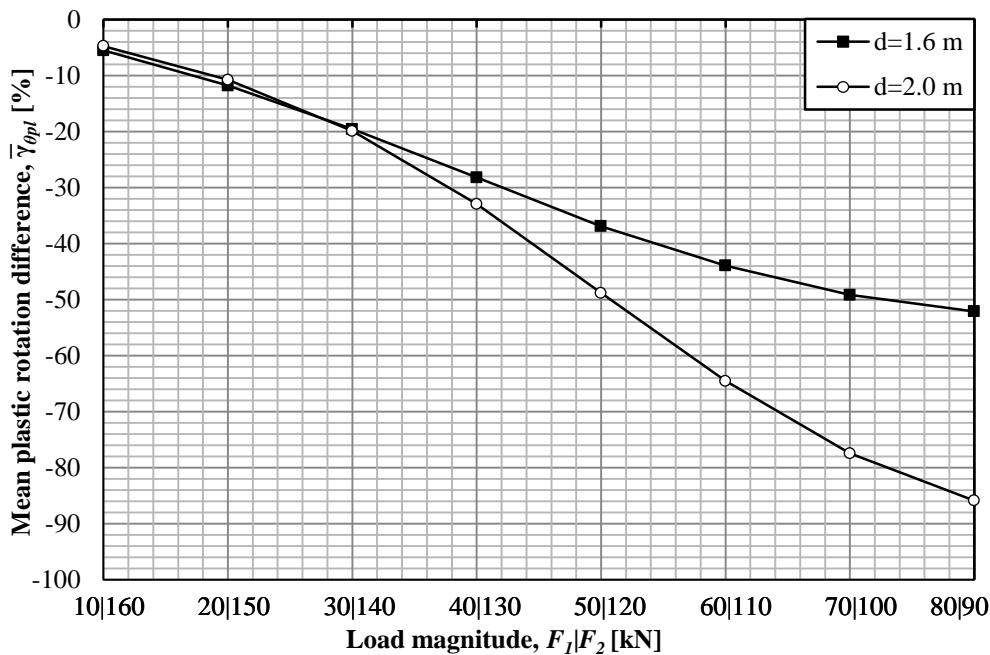
Figure 6.62 *Mean difference in plastic rotation $\gamma_{\theta pl}$ between a $d = 1.2$ m and, $d = 1.6$ m and $d = 2.0$ m.*

It can be seen in Figure 6.62 that an increased distance d resulted in a significant decrease in plastic rotation. The difference in plastic rotation increased with decreasing difference between the two forces F_1 and F_2. This behaviour was expected since the distance between a force of a great magnitude and a force of a small magnitude should not influence the accumulated damage to a great extent. When both forces are of a relative high magnitude, the distance should influence the accumulated damage to a greater extent, which was the case.

6.6 Summation

This section covers a comparison between the moving concentrated forces presented in Section 6.3 to 6.4. A single and a pair of moving concentrated forces are compared with static forces of the same magnitudes. As a final part of this section, the results presented in Chapter 6 are discusses.

6.6.1 Comparison – Moving forces

This section covers the investigated forces on the cantilever structure presented in Section 6.3 to 6.4 and evaluates the differences and similarities between them. These sections have covered the four main load cases:

- A single moving concentrated force – Constant magnitude
- A single moving concentrated force – Varying magnitudes
- Two moving concentrated forces – Equal magnitudes
- Two moving concentrated forces – Different magnitudes

The case of two moving concentrated forces of different magnitudes can be seen as an intermediate combination of the case of two moving concentrated forces of equal magnitudes and a single moving concentrated force of constant magnitudes. The case of a single moving concentrated force of constant magnitude can be seen as an extreme case of two moving concentrated force of different magnitudes. The other extreme case is when the different force magnitudes approach a mean value, which is the case of two moving forces of equal magnitudes. This means that the plastic rotation obtained by the two moving concentrated forces of different magnitudes should be found between the two extreme cases as explained above. This was also the case which can be seen in Figure 6.63 to Figure 6.65 where these analyses are presented together.
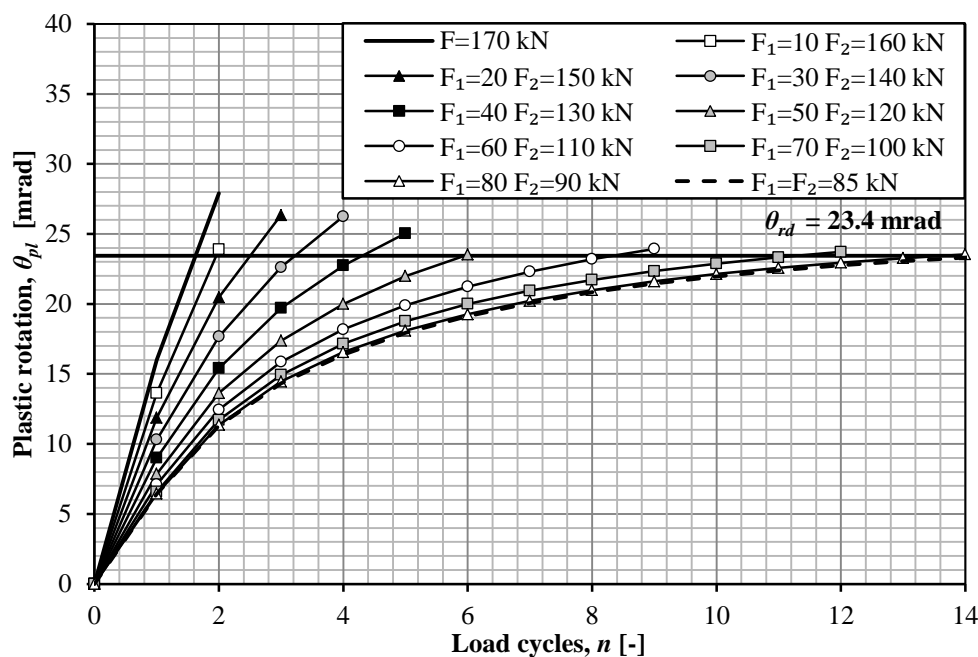
Figure 6.63   Plastic rotation for different load combinations of a pair of moving concentrated forces of varying magnitudes for d = 1.2 m.
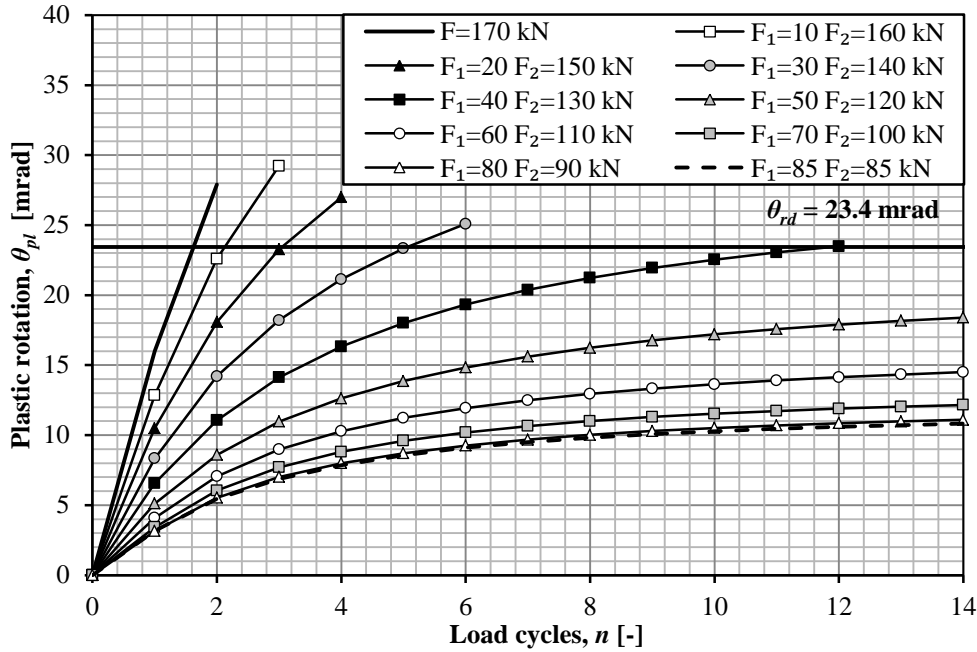
Figure 6.64   Plastic rotation for different load combinations of a pair of moving concentrated forces of varying magnitudes for d = 1.6 m.
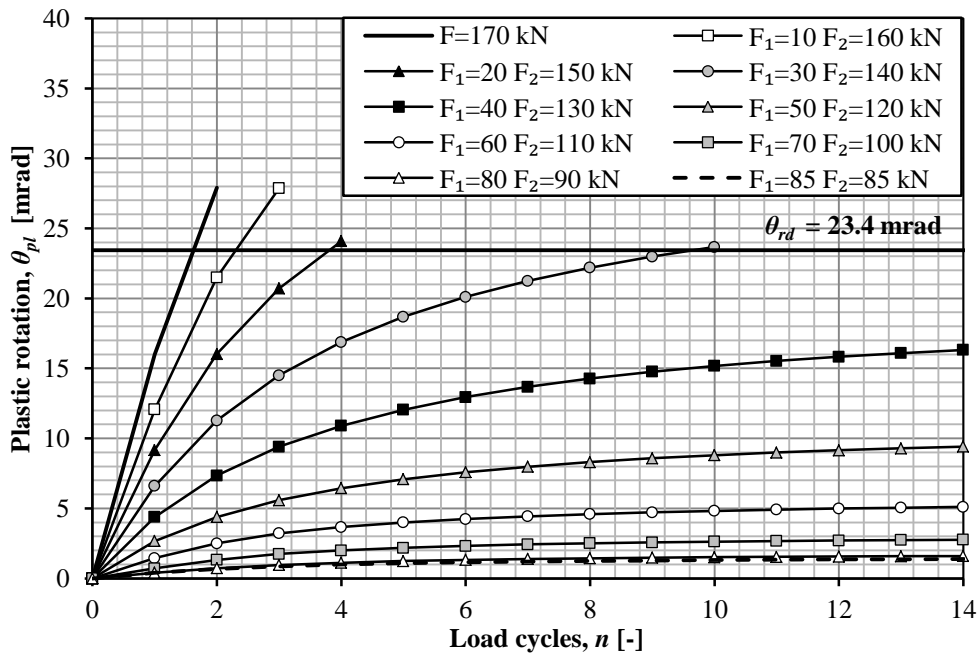
Figure 6.65   Plastic rotation for different load combinations of a pair of moving concentrated forces of varying magnitudes for d = 2.0 m.

It can be seen in Figure 6.63 to Figure 6.65 that the results where $F_1=F_2=85$ kN corresponded well to the case where $F_1=80$ kN and $F_2=90$ kN for all distances d. The plastic rotation obtained by $F=170$ kN was slightly higher than the case where $F_1=10$ kN and $F_2=160$ kN for all distances d. These results indicate that a difference between the two moving concentrated forces of different magnitudes of 10 kN ($F_1=80$ kN and $F_2=90$ kN) was small enough not to influence the plastic rotation further. This corresponded well to what was expected. These results also indicate that it was advantageous for the cantilever structure to separate the total force into two

CHALMERS, *Civil and Environmental Engineering*, Master's Thesis 2014:73

separate forces, even if the difference was relatively small. The advantageous effect of dividing the total force into two separate forces increased with the increased distance *d* which was reasonable.

These analyses were only conducted for one total force F_{tot} =170 kN for the two moving forces of different magnitudes but the advantageous effect of dividing the total force into two separated forces was believed to increase with an increased total force. It was also treated in previous sections that a further increase of the distance *d* is advantageous for the cantilever structure.

6.6.2 Comparison – Static vs. moving forces

It is clear that a moving concentrated force caused significantly more plastic rotation to the cantilever structure than what was caused by a static force of the same magnitude. It was shown in Section 6.3 to 6.4 that the plastic rotation reached a stable state after a number of load cycles. This indicates that a moving concentrated force have an upper limit of the amount of plastic rotation it can cause. This upper limit may be situated above the plastic rotation capacity of the structure but, as have been illustrated in Section 6.3 to 6.4, were in most cases for forces of great magnitudes situated below this limit.

It is also clear that there is a significant difference between the plastic rotation caused by static and moving concentrated forces immediately after the first completed load cycle. This means that all values of the plastic rotation caused by a moving concentrated force must be present within these upper and lower limits as can be seen in Figure 6.66.
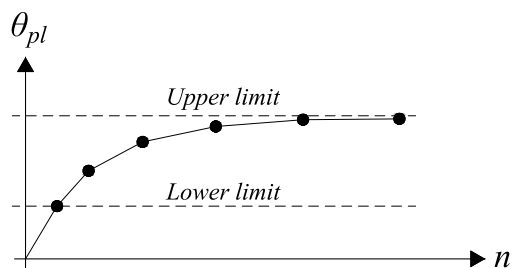
Figure 6.66   Upper and lower limit of plastic rotation for moving concentrated forces

In order to compare the moving forces to the static forces, a cumulative factor $\gamma_{\theta pl.mov}$ was defined according to Equation (6-38). The cumulative factor describes the relation between the plastic rotation caused by a moving concentrated force and the plastic rotation caused by a static force.

$$\gamma_{\theta plmov} = \frac{\theta_{pl.mov.n}}{\theta_{pl.stat}}$$
(6-38)

In order to evaluate the distribution of this factor, two sub factors $\gamma_{\theta pl.mov.min}$ and $\gamma_{\theta pl.mov.max}$ was defined. These factors were calculated for all forces that reached a stable state (reached its maximum plastic rotation) in the conducted analyses. The factors were calculated using Equation (6-39) and (6-40), respectively, which is shown in Figure 6.67.

$$\gamma_{\theta plmov.\max} = \frac{\theta_{pl.mov.n=150}}{\theta_{pl.stat}} \qquad (6\text{-}39)$$

$$\gamma_{\theta plmov.\min} = \frac{\theta_{pl.mov.n=1}}{\theta_{pl.stat}} \qquad (6\text{-}40)$$

Where $\theta_{pl.stat}$ = the plastic rotation caused by a static force of the same magnitude as a moving force

$\theta_{pl.mov.n}$ = the plastic rotation caused by a moving force for each load cycle n

It is clear from Figure 6.67 that the plastic rotation caused by a moving concentrated force was within the range of 2 to 20 times larger than the plastic rotation caused by a static force. It is also clear that an increased distance d between the forces and an increased total applied force F_{tot} yielded plastic rotations closer to what was predicted by the static forces. How the cumulative factor developed for a single moving concentrated force is shown in Figure 6.68. For the development of the cumulative factor for two moving concentrated forces, the reader is referred to Appendix G.
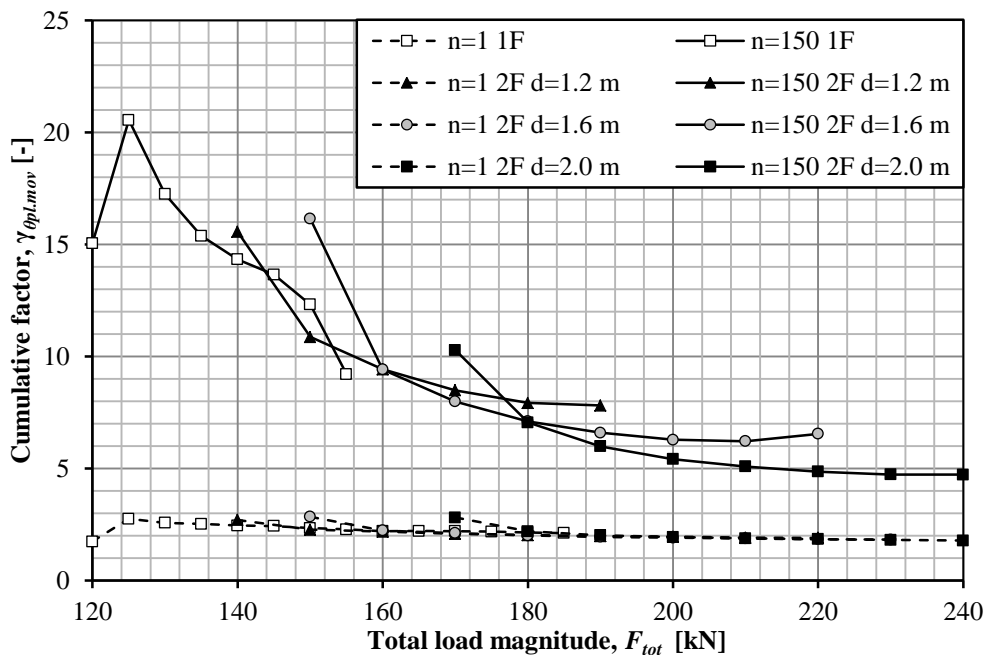
Figure 6.67 Maximum and minimum values of the cumulative factor $\gamma_{\theta pl.mov}$ for a single and a pair of moving concentrated forces.
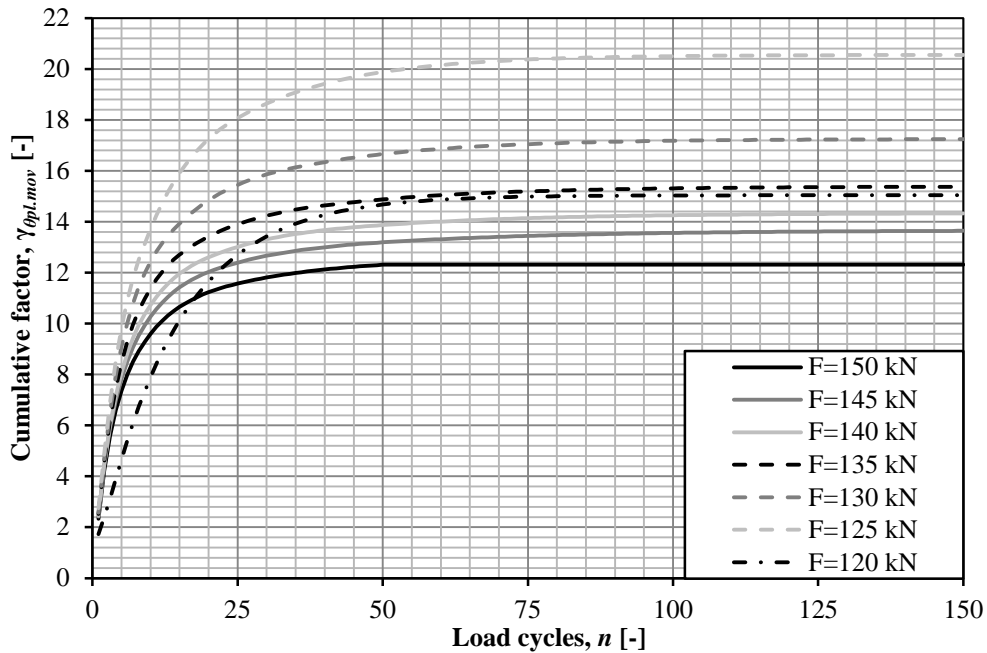
Figure 6.68 Development of the cumulative factor $\gamma_{\theta pl.mov}$ for a single moving concentrated force for 150 load cycles.

6.6.3 Discussion

It was first discovered in Section 6.3 that the development of plastic rotation in the cantilever structure reached a stable state where the influence of the applied force decreased as the number of load cycles increased. The behaviour of the slab resembled the linear elastic behaviour even though the slab was still in the plastic state. This behaviour was then found for all types of load magnitudes, load combinations and load application orders studied in this Thesis. When this behaviour of the slab was reached differs for all the above stated variables but for a large amount of the studied forces, this was found before the plastic rotation capacity was reached.

It was discovered that a traditional superposition approach of moving concentrated forces significantly overestimated the plastic rotation. This overestimation was based on the fact that the superposition approach did not account for the decreased effect of the applied forces as the number of load cycles increased. This means that the error was increased as the number of load series were increased in the superposition approach. It was also shown that the error was almost linearly increased with an increase of the applied force.

It was shown in Section 6.2 to 6.5 that there was a significant difference between the plastic rotation caused by static and moving concentrated forces. The plastic rotation caused by a moving force could be as high as 20 times the plastic rotation caused by a static force of the same magnitude. This difference might be greater for forces that were not covered in this Thesis. It was shown that this difference decreased as the force magnitude increased and also decreased with increased distance *d* between a pair of moving concentrated forces.

CHALMERS, *Civil and Environmental Engineering*, Master's Thesis 2014:73

7 Cumulative plastic rotation – Simply supported slab

The aim of this chapter, as was mentioned in Chapter 6, was to increase the understanding of development of accumulated damage in long slabs which are subjected to moving concentrated forces of magnitudes below, at or above what is predicted by the serviceability limit state as have been described in Section 6.1.1. The response of static forces was, as in Chapter 6, studied for comparison purposes and as reference results. The response of a single moving concentrated force was thereafter studied and then expanded to two moving concentrated forces. The forces were, as in Chapter 6, applied with constant and varying magnitudes and the distance between the two moving concentrated forces was altered in order to cover a broader spectrum of possible load combinations.

The simply supported one-way slab studied in Chapter 5 was for these analyses modelled without a symmetry boundary in the *y*-direction since such a boundary could not reflect the moving forces of interest in this Thesis. The symmetry boundary in *x*-direction was, however, kept due to the restriction of nodes in the student version of ADINA. As for the cantilever slab in Chapter 6, numerical problems occurred and the measures taken were the same as stated in that chapter. The width of the slab was therefore set to 12 m on the same basis and background as stated in Chapter 6.

The methodology and the results presented in this chapter correspond well to what was defined and observed in Chapter 6. Due to this fact, these are in this chapter presented in a more compact form and the reader is referred to Chapter 6 for comparison and additional information regarding these matters.
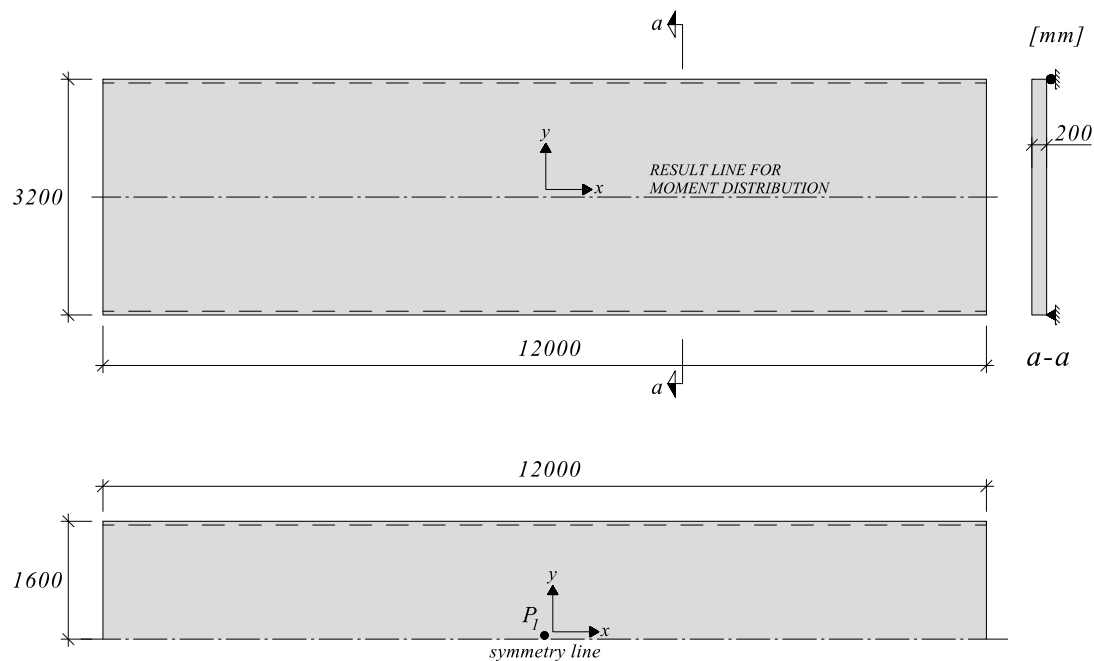
Figure 7.1   Geometry and dimensions of the studied simply supported one-way slab.

7.1 Methodology

This section covers the methodology used for the studies related to the development of plastic rotation. The background and the practical application of these studies, the moment-curvature relations, the FE model and the influence of the torsional stiffness are also treated in this section.

7.1.1 Background

The aim of this study was the same as stated in Section 6.1.1. This study was also directed towards load magnitudes below, at or above what is predicted by the serviceability limit state. For additional information of the background of this study, the reader is referred to Section 6.1.1.

As observed in Chapter 5, moments higher than predicted by a simplified linear elastic analysis occurred when a more refined analysis was conducted. This difference was derived from the orthotropic stiffness which was a result from varying reinforcement amounts in different directions. This behaviour was also here observed for the linear elastic orthotropic case in Figure 5.6 and is also illustrated here in Figure 7.2.
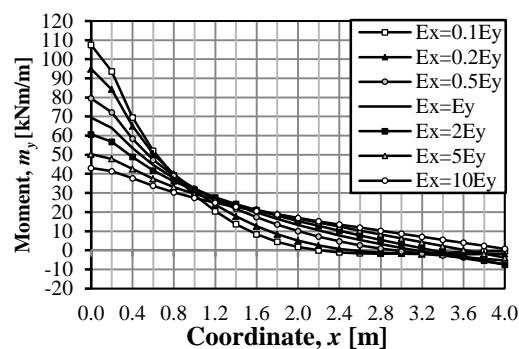
Figure 7.2   Linear elastic orthotropic moment distribution.

7.1.2 Moment-curvature relations

The restrictions and modelling choices made for the cantilever structure in Section 6.1.2 generally also applies here and are therefore omitted in this section. For the background of the modelling choices the reader is referred to Appendix C.

The bilinear plastic moment-curvature relation for the slab was here based on the elastic response of an isotropic, cracked, simply supported slab subjected to a concentrated force of 100 kN at the centre of the slab. This can be compared with the force magnitude of 200 kN that was applied on the cantilever structure in Chapter 6. The reason for this difference can be derived from the fact that the simply supported structure was subjected to the force in the symmetry boundary which yielded a total force of 200 kN.

The elastic part of the moment-curvature relation used for these analyses was the moment-curvature relation used for the case Cracked of the simply supported slab in SLS, presented in Chapter 5. The elastic part of the moment-curvature relation and the corresponding moment distribution in the fixed support is illustrated in Figure 7.3.
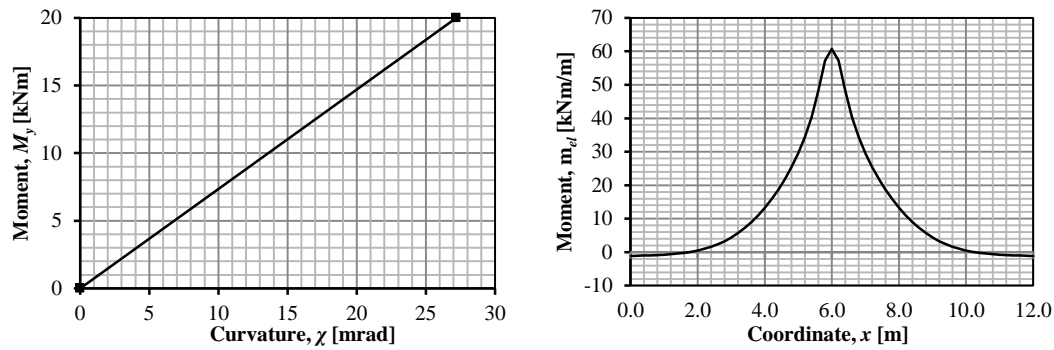
Figure 7.3   Elastic moment-curvature relation and the corresponding moment distribution in the centre of the slab.

It can here be noted in Figure 7.3 that the moment distribution had a sharp peak in the centre of the slab. This in contrast to the moment distribution obtained for the cantilever structure. The reason for this discrepancy can be derived from the fact that the moment distribution was measured directly below the location of the load application in this case. The force was also applied differently in this analysis compared to the cantilever structure. This is treated below.

The force was in this case applied in six nodes instead of a single node, which was the case for the cantilever structure in Chapter 6. The reason for this load application can be derived from the fact that a load application in a single node is a simplification that yielded unrealistic force concentrations and thus unrealistic plastic rotations. Such a simplification yielded satisfactory results for the cantilever structure in Chapter 6 since the plastic rotation was measured a certain distance from the location of the force application. For additional information about the load application, the reader is referred to Appendix C.

How the plastic moment M_{pl} was derived was covered in Section 6.1.2 and is not further discussed here.

To summarize, the bilinear plastic moment-curvature relation used in this section was based on:

- The elastic response of an isotropic, cracked cross-section
- The plastic moment M_{pl}, based on the elastic response of the structure
- The plastic rotation capacity θ_{rd} of the cross-section

The two moment-curvature relations used as input for the analyses in this section is illustrated in Figure 7.4
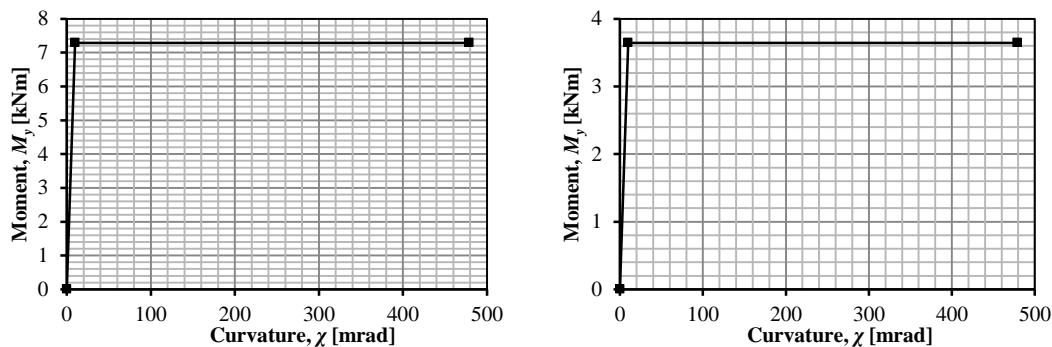
Figure 7.4   Bilinear plastic moment-curvatures used for the analyses in this section.

For additional and a more profound description on the modelling choices made for these analyses, the reader is referred to Appendix C. The construction of the plastic moment and the design of the plastic rotation capacity are also treated in Appendix C.

7.1.3 Finite element model

How the simply supported one-way slab was modelled for the analyses in this section and how the moving forces were applied is illustrated in Figure 7.5.
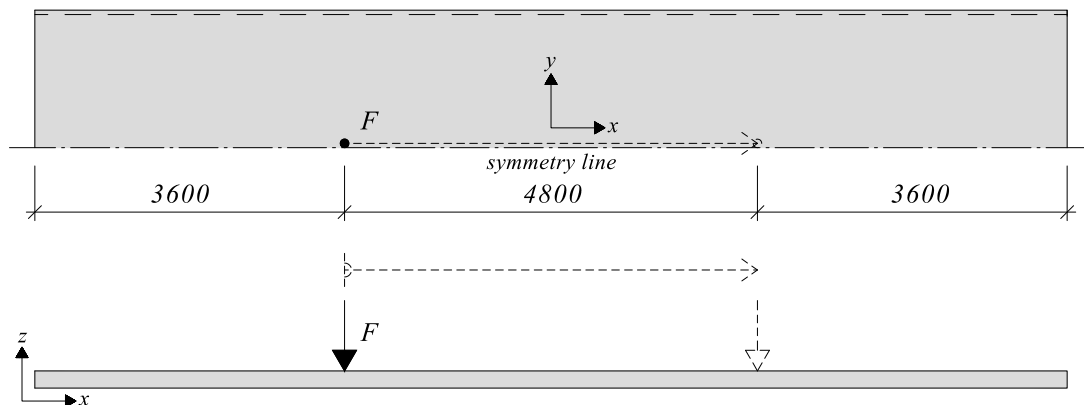
Figure 7.5   Geometry and dimensions of the studied simply supported slab for a single moving concentrated force.

The finite element models used for the simply supported one-way structure were in most cases the same as the cantilever structure in Section 6.1.3. Large parts are therefore omitted in this section and the reader is referred to Section 6.1.3 for additional information of the FE model.

The plastic rotation and the development of plastic rotation in the centre of the slab were of interest in this study and are therefore presented in this section in the result point P_1, illustrated in Figure 7.1. When the development of the plastic rotation along the centre line of the slab is illustrated in this section, the coordinate $x = 0$ refer to the centre of the slab (due to the symmetry behaviour of the structure).

Since the plastic rotation in the centre of the symmetry boundary was of interest, the point loads were positioned in the line where the plastic rotation was measured. Contrary to the cantilever slab where the plastic rotation was measured a certain distance from the point load, attention had to be directed to how the point load was modelled to yield reasonable results. This was briefly treated in Section 7.1.2 and the reader is referred to Appendix C for additional information regarding this matter.

The plastic rotation was calculated in the same approximate approach as presented in Section 6.1.3. The rotation in the first node was also here prescribed by the boundary conditions to zero, which influenced the angle of the triangle. The angle α, i.e. the plastic rotation, was calculated from the triangle created by the deflected nodes, which can be seen in Figure 7.6.
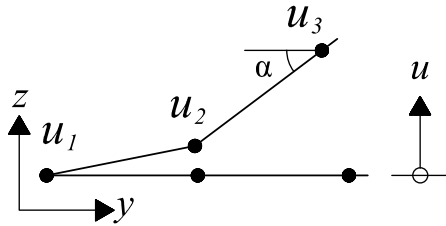
Figure 7.6   The approximate approach for calculating the plastic rotation θ_{pl} in the centre of the symmetry boundary in the simply supported one-way slab.

The angle α and thus the plastic rotation θ_{pl}, was calculated from the deflection in the second and third node due to how the ADINA software treats the plastic curvature in the FE model. The angle α was dependent on the mesh density since a finer mesh provides a better approximation. The orthotropic mesh density described above yielded satisfactory results and an increase of the mesh density did not influence the results significantly. For additional information regarding how ADINA treats the plastic curvature and how the results could have been obtained, the reader is referred to Section 6.1.3 and Appendix D.

7.1.4 Torsional stiffness

The torsional stiffness was for these analyses also set to 1/16 of the elastic stiffness of a concrete beam with a width and height of 0.2 m. The choice of torsional stiffness was also here believed to be conservative and for additional information about this matter, the reader is referred to Section 6.1.4 and Appendix B.

7.2 Response of a single and two static forces

The response and the development of plastic rotation for a single and two static forces of varying magnitudes are treated in this section. The aim of this section was to study how the simply supported one-way structure behaved under static forces so that the development of plastic rotation caused by moving concentrated forces could be compared and evaluated. This evaluation is treated in Section 7.6.2.

The simply supported slab was subjected to single forces F of the following magnitudes:

$$F = \begin{bmatrix} 55\ 60\ 65 \ldots 135\ 140\ 145 \end{bmatrix} \text{kN} \tag{7-1}$$

The forces that were applied on the slab had a range of 55 kN, where no plastic rotation occurred, and 145 kN which was the force of the smallest magnitude to cause failure due to plastic rotation θ_{pl}. The forces were applied in the centre of the slab which can be seen in Figure 7.11.

[mm]
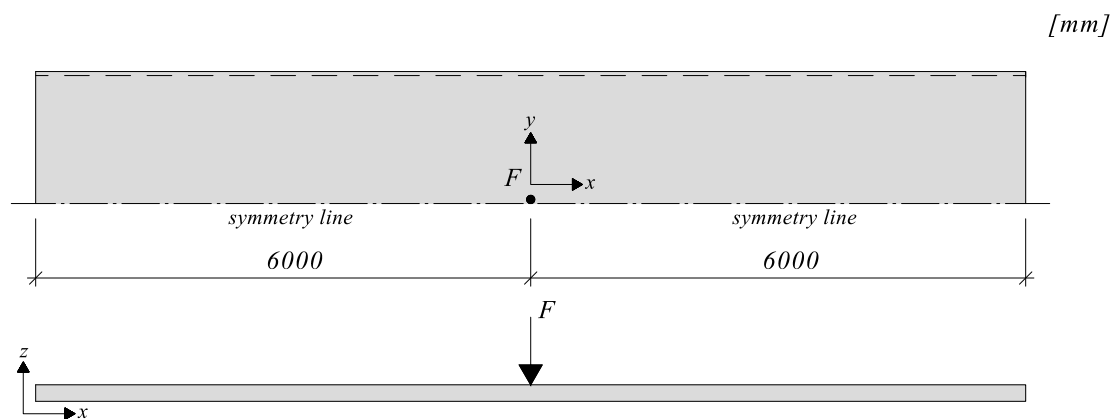
Figure 7.7   Geometry and dimensions of the studied simply supported slab subjected to a single static concentrated force.

The slab was also subjected to two concentrated forces F_1 and F_2 that varied according to the following magnitudes:

$$F_1 = F_2 = \begin{bmatrix} 40\ 45\ 50 \ldots 85\ 90\ 95 \end{bmatrix} \text{kN} \tag{7-2}$$

The distance between the two forces was kept from Section 6.2 and was therefore altered according to:

$$d = \begin{bmatrix} 1.2\ 1.6\ 2.0 \end{bmatrix} \text{m} \tag{7-3}$$

The forces that were applied on the slab had a range of 40 kN, where no plastic rotation occurred for $d = 1.2$ m, and 95 kN which was the force of the smallest magnitude to cause failure due to plastic rotation for $d = 2.0$ m. The forces were also here applied in the centre of the slab which can be seen in Figure 7.8.
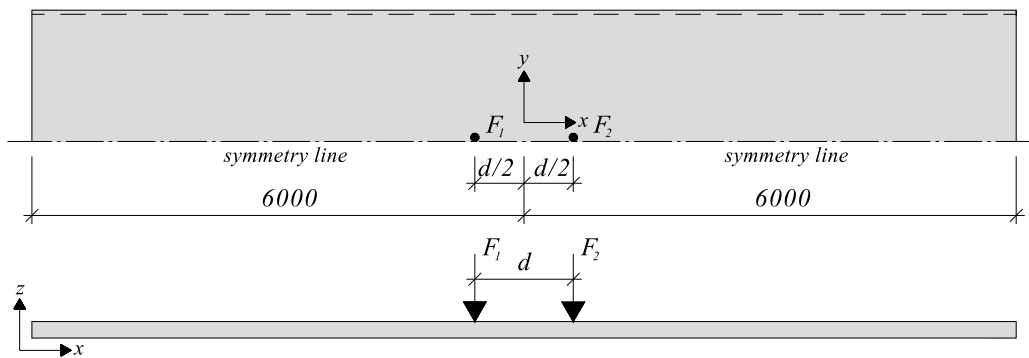
Figure 7.8   Geometry and dimensions of the studied simply supported slab subjected to a pair of static concentrated forces.

The results from the analyses are shown in Figure 7.13 where it is clearly shown, as for the cantilever structure in Section 6.2, that it was advantageous for the cantilever structure with an increased distance between the two concentrated forces.
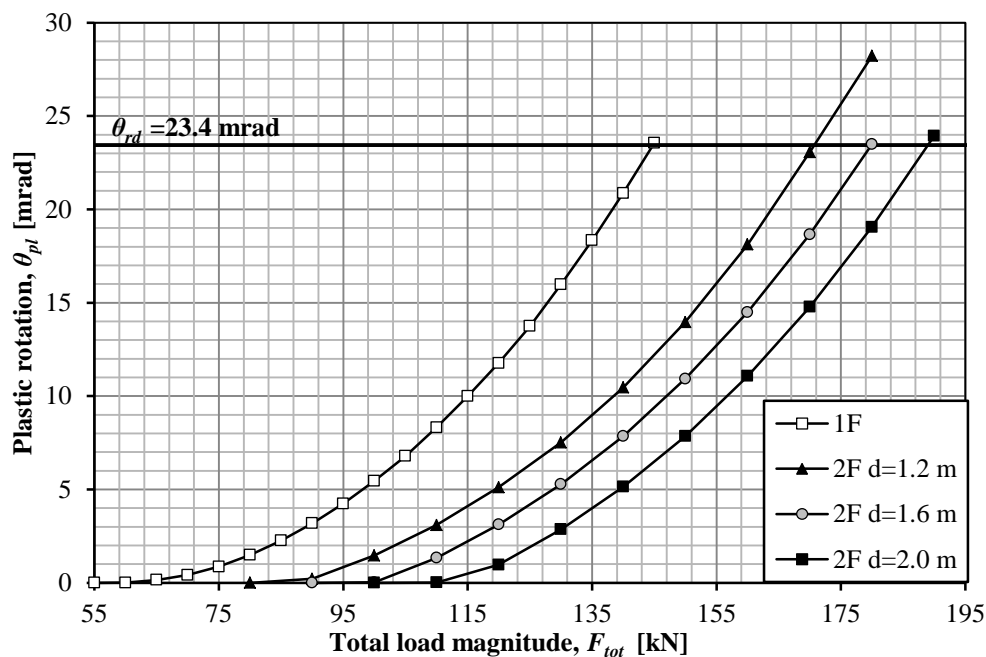
Figure 7.9   Plastic rotation at the centre of the simply supported slab for different magnitudes of static forces.

As a validation of the model, the simply supported structure was subjected to a single static force of 115 kN that were applied over ten load cycles (applied and removed ten times). As stated in Section 6.2, a static force should in theory cause a plastic rotation that does not develop when the number of load applications increases. This is also how the model behaved, as can be seen in Figure 7.10, and it is clear that the model was more stable than the cantilever structure in Section 6.2.
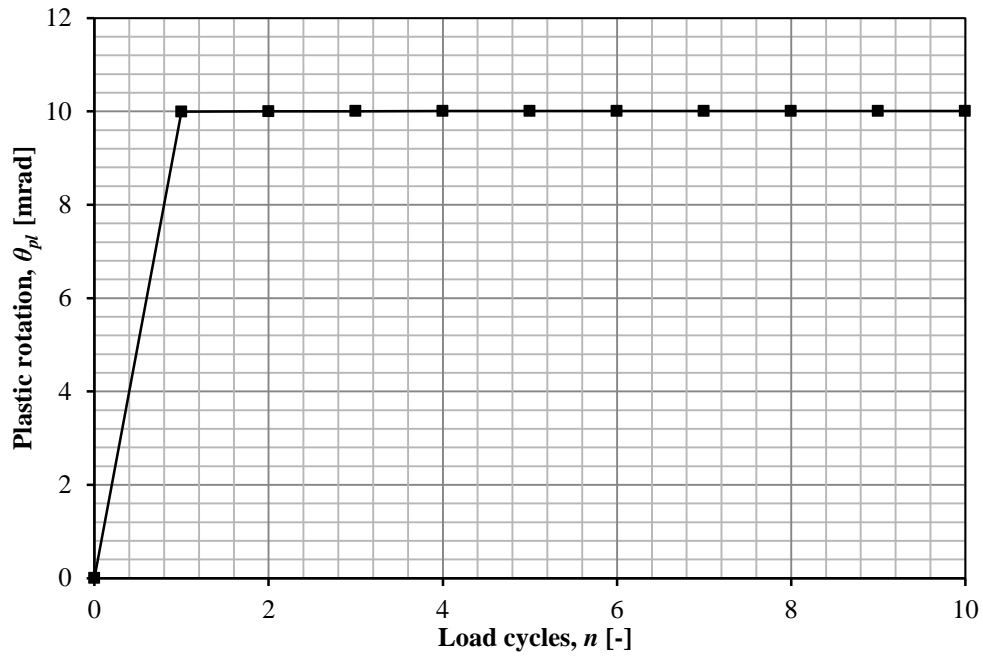
Figure 7.10   Plastic rotation at the centre of the simply supported slab for a static force F=115 kN during ten load cycles.

7.3 Response of a single moving force

The response and the development of accumulated damage, i.e. plastic rotation, for a single moving concentrated force of constant and varying magnitudes is treated in this section. A comparison between the different load cases and how a superposition approach corresponds to the behaviour of the slab from the conducted analyses is also treated in this section. The results obtained in these analyses corresponded well to those obtained in Section 6.3 for the cantilever structure. The results are therefore presented here in a more compact form and the reader is referred to Section 6.3 for comparison and additional information regarding the analyses.
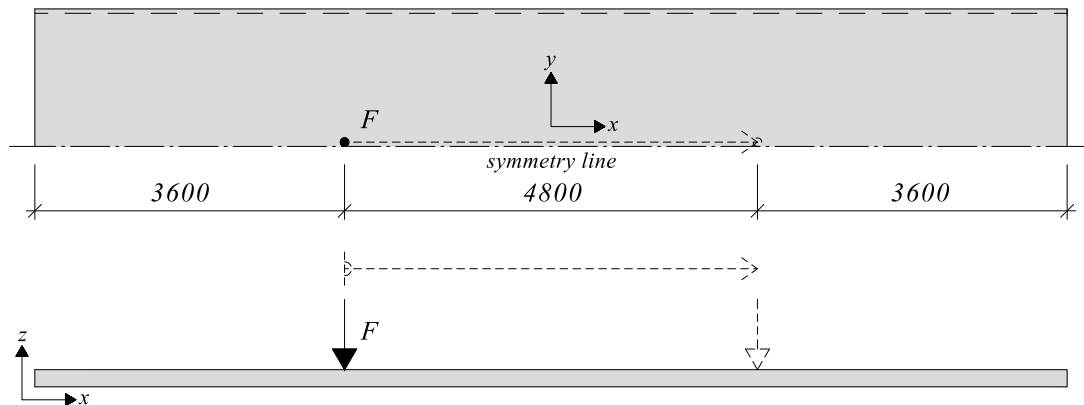
Figure 7.11   Geometry and dimensions of the studied simply supported slab for a single moving concentrated force.

7.3.1 Load magnitudes – Constant

The slab in Figure 7.11 was exposed to a range of moving concentrated forces *F* of different magnitudes:

$$F = \begin{bmatrix} 55 & 60 & 65 & ... & 115 & 120 & 125 \end{bmatrix} \text{kN} \tag{7-4}$$

As can be seen in Figure 7.12, a high load magnitude led to failure in a small number of load cycles while a low load magnitude led to failure with a higher number of load cycles. This behaviour corresponded to the expected behaviour of the structure and what was observed in Section 6.3.

The simply supported slab was also subjected to 150 load cycles *n* for each load magnitude *F* if failure of the structure did not occur within that range.

Forces with a magnitude ranging from 110 kN to 125 kN reached failure in two or less load cycles which is shown in Figure 7.13 for scale purposes.
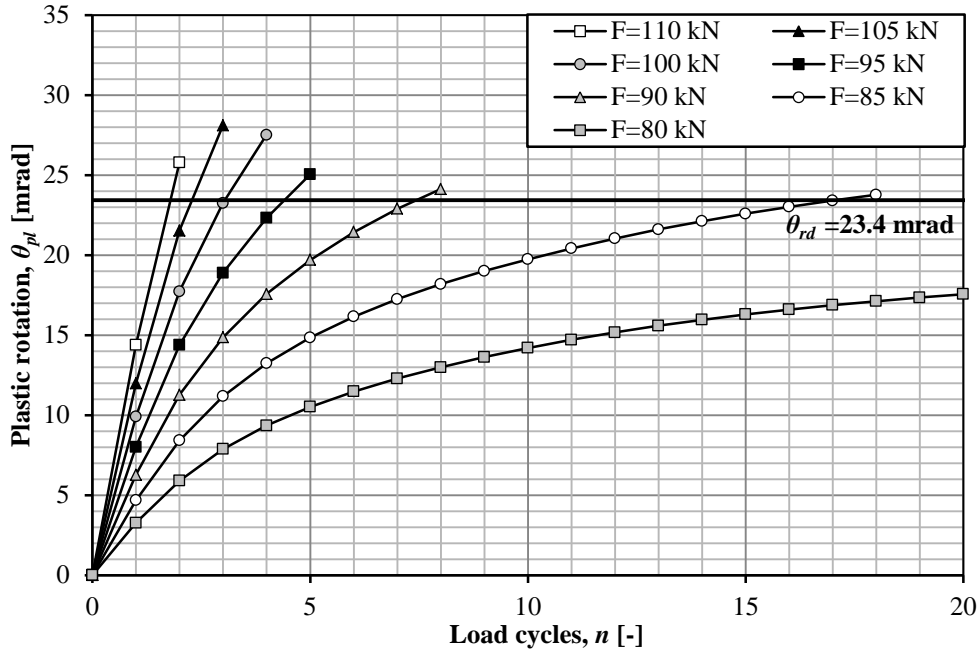
Figure 7.12   Plastic rotation for different magnitudes of moving concentrated forces.
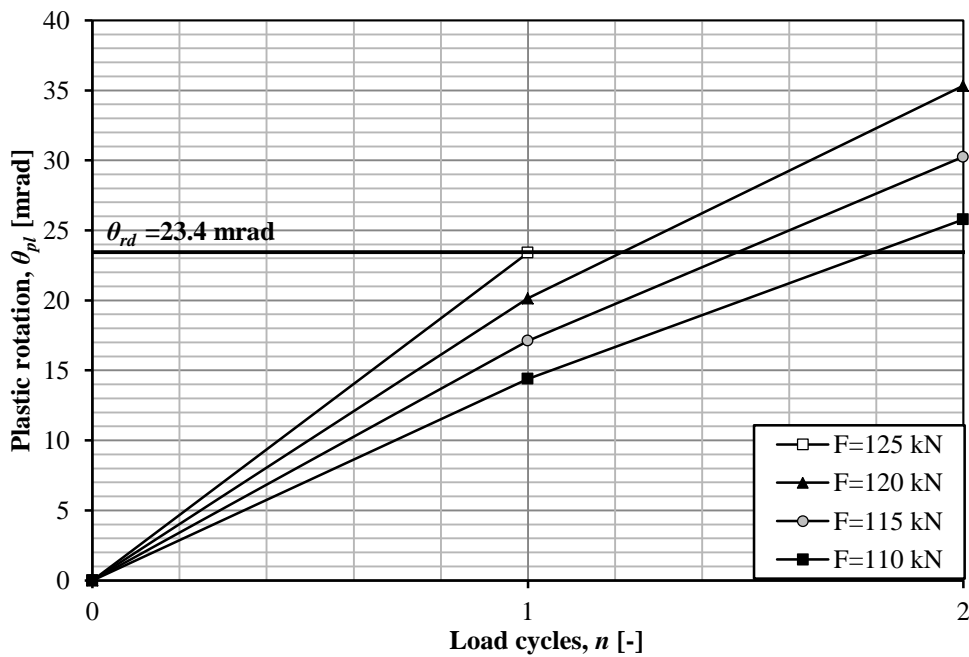
Figure 7.13   Plastic rotation for different magnitudes of moving concentrated forces.

It is also here clear that the magnitude of the applied force F had a substantial influence on the number of load cycles the simply supported slab could sustain before the occurrence of failure due to plastic rotation. The number of load cycles to failure n_u for different magnitudes of the total force is shown in Figure 7.14.

CHALMERS, *Civil and Environmental Engineering*, Master's Thesis 2014:73
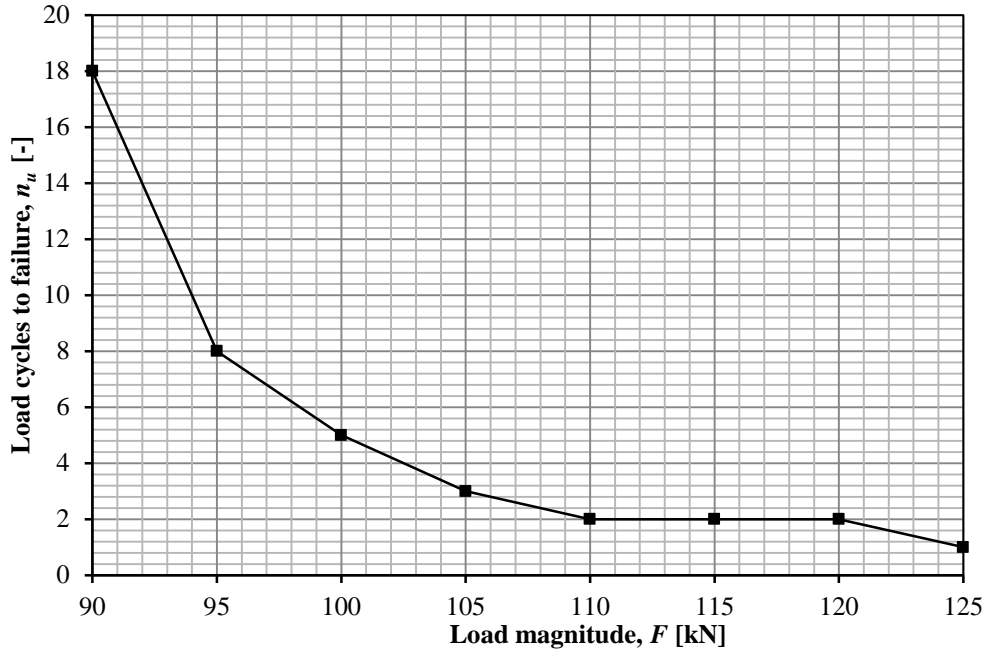
Figure 7.14 *Number of load cycles to failure for different magnitudes of moving concentrated forces.*

As in the case of the cantilever structure, plastic rotation for a certain load magnitude was obtained during the early load cycles while an increased number of load cycles approached a stable value of the plastic rotation. The plastic rotation approached a stable state where the occurrence of failure was unlikely to take place within a number of load cycles that could be analysed in this Thesis.

The critical force F_{crit} was in the case of a single static moving concentrated force somewhere between 80 kN and 85 kN. This behaviour can be seen in Figure 7.15.
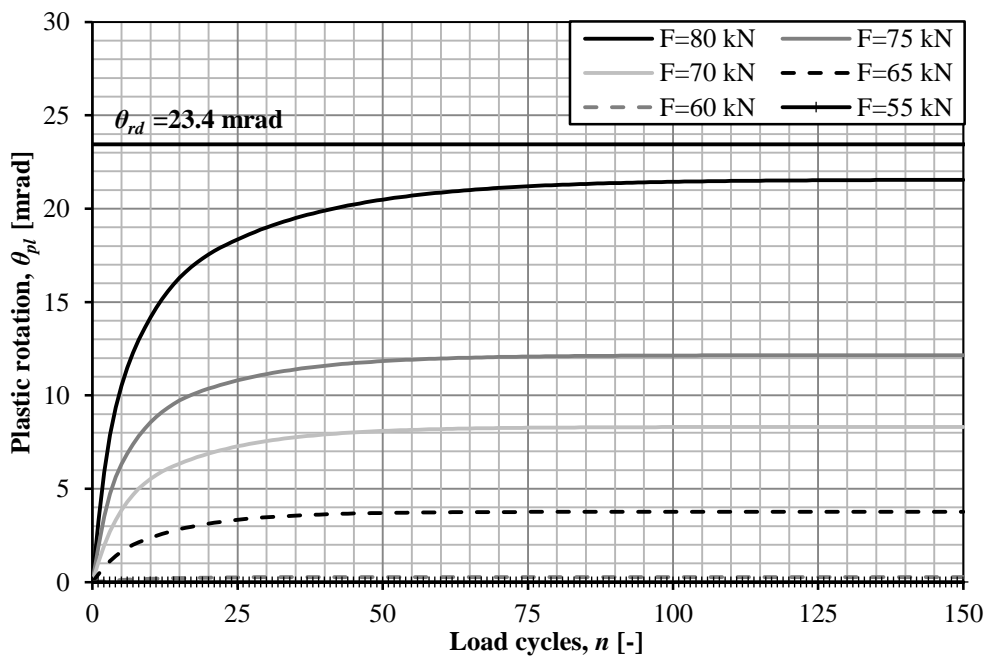
Figure 7.15 *Plastic rotation for different magnitudes of moving concentrated forces.*

The reason for the phenomenon shown in Figure 7.15 is the same as described in Section 6.3.1 for the cantilever structure.

The theory shown in Figure 6.21 in Section 6.3.1 was investigated for a moving concentrated force with a magnitude of 70 kN for an increasing number of load cycles. The plastic rotation along the centre of the slab is shown in Figure 7.16 where it is clearly visible that the simply supported slab approached a linear elastic behaviour with an increased number of load cycles. As for the cantilever slab, it can be seen that the plastic rotation did not reach its maximum in the centre of the slab during the early load cycles. It is also clear that the simply supported structure demanded a greater number of load cycles before the maximum plastic rotation was found in the centre of the slab. The reason for this was assumed to be derived from how the forces were applied and the reason for the overall behaviour can be found in Section 6.3.1.
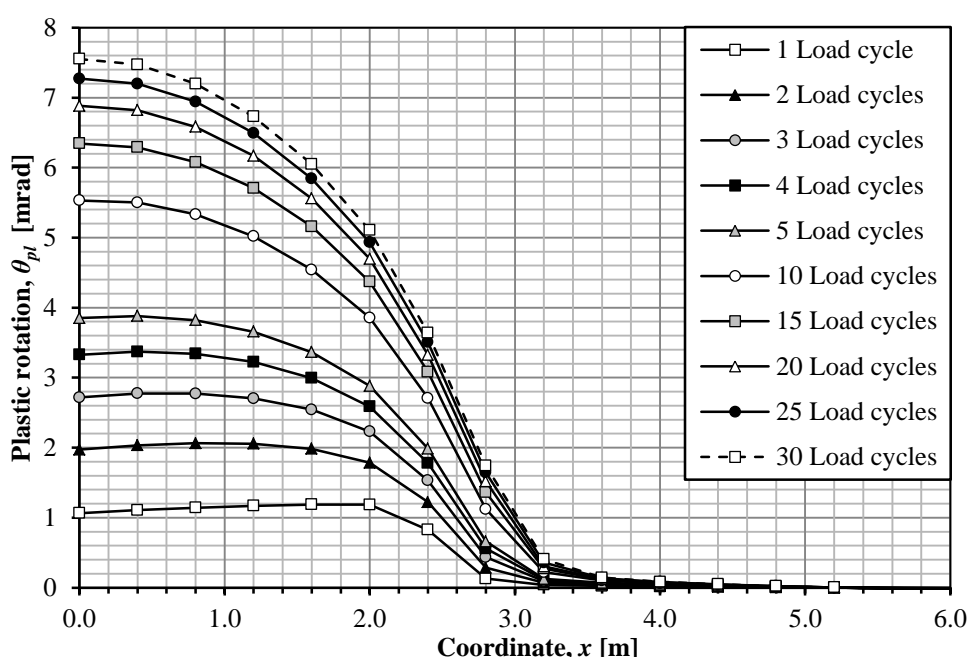
Figure 7.16 Development of plastic rotation θ_{pl} along the centre line for a load magnitude of 70 kN.

7.3.2 Load magnitudes – Varying

The analyses for the constant load magnitudes for a single moving concentrated force illustrated how the plastic rotation developed in the simply supported structure. As described in Section 6.3.2, the case where a bridge structure is subjected to a constant force above the serviceability limit state must be considered as an extreme case. The simply supported structure was therefore subjected to two different load combinations, LC_A and LC_B. The same approach and notations used in the case of the cantilever structure in Section 6.3.2 was used for these analyses.

The load combinations and how these are defined was discussed in Section 6.3.2 and are here presented without further discussion as a support for the results presented below. Load combination LC_{A1} is here again defined in Equation (7-5) and is illustrated in Figure 7.17. Load combination LC_{A2} is here again defined in Equation (7-6) and is illustrated in Figure 7.18.

$$F_{1,n=1} > F_{2,n=5} \tag{7-5}$$
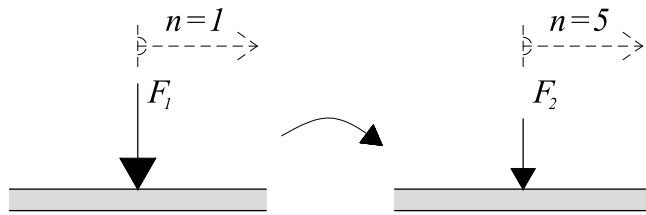
Figure 7.17   Load combination A$_1$, LC$_{A1}$

$$F_{1,n=5} < F_{2,n=1} \tag{7-6}$$
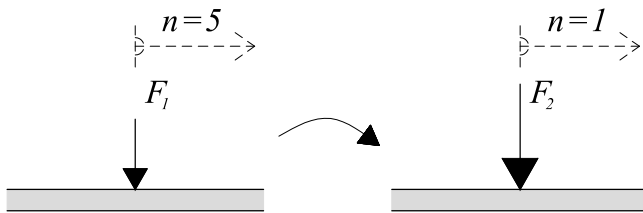
Figure 7.18   Load combination A$_2$, LC$_{A2}$

The magnitude of the larger force was set to 110 kN and the magnitude of the inferior force was set to a range of 60 kN to 90 kN. The background of the chosen range of the load magnitudes for the load combinations was treated in Section 6.3.2.

As can be seen in Figure 7.19, and which have been observed for the cantilever structure, the development of plastic rotation is dependent on the load history.
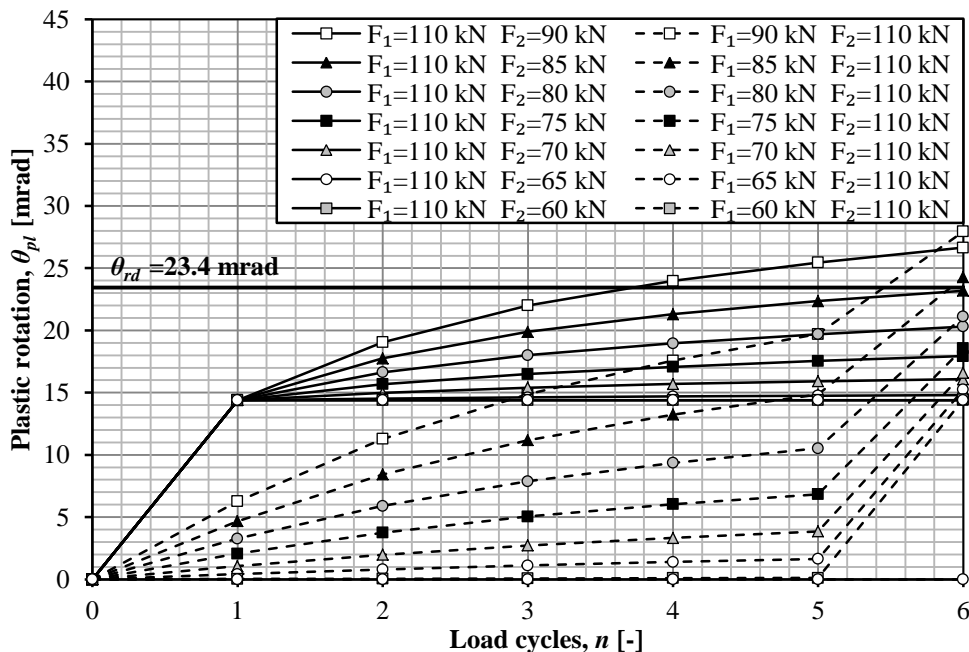
Figure 7.19   Plastic rotation for varying magnitudes of moving concentrated forces for six load cycles.

It is clear from Figure 7.19 that there is a small, but noticeable, difference in plastic rotation after six load cycles between the two different load combinations. The plastic

rotation was also here measured after six load cycles the difference was calculated according to Equation (6-13), defined in Section 6.3.2. The difference is shown in in Figure 7.20 and the reader is referred to Appendix H for tabulated values.
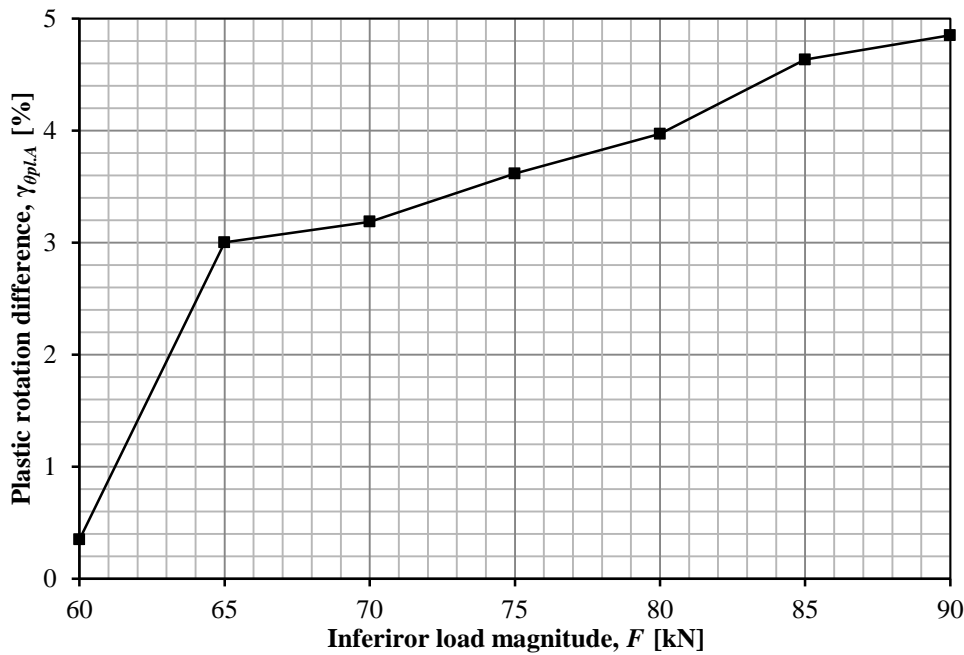
Figure 7.20   Difference in plastic rotation $\gamma_{\theta pl.A}$ between load combination A_1 and A_2, shown in percent for different magnitudes of the inferior forces.

The second load combination, LC_B consisted of two constant loads of two different magnitudes, but applied in three steps. This load combination was also defined and discussed in Section 6.3.2 and are here presented without further discussion as a support for the results presented below.

$$F_1 = F_{1,n=3} = F_{2,n=2} \tag{7-7}$$

$$F_2 = F_{2,n=1} > F_1 \tag{7-8}$$
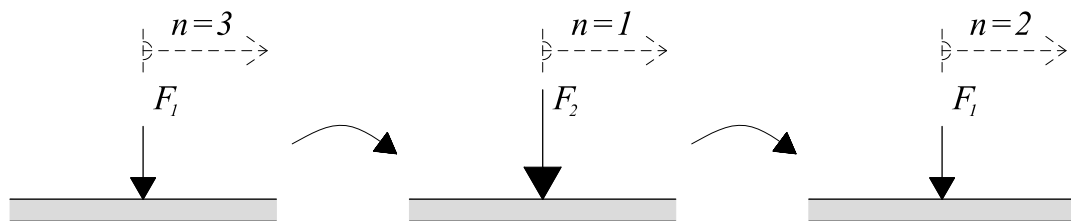
Figure 7.21   Load combination B, LC_B

The magnitudes of the larger and the smaller forces were the same as in the case of the first load combination, LC_A and were based on the same background theory.

It can be seen in Figure 7.22 that the behaviour of the slab approached the behaviour of a single moving concentrated force of 110 kN, which is reasonable.
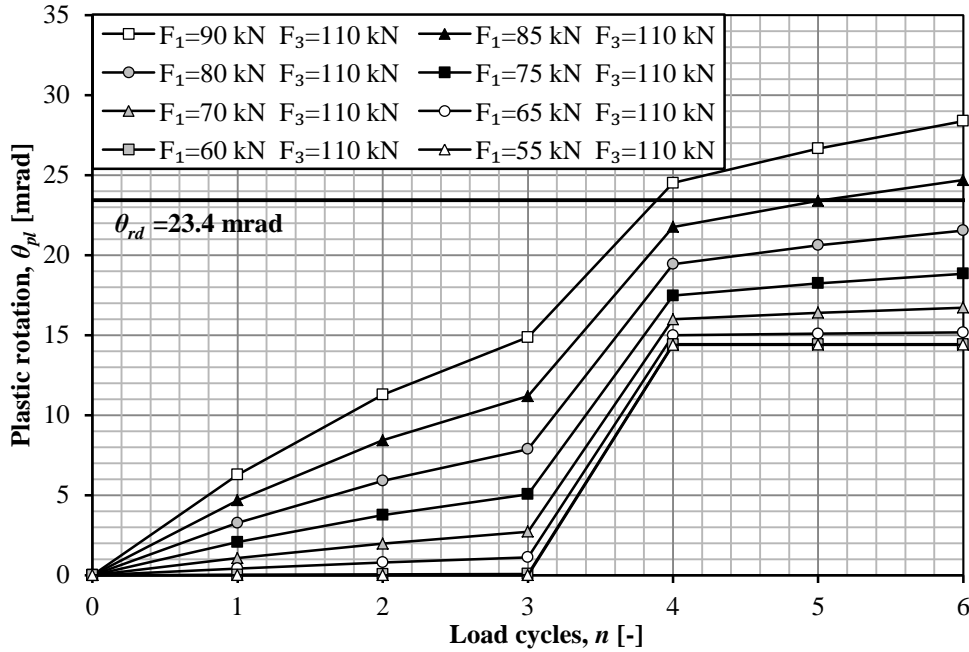
Figure 7.22 Plastic rotation for varying magnitudes of moving concentrated forces for six load cycles.

7.3.3 Comparison

In order to determine the most critical load combination with respect to plastic rotation that was studied in Section 7.3.2, these are compared in Figure 7.23. The comparison conducted in this section corresponds to the comparisons made in Section 6.3.3 and the reader is thus referred to that section for equations and definitions.
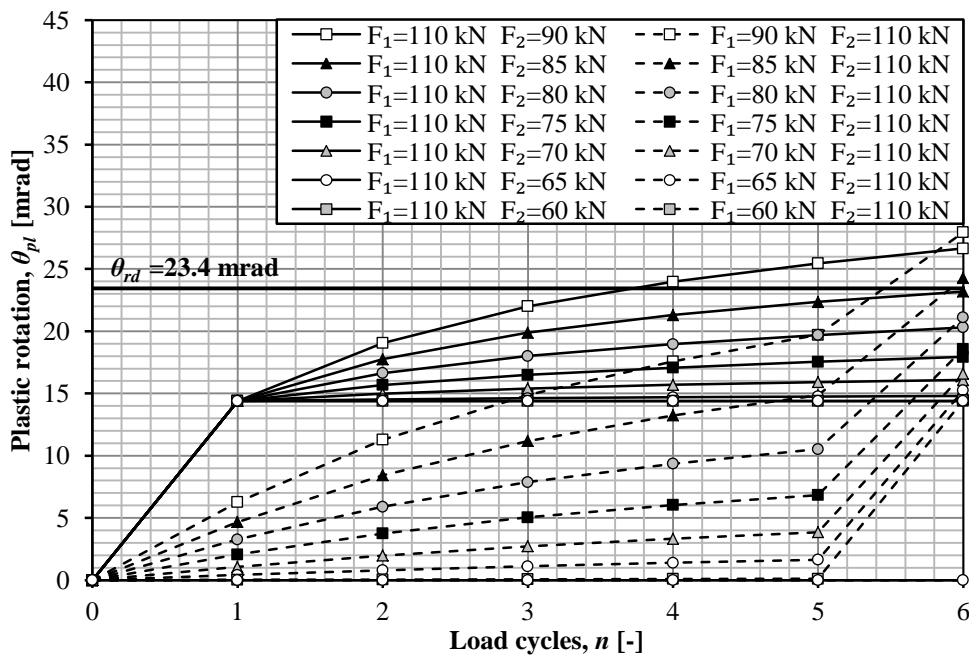
Figure 7.23 Plastic rotation for varying magnitudes of moving concentrated forces for six load cycles.

It is clear from Figure 7.23 that there is a small, but noticeable, difference in plastic rotation after six load cycles between the three different load combinations. The plastic rotation was measured for load combination LC_{A1}, LC_{A2} and LC_B after six load cycles and the difference was calculated according to Equation (6-16) and (6-17), defined in Section 6.3.3. The difference is shown in in Figure 7.24 and the reader is referred to Appendix H for tabulated values.
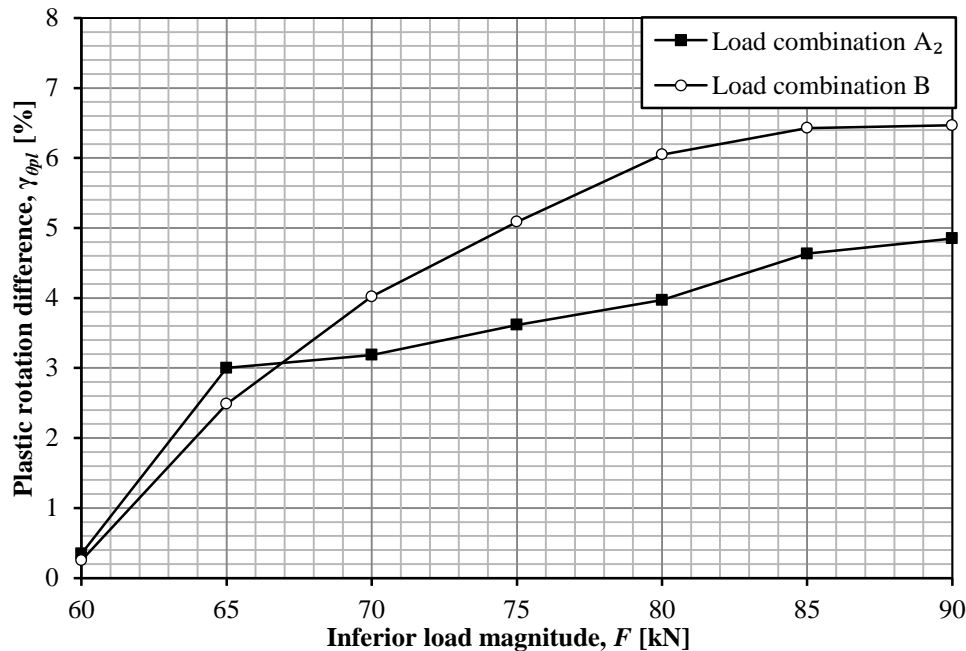
Figure 7.24 *Difference in plastic rotation $\gamma_{\theta pl}$ between load combination A_1, and load combination A_2 and B, shown in percent for different magnitudes of the inferior forces.*

It can be seen in Figure 7.24 that load combination LC_B resulted in the highest plastic rotation of the slab after six load cycles for inferior forces of a magnitude greater than 65 kN. For inferior forces of a magnitude below this value, load combination LC_{A2} yielded the highest plastic rotation of the slab after six load cycles. These results indicate that the most likely load combination of the structure, LC_B, for the majority of the investigated forces, was the one to cause the highest plastic rotation. This was also observed for the cantilever structure in Section 6.3.3.

It should also here be noted that the difference between the two load combinations is small and the results should therefore be treated with care.

7.3.4 Traditional superposition approach

As for the cantilever structure, it was clearly shown that the development of plastic rotation is dependent on the load history which indicates that a traditional superposition method is not recommended. The error of a superposition approach was here evaluated for the two load combinations LC_A and LC_B. The result from the superposition approach were obtained by merging results from Section 7.3.1 where all the loads were applied on an unloaded, simply supported slab. For the background theory of the superposition approach used in this section, the reader is referred to Section 6.3.4.

The development of plastic rotation for LC_{A1}, which was shown in Figure 7.19, was extended to 20 load cycles and is shown in Figure 7.25. The results for the different load magnitudes from Section 7.3.1 were used in order to obtain a plastic rotation development based on a superposition method. This is shown in Figure 7.26.
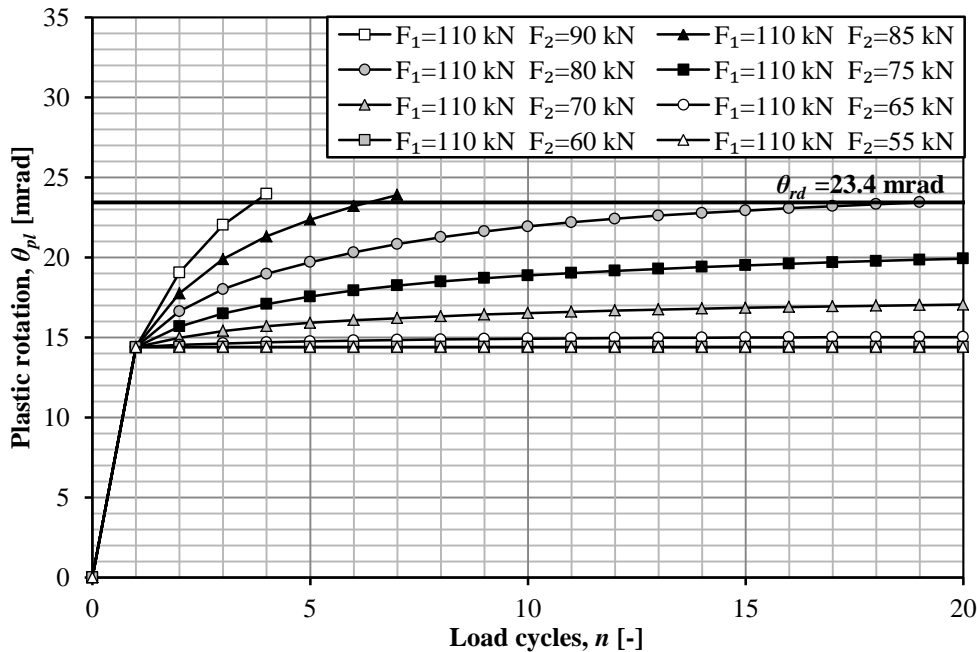
Figure 7.25   Plastic rotation for load combination LC_{A1}.
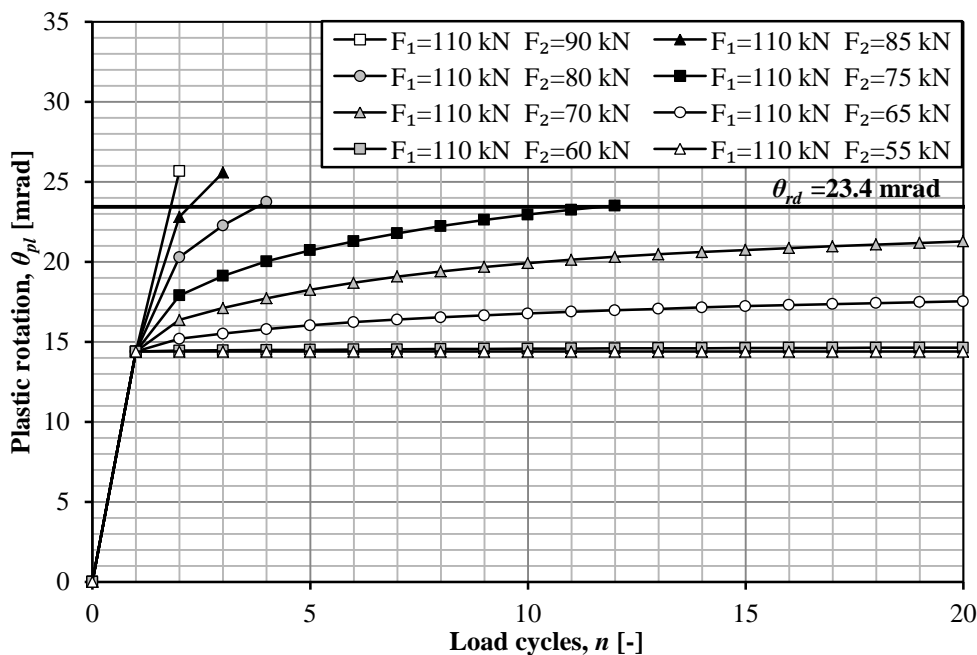
Figure 7.26   Plastic rotation for load combination LC_{A1}, based on a traditional superposition approach.

It is clear from Figure 7.25 and Figure 7.26 that there is a significant difference between the result from the analyses and the results from a superposition approach. The plastic rotation was measured after six load cycles and the difference was calculated according to Equation (6-18), defined in Section 6.3.4. The difference is shown in in Figure 7.27 and the reader is referred to Appendix H for tabulated values.
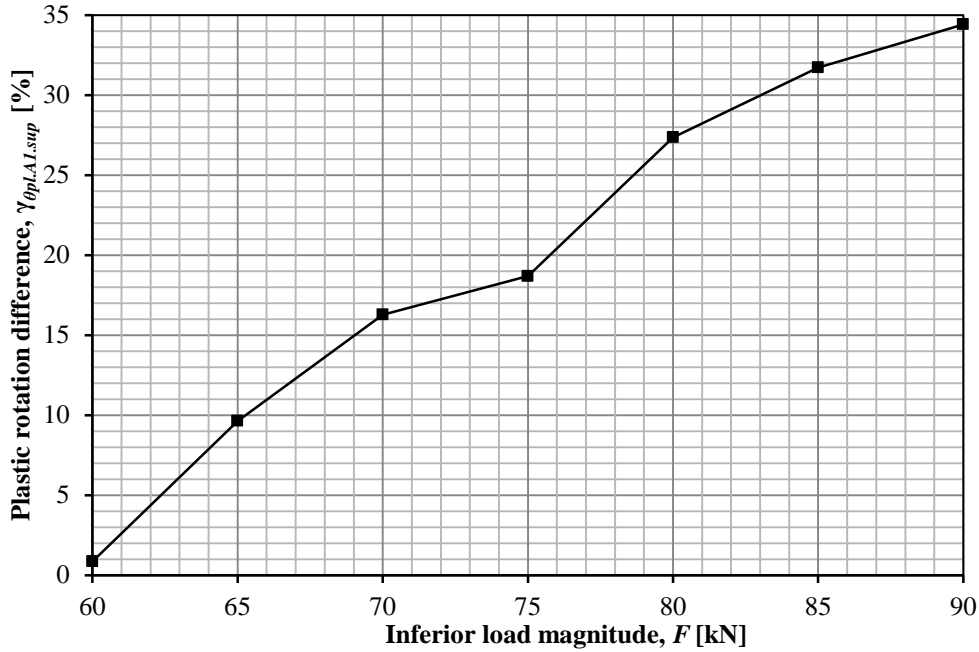
Figure 7.27 Difference in plastic rotation $\gamma_{\theta pl.A1.sup}$ for load application A_1 between results from an analysis and results from a superposition approach, shown in percent for different magnitudes of the inferior forces.

As can be seen in Figure 7.27, the value obtained for $F = 75$ kN exhibited a deviant behaviour. The analyses were thoroughly examined but no indication of an error was discovered. This value was however assumed to be amiss which influenced the results illustrated in Figure 7.30 and Figure 7.31.

The development of plastic rotation for LC_B, which is shown in Figure 7.22, is also shown in Figure 7.28 for comparison purposes. The plastic rotation development based on the superposition method is shown in Figure 7.29. The same superposition approach that was used for the load combination LC_{A1} was also used in this case.
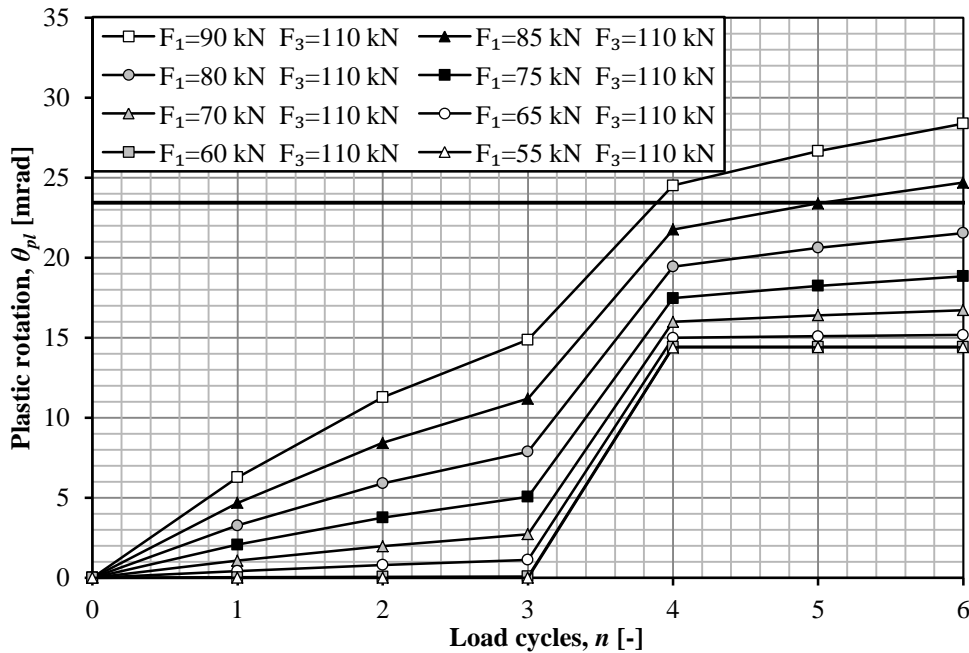
Figure 7.28 Plastic rotation for load combination LC_B.
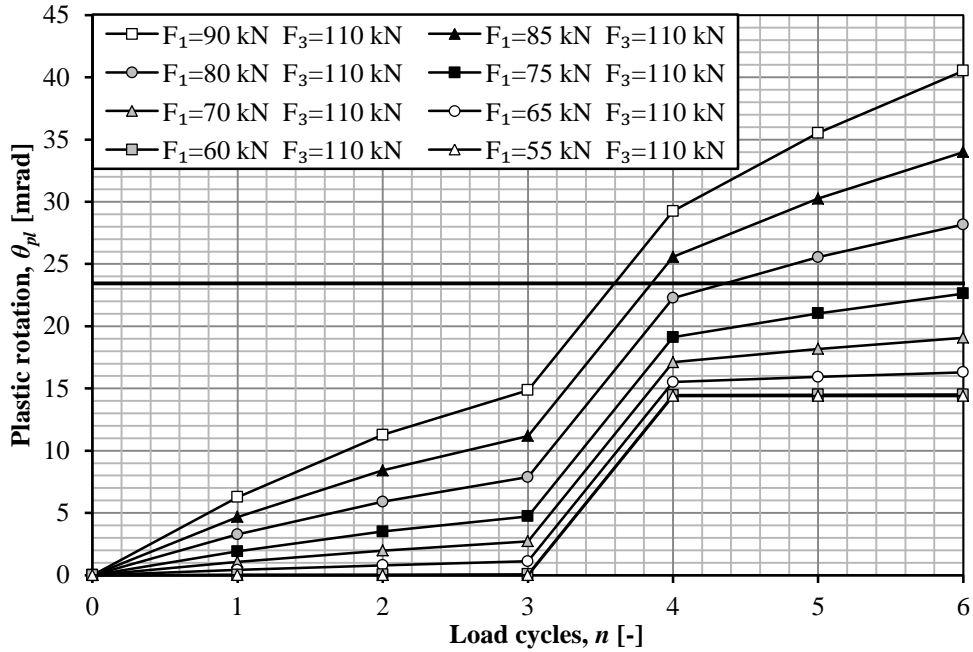
Figure 7.29 Plastic rotation for load combination LC$_B$, based on a traditional superposition approach.

It is clear from Figure 7.28 and Figure 7.29 that there is a significant difference between the result from the analyses and the results from a superposition approach. The plastic rotation was measured after six load cycles and the difference was calculated according to Equation (6-19), defined in Section 6.3.4. The difference is shown in Figure 7.30 and the reader is referred to Appendix H for tabulated values.
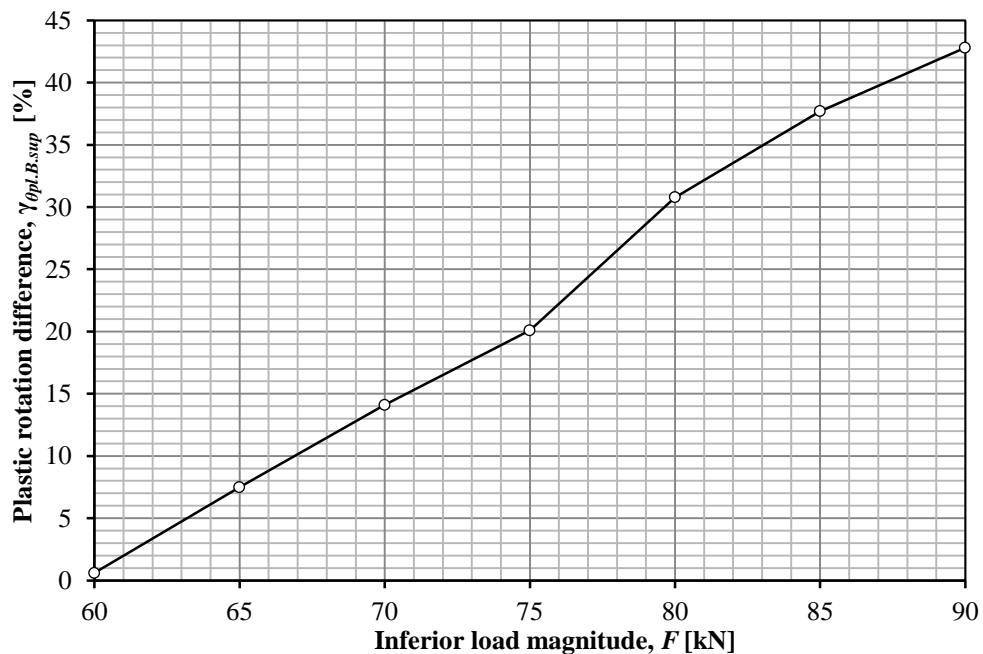
Figure 7.30 Difference in plastic rotation $\gamma_{\theta pl.B.sup}$ after six load cycles for load combination B between results from an analysis and results from a superposition approach.

If Figure 7.27 and Figure 7.30 are combined, the difference in percentage between the analyses and the superposition approach for load combination LC_A and LC_B can be shown in Figure 7.31.
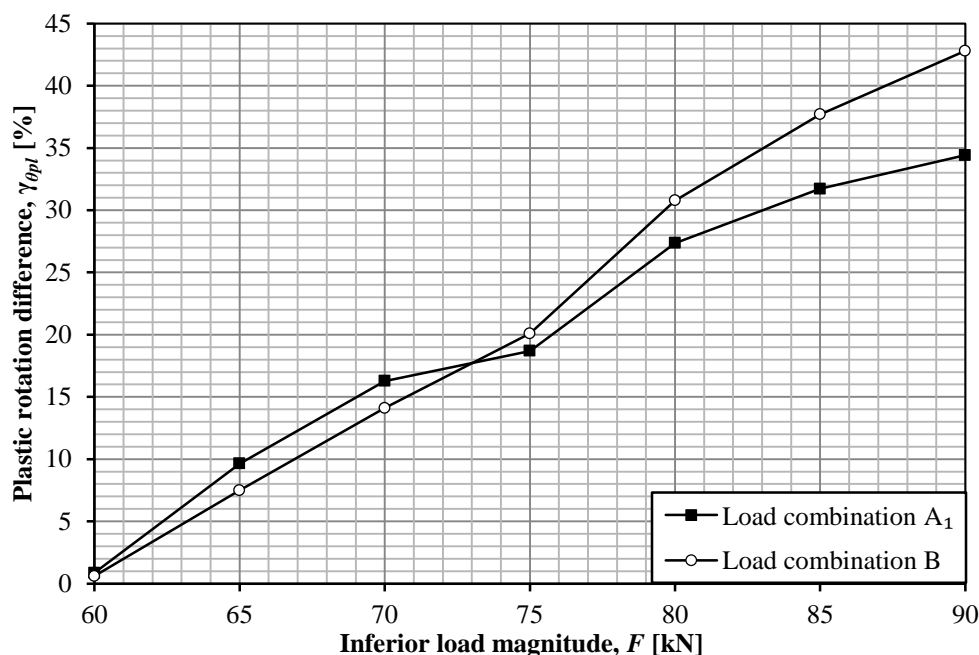
Figure 7.31 *Difference in plastic rotation $\gamma_{\theta pl.sup}$ for load combination A_1 and B between results from an analysis and results from a superposition approach, shown in percent for different magnitudes of the inferior forces.*

It is clear that the superposition approach overestimated the plastic rotation in the structure for both load combination LC_A and LC_B. This was also shown for the cantilever structure in Section 6.3.4 and was expected since the adaptation of the slab due to repeated loading was not fully captured by the superposition approach. The difference in plastic rotation between the analyses and the superposition approach was greater for load combination LC_B for larger loads and for LC_A for loads of smaller magnitudes.

In the case of the cantilever structure in Section 6.3.4, load combination LC_B yielded a larger difference in plastic rotation than load combination LC_A. The reason for the difference was believed to be derived from the fact that the plastic rotation from each load was overestimated and load combination B consisted of three separate loads instead of two separate loads which was the case for load combination A. This was obviously not the case for all magnitudes of the inferior forces for the simply supported structure. It can however be seen that the difference increased with an increased value of the inferior force which was the case for the cantilever structure.

7.4 Response of two moving forces – Equal magnitudes

The slab in this analysis was modelled with the same geometry and moment-curvature relations as the slab in Section 7.3. The results obtained in this section corresponded well to those obtained in Section 6.4 for the cantilever structure. The results are therefore presented here in a more compact form and the reader is referred to Section 6.4 for comparison and additional information regarding the analyses.
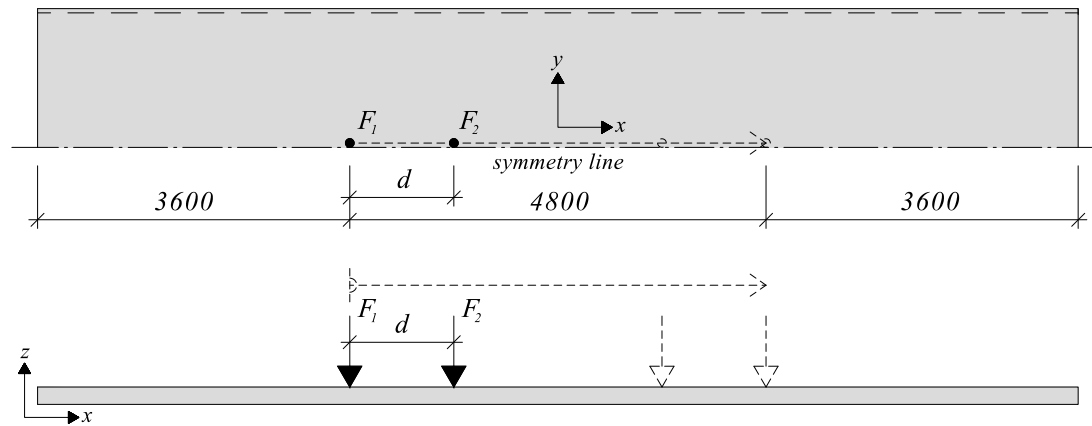
Figure 7.32   Geometry and dimensions of the studied simply supported slab for two concentrated forces.

The modelling choices and moment-curvature relation from the analysis of a single static moving concentrated force was also used in this analysis.

The sum of the loads applied on the slab in this analysis differed between the distances d between the pair of concentrated forces. The distance between the forces was altered according to Equation (7-9) and the influence of this parameter is treated in Section 7.4.1 to 7.4.3.

$$d = \begin{bmatrix} 1.2 \, 1.6 \, 2.0 \end{bmatrix} \text{m} \tag{7-9}$$

7.4.1 Constant distance, $d = 1.2$ m

In the case of a constant distance of $d = 1.2$ m, the applied forces F_1 and F_2 varied according to the following magnitudes:

$$F_1 = F_2 = \begin{bmatrix} 40 \, 45 \, 50 \, ... \, 65 \, 70 \, 75 \end{bmatrix} \text{kN} \tag{7-10}$$

Where:

$$F_{tot} = F_1 + F_2 \tag{7-11}$$

As in the case of a single moving concentrated force, the analyses were conducted with 150 load cycles n for each pair of concentrated forces if failure of the simply supported slab did not occur within this range. The plastic rotation in the centre of the slab for different magnitudes of forces is shown in Figure 7.33.
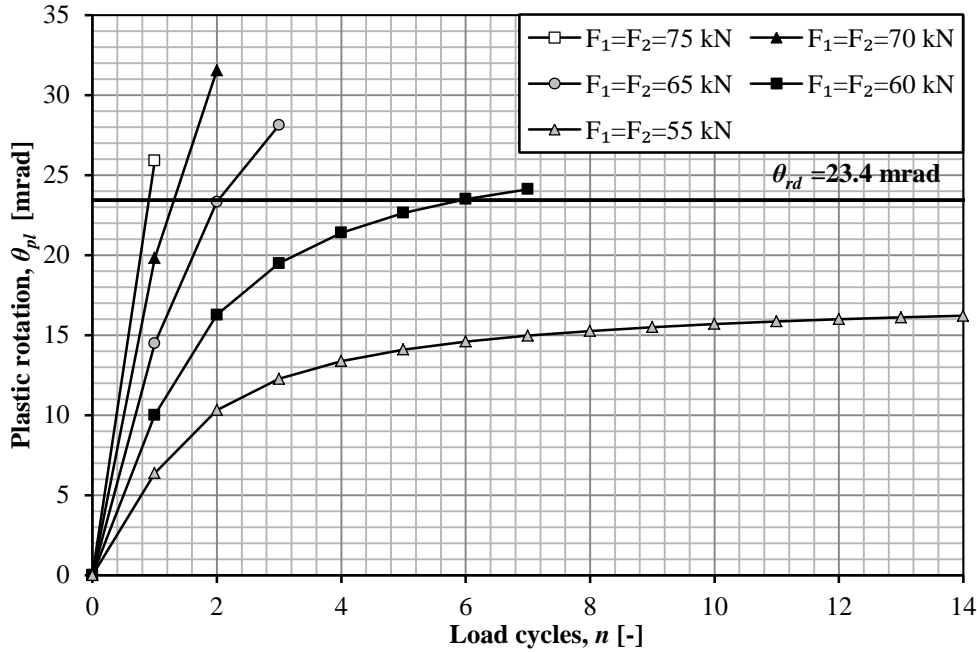
Figure 7.33 Plastic rotation for different magnitudes of a pair of moving concentrated forces.

The number of load cycles to failure n_u for different magnitudes of the applied forces is shown in Figure 7.34.
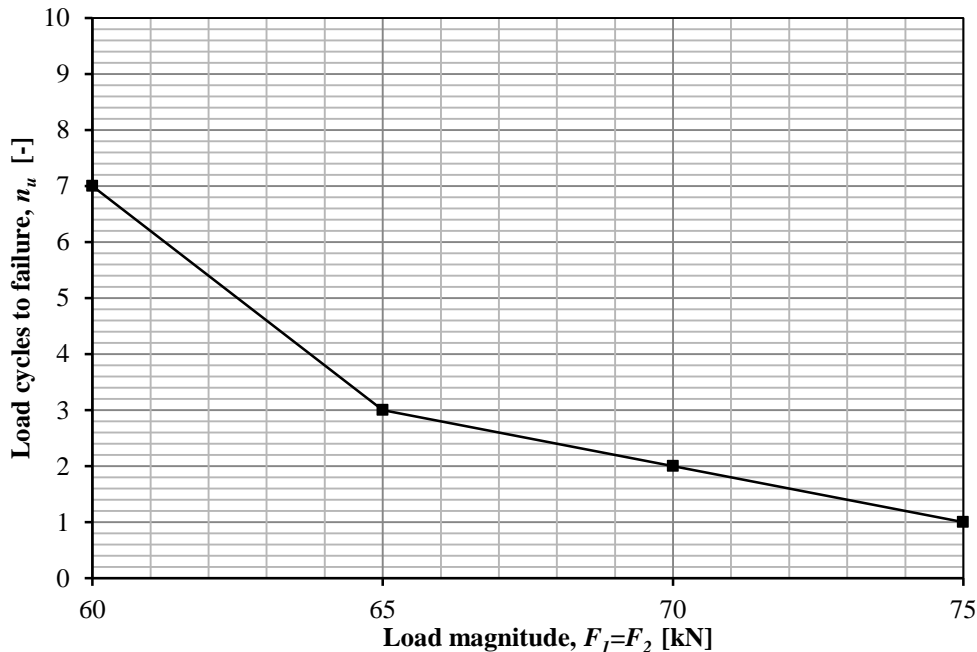
Figure 7.34 Number of load cycles to failure for different magnitudes of a pair of moving concentrated forces for d = 1.2 m.

As in the case of a single moving concentrated force, the plastic rotation approached a stable value where the occurrence of failure was unlikely to occur within the number of load cycles studied in this Thesis. This was the case when the total force was below the critical force F_{crit} which in this case was somewhere between 55 kN and 60 kN. The reason for this phenomenon was described in Section 6.3.1.
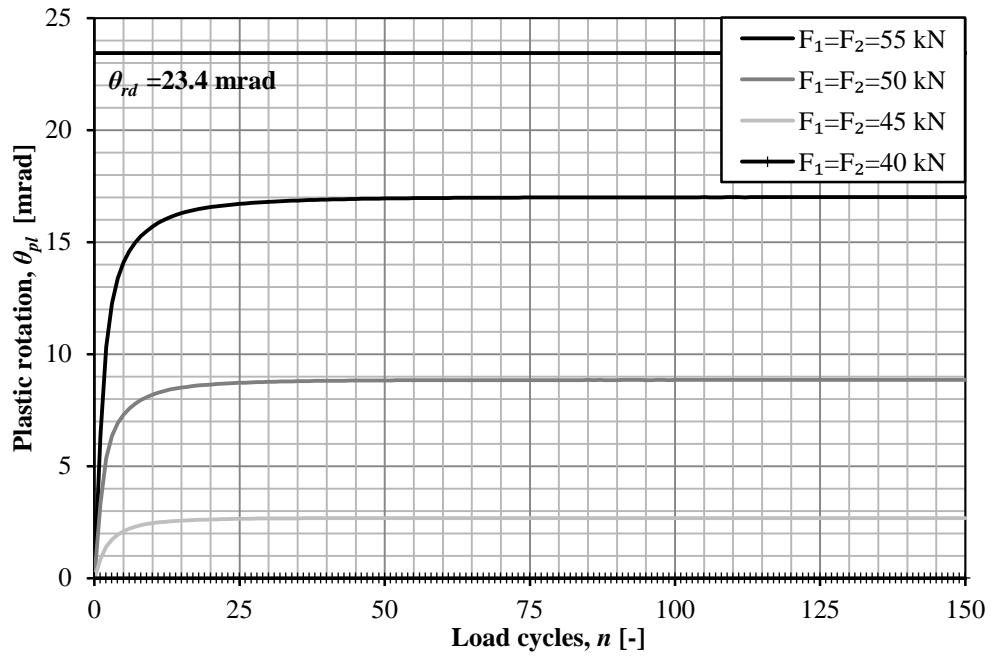
Figure 7.35 Plastic rotation for different magnitudes of a pair of moving concentrated forces

7.4.2 Constant distance, $d = 1.6$ m

In the case of a constant distance of $d = 1.6$ m, the applied forces F_1 and F_2 varied according to the following magnitudes:

$$F_1 = F_2 = [45\ 50\ 55\ ...\ 70\ 75\ 80]\ \text{kN} \tag{7-12}$$

The plastic rotation in the centre of the slab for different magnitudes of forces is shown in Figure 7.36.
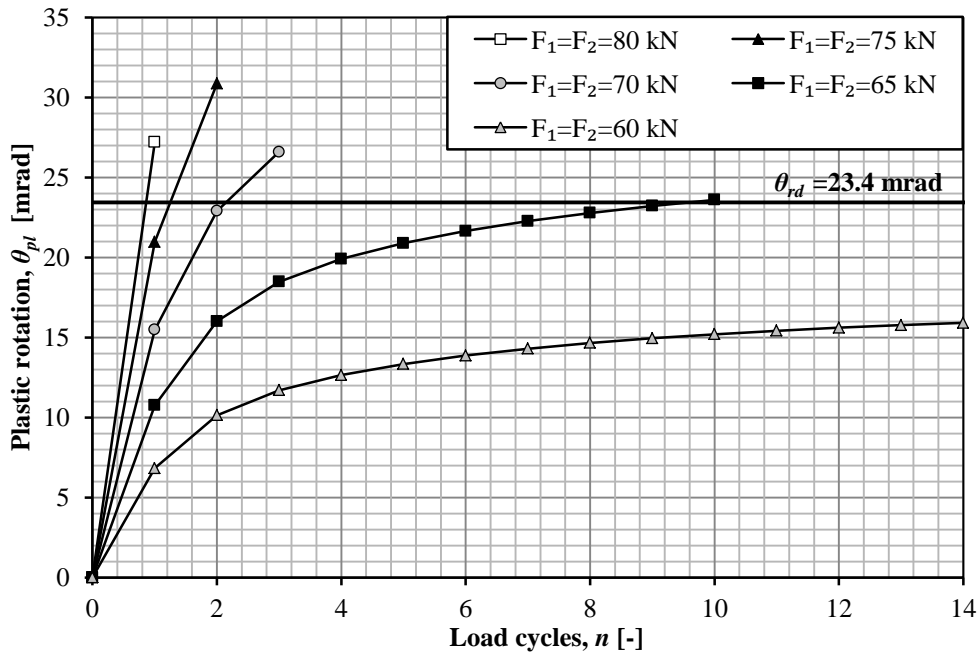
Figure 7.36 Plastic rotation for different magnitudes of a pair of moving concentrated forces.
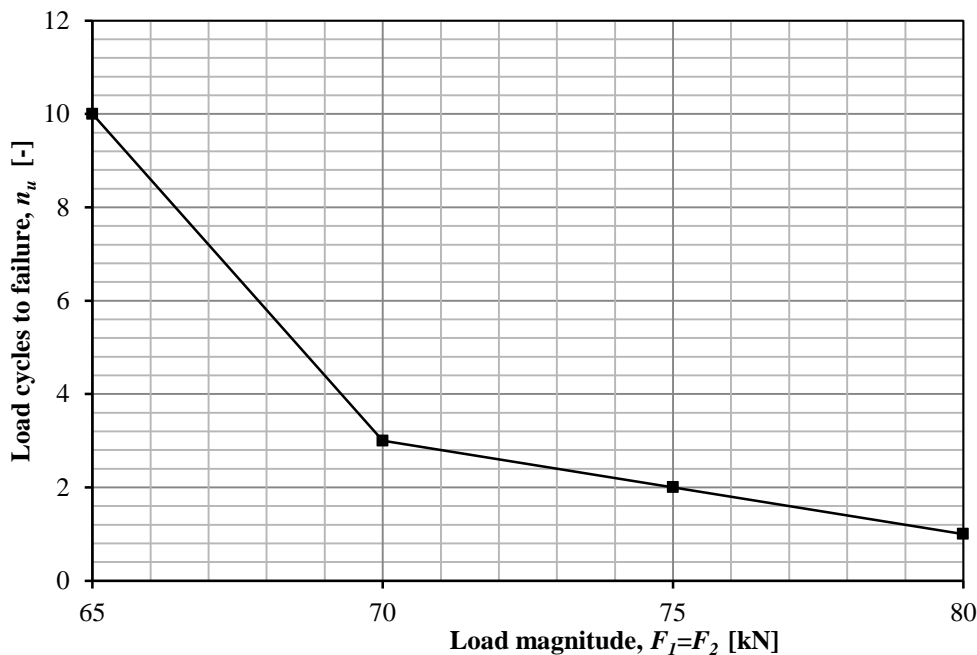
Figure 7.37 Number of load cycles to failure for different magnitudes of a pair of moving concentrated forces for $d = 1.6$ m.

The critical force F_{crit} was in this case somewhere between 60 kN and 65 kN.
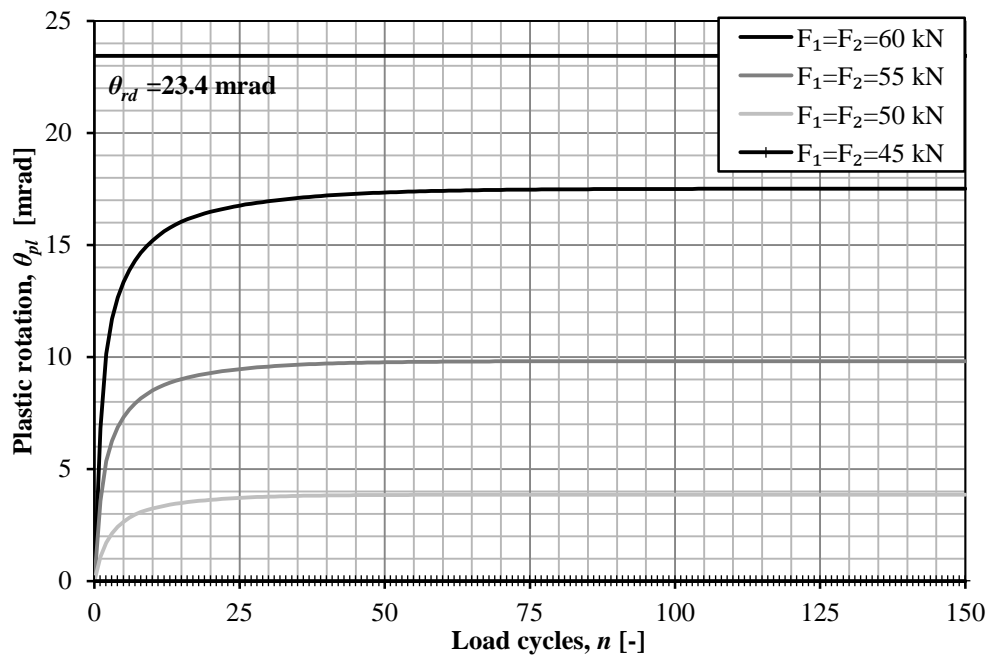
Figure 7.38 Plastic rotation for different magnitudes of a pair of moving concentrated forces.

7.4.3 Constant distance, $d = 2.0$ m

In the case of a constant distance of $d = 2.0$ m, the applied forces F_1 and F_2 varied according to the following magnitudes:

$$F_1 = F_2 = [45\ 50\ 55\ ...\ 75\ 80\ 85]\ \text{kN} \tag{7-13}$$

The plastic rotation in the centre of the slab for different magnitudes of forces is shown in Figure 7.41
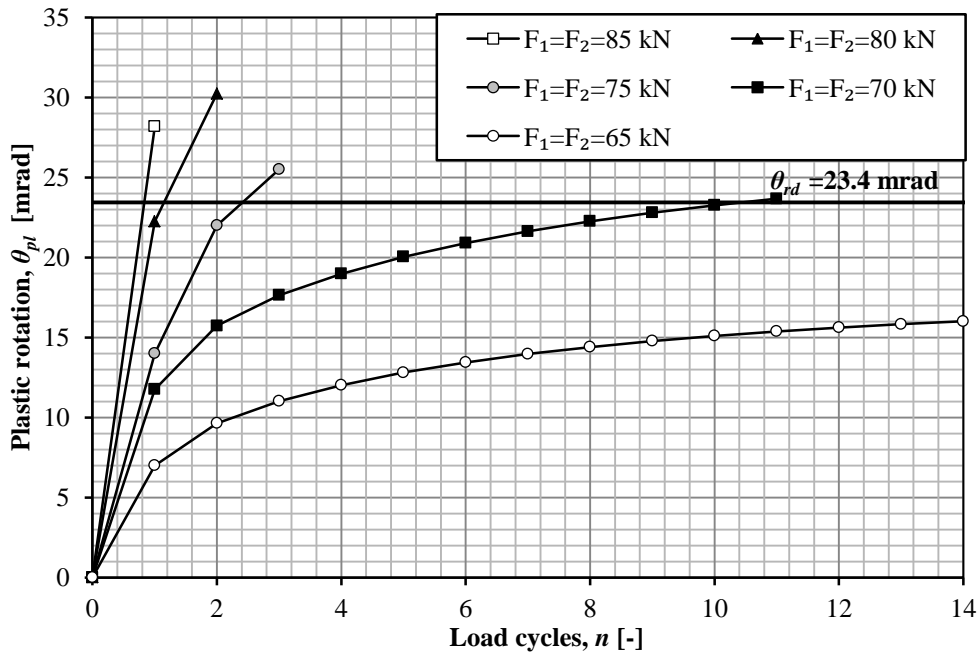
Figure 7.39   Plastic   rotation   for   different   magnitudes   of   a   pair   of   moving concentrated forces.
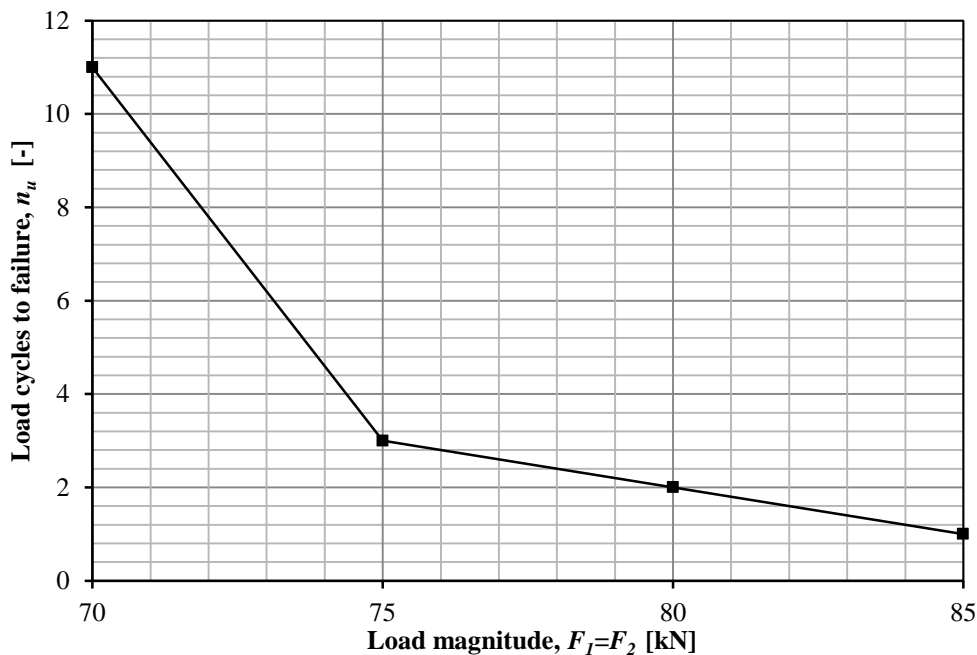
Figure 7.40   Number of load cycles to failure for different magnitudes of a pair of moving concentrated forces for $d = 2.0$ m.

The critical force F_{crit} was in this case somewhere between 65 kN and 70 kN.
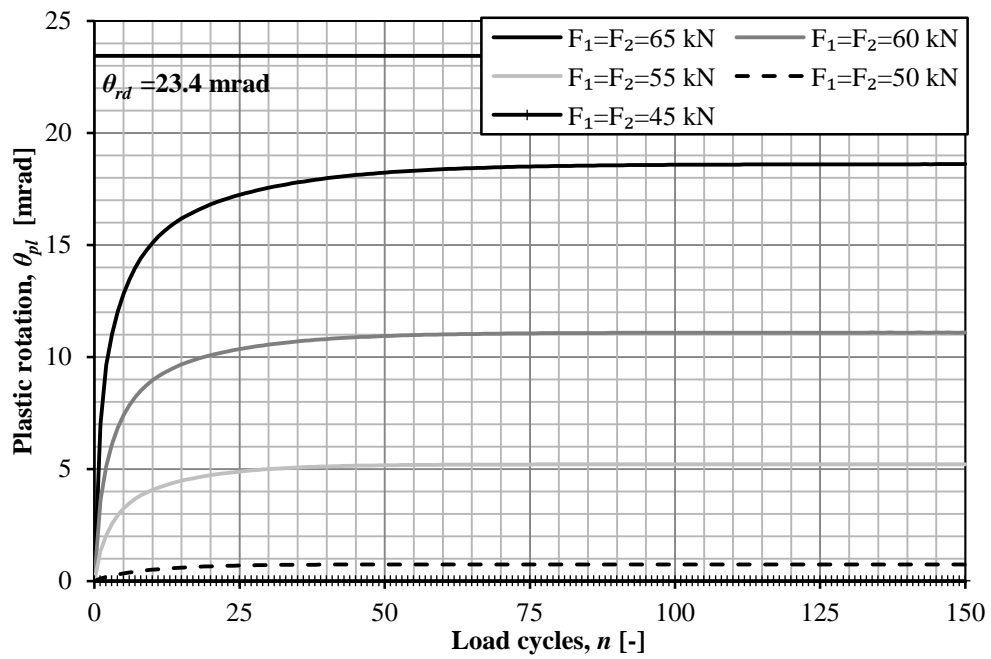
Figure 7.41 Plastic rotation for different magnitudes of a pair of moving concentrated forces.

7.4.4 Comparison

In order to compare the plastic rotation caused by the different loads and load magnitudes, the number of load cycles to cause failure n_u was compared with the total load magnitude F_{tot} from Equation (7-11) for the different loads applied on the simply supported slab. This behaviour is shown in Figure 7.42. The methodology used in this section was kept from Section 6.4.4 which the reader is referred to for comparison and additional information.
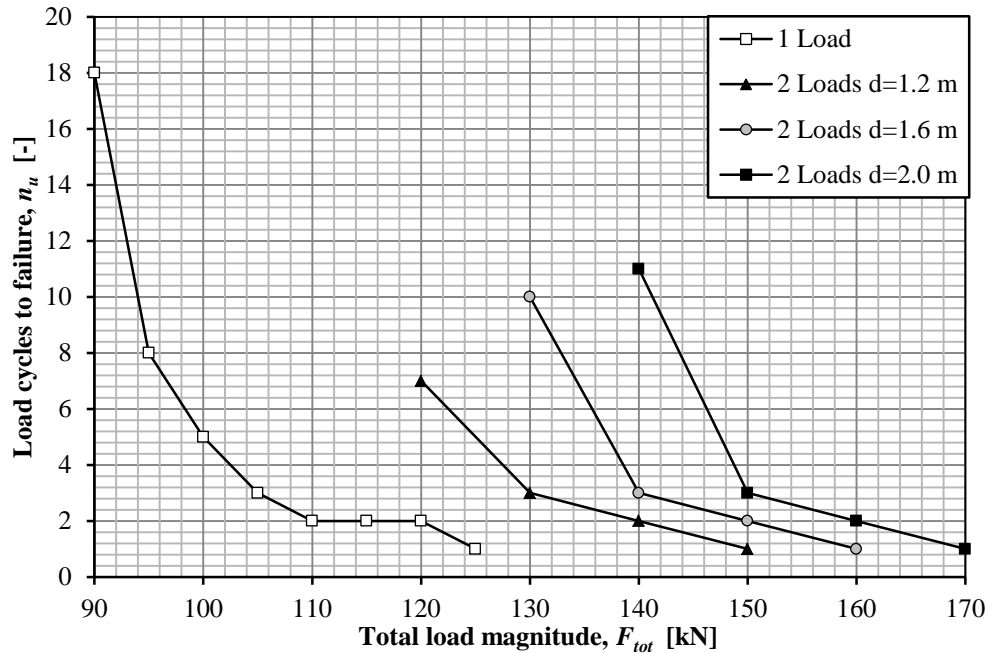
Figure 7.42   Number of load cycles to failure for different loads and load magnitudes.

It is clearly shown in Figure 7.42 that was is advantageous for the simply supported slab, from the perspective of plastic rotation, with an increased distance between a pair of concentrated forces. It is also clearly shown that the case of two concentrated forces was advantageous in comparison to the case of a single moving concentrated force with the same load magnitude. As the concentrated force was separated into two forces and the distance between those two increased, the total load magnitude and number of load cycles to failure increased.

In order to compare the number of load cycles to cause failure for the different loads and load magnitudes, a load magnitude factor $\gamma_{\theta plu.F}$ was defined as in Section 6.4.4:

$$\gamma_{\theta plu.F} = \frac{F_{tot}(n_u)}{F_{el}} \tag{7-14}$$

Where F_{tot} = the total applied force

$\quad\quad\quad F_{el}$ = the force of greatest magnitude not to cause any plastic rotation for a single moving concentrated force, in this case 55 kN

$\quad\quad\quad n_u$ = the number of load cycles to failure for each applied force

It was possible, from this relation, to predict the vulnerability of the slab, i.e. how much the moving concentrated forces could be increased in magnitude before failure due to plastic rotation occurs. This relation is shown in Figure 7.43.
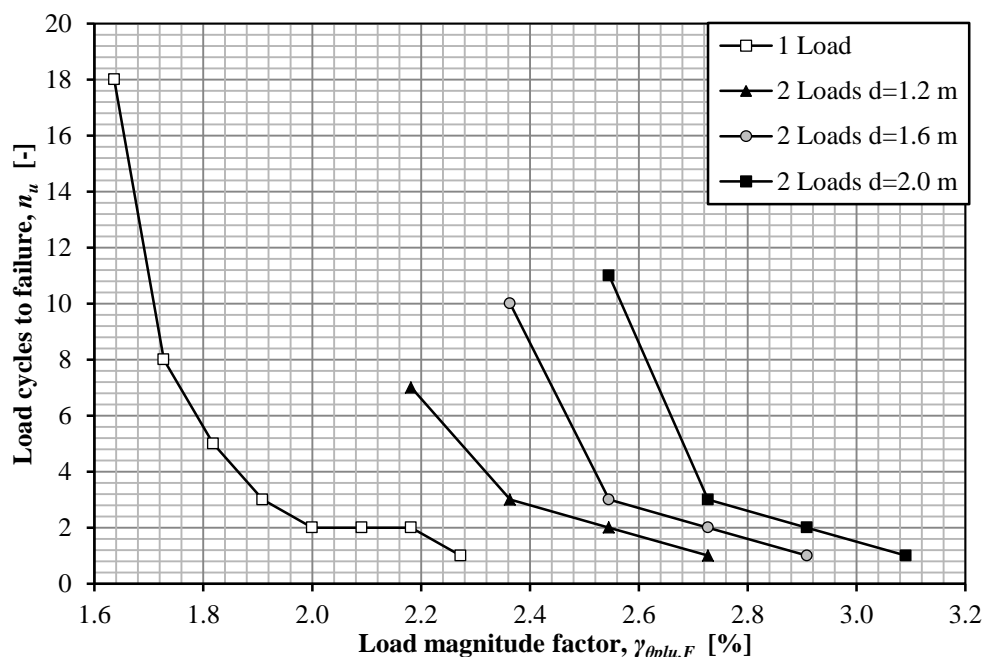
Figure 7.43 Number of load cycles to failure for a load magnitude factor $\gamma_{\theta plu.F}$ related to the load F_{el}.

It can be seen in Figure 7.43 that the moving concentrated force of the highest magnitude not to cause any plastic rotation in the structure could be increased by 63 % before failure of the simply supported slab occurred within 150 load cycles. If the total force was separated into two concentrated forces with a distance of 1.2 m instead, the total applied load could be increased by 118 % before failure of the simply supported slab occurred within 150 load cycles. An increase of the distance between the two concentrated forces generated an increase in total load magnitude before failure occurred.

As in the case of the cantilever structure in Section 7.4, it is reasonable to assume that there is a distance d between the pair of moving concentrated forces such that the simply supported structure experiences the force pair as two single forces. This behaviour was not studied for this structure due to the limited timeframe of this Thesis. It is however reasonable to assume that the smallest distance d_{crit} for the slab to experience the force pair as two single forces is smaller than the critical distance for the cantilever structure. This can be derived from Figure 7.43 where it is clearly shown that the applied forces can be significantly more increased that the forces for the cantilever structure and thus have an advantageous distribution of the plastic rotation.

7.5 Response of two moving forces – Different magnitudes

The slab shown in Figure 7.32 was in this analysis subjected to a number of forces F of different magnitudes in order to study the influence of such load combinations. The methodology used in this section was kept from Section 6.5 and is therefore presented here in a more compact form. In order to study the influence of varying load magnitudes within the pair of moving concentrated forces, the total applied force F_{tot} was set to:

$$F_{tot} = F_1 + F_2 = 120 \text{ kN} \tag{7-15}$$

Where:

$$F_1 \neq F_2 \tag{7-16}$$

$$F_1 = \begin{bmatrix} 10 \ 20 \ 30 \ 40 \ 50 \end{bmatrix} \text{kN} \tag{7-17}$$

$$F_2 = \begin{bmatrix} 110 \ 100 \ 90 \ 80 \ 70 \end{bmatrix} \text{kN} \tag{7-18}$$

Where F_1 was the second force of the force pair to load the slab which can be seen in Figure 7.32. The magnitude of the force F_2 was, for this load application order, always greater than the force F_1 according to Equation (7-19) and Figure 7.44

$$F_1 < F_2 \tag{7-19}$$
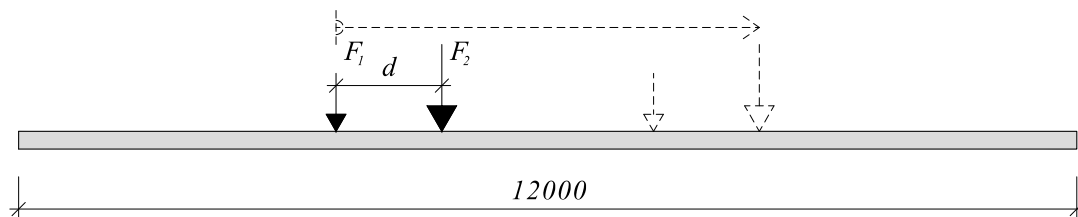
Figure 7.44   The first load application order LAO$_1$ of the studied slab.

The plastic rotation caused by the applied force pair was not significantly influenced by the load application order. A study of this influence is treated in Appendix E and the analyses in this section follow the first load application order, LAO_1, which is stated in Equation (7-15) to (7-19).

7.5.1 Constant distance, d = [1.2 1.6 2.0] m

The distance d between the force pair applied on the cantilever slab was kept from the previous analyses in Section 7.4 and the results from the analyses are shown in Figure 7.45 to Figure 7.47:
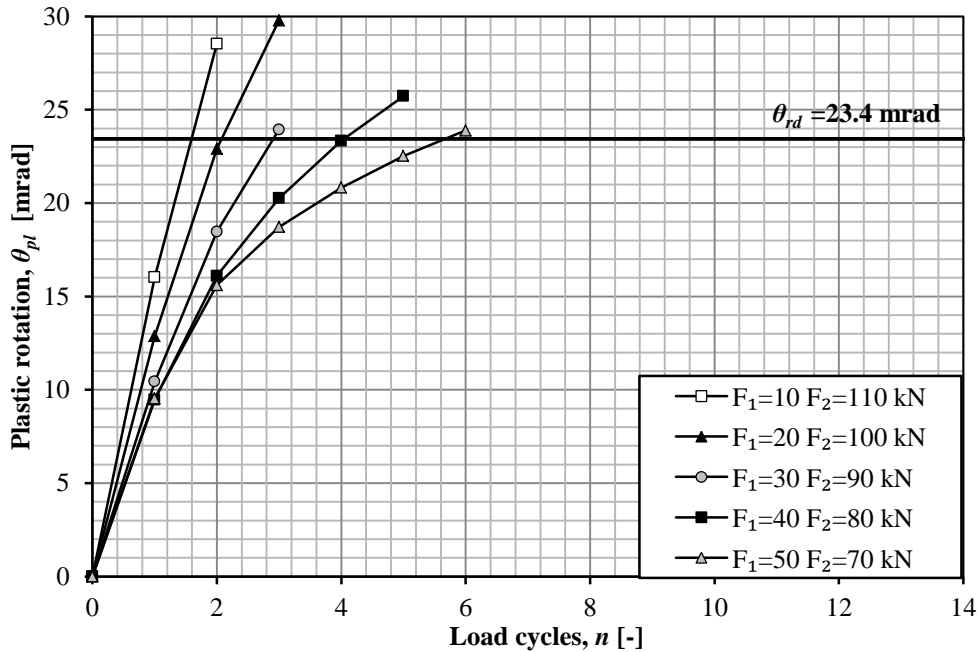
Figure 7.45   Plastic rotation for different load combinations of a pair of moving concentrated forces of varying magnitudes for d = 1.2 m.
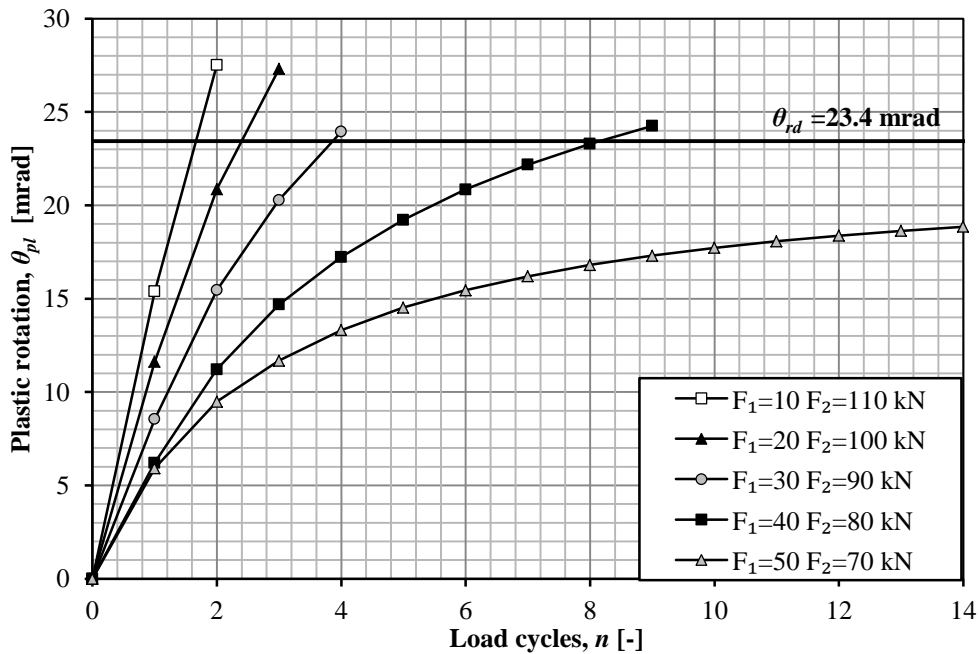
Figure 7.46   Plastic rotation for different load combinations of a pair of moving concentrated forces of varying magnitudes for d = 1.6 m.
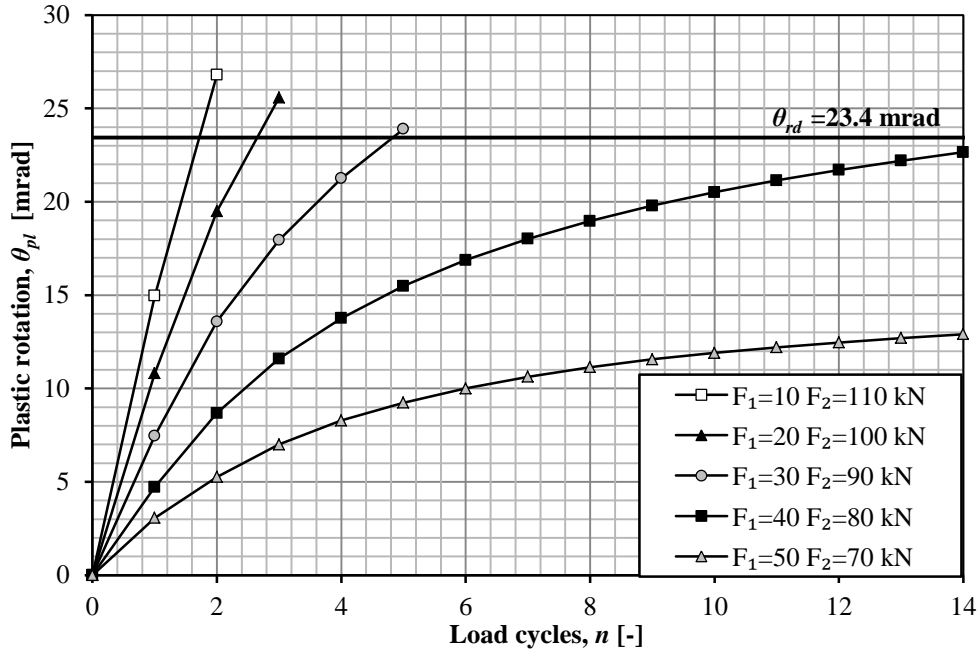
Figure 7.47 Plastic rotation for different load combinations of a pair of moving concentrated forces of varying magnitudes for d = 2.0 m.

As expected, and as observed in Section 7.4, it was advantageous for the simply supported structure with an increased distance between the moving concentrated forces. It is also clear that it was advantageous for the simply supported structure with a more evenly distributed force application.

From Figure 7.45 to Figure 7.47, it can be seen that:

- For the distance $d = 1.2$ m, all investigated load combinations led to failure within 14 load cycles or less.
- For the distance $d = 1.6$ m, four of the investigated load combinations led to failure within 14 load cycles or less.
- For the distance $d = 2.0$ m, three of the investigated load combinations led to failure within 14 load cycles or less.

How the plastic rotation developed in the centre of the slab during the first 10 load cycles for $d = 1.2$ m is illustrated in Figure 7.48.

It can be seen in Figure 7.48 that the load combinations with a large difference in force magnitudes between the two forces led to failure during a few load cycles. The plastic rotation for these loads greatly exceeded the plastic rotation capacity for the cross-section but is presented here in order to evaluate how the accumulated damage developed in the centre of the simply supported structure. It can be seen that the accumulated damage for the forces of more equal magnitudes approached a stable state more rapidly than the force pair with a bigger difference in magnitude between the two forces. This was also observed in Figure 7.45 where the distance between the curves decreased as the forces approached a mean value.
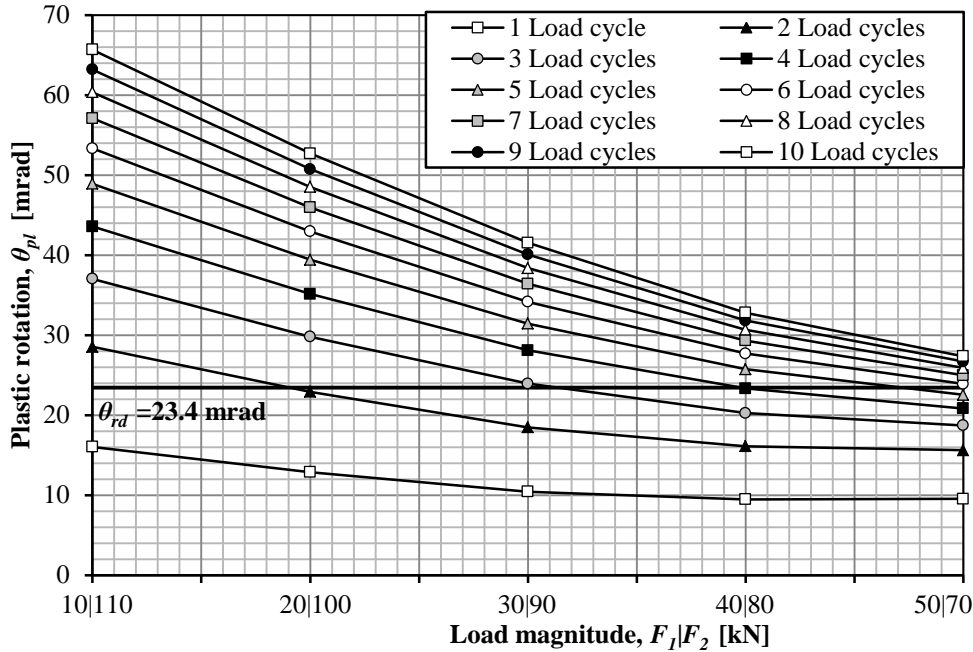
Figure 7.48 Development of plastic rotation for different load combinations of a pair of moving concentrated forces of varying magnitudes for d = 1.2 m.

7.5.2 Comparison

In order to determine how the plastic rotation was influenced by the distance d between the moving forces of varying magnitudes, the different analyses were compared below. The plastic rotation obtained from the analyses with $d = 1.6$ m and $d = 2.0$ m was compared to the plastic rotation with $d = 1.2$ m according to Equation (6-32) and (6-33), defined in Section 6.5.2. The difference is shown in Figure 7.49 and Figure 7.50 and the reader is referred to Appendix H for tabulated values.
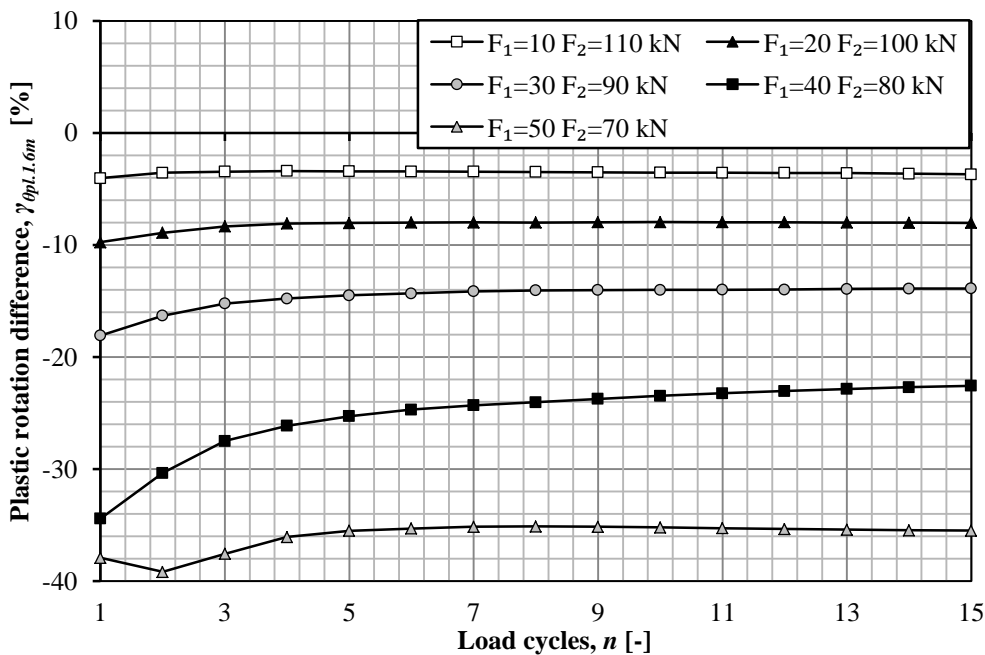
Figure 7.49 Difference in plastic rotation $\gamma_{\theta pl.1.6m}$ for different load combinations between d = 1.2 m and d = 1.6 m.
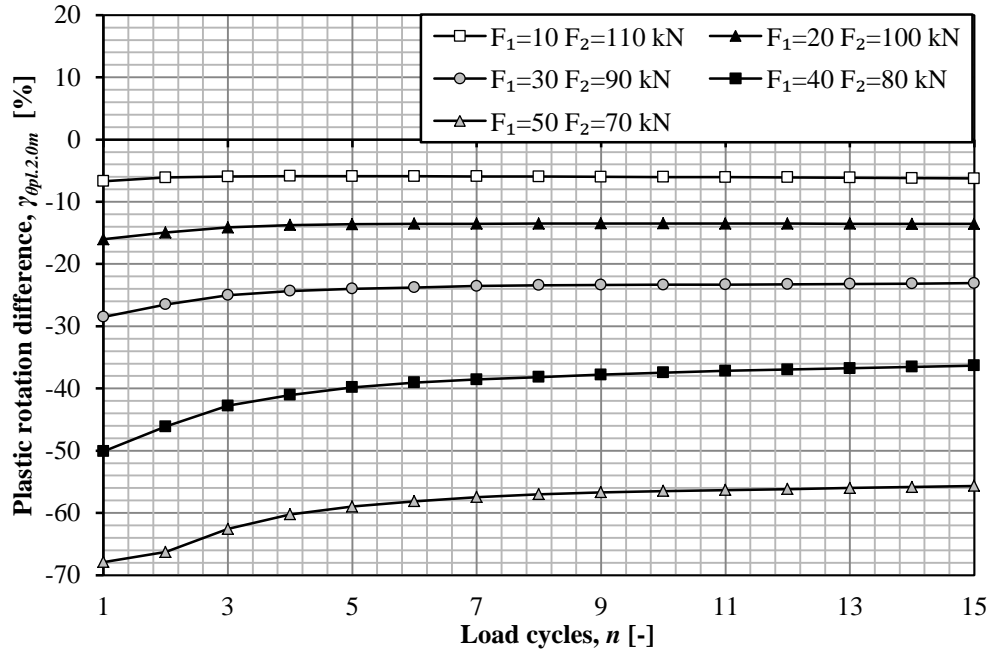
Figure 7.50 Difference in plastic rotation $\gamma_{\theta pl.2.0m}$ for different load combinations between $d = 1.2$ m and $d = 2.0$ m.

It was here observed, as in Section 6.5.2 that the difference in plastic rotation was almost constant for each separate load combination and distance after a few load cycles. The mean plastic rotation difference was therefore of interest and defined as in Section 6.5.2. The mean plastic rotation difference was calculated according to Equation (6-34) to (6-37), presented in Section 6.5.2. The difference is shown in Figure 7.51 and the reader is referred to Appendix H for tabulated values.
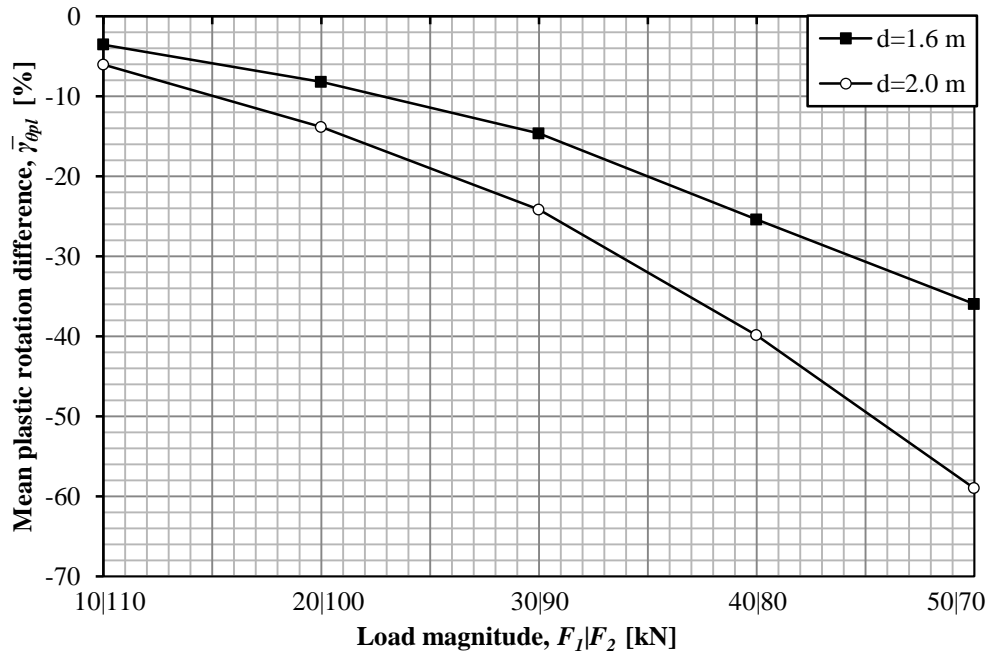
Figure 7.51 Mean difference in plastic rotation $\gamma_{\theta pl}$ between $d = 1.2$ m and, $d = 1.6$ m and $d = 2.0$ m.

It can be seen in Figure 7.51 that an increased distance d resulted in a significant decrease in plastic rotation. The difference in plastic rotation increased with decreased

CHALMERS, *Civil and Environmental Engineering*, Master's Thesis 2014:73

difference between the two forces F_1 and F_2. This behaviour was expected since the distance between a force of a great magnitude and a force of a small magnitude should not influence the accumulated damage to a great extent. When both forces are of a relative high magnitude, the distance should influence the accumulated damage to a greater extent, which was the case.

7.6 Summation

This section covers a comparison between the moving concentrated forces presented in Section 7.3 to 7.5. A single and a pair of moving concentrated forces are compared with static forces of the same magnitudes. As a final part of this section, the results presented in Chapter 7 are discussed.

7.6.1 Comparison – Moving forces

This section covers the investigated forces on the simply supported structure presented in the Section 7.3 to 7.5 and evaluates the differences and similarities between them. These sections have covered the two main load cases:

- A single moving concentrated force – Constant magnitude
- A single moving concentrated force – Varying magnitudes
- Two moving concentrated forces – Equal magnitudes
- Two moving concentrated forces – Different magnitudes

As discussed in Section 6.6.1, the results from the pair of moving concentrated forces of different magnitudes should yield plastic rotation greater than what is caused by a pair of moving forces of equal magnitudes and less that what is caused by a single moving force. This can be seen in Figure 7.52 to Figure 7.54 where these analyses are presented together.
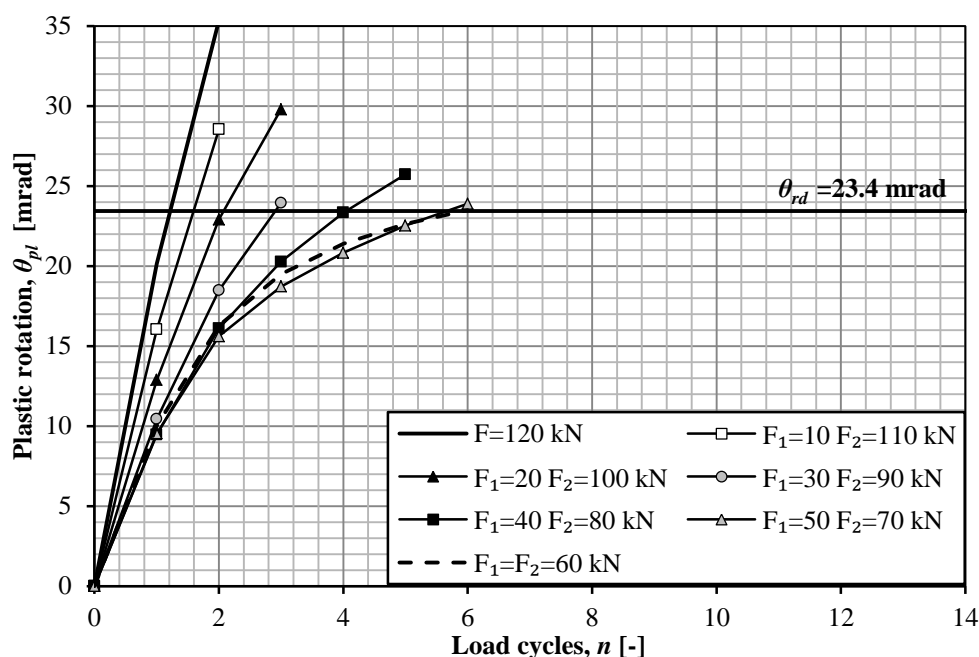
Figure 7.52 Plastic rotation for different load combinations of a pair of moving concentrated forces of varying magnitudes for d=1.2 m.
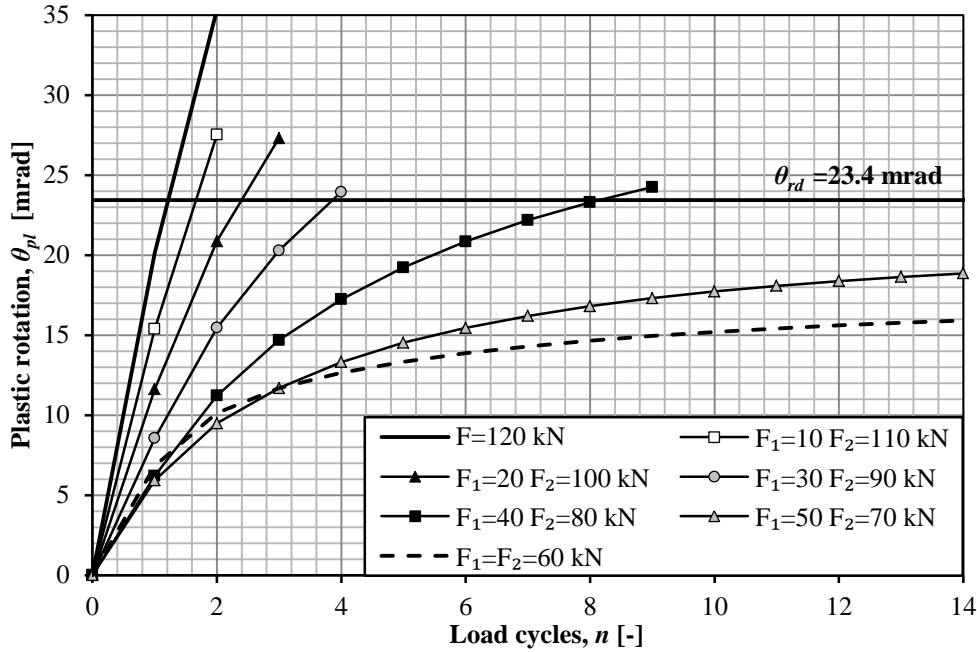
Figure 7.53 Plastic rotation for different load combinations of a pair of moving concentrated forces of varying magnitudes for d=1.6 m.
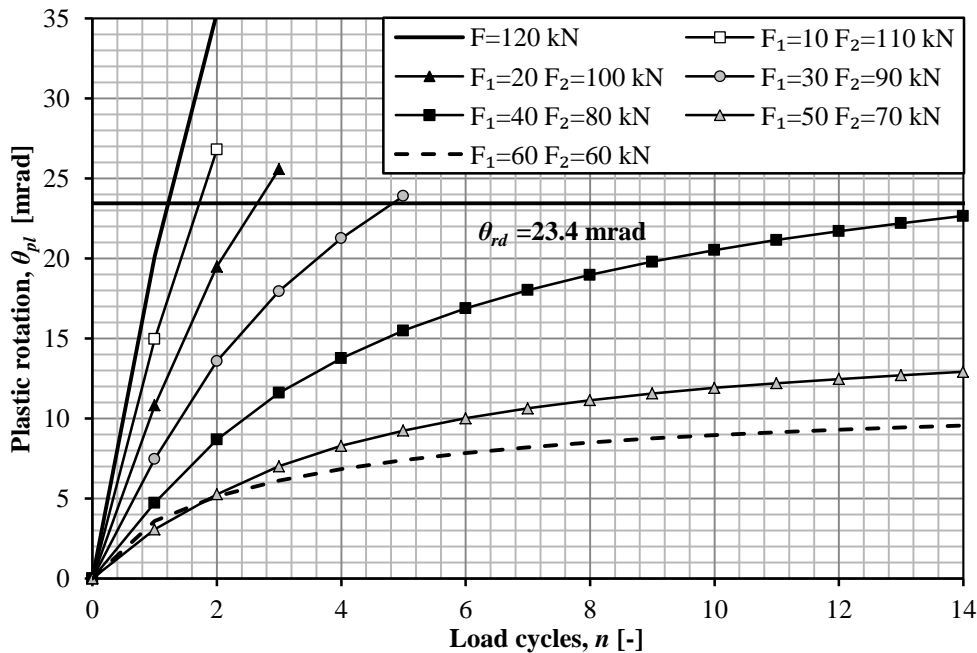
Figure 7.54 Plastic rotation for different load combinations of a pair of moving concentrated forces of varying magnitudes for d=2.0 m.

It can be seen in Figure 7.52 to Figure 7.54 that the results where $F_1=F_2=60$ kN yielded higher plastic rotation than the case where $F_1=50$ kN and $F_2=70$ kN during the first load cycles. However, the accumulated damage caused by the load combination of two concentrated forces of different magnitudes was thereafter greater than the case where $F_1=F_2=60$ kN. The results indicates that the two equal forces were more critical to the development of the plastic rotation during the early load cycles and that the simply supported slab thereafter adapted to the load magnitude quicker than in the case of two different forces. The effect of the larger force

($F_2 = 70$ kN) was in this case decisive for the development of the plastic rotation which caused this load combination to develop more plastic rotation after a few load cycles than the case of two equal forces.

The plastic rotation obtained by $F = 120$ kN was slightly higher than the case where $F_1 = 10$ kN and $F_2 = 110$ kN for all distances d.

These analyses were only conducted for one total force $F_{tot} = 120$ kN for the two moving concentrated forces of different magnitudes but the advantageous effect of separating the total force into two separated forces are believed to increase with an increased total force.

7.6.2 Comparison – Static vs. moving forces

As in the case of the cantilever structure, it is clear that a moving concentrated force causes significantly more plastic rotation than what is caused by a static force of the same magnitude. The development factor used for the cantilever structure in Section 6.6.2 was here used in the same way and based on the same observations.

As for the cantilever structure, the distribution of the development factor $\gamma_{\theta pl.mov}$ was divided into two sub factors $\gamma_{\theta pl.mov.min}$ and $\gamma_{\theta pl.mov.max}$. These factors represent the minimum and maximum difference in plastic rotation between static and moving forces of the same magnitudes. For the definition of these factors, the reader is referred to Section 6.6.2.

The development factors were also here calculated for all forces that reached a stable state (reached its maximum plastic rotation) in the conducted analyses and the results is shown in Figure 7.55.
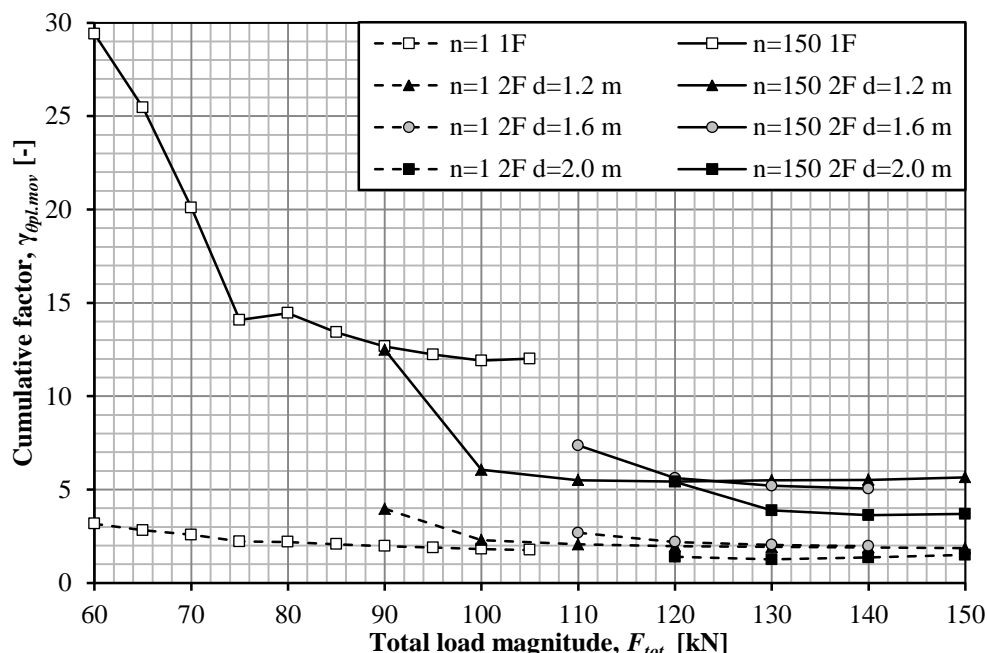
Figure 7.55 Maximum and minimum values of the cumulative factor $\gamma_{\theta pl.mov}$ for a single and a pair of moving concentrated forces.

It is clear from Figure 7.55. that the plastic rotation caused by a moving concentrated force was within the range of 1.5 to 30 times larger than the plastic rotation caused by a static force. It is also in this case clear that an increased distance d between the

forces and an increased total applied force F_{tot} yielded plastic rotations closer to what was predicted by static forces. How the cumulative factor developed for a single moving concentrated force is shown in Figure 7.56. For the development of the cumulative factor for two moving concentrated forces, the reader is referred to Appendix G.
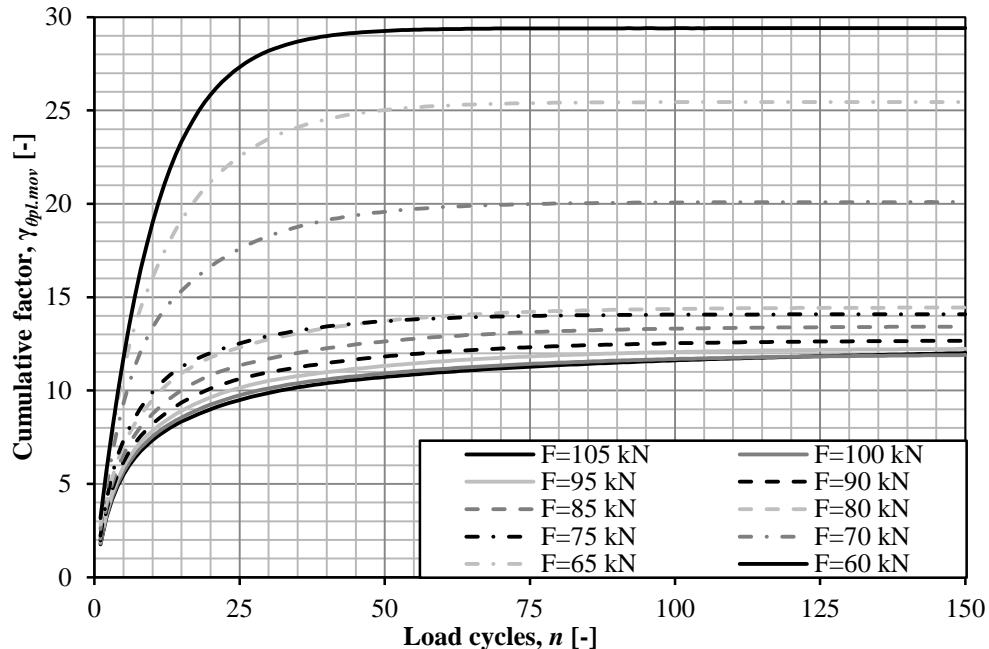
Figure 7.56 Development of the cumulative factor $\gamma_{\theta pl.mov}$ for a single moving concentrated force.

7.6.3 Discussion

In general, the results presented in Chapter 7 follow the same pattern as in Chapter 6 and are here briefly discussed. For a more detailed discussion and for additional information the reader is referred to Section 6.6.3.

The simply supported one-way structure reached a stable state, with respect to the plastic rotation development, when the number of load cycles n was increased.

A traditional superposition approach of moving concentrated forces significantly overestimated the plastic rotation. The magnitude of the overestimation corresponded well to what was obtained from the cantilever structure, but with a slightly different behaviour. The difference for the cantilever structure indicated a linear behaviour while the difference seemed to diminish as the load magnitude increased for the simply supported structure.

It was also for the simply supported structure shown that there was a significant difference between the plastic rotation caused by static and moving concentrated forces. The plastic rotation caused by a moving force could be as high as 30 times the plastic rotation caused by a static force of the same magnitude. It was also for this structure shown that this difference decreased as the force magnitude increased and also decreased with increased distance d between a pair of moving concentrated forces.

8 Evaluation and discussion of results

This chapter covers the evaluation and discussion of the obtained results, presented in this Thesis. Section 8.1 covers the results from Chapter 4 and 5, focused on the moment distribution in the serviceability limit state for slabs subjected to static concentrated forces. Section 8.2 covers the results from Chapter 6 and 7, focused on the development of cumulative plastic rotation θ_{pl} in slabs subjected to moving concentrated static forces.

8.1 Moment distribution in SLS

For studies related to moment distribution in SLS, several cases were studied which were intended to represent different scenarios which may appear in a bridge structure. The different scenarios included a variety of stiffness in different directions due to varying reinforcement amounts or normal stresses in those directions. The non-linear analyses were divided into three different categories, namely Uncracked, Neutral and Cracked. The names of the three categories imply on the state and corresponding stiffness in the longitudinal direction of the slab, i.e. the *x*-direction in the figures presented in this section. The variety of stiffness may be derived from the global bending moment for a beam bridge structure where, for example, a positive global moment compresses the upper flange of the cross-section. Further, two different levels of the cracking moment were chosen. See Section 4.1 for the methodology used.

Two different structures were studied, a cantilever slab and a simply supported one-way slab. Both structures were studied with a single concentrated force and two concentrated forces, see Figure 8.1.
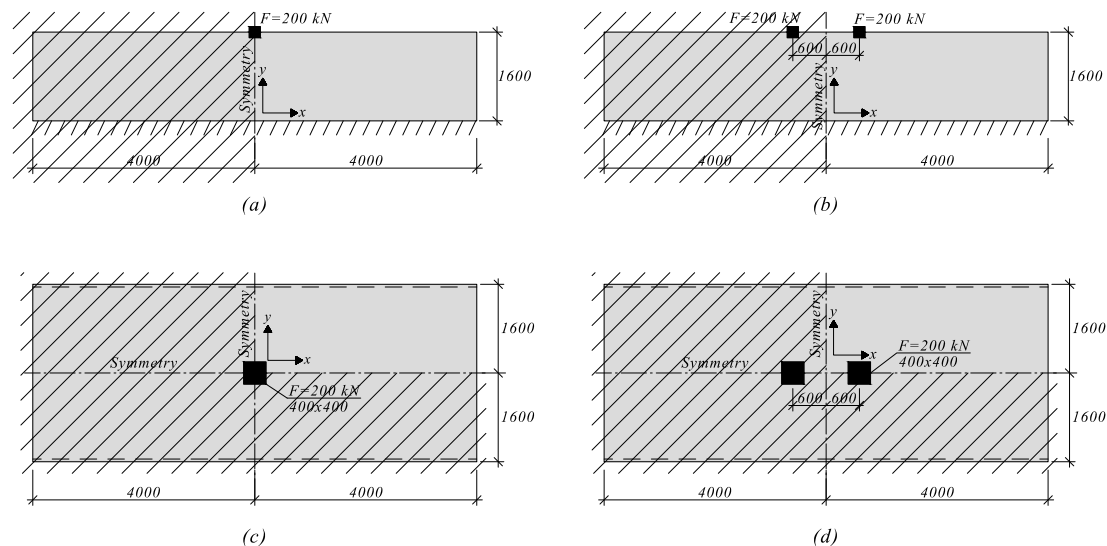
Figure 8.1   *The studied structures and load applications; (a) cantilever slab, single force (b) cantilever slab, two forces (c) simply supported slab, single force (d) simply supported slab, two forces*

In this section, a summary of the maximum moments obtained from the analyses is made for easier comparison. Further, the responses of the structures are investigated with the help of contour plots which display in which branch of the trilinear moment-curvature relation the beam elements are situated. Finally, the results are compared to the recommendations in Pacoste *et al.* (2012).

8.1.1 Maximum moment

The maximum moments obtained from the analyses were of most interest and the results are therefore summarized in column graphs for easier comparison; see Figure 8.2 to Figure 8.5. The values are expressed as a factor of the isotropic linear solution obtained from the beam grillage model.
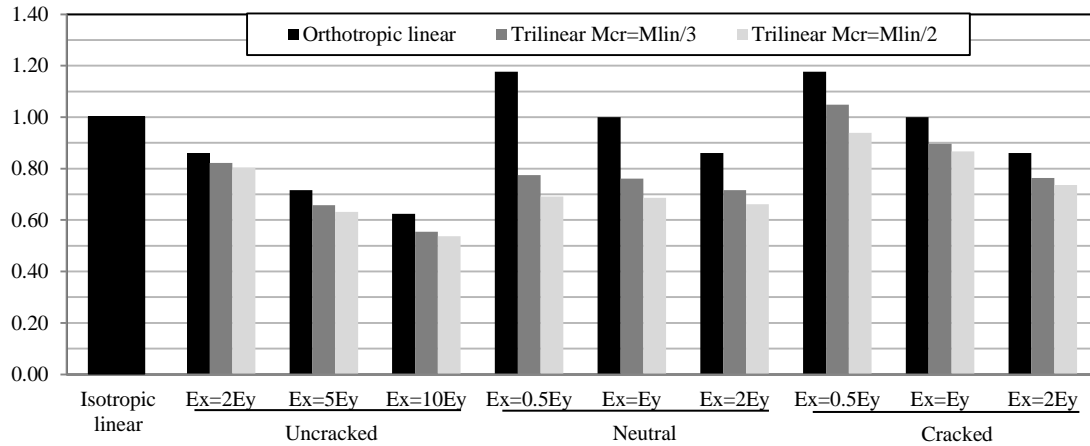
Figure 8.2   Maximum moments; cantilever slab, single concentrated force.
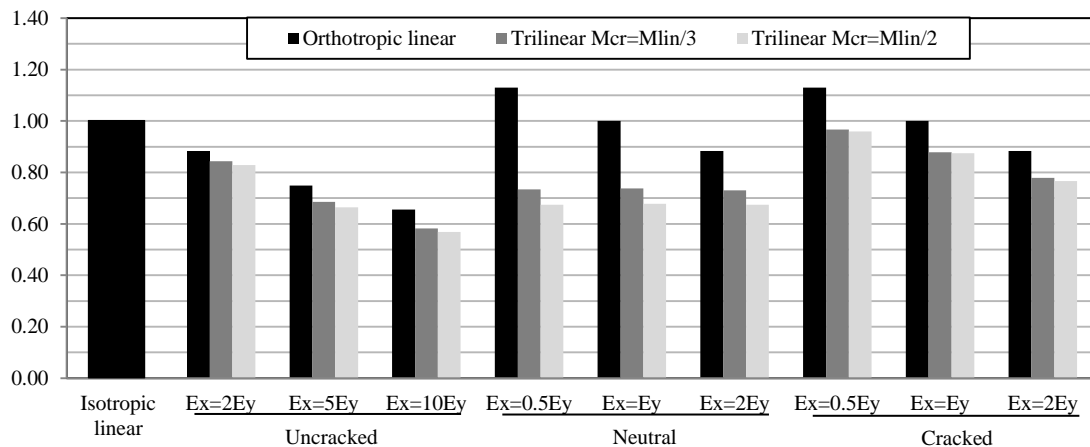
Figure 8.3   Maximum moments; cantilever slab, two concentrated forces.
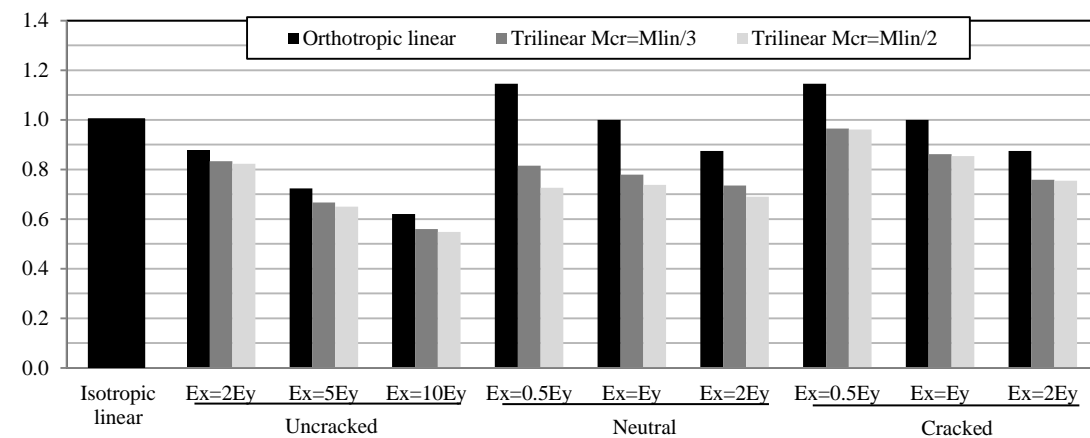
Figure 8.4   Maximum moments; simply supported one-way slab, single concentrated force.
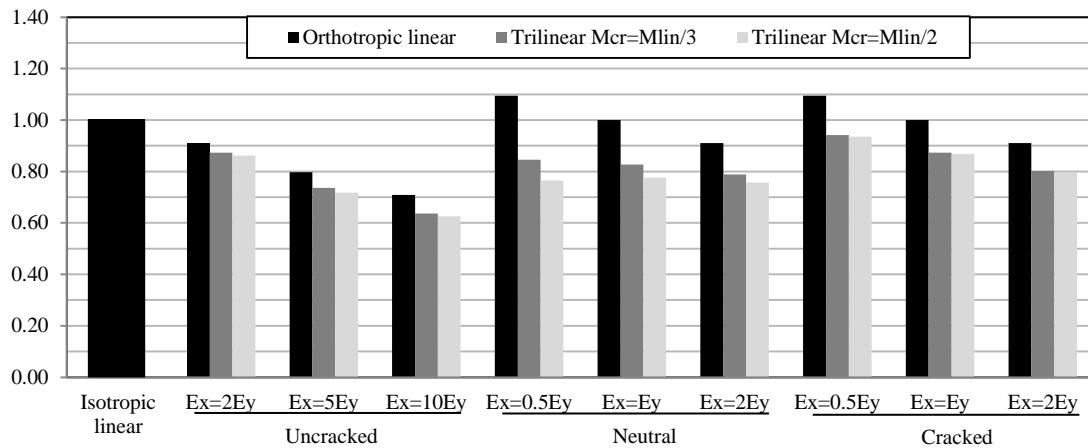
Figure 8.5   Maximum moments; simply supported one-way slab, two concentrated forces.

It was observed that for all different cases, the orthotropic linear solution was conservative with respect to the non-linear solutions. This is logical due to the fact that the positive influence from uncracked sections was ignored. In the cases Uncracked and Cracked, the response in the x-direction was linear, which is a reason why the non-linear solutions were more similar to the orthotropic linear solutions than for the case Neutral.

In the case Uncracked, it is shown that the maximum moment was decreased by about 20 to 25 % for the stiffness proportion $E_x=5E_y$, which is a reasonable stiffness proportion between uncracked and cracked reinforced concrete. The case Uncracked was intended to represent a region of a bridge structure which is uncracked in the longitudnal directions due to global forces, see Figure 4.3. This region may be quite large depending on the structure, which means that there could be a significant gain in taking this stiffness proportion into account, even with a linear orthotropic model.

The non-linear solutions for the case Neutral are very similar, independent on stiffness proportions. This is most likely due to the fact that uncracked parts of the structure dominates the behaviour, and would mean that the solution would tend to approach the orthotropic linear solution if the structure was already cracked from an earlier applied load. The non-linear solutions could thus be too liberal for design of a bridge, where moving loads may cause cracking along an extensive part of the structure, which also applies for the case Cracked. It was also shown in Section 5.2.3, that if the load was of a higher magnitude in relation to the cracking moment, the solutions would be more affected by the stiffness proportions.

For the cases Neutral and Cracked, both main directions had the stiffness of cracked reinforced concrete when the load was applied. The stiffness proportion was thus a result of varying reinforcement amounts in the two directions. Unlike the case Uncracked, where one direction had the stiffness of uncracked concrete throughout the analysis, the range of stiffness proportion was smaller. This is why only a range of stiffness proportion from $E_x=0.5E_y$ to $E_x=2E_y$ were chosen. The orthotropic linear solutions show a variation of about 10 to 15 % of the maximum moment compared to the isotropic linear solution. This means that the actual moment in the slab could be underestimated by an isotropic linear elastic analysis. Even though the non-linear analyses show a lower moment than the isotropic solution for the majority of cases, the solution could still be too liberal if the structure is already cracked due to earlier loading as previously mentioned.

8.1.2 Contour plots

In order to investigate and interpret the results, the curvature in the beam elements of the finite element model was measured and illustrated as contour plots. The plots follow the orientation presented in Figure 8.1. Each element was given a colour depending on which branch of the moment-curvature relation the beam element was situated in, see Figure 8.6. The plots presented in this section were based on the results from cases with the chosen magnitude of the cracking moment $M_{cr}=M_{lin}/3$.
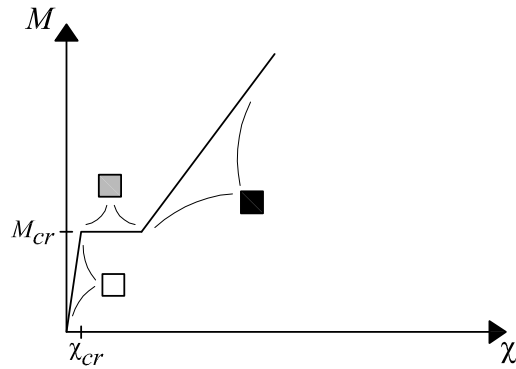
Figure 8.6   Colour distinction for contour plots

8.1.2.1   Case Uncracked

The contour plots from the case Uncracked for a single concentrated force are shown in Figure 8.7. Note that, since all elements in the *x*-direction had an uncracked stiffness, only elements that were orientated in the *y*-direction are plotted.
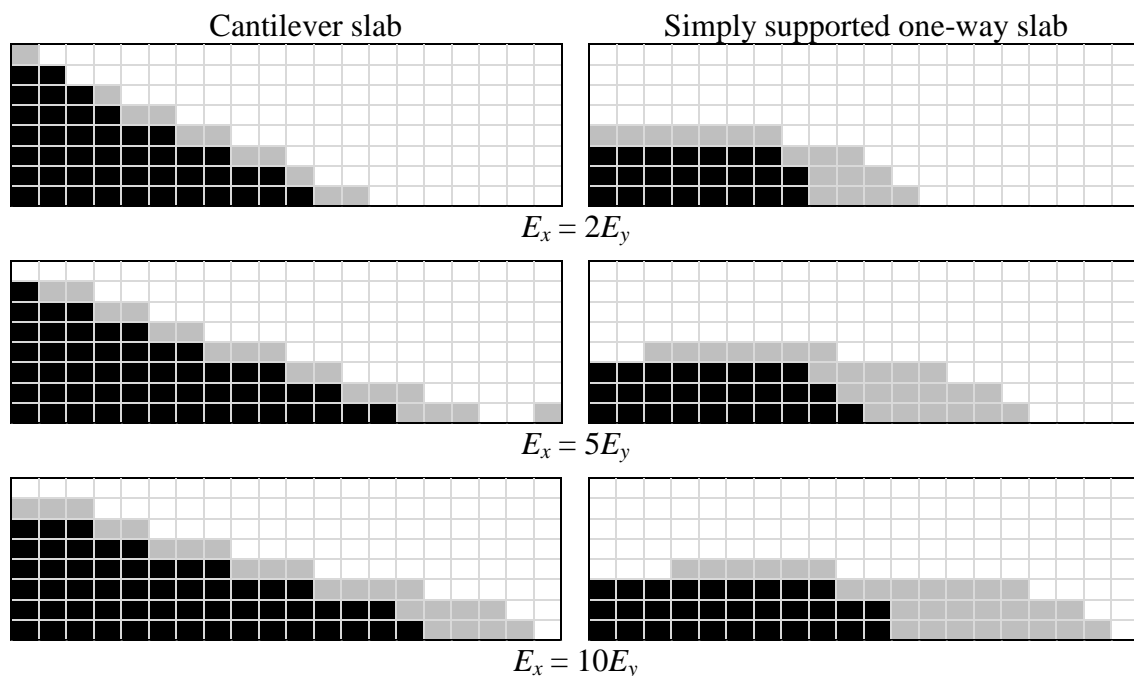
Figure 8.7   Contour plot for the case Uncracked with a single concentrated force. Beam elements orientated in the y-direction.

In the case Uncracked, the stiffness in the *x*-direction was locked to the stiffness of uncracked concrete. This means that, as the stiffness factor $\alpha = E_x / E_y$ increased, the

y-direction got weaker. The plots show that, as the *y*-direction got weaker, additional elements along the length of the slab were activated.

8.1.2.2   Case Neutral

As seen in Section 8.1.1, the maximum moments for the case Neutral were similar, independent on stiffness proportions. The contour plots are divided into beam elements in *x*- and *y*-direction. Cracking along each main direction can then be observed. The contour plots for the cantilever slab from the case Neutral are presented in Figure 8.8.
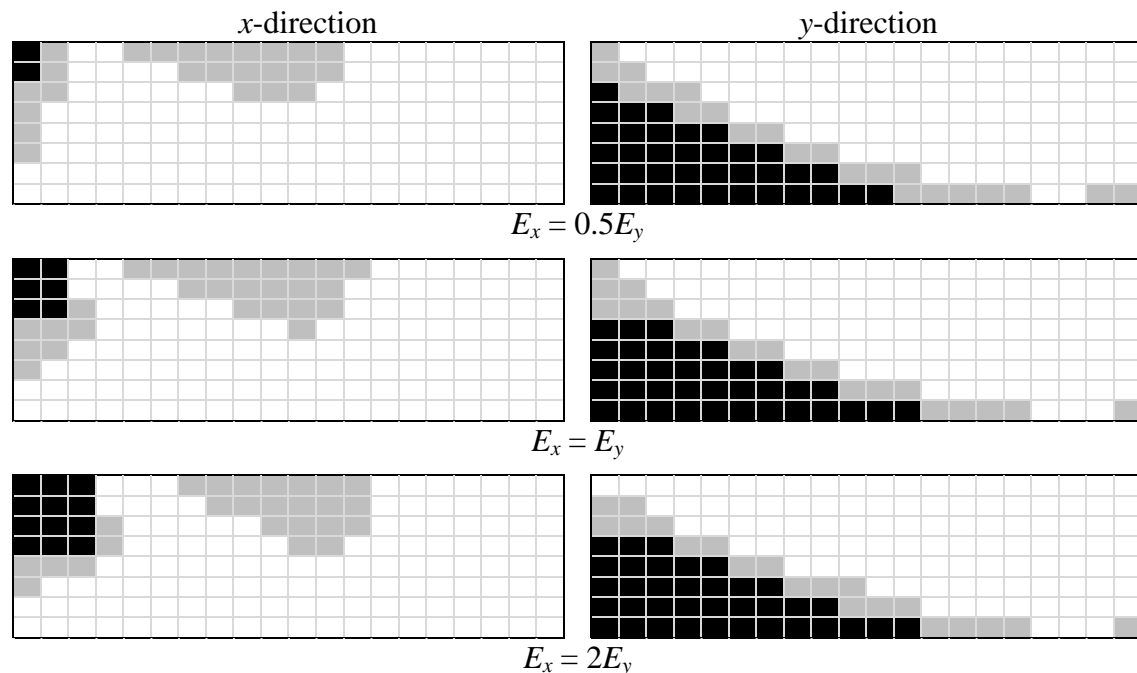
Figure 8.8   Contour plot for the case Neutral, cantilever slab with a single concentrated force.

The results show that most cracking occurred in the *y*-direction along the fixed edge and that a large part of the structure close to the applied load reached the state II stiffness. In the *x*-direction, only elements directly under the concentrated force reached a state II stiffness. Note that the cracks under the applied load were bottom cracks, while the cracks to the right of the applied load were top cracks. This explains the uncracked area in between, since it is an area in which the moment changes from positive to negative. This means that for a moving load, there will be both bottom and top cracks along the entire structure. As discussed in Section 8.1.1, the non-linear solution can thus be too liberal if the structure is already cracked due to earlier loading.

Contrary to the moment distribution, the curvature contour plot show a distinct difference between the three different stiffness proportions. Namely, that as the *x*-direction increased in stiffness and thus attracted additional loads which resulted in a larger area which reached the state II stiffness.

8.1.2.3 Case Cracked

In the case Cracked, the *x*-direction had a linear moment-curvature relation which represents the stiffness of cracked concrete with varying reinforcement amounts. Since the relation was linear, all elements orientated in the *x*-direction had the same stiffness. In Figure 8.9, the contour plots for the case Cracked with a single concentrated force are presented. Only beam elements orientated in the *y*-direction is displayed.

$$E_x = 0.5E_y$$

$$E_x = E_y$$

$$E_x = 2E_y$$
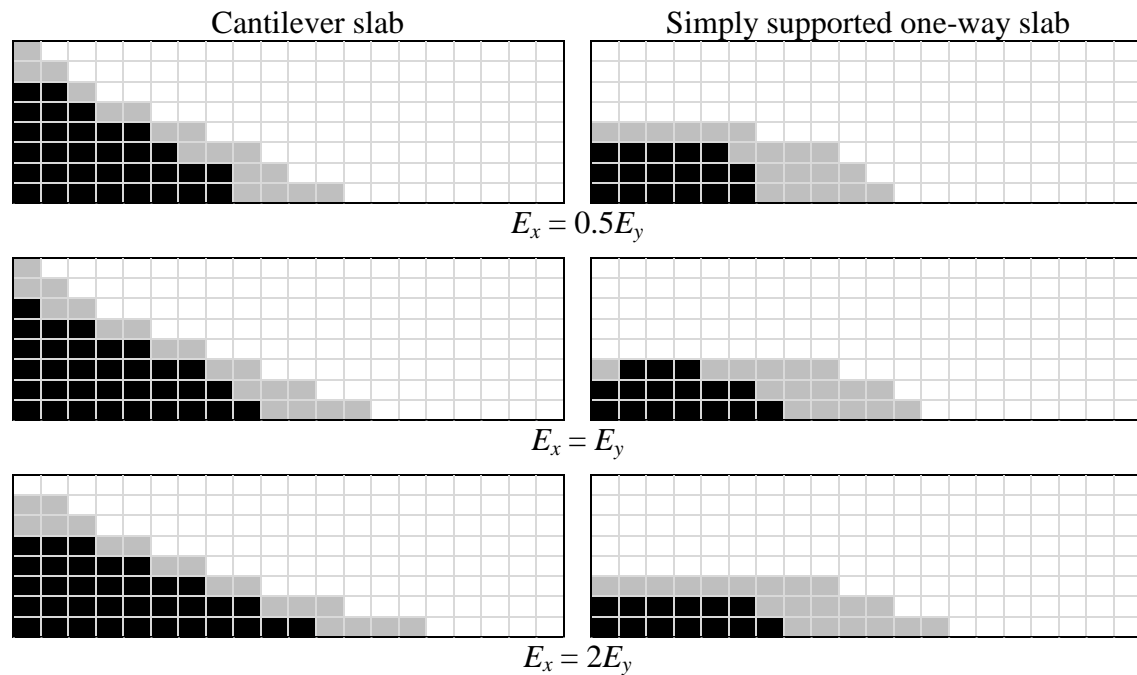
Figure 8.9   *Contour plot for the case Cracked with a single concentrated force.*
            Beam elements orientated in the y-direction.

As in the case Uncracked, the extent of the cracked regions were increased as the *y*-direction became weaker in proportion to the *x*-direction. It is however not as clear as in the case Uncracked. The reason is most likely due to the larger range of stiffness proportions in the case Uncracked.

8.1.3 Effective moment distribution width

An objective of this Thesis was to evaluate the recommendations given in Pacoste *et al.* (2012), see Section 3.4.2. In Pacoste, the recommendations are stated in terms of effective moment distribution width w_{eff}, which can be computed as:

$$w_{eff} = \frac{M_{y.tot}}{m_{y,\max}}$$

(8-1)

Where: w_{eff} = effective width for moment distribution

$M_{y.tot}$ = total moment in y-direction

$m_{y,\max}$ = maximum moment m_y measured in analysis

The distribution width w_{eff} from the linear solutions in Chapter 4 and 5 are presented in Figure 8.10. Note that no scenarios in this study include values of the stiffness factor α below 0.5. A value of, for example $\alpha = 0.1$, would mean that the slab had an uncracked stiffness in the y-direction, while it had a cracked stiffness in the x-direction. This could be accomplished by prestressing the concrete in the y-direction. However, this scenario was not discussed in this Thesis.
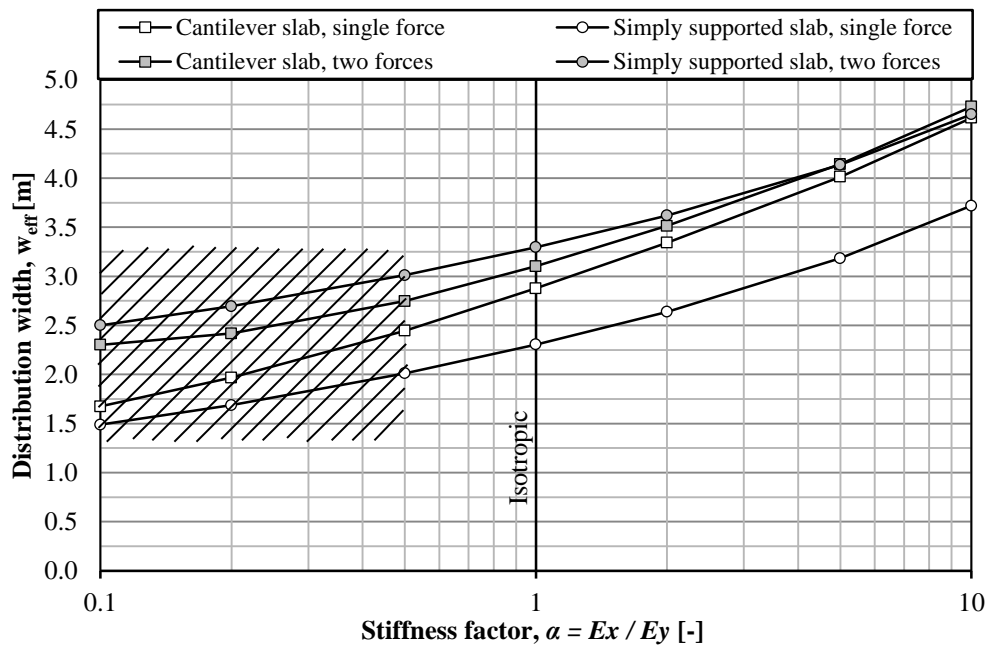
Figure 8.10 Effective moment distribution width from linear elastic orthotropic cases.

The moment distribution widths for the trilinear solutions were omitted since the orthotropic linear solutions describe the trilinear solutions fairly well for the majority of cases. Also, with respect to the maximum moment from the trilinear solutions, the linear orthotropic solution is conservative.

The recommended values of the moment distribution width were calculated from simple relations stated in Section 3.4.2. The relations include the thickness of the slab which in this Thesis was chosen to 0.2 m. However, a range of stiffness proportions were chosen and the levels of the cracking moment were chosen as a factor of the orthotropic linear solution, see Section 4.1.1. Thus, the only parameter the height of

the slab affects is the torsional stiffness which was chosen conservatively, see Section 4.1.3.

The relations also include the width of the applied load. For the cantilever slab, the concentrated force was modelled as a point load acting on a single node. However, for the simply supported slab the load was spread over an area of 0.4 x 0.4 m², which was chosen according to the load model described in Section 5.1. Therefore, when calculating the recommended value, $b = 0.4$ m was chosen. No surfacing material were discussed and was chosen to $t = 0$ m.

For the cantilever slab subjected to a single concentrated force, the recommended distribution width was calculated as:

$$w_{eff} = 2h + b + t = 2 \cdot 0.2 + 0.4 + 0 = 0.8 \text{ m} \tag{8-2}$$

For the cantilever slab subjected to two concentrated forces, the recommended distribution width was calculated as:

$$w_{eff} = 2 \cdot x_R + 2h + b + t = 2 \cdot 0.6 + 2 \cdot 0.2 + 0.4 + 0 = 2.0 \text{ m} \tag{8-3}$$

For the simply supported one-way slab subjected to a single concentrated force, the recommended distribution width was chosen according to:

$$\min\left(3h, \frac{l}{10}\right) \leq w_{eff} \leq \min\left(5h, \frac{l}{5}\right) \tag{8-4}$$

$$\min\left(3 \cdot 0.2, \frac{3.2}{10}\right) \leq w_{eff} \leq \min\left(5 \cdot 0.2, \frac{3.2}{5}\right) \tag{8-5}$$

$$0.32 \text{ m} \leq w_{eff} \leq 0.64 \text{ m} \tag{8-6}$$

The case with several concentrated forces was not treated in Pacoste *et al.* (2012) for simply supported one-way slabs. However, following the methodology used for cantilever slabs, the recommended distribution width was chosen according to:

$$2 \cdot x_R + \min\left(3h, \frac{l}{10}\right) \leq w_{eff} \leq 2 \cdot x_R + \min\left(5h, \frac{l}{5}\right) \tag{8-7}$$

$$2 \cdot 0.6 + \min\left(3 \cdot 0.2, \frac{3.2}{10}\right) \leq w_{eff} \leq 2 \cdot 0.6 + \min\left(5 \cdot 0.2, \frac{3.2}{5}\right) \tag{8-8}$$

$$1.52 \text{ m} \leq w_{eff} \leq 1.84 \text{ m} \tag{8-9}$$

A minimum value was however calculated for a single force as:

$$w_{eff.\min} = 2h + b = 2 \cdot 0.2 + 0.4 = 0.8 \text{ m} \tag{8-10}$$

And for two forces as:

$$w_{eff.\min} = 2 \cdot x_R + 2h + b = 2 \cdot 0.6 + 2 \cdot 0.2 + 0.4 = 2.0 \text{ m} \tag{8-11}$$

The recommended values were well below the calculated values presented in Figure 8.10. It should be noted that a low value of the torsional stiffness of the beam elements was chosen in the analyses, which was believed to be conservative, see Section 4.1.3. If a larger torsional stiffness would be chosen, the results would display a better distribution of the forces which means that the effective distribution width would increase even more.

If the thickness of the slab was set to 0.4 m, instead of the chosen 0.2 m, the recommended values would increase, see Table 8.1.

Table 8.1   Recommended values of moment distribution width according to Pacoste et al. using a slab thickness of 0.4 m.

Cantilever slab, single force	$w_{eff} = 1.2$ m
Cantilever slab, two forces	$w_{eff} = 2.4$ m
Simply supported slab, single force	$w_{eff} = 1.2$ m
Simply supported slab, two forces	$w_{eff} = 2.4$ m

Table 8.1 shows that the recommendations were conservative for the studies made, even with a slab thickness of 0.4 m. It should be noted that with an increased height, the torsional stiffness would have increased and thus resulted in a wider distribution of the forces. For easier comparison, both the calculated and the recommended values are shown in Figure 8.11.
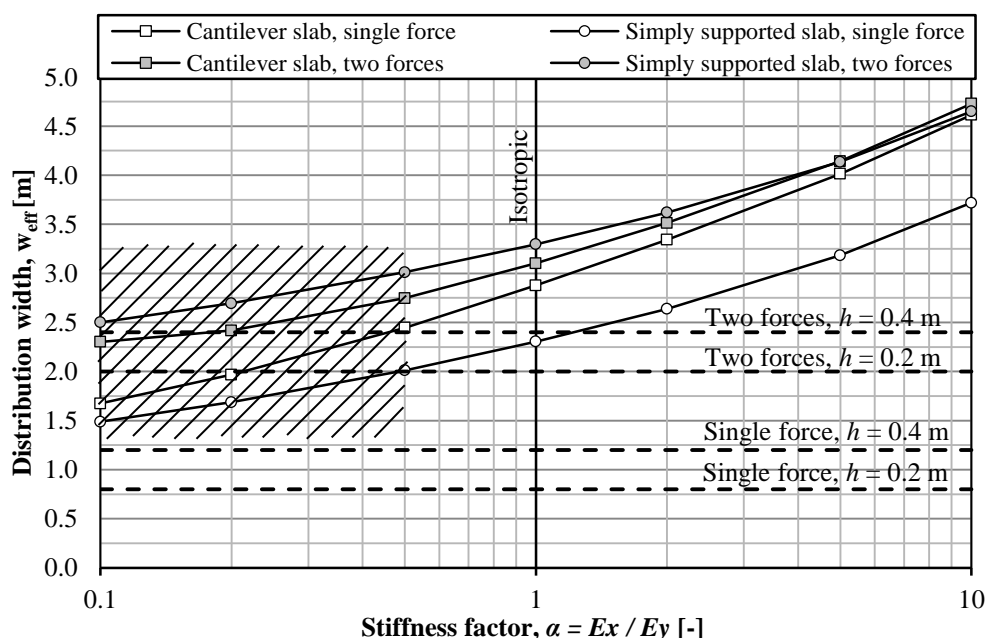
Figure 8.11   Effective moment distribution width from linear elastic orthotropic cases combined with the recommended values from Pacoste et al.

8.2 Cumulative plastic rotation

This section covers the evaluation and discussion from the results obtained in Chapter 6 and 7. The development of cumulative plastic rotation was studied for a cantilever and a simply supported one-way concrete slab, illustrated in Figure 8.12. The plastic rotations are for some analyses in this section significantly higher than the defined plastic rotation capacity θ_{rd} used in this Thesis and are also significantly higher than plastic rotations that can be expected in real structures. These values are however presented and used due to comparison purposes.
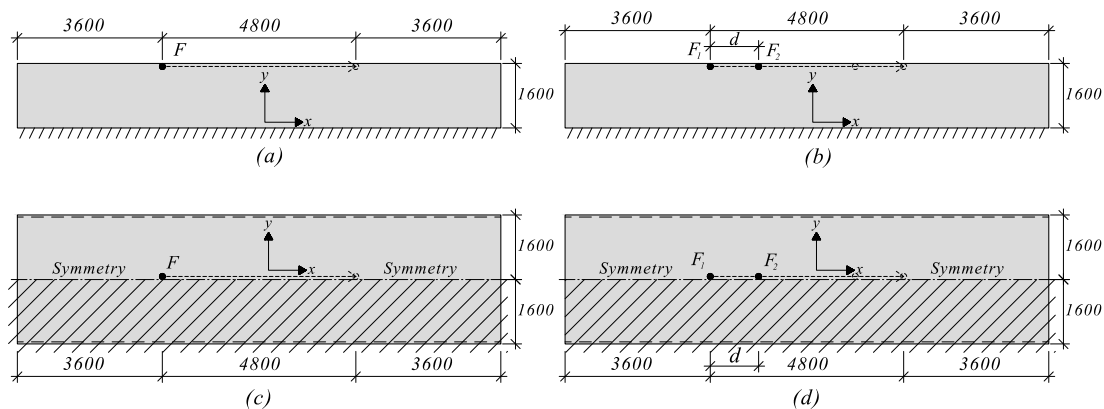
Figure 8.12 The studied structures and load applications; (a) cantilever slab, single moving force (b) cantilever slab, two moving forces (c) simply supported slab, single moving force (d) simply supported slab, two moving forces

The development of plastic rotation was studied for the following four main load combinations:

- A single moving concentrated force – Constant magnitude
- A single moving concentrated force – Varying magnitudes
- Two moving concentrated forces – Equal magnitudes ($F_1 = F_2$)
- Two moving concentrated forces – Different magnitudes ($F_1 \neq F_2$)

Where the following parameters was altered:

- Load magnitudes, *F*, for all forces
- Load application order, *LAO*, of all forces
- Distance, *d*, between the two moving concentrated forces

8.2.1 Plastic rotation development – Moving forces

The development of plastic rotation for the load combinations presented above is illustrated for the cantilever and the simply supported structure in Figure 8.13 and Figure 8.14, respectively. It can be seen that the plastic rotation approached a stable state for both structures when the number of load cycles were increased. This means that a load that causes accumulated damage to the structures becomes less significant as the number of load cycles increases. This phenomenon was discovered for all the studied load combinations and load applications in this Thesis.

The single force could, for both structures, not be studied for the same amount of load cycles as the load combination consisting of two forces since the analyses were too unstable for such a high degree of plastic rotation. The values were instead estimated by the superposition approach in Section 8.2.4, proposed for further studies.
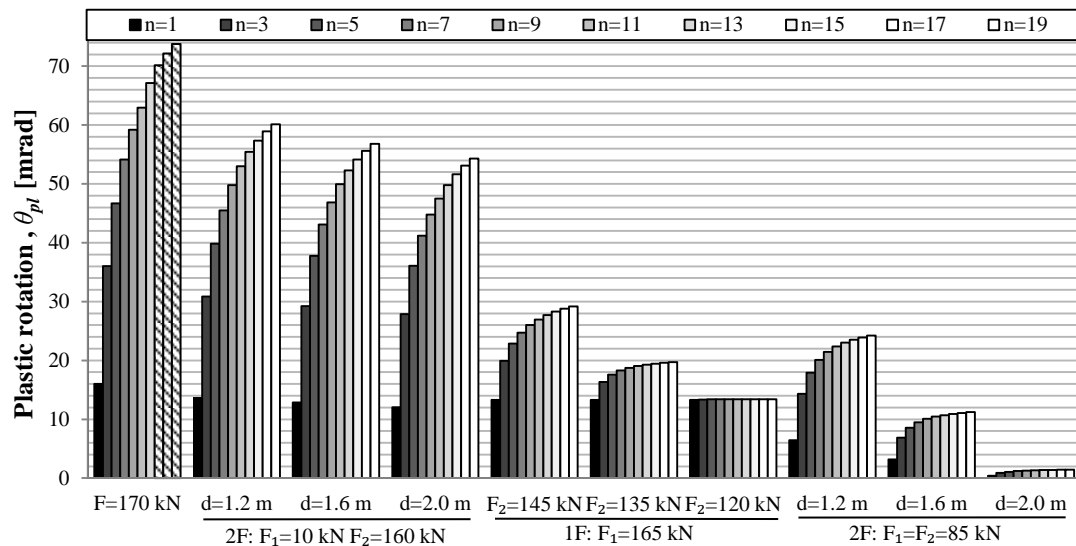
Figure 8.13 Development of plastic rotation θ_{pl}, for the first 19 load cycles for different load combinations. Cantilever structure.
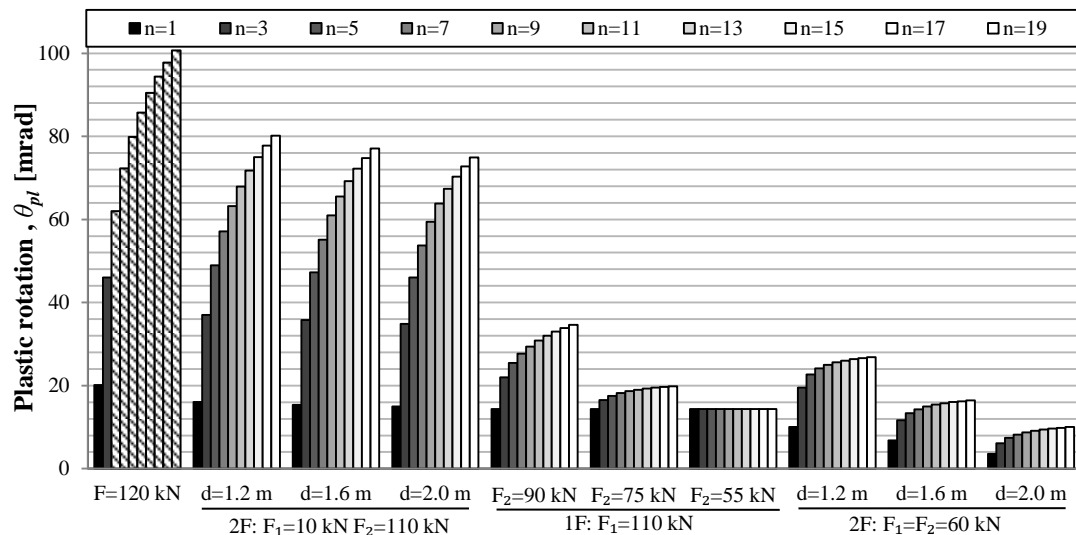
Figure 8.14 Development of plastic rotation θ_{pl}, for the first 19 load cycles for different load combinations. Simply supported one-way structure.

It can be seen in Figure 8.13 and Figure 8.14, that a single moving concentrated force was the most critical for the structures with respect to the development of plastic rotation. If the single force was separated into two forces where one was significantly larger than the other, the damage done to the structure decreased. The damage further decreased if the two forces of different magnitudes approached an equal force distribution. The damage done to the structure was, for all cases, decreased if the distance between the two forces increased. This behaviour was expected. The adaptation to the damage, and thus the decreased influence of the applied forces, was however not anticipated.

As have been noted above, the distance *d* between the force pair was essential to the development of accumulated damage in the structure. A plastic rotation factor $\gamma_{\theta pl}$, defined as a relation of the plastic rotation caused by a single moving force and two moving forces of the same total magnitude, is illustrated in Figure 8.15 and Figure 8.16.
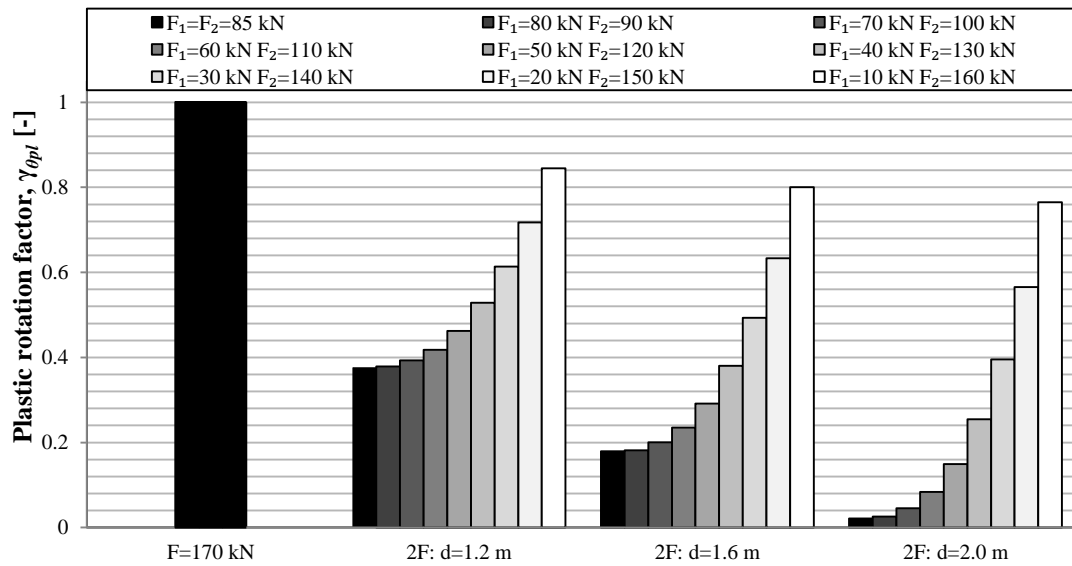
Figure 8.15   Plastic rotation factor $\gamma_{\theta pl}$. Cantilever structure.
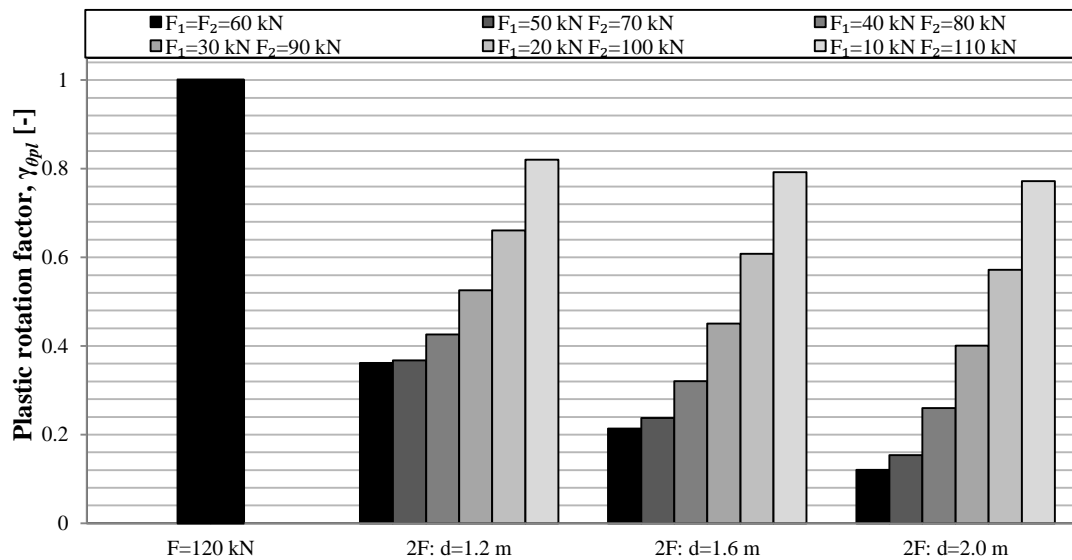
Figure 8.16   Plastic rotation factor $\gamma_{\theta pl}$. Simply supported structure.

It can be seen in Figure 8.15 and Figure 8.16 that the plastic rotation caused by a pair of moving concentrated forces merely constituted a smaller proportion of what was caused by a single moving force of the same total magnitude.

If the distance between the two forces was increased enough, the structure experienced the force pair as two single forces. This can be seen in Figure 8.17 where the total load magnitude F_{tot} (the sum of the force pair), not to cause any plastic rotation or failure due to plastic rotation after one load cycle, is illustrated for an increased distance d.
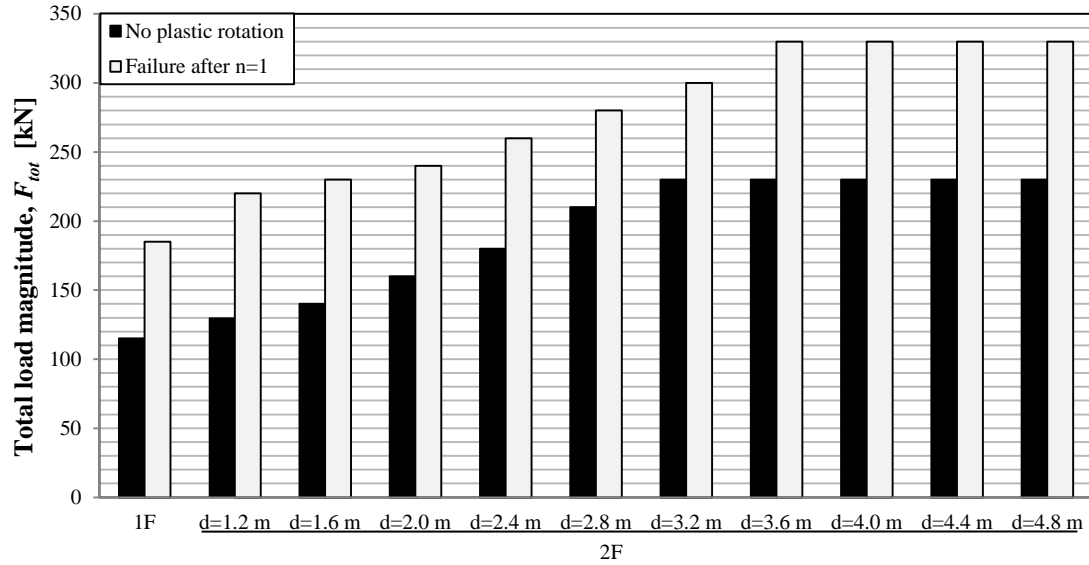
Figure 8.17   Total load magnitude F$_{tot}$ for different distances between the moving concentrated forces of equal magnitudes. Cantilever structure.

The study of the influence of the distance between the pair of moving concentrated forces were only conducted on the cantilever structure but it is reasonable to assume that the simply supported structure exhibit a similar behaviour.

8.2.2   Plastic rotation development – Static vs. moving forces

In traditional analysis and design, static forces are most commonly used. The subject of comparing the plastic rotation caused by static and moving forces was therefore of interest. In order to compare these two types of forces, a cumulative factor $\gamma_{.\theta pl.mov}$ was defined. This factor represents the difference between the plastic rotation caused by a moving force and the plastic rotation caused by a static force of the same magnitude.

As have been observed Chapter 6, 7 and partly in Section 8.2.1, the development of plastic rotation reaches a stable state where the plastic rotation in the structure did not increase with an increased number of load cycles. This means that there is an upper and lower limit of plastic rotation caused by a moving force and thus an upper and lower limit of the cumulative factor, here denoted as $\gamma_{\theta pl.mov.max}$ and $\gamma_{\theta pl.mov.min}$. The lower limit was set to the plastic rotation after the first load cycle and the upper limit was set to the plastic rotation after load cycle number 150. The analyses could not be conducted for 150 load cycles for all load magnitudes due to the unstable nature of the FE models at such a high degree of plastic rotation. The analyses conducted are presented in Figure 8.18 and Figure 8.19.

$$\gamma_{\theta pl.mov.\max} = \frac{\theta_{pl.mov.n=150}}{\theta_{pl.stat}}$$ (8-12)

$$\gamma_{\theta pl.mov.\min} = \frac{\theta_{pl.mov.n=1}}{\theta_{pl.stat}}$$ (8-13)
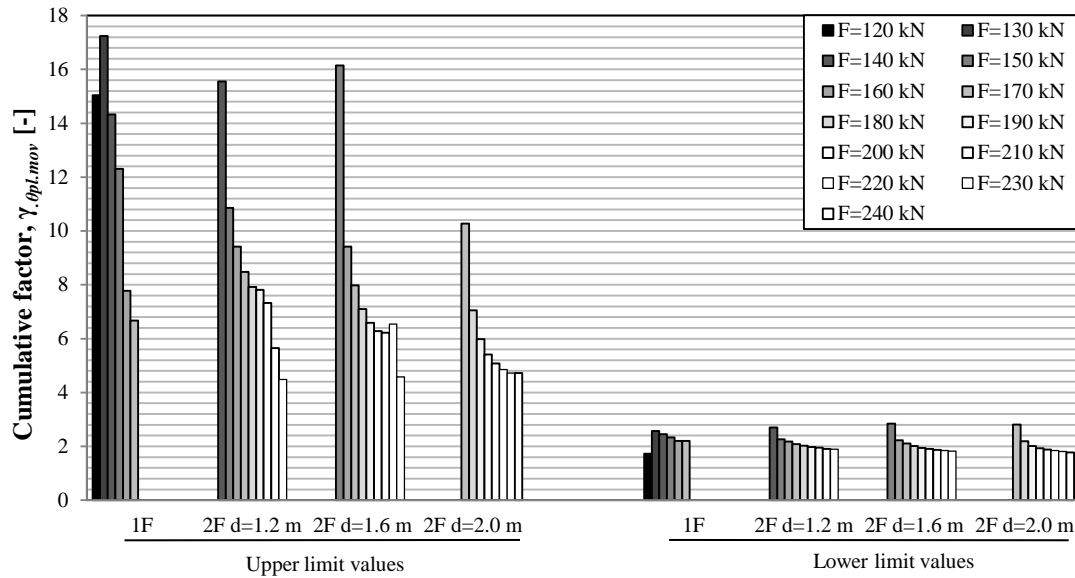
Figure 8.18   Cumulative factors. Cantilever structure.
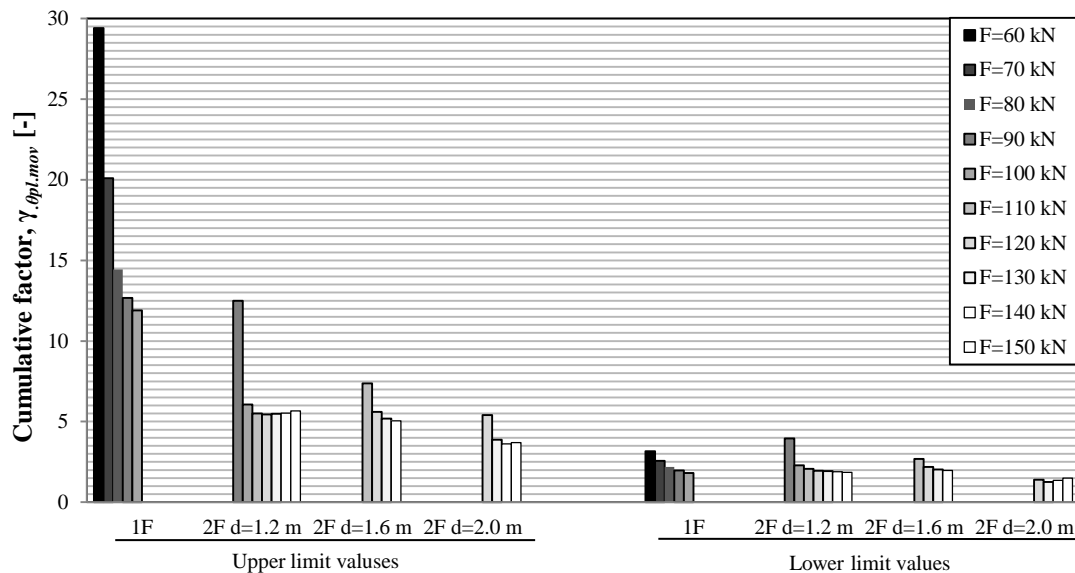
Figure 8.19   Cumulative factors. Simply supported structure.

From Figure 8.18 and Figure 8.19, it can be seen that the upper limit of the cumulative factor decreases with increased load magnitude and increased distance *d* between the pair of moving concentrated forces. The lower limit of the cumulative factor behaves similarly but to a lesser extent and exhibits a more stable behaviour. This behaviour applies for both structures studied in this Thesis. Two crucial observations can be made from these results:

- Static forces yielded plastic rotations closer to what was obtained from moving forces when the magnitude was increased and the distance between the moving concentrated forces were increased.
- The moving forces caused plastic rotation that was 1.5 to 30 times greater than what was caused by static forces of the same magnitudes.

It is also crucial to observe that the maximum value of the lower limit values was in the magnitude of 4. This means that a moving concentrated force that is applied once,

which is reasonable to assume, can cause plastic rotations four times greater than a static force of the same magnitude. This indicates that the load application (static or moving) is vital when estimating the structural response and the corresponding damage.

8.2.3 Traditional superposition approach

It was observed in Section 8.2.1 that the load history was of great importance for the case of cumulative damage for both structures. It was therefore essential to study if a traditional superposition approach could be utilized when estimating future damage on a structure where a damaging process has been initiated. The superposition approach used in this Thesis is illustrated in Figure 8.20.
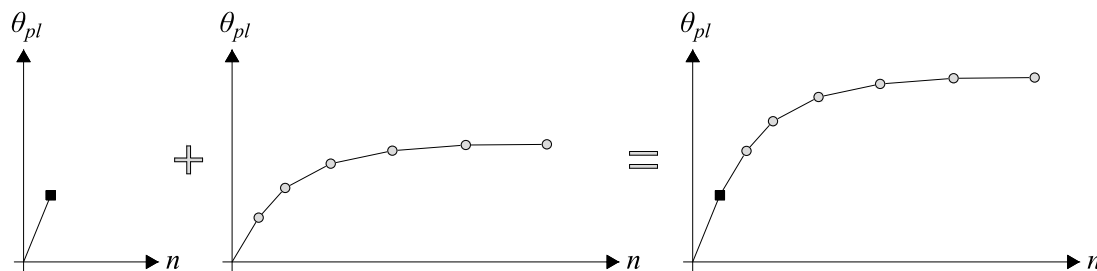
Figure 8.20   The superposition approach used in this Thesis.

In order to study if a superposition approach is a valid method for the development of plastic rotation; the structures were subjected to the three following load combinations of single forces:

LC_{A1}: One large force ($n = 1$) followed by one smaller force ($n = 5$)

LC_{A2}: One small force ($n = 5$) followed by one large force ($n = 1$)

LC_B: One small force ($n = 3$) followed by one large force ($n = 1$) followed by one small force ($n = 2$)

Where n was the number of load cycles for each applied force F.

It can be seen in Figure 8.21 and Figure 8.22 that a traditional superposition approach greatly overestimated the plastic rotation. The figures illustrate the plastic rotation after six load cycles for the load combinations stated above. There is a slight difference between the plastic rotations caused by these combinations and it can be seen that it was advantageous for the structure to be subjected to the larger force when the accumulated damage was small.

The worst case was not the opposite of this, i.e. to apply the larger force when the accumulated damage in the structure was large. The most disadvantageous load combination was to apply a large force right after a damaging process had been initiated. This means that the most advantageous and disadvantageous load combinations were separated by only one force that caused plastic rotation.

It should however be noted that the difference is small and these results should therefore be treated with care.
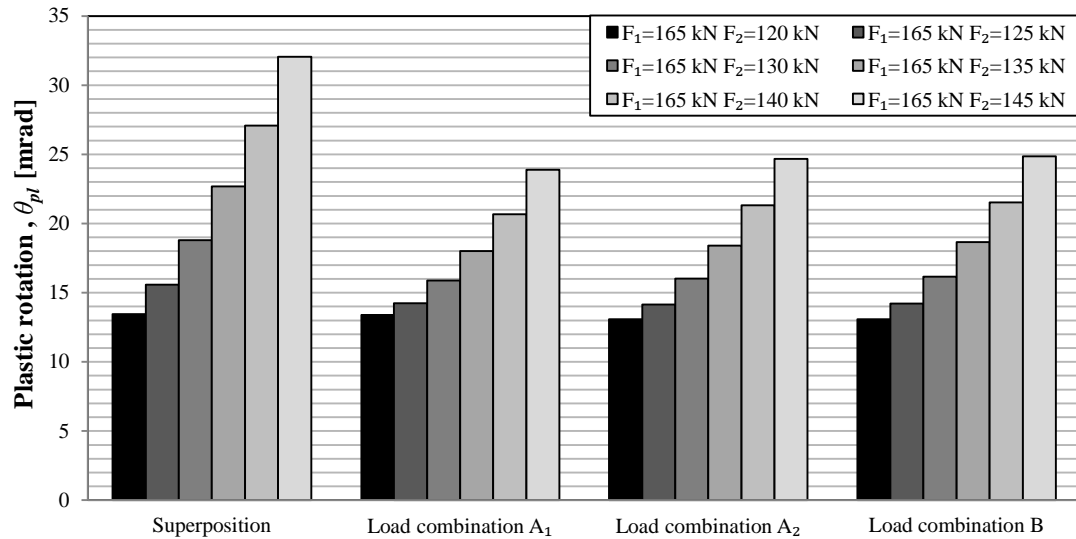
Figure 8.21   Plastic rotation θ_{pl} after six load cycles. Cantilever structure.
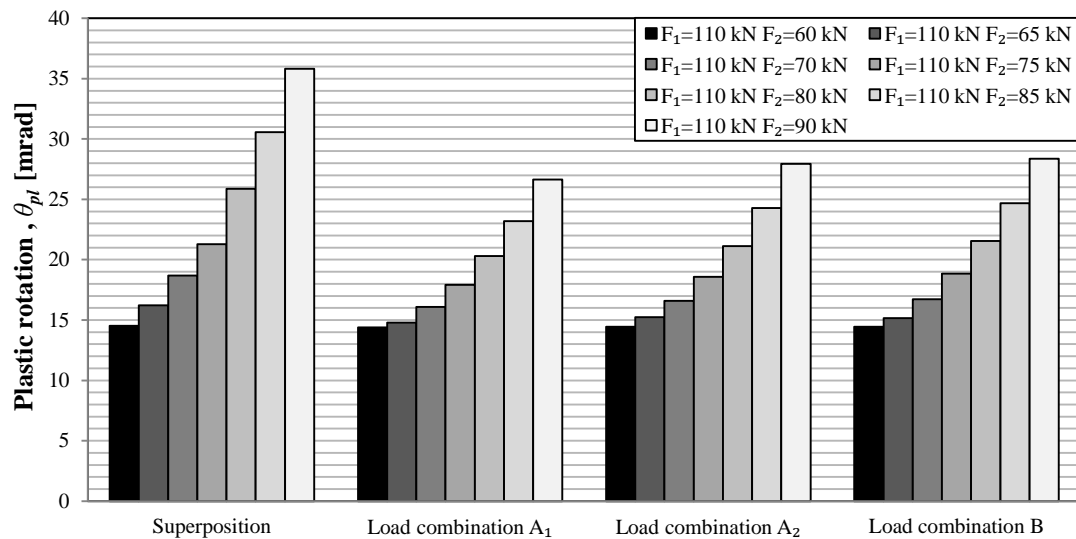
Figure 8.22   Plastic rotation θ_{pl} after six load cycles. Simply supported structure.

8.2.4 Proposed superposition approach

It has been illustrated in Section 8.2.3 that a traditional superposition approach is not recommended (or even valid) for the development of plastic rotation. It was however discovered that an alternative superposition approach could be utilized in order to predict the development of future damages. This superposition approach is based on the plastic rotation obtained after the first load cycle and it is possible, from this value, to predict the future development of plastic rotation in the structures studied in this Thesis. This discovery was made in the final stage of this Thesis and was therefore not thoroughly studied. The aim of this section is therefore to provide fundamental knowledge of this superposition approach in order to initiate further studies within the subject.

As stated above, the proposed superposition approach was based on the plastic rotation caused by the first load cycle which is illustrated in Figure 8.23.
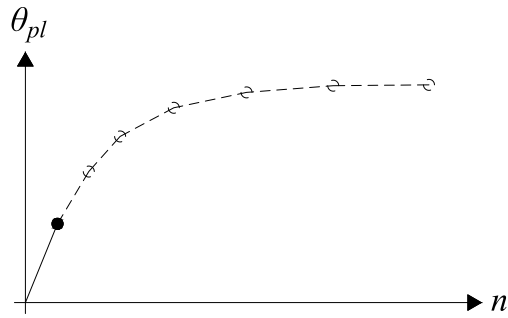
Figure 8.23   Proposed superposition approach.

For each load cycle *n* of a single and two moving concentrated forces of varying and equal magnitudes, a development factor $\gamma_{D.\theta pl.n}$ was defined according to Equation (8-14):

$$\gamma_{D.\theta pl.n} = \frac{\theta_{pl.n}}{\theta_{pl.n=1}} \tag{8-14}$$

A mean value for all development factors was defined according to:

$$\bar{\gamma}_{D.\theta pl.n} = \frac{\sum \gamma_{D.\theta pl.n}}{n_F} \tag{8-15}$$

Where n_F was defined as the number of load magnitudes, and thus analyses, that were conducted for 150 load cycles (a stable state of the plastic rotation was defined at $n = 150$). These mean development factors were used in order to predict the plastic rotation development of a range of single moving forces. This development is illustrated for the cantilever ($n_F = 9$, 120-160 kN) and the simply supported structure ($n_F = 10$, 60-105 kN) in Figure 8.24 and Figure 8.25, respectively.
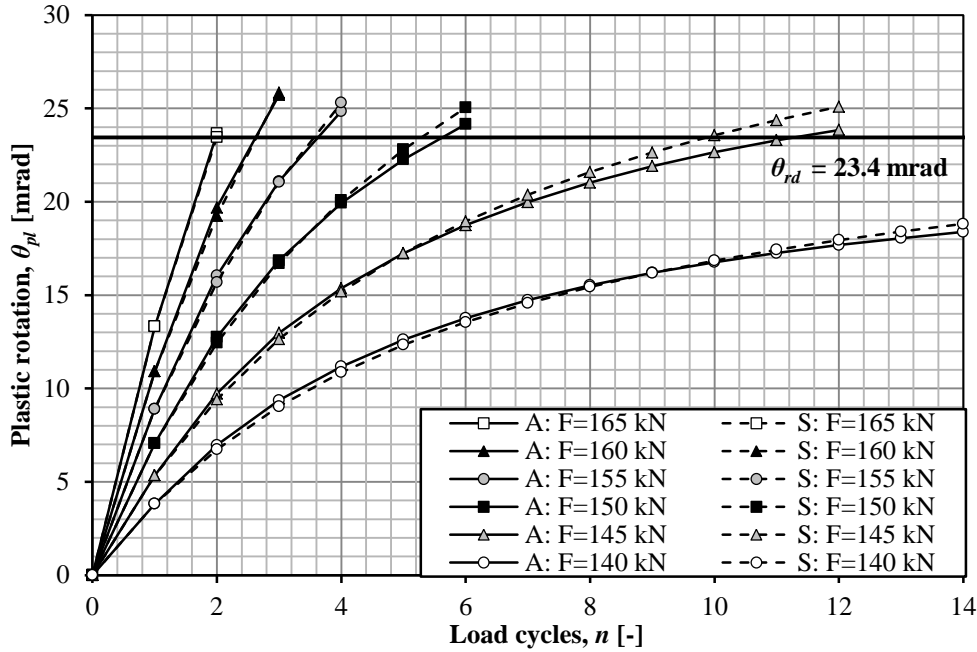
Figure 8.24 Plastic rotation development for the results obtained from analyses (A) and the proposed superposition (S) approach. Cantilever structure.
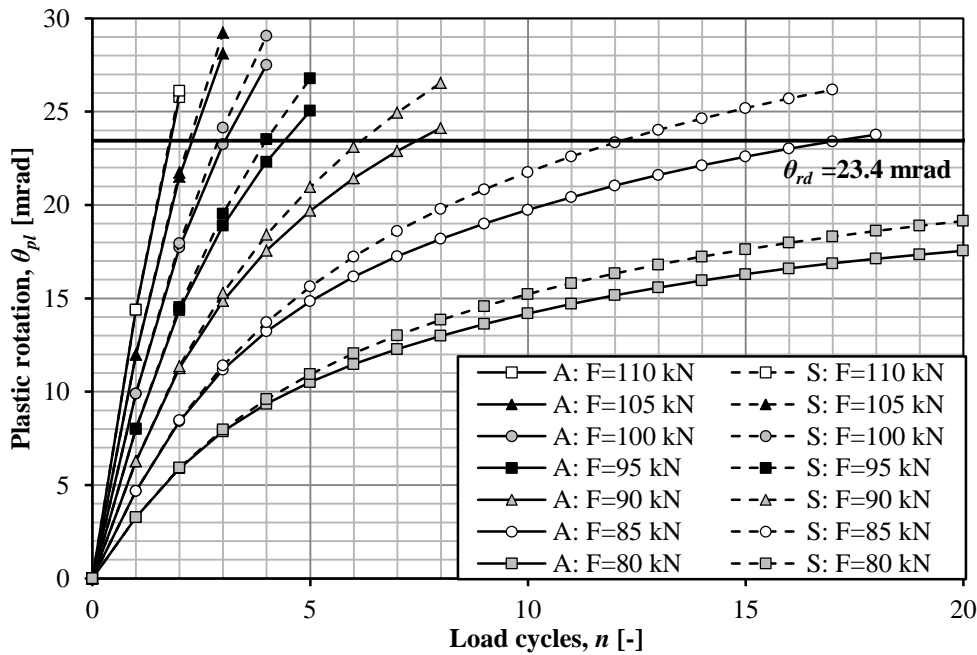
Figure 8.25 Plastic rotation development for the results obtained from analyses (A) and the proposed superposition (S) approach. Simply supported structure.

It can be seen in Figure 8.24 and Figure 8.25 that the results from the proposed superposition approach corresponds rather well to the results obtained from the analyses. This is reasonable since the mean development factor was merely a mean value of the development of the presented forces. The mean factor was, however, of great interest since it indicates that there is one factor for each load cycle from where it is possible to predict the plastic rotation development for a range of force magnitudes. In other words; if the development factor is defined for a small number of

magnitudes, it is possible to predict the plastic rotation caused by forces of inferior or greater magnitudes. The factor is however case specific and therefore has to be evaluated for each load combination and application. The development factor is illustrated in Figure 8.26 and Figure 8.27 for a single force of constant magnitude and two concentrated forces of equal and different magnitudes.
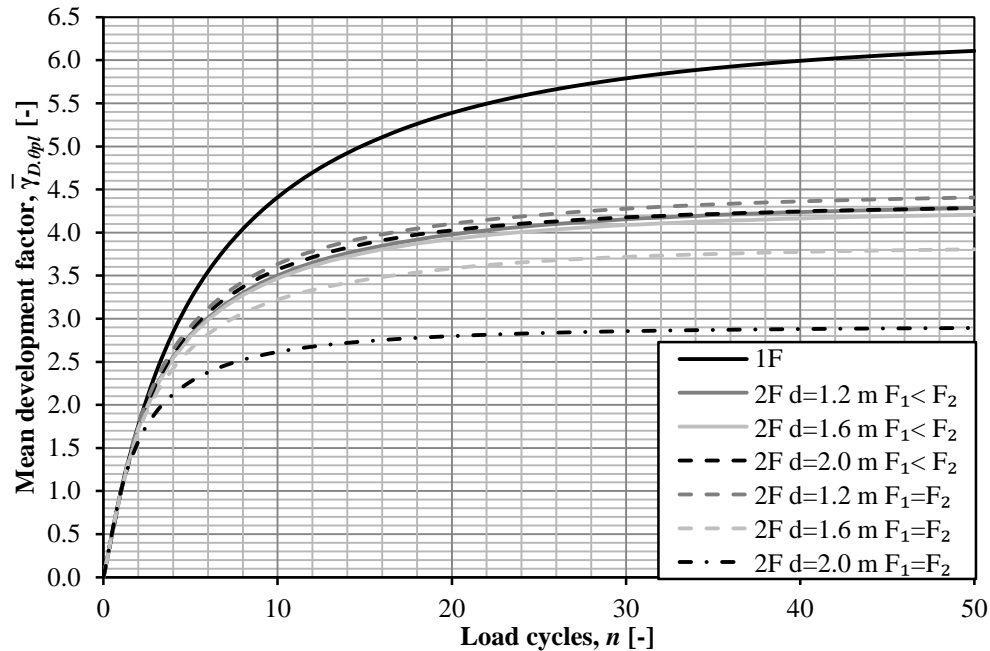
Figure 8.26 Mean plastic development factor. Cantilever structure.
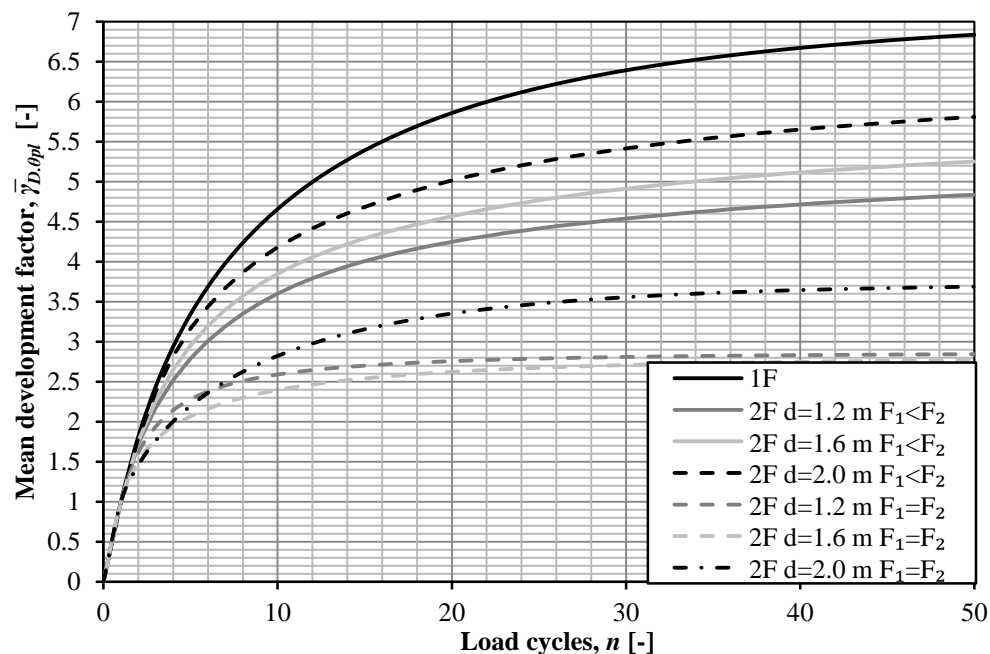
Figure 8.27 Mean plastic development factor. Simply supported structure.

As can be seen in Figure 8.26 and Figure 8.27, the development factor differs between the two studied structures.

It is possible from each separate curve to predict the plastic rotation development of a vast range of force magnitudes. With a larger number of structures, load combinations

and load magnitudes, it should be possible to normalize the development factors to a relatively narrow spectrum. Consequently, it may, from such a spectrum of development factors, be possible to predict the plastic rotation for a large number of ordinary bridge structures and load combinations to a satisfactory extent. Hence, this development could accordingly be related to the cumulative factors, as presented and discussed in Section 8.2.2, and thus be related to static forces of equal magnitudes. In summation; this approach could be used to estimate the plastic rotation development for moving forces, based on the plastic rotation caused by a single static force. This would be advantageous since static forces are less time consuming and cumbersome than moving forces and thus convenient for conventional bridge design analysis. This approach is illustrated in Figure 8.28.
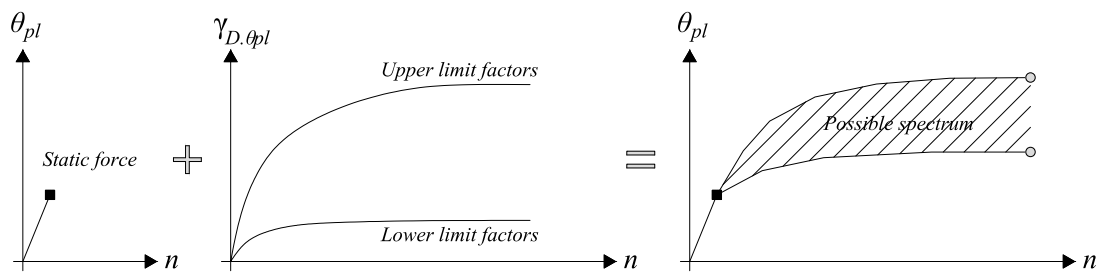
Figure 8.28 Illustration of how the proposed superposition approach can be developed and used.

It can be concluded that no development factors have been presented for forces of varying magnitudes which is the most probable load combination on a bridge structure. It is however believed to be possible, from the superposition approach proposed in this Thesis, to relate a development factor to an existing damage θ_{pl} and the plastic rotation capacity θ_{rd}. Consequently, it should, from such a relation, be possible to estimate future damages caused by forces of varying magnitudes and thus cover a wide spectrum of possible load combinations that are of interest in the bridge design community.

8.3 Shear force distribution

The shear force distribution has not been discussed in this Thesis, but is presented for the interested reader in Appendix I for the studies related to moment distribution in SLS. However, some unexpected irregularities were discovered in the shear force distributions and are therefore pointed out in this section. One such irregularity is that for the linear elastic analyses, with a single concentrated force positioned in the center of the slab, the maximum shear force was not obtained in the center, where the maximum moment is positioned. The shear force distributions for the cantilever slab in the linear elastic case are presented in Figure 8.29a. Further, unexpected local peak values were obtained in the non-linear analyses. These peaks are positioned at locations where the moment-curvature relations in the beam elements are in, or close to the horizontal part of the trilinear relation, see Figure 8.29b.

(a)   *(b)*
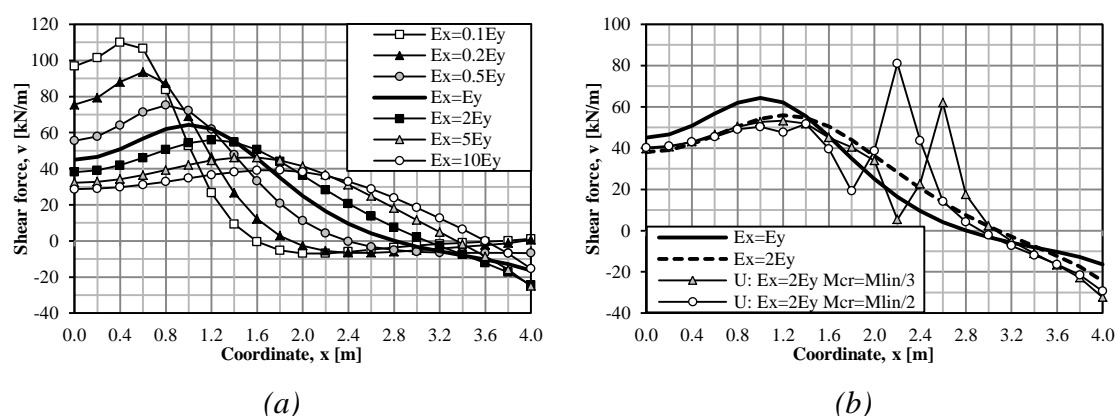
Figure 8.29 Shear force distribution, cantilever slab with a single force. (a) Linear elastic case (b) Case Uncracked $E_x = 2E_y$

The shift in position of the maximum shear force in the linear elastic case seems to be a product of the beam grillage model, and is not obtained in a corresponding shell element model. It was shown in this Thesis that the torsional stiffness of the beam elements had a significant influence on the structural response of a beam grillage model. The effect discussed above is present even for an elastic (uncracked) torsional stiffness, but is magnified with lowered torsional stiffness. The peak values shown in Figure 8.29b was not obtained in Lim (2013) for similar analyses. This is most probably due to the fact that an elastic (uncracked) torsional stiffness was utilized in the beam elements.

The majority of results in this Thesis are based on bending action, which is believed to be more accurately described by the beam grillage model than the shear force distribution. However, the effects described above should be further studied in order to verify the use of a beam grillage model for non-linear analysis.

9 Concluding remarks

The conclusions derived in this Thesis and proposals for further studies within the field are presented in this chapter.

9.1 Conclusions

This Thesis studied the response of reinforced concrete slabs subjected to concentrated forces. Two main aspects were studied, namely moment distribution in the serviceability limit state and cumulative plastic rotation where the latter arises from cyclic moving forces.

A beam grillage model in liaison with multi-linear moment-curvature relations that defined the material response was utilized. However, difficulties arose regarding the choice of the torsional stiffness and how it should be implemented in such an analysis. A parametric study performed in this Thesis showed that the torsional stiffness has a significant effect on the structural response in a beam grillage model. Further, unexpected irregularities were discovered in the shear force distribution when utilizing a beam grillage model.

Studies related to moment distribution in SLS showed that results from a linear orthotropic model correspond to those obtained from a multi-linear model. A model which takes uncracked parts of the structure into account, only display a marginally lower maximum moment. However, an orthotropic stiffness which may arise from varying normal stresses in the two main directions of a slab was shown to have a significant effect on the moment distribution. Results indicated that the maximum moment could be reduced by approximately 20-25 %, if the transverse direction of the slab had the stiffness of uncracked concrete, while the studied direction had a stiffness of cracked reinforced concrete. Further, the recommendations given for moment redistribution in Pacoste *et al.* (2012) were shown to be conservative for the studied cases. However, it is difficult to predict to what extent the recommendations are conservative due to the difficulties in estimating the torsional stiffness of the beam elements used in the model.

Studies related to cumulative plastic rotation demonstrated that the structures studied in this Thesis adapted to the accumulated damages and was stabilized; i.e. the influence of the applied forces decreased with an increased number of load cycles. Studies showed that there was a significant difference between the plastic rotation caused by static and moving concentrated forces. Due to this significant difference, it is recommended to treat static forces that may cause plastic rotation, such as heavy industrial transportation, with caution. It was shown in this Thesis that the maximum moment may be underestimated due to simplifications in the linear elastic analysis. This underestimation may cause unintended plastic rotation to occur, even for design loads. This further stresses the importance of a cautious approach when authorizing permits for heavy transportation that is generally not allowed on the structure.

Results obtained in this Thesis indicate that a traditional superposition approach of load combinations greatly overestimates the plastic rotation development. An alternative superposition approach, based on the plastic rotation after the first load cycle, was therefore proposed in this Thesis. This approach requires further studies in order to expand the method to a broad spectrum of load combinations and structures which may be of great interest for the bridge design community.

9.2 Further studies

A beam grillage model in liaison with linear moment-curvature relations that defines the material response is a common approach in FE analysis today. However, there seems to be a limited amount of documented studies of the behaviour of such a model in liaison with non-linear moment-curvature relations. Consequently, further studies within the field are essential in order to validate the method. The method described could be a powerful tool for non-linear analysis due to its simplicity and numerical stability.

The torsional stiffness of the beam elements in the grillage model was shown to have a significant influence of the structural response. Since difficulties arose regarding how to treat this problem it is proposed to further study the influence of torsional stiffness in reinforced concrete slabs and how it can be treated in a grillage model.

The shear force distribution was not discussed in this Thesis. However, some irregularities were discovered in the solutions. These irregularities should also be further studied in order to verify the use of a beam grillage model.

The studies of plastic rotation development were directed towards the bearing capacity of structures and showed that the plastic rotation accumulates for cyclic loads. Furthermore, it is of interest to study how this type of loading correlates to a reduced service life of the structure, due to the induced damage. Consequently, it ought to be of great societal interest to quantify the actual cost, based on the reduced service life of the structure, of authorizing heavy transportation.

The proposed superposition approach for moving cyclic load was just briefly studied in this Thesis. A study conducted on additional structures with varying geometries, load combinations and load magnitudes could yield further knowledge on how to estimate the plastic rotation development based on static forces.

10 References

ADINA (2012) *Theory and Modelling Guide,* Vol 1: ADINA Solids & Structures Report ARD 11-8, ADINA R & D, Inc., Watertown, MA. USA.

B7 (1968) *Bestämmelser för betongkonstruktioner - Allmänna konstruktions-bestämmelser*, Statens betongkommitté, Svensk byggtjänst, Stockholm, Sweden.

BBK 04 (2004) *Boverkets handbok om betongkonstruktioner, BBK 04*, Boverket, Sweden.

Bro (2004) *Vägverkets allmänna tekniska beskrivning för nybyggande och förbättring av broar*, Vägverket, Sweden.

CEN (2003) *Eurocode 1: Action on structures – Part 2: Traffic loads on bridges*, European Comittee for Standardization, Brussels, Belgium.

CEN (2004) *Eurocode 2: Design of concrete Structures – Part 1-1: General rules and rules for buildings,* European Comittee for Standardization, Brussels, Belgium.

Davidsson M. (2003) *Strukturanalys av betongkonstruktioner med finita elementmetoden*, Brosamverkan Väst, Göteborg, Sweden.

Engström B. (2011) *Design and analysis of continuous beams and columns*, Report 2007:3, Edition 2011. Division of Structural Engineering, Concrete Structures, Chalmers University of Technology, Göteborg, Sweden.

Hedman O., Losberg A. (1976) *Skjuvhållfasthet hos tunna betongplattor belastade med rörliga punktlaster*, Preliminär delrapport till Vägverket, Sweden.

Lim S. (2013) *Redistribution of force concentrations in reinforced concrete cantilever slab using 3D non-linear FE analyses,* Division of Structural Engineering, Concrete Structures, Chalmers University of Technology, Göteborg, Sweden.

Lopes A.V., Lopes M.R., Carmo R. (2014) *Stiffness of reinforced concrete slabs subjected to torsion*, Department of Civil Engineering, University of Coimbra

Nowak A. S. (1993) *Live load model for highway bridges.* Structural safety vol 13, pp 53-56.

Pacoste C., Plos M., Johansson M. (2012) *Recommendations for finite element analysis for the design of reinforced concrete slabs.* Royal Institute of Technology, Stockholm, Sweden.

Siegert D., Estivin M., Billo J., Barin F. and Toutlemonde F. (2008) *Extreme Effects of the Traffic Loads on a Prestressed Concrete Bridge*. In Jacob B., editor, 10th International Conference of Heavy Vehicle, pp 379-387, Paris France.

Treacy M. A. & Brühwiler E. (2013) *Extreme action effects in reinforces concrete bridges from monitoring.* International Association for Bridge and Structural Engineering, vol 99, pp 144-145.

Zhou Y. X., Schmidt F., Jacob B., Toutlemonde F. (2014) *Accurate and up-to-date evaluation of extreme load effects for bridge assessment.* Transport Research Arena, Paris, France, vol 1.

Appendix A   Modelling Choices

This chapter covers the modelling choices that were made concerning mesh densities, beam widths for the beam grillage models etc. Since one aim of this Thesis is to study the moment distribution and redistribution in SLS, most modelling choices were based on moment distribution.

A.1 Cantilever slab

This section covers the chosen mesh densities for both the shell element model and the beam grillage model.

A.1.1 Shell element model

For the shell element model, mesh sizes of 0.1, 0.2 and 0.4 m were studied. The moment distributions along the fixed edge are shown in Figure A.1. The shell model was only used for a linear isotropic elastic analysis. A modulus of elasticity $E = 33$ GPa was used as input.
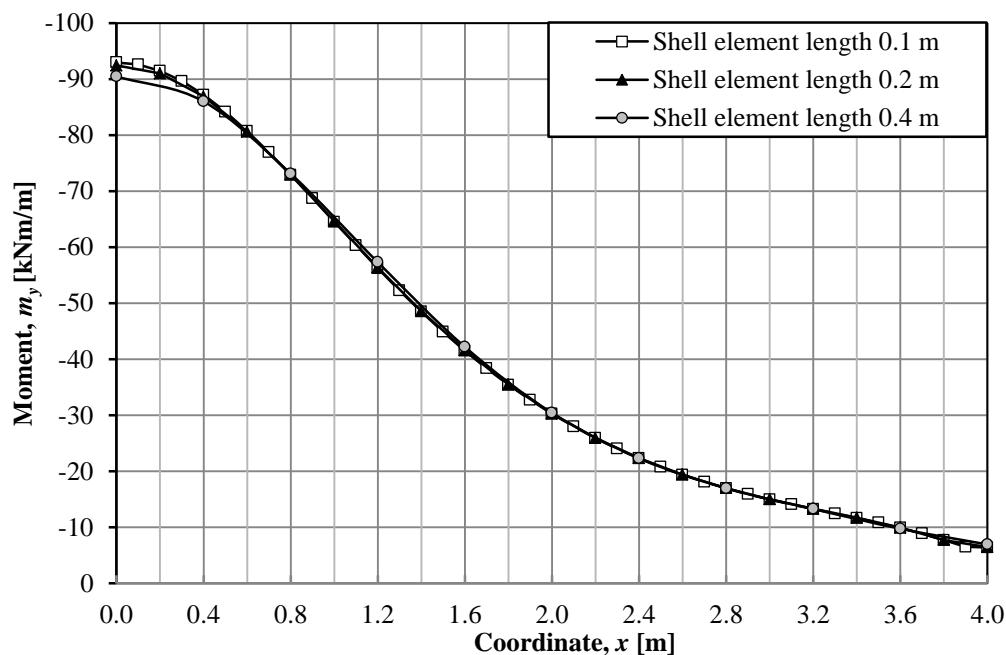
Figure A.1   Moment distribution along the fixed edge, shell element model.

It was concluded that the model with 0.2 m mesh size yielded satisfying results and was, due to the converged behaviour, chosen for further analysis.

A.1.2 Beam grillage model

In order to determine an appropriate beam grillage model, beam widths of 0.1, 0.2 and 0.4 m were compared to the shell element model. It should here be noted that the mesh size of the beams was set to the width of the beam elements so that nodes were positioned at the intersection between two beams. For linear elastic analysis, there was no difference in the results obtained for beams with smaller mesh size, i.e.

additional nodes between the intersections. The analysis was isotropic and a modulus of elasticity $E = 33$ GPa was used as input. The beam elements were modelled with a linear elastic material and a rectangular cross-section in ADINA, which means that ADINA calculated the torsional stiffness of the beam element from the modulus of elasticity and the geometry of the cross-section. A comparison of the moment distribution between the beam grillage models and the shell element model is shown in Figure A.2.
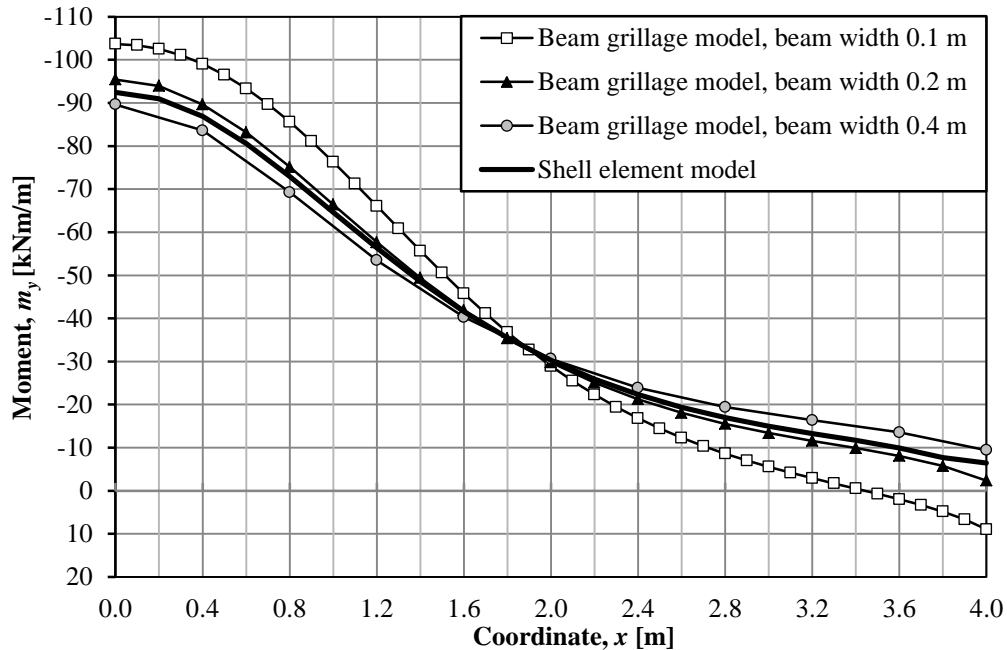
Figure A.2   Comparison between shell element model and beam grillage models with varying beam widths.

The maximum moment was of most interest in this Thesis and it was believed that the shell element model yielded the most reasonable results for a linear elastic analysis. Therefore, the model that corresponded best with the shell element model, comparing the maximum moments, was chosen for further analysis. It was concluded that the beam grillage model with beam width 0.2 m yielded satisfying results in the isotropic linear elastic case. Therefore, a beam grillage model with a beam width of 0.2 m was chosen for further analysis. The difference between the obtained results can be derived from the influence of the torsional stiffness which is studied in Appendix B. The choice of 0.2 m beam width was also made in Lim (2013) for similar studies.

A.2 Simply supported slab

This section covers the chosen mesh densities and load application for the simply supported one-way slab.

A.2.1 Shell element model

For the shell element model, mesh sizes of 0.1 and 0.2 m were studied. The moment distributions for both cases are shown in Figure A.3. The shell model was only used for linear elastic analysis. The analysis was isotropic and a modulus of elasticity $E = 33$ GPa was used as input.
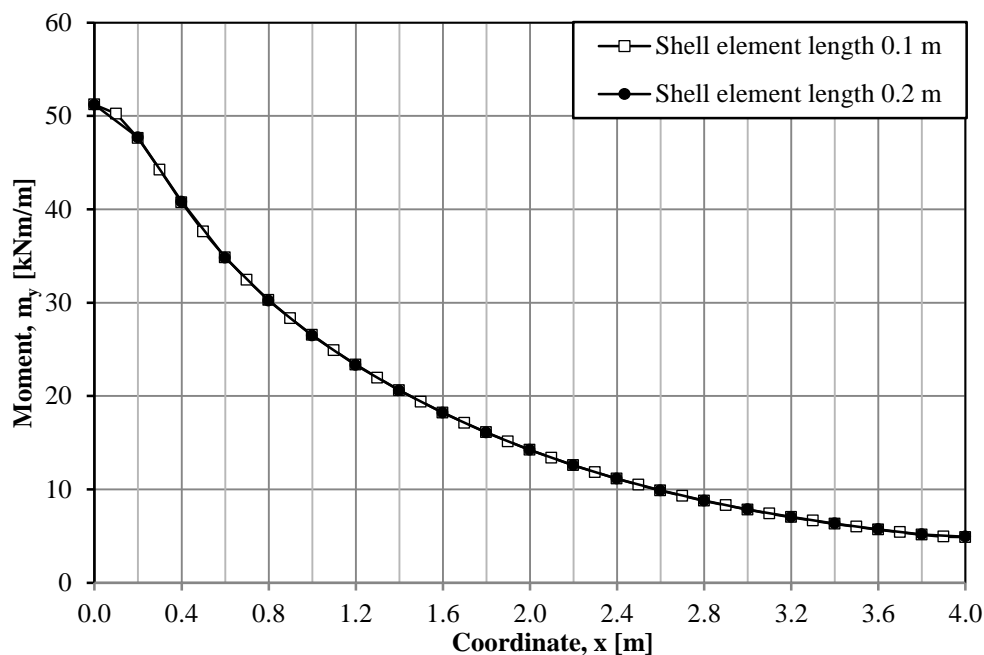
Figure A.3   Moment distribution along the centre of the slab, shell element model.

It was concluded that the model with 0.2 m mesh size yielded satisfying results and was, due to the converged behaviour, chosen for further analysis.

A.2.2 Beam grillage model

In order to determine an appropriate beam grillage model, beam widths of 0.1 and 0.2 m were compared with the shell element model. Models of greater widths were not of interest due to the load application, where the concentrated force was distributed over an area of 0.2 x 0.2 m^2 in the double-symmetric model. It should here be noted that the mesh size of the beams were equal to the width of the beams so that the nodes were positioned at the intersection between two beam elements. The analysis was isotropic and a modulus of elasticity $E = 33$ GPa was used as input. The beam elements were modelled with a material and cross-section in ADINA, which means that ADINA calculated the torsional stiffness of the beam element from the modulus of elasticity and the geometry of the cross-section. A comparison of moment distribution between the beam grillage model and the shell element model is shown in Figure A.4.
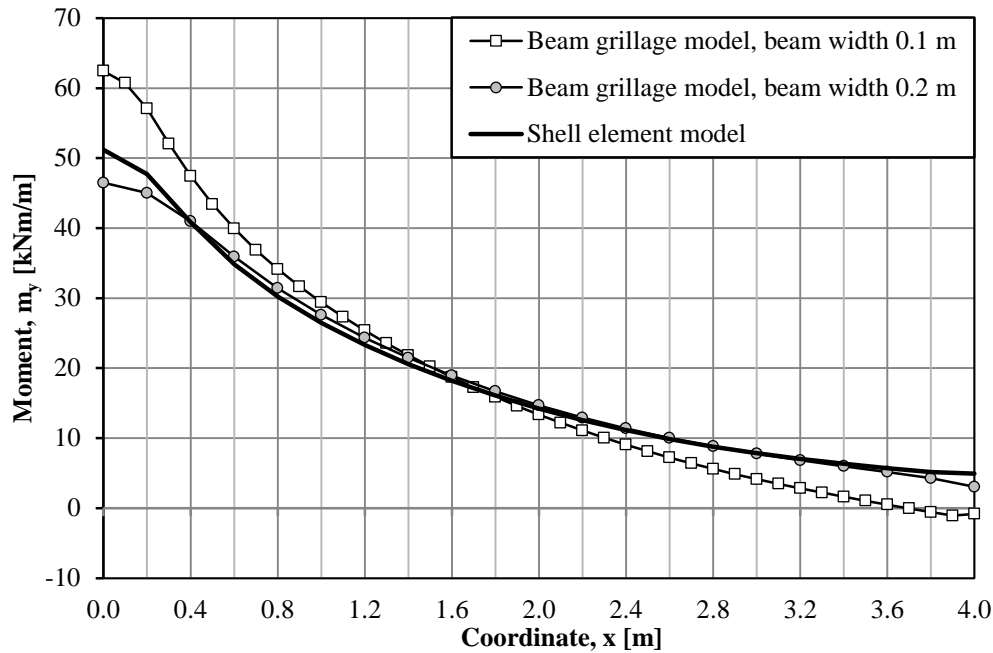
Figure A.4 Comparison between shell element model and beam grillage models with varying beam widths.

The maximum moment is of most interest in this Thesis. And it is believed that the shell element model yields the most reasonable results for a linear elastic analysis. Therefore, the model that corresponded best with the shell element model, comparing the maximum moments, was chosen for further analysis. It was concluded that the beam grillage model with beam width 0.2 m yielded satisfying results in the isotropic linear elastic case. Therefore, a beam grillage model with a beam width of 0.2 m was chosen for further analysis. The difference between the obtained results can, as in the case of the cantilever structure, be derived from the influence of the torsional stiffness which is studied in Appendix B.

A.2.3 Influence of load model

For the cantilever slab, the load model did not affect the moment distribution to a noticeable extent. This, because the moment was measured a certain distance from the applied load. However, for the case of the simply supported slab, the moment was measured in a line that crossed the applied load. It was therefore important to choose an appropriate load model that yields reasonable results.

The shell element model was modelled with a pressure load which is intuitively the most reasonable way to model a concentrated force coming from a tire of a vehicle. However, this was not possible when utilizing beam elements. A study was therefore conducted in order to investigate the response from different load models on the beam grillage model, see Figure A.5.
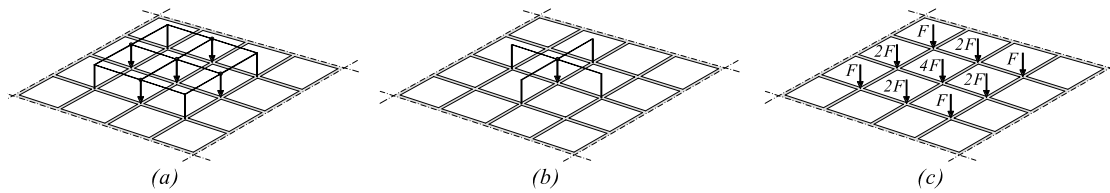
Figure A.5   Load models; (a) grid of line loads, (b) two crossing line loads, (c) point loads acting on several adjacent nodes.

Again, the shell element model was used to compare the three different load models, see Figure A.6.
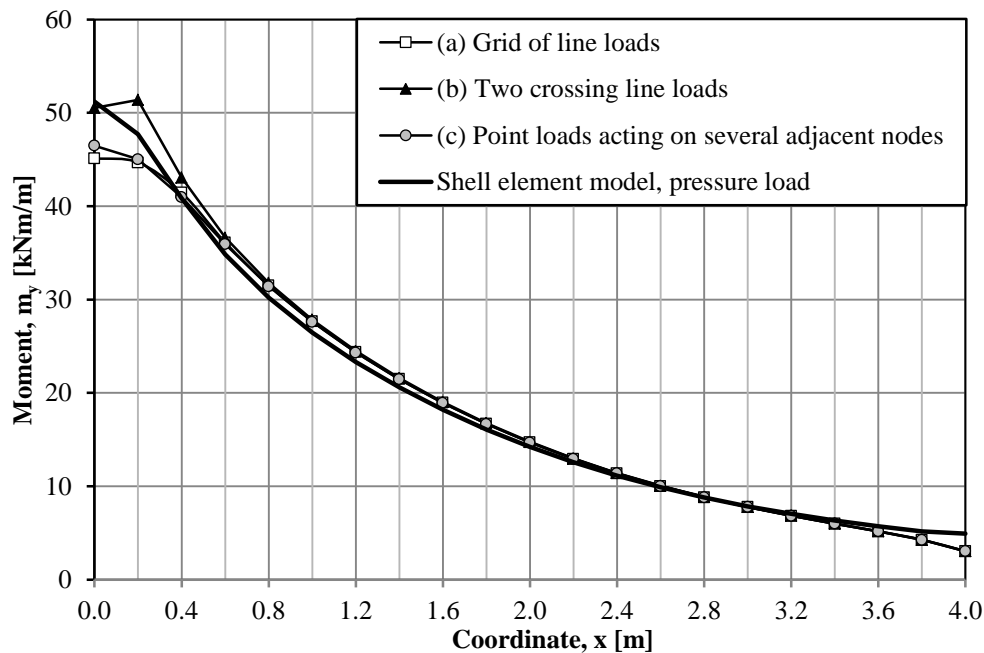
Figure A.6   Comparison of load models.

It was concluded that the shape of the moment distribution from the load model with several adjacent point loads corresponded to the shell element model to the greatest extent. Even though the maximum moment obtained from two crossing line loads were the best fit, the shape was assumed to be unrealistic. The shape probably originated from torsional rigidity errors in the half beam, positioned in the symmetry boundary line. The model with several adjacent point loads also had the advantage of yielding the same total moment as that of a pressure load. The total moment from two crossing line loads was larger due to the fact that additional load was concentrated in the middle of the slab. Therefore, the load model with four point loads was chosen for further analysis.

Appendix B   Torsional stiffness in beam grillage models

This chapter covers the study of the influence of torsional stiffness on beam elements in a beam grillage model. The first section covers the influence of torsional stiffness on moment distribution in SLS. The second section covers the influence of torsional stiffness on plastic rotation development.

Difficulties arose regarding the torsional stiffness when the slabs, presented in this Thesis, were modelled with beam grillage models. The main difficulty was to design the torsional stiffness that was to be used for input values for the beam elements. In Appendix A, it was shown that the beam grillage model, where the widths of the beams were equal to the height of the slab, gave results similar to the linear elastic shell element model. However, since the non-linear behaviour was of interest in this Thesis, multilinear moment-curvature relations were used in order to capture the material response of the structures. The moment-curvature relations were calculated analytically for an equivalent beam with a width equal to the distance between the beam elements, which was believed to be an acceptable approximation. However, the torsional stiffness of slabs is more complicated, and the difference between a grillage model and a plate is more pronounced. It was therefore motivated to perform a parametric study of the influence of the torsional stiffness of the beam elements in the beam grillage model.

For the studies in this section, different magnitudes of the torsional stiffness of the beam elements were chosen. The elastic stiffness, i.e. the stiffness based on the modulus of elasticity and the gross geometry of the cross-section was chosen as reference. A factor 1/8, 1/16 and 0 of the elastic stiffness was thereafter studied.

B.1 Moment distribution in SLS

The study directed towards moment distribution in SLS was performed on the cantilever slab in Chapter 4 and the moment-curvature model was utilized in both main directions of the structure. Both difference in moment distribution and plastic rotation was here of interest.

Linear moment-curvature relations were used which was based on a reference stiffness of 0.5 % reinforcement amount, see Section 4.1.1. A concentrated force of the magnitude $F = 200$ kN was applied, see Figure 4.6. The results from the study with varying torsional stiffness are presented in Figure B.1.
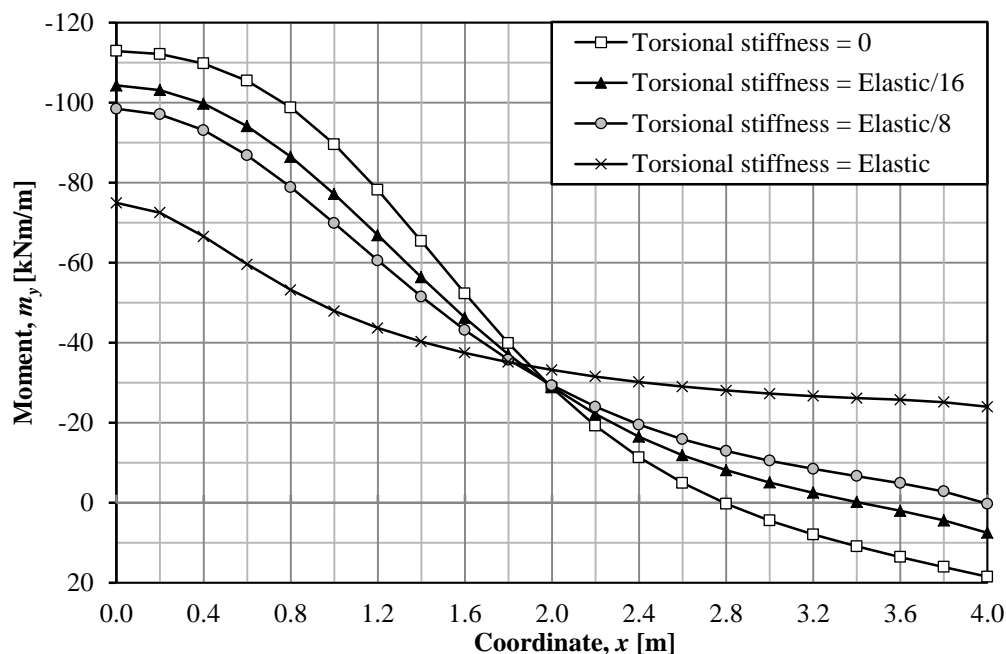
Figure B.1   Moment distribution with varying torsional stiffness for the cantilever slab.

As can be seen in Figure B.1, the moment distribution was significantly influenced by the torsional stiffness of the beam elements. The maximum moment was approximately 50 % greater for the case with no torsional stiffness compared to the elastic stiffness. It should here be noted that the real torsional stiffness of a slab is not linear, which has been assumed in this study, and will change with increased cracking.

The influence of the torsional stiffness when analysing plastic rotation in a slab with the help of beam grillage models was also studied. In Lim (2013), an elastic torsional stiffness was used throughout the Thesis, even for elements which was in the post-cracking state. Both bilinear and trilinear moment-curvature relations were used in the study, and the cantilever slab was of equal dimensions as the one studied here. Also, the applied load was of equal magnitude, i.e. $F = 200$ kN. Similar to the case in Lim, the plastic moment capacity for each beam element was chosen to 60 % of the maximum moment, measured in the linear elastic case with elastic torsional stiffness. For the trilinear case, the cracking moment was chosen to $M_{cr}=M_{lin}/3$. The stiffness in state II was chosen to the reference value based on a reinforcement amount of 0.5 %, see Section 4.1.1. The results from the study are presented in Figure B.2.

CHALMERS, *Civil and Environmental Engineering*, Master's Thesis 2014:73
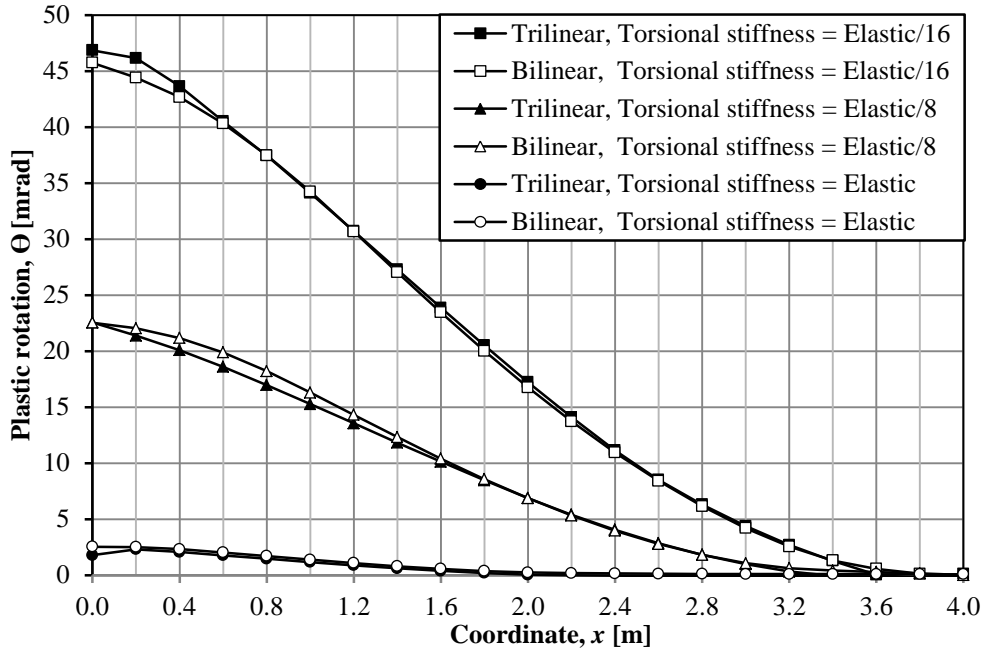
Figure B.2   Plastic rotation with varying torsional stiffness.

The results indicate only a small difference between the bilinear and trilinear cases. For the elastic torsional stiffness, results similar to the ones presented by Lim were obtained. Note that a different state II stiffness was used in this study compared to Lim, which can explain the small deviation between the results. However, the study shows that with decreasing torsional stiffness, the plastic rotation is considerably increased. The case with zero torsional stiffness became too numerically unstable and the analysis was aborted.

This study shows that great care should be taken when the torsional stiffness is chosen. An elastic torsional stiffness will most likely yield results which are not conservative in the post-cracking state, while zero torsional stiffness probably is too conservative and will yield unrealistic deformations, since the stiffness of the slab is greatly reduced.

B.2 Cumulative plastic rotation

The study directed towards cumulative plastic rotation was performed on the cantilever slab in Chapter 6 and the moment-curvature model was also here utilized in both main directions of the structure. Since the study was performed for cumulative plastic rotation, only the results from a completely unloaded slab (i.e. between each completed load cycle) were of interest and the moment distribution was therefore omitted in this section. A study of the plastic rotation obtained from a single static force was also conducted for comparison purposes.

As in Section B.1, the linear moment-curvature relations were used with the same reference stiffness, see Section 4.1.1. Concentrated forces of the magnitudes $F = 135$ kN and $F = 150$ kN was applied on the cantilever structure. The smaller force yielded no plastic rotation for an elastic torsional stiffness and a factor of 1/8 of the elastic stiffness. The case with zero torsional stiffness was also here aborted due to the unstable behaviour of the structure. The applied force was therefore increased to 150 kN and the results from the study are shown for a torsional stiffness of 1/8 and 1/16 of the elastic stiffness in Figure B.3 and Figure B.4, respectively. The elastic torsional stiffness did not yield any plastic rotation and the case with zero torsional stiffness was also here aborted on the same basis as stated above.

As can be seen in Figure B.3 and Figure B.4, the plastic rotation was significantly influenced by the torsional stiffness of the beam elements. It can also be seen that the plastic rotation did not develop over the total length of the structure which can be derived from how the forces were applied, see Chapter 6. As have been stated in Section 6.3.1, the structure adapted to the applied forces and thus appeared to behave linear elastically. The structure was, in fact, in the plastic state and approached a stable state where the development of plastic rotation did not increase significantly for additional load cycles. The maximum plastic rotation, for the case of 1/16 of the elastic stiffness, was for all load cycles 140 to 170 % greater than what was obtained for 1/8 of the elastic stiffness.
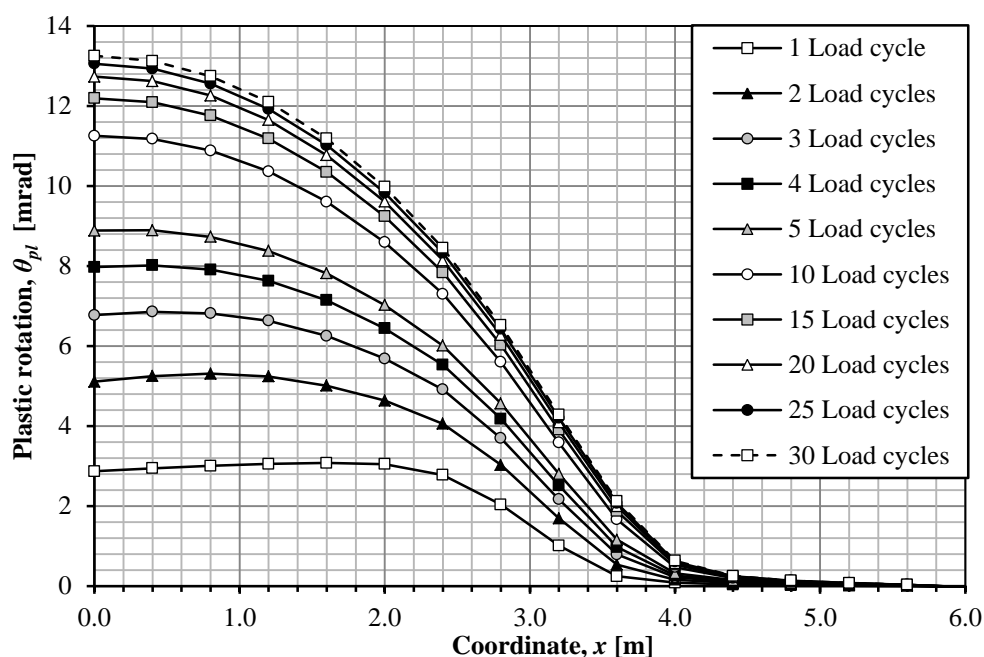
Figure B.3   Plastic rotation development for a torsional stiffness factor of 1/8.
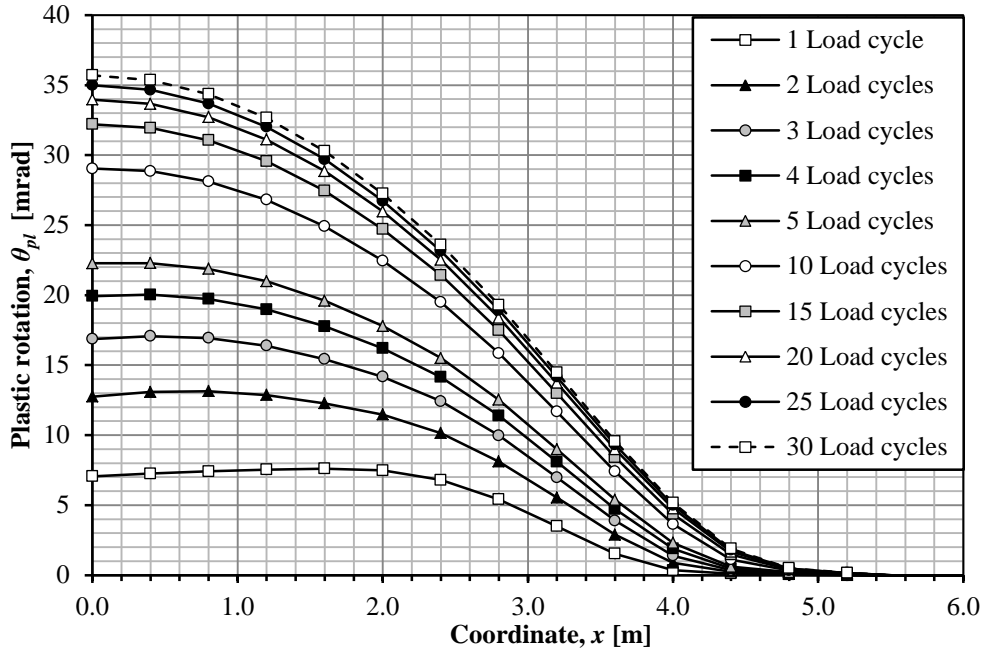
Figure B.4   Plastic rotation development for a torsional stiffness factor of 1/16.

The results from the analysis for a single static force are shown in Figure B.5. In accordance with the results presented in Figure B.3 and Figure B.4, the torsional stiffness was also for static forces of significant importance. The difference in plastic rotation between the static forces was roughly 150 % which corresponded well to what was observed for the moving concentrated forces.
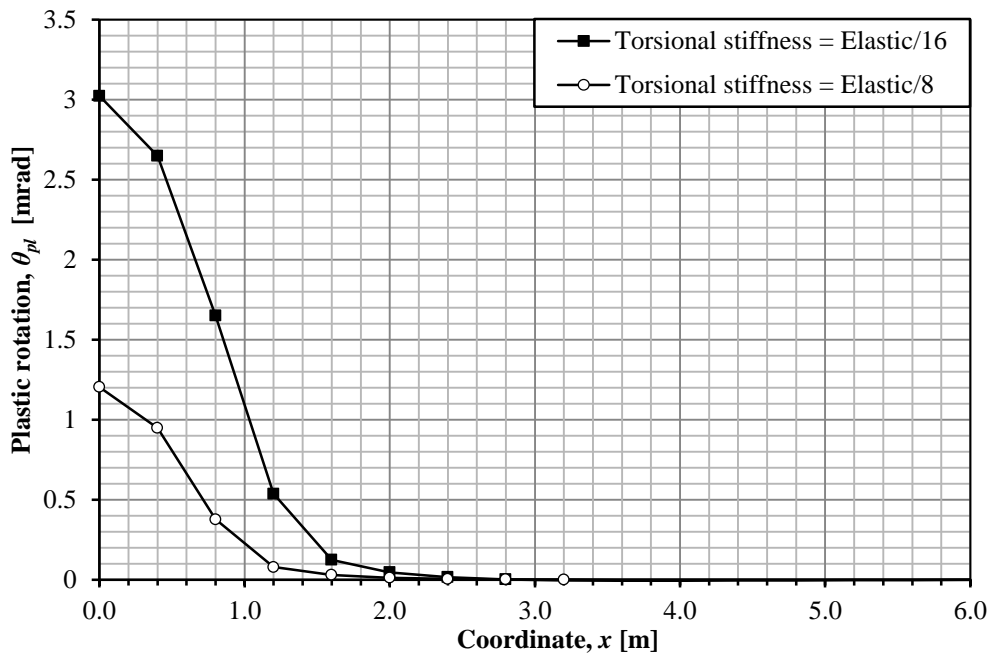
Figure B.5   Plastic rotation for a static concentrated force.

The plastic rotation was, in the case of 1/8 of the elastic stiffness, roughly 140 % greater for a single moving force than for a single static force. This means that the difference was of such magnitude after the first load cycle was completed for the moving force. The difference was thereafter increased towards 1000 %, when the plastic rotation was stabilized after 30 load cycles. For the case of 1/16 of the elastic

stiffness, the difference ranged from 130 to 1100 % for the same spectrum of load cycles. This behaviour was also observed in Section 6.6.2 where the difference decreased with increased load magnitude of the applied force.

It was from this study concluded that the torsional stiffness influences the plastic rotation and the development of plastic rotation to a significant extent. The influence was for the studied load magnitudes not increased as the number of load cycles increased for the moving concentrated forces. However, due to the large difference in the obtained plastic rotation, the torsional stiffness was also for these analyses chosen to 1/16 of the elastic stiffness. This stiffness was believed to be conservative and was utilized throughout the Thesis.

Appendix C Moment-curvature relations

This chapter covers the moment-curvature relations used for the analyses in Chapter 4 to 7 and how these were derived. The first section covers the moment-curvature relations used for the moment distribution in SLS while the second section covers the moment-curvature relations used for the analyses of plastic rotation development.

C.1 Moment distribution in SLS

The moment-curvature relations used in the Chapter 4 and 5, regarding moment distribution in the service state, are presented in this section. For the methodology behind the construction of these relations, the reader is referred to Section 4.1.

Due to numerical stability reasons, a slight inclination was chosen for the second branch of the trilinear relations, such that $M_2 = 1.05 M_{cr}$. Where M_2 is the moment at the intersection between the second and third line. Tests showed that this inclination did not affect the results to a significant extent.

C.1.1 Linear elastic analyses

For linear elastic analysis, the moment-curvature relation is equal for both the cantilever slab and the simply supported slab. The stiffness of an uncracked concrete section with a height and width of 0.2 m was used as a reference. The reference stiffness was used in both directions for the case $E_x = E_y$, and kept constant in the y-direction while the stiffness in the x-direction varied, as presented in Figure C.1. The relations are presented both in a figures and in the form of tabulated values, where linear interpolation can be utilized for intermediate values.

$E_x = 0.1E_y$		$E_x = 2E_y$	
Moment [Nm]	Curvature [1/m]	Moment [Nm]	Curvature [1/m]
0	0	0	0
20000	0.0455	20000	0.00228
$E_x = 0.2E_y$		$E_x = 5E_y$	
0	0	0	0
20000	0.0227	20000	0.0009
$E_x = 0.5E_y$		$E_x = 10E_y$	
0	0	0	0
20000	0.0091	20000	0.00046
$E_x = E_y$			
0	0		
20000	0.00454		
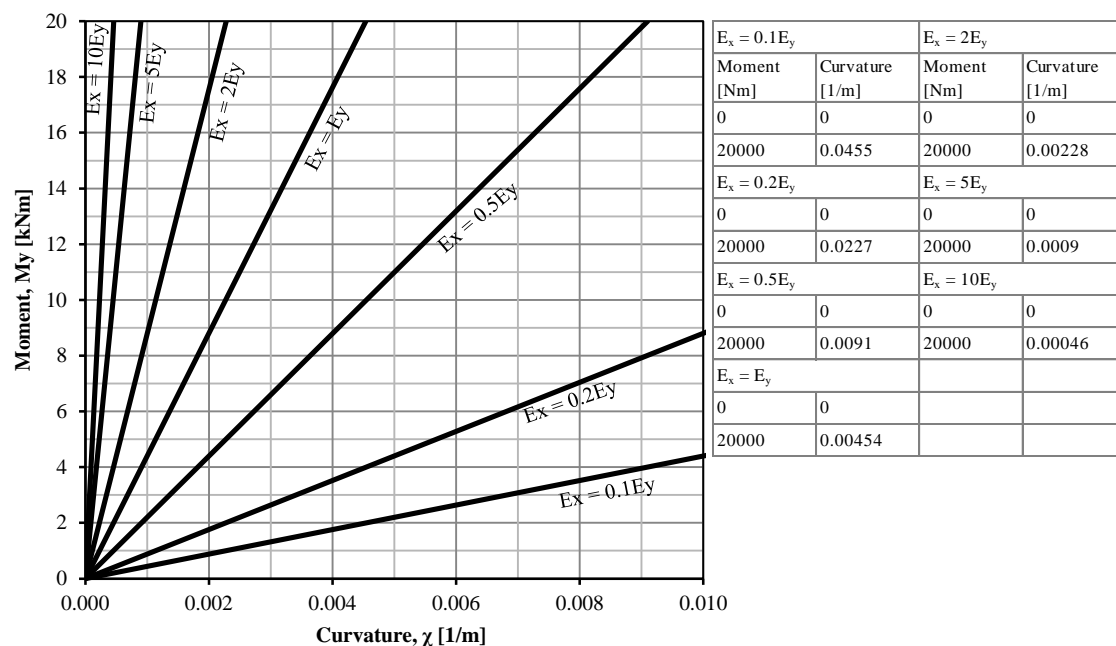
Figure C.1 Moment-curvature relations in the x-direction for linear elastic analyses.

C.1.2 Case Uncracked

The moment-curvature relations for the case Uncracked are presented in this section. The stiffness in the x-direction was kept constant as the stiffness of an uncracked concrete section with a height and width of 0.2 m. Since two levels of the cracking moment M_{cr} was chosen as factors of the maximum moment in the linear solution, the relations are different for the cantilever slab and the simply supported slab, and also for a single force and two forces. The relations are presented as graphs in Figure C.2 to Figure C.5, and as tabulated values in Table C.1 and Table C.2.
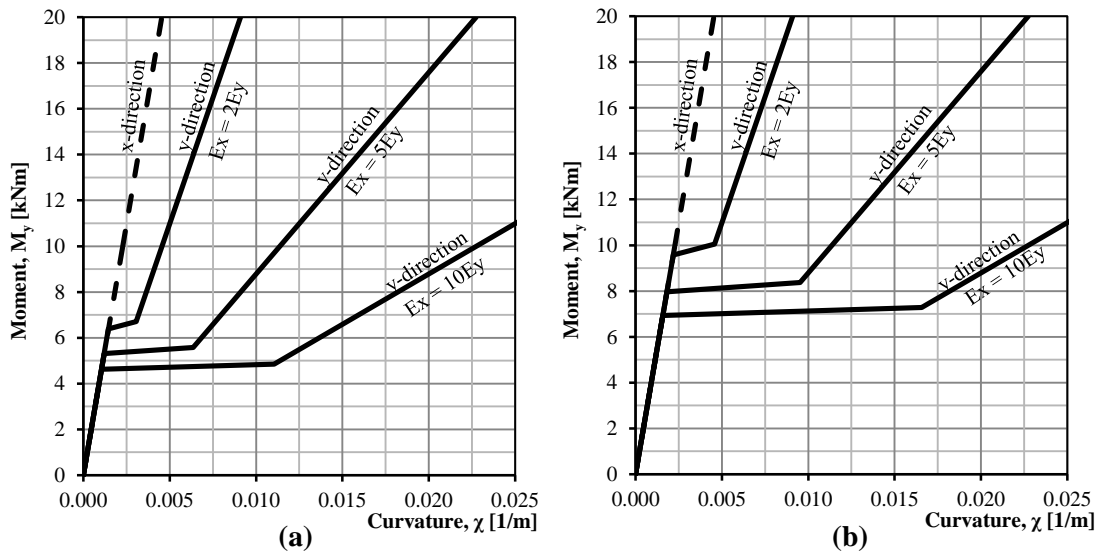
Figure C.2   Moment-curvature relations for the cantilever slab with a single concentrated force, case Uncracked. (a) $M_{cr} = M_{lin}/3$, (b) $M_{cr} = M_{lin}/2$
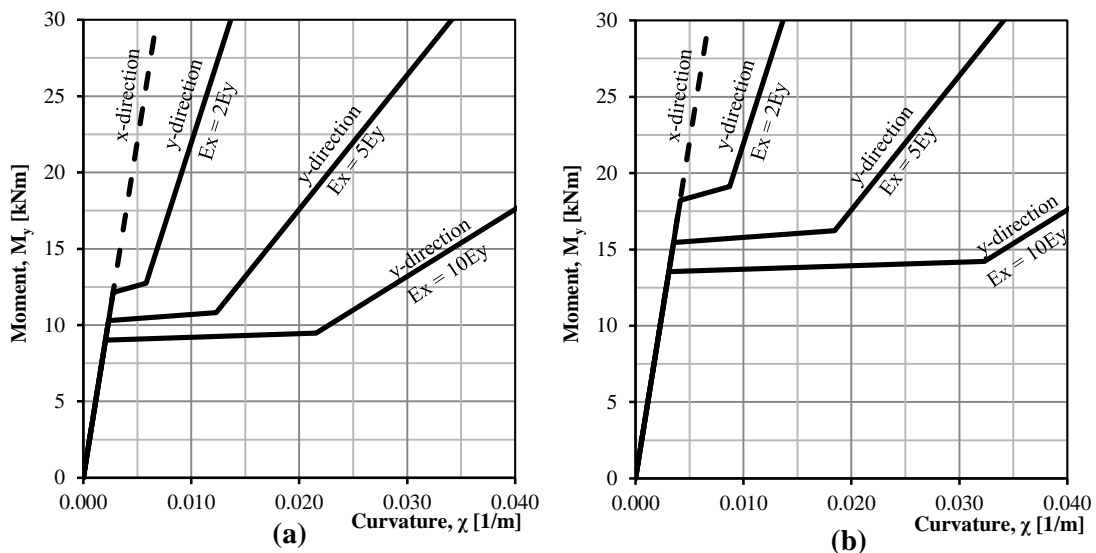
Figure C.3   Moment-curvature relations for the cantilever slab with two concentrated forces, case Uncracked. (a) $M_{cr} = M_{lin}/3$, (b) $M_{cr} = M_{lin}/2$
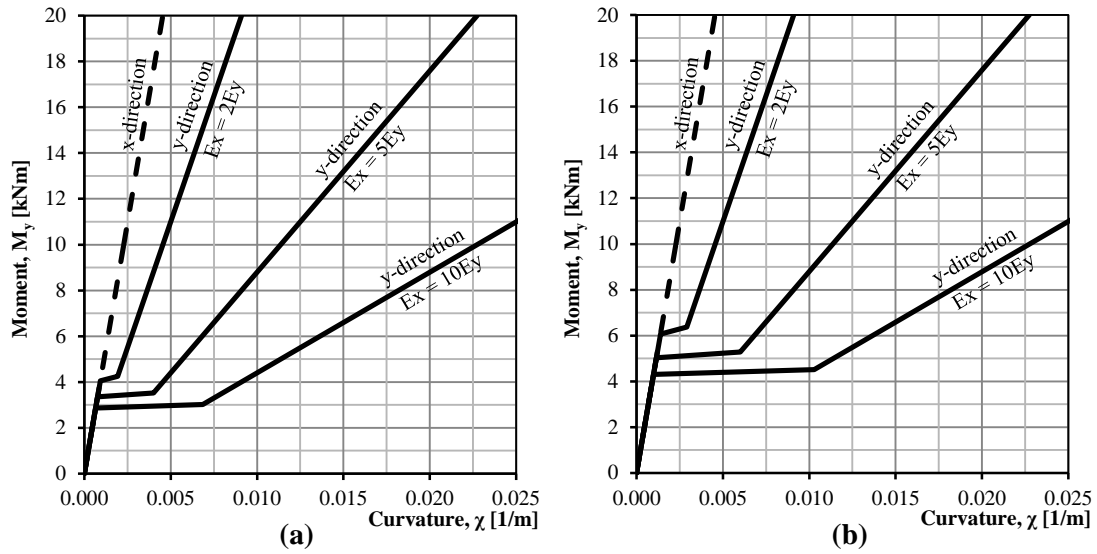
Figure C.4   Moment-curvature relations for the simply supported one-way slab with a single concentrated force, case Uncracked. (a) $M_{cr} = M_{lin}/3$, (b) $M_{cr} = M_{lin}/2$
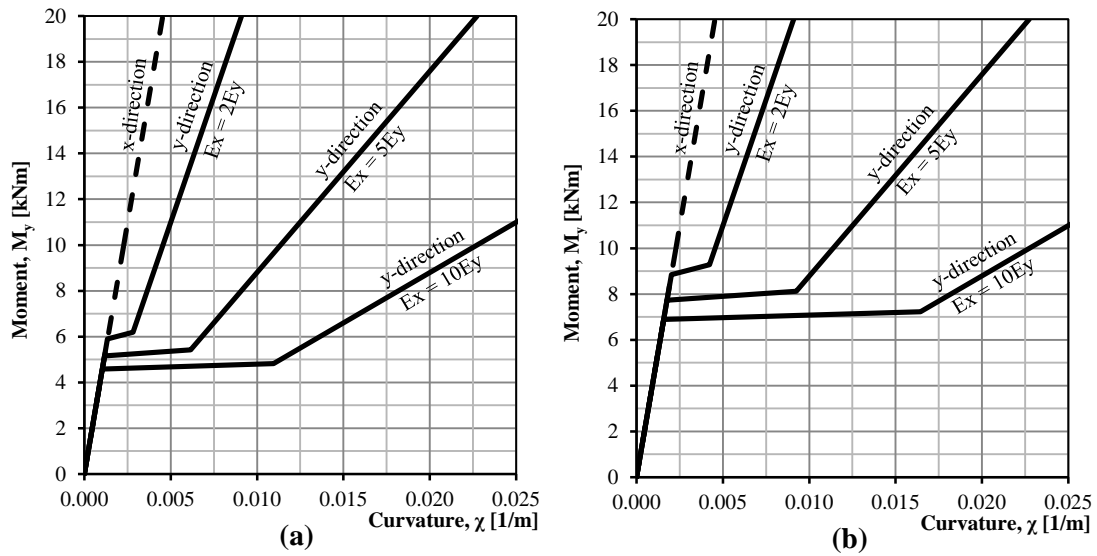
Figure C.5   Moment-curvature relations for the simply supported one-way slab with two concentrated forces, case Uncracked. (a) $M_{cr} = M_{lin}/3$, (b) $M_{cr} = M_{lin}/2$

Table C.1   Moment-curvature relations used in the x-directions, case Uncracked.

Moment [Nm]	Curvature [1/m]
0	0
20000	0.00454

Table C.2   Moment-curvature relations used in the y-directions, case Uncracked.

Cantilever slab, single concentrated force

$M_{cr} = M_{lin}/3$						$M_{cr} = M_{lin}/2$					
$E_x = 2E_y$		$E_x = 5E_y$		$E_x = 10E_y$		$E_x = 2E_y$		$E_x = 5E_y$		$E_x = 10E_y$	
Moment	Curvature	Moment	Curvature	Moment	Curvature	Moment	Curvature	Moment	Curvature	Moment	Curvature
[Nm]	[1/m]	[Nm]	[1/m]	[Nm]	[1/m]	[Nm]	[1/m]	[Nm]	[1/m]	[Nm]	[1/m]
0	0	0	0	0	0	0	0	0	0	0	0
6382	0.00145	5314	0.00121	4624	0.00105	9572	0.00218	7971	0.00181	6936	0.00158
6701	0.00305	5580	0.00635	4855	0.01104	10051	0.00457	8370	0.00952	7282	0.01657
20000	0.00910	20000	0.02275	20000	0.04550	20000	0.00910	20000	0.02275	20000	0.04550

Cantilever slab, two concentrated forces

$M_{cr} = M_{lin}/3$						$M_{cr} = M_{lin}/2$					
$E_x = 2E_y$		$E_x = 5E_y$		$E_x = 10E_y$		$E_x = 2E_y$		$E_x = 5E_y$		$E_x = 10E_y$	
Moment	Curvature	Moment	Curvature	Moment	Curvature	Moment	Curvature	Moment	Curvature	Moment	Curvature
[Nm]	[1/m]	[Nm]	[1/m]	[Nm]	[1/m]	[Nm]	[1/m]	[Nm]	[1/m]	[Nm]	[1/m]
0	0	0	0	0	0	0	0	0	0	0	0
12144	0.00276	10299	0.00234	9022	0.00205	18216	0.00414	15448	0.00351	13533	0.00308
12751	0.00580	10814	0.01230	9473	0.02155	19126	0.00870	16221	0.01845	14210	0.03233
20000	0.00910	20000	0.02275	20000	0.04550	20000	0.00910	20000	0.02275	20000	0.04550

Simply supported one-way slab, single concentrated force

$M_{cr} = M_{lin}/3$						$M_{cr} = M_{lin}/2$					
$E_x = 2E_y$		$E_x = 5E_y$		$E_x = 10E_y$		$E_x = 2E_y$		$E_x = 5E_y$		$E_x = 10E_y$	
Moment	Curvature	Moment	Curvature	Moment	Curvature	Moment	Curvature	Moment	Curvature	Moment	Curvature
[Nm]	[1/m]	[Nm]	[1/m]	[Nm]	[1/m]	[Nm]	[1/m]	[Nm]	[1/m]	[Nm]	[1/m]
0	0	0	0	0	0	0	0	0	0	0	0
4045	0.00092	3350	0.00076	2868	0.00065	6067	0.00138	5026	0.00114	4302	0.00098
4247	0.00193	3518	0.00400	3011	0.00685	6371	0.00290	5277	0.00600	4517	0.01028
20000	0.00910	20000	0.02275	20000	0.04550	20000	0.00910	20000	0.02275	20000	0.04550

Simply supported one-way slab, two concentrated forces

$M_{cr} = M_{lin}/3$						$M_{cr} = M_{lin}/2$					
$E_x = 2E_y$		$E_x = 5E_y$		$E_x = 10E_y$		$E_x = 2E_y$		$E_x = 5E_y$		$E_x = 10E_y$	
Moment	Curvature	Moment	Curvature	Moment	Curvature	Moment	Curvature	Moment	Curvature	Moment	Curvature
[Nm]	[1/m]	[Nm]	[1/m]	[Nm]	[1/m]	[Nm]	[1/m]	[Nm]	[1/m]	[Nm]	[1/m]
0	0	0	0	0	0	0	0	0	0	0	0
5894	0.00134	5157	0.00117	4588	0.00104	18216	0.00414	15448	0.00351	13533	0.00308
6188	0.00282	5415	0.00616	4818	0.01096	19126	0.00870	16221	0.01845	14210	0.03233
20000	0.00910	20000	0.02275	20000	0.04550	20000	0.00910	20000	0.02275	20000	0.04550

C.1.3 Case Neutral

The moment-curvature relations for the case Neutral are presented in this section. The stiffness in state II was kept constant in the y-direction for the different stiffness proportions, while the stiffness in state II varied with the stiffness factor α in the x-direction. However, the level of the cracking moment M_{cr} varied for both directions. The relations are presented as graphs in Figure C.6 to Figure C.9, and as tabulated values in Table C.3 and Table C.4.
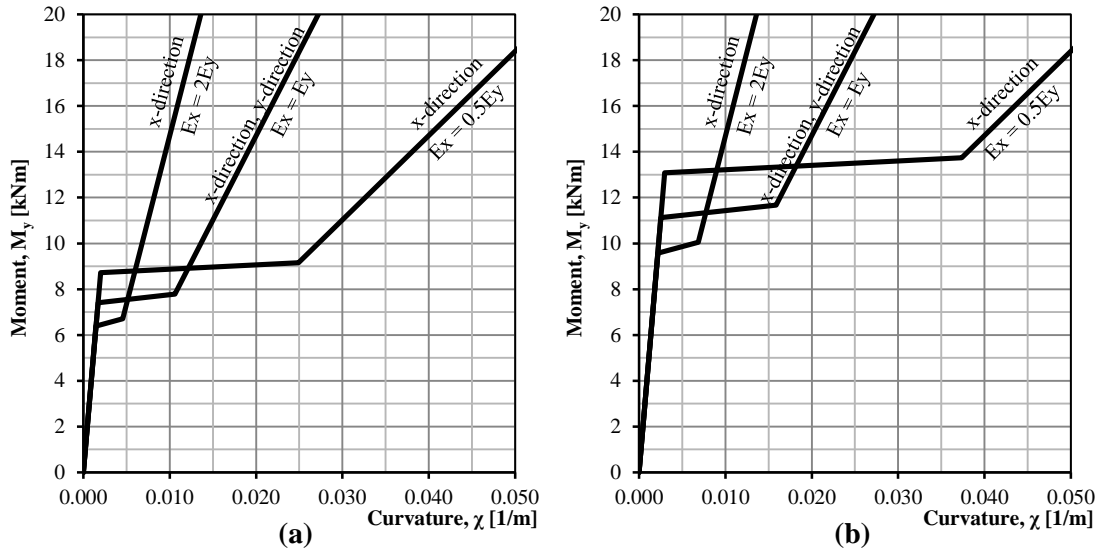
Figure C.6   Moment-curvature relations for the cantilever slab with a single concentrated force, case Neutral. (a) $M_{cr} = M_{lin}/3$, (b) $M_{cr} = M_{lin}/2$
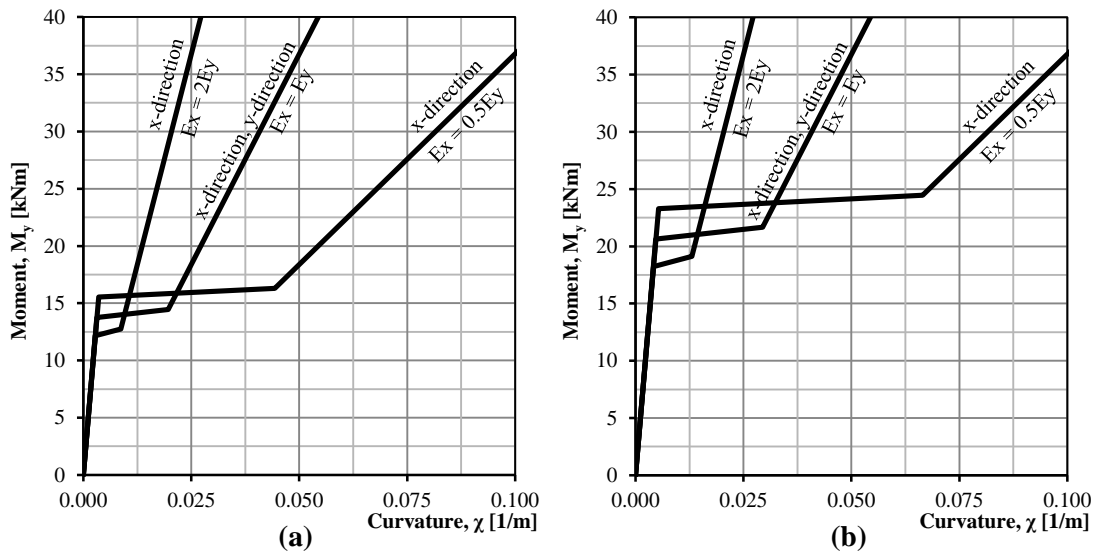
Figure C.7   Moment-curvature relations for the cantilever slab with two concentrated forces, case Neutral. (a) $M_{cr} = M_{lin}/3$, (b) $M_{cr} = M_{lin}/2$
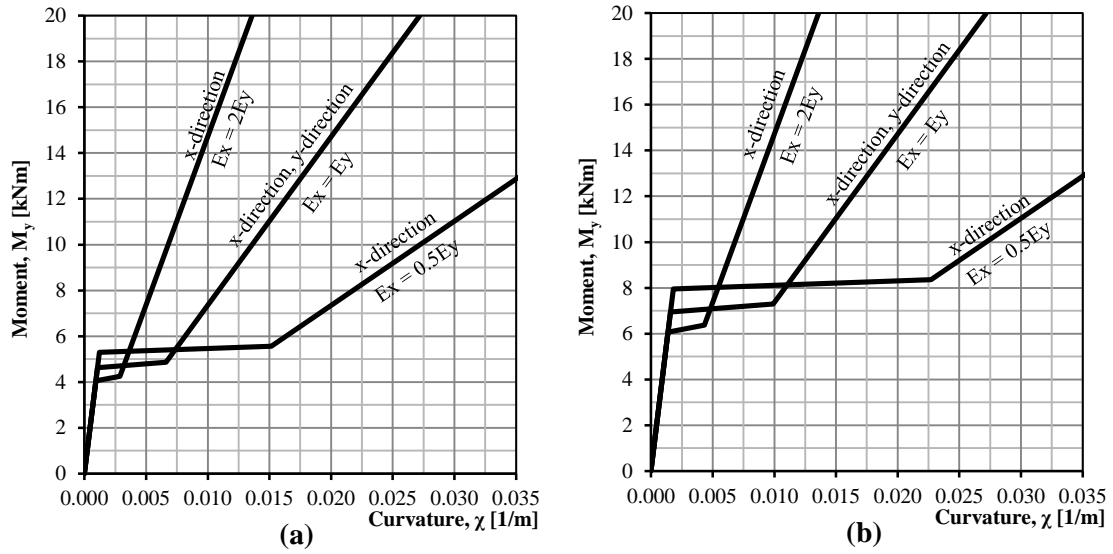
Figure C.8   Moment-curvature relations for the simply supported one-way slab with a single concentrated force, case Neutral. (a) $M_{cr} = M_{lin}/3$, (b) $M_{cr} = M_{lin}/2$
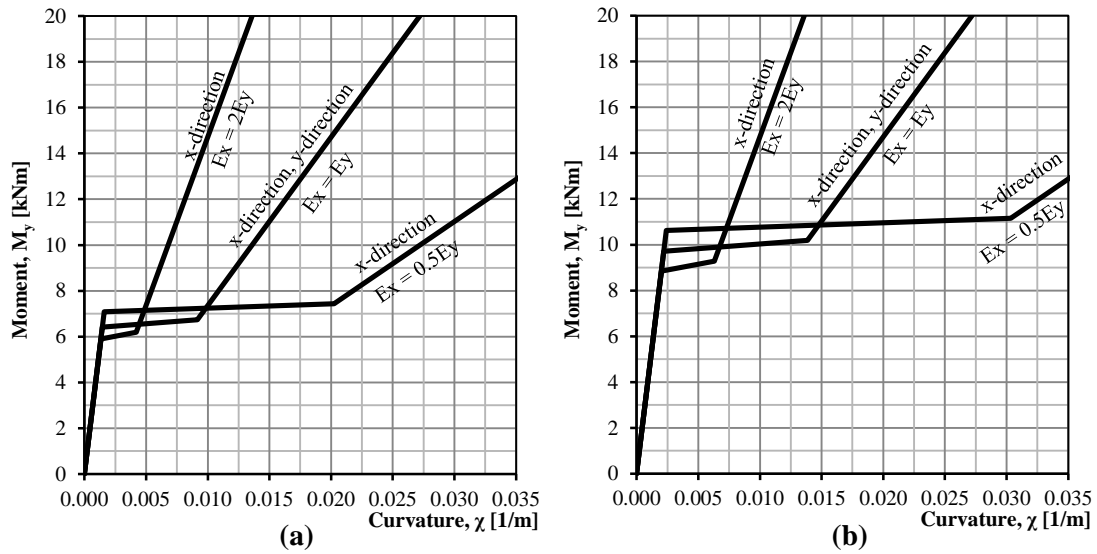
Figure C.9   Moment-curvature relations for the simply supported one-way slab with two concentrated forces, case Neutral. (a) $M_{cr} = M_{lin}/3$, (b) $M_{cr} = M_{lin}/2$

CHALMERS, *Civil and Environmental Engineering*, Master's Thesis 2014:73

Table C.3   Moment-curvature relations used in the x-directions, case Neutral.

Cantilever slab, single concentrated force											
$M_{cr} = M_{lin}/3$						$M_{cr} = M_{lin}/2$					
$E_x = 0.5E_y$		$E_x = E_y$		$E_x = 2E_y$		$E_x = 0.5E_y$		$E_x = E_y$		$E_x = 2E_y$	
Moment	Curvature	Moment	Curvature	Moment	Curvature	Moment	Curvature	Moment	Curvature	Moment	Curvature
[Nm]	[1/m]	[Nm]	[1/m]	[Nm]	[1/m]	[Nm]	[1/m]	[Nm]	[1/m]	[Nm]	[1/m]
0	0	0	0	0	0	0	0	0	0	0	0
8725	0.00198	7413	0.00168	6382	0.00145	13087	0.00297	11120	0.00253	9572	0.00218
9161	0.02492	7784	0.01059	6701	0.00456	13741	0.03738	11676	0.01588	10051	0.00683
20000	0.05440	20000	0.02720	20000	0.01360	20000	0.05440	20000	0.02720	20000	0.01360

Cantilever slab, two concentrated forces											
$M_{cr} = M_{lin}/3$						$M_{cr} = M_{lin}/2$					
$E_x = 0.5E_y$		$E_x = E_y$		$E_x = 2E_y$		$E_x = 0.5E_y$		$E_x = E_y$		$E_x = 2E_y$	
Moment	Curvature	Moment	Curvature	Moment	Curvature	Moment	Curvature	Moment	Curvature	Moment	Curvature
[Nm]	[1/m]	[Nm]	[1/m]	[Nm]	[1/m]	[Nm]	[1/m]	[Nm]	[1/m]	[Nm]	[1/m]
0	0	0	0	0	0	0	0	0	0	0	0
15531	0.00353	13749	0.00312	12144	0.00276	23297	0.00529	20623	0.00469	18216	0.00414
16308	0.04436	14436	0.01963	12751	0.00867	24462	0.06654	21654	0.02945	19126	0.01301
40000	0.10880	40000	0.05440	40000	0.02720	40000	0.10880	40000	0.05440	40000	0.02720

Simply supported one-way slab, single concentrated force											
$M_{cr} = M_{lin}/3$						$M_{cr} = M_{lin}/2$					
$E_x = 0.5E_y$		$E_x = E_y$		$E_x = 2E_y$		$E_x = 0.5E_y$		$E_x = E_y$		$E_x = 2E_y$	
Moment	Curvature	Moment	Curvature	Moment	Curvature	Moment	Curvature	Moment	Curvature	Moment	Curvature
[Nm]	[1/m]	[Nm]	[1/m]	[Nm]	[1/m]	[Nm]	[1/m]	[Nm]	[1/m]	[Nm]	[1/m]
0	0	0	0	0	0	0	0	0	0	0	0
5302	0.00120	4629	0.00105	4045	0.00092	7953	0.00181	6943	0.00158	6067	0.00138
5567	0.01514	4860	0.00661	4247	0.00289	8350	0.02271	7290	0.00991	6371	0.00433
20000	0.05440	20000	0.02720	20000	0.01360	20000	0.05440	20000	0.02720	20000	0.01360

Simply supported one-way slab, two concentrated forces											
$M_{cr} = M_{lin}/3$						$M_{cr} = M_{lin}/2$					
$E_x = 0.5E_y$		$E_x = E_y$		$E_x = 2E_y$		$E_x = 0.5E_y$		$E_x = E_y$		$E_x = 2E_y$	
Moment	Curvature	Moment	Curvature	Moment	Curvature	Moment	Curvature	Moment	Curvature	Moment	Curvature
[Nm]	[1/m]	[Nm]	[1/m]	[Nm]	[1/m]	[Nm]	[1/m]	[Nm]	[1/m]	[Nm]	[1/m]
0	0	0	0	0	0	0	0	0	0	0	0
7083	0.00161	6421	0.00146	5894	0.00134	10624	0.00241	9708	0.00221	8841	0.00201
7437	0.02023	6742	0.00917	6188	0.00421	11155	0.03034	10193	0.01386	9283	0.00631
20000	0.05440	20000	0.02720	20000	0.01360	20000	0.05440	20000	0.02720	20000	0.01360

Table C.4   Moment-curvature relations used in the y-directions, case Neutral.

Cantilever slab							
Single concentrated force				Two concentrated forces			
$M_{cr} = M_{lin}/3$		$M_{cr} = M_{lin}/2$		$M_{cr} = M_{lin}/3$		$M_{cr} = M_{lin}/2$	
Moment	Curvature	Moment	Curvature	Moment	Curvature	Moment	Curvature
[Nm]	[1/m]	[Nm]	[1/m]	[Nm]	[1/m]	[Nm]	[1/m]
0	0	0	0	0	0	0	0
7413	0.00168	11120	0.00253	13749	0.00312	20623	0.00469
7784	0.01059	11676	0.01588	14436	0.01963	21654	0.02945
20000	0.02720	20000	0.02720	40000	0.05440	40000	0.05440
Simply supported one-way slab							
Single concentrated force				Two concentrated forces			
$M_{cr} = M_{lin}/3$		$M_{cr} = M_{lin}/2$		$M_{cr} = M_{lin}/3$		$M_{cr} = M_{lin}/2$	
Moment	Curvature	Moment	Curvature	Moment	Curvature	Moment	Curvature
[Nm]	[1/m]	[Nm]	[1/m]	[Nm]	[1/m]	[Nm]	[1/m]
0	0	0	0	0	0	0	0
4629	0.00105	6943	0.00158	6421	0.00146	9708	0.00221
4860	0.00661	7290	0.00991	6742	0.00917	10193	0.01386
20000	0.02720	20000	0.02720	20000	0.02720	20000	0.02720

C.1.4 Case Cracked

The moment-curvature relations for the case Cracked are presented in this section. The stiffness in state II was kept constant in the y-direction for the different stiffness proportions, while the stiffness in state II varied with the stiffness factor α in the x-direction. The relation in the x-direction is linear which was meant to represent a cracked stiffness before the load is applied, while the slab is uncracking from start in the y-direction. The relations are presented as graphs in Figure C.10 to Figure C.13, and as tabulated values in Table C.5 and Table C.6.
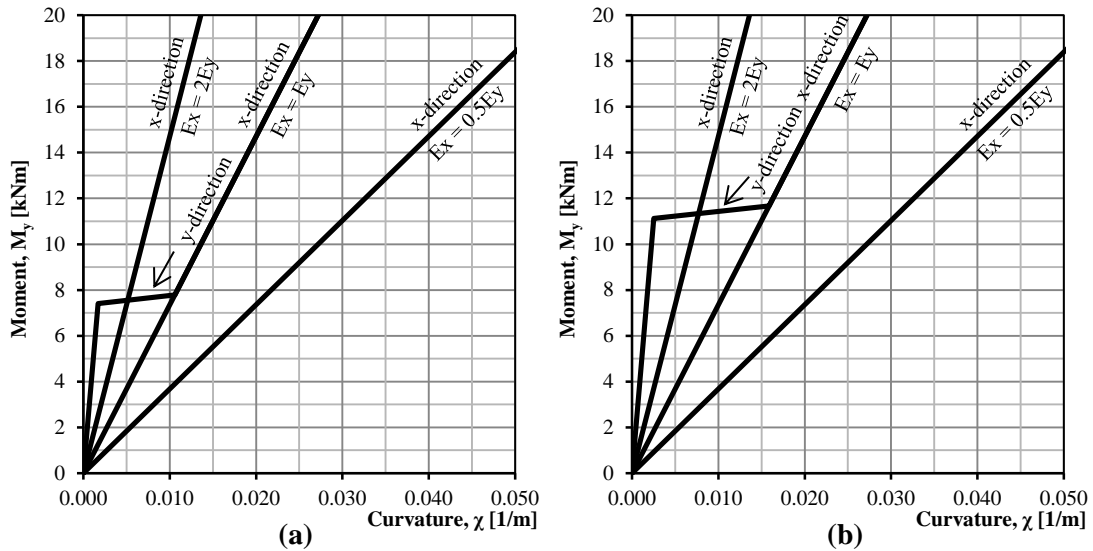
Figure C.10 Moment-curvature relations for the cantilever slab with a single concentrated force, case Cracked. (a) $M_{cr} = M_{lin}/3$, (b) $M_{cr} = M_{lin}/2$
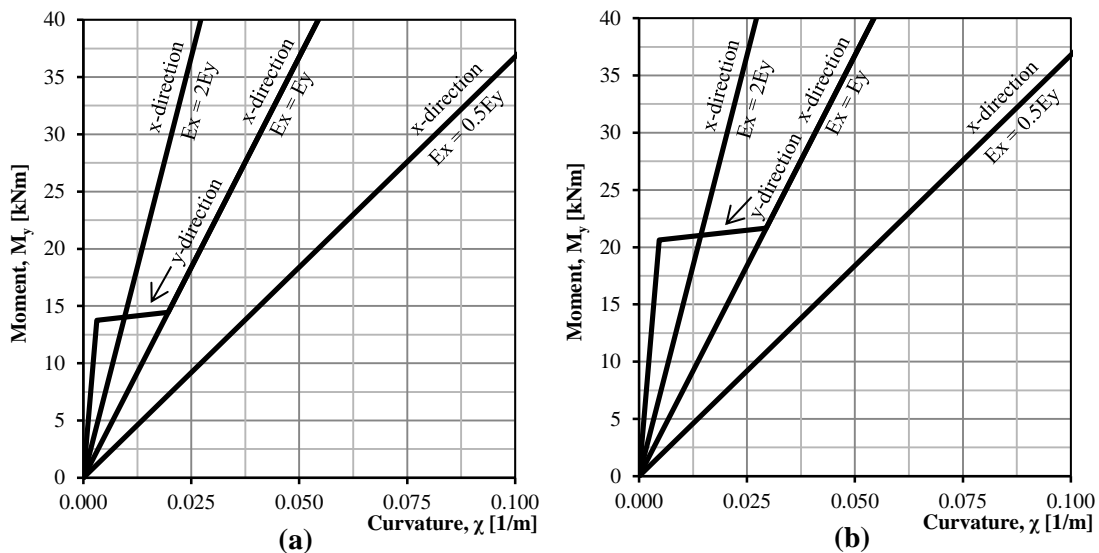
Figure C.11 Moment-curvature relations for the cantilever slab with two concentrated forces, case Cracked. (a) $M_{cr} = M_{lin}/3$, (b) $M_{cr} = M_{lin}/2$
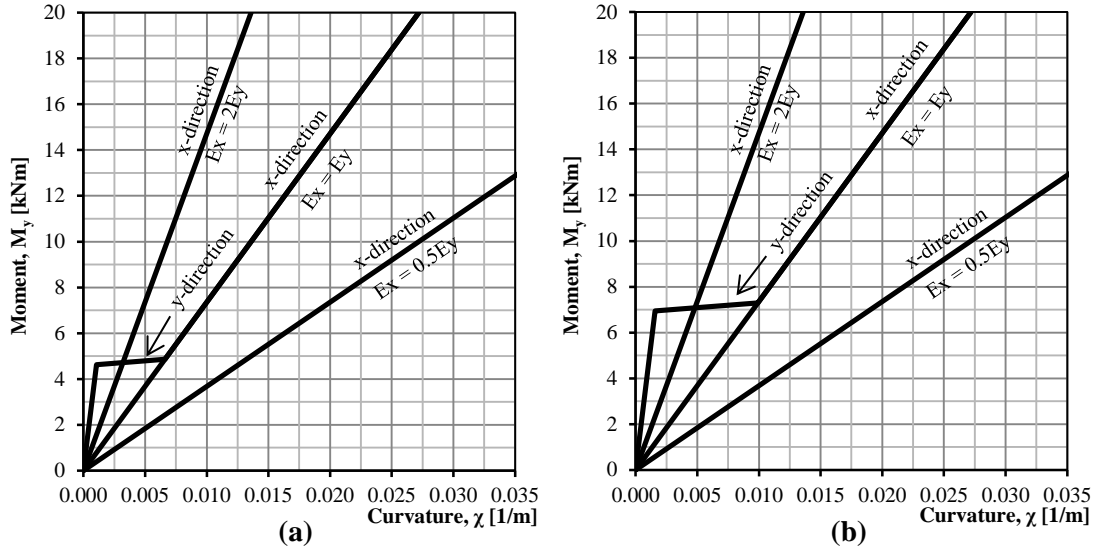
Figure C.12 Moment-curvature relations for the simply supported one-way slab with a single concentrated force, case Cracked. (a) $M_{cr} = M_{lin}/3$, (b) $M_{cr} = M_{lin}/2$
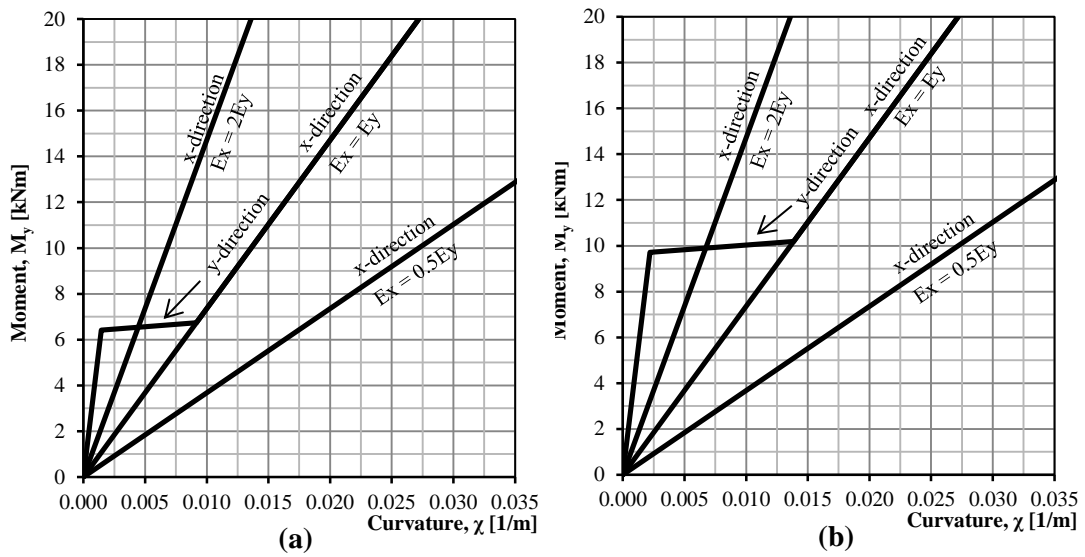
Figure C.13 Moment-curvature relations for the simply supported one-way slab with two concentrated force, case Cracked. (a) $M_{cr} = M_{lin}/3$, (b) $M_{cr} = M_{lin}/2$

Table C.5   Moment-curvature relations used in the x-directions, case Cracked.

Cantilever slab, single concentrated force											
$M_{cr} = M_{lin}/3$						$M_{cr} = M_{lin}/2$					
$E_x = 0.5E_y$		$E_x = E_y$		$E_x = 2E_y$		$E_x = 0.5E_y$		$E_x = E_y$		$E_x = 2E_y$	
Moment	Curvature	Moment	Curvature	Moment	Curvature	Moment	Curvature	Moment	Curvature	Moment	Curvature
[Nm]	[1/m]	[Nm]	[1/m]	[Nm]	[1/m]	[Nm]	[1/m]	[Nm]	[1/m]	[Nm]	[1/m]
0	0	0	0	0	0	0	0	0	0	0	0
20000	0.0544	20000	0.0272	20000	0.0136	20000	0.0544	20000	0.0272	20000	0.0136

Cantilever slab, two concentrated forces											
$M_{cr} = M_{lin}/3$						$M_{cr} = M_{lin}/2$					
$E_x = 0.5E_y$		$E_x = E_y$		$E_x = 2E_y$		$E_x = 0.5E_y$		$E_x = E_y$		$E_x = 2E_y$	
Moment	Curvature	Moment	Curvature	Moment	Curvature	Moment	Curvature	Moment	Curvature	Moment	Curvature
[Nm]	[1/m]	[Nm]	[1/m]	[Nm]	[1/m]	[Nm]	[1/m]	[Nm]	[1/m]	[Nm]	[1/m]
0	0	0	0	0	0	0	0	0	0	0	0
40000	0.1088	40000	0.0544	40000	0.0272	40000	0.1088	40000	0.0544	40000	0.0272

Simply supported one-way slab, single concentrated force											
$M_{cr} = M_{lin}/3$						$M_{cr} = M_{lin}/2$					
$E_x = 0.5E_y$		$E_x = E_y$		$E_x = 2E_y$		$E_x = 0.5E_y$		$E_x = E_y$		$E_x = 2E_y$	
Moment	Curvature	Moment	Curvature	Moment	Curvature	Moment	Curvature	Moment	Curvature	Moment	Curvature
[Nm]	[1/m]	[Nm]	[1/m]	[Nm]	[1/m]	[Nm]	[1/m]	[Nm]	[1/m]	[Nm]	[1/m]
0	0	0	0	0	0	0	0	0	0	0	0
20000	0.0544	20000	0.0272	20000	0.0136	20000	0.0544	20000	0.0272	20000	0.0136

Simply supported one-way slab, two concentrated forces											
$M_{cr} = M_{lin}/3$						$M_{cr} = M_{lin}/2$					
$E_x = 0.5E_y$		$E_x = E_y$		$E_x = 2E_y$		$E_x = 0.5E_y$		$E_x = E_y$		$E_x = 2E_y$	
Moment	Curvature	Moment	Curvature	Moment	Curvature	Moment	Curvature	Moment	Curvature	Moment	Curvature
[Nm]	[1/m]	[Nm]	[1/m]	[Nm]	[1/m]	[Nm]	[1/m]	[Nm]	[1/m]	[Nm]	[1/m]
0	0	0	0	0	0	0	0	0	0	0	0
20000	0.0544	20000	0.0272	20000	0.0136	20000	0.0544	20000	0.0272	20000	0.0136

Table C.6   Moment-curvature relations used in the y-directions, case Cracked.

Cantilever slab							
Single concentrated force				Two concentrated forces			
$M_{cr} = M_{lin}/3$		$M_{cr} = M_{lin}/2$		$M_{cr} = M_{lin}/3$		$M_{cr} = M_{lin}/2$	
Moment	Curvature	Moment	Curvature	Moment	Curvature	Moment	Curvature
[Nm]	[1/m]	[Nm]	[1/m]	[Nm]	[1/m]	[Nm]	[1/m]
0	0	0	0	0	0	0	0
7413	0.00168	11120	0.00253	13749	0.00312	20623	0.00469
7784	0.01059	11676	0.01588	14436	0.01963	21654	0.02945
20000	0.02720	20000	0.02720	40000	0.05440	40000	0.05440
Simply supported one-way slab							
Single concentrated force				Two concentrated forces			
$M_{cr} = M_{lin}/3$		$M_{cr} = M_{lin}/2$		$M_{cr} = M_{lin}/3$		$M_{cr} = M_{lin}/2$	
Moment	Curvature	Moment	Curvature	Moment	Curvature	Moment	Curvature
[Nm]	[1/m]	[Nm]	[1/m]	[Nm]	[1/m]	[Nm]	[1/m]
0	0	0	0	0	0	0	0
4629	0.00105	6943	0.00158	6421	0.00146	9708	0.00221
4860	0.00661	7290	0.00991	6742	0.00917	10193	0.01386
20000	0.02720	20000	0.02720	20000	0.02720	20000	0.02720

C.2 Cumulative plastic rotation

This section covers the bilinear moment-curvature relations that were used for the cumulative plastic rotation analyses. The modelling choices, limitations in ADINA, the plastic rotation capacity θ_{rd} and how the moment-curvature relation was derived are also treated in this section.

C.2.1 Modelling choices

The trilinear elastic model used in Chapter 4 and 5 could not be adapted to a plastic analysis. The plastic analysis provided in ADINA does not allow the stiffness of a material in a phase to be higher than the previous phase, i.e. the derivative of the moment-curvature functions must decrease as the curvature increases, ADINA (2012). When unloaded, the inclination of the unloading curve is equal to the inclination of the first defined curve in the moment-curvature relation. How this applies geometrically is illustrated in Figure C.14.
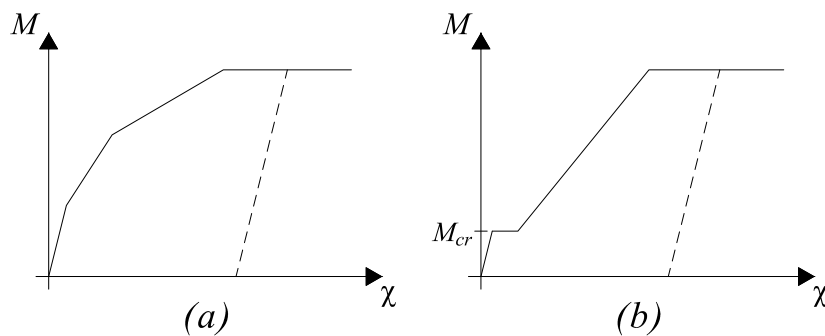
Figure C.14 Moment-curvature input for ADINA with the unloading response as a dashed line for: (a) moment-curvature relation allowed by ADINA, and (b) moment-curvature relation declined by ADINA.

Since the trilinear elastic part of the model in Figure C.14b could not be adapted to a quadlinear plastic analysis, a bilinear moment-curvature relation was used instead. This simplification of the moment-curvature relation is illustrated in Figure C.15.
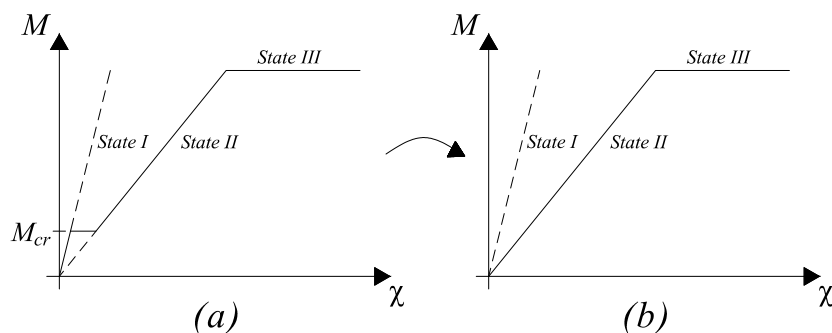
Figure C.15 Moment-curvature relations for (a) a quadlinear plastic analysis, and (b) a bilinear plastic analysis.

The moment-curvature relation used for the plastic analyses in this report was constructed from the bilinear plastic model in Figure C.15b and the plastic rotation capacity θrd, treated in Appendix C.2.2.

As an alternative to the chosen moment-curvature relation, a quadlinear model that includes the effect of tension stiffening, as can be seen in Figure C.16 could have been used. However, this model was omitted due to the two main reasons stated below:

- The tension stiffening effect was believed to be small in these analyses.
- The unloading curve was believed to be better represented by a state II model than a state I model.

The tension stiffening effect was believed to be small since the analyses mainly focused on cumulative damage in the structure. With up to 150 load cycles n, the overall effect of tension stiffening would decrease with each completed load cycle. As an effect of the curve shown in Figure C.16, the unloading curve would have a much steeper inclination than obtained by the moment-curvature relation in Figure C.15b.

Since one aim of this Thesis is to study cumulative damage, the state II model was believed to represent the true unloading curve to a greater extent than the state I model. Since large plastic rotations were to be studied, an increased number of beam elements in the beam grillage model would reach the yield state (state III). It is therefore safe to assume that the investigated sections in a real structure would experience high stresses and therefore behave more like a fully cracked, than an uncracked, section when unloaded.
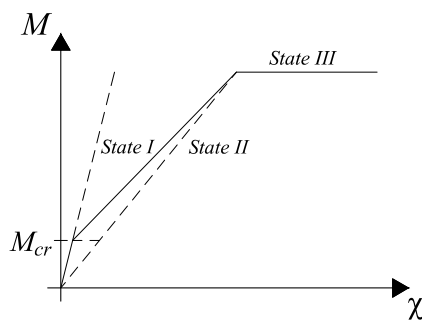
Figure C.16 Trilinear plastic moment-curvature relation including the effect of tension stiffening.

C.2.2 Plastic rotation capacity

The plastic rotation capacity θ_{rd} of a cross-section is a function of the geometry of the cross-section b, the reinforcement amount A_s, the concrete strength class f_{ck} and reinforcing steel class and strength f_{yd}. The cantilever slab and the simply supported slab do not differ in the above stated input data and therefore have the same sustainability towards accumulated damage. Due to this fact, both structures are treated together below. The theory of the plastic rotation capacity of a cross-section and how it is determined in Eurocode 2, CEN (2004) is treated in Section 2.2.6.

The total amount of reinforcement was set to 0.5 % which is treated in Section 4.1.1 and yielded:

$$A_s = 0.005 \cdot A_c = 0.005 \cdot 1 \cdot 0.2 = 1000 \cdot 10^{-6}\,\mathrm{m}^2 \tag{C-1}$$

Concrete C30/37 and reinforcing steel B500B yielded:

$$f_{yd} = \frac{f_{yk}}{\gamma_s} = \frac{500 \cdot 10^6}{1.15} = 434.8 \text{ MPa} \tag{C-2}$$

$$f_{cd} = \frac{f_{ck}}{\gamma_c} = \frac{30 \cdot 10^6}{1.5} = 20 \text{ MPa} \tag{C-3}$$

Where:

$$\gamma_s = 1.15 \tag{C-4}$$

$$\gamma_c = 1.5 \tag{C-5}$$

Which yielded:

$$x_u = \frac{f_{yd} \cdot A_s}{\alpha_R \cdot f_{cd} \cdot b} = \frac{434.8 \cdot 10^6 \cdot 1000 \cdot 10^{-6}}{0.810 \cdot 20 \cdot 10^6 \cdot 1} = 0.027 \text{ m} \tag{C-6}$$

$$\frac{x_u}{d} = \frac{0.027}{0.164} = 0.164 \tag{C-7}$$

From Figure C.17, with $x_u/d = 0.164$, Class B steel and concrete strength class C30/37, $\theta_{pl,d}$ was obtained as:

$$\theta_{pl,d} = 13 \cdot 10^{-3} \text{ rad} \tag{C-8}$$
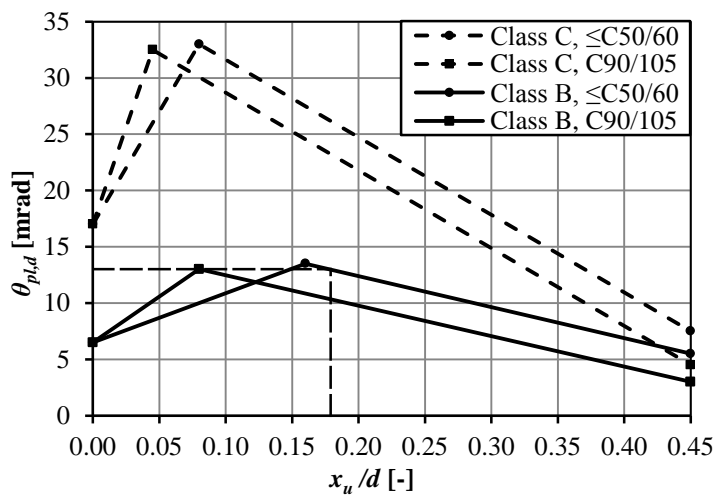
Figure C.17 Plastic rotation capacity for reinforcement class B and C.

The shear slenderness λ was determined according to:

$$\lambda = \frac{l_0}{d} = \frac{1.6}{0.164} = 9.76 \tag{C-9}$$

$$k_\lambda = \sqrt{\frac{\lambda}{3}} = \sqrt{\frac{9.76}{3}} = 1.80 \tag{C-10}$$

The plastic rotation capacity of the cross-section was determined according to:

$$\theta_{rd} = k_\lambda \cdot \theta_{pl,d} = 1.80 \cdot 13 \cdot 10^{-3} = 23.44 \cdot 10^{-3} \text{ rad}$$ (C-11)

The plastic rotation capacity $\theta_{rd} = 23.44$ mrad was used throughout this Thesis.

C.2.3 Cantilever slab – A single moving concentrated force

The plastic bilinear moment-curvature relation for the cantilever slab subjected to a single moving force of constant and varying load magnitudes was established from the linear elastic behaviour of an isotropic, cracked slab. The cantilever structure was subjected to a force $F = 200$ kN in the centre of the primary free edge, as can be seen in Figure C.18.
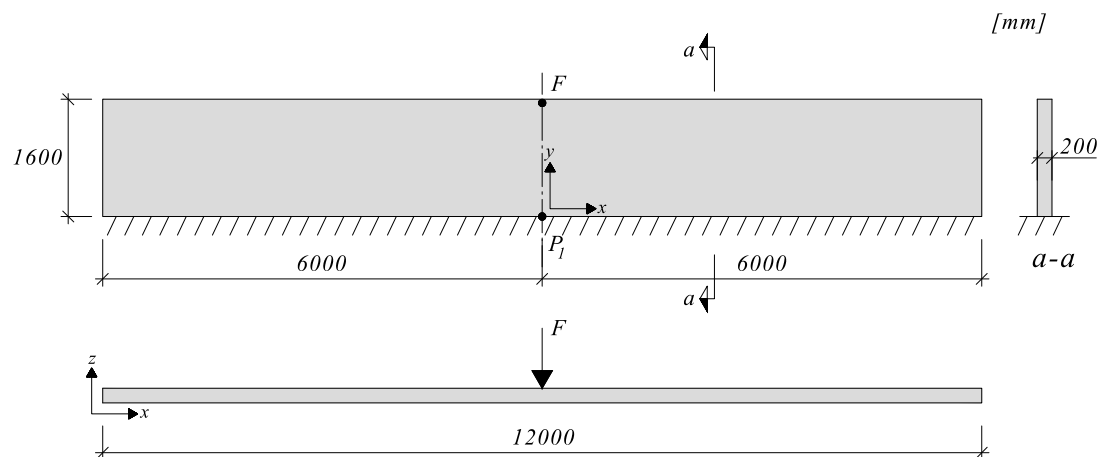
Figure C.18 Geometry and location of the applied force of the studied cantilever slab.

The width of the slab was chosen to 12 m in order to avoid numerical problems that were obtained with a slab with an 8 m width. For the shorter slab, disturbances of the slab occurred near the free edges and a wider slab was therefore chosen since the scope of this Thesis is to investigate the behaviour of a long slab. This is further treated in Section 6.1.3.

The load model consisted of one concentrated static force, applied in a single node using a total of 500 time steps, which gives a load increment of 2.5 kN per time step.

The moment-curvature relation used for this analysis was the isotropic, cracked stiffness used in Chapter 4 and 5, which can be seen in Figure C.19.
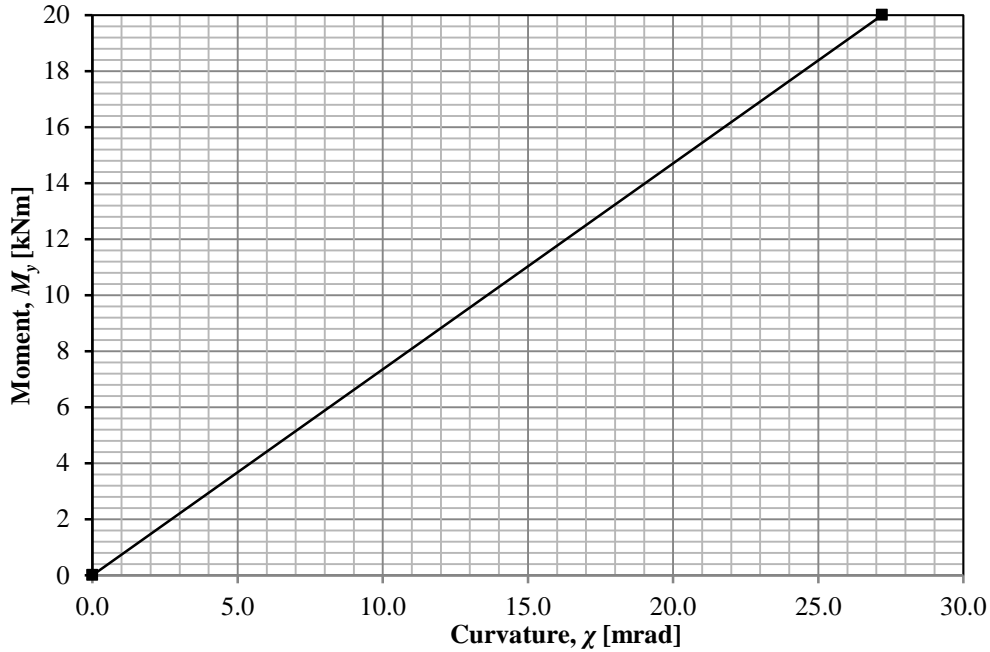
Figure C.19 Elastic moment-curvature for an isotropic, cracked cross-section, used in order to establish the bilinear plastic moment-curvature relation.

From the load application, the moment distribution along the fixed edge was obtained which is shown in Figure C.20.
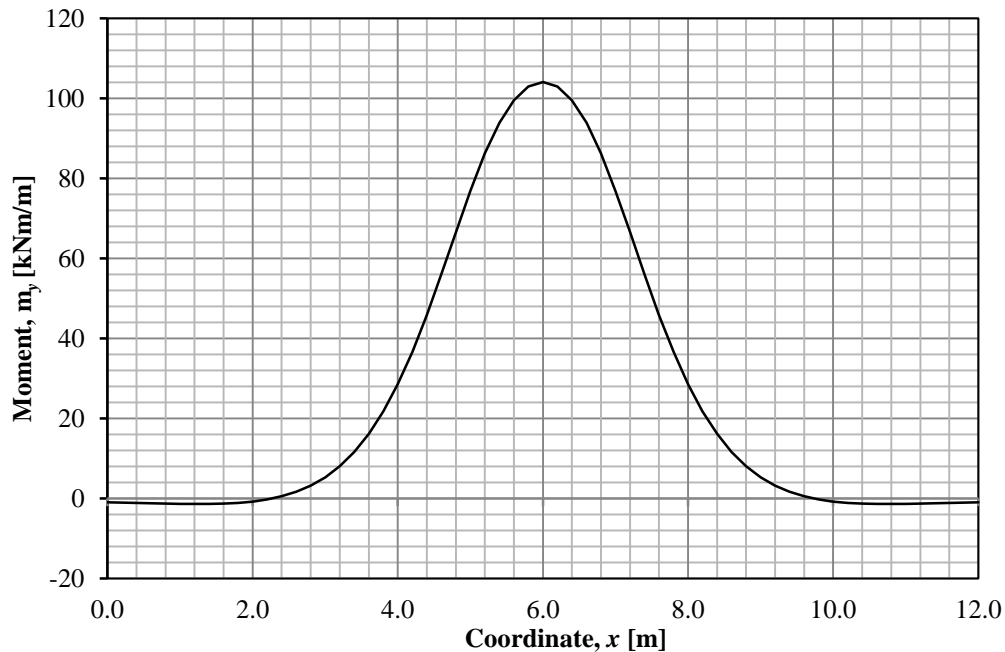
Figure C.20 Moment distribution for the studied slab with an applied concentrated force of 200 kN.

The maximum moment from the isotropic, cracked analysis was used in order to establish the yield moment for the bilinear plastic analysis where:

$$m_{el} = 104.1 \text{ kNm/m} \tag{C-12}$$

The plastic moment m_{pl} was chosen to 60% of the maximum elastic moment m_{el} which yields:

$$m_{pl} = 0.6 \cdot 104.1 = 62.46 \text{ kNm/m} \tag{C-13}$$

In order to obtain the plastic moment for each beam in the beam grillage model in this analysis, the plastic moment m_{pl} was multiplied by the beam width according to:

$$M_{pl} = m_{pl} \cdot b = 62.46 \cdot 0.2 = 12.49 \text{ kNm} \tag{C-14}$$

The choice of the plastic moment m_{pl} was based on a recommendation by Pacoste *et al.* (2012) where the following limits for redistribution of reinforcement moments were proposed:

$$0.6 \cdot M_{elastic} \leq M_{plastic} \leq M_{elastic} \tag{C-15}$$

Failure of the cantilever slab was defined as in Appendix C.2.2 where the plastic rotation capacity θ_{rd} was determined for a cross-section with a reinforcement amount of 0.5 % where:

$$\theta_{rd} = 23.44 \text{ mrad} \tag{C-16}$$

The bilinear moment-curvature relation used in this analysis is based on a combination of the elastic response of a cracked cross-section m_{el}, the plastic moment m_{pl} described in Equation (C-13) and the failure due to plastic rotation, defined as the plastic rotation capacity θ_{rd} described in Equation (C-16). The bilinear moment-curvature relation from the above stated input was combined and is shown in Figure C.21.
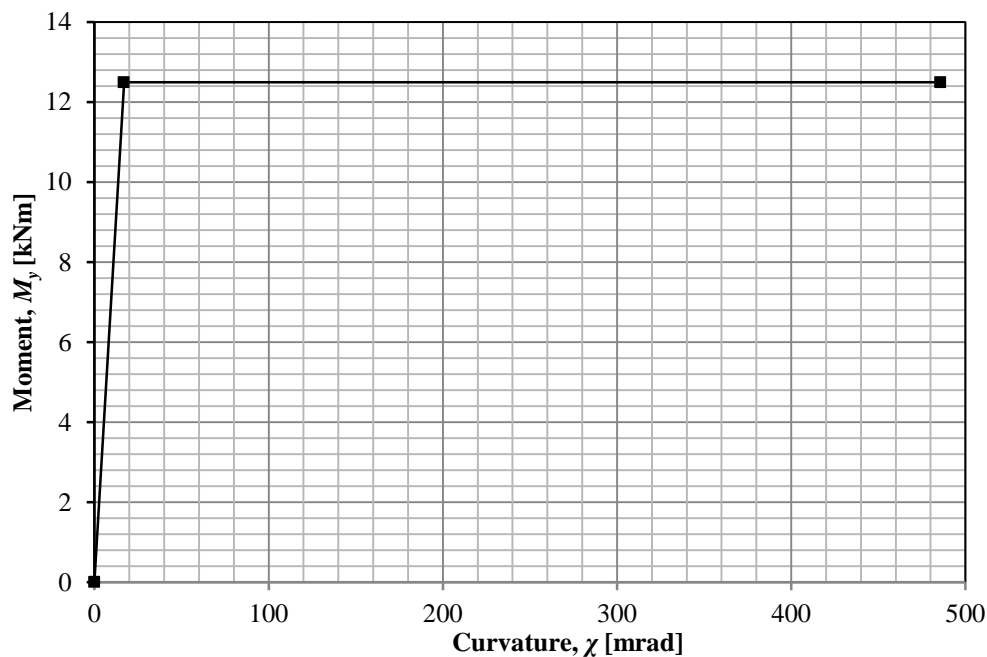
Figure C.21 Bilinear plastic moment-curvature relation for the studied cantilever slab. Valid for the majority of the beams in the beam grillage model.

The above stated moment-curvature relation applies for the majority of the beams in the beam grillage model. As can be seen in Equation (C-13), the moment-curvature relation applies for beams with a width of 0.2 m. As have been stated in Section 6.1.3, the beam grillage models were modelled with beams of half the width in the boundaries. This yields moment-curvature relations for these beams with the same elastic response and plastic rotation capacity but with a plastic moment m_{pl} that is 50 % of a full cross-section. The moment-curvature relation for the beams in the boundaries is shown in Figure C.22.
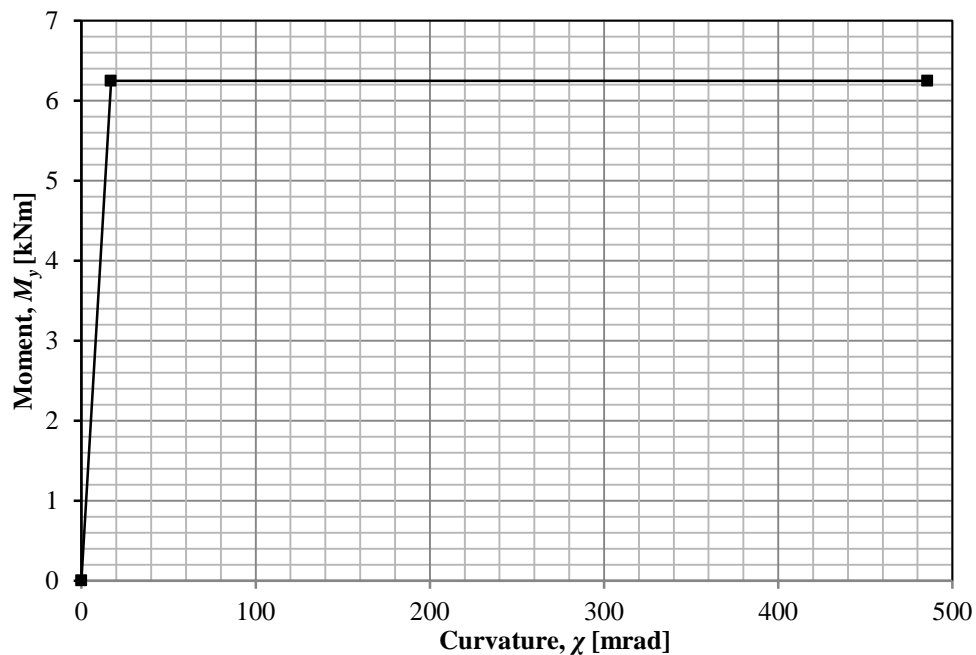
Figure C.22 Bilinear plastic moment-curvature relation for the studied cantilever slab. Valid for beams in the boundaries in the beam grillage model.

C.2.4 Cantilever slab – Two moving concentrated forces

The plastic bilinear moment-curvature relation for the cantilever slab subjected to a single moving force of constant and varying magnitudes was also used for these analyses. There are mainly two reasons for this choice of moment-curvature relation:

- Comparison purposes between a single and two moving concentrated forces.
- Comparison purposes within the two moving concentrated forces.

If a moment-curvature relation were to be constructed for two moving concentrated forces, no comparison between this load case and the load case for a single moving concentrated force could have been made. Since one aim of this Thesis is to study how long slabs behave for cumulative damage, it was essential to make comparisons between different load cases. The aim of this Thesis is also to investigate how the cumulative damage is affected by the distance d between the two moving concentrated forces. With individual moment-curvature relations for each distance, a comparison study between these would be less obvious.

C.2.5 Simply supported slab – A single moving concentrated force

The plastic bilinear moment-curvature relation for the simply supported one-way slab subjected to a single moving concentrated force of constant and varying load magnitudes was established from the linear elastic behaviour of an isotropic, cracked slab. The cantilever structure was subjected to a total force $F = 200$ kN in the centre of the slab, as in the case of the cantilever structure. Due to the symmetry boundary, the total applied force F_{tot} in the analysis was set to 100 kN, as can be seen in Figure C.23.
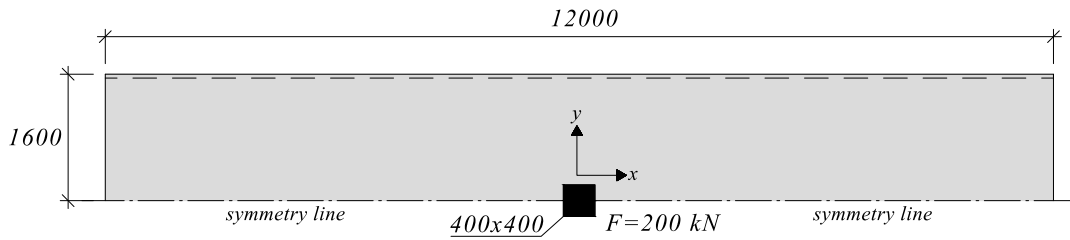
Figure C.23 Geometry and location of the applied force of the studied simply supported one-way slab.

As in the case of the cantilever structure, the width of the slab was chosen to 12 m in order to avoid numerical problems.

The load model used can be seen in Figure C.24 which consists of six concentrated static forces that were applied using a total of 500 time steps, which gave a load increment of 1.25 kN per time step. The six concentrated forces represented one concentrated force, applied over a surface of 0.4 x 0.4 m^2. Due to the symmetry boundary, this area was set to 0.4 x 02 m^2.
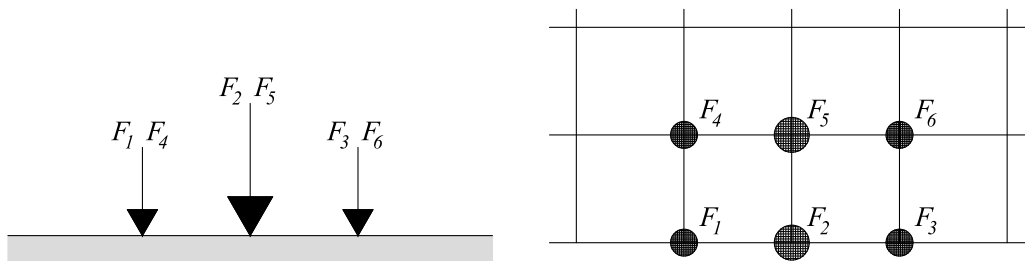
Figure C.24 Load model and force distribution used for beam grillage model.

Since the six concentrated forces represented a surface load, applied on a beam grillage model, the forces corresponds to the force contributions from the represented areas. Due to this load interpretation, the two mid-forces received force contributions from two areas and were therefore greater than the remaining forces. How the forces were applied on the beam grillage model can be seen in the Figure C.24.

The total number of force contributions was eight, four from each surface, which was distributed over six forces. This gave the following force relations:

$$F_1 = F_3 = F_4 = F_6 = \frac{F_{tot}}{8} \tag{C-17}$$

$$F_2 = F_5 = 2 \cdot \frac{F_{tot}}{8} \tag{C-18}$$

The moment-curvature relation used for this analysis was the cracked stiffness used in Chapter 4 and 5, which can be seen in Figure C.25.
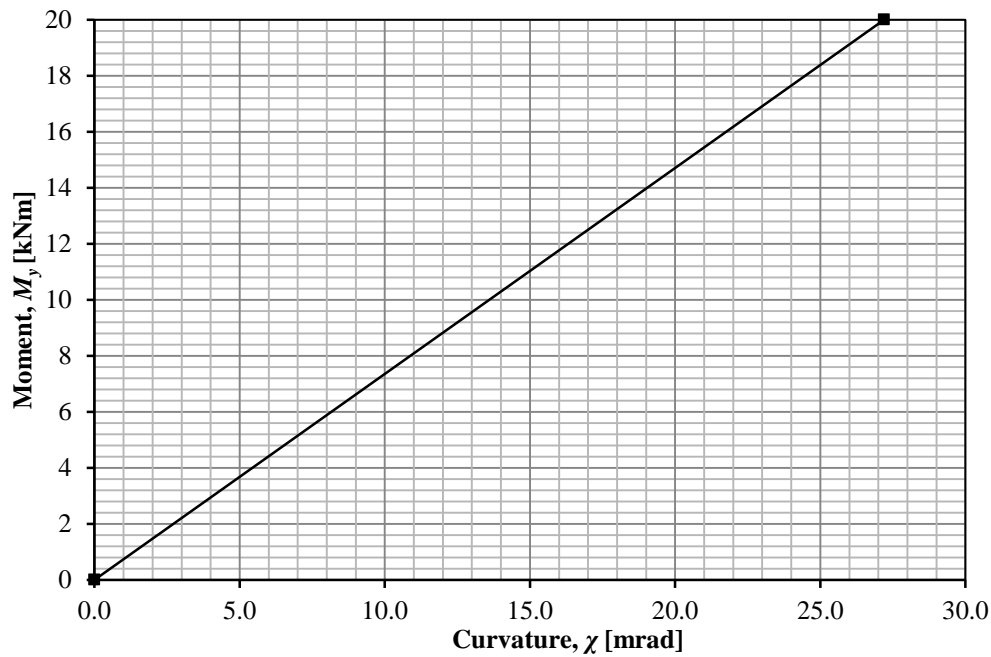
Figure C.25 Elastic moment-curvature for a cracked cross-section, used in order to establish the bilinear plastic moment-curvature relation.

From the load application, the moment distribution along the mid-section of the slab was established which is shown in Figure C.26. The peak moment was more distinct than in the case of the cantilever slab. The reason for this can be derived from the fact that the moment distribution was measured in the same line as where the forces were applied.
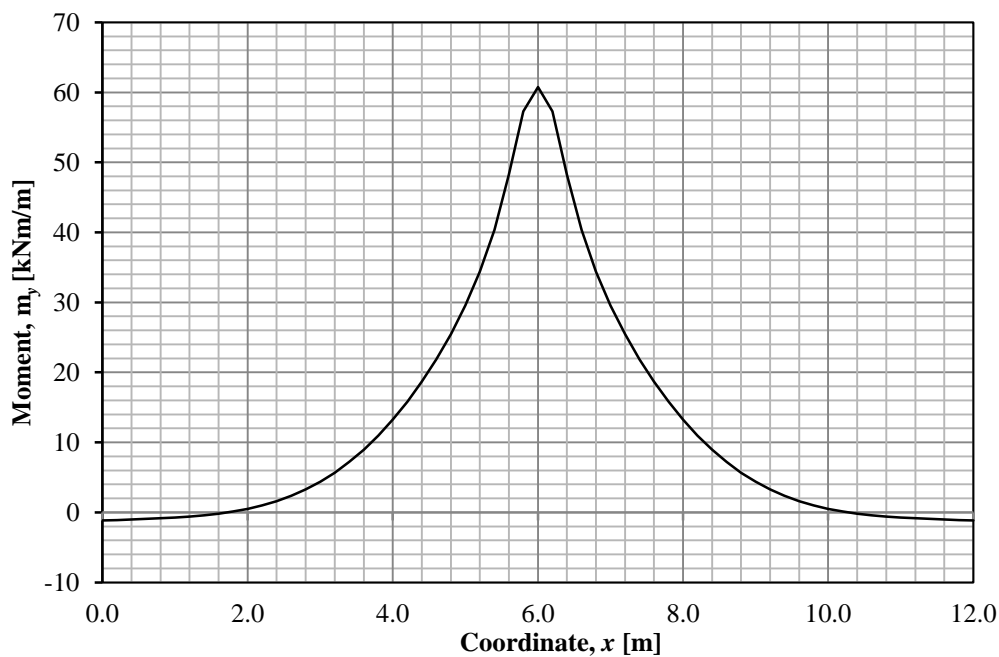
Figure C.26 Moment distribution for the studied slab with an applied concentrated force of 100 kN.

The maximum moment from the isotropic, cracked analysis was used in order to establish the yield moment for the bilinear plastic analysis. The procedure was the same as stated for the cantilever structure in Appendix C.2.3 and is here presented in a simplified and more compact form:

$$m_{el} = 60.75 \text{ kNm/m} \tag{C-19}$$

$$m_{pl} = 0.6 \cdot 60.75 \cdot 1 = 36.45 \text{ kNm/m} \tag{C-20}$$

$$M_{pl} = m_{pl} \cdot b = 36.45 \cdot 0.2 = 7.29 \text{ kNm} \tag{C-21}$$

Failure of the simply supported slab was also here defined as in Appendix C.2.2 where the plastic rotation capacity θ_{rd} was determined for a cross-section with a reinforcement amount of 0.5% where:

$$\theta_{rd} = 23.44 \text{ mrad} \tag{C-22}$$

The bilinear moment-curvature relation used in this analysis was, as in the case of the cantilever structure, based on a combination of the elastic response of a cracked cross-section m_{el}, the plastic moment m_{pl} described in Equation (C-20) and the failure due to plastic rotation, defined as the plastic rotation capacity θ_{rd}, described in Equation (C-22). The bilinear moment-curvature relation from the above stated input was combined and is shown in Figure C.27.
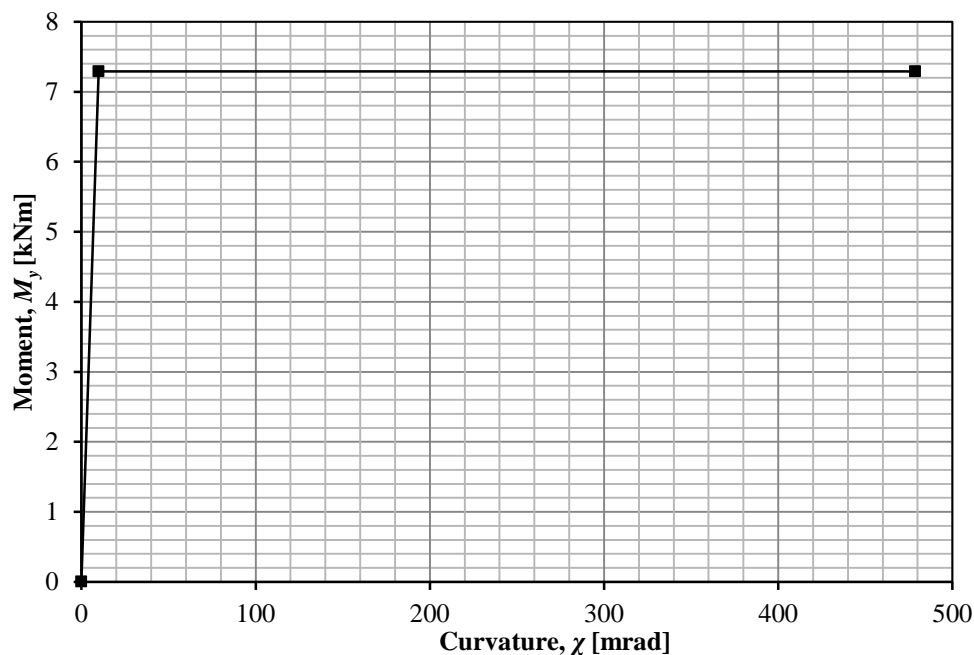
Figure C.27 Bilinear plastic moment-curvature relation for the studied cantilever slab. Valid for the majority of the beams in the beam grillage model.

The above stated moment-curvature relation applies for the majority of the beams in the beam grillage model. As in the case of the cantilever structure, the moment-curvature relation presented in Figure C.27 does not apply for beams in the boundaries. The moment-curvature model for these beams in the beam grillage model is presented in Figure C.28.
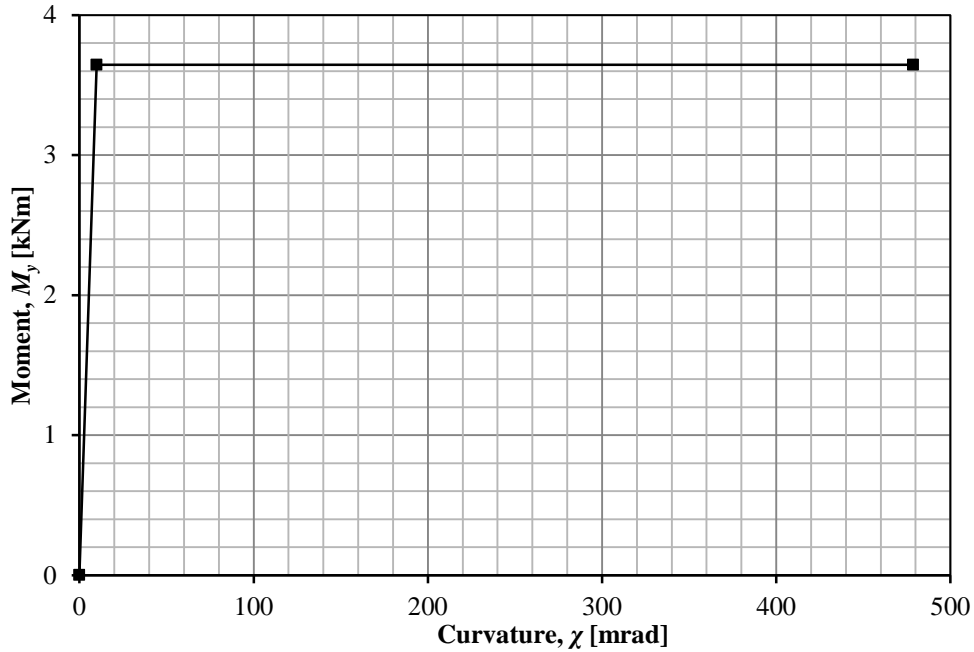
Figure C.28 Bilinear plastic moment-curvature relation for the studied cantilever slab. Valid for the beams in the boundaries and the symmetry boundaries in the beam grillage model.

C.2.6 Simply supported slab – Two moving concentrated forces

The plastic bilinear moment-curvature relation for the simply supported one-way slab subjected to a single moving force of constant and varying magnitudes was also used for these analyses. The reasons for this choice were the same as stated in Appendix C.2.4 for the cantilever structure:

- Comparison purposes between a single and two moving concentrated forces.
- Comparison purposes within the two moving concentrated forces.

Appendix D Approximation of plastic rotation

This chapter covers the approximate approach that was used in this Thesis to measure plastic rotation in the cantilever and simply supported structure. This chapter also covers how this approximate approach differs from the results obtained from the option provided by ADINA.

D.1 Background of the approximation

ADINA provides an option for obtaining the plastic curvature in the integration points over the elements. If the plastic curvature is summarized over the element length, the plastic rotation in the structure is obtained. The results from the option provided from ADINA is, however rather cumbersome when exporting the obtained data for external analysis. As an alternative to obtaining the plastic curvature and thus the plastic rotation directly from ADINA, deflections in the nodes can be measured and an angle α created by these nodes can be determined. If the angle α is measured after each load cycle is completed, i.e. when the cantilever slab is completely unloaded, it represents the plastic rotation θ_{pl} accumulated during that load cycle. This method is the approximate approach used throughout this Thesis that is further examined below.

Since the approximate approach is dependent on the distance between the nodes in order to calculate the plastic rotation, the mesh densities influence the results. The mesh density for the two structures was set so that the element length was 0.2 m for the majority of the elements in the structures. The mesh density was however increased so that the element length was 0.05 m where the plastic rotation was calculated. The choice was based on the observations made by Lim (2013) and a parametric study was performed in this Thesis indicated that the choice was reasonable and yielded satisfying results. This decreased element length was therefore used at the cantilever support and in the centre of the simply supported structure, see Figure D.1 and Figure D.5

The influence of further increased mesh densities did not yield results that differed significantly from the ones obtained from the above stated mesh used in this Thesis. The above stated mesh was therefore evaluated as satisfactory for the analyses conducted in this Thesis.

D.2 Cantilever slab
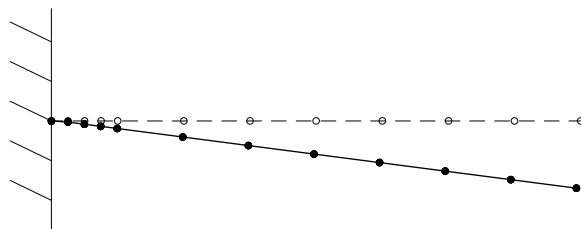
Figure D.1   Deflected shape and mesh density for the cantilever structure

The approximate approach to determine the plastic rotation was to measure the deflection in the second and third node, u_2 and u_3 after each completed load cycle.

$$\Delta u = u_2 - u_3 \tag{D-1}$$

The angle α, i.e. the plastic rotation, was calculated from the triangle created by the deflected nodes.

$$\alpha = \tan(\frac{\Delta u}{l_{ele}}) \tag{D-2}$$

Where $l_{ele} = 0.050$ m, which is the length of each element at the fixed support, see Figure D.1.
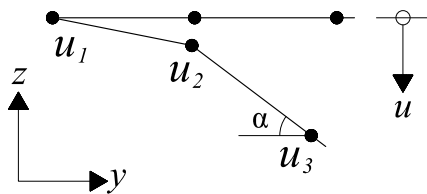
Figure D.2   Geometrical interpretation of the plastic rotation for the cantilever structure.

The rotation in the first node u_1 was prescribed to zero by the boundary conditions which influenced the angle of the triangle and thus results in an approximation. The approximation is shown in Figure D.3.
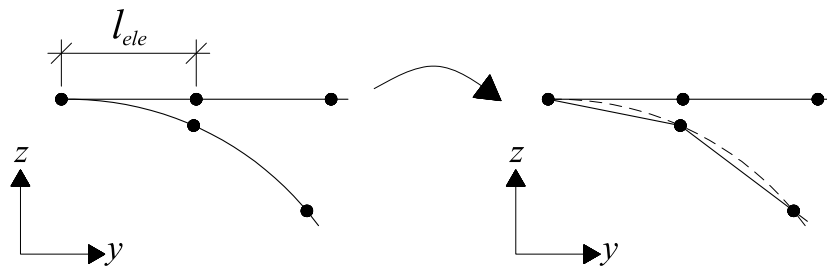
Figure D.3   Approximation of the plastic rotation for the cantilever structure.

The background for calculating the angle based on the deflection in the second and third node was derived from how ADINA treats plastic curvature in beam elements. The reader is referred to Section 6.1.3 for additional information on this matter.

In order to evaluate the influence of the above stated approximation, the cantilever structure in Chapter 6 was subjected to a single moving concentrated force of the following magnitudes:

$$F = \begin{bmatrix} 140 & 145 & 150 & 155 & 160 & 165 \end{bmatrix} \text{kN} \tag{D-3}$$

This range of force magnitudes covered the largest force not to cause failure within 150 load cycles to the smallest force to cause failure after two load cycles. The result from the approximation was used throughout this Thesis and is shown in Figure 6.17.

The analyses for the different forces were conducted for 150 load cycles if failure of the structure did not occur within that range. The plastic rotation obtained by the option provided by ADINA and the approximation stated above is shown in Figure D.4.
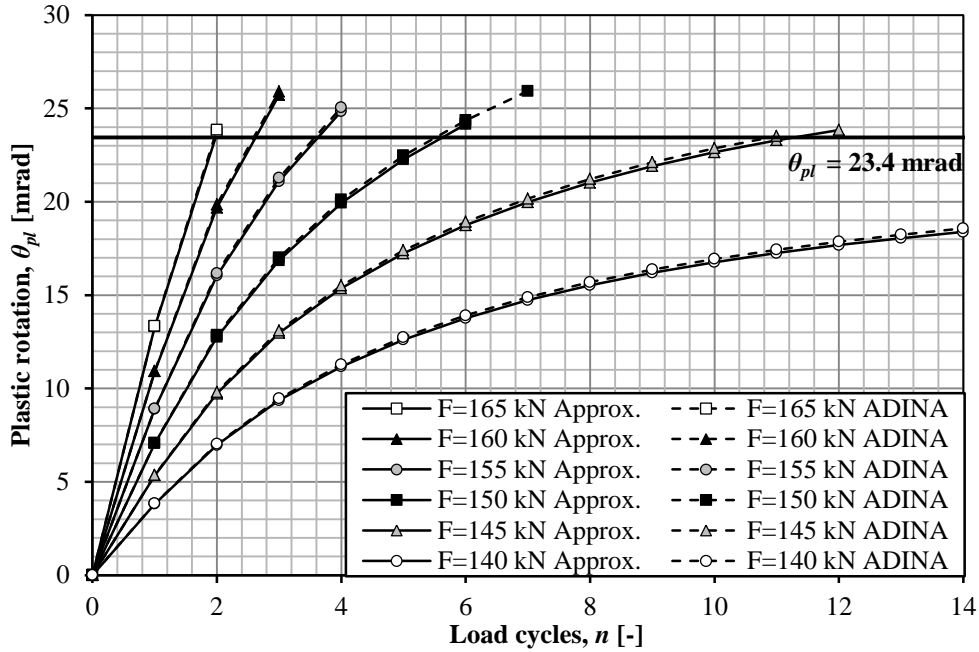
Figure D.4   Plastic rotation for different magnitudes of moving concentrated forces.

As can be seen in Figure D.4, the approximate approach yields satisfactory results for the development of plastic rotation for a single moving force on the cantilever structure. It was from these results concluded that the approximate approach was satisfactory for the load cantilever structure and combinations studied in this Thesis.

D.3 Simply supported slab
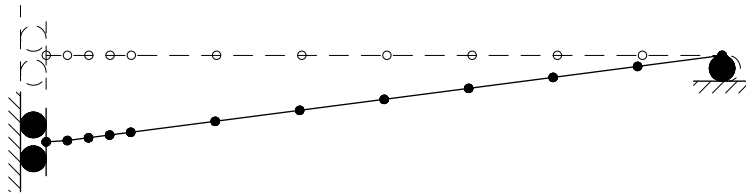
Figure D.5   Deflected shape and mesh density for the simply supported one-way structure.

The approximate approach to determine the plastic rotation was to measure the deflection in the second and third node, u_2 and u_3 after each completed load cycle.

$$\Delta u = u_3 - u_2 \tag{D-4}$$

The angle α, i.e. the plastic rotation, was calculated from the triangle created by the deflected nodes.

$$\alpha = \tan(\frac{\Delta u}{l_{ele}}) \tag{D-5}$$

Where $l_{ele} = 0.050$ m, which is the length of each element in the centre of the slab.
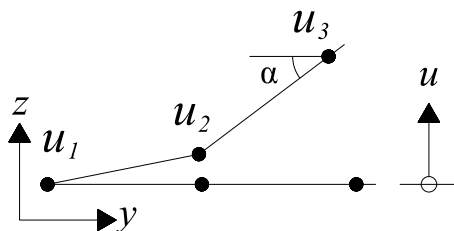
Figure D.6   Geometrical interpretation of the plastic rotation for the simply supported one-way structure.

The rotation in the first node u_1 was also here prescribed to zero by the boundary conditions which influenced the angle of the triangle and thus results in an approximation. The approximation is shown in Figure D.7.
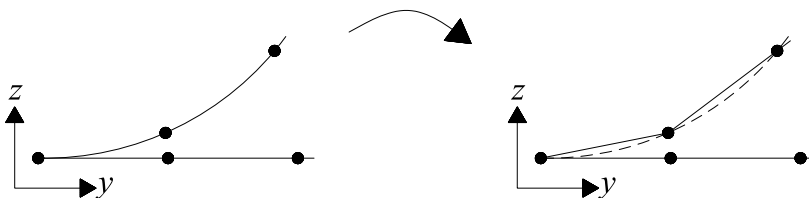
Figure D.7   Approximation of the plastic rotation for the simply supported one-way structure.

In order to evaluate the influence of the above stated approximation, the simply supported structure in Chapter 7 was subjected to a single moving concentrated force of the following magnitudes:

$$F = \begin{bmatrix} 80 & 85 & 90 & 95 & 100 & 105 & 110 \end{bmatrix} \text{kN} \tag{D-6}$$

The background for the range of forces was covered in Appendix D.2. The results from the approximation were used throughout this Thesis and are shown in Figure 7.12.

The analyses for the different forces were also here conducted for 150 load cycles if failure of the structure did not occur within that range. The plastic rotation obtained by the option provided by ADINA and the approximation stated above is shown in Figure D.8.
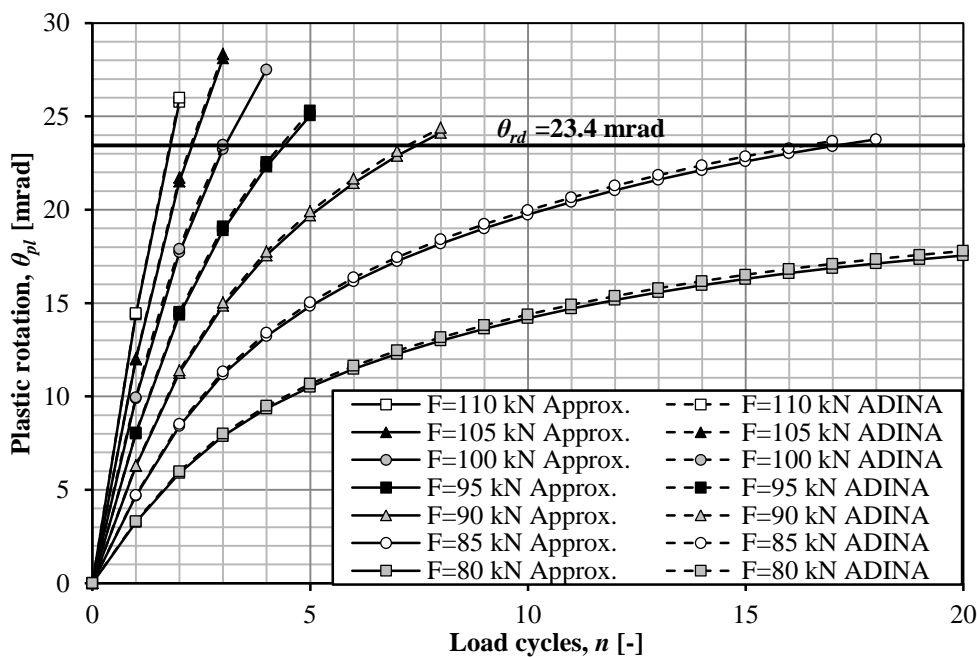
Figure D.8   Plastic rotation for different magnitudes of moving concentrated forces.

It can also here be seen that the approximation yields satisfactory results which motivates the use of the approximation for the simply supported structure in this Thesis.

Appendix E   Load application order

This chapter covers the load application order of a pair of moving concentrated forces with a constant distance $d = 1.2$ m and how this influenced the plastic rotation in a cantilever and a simply supported one-way structure. This chapter also covers the difference in plastic rotation between these load application orders which served as a foundation for the load application order used for the analyses in this Thesis.

The load application order is in this Thesis defined as the order of how two forces of different magnitudes are applied on the structure. There are in this case two possible load application orders, here denoted LAO_1 and LAO_2, where the first force was greater than the second and vice versa. Equation (E-1) and (E-2) defines the first and second load application order respectively and these are also illustrated in Figure E.1 and Figure E.2 respectively.

$$F_1 < F_2 \tag{E-1}$$
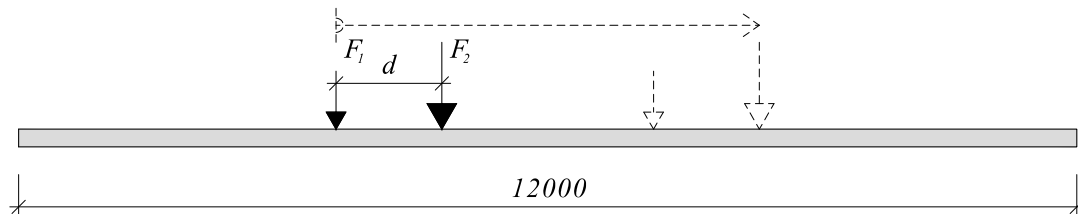
Figure E.1   Force layout for the first load application order, LAO_1

$$F_1 > F_2 \tag{E-2}$$
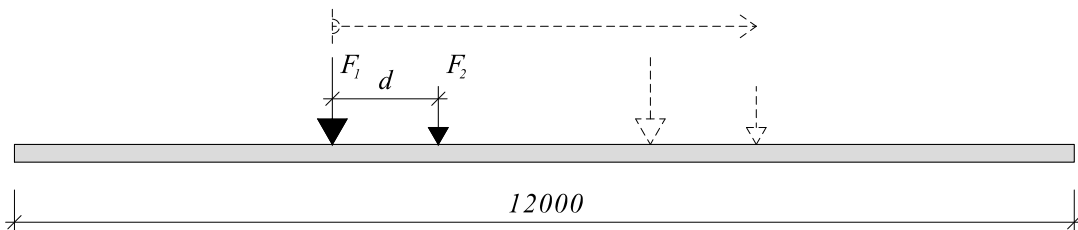
Figure E.2   Force layout for the second load application order, LAO_2

E.1 Cantilever slab

The load application order, i.e. how a pair of moving concentrated forces are applied and how this influences the development of the plastic rotation in the cantilever structure is here evaluated. The study was conducted on the cantilever structure presented in Section 6.5 for a pair of moving concentrated forces of different magnitudes.

The total applied force F_{tot} was kept constant so that:

$$F_{tot} = F_1 + F_2 = 170 \text{ kN} \tag{E-3}$$

Where:

$$F_1 \neq F_2 \tag{E-4}$$

Where the first load application order LAO_1 had the following force layout:

$$F_1 = \begin{bmatrix} 10\ 20\ 30\ 40\ 50\ 60\ 70\ 80 \end{bmatrix} \text{kN} \tag{E-5}$$

$$F_2 = \begin{bmatrix} 160\ 150\ 140\ 130\ 120\ 110\ 100\ 90 \end{bmatrix} \text{kN} \tag{E-6}$$

The second load application order LAO_2 had the following force layout:

$$F_1 = \begin{bmatrix} 160\ 150\ 140\ 130\ 120\ 110\ 100\ 90 \end{bmatrix} \text{kN} \tag{E-7}$$

$$F_2 = \begin{bmatrix} 10\ 20\ 30\ 40\ 50\ 60\ 70\ 80 \end{bmatrix} \text{kN} \tag{E-8}$$

The two different load application orders are treated and compared in Appendix E.1.1 to E.1.3.

E.1.1 Load application order LAO₁, F₁< F₂

The plastic rotation is shown in Figure E.3 and the development of the plastic rotation during the first ten load cycles is illustrated in Figure E.4.
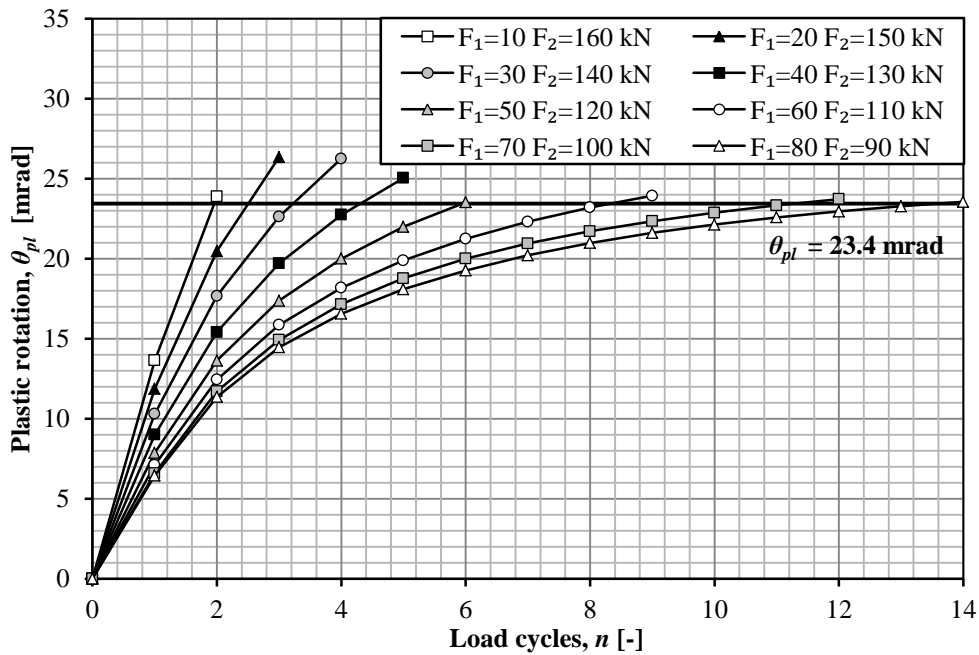
Figure E.3   Plastic rotation for different load combinations for the first load application order LAO₁.
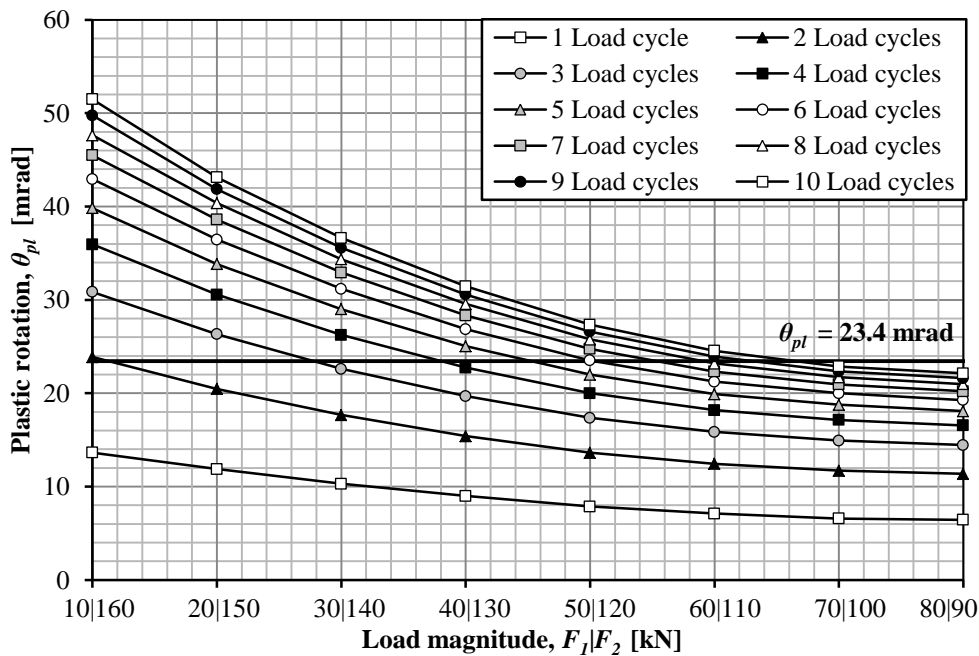
Figure E.4   Development of plastic rotation for different load combinations for the first load application order LAO₁.

E.1.2 Load application order LAO₂, F₁ > F₂

The plastic rotation in the centre of the slab can is shown in Figure E.5 and the development of the plastic rotation during the first ten load cycles is illustrated in Figure E.6.
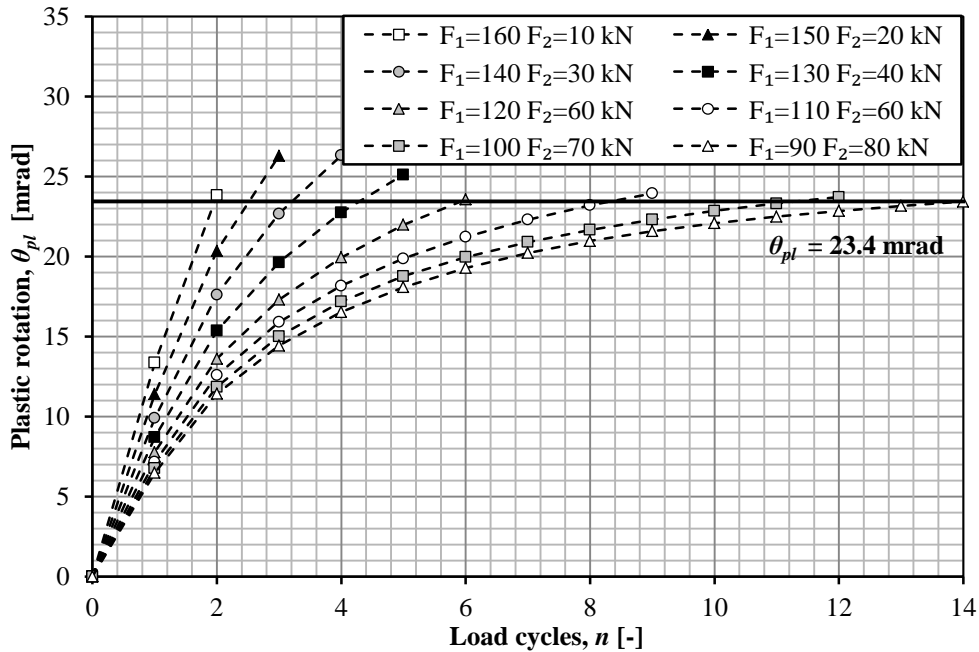
Figure E.5   Plastic rotation for different load combinations for the first load application order LAO₂.
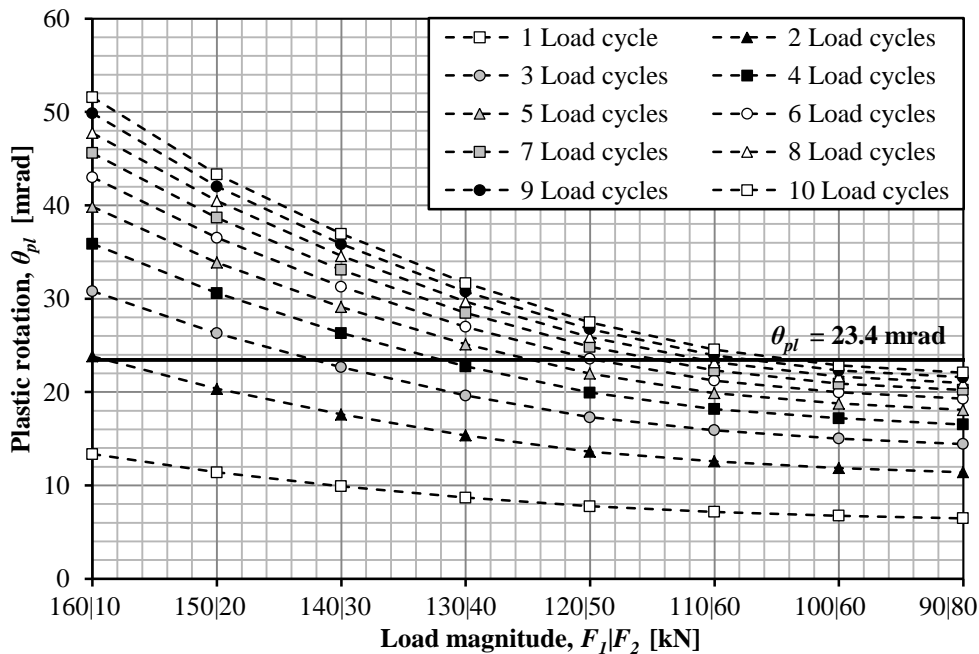
Figure E.6   Development of plastic rotation for different load combinations for the first load application order LAO₂.

E.1.3 Comparison of load application orders

The two load application orders are here compared in order to evaluate the influence it has on the development of plastic rotation. As can be seen in Figure E.7, the load application order has a small influence on the plastic rotation development of the structure. It is clear that the greatest difference in plastic rotation arises after the first load cycle for the load combinations with the greatest load magnitude differences.
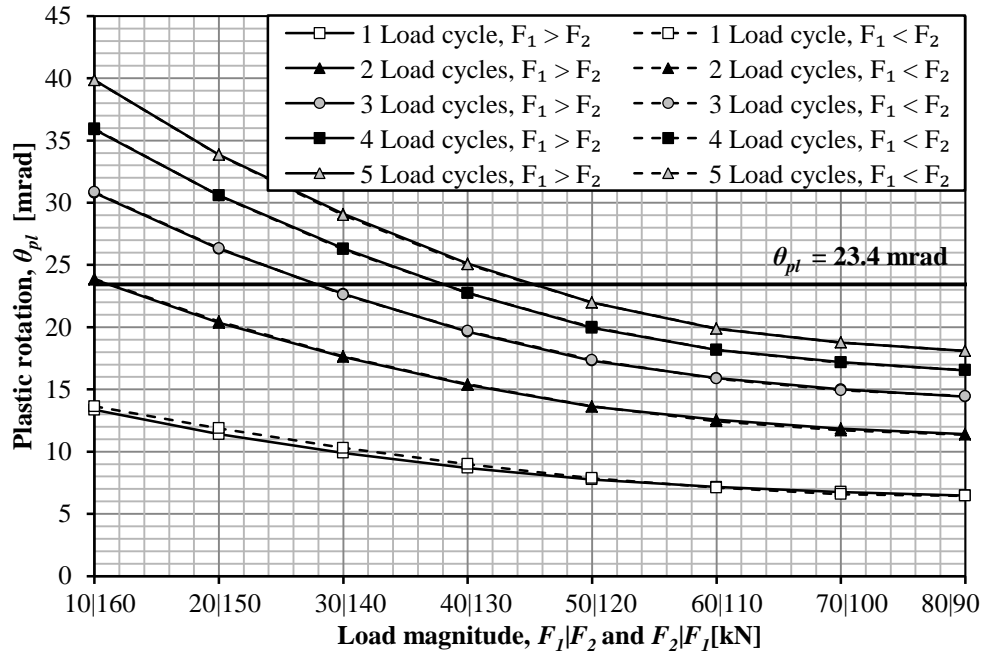
Figure E.7   Development of plastic rotation for different load combinations for the first and second load application order for the first five load cycles.

The difference in plastic rotation $\gamma_{\theta pl.LAO}$ between the two load application orders was calculated according to Equation (E-9):

$$\gamma_{\theta pl.LAO} = \frac{\theta_{pl.LAO2} - \theta_{pl.LAO1}}{\theta_{pl.LAO1}} \tag{E-9}$$

The result from Equation (E-9) is shown in Figure E.8 where it is clearly illustrated that there is no obvious connection between the load application order and the development of plastic rotation.

If, however, only load cycle number seven to ten is shown, a clearer pattern arises as can be seen in Figure E.9 and a tendency of convergence arises. It appears from this figure that LAO_1 is advantageous for the structure when the load magnitude difference is significant to intermediate. As the load magnitude difference decreases, the difference of the plastic rotation from the two load application orders also decreases. This behaviour is natural since the difference between the force magnitudes are small and the load application order should therefore not be significant.
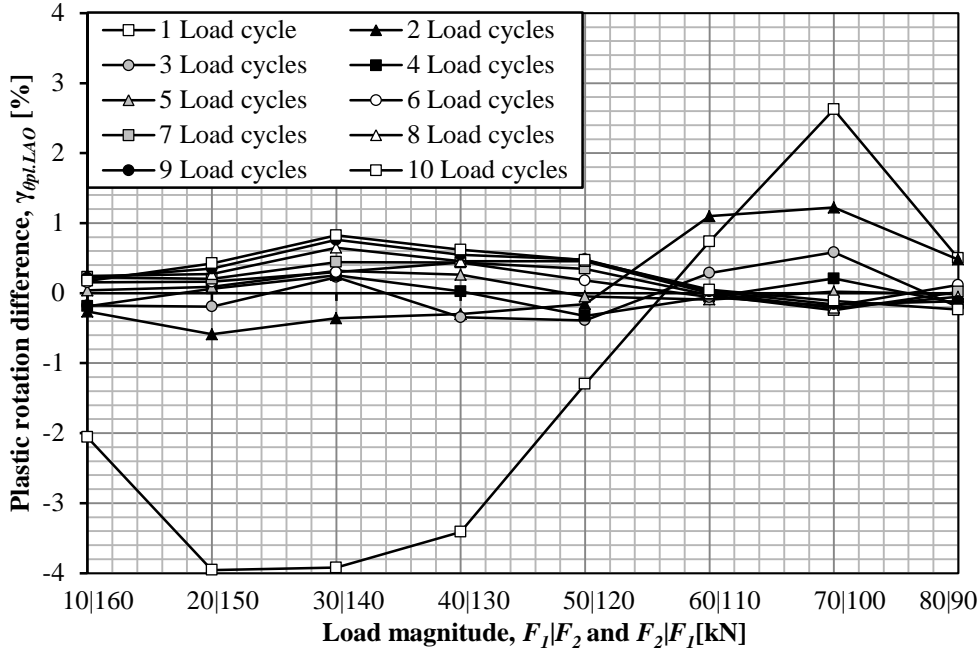
Figure E.8   Difference in plastic rotation γ_{LAO} for the first ten load cycles between the results from LAO_1 and LAO_2 for the first ten load cycles.
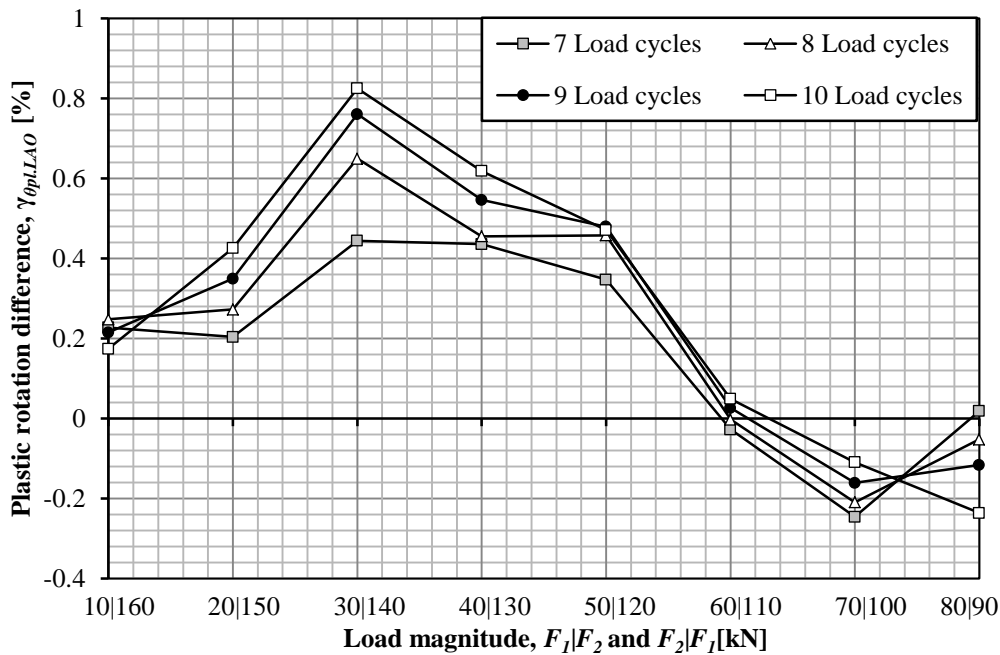
Figure E.9   Difference in plastic rotation γ_{LAO} for the first ten load cycles between the results from LAO_1 and LAO_2 for load cycle seven to ten.

The second load application order LAO_2 causes greater plastic rotation for the majority of the studied load combinations and load cycles. It should here be noted that the difference is small and a bit unstable. The load application order used in this Thesis was chosen to LAO_1.

E.2 Simply supported slab

The load application order and how this influenced the development of the plastic rotation in the simply supported structure is here evaluated. The study was conducted on the simply supported structure in Chapter 7 for a pair of moving concentrated forces of different magnitudes.

The total applied force F_{tot} was also here kept constant so that:

$$F_{tot} = F_1 + F_2 = 120 \text{ kN} \tag{E-10}$$

Where:

$$F_1 \neq F_2 \tag{E-11}$$

Where the first load application order LAO_1 had the following force layout:

$$F_1 = \begin{bmatrix} 10 \ 20 \ 30 \ 40 \ 50 \end{bmatrix} \text{kN} \tag{E-12}$$

$$F_2 = \begin{bmatrix} 110 \ 100 \ 90 \ 80 \ 70 \end{bmatrix} \text{kN} \tag{E-13}$$

The second load application order LAO_2 had the following force layout:

$$F_1 = \begin{bmatrix} 110 \ 100 \ 90 \ 80 \ 70 \end{bmatrix} \text{kN} \tag{E-14}$$

$$F_2 = \begin{bmatrix} 10 \ 20 \ 30 \ 40 \ 50 \end{bmatrix} \text{kN} \tag{E-15}$$

The two different load application orders are treated and compared in Appendix E.2.1 to E.2.3

E.2.1 Load application order LAO₁, F₁ < F₂

The plastic rotation is shown in Figure E.10 and the development of the plastic rotation during the first ten load cycles is illustrated in Figure E.11.
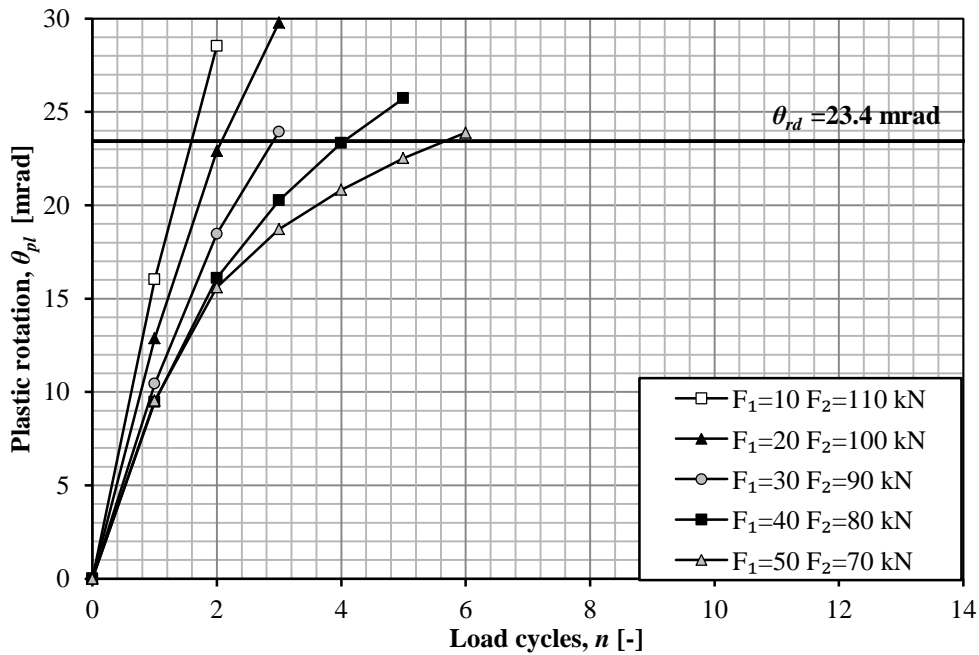
Figure E.10 Plastic rotation for the first load application order, LAO₁.
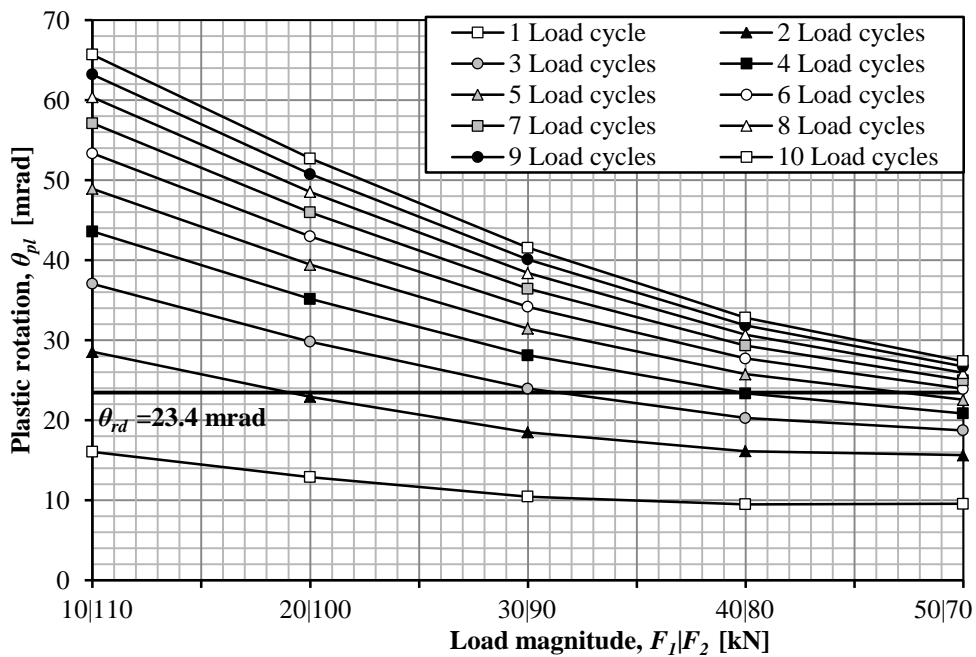
Figure E.11 Development of plastic rotation for the first load application order, LAO₁.

E.2.2 Load application order LAO₂, F₁ > F₂

The plastic rotation is shown in Figure E.12 and the development of the plastic rotation during the first ten load cycles is illustrated in Figure E.13.
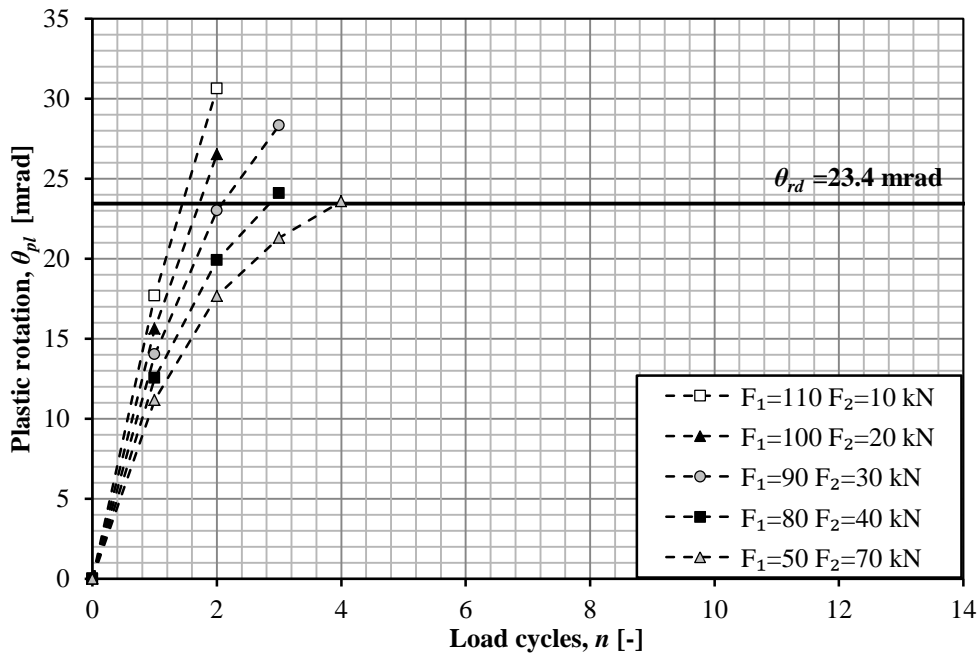
Figure E.12 Plastic rotation for the second load application order, LAO₂.
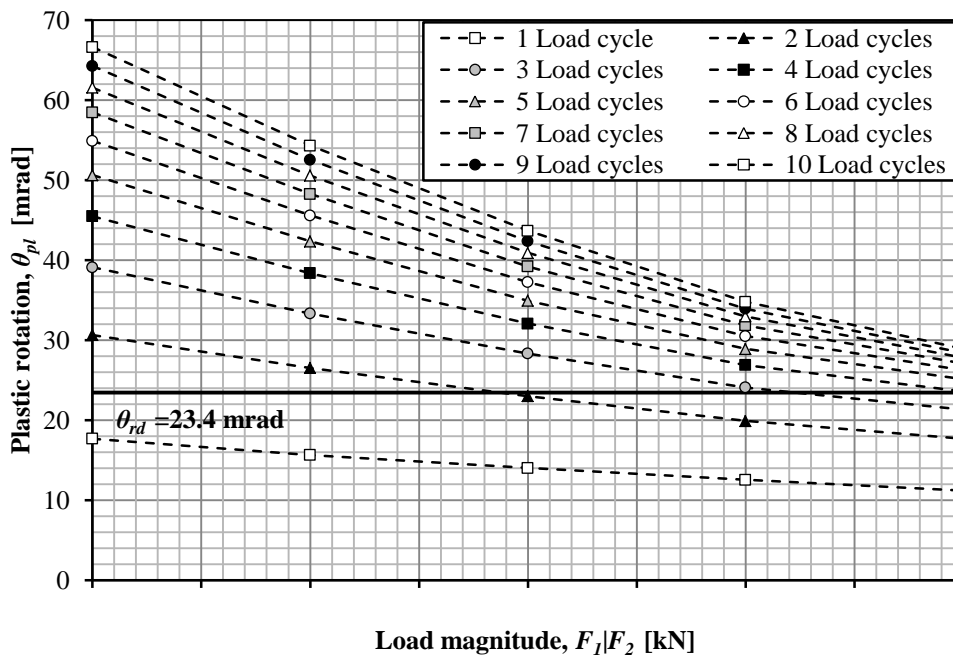
Figure E.13 Development of plastic rotation for the second load application order, LAO₂.

E.2.3 Comparison of load application orders

The two load application orders are here compared in order to evaluate the influence it had on the development of plastic rotation. As can be seen in Figure E.14, the load application order has a noticeable influence on the plastic rotation development of the structure. It is clear that the greatest difference in plastic rotation arises after the first load cycle for the load combinations with intermediate load magnitude differences.
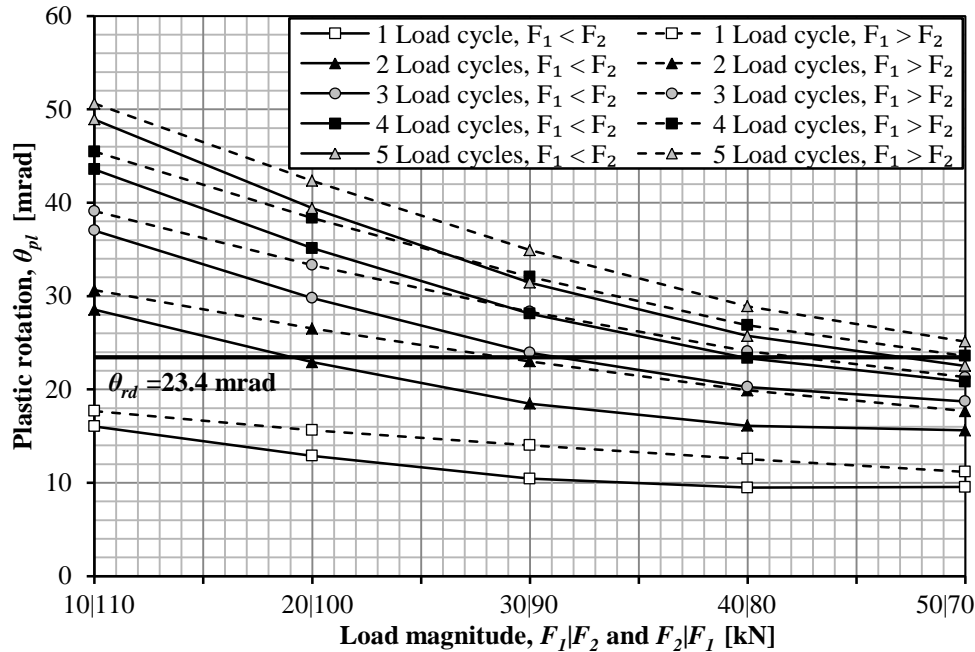
Figure E.14 Development of plastic rotation for different load combinations for the first and second load application order for the first five load cycles.

The difference in plastic rotation $\gamma_{\theta pl.LAO}$ between the two load application orders was calculated according to Equation (E-16):

$$\gamma_{\theta pl.LAO} = \frac{\theta_{pl.LAO2} - \theta_{pl.LAO1}}{\theta_{pl.LAO1}} \tag{E-16}$$

The result from Equation (E-16) is shown in Figure E.15 where it is clearly shown that the difference in plastic rotation between the two load application orders is diminished as the number of load cycles is increased. It can be seen in the figure that LAO_1 is advantageous for the structure for all investigated load combinations. The difference in plastic rotation seems to reach a stable state after a few load cycles where the difference is slightly bigger for larger differences between the force magnitudes. The second load application order LAO_2 causes greater plastic rotation for all investigated load combinations and load cycles.

The load application LAO_1 was however chosen for the analyses presented in this Thesis due to comparison purposes to the cantilever structure.
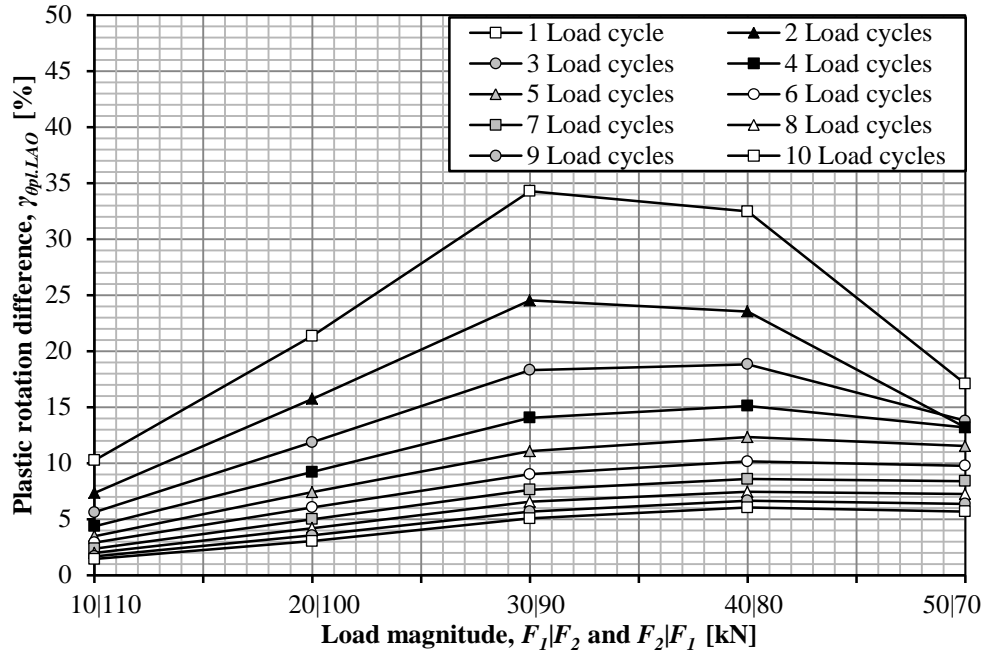
Figure E.15 Difference in plastic rotation γ_{LAO} for the first ten load cycles between the results from LAO_1 and LAO_2 for the first ten load cycles.

Appendix F Influence of distance, *d*

This chapter covers the study conducted on the cantilever structure in Section 6.4.5 where the influence of the distance *d* between a pair of moving concentrated forces was evaluated. The results presented in this chapter is not discussed to a great extent but are presented for the interested reader.

In order to evaluate how the distance influenced the plastic rotation of the structure, the distance between the pair of moving concentrated forces was altered according to:

$$d = \begin{bmatrix} 1.2\ 1.6\ 2.0\ 2.4\ 2.8\ 3.2\ 3.6\ 4.0\ 4.4\ 4.8 \end{bmatrix} \text{m} \qquad \text{(F-1)}$$

The cantilever structure was subjected to forces from 65 kN to 165 kN according to the following magnitudes:

$$F_1 = F_2 = \begin{bmatrix} 65\ 70\ 75\ ...\ 155\ 160\ 165 \end{bmatrix} \text{kN} \qquad \text{(F-2)}$$

The total applied load F_{tot} of the forces F_1 and F_2 is defined in Equation (F-3):

$$F_{tot} = F_1 + F_2 \qquad \text{(F-3)}$$
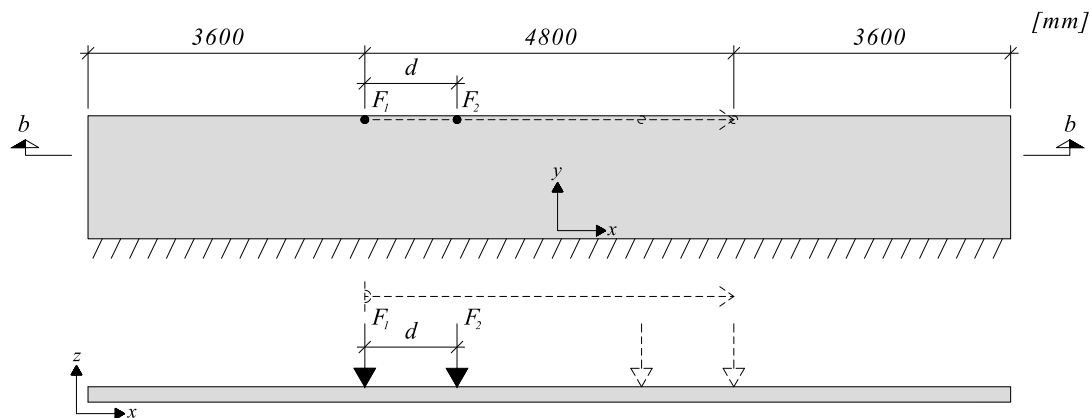
Figure F.1   Geometry and dimensions of the studied cantilever slab for two concentrated forces of equal magnitudes.

The analyses were conducted for 150 load cycles *n* for each pair of concentrated forces if failure of the cantilever slab did not occur within this range. The plastic rotation in the centre of the slab for different magnitudes of forces and distances between the forces is shown in Figure F.2 to Figure F.21.
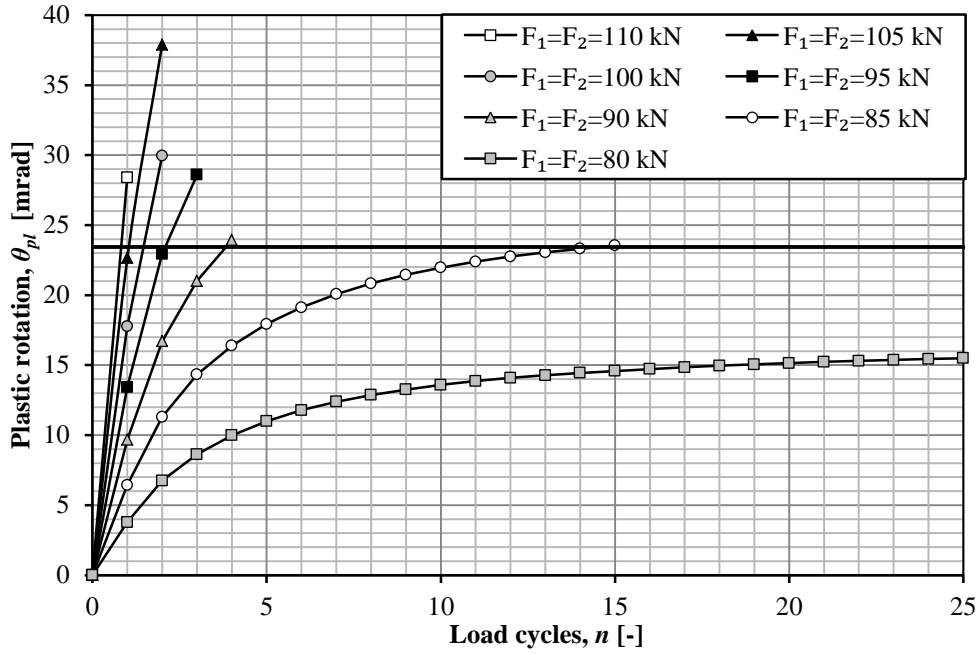
Figure F.2   Plastic rotation in the centre of the cantilever slab for d = 1.2 m.
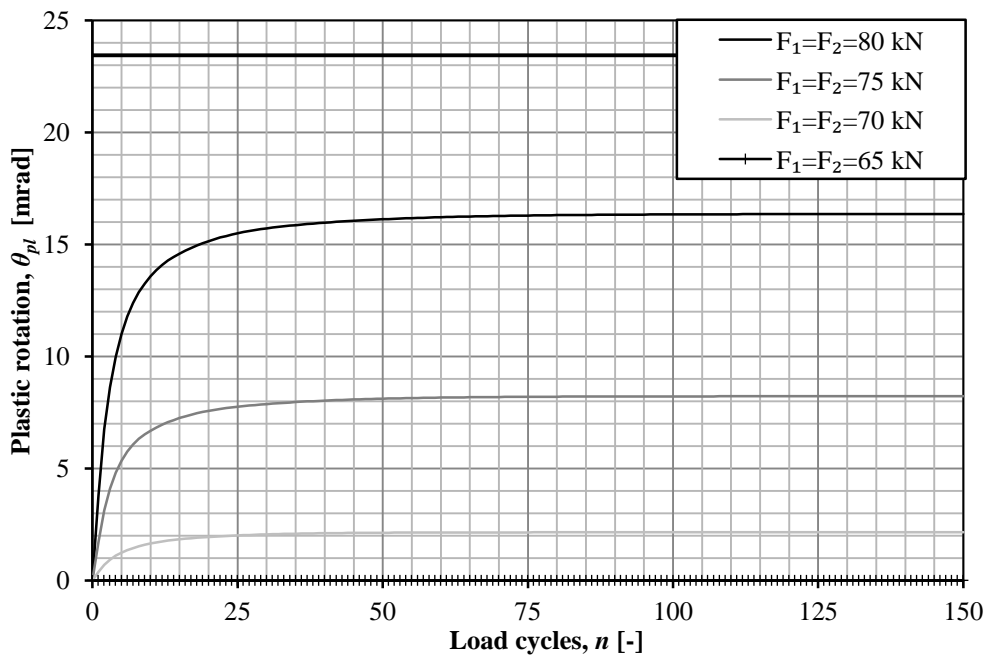
Figure F.3   Plastic rotation in the centre of the cantilever slab for d = 1.2 m.

CHALMERS, *Civil and Environmental Engineering*, Master's Thesis 2014:73
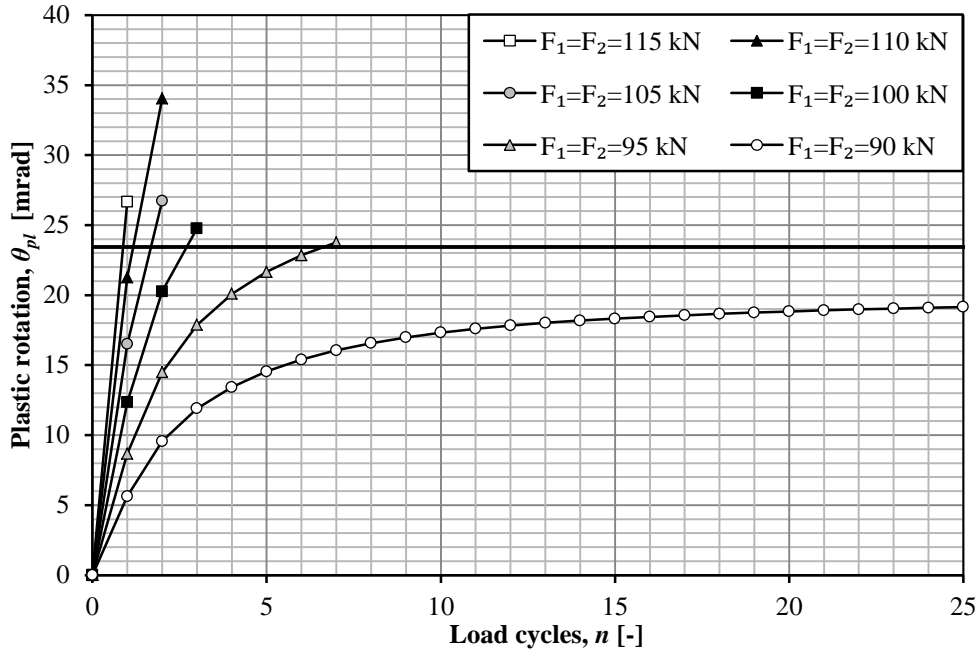
Figure F.4   Plastic rotation in the centre of the cantilever slab for d = 1.6 m.
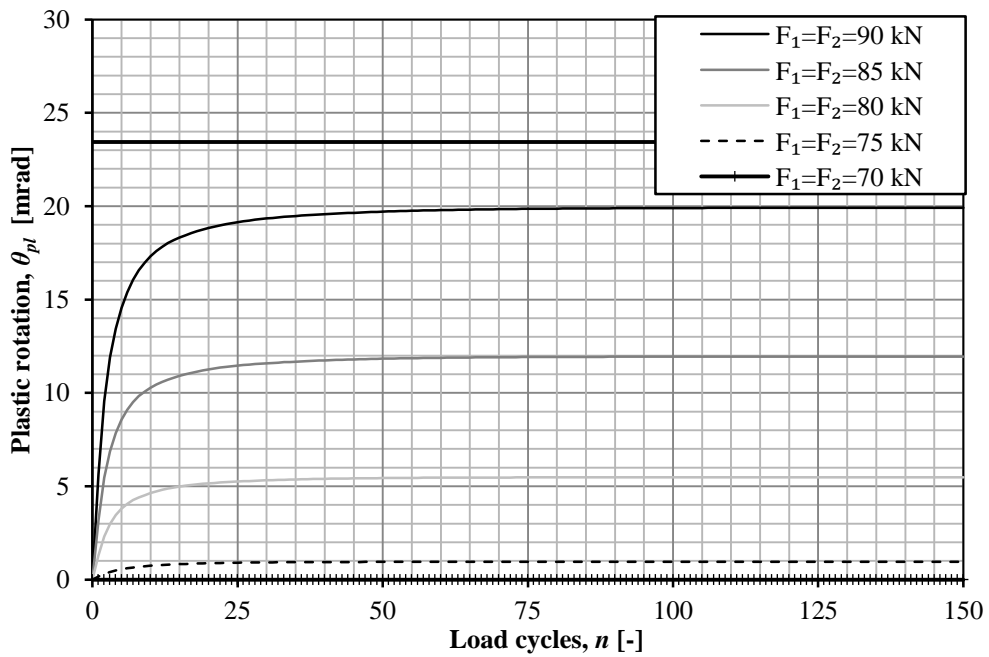
Figure F.5   Plastic rotation in the centre of the cantilever slab for d = 1.6 m.
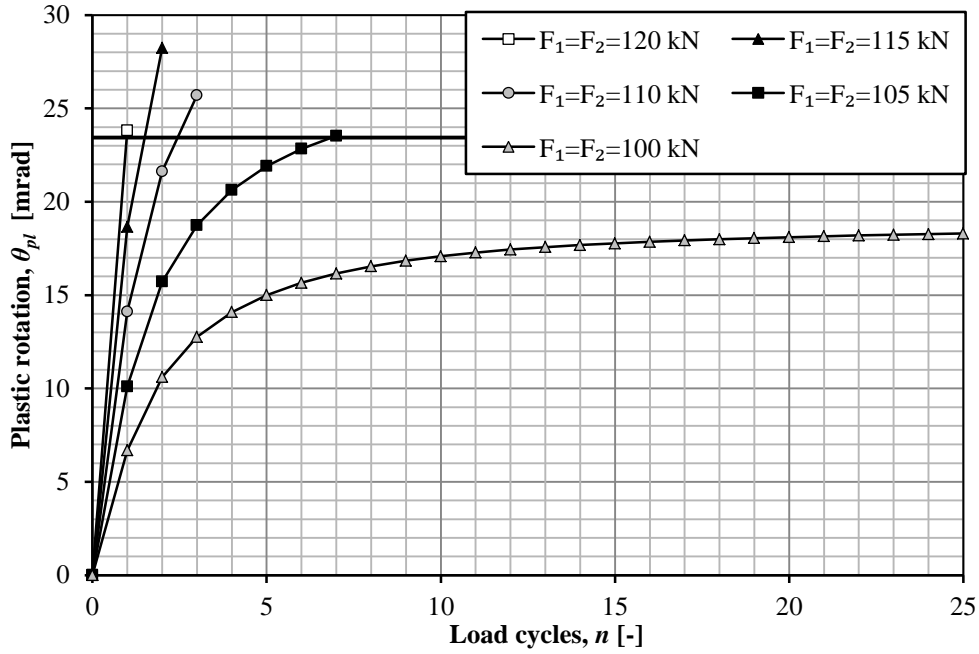
Figure F.6   Plastic rotation in the centre of the cantilever slab for d = 2.0 m.
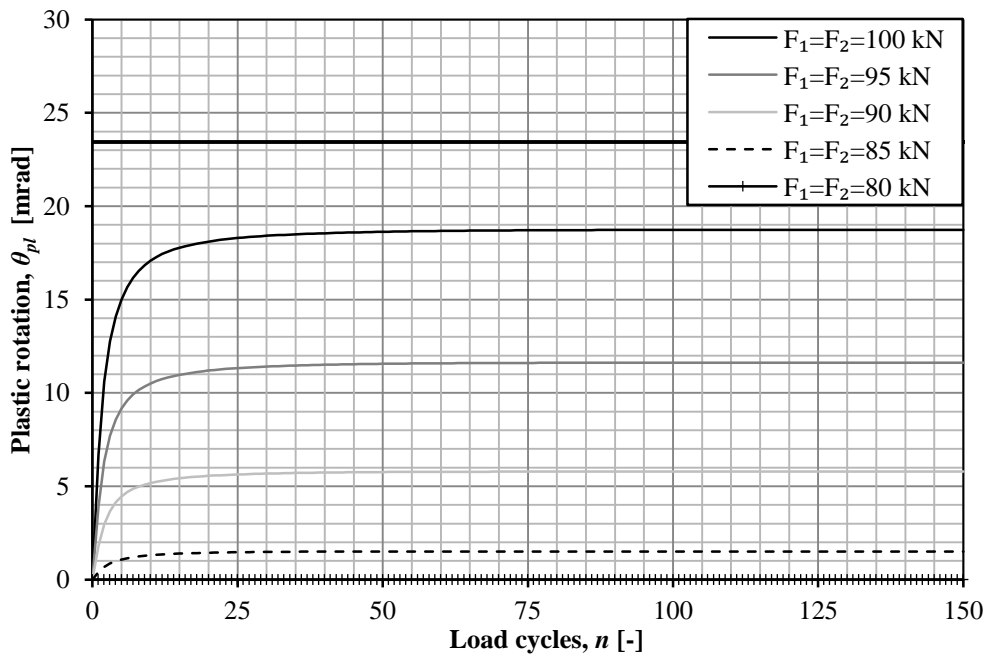
Figure F.7   Plastic rotation in the centre of the cantilever slab for d = 2.0 m.
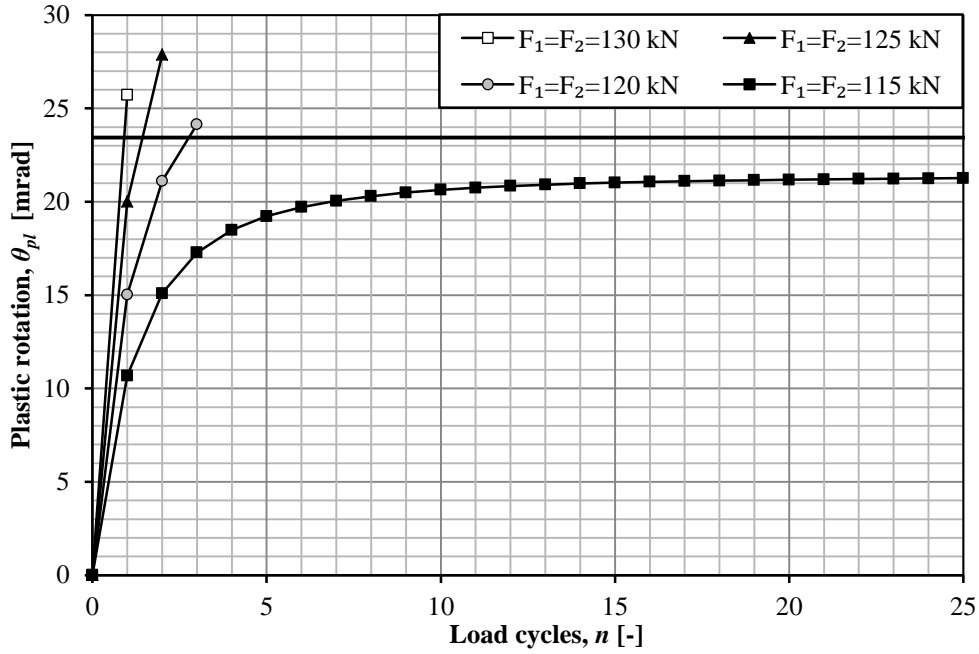
Figure F.8   Plastic rotation in the centre of the cantilever slab for d = 2.4 m.
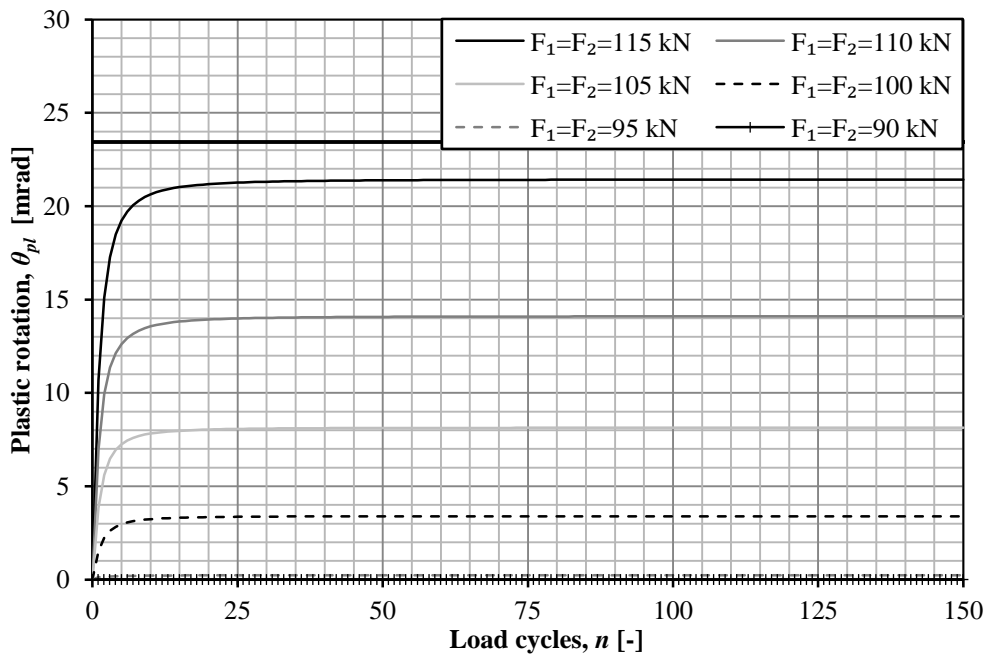
Figure F.9   Plastic rotation in the centre of the cantilever slab for d = 2.4 m.
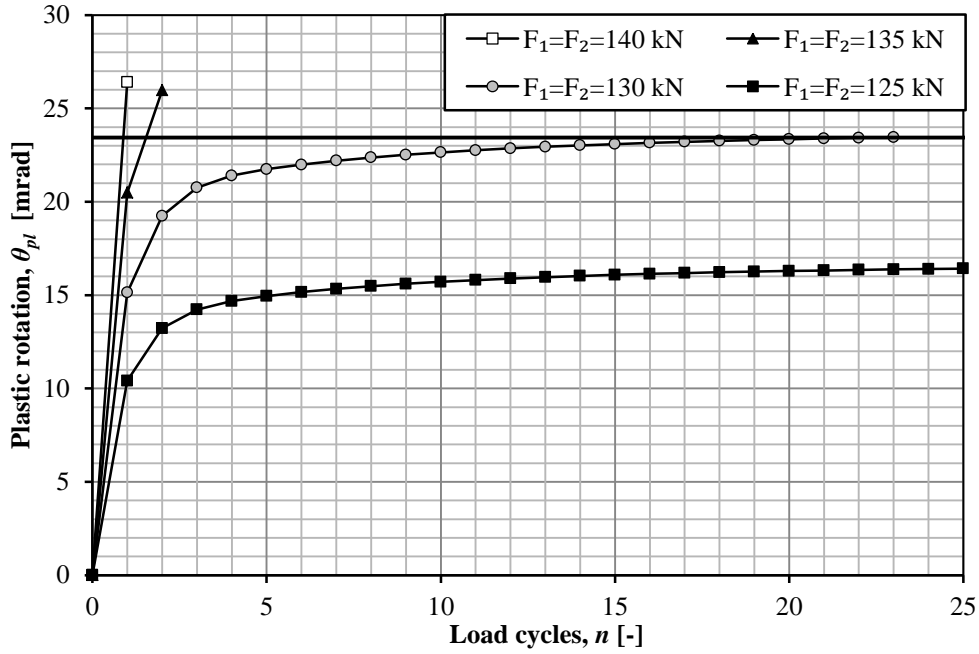
Figure F.10   Plastic rotation in the centre of the cantilever slab for d = 2.8 m.
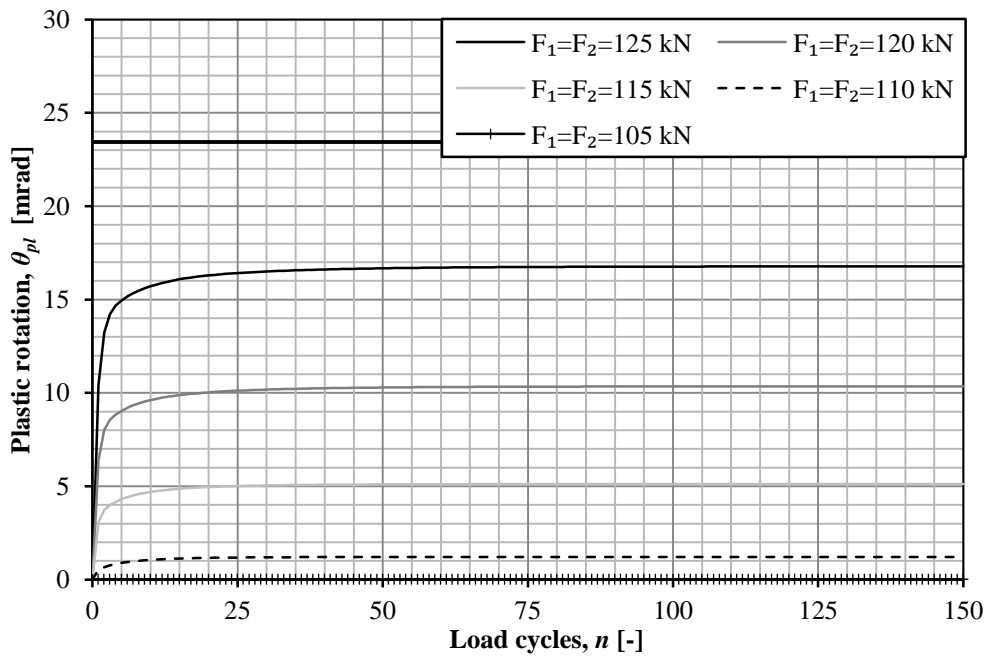
Figure F.11   Plastic rotation in the centre of the cantilever slab for d = 2.8 m.

CHALMERS, *Civil and Environmental Engineering*, Master's Thesis 2014:73
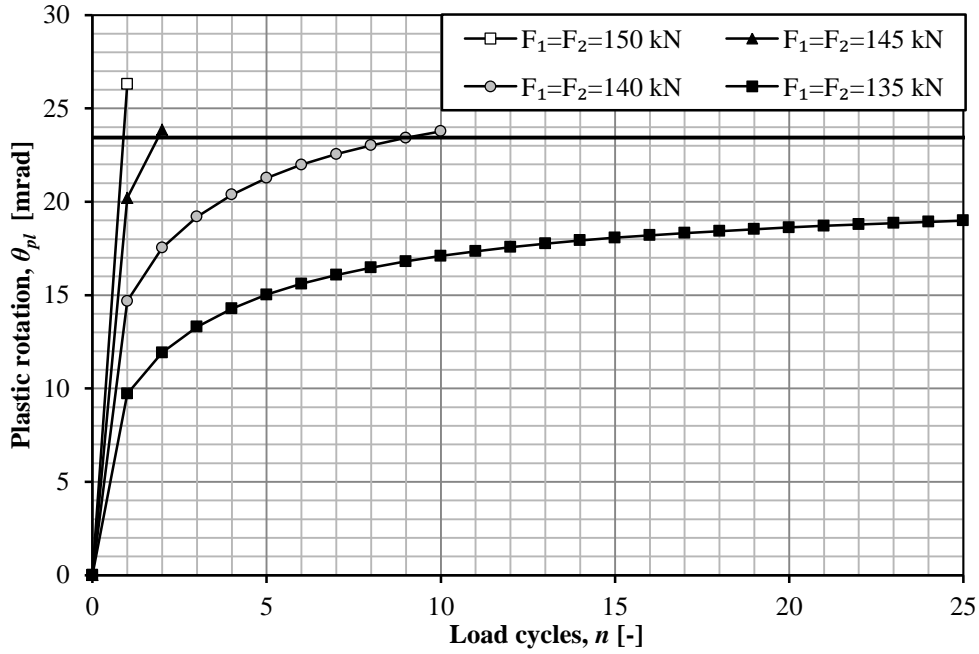
Figure F.12   Plastic rotation in the centre of the cantilever slab for d = 3.2 m.
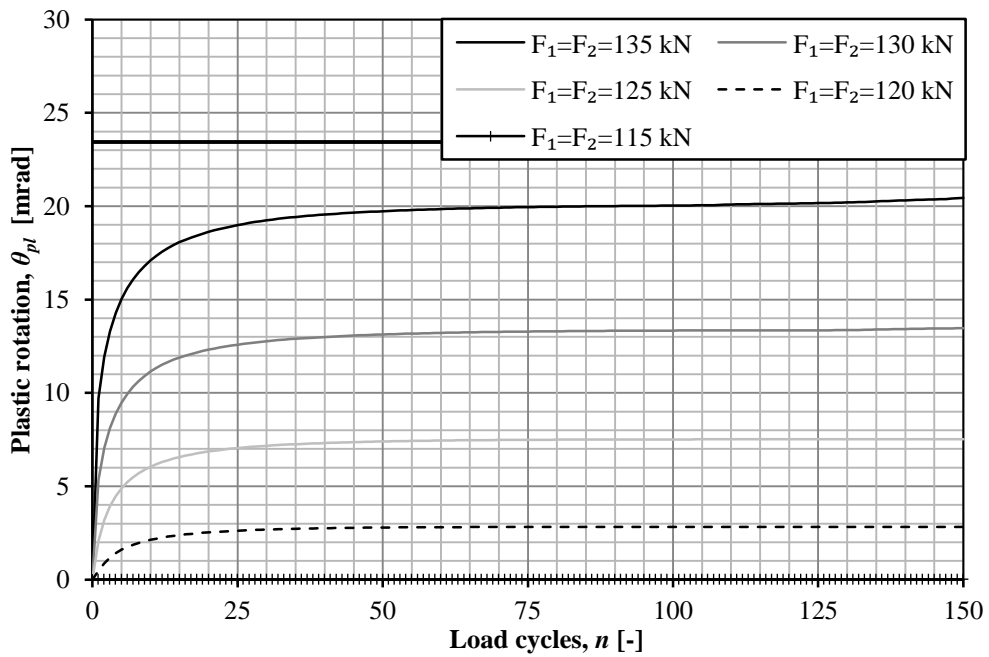
Figure F.13   Plastic rotation in the centre of the cantilever slab for d = 3.2 m.
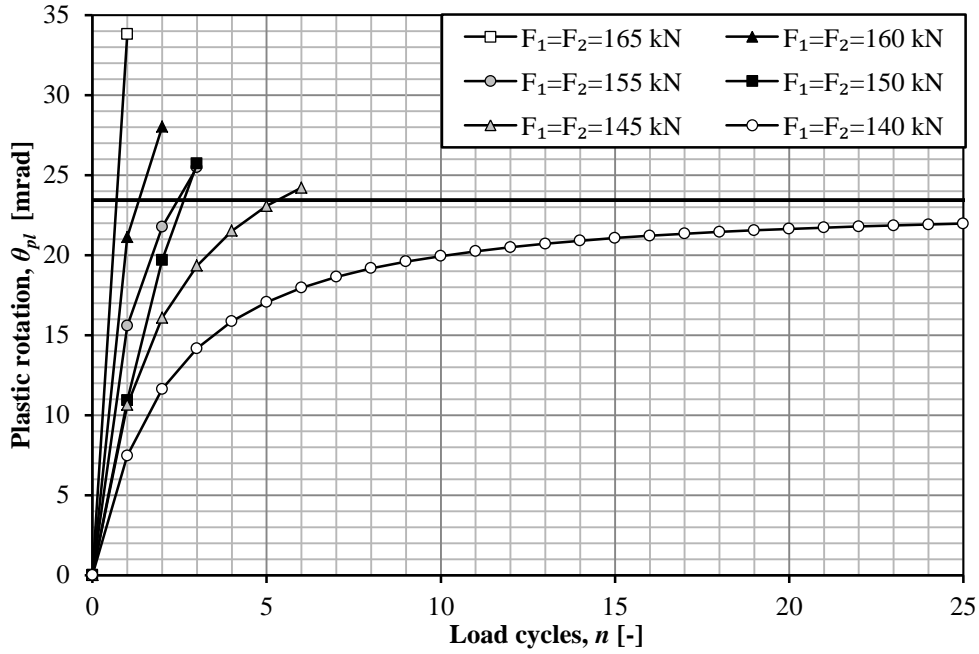
Figure F.14   Plastic rotation in the centre of the cantilever slab for d = 3.6 m.
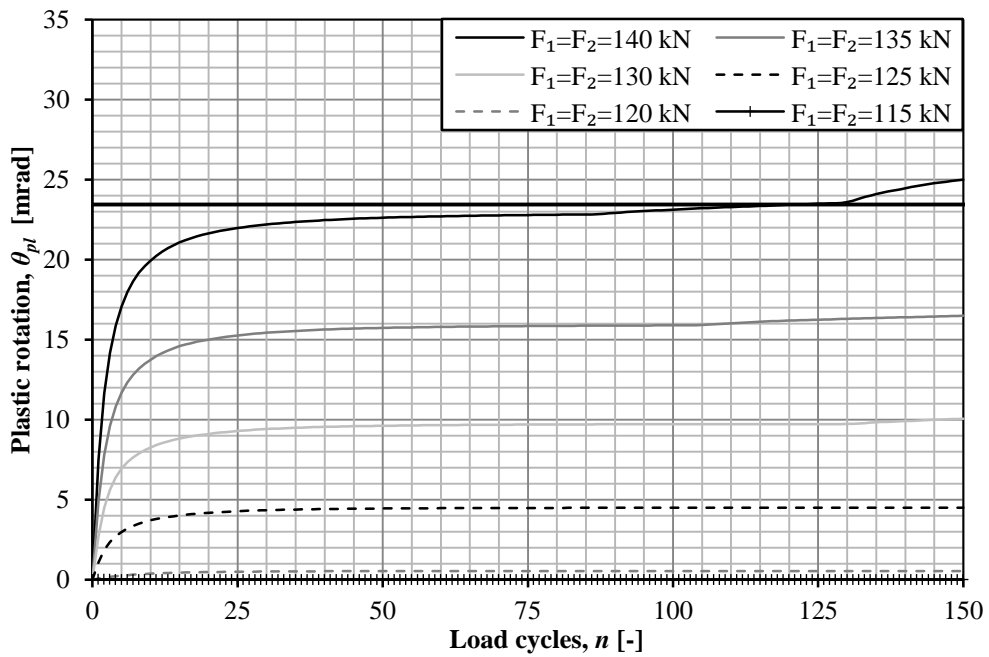
Figure F.15   Plastic rotation in the centre of the cantilever slab for d = 3.6 m.

CHALMERS, *Civil and Environmental Engineering*, Master's Thesis 2014:73
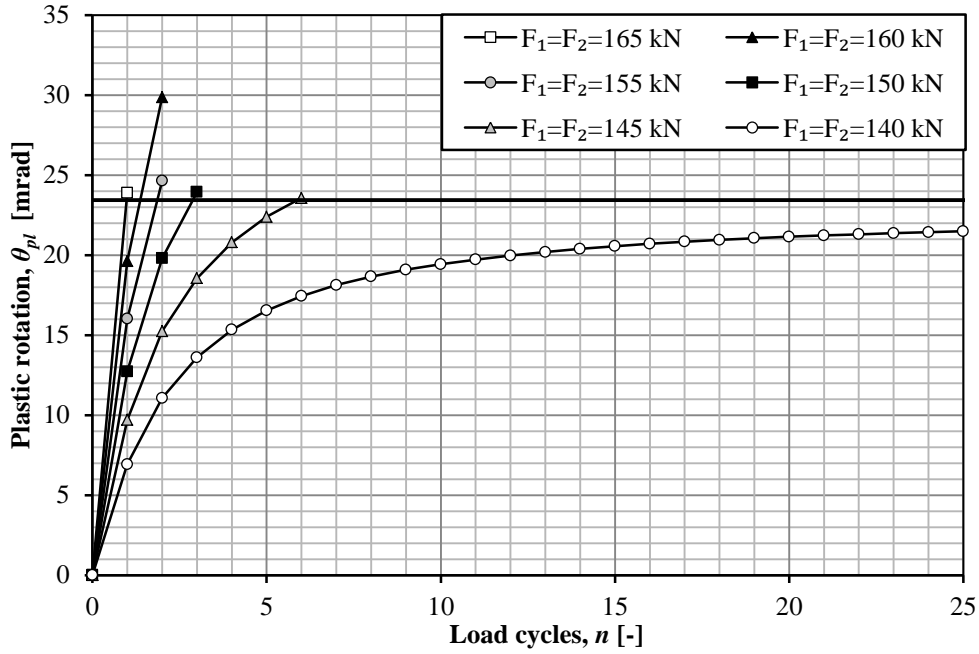
Figure F.16 Plastic rotation in the centre of the cantilever slab for d = 4.0 m.
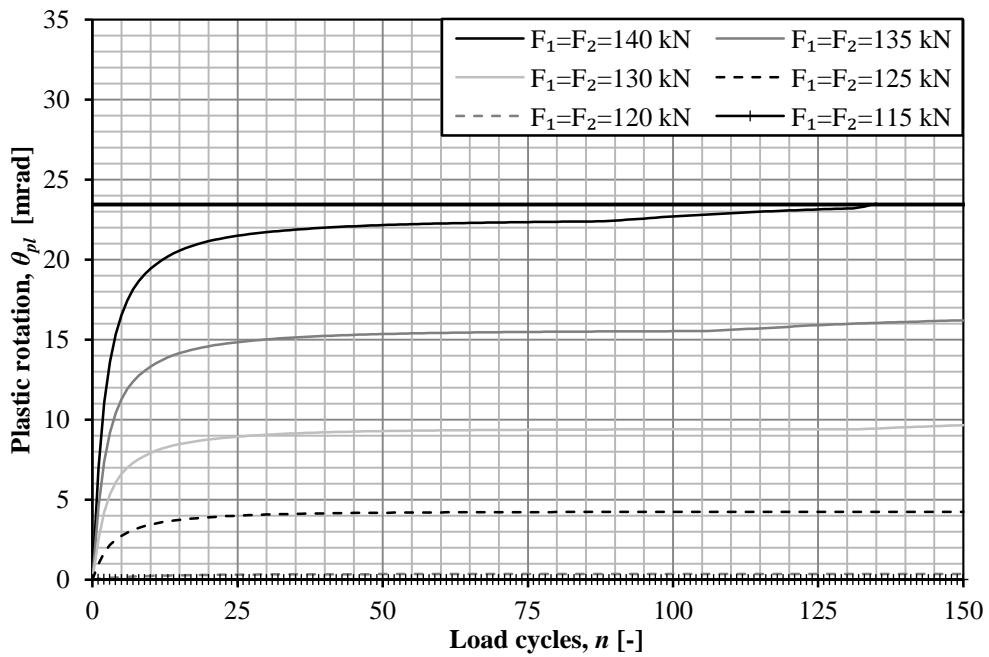
Figure F.17 Plastic rotation in the centre of the cantilever slab for d = 4.0 m.
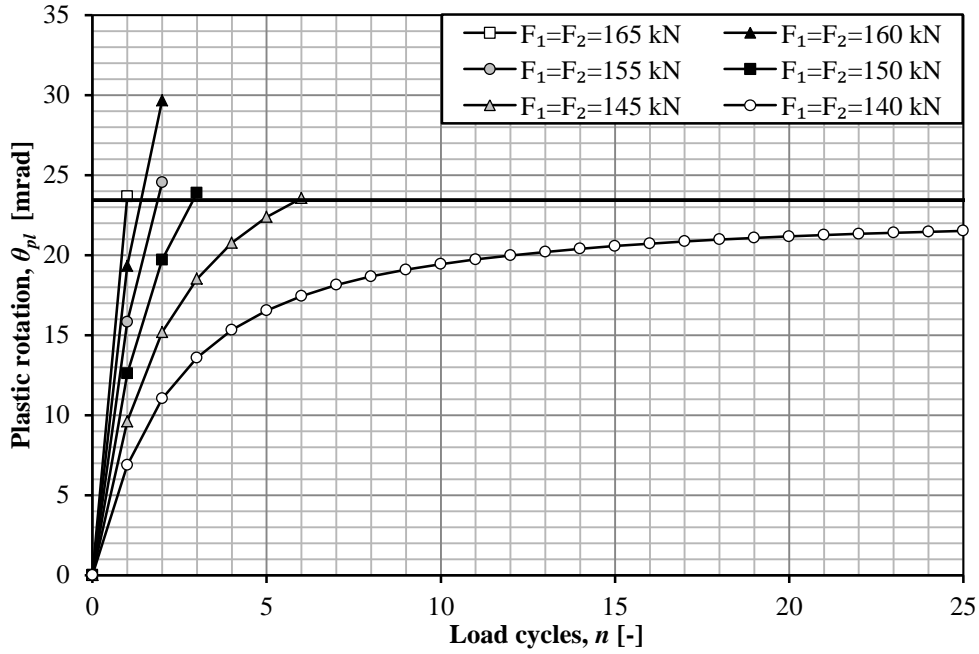
Figure F.18   Plastic rotation in the centre of the cantilever slab for d = 4.4 m.
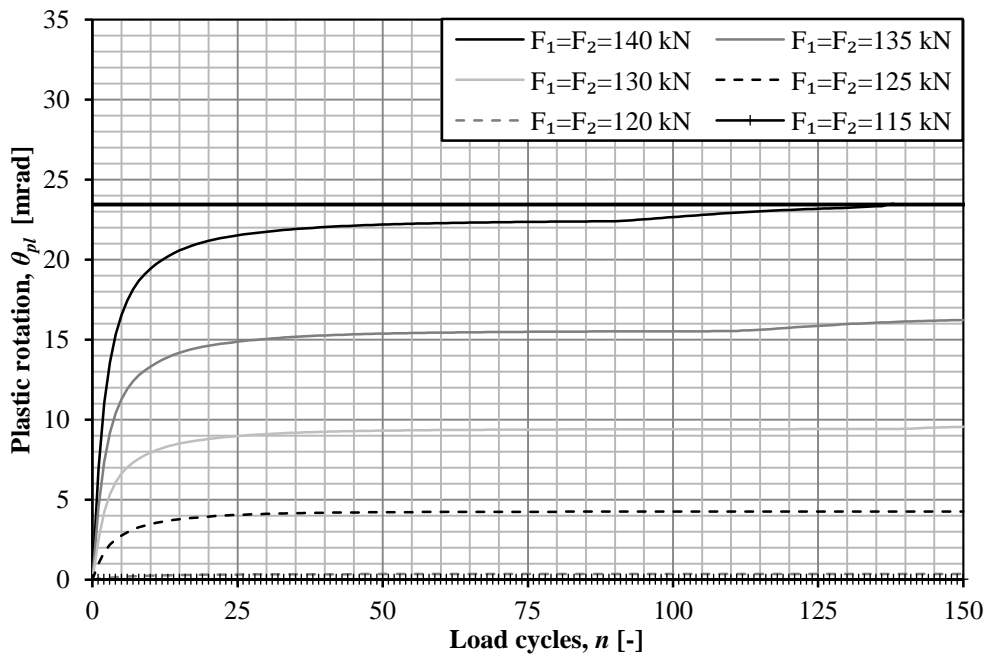
Figure F.19   Plastic rotation in the centre of the cantilever slab for d = 4.4 m.

CHALMERS, *Civil and Environmental Engineering*, Master's Thesis 2014:73
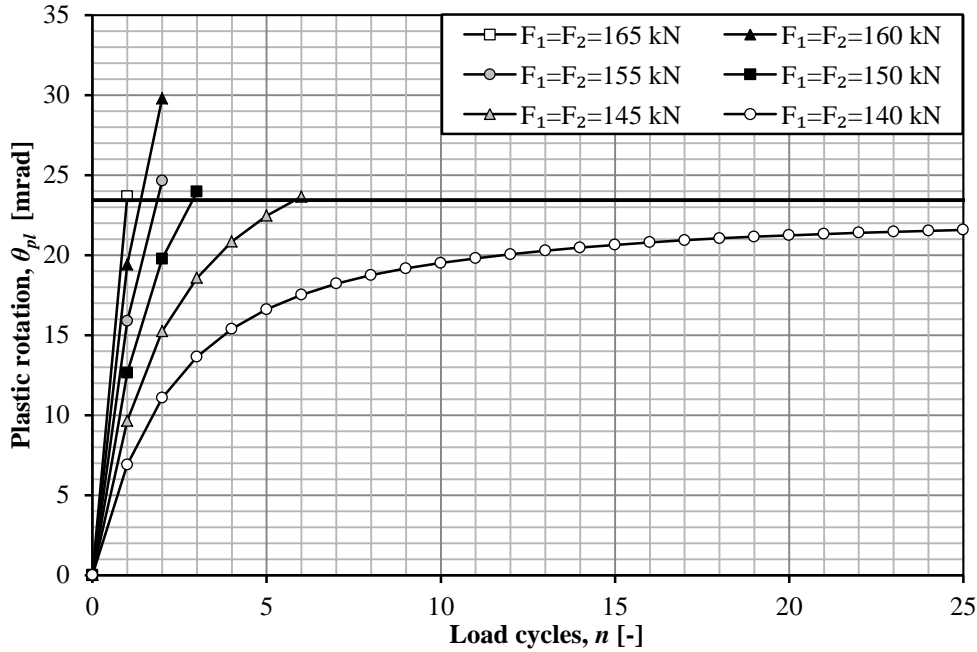
Figure F.20 Plastic rotation in the centre of the cantilever slab for d = 4.8 m.
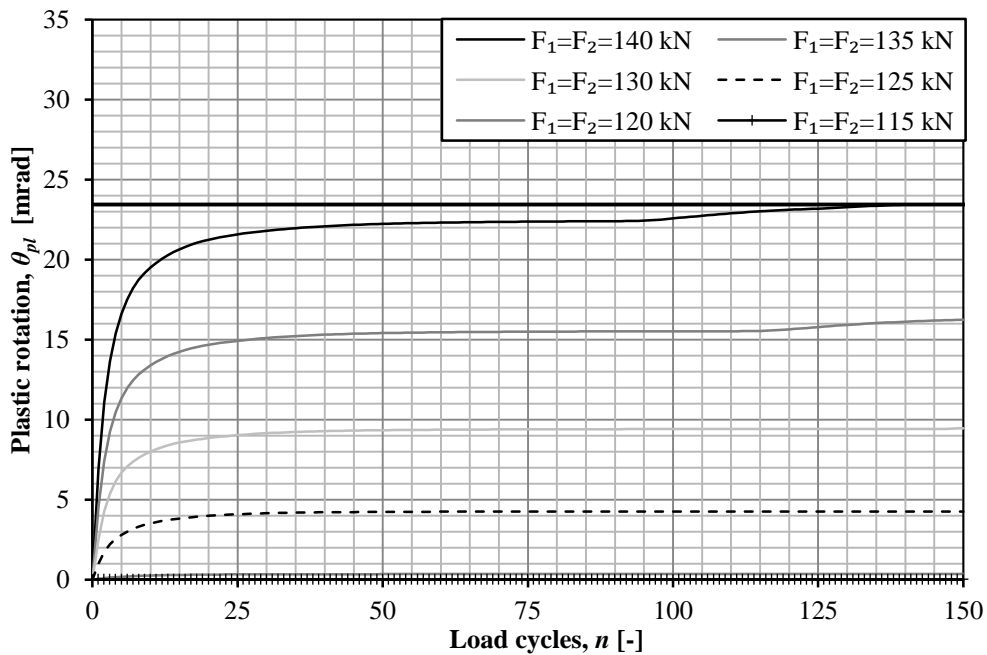
Figure F.21 Plastic rotation in the centre of the cantilever slab for d = 4.8 m.

As can be seen in Figure F.13, Figure F.15, Figure F.17, Figure F.19 and Figure F.21 there is an increase in plastic rotation after a certain load cycles. This phenomenon can be observed when the plastic rotation at the fixed support has developed to such an extent that the slab starts to behave differently. The forces are in this state carried in x-direction, perpendicular to the direction towards the support, since the majority of the centre part of the slab cannot carry any additional force. This would not be the case in a long slab which is of interest in this report and the results after this critical section is therefore omitted in this Thesis.

The number of load cycles to failure n_u for each distance d and total load magnitude F_{tot} is summarized in Table F.1. The largest applied total force for each distance, not

to cause any plastic rotation, is also summarized in this table. These extreme values are shown in Figure F.22.

Table F.1 *Number of load cycles to failure n_u for different values of the total applied force and distance.*

F_{tot} [kN]	Distance d									
	1.2	1.6	2.0	2.4	2.8	3.2	3.6	4.0	3.6	4.0
130	∞									
135	-									
140	-	∞								
145	-	-								
150	-	-								
155	-	-								
160	-	-	∞							
165	-	-	-							
170	15	-	-							
180	4	-	-	∞						
190	3	7	-	-						
200	2	3	-	-						
210	2	2	7	-	∞					
220	**1**	2	3	-	-					
230		**1**	2	-	-	∞	∞	∞	∞	∞
240			**1**	3	-	-	-	-	-	-
250				2	-	-	-	-	-	-
260				**1**	23	-	-	-	-	-
270					2	-	-	-	-	-
280					**1**	10	-	-	-	-
290						2	6	6	6	6
300						**1**	3	3	3	3
310							3	2	2	2
320							2	2	2	2
330							**1**	**1**	**1**	**1**
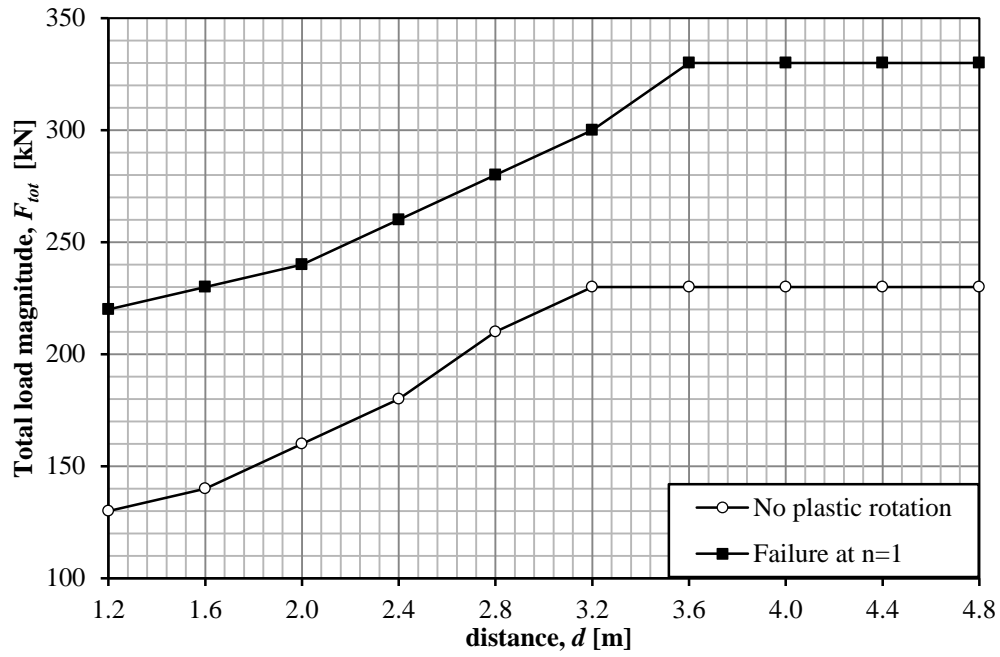
Figure F.22 Relation between total load magnitude F$_{tot}$ and distance d for forces not to cause any plastic rotation and failure after one load cycle.

Appendix G   Comparison – Static vs. moving forces

This chapter covers the cumulative factor $\gamma_{\theta pl.mov}$ for a single static and a pair of concentrated forces of different magnitudes. The results from these analyses are in this chapter presented for the cantilever and the simply supported one-way structure. The results are not discussed but are just presented for the interested reader.

As described in Section 6.6.2 in 7.6.2, the difference between static and moving concentrated forces was of interest. The distance d between the pair of moving concentrated forces varied according to Equation (G-1):

$$d = \begin{bmatrix} 1.2 & 1.6 & 2.0 \end{bmatrix} \, \text{m} \tag{G-1}$$

The cumulative factor was defined as the relation between the plastic rotation caused by a moving concentrated force and a static force of the same magnitude. This relation is stated in Equation (G-2):

$$\gamma_{\theta plmov} = \frac{\theta_{pl.mov.n}}{\theta_{pl.stat}} \tag{G-2}$$

G.1.1 Cantilever slab
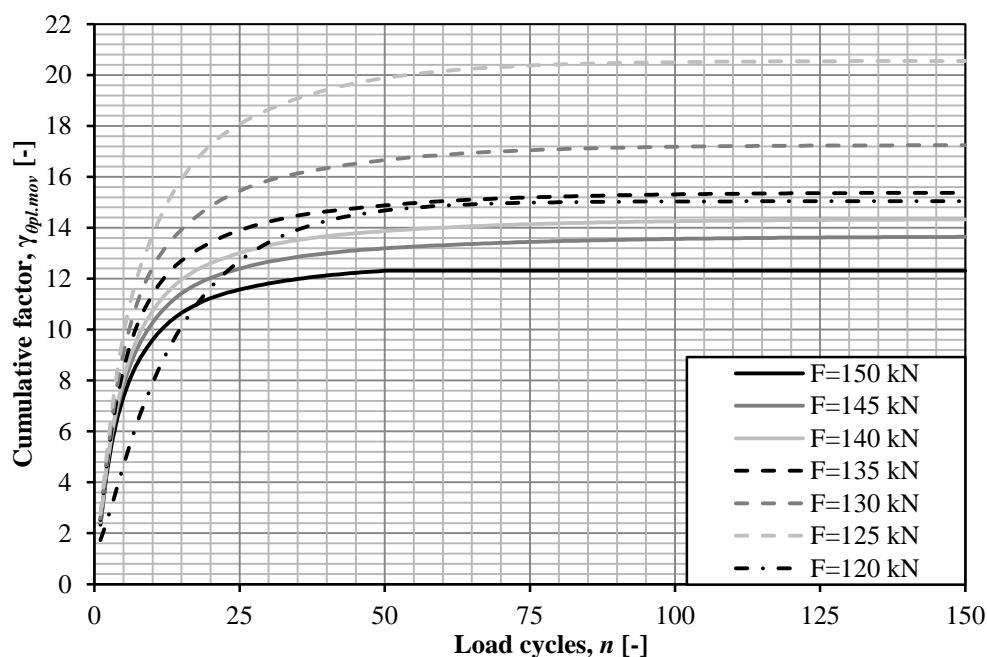
Figure G.1   Development of the cumulative factor $\gamma_{\theta pl.mov}$ for a single moving concentrated force.
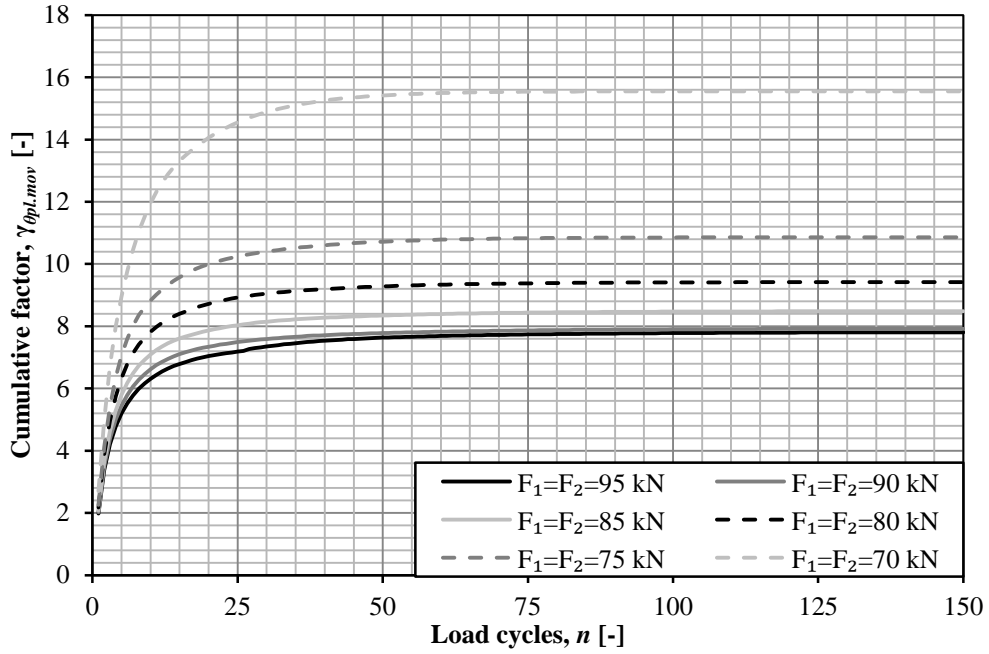
Figure G.2 Development of the cumulative factor $\gamma_{\theta pl.mov}$ for two moving concentrated forces with d = 1.2 m.
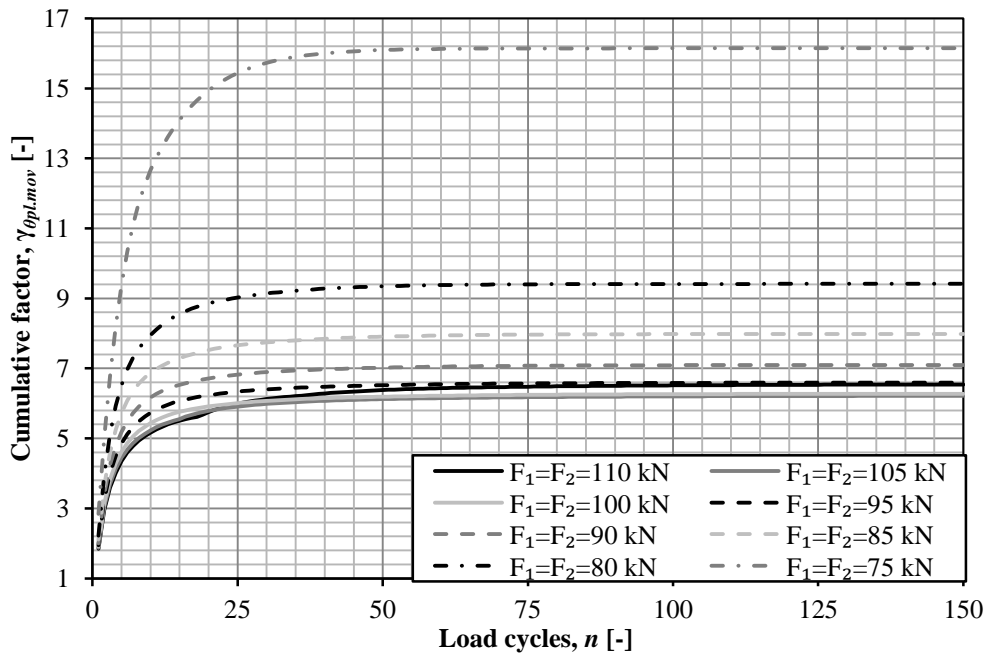
Figure G.3 Development of the cumulative factor $\gamma_{\theta pl.mov}$ for two moving concentrated forces with d = 1.6 m.

CHALMERS, *Civil and Environmental Engineering*, Master's Thesis 2014:73
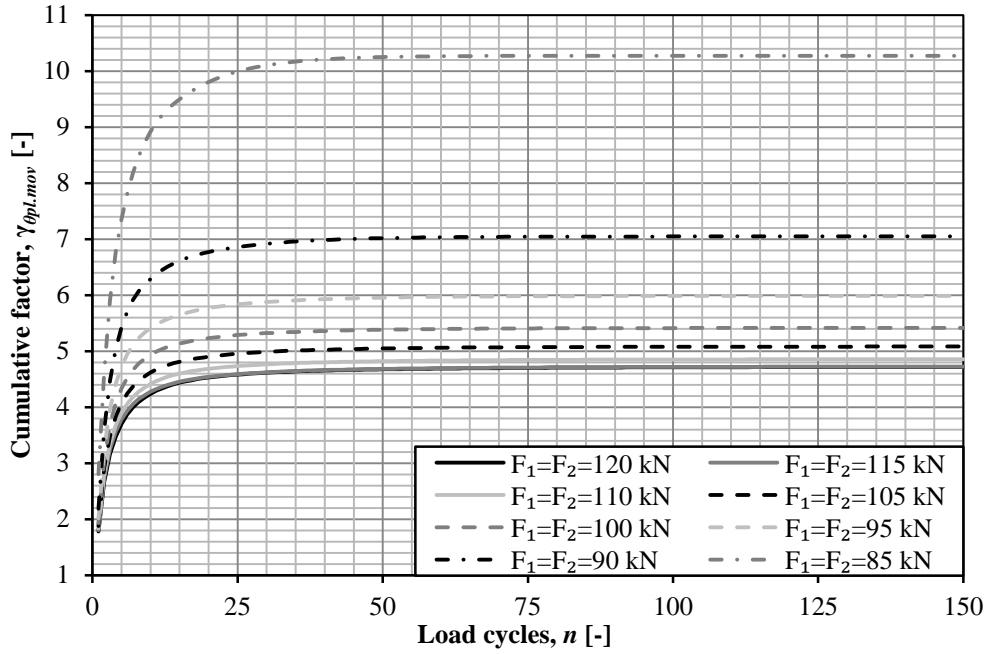
Figure G.4   *Development of the cumulative factor* $\gamma_{\theta pl.mov}$ *for two moving concentrated forces with d = 2.0 m.*

G.1.2 Simply supported slab
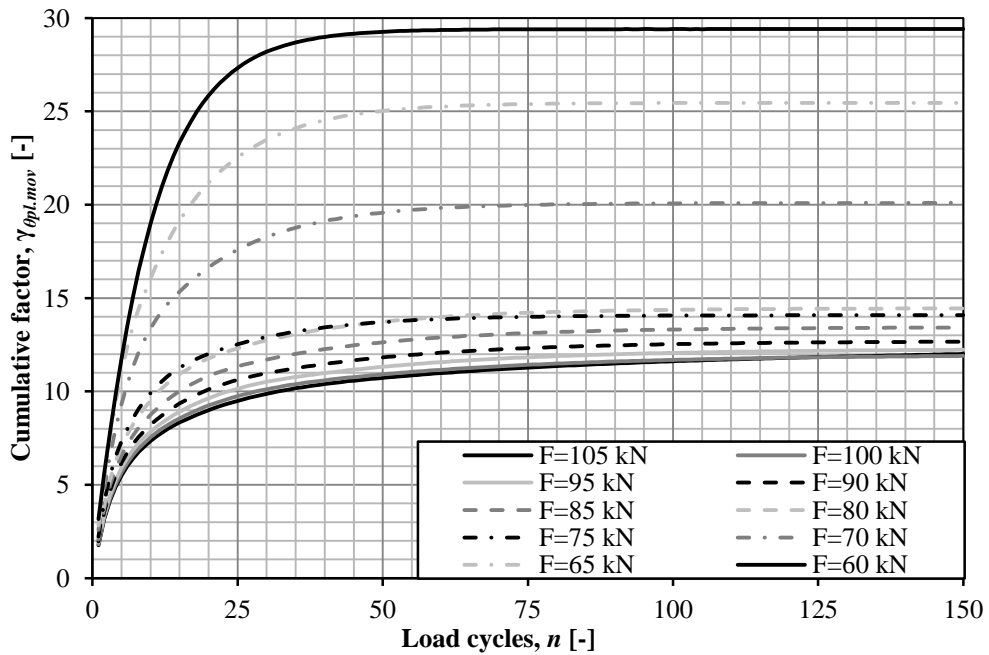
Figure G.5   *Development of the cumulative factor* $\gamma_{\theta pl.mov}$ *for a single moving concentrated force.*
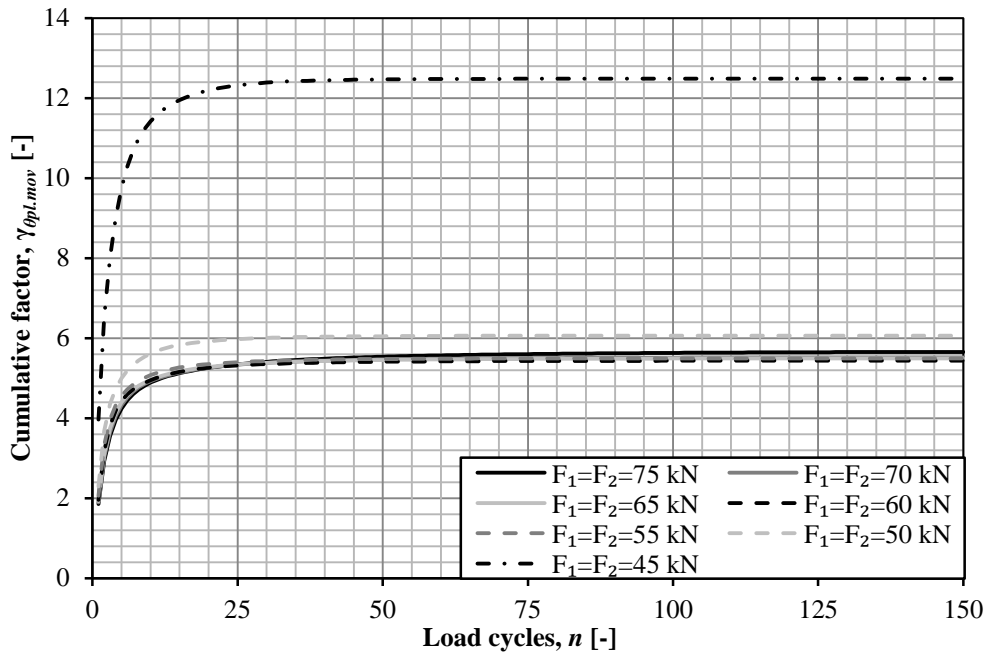
Figure G.6   Development   of   the   cumulative   factor $\gamma_{\theta pl.mov}$ for   two   moving concentrated forces with d = 1.2 m.
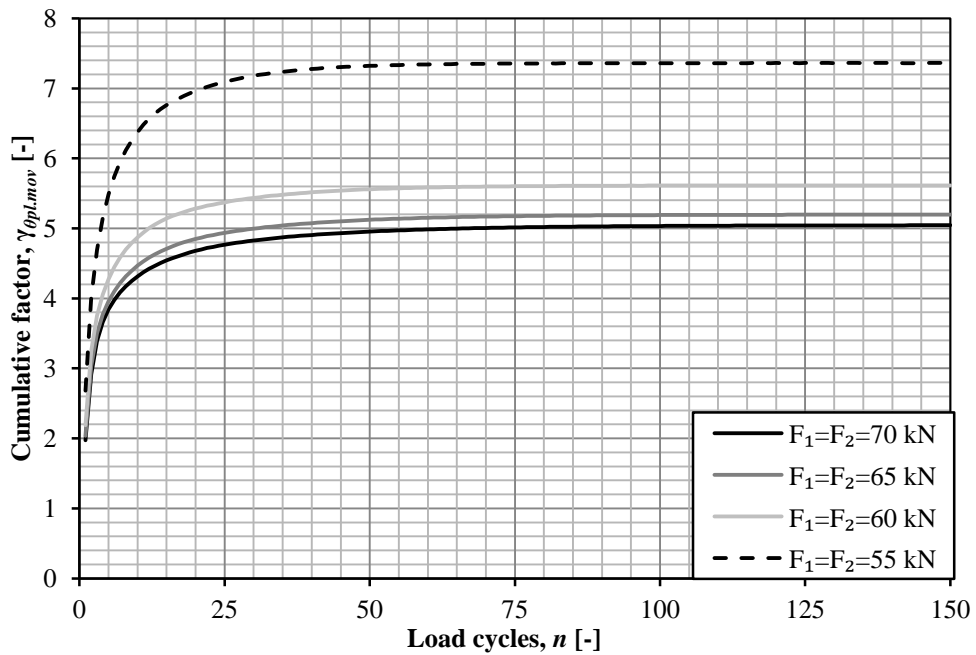
Figure G.7   Development   of   the   cumulative   factor $\gamma_{\theta pl.mov}$ for   two   moving concentrated forces with d = 1.6 m.
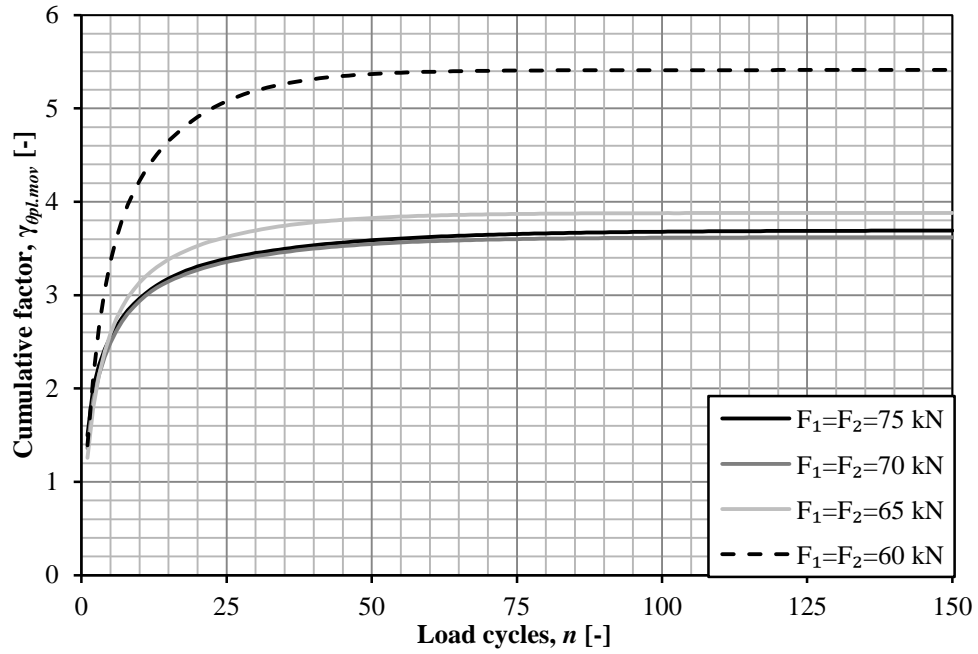
Figure G.8   Development of the cumulative factor $\gamma_{\theta pl.mov}$ for two moving concentrated forces with $d = 2.0$ m.

Appendix H   Tabulated values

This Chapter covers tabulated values to the comparison studies conducted in Chapter 6 and 7. The values presented in the tables in Section H.1 and H.2 was used to construct the figures in Chapter 6 and 7. The values should here be seen as additional information for the interested reader and is not commented and discussed to a great extent. The figures and equations in Section H.1 and H.2 are the same as illustrated and defined in Chapter 6 and 7 and are here presented as a help and for orientation purposes for the reader.

H.1 Cantilever slab

This section covers the tabulated values to the comparison studies conducted in Chapter 6.

H.1.1 Load magnitudes – Varying

Figure H.1 consists of Figure 6.25 and Figure 6.26.
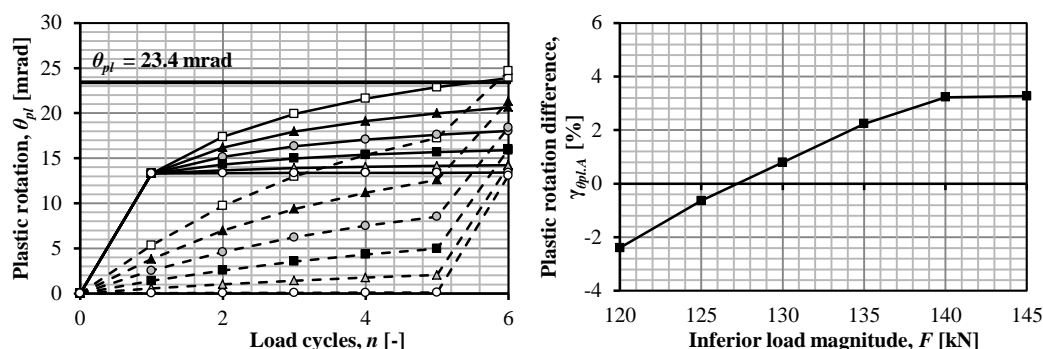
Figure H.1   Plastic rotation development and difference in plastic rotation $\gamma_{\theta pl.A}$ between load combination A_1 and A_2.

$$\gamma_{\theta pl.A} = \frac{\theta_{pl.A2} - \theta_{pl.A1}}{\theta_{pl.A1}} \tag{H-1}$$

Table H.1   Plastic rotation $\theta_{pl,A}$ and difference in plastic rotation $\gamma_{\theta pl.A}$ after six load cycles for a single moving concentrated force of varying magnitudes.

F_2 [kN]	$\theta_{pl.A1}$ [mrad]	$\theta_{pl.A2}$ [mrad]	$\gamma_{\theta pl.A}$ [%]
120	13.40	13.07	-2.5
125	14.24	14.15	-0.7
130	15.89	16.01	0.8
135	18.01	18.41	2.2
140	20.66	21.33	3.1
145	23.89	24.69	3.2

H.1.2 Comparison of single forces – Varying

Figure H.2 consists of Figure 6.29 and Figure 6.30.
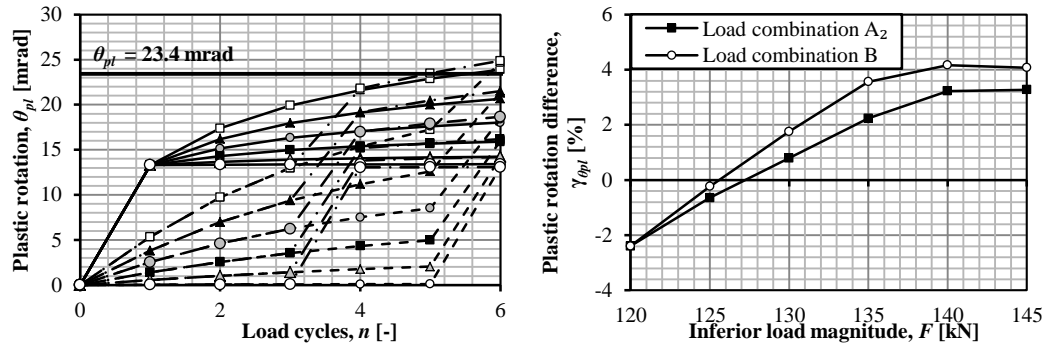
Figure H.2   Plastic rotation development and difference in plastic rotation $\gamma_{\theta pl.A}$ between load combination A_1 and load combination A_2 and B.

$$\gamma_{\theta pl.A} = \frac{\theta_{pl.A2} - \theta_{pl.A1}}{\theta_{pl.A1}} \tag{H-2}$$

$$\gamma_{\theta pl.B} = \frac{\theta_{pl.B} - \theta_{pl.A1}}{\theta_{pl.A1}} \tag{H-3}$$

Table H.2   Plastic rotation θ_{pl} and difference in plastic rotation $\gamma_{\theta pl}$ after six load cycles for a single moving concentrated force of varying magnitudes.

F [kN]	$\theta_{pl.A1}$ [mrad]	$\theta_{pl.A2}$ [mrad]	$\theta_{pl.B}$ [mrad]	$\gamma_{\theta pl.A}$ [%]	$\gamma_{\theta pl.B}$ [%]
120	13.40	13.07	13.08	-2.5	-2.5
125	14.24	14.15	14.20	-0.7	-0.2
130	15.89	16.01	16.17	0.8	1.7
135	18.01	18.41	18.65	2.2	3.4
140	20.66	21.33	21.52	3.1	4.0
145	23.89	24.67	24.86	3.2	3.9

H.1.3 Traditional superposition approach

Figure H.3 consists of Figure 6.33 and Figure 6.34.
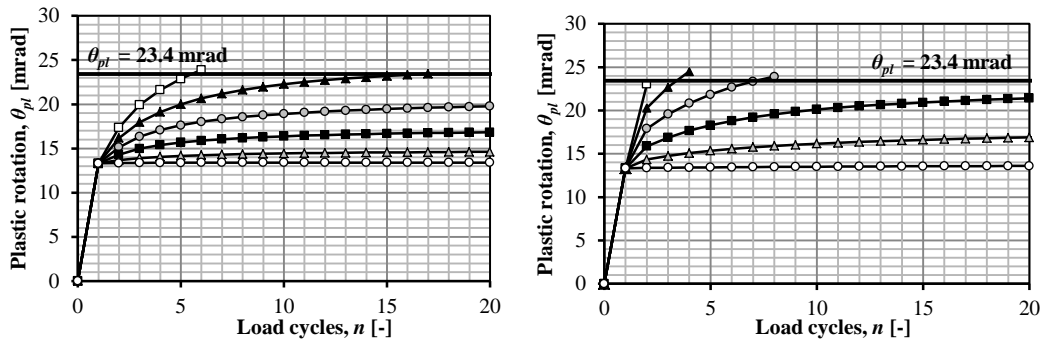
Figure H.3   Plastic rotation development from analyses and a traditional superposition approach. Load combination A₁.

$$\gamma_{\theta pl.A1.\text{sup}} = \frac{\theta_{pl.A1.\text{sup}} - \theta_{pl.A1.ana}}{\theta_{pl.A1.ana}} \tag{H-4}$$

Table H.3   Plastic rotation and difference in plastic rotation γ_{θpl.A1.sup} after six load cycles for a single moving concentrated force of varying magnitudes

F [kN]	$\theta_{pl.A1.ana}$ [mrad]	$\theta_{pl.A1.\text{sup}}$ [mrad]	$\gamma_{\theta pl.A.\text{sup}}$ [%]
120	13.39	13.45	0.4
125	14.24	15.57	9.4
130	15.89	18.78	18.3
135	18.01	22.68	25.9
140	20.66	27.08	31.1
145	23.89	32.06	34.2

Figure H.4 is a miniature of Figure 6.35.
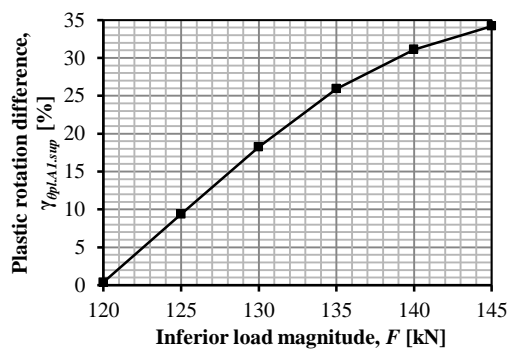
Figure H.4   Difference in plastic rotation γ_{θpl.A1.sup} for load combination A₁ between the results from an analysis and a traditional superposition approach.

Figure H.5 consists of Figure 6.36 and Figure 6.37.
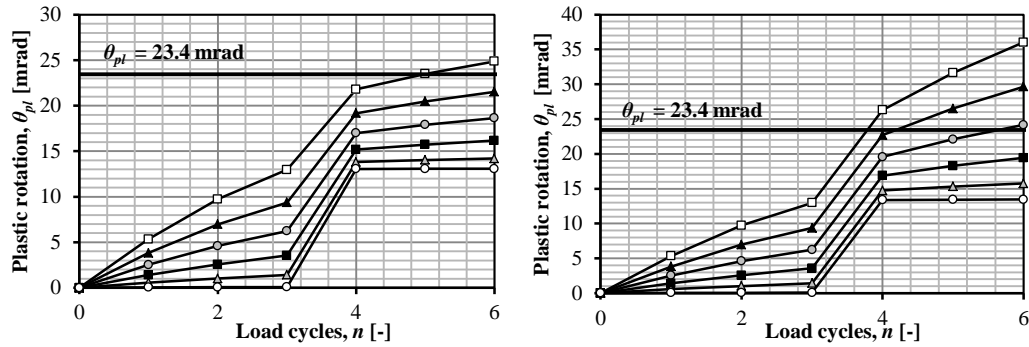
Figure H.5   *Plastic rotation development from analyses and a traditional superposition approach. Load combination B.*

$$\gamma_{\theta pl.B.\text{sup}} = \frac{\theta_{pl.B.\text{sup}} - \theta_{pl.B.ana}}{\theta_{pl.B.ana}} \tag{H-5}$$

Table H.4   *Plastic rotation and difference in plastic rotation $\gamma_{\theta pl.B.sup}$ after six load cycles for a single moving concentrated force on a cantilever slab.*

F [kN]	$\theta_{pl.B.ana}$ [mrad]	$\theta_{pl.B.\text{sup}}$ [mrad]	$\gamma_{\theta pl.B.\text{sup}}$ [%]
120	13.08	13.45	2.8
125	14.20	15.75	10.9
130	16.17	19.43	20.2
135	18.65	24.15	29.5
140	21.52	29.65	37.8
145	24.86	39.91	44.9

Figure H.6 consists of Figure 6.38 and Figure 6.39.
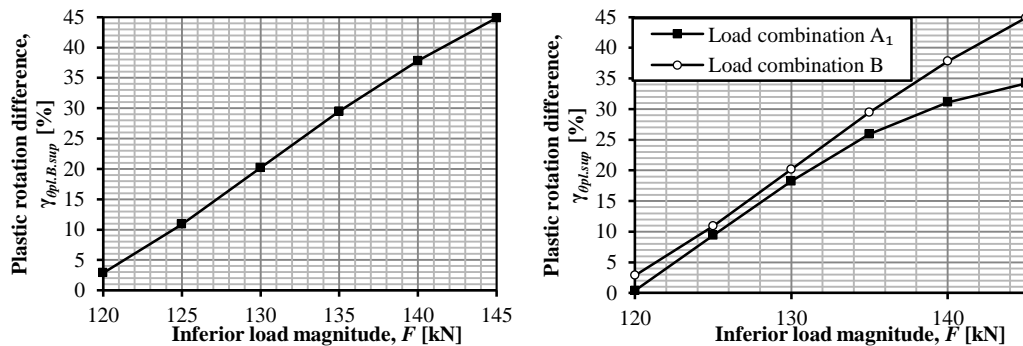
Figure H.6   *Difference in plastic rotation $\gamma_{\theta pl.B1.sup}$ for load combination B between the results from an analysis and a traditional superposition approach. The right figure is a combination of load combination A_1 and B.*

H.1.4 Comparison of two forces – Varying

$$\gamma_{\theta pl.1.6m} = \frac{\theta_{pl.1.6m} - \theta_{pl.1.2m}}{\theta_{pl.1.2m}} \tag{H-6}$$

$$\gamma_{\theta pl.2.0m} = \frac{\theta_{pl.2.0m} - \theta_{pl.1.2m}}{\theta_{pl.1.2m}} \tag{H-7}$$

Figure H.7 consists of Figure 6.60 and Figure 6.61.
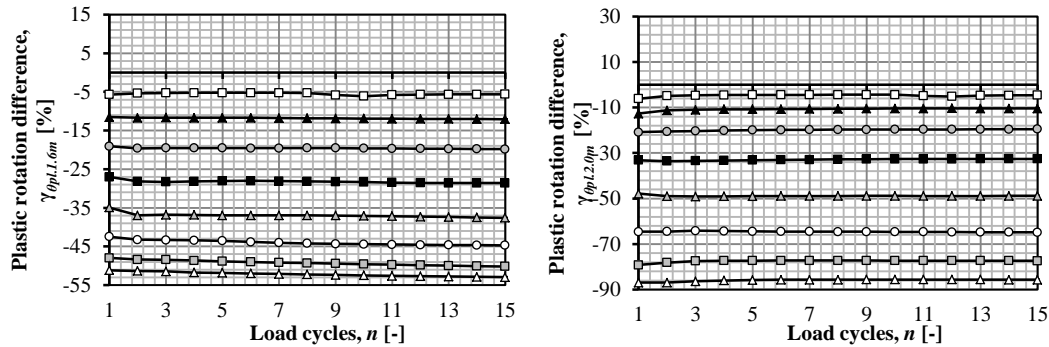
Figure H.7 *Difference in plastic rotation $\gamma_{\theta pl.1.6m}$ and $\gamma_{\theta pl.2.0m}$ for a pair of moving forces of different magnitudes.*

$$\bar{\gamma}_{\theta pl.1.6m} = \frac{\bar{\theta}_{pl.1.6m} - \bar{\theta}_{pl.1.2m}}{\bar{\theta}_{pl.1.2m}} \tag{H-8}$$

$$\bar{\gamma}_{\theta pl.2.0m} = \frac{\bar{\theta}_{pl.2.0m} - \bar{\theta}_{pl.1.2m}}{\bar{\theta}_{pl.1.2m}} \tag{H-9}$$

Where:

$$\bar{\theta}_{pl.1.6m} = \frac{\sum_{0}^{n} \theta_{pl.1.6m}}{n} \tag{H-10}$$

$$\bar{\theta}_{pl.2.0m} = \frac{\sum_{0}^{n} \theta_{pl.2.0m}}{n} \tag{H-11}$$

Table H.5 *Mean plastic rotation difference for all load combinations and load cycles for a pair of moving concentrated forces of varying magnitudes.*

F_1 [kN]	$\bar{\gamma}_{\theta pl.1.6m}$ [%]	$\bar{\gamma}_{\theta pl.2.0m}$ [%]
10	-5.5	-4.7
20	-11.8	-10.8
30	-19.6	-19.9

40	-28.2	-32.9
50	-36.9	-48.8
60	-44.0	-64.5
70	-49.2	-77.5
80	-52.1	-85.9

Figure H.8 is a miniature of Figure 6.62.
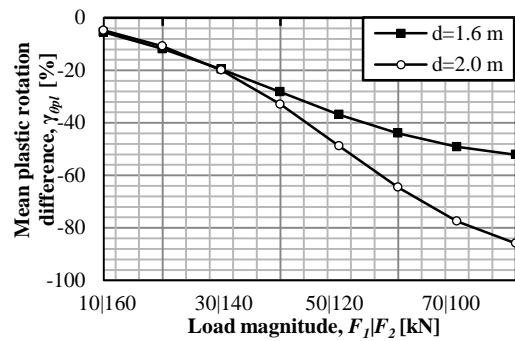
Figure H.8   Mean difference in plastic rotation between a distance of 1.2 m and, 1.6 m and 2.0 m.

H.2 Simply supported slab

This section covers the tabulated values to the comparison studies conducted in Chapter 7

H.2.1 Load magnitudes – Varying

Figure H.9 consists of Figure 7.19 and Figure 7.20.
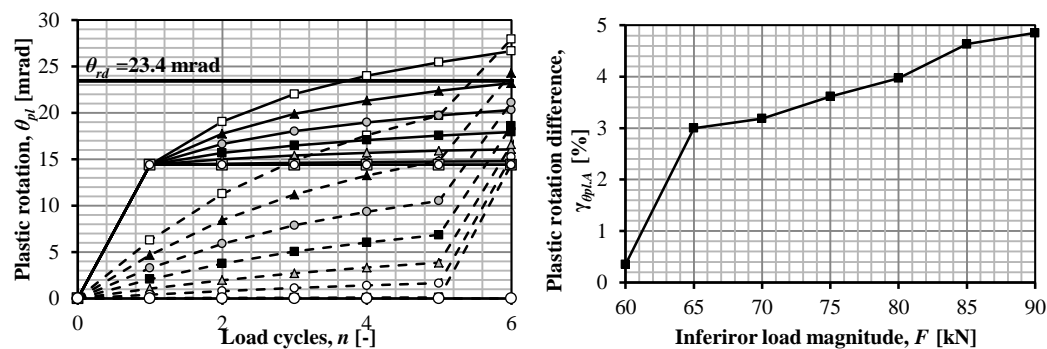
Figure H.9   Plastic rotation development and difference in plastic rotation $\gamma_{\theta pl.A}$ between load combination A_1 and A_2.

$$\gamma_{\theta pl.A} = \frac{\theta_{pl.A2} - \theta_{pl.A1}}{\theta_{pl.A1}} \tag{H-12}$$

Table H.6   Plastic rotation $\theta_{pl.A}$ and difference in plastic rotation $\gamma_{\theta pl.A}$ after six load cycles for a single moving concentrated force of varying magnitudes.

F_2 [kN]	$\theta_{pl.A1}$ [mrad]	$\theta_{pl.A2}$ [mrad]	$\gamma_{\theta pl.A}$ [%]
60	14.40	14.45	0.4
65	14.80	15.24	3.0
70	16.08	16.59	3.2
75	17.93	18.58	3.6
80	20.31	21.12	4.0
85	23.20	24.27	4.6
90	26.65	27.94	4.9

H.2.2 Comparison of single forces – Varying

Figure H.10 consists of Figure 7.23 and Figure 7.24.
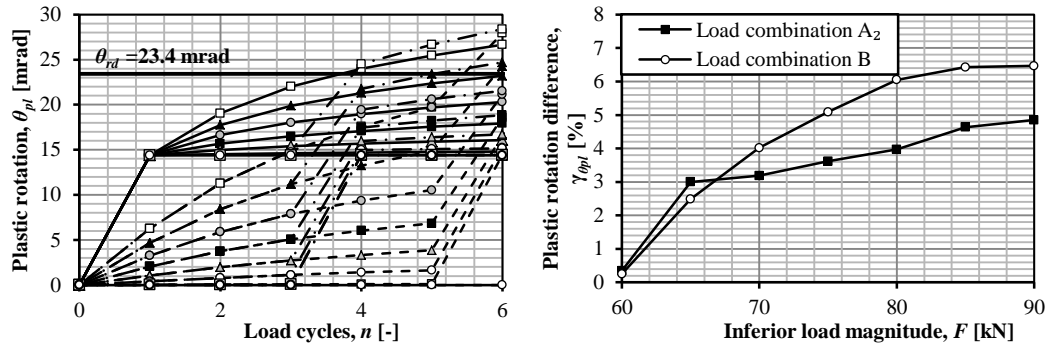
Figure H.10 Plastic rotation development and difference in plastic rotation $\gamma_{\theta pl.A}$ between load combination A_1 and load combination A_2 and B.

$$\gamma_{\theta pl.A} = \frac{\theta_{pl.A2} - \theta_{pl.A1}}{\theta_{pl.A1}} \tag{H-13}$$

$$\gamma_{\theta pl.B} = \frac{\theta_{pl.B} - \theta_{pl.A1}}{\theta_{pl.A1}} \tag{H-14}$$

Table H.7   Plastic rotation and difference in plastic rotation $\gamma_{\theta pl}$ after six load cycles for a single moving concentrated force of varying magnitudes.

F [kN]	$\theta_{pl.A1}$ [mrad]	$\theta_{pl.A2}$ [mrad]	$\theta_{pl.B}$ [mrad]	$\gamma_{\theta pl.A}$ [%]	$\gamma_{\theta pl.B}$ [%]
60	14.40	14.45	14.43	0.3	0.3
65	14.80	15.24	15.17	3.0	2.5
70	16.08	16.59	16.72	3.2	4.0
75	17.93	18.58	18.84	3.6	5.1
80	20.31	21.12	21.54	4.0	6.1
85	23.20	24.27	24.69	4.6	6.4
90	26.65	27.95	28.38	4.9	6.5

H.2.3 Traditional superposition approach

Figure H.11 consists of Figure 7.25 and Figure 7.26.
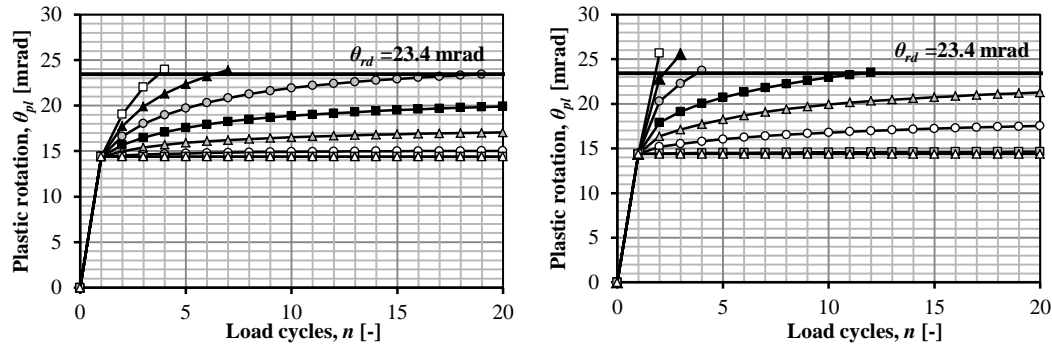
Figure H.11 Plastic rotation development from analyses and a traditional superposition approach. Load combination A_1.

$$\gamma_{\theta pl.A1.\text{sup}} = \frac{\theta_{pl.A1.\text{sup}} - \theta_{pl.A1.ana}}{\theta_{pl.A1.ana}} \tag{H-15}$$

Table H.8 Plastic rotation and difference in plastic rotation $\gamma_{\theta pl.A1.sup}$ after six load cycles for a single moving concentrated force of varying magnitudes

F [kN]	$\theta_{pl.A1.ana}$ [mrad]	$\theta_{pl.A1.\text{sup}}$ [mrad]	$\gamma_{\theta pl.A1.\text{sup}}$ [%]
60	14.39	14.52	0.9
65	14.80	16.23	9.6
70	16.08	18.69	16.3
75	17.93	21.28	18.7
80	20.31	25.87	27.4
85	23.20	30.55	31.7
90	26.65	35.83	34.4

Figure H.12 is a miniature of Figure 7.27
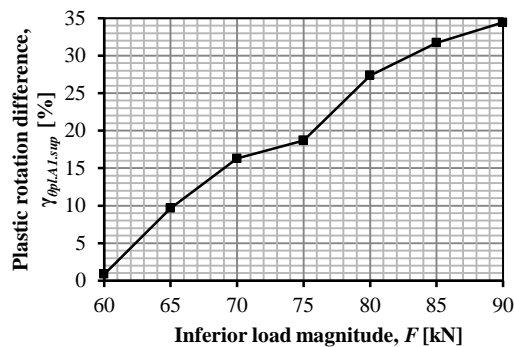
Figure H.12 Difference in plastic rotation $\gamma_{\theta pl.A1.sup}$ for load combination A_1 between the results from an analysis and a traditional superposition approach.

Figure H.13 consists of Figure 7.28 and Figure 7.29.
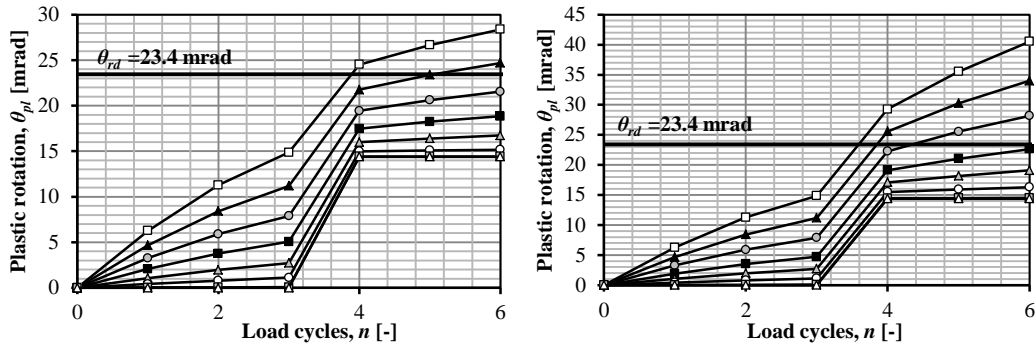
Figure H.13 Plastic rotation development from analyses and a traditional superposition approach. Load combination B.

$$\gamma_{\theta pl.B.\text{sup}} = \frac{\theta_{pl.B.\text{sup}} - \theta_{pl.B.ana}}{\theta_{pl.B.ana}} \tag{H-16}$$

Table H.9   Plastic rotation and difference in plastic rotation $\gamma_{\theta pl.B.sup}$ after six load cycles for a single moving concentrated force of varying magnitudes.

$F\ [\mathrm{kN}]$	$\theta_{pl.B.ana}\ [\mathrm{mrad}]$	$\theta_{pl.B.\text{sup}}\ [\mathrm{mrad}]$	$\gamma_{\theta pl.B.\text{sup}}\ [\%]$
60	14.43	14.52	0.6
65	15.17	16.30	7.5
70	16.72	19.08	14.1
75	18.84	22.63	20.1
80	21.54	28.17	30.8
85	24.69	33.99	37.7
90	28.38	40.52	42.8

Figure H.14 consists of Figure 7.30 and Figure 7.31.
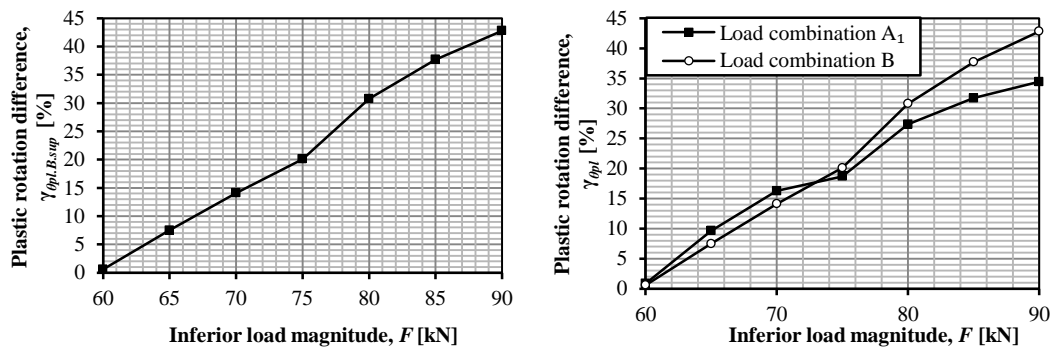
Figure H.14 Difference in plastic rotation $\gamma_{\theta pl.B1.sup}$ for load combination B between the results from an analysis and a traditional superposition approach. The right figure is a combination of load combination A_1 and B.

H.2.4 Comparison of two forces – Varying

$$\gamma_{\theta pl.1.6m} = \frac{\theta_{pl.1.6m} - \theta_{pl.1.2m}}{\theta_{pl.1.2m}} \tag{H-17}$$

$$\gamma_{\theta pl.2.0m} = \frac{\theta_{pl.2.0m} - \theta_{pl.1.2m}}{\theta_{pl.1.2m}} \tag{H-18}$$

Figure H.15 consists of Figure 7.49 and Figure 7.50.
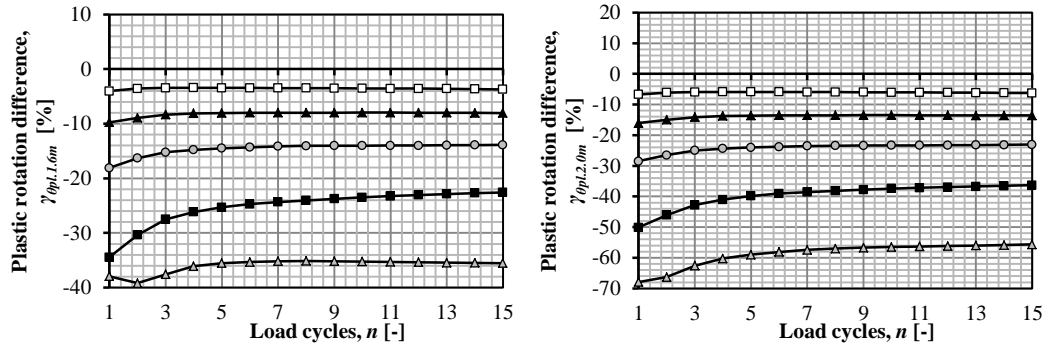
Figure H.15 Difference in plastic rotation $\gamma_{\theta pl.1.6m}$ and $\gamma_{\theta pl.2.0m}$ for a pair of moving forces of different magnitudes.

$$\bar{\gamma}_{\theta pl.1.6m} = \frac{\bar{\theta}_{pl.1.6m} - \bar{\theta}_{pl.1.2m}}{\bar{\theta}_{pl.1.2m}} \tag{H-19}$$

$$\bar{\gamma}_{\theta pl.2.0m} = \frac{\bar{\theta}_{pl.2.0m} - \bar{\theta}_{pl.1.2m}}{\bar{\theta}_{pl.1.2m}} \tag{H-20}$$

Where:

$$\bar{\theta}_{pl.1.6m} = \frac{\sum_{0}^{n} \theta_{pl.1.6m}}{n} \tag{H-21}$$

$$\bar{\theta}_{pl.2.0m} = \frac{\sum_{0}^{n} \theta_{pl.2.0m}}{n} \tag{H-22}$$

Table H.10 Mean plastic rotation difference for all load combinations and load cycles for a pair of moving concentrated forces of varying magnitudes.

F_1 [kN]	$\bar{\gamma}_{\theta pl.1.6m}$ [%]	$\bar{\gamma}_{\theta pl.2.0m}$ [%]
10	-3.55	-6.1
20	-8.22	-13.9
30	-14.67	-24.2

| 40 | -25.42 | -39.9 |
| 50 | -35.99 | -59.0 |

Figure H.16 is a miniature of Figure 7.51
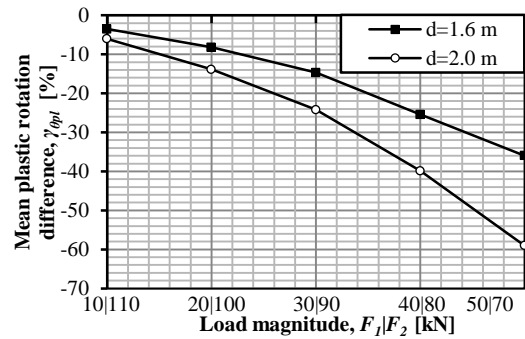
Figure H.16 Mean difference in plastic rotation between a distance of 1.2 m and, 1.6 m and 2.0 m.

Appendix I   Shear force distribution

The shear force distributions from the chapters concerning moment distribution in SLS are presented here; see Table I.1 to Table I.4. The results are not discussed but are shown for the interested reader. The results are presented in the same order as the moment distributions.

Table I.1   Cantilever slab, single concentrated force.

Neutral, $E_x = 2E_y$

Cracked, $E_x = 0.5E_y$

Cracked, $E_x = E_y$

Cracked, $E_x = 2E_y$
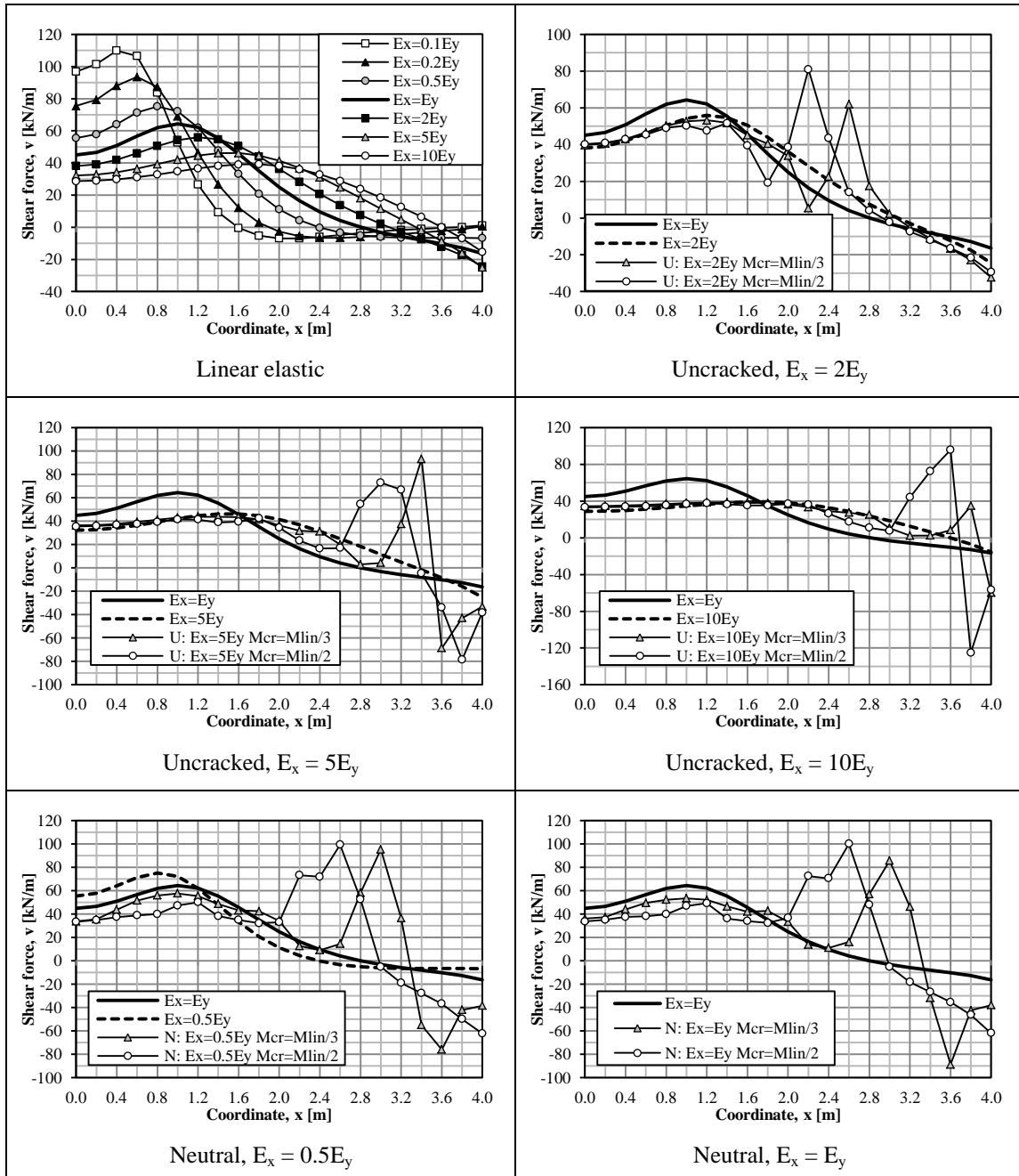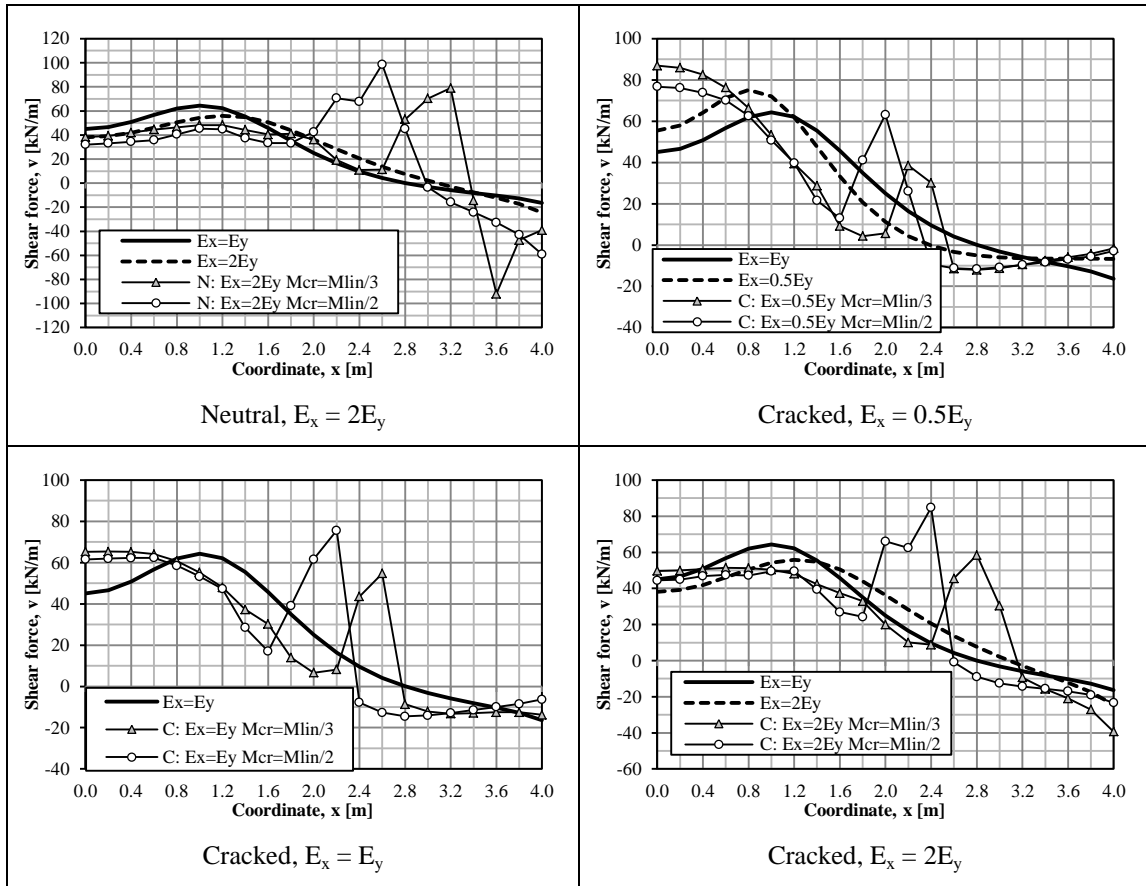
Table I.2   *Cantilever slab, two concentrated forces.*

Linear elastic

Uncracked, $E_x = 2E_y$

CHALMERS, *Civil and Environmental Engineering*, Master's Thesis 2014:73

Uncracked, $E_x = 5E_y$

Uncracked, $E_x = 10E_y$

Neutral, $E_x = 0.5E_y$

Neutral, $E_x = E_y$

Neutral, $E_x = 2E_y$

Cracked, $E_x = 0.5E_y$

Cracked, $E_x = E_y$

Cracked, $E_x = 2E_y$
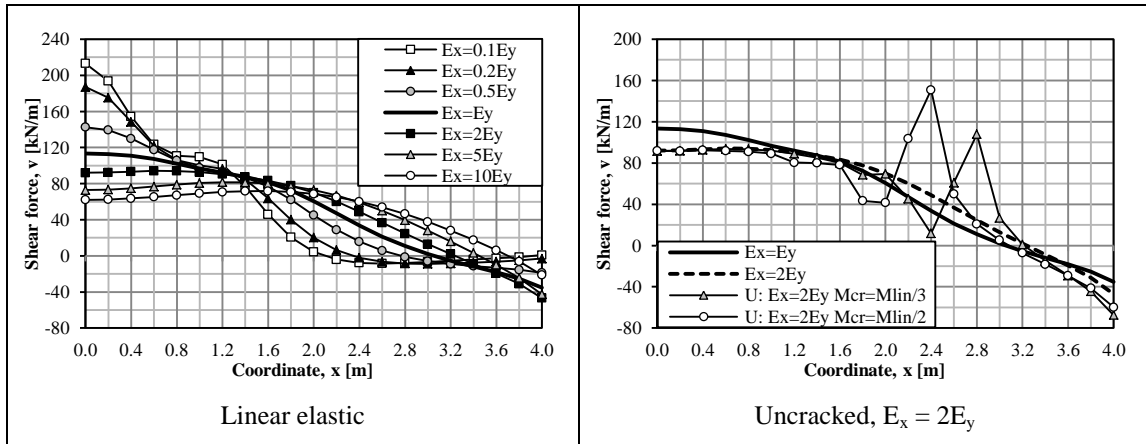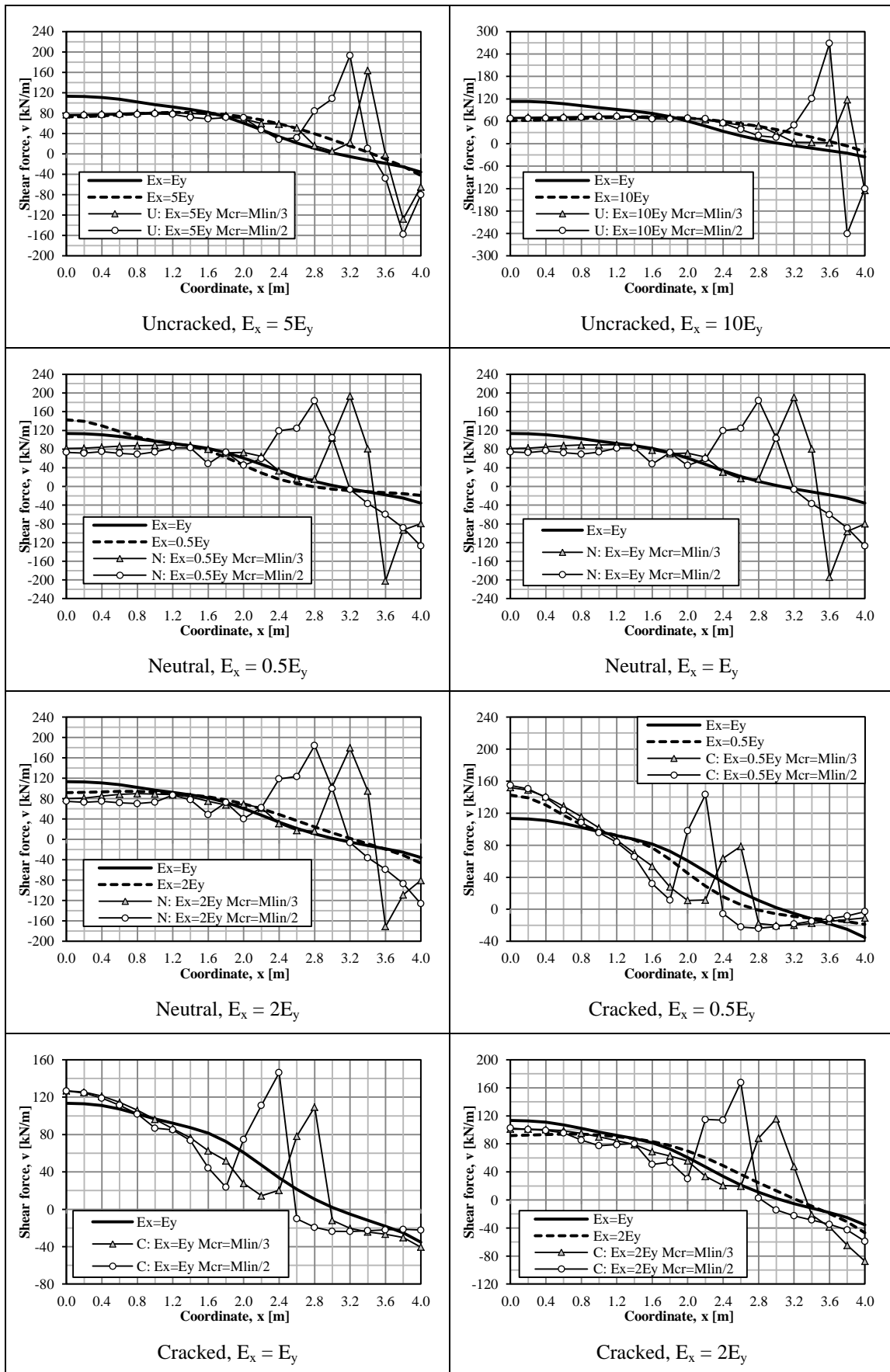
Table I.3   Simply supported slab, single concentrated force.

Linear elastic

Uncracked, $E_x = 2E_y$

Uncracked, $E_x = 5E_y$

Uncracked, $E_x = 10E_y$

Neutral, $E_x = 0.5E_y$

Neutral, $E_x = E_y$

Neutral, $E_x = 2E_y$

Cracked, $E_x = 0.5E_y$

Cracked, $E_x = E_y$ Cracked, $E_x = 2E_y$
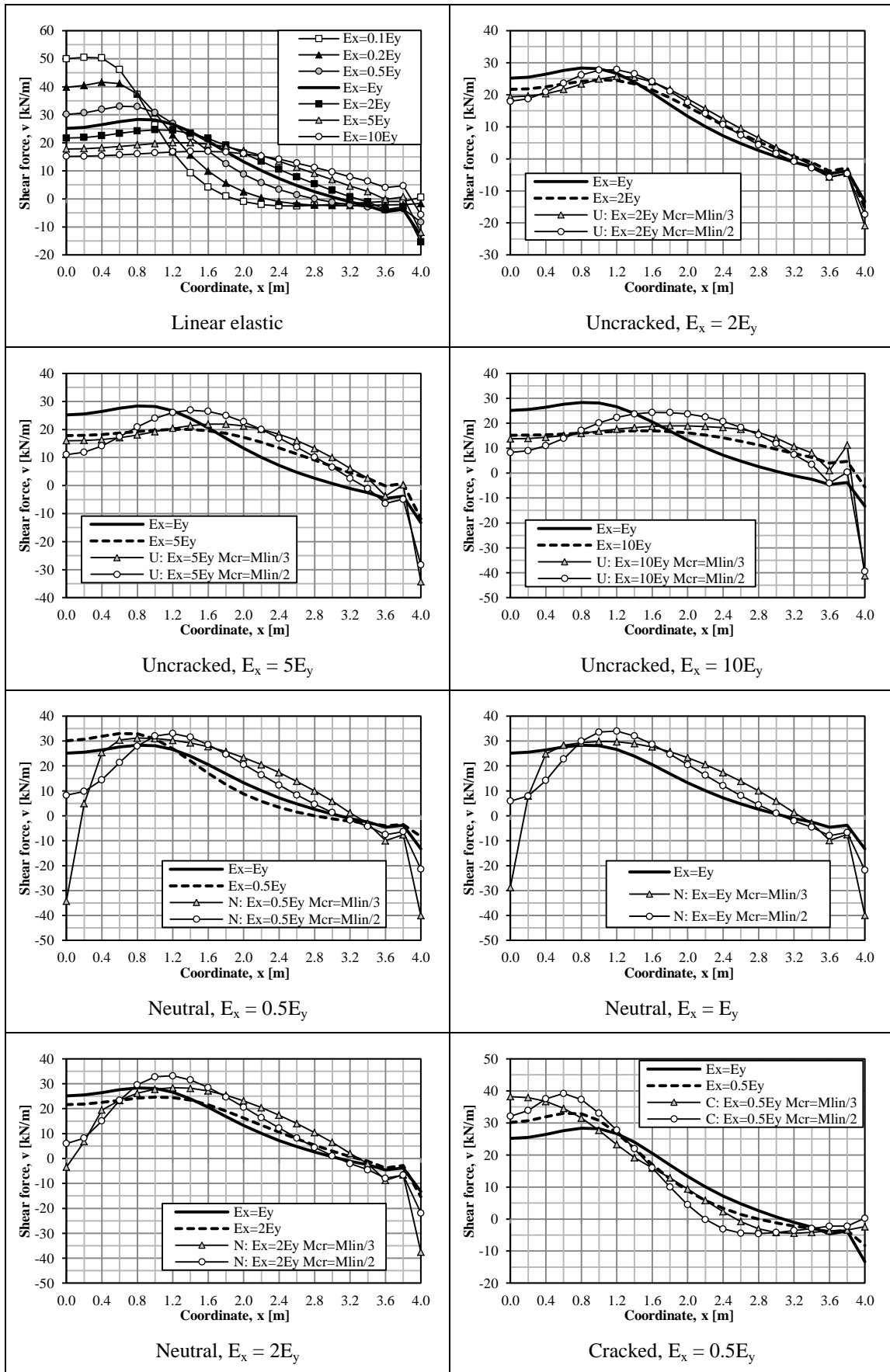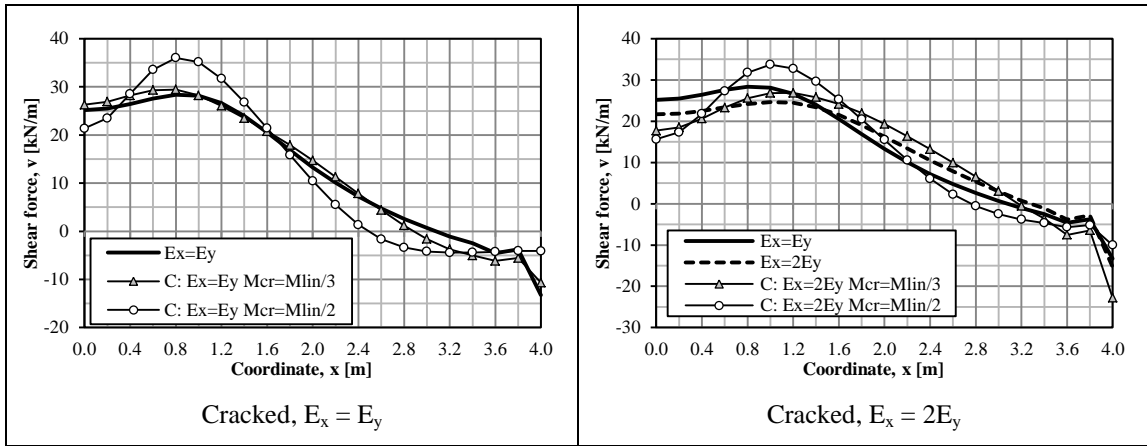
Table I.4   *Simply supported slab, two concentrated forces.*

Linear elastic   Uncracked, $E_x = 2E_y$

Uncracked, $E_x = 5E_y$ Uncracked, $E_x = 10E_y$

Neutral, $E_x = 0.5E_y$

Neutral, $E_x = E_y$

Neutral, $E_x = 2E_y$

Cracked, $E_x = 0.5E_y$

Cracked, $E_x = E_y$

Cracked, $E_x = 2E_y$
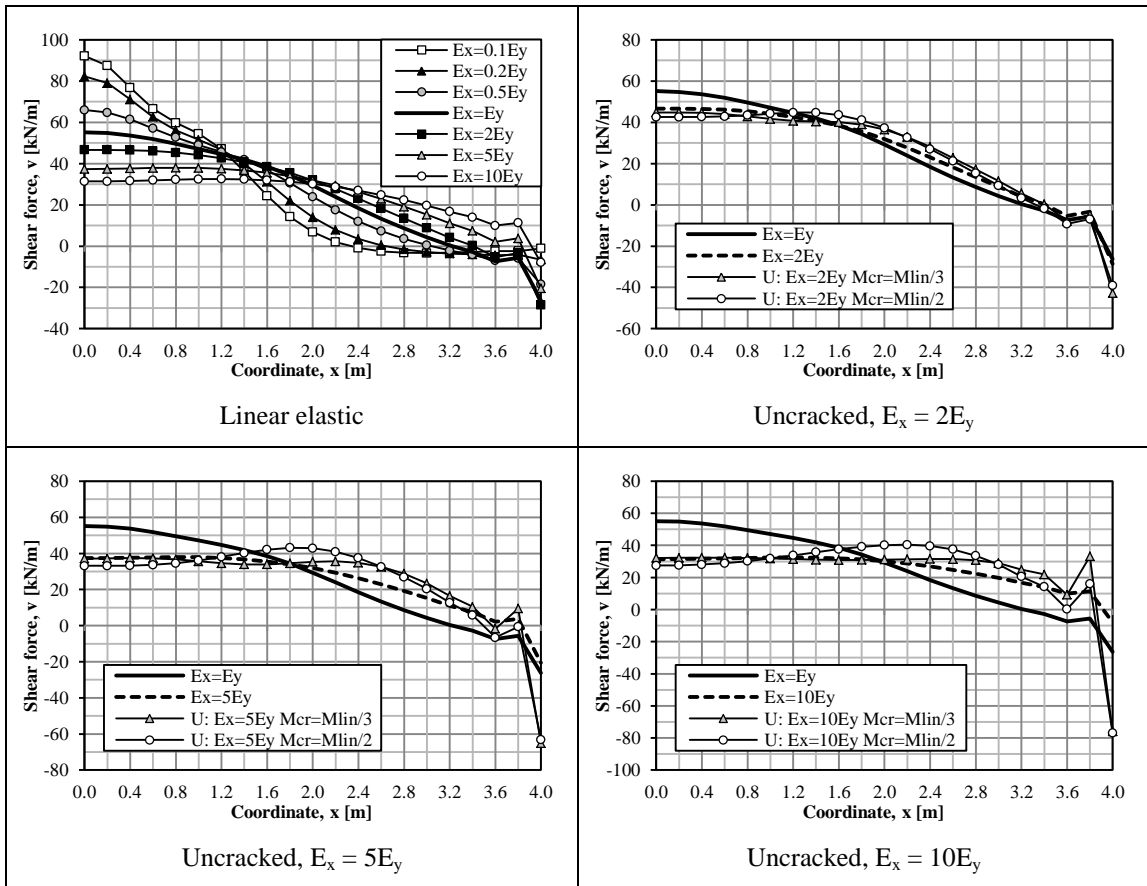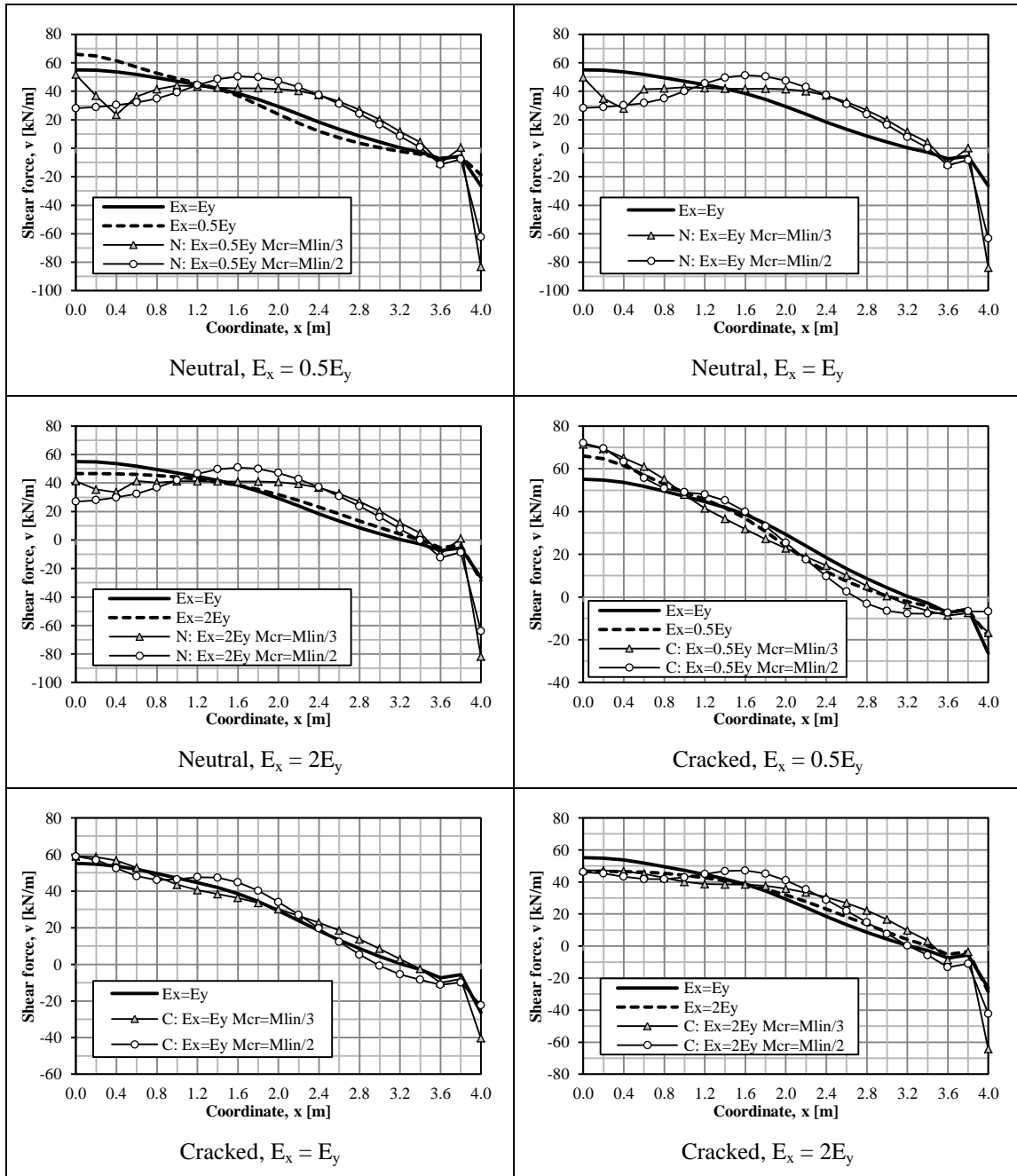
Appendix J   Input files for ADINA

The input files (.in-files) used for the ADINA software in this Thesis is presented in this chapter for the two following examples:

- Moment distribution in SLS - Simply supported slab
  - A single static force $F = 125$ kN
  - Case uncracked
  - $M_{cr} = M_{lin} / 3$
  - $E_x = 5E_y$
- Cumulative plastic rotation - Cantilever slab
  - A single moving concentrated force $F = 120$ kN
  - 150 load cycles n
  - Orthotropic mesh

For additional input data and the results obtained from the two analyses presented above, the reader is referred to Appendix C, and Chapter 5 and 6 respectively. Due to the great number of time functions and load applications used for the analysis of cumulative plastic rotation, these have been significantly shortened.

J.1 Moment distribution – Simply supported slab

```
*****************************************************
*****************************************************
********************* ANALYSIS ********************
*****************************************************
*****************************************************

*--- ADINA: AUI version 8.9.2 ---*
DATABASE NEW SAVE=NO PROMPT=NO
FEPROGRAM ADINA
CONTROL FILEVERSION=V89

AUTOMATIC TIME-STEPPING MAXSUBD=10
ACCURACY=NO,
   DISTOL=0.00100000000000000 DTMAX=3.00000000000000,
   RESTORE=AUTOMATIC RESPS=NO
RESFAC=0.000100000000000000,
   DIVFAC=2.00000000000000 LSMASSF=1.00000000000000

MASTER ANALYSIS=STATIC MODEX=EXECUTE
TSTART=0.00000000000000 IDOF=0,
   OVALIZAT=NONE FLUIDPOT=AUTOMATIC
CYCLICPA=1 IPOSIT=STOP,
   REACTION=YES INITIALS=NO FSINTERA=NO
IRINT=DEFAULT CMASS=NO,
   SHELLNDO=AUTOMATIC AUTOMATI=ATS
SOLVER=SPARSE,
   CONTACT-=CONSTRAINT-FUNCTION
TRELEASE=0.00000000000000,
   RESTART-=NO FRACTURE=NO LOAD-CAS=NO LOAD-
PEN=NO SINGULAR=YES,
   STIFFNES=0.000100000000000000 MAP-OUTP=NONE
MAP-FORM=NO,
   NODAL-DE=" POROUS-C=NO ADAPTIVE=0 ZOOM-
LAB=1 AXIS-CYC=0,
   PERIODIC=NO VECTOR-S=GEOMETRY EPSI-FIR=NO
STABILIZ=NO,
   STABFACT=1.00000000000000E-10 RESULTS=PORTHOLE
FEFCORR=NO,
   BOLTSTEP=1 EXTEND-S=YES CONVERT-=NO
DEGEN=YES TMC-MODE=NO,
   ENSIGHT-=NO IRSTEPS=1 INITIALT=NO TEMP-INT=NO
ESINTERA=NO,
   OP2GEOM=NO
```

```
*****************************************************
*****************************************************
**************** TIMEFUNCTIONS ******************
*****************************************************
*****************************************************

*** TIME STEP & FUNCTION ***
TIMESTEP NAME=DEFAULT
@CLEAR
500        1
@

TIMEFUNCTION NAME=1
@CLEAR
0     0
500    1
@

*****************************************************
*****************************************************
****************** GEOMETRY ******************
*****************************************************
*****************************************************

****************** NODES ******************

COORDINATES POINT SYSTEM=0
*** POINTS ON X AXIS ***
1 0.00 0.00 0.00 0
2 0.20 0.00 0.00 0
3 0.40 0.00 0.00 0
4 0.60 0.00 0.00 0
5 0.80 0.00 0.00 0
6 1.00 0.00 0.00 0
7 1.20 0.00 0.00 0
8 1.40 0.00 0.00 0
9 1.60 0.00 0.00 0
10 1.80 0.00 0.00 0
11 2.00 0.00 0.00 0
12 2.20 0.00 0.00 0
13 2.40 0.00 0.00 0
14 2.60 0.00 0.00 0
15 2.80 0.00 0.00 0
16 3.00 0.00 0.00 0
17 3.20 0.00 0.00 0
18 3.40 0.00 0.00 0
19 3.60 0.00 0.00 0
20 3.80 0.00 0.00 0
21 4.00 0.00 0.00 0
```

*** POINTS ON Y=1.4 ***
101 0.00 1.40 0.00 0
102 0.20 1.40 0.00 0
103 0.40 1.40 0.00 0
104 0.60 1.40 0.00 0
105 0.80 1.40 0.00 0
106 1.00 1.40 0.00 0
107 1.20 1.40 0.00 0
108 1.40 1.40 0.00 0
109 1.60 1.40 0.00 0
110 1.80 1.40 0.00 0
111 2.00 1.40 0.00 0
112 2.20 1.40 0.00 0
113 2.40 1.40 0.00 0
114 2.60 1.40 0.00 0
115 2.80 1.40 0.00 0
116 3.00 1.40 0.00 0
117 3.20 1.40 0.00 0
118 3.40 1.40 0.00 0
119 3.60 1.40 0.00 0
120 3.80 1.40 0.00 0
121 4.00 1.40 0.00 0

*** POINTS ON Y=1.6 ***
151 0.00 1.60 0.00 0
152 0.20 1.60 0.00 0
153 0.40 1.60 0.00 0
154 0.60 1.60 0.00 0
155 0.80 1.60 0.00 0
156 1.00 1.60 0.00 0
157 1.20 1.60 0.00 0
158 1.40 1.60 0.00 0
159 1.60 1.60 0.00 0
160 1.80 1.60 0.00 0
161 2.00 1.60 0.00 0
162 2.20 1.60 0.00 0
163 2.40 1.60 0.00 0
164 2.60 1.60 0.00 0
165 2.80 1.60 0.00 0
166 3.00 1.60 0.00 0
167 3.20 1.60 0.00 0
168 3.40 1.60 0.00 0
169 3.60 1.60 0.00 0
170 3.80 1.60 0.00 0
171 4.00 1.60 0.00 0

*** POINTS ON Y AXIS ***
201 0.00 0.20 0.00 0
202 0.00 0.40 0.00 0
203 0.00 0.60 0.00 0
204 0.00 0.80 0.00 0
205 0.00 1.00 0.00 0
206 0.00 1.20 0.00 0

*** POINTS ON X=4 ***
301 4.00 0.20 0.00 0
302 4.00 0.40 0.00 0
303 4.00 0.60 0.00 0
304 4.00 0.80 0.00 0
305 4.00 1.00 0.00 0
306 4.00 1.20 0.00 0

*** AUXILLARY POINTS ***
1001 -0.20 -0.20 0.00 0
@

*********************** LINES ***********************

*** LINES IN Y-DIRECTION ***
LINE STRAIGHT NAME=1 P1=1 P2=101
LINE STRAIGHT NAME=2 P1=2 P2=102
LINE STRAIGHT NAME=3 P1=3 P2=103
LINE STRAIGHT NAME=4 P1=4 P2=104
LINE STRAIGHT NAME=5 P1=5 P2=105
LINE STRAIGHT NAME=6 P1=6 P2=106
LINE STRAIGHT NAME=7 P1=7 P2=107
LINE STRAIGHT NAME=8 P1=8 P2=108
LINE STRAIGHT NAME=9 P1=9 P2=109
LINE STRAIGHT NAME=10 P1=10 P2=110
LINE STRAIGHT NAME=11 P1=11 P2=111
LINE STRAIGHT NAME=12 P1=12 P2=112
LINE STRAIGHT NAME=13 P1=13 P2=113
LINE STRAIGHT NAME=14 P1=14 P2=114
LINE STRAIGHT NAME=15 P1=15 P2=115
LINE STRAIGHT NAME=16 P1=16 P2=116

LINE STRAIGHT NAME=17 P1=17 P2=117
LINE STRAIGHT NAME=18 P1=18 P2=118
LINE STRAIGHT NAME=19 P1=19 P2=119
LINE STRAIGHT NAME=20 P1=20 P2=120
LINE STRAIGHT NAME=21 P1=21 P2=121

LINE STRAIGHT NAME=51 P1=101 P2=151
LINE STRAIGHT NAME=52 P1=102 P2=152
LINE STRAIGHT NAME=53 P1=103 P2=153
LINE STRAIGHT NAME=54 P1=104 P2=154
LINE STRAIGHT NAME=55 P1=105 P2=155
LINE STRAIGHT NAME=56 P1=106 P2=156
LINE STRAIGHT NAME=57 P1=107 P2=157
LINE STRAIGHT NAME=58 P1=108 P2=158
LINE STRAIGHT NAME=59 P1=109 P2=159
LINE STRAIGHT NAME=60 P1=110 P2=160
LINE STRAIGHT NAME=61 P1=111 P2=161
LINE STRAIGHT NAME=62 P1=112 P2=162
LINE STRAIGHT NAME=63 P1=113 P2=163
LINE STRAIGHT NAME=64 P1=114 P2=164
LINE STRAIGHT NAME=65 P1=115 P2=165
LINE STRAIGHT NAME=66 P1=116 P2=166
LINE STRAIGHT NAME=67 P1=117 P2=167
LINE STRAIGHT NAME=68 P1=118 P2=168
LINE STRAIGHT NAME=69 P1=119 P2=169
LINE STRAIGHT NAME=70 P1=120 P2=170
LINE STRAIGHT NAME=71 P1=121 P2=171

*** LINES IN X-DIRECTION ***
LINE STRAIGHT NAME=201 P1=1 P2=21
LINE STRAIGHT NAME=202 P1=201 P2=301
LINE STRAIGHT NAME=203 P1=202 P2=302
LINE STRAIGHT NAME=204 P1=203 P2=303
LINE STRAIGHT NAME=205 P1=204 P2=304
LINE STRAIGHT NAME=206 P1=205 P2=305
LINE STRAIGHT NAME=207 P1=206 P2=306

LINE STRAIGHT NAME=210 P1=151 P2=152
LINE STRAIGHT NAME=211 P1=152 P2=153
LINE STRAIGHT NAME=212 P1=153 P2=154
LINE STRAIGHT NAME=213 P1=154 P2=155
LINE STRAIGHT NAME=214 P1=155 P2=156
LINE STRAIGHT NAME=215 P1=156 P2=157
LINE STRAIGHT NAME=216 P1=157 P2=158
LINE STRAIGHT NAME=217 P1=158 P2=159
LINE STRAIGHT NAME=218 P1=159 P2=160
LINE STRAIGHT NAME=219 P1=160 P2=161
LINE STRAIGHT NAME=220 P1=161 P2=162
LINE STRAIGHT NAME=221 P1=162 P2=163
LINE STRAIGHT NAME=222 P1=163 P2=164
LINE STRAIGHT NAME=223 P1=164 P2=165
LINE STRAIGHT NAME=224 P1=165 P2=166
LINE STRAIGHT NAME=225 P1=166 P2=167
LINE STRAIGHT NAME=226 P1=167 P2=168
LINE STRAIGHT NAME=227 P1=168 P2=169
LINE STRAIGHT NAME=228 P1=169 P2=170
LINE STRAIGHT NAME=229 P1=170 P2=171

LINE STRAIGHT NAME=250 P1=101 P2=102
LINE STRAIGHT NAME=251 P1=102 P2=103
LINE STRAIGHT NAME=252 P1=103 P2=104
LINE STRAIGHT NAME=253 P1=104 P2=105
LINE STRAIGHT NAME=254 P1=105 P2=106
LINE STRAIGHT NAME=255 P1=106 P2=107
LINE STRAIGHT NAME=256 P1=107 P2=108
LINE STRAIGHT NAME=257 P1=108 P2=109
LINE STRAIGHT NAME=258 P1=109 P2=110
LINE STRAIGHT NAME=259 P1=110 P2=111
LINE STRAIGHT NAME=260 P1=111 P2=112
LINE STRAIGHT NAME=261 P1=112 P2=113
LINE STRAIGHT NAME=262 P1=113 P2=114
LINE STRAIGHT NAME=263 P1=114 P2=115
LINE STRAIGHT NAME=264 P1=115 P2=116
LINE STRAIGHT NAME=265 P1=116 P2=117
LINE STRAIGHT NAME=266 P1=117 P2=118
LINE STRAIGHT NAME=267 P1=118 P2=119
LINE STRAIGHT NAME=268 P1=119 P2=120
LINE STRAIGHT NAME=269 P1=120 P2=121

```
*************************************************
*************************************************
********* MOMENT-CURVATURE RELATIONS **********
*************************************************
*************************************************

*** GROUP 1: Used for beams in X-direction***
TWIST-MOMENT NAME=1
@CLEAR
0          0
0.043      10000
@


MOMENT-TWIST NAME=1
@CLEAR
0          1
1E6        1
@

*** Bending moment, S-direction
CURVATURE-MO NAME=2
@CLEAR
0.00227              10000
0.00454              20000
@

MOMENT-CURVA NAME=2
@CLEAR
0          2
1E6        2
@

*** Bending moment, T-direction
CURVATURE-MO NAME=3
@CLEAR
0.00227              10000
0.00454              20000
@

MOMENT-CURVA NAME=3
@CLEAR
0          3
1E6        3
@

RIGIDITY-MOM NONLINEAR-ELASTIC NAME=1
RIGIDITY=1,
   MOMENT-R=1 MOMENT-S=2 MOMENT-T=3 DENSITY=0,
   MASS-ARE=0 MASS-RIN=0,
   MASS-SIN=0 MASS-TIN=0,
   ALPHA=0

*** GROUP 2: Used for beams in Y-direction ***
TWIST-MOMENT NAME=4
@CLEAR
0          0
0.043      10000
@


MOMENT-TWIST NAME=4
@CLEAR
0          4
1E6        4
@

*** Bending moment, S-direction
CURVATURE-MO NAME=5
@CLEAR
-0.02275   -20000
-0.00400   -3518
-0.00076   -3350
0          0
0.00076    3350
0.00400    3518
0.02275    20000

@

MOMENT-CURVA NAME=5
@CLEAR
0          5
1E6        5
@
```

*** Bending moment, T-direction
CURVATURE-MO NAME=6
@CLEAR
0.00227   10000
0.00454   20000
@

MOMENT-CURVA NAME=6
@CLEAR
0   6
1E6   6
@

RIGIDITY-MOM NONLINEAR-ELASTIC NAME=2
RIGIDITY=1,
   MOMENT-R=4 MOMENT-S=5 MOMENT-T=6 DENSITY=0,
   MASS-ARE=0 MASS-RIN=0,
   MASS-SIN=0 MASS-TIN=0,
   ALPHA=0

*** GROUP 3: Used for beam along X-axis in symmetry line ***
TWIST-MOMENT NAME=7
@CLEAR
0   0
0.215   10000
@

MOMENT-TWIST NAME=7
@CLEAR
0   7
1E6   7
@

*** Bending moment, S-direction
CURVATURE-MO NAME=8
@CLEAR
0.00454   10000
0.00908   20000
@

MOMENT-CURVA NAME=8
@CLEAR
0   8
1E6   8
@

*** Bending moment, T-direction
CURVATURE-MO NAME=9
@CLEAR
0.00454   10000
0.00908   20000
@

MOMENT-CURVA NAME=9
@CLEAR
0   9
1E6   9
@

RIGIDITY-MOM NONLINEAR-ELASTIC NAME=3
RIGIDITY=1,
   MOMENT-R=7 MOMENT-S=8 MOMENT-T=9 DENSITY=0,
   MASS-ARE=0 MASS-RIN=0,
   MASS-SIN=0 MASS-TIN=0,
   ALPHA=0

*** GROUP 4: Used for beam along Y-axis in symmetry line ***
TWIST-MOMENT NAME=10
@CLEAR
0   0
0.215   10000
@

MOMENT-TWIST NAME=10
@CLEAR
0   10
1E6   10
@

```
*** Bending moment, S-direction
CURVATURE-MO NAME=11
@CLEAR
-0.045500   -20000
-0.004002   -1759
-0.000761   -1675
0           0
0.000761    1675
0.004002    1759
0.045500    20000

@

MOMENT-CURVA NAME=11
@CLEAR
0           11
1E6         11
@

*** Bending moment, T-direction
CURVATURE-MO NAME=12
@CLEAR
0.00454              10000
0.00908              20000
@

MOMENT-CURVA NAME=12
@CLEAR
0           12
1E6         12
@

*********** MOMENT-CURVATURE GROUPS ************

RIGIDITY-MOM NONLINEAR-ELASTIC NAME=4
RIGIDITY=1,
    MOMENT-R=10 MOMENT-S=11 MOMENT-T=12
DENSITY=0,
    MASS-ARE=0 MASS-RIN=0,
    MASS-SIN=0 MASS-TIN=0,
    ALPHA=0

*** ELEMENT GROUPS ***
EGROUP BEAM NAME=1 SUBTYPE=THREE-D
DISPLACE=DEFAULT MATERIAL=1 RINT=5,
    SINT=7 TINT=DEFAULT RESULTS=FORCES
INITIALS=NONE CMASS=DEFAULT,
    RIGIDEND=NONE MOMENT-C=YES RIGIDITY=1
MULTIPLY=1000000.00000000,
    RUPTURE=ADINA OPTION=NONE BOLT-
TOL=0.00000000000000 DESCRIPT=,
'NONE' SECTION=1 PRINT=DEFAULT SAVE=DEFAULT
TBIRTH=0.00000000000000,
    TDEATH=0.00000000000000 SPOINT=4
BOLTFORC=0.00000000000000,
    BOLTNCUR=0 TMC-MATE=1 BOLT-NUM=0 BOLT-
LOA=0.00000000000000,
    WARP=NO

EGROUP BEAM NAME=2 SUBTYPE=THREE-D
DISPLACE=DEFAULT MATERIAL=2 RINT=5,
    SINT=7 TINT=DEFAULT RESULTS=FORCES
INITIALS=NONE CMASS=DEFAULT,
    RIGIDEND=NONE MOMENT-C=YES RIGIDITY=2
MULTIPLY=1000000.00000000,
    RUPTURE=ADINA OPTION=NONE BOLT-
TOL=0.00000000000000 DESCRIPT=,
'NONE' SECTION=2 PRINT=DEFAULT SAVE=DEFAULT
TBIRTH=0.00000000000000,
    TDEATH=0.00000000000000 SPOINT=4
BOLTFORC=0.00000000000000,
    BOLTNCUR=0 TMC-MATE=1 BOLT-NUM=0 BOLT-
LOA=0.00000000000000,
    WARP=NO
```

```
EGROUP BEAM NAME=3 SUBTYPE=THREE-D
DISPLACE=DEFAULT MATERIAL=2 RINT=5,
    SINT=7 TINT=DEFAULT RESULTS=FORCES
INITIALS=NONE CMASS=DEFAULT,
    RIGIDEND=NONE MOMENT-C=YES RIGIDITY=3
MULTIPLY=1000000.00000000,
    RUPTURE=ADINA OPTION=NONE BOLT-
TOL=0.00000000000000 DESCRIPT=,
'NONE' SECTION=2 PRINT=DEFAULT SAVE=DEFAULT
TBIRTH=0.00000000000000,
    TDEATH=0.00000000000000 SPOINT=4
BOLTFORC=0.00000000000000,
    BOLTNCUR=0 TMC-MATE=1 BOLT-NUM=0 BOLT-
LOA=0.00000000000000,
    WARP=NO

EGROUP BEAM NAME=4 SUBTYPE=THREE-D
DISPLACE=DEFAULT MATERIAL=2 RINT=5,
    SINT=7 TINT=DEFAULT RESULTS=FORCES
INITIALS=NONE CMASS=DEFAULT,
    RIGIDEND=NONE MOMENT-C=YES RIGIDITY=4
MULTIPLY=1000000.00000000,
    RUPTURE=ADINA OPTION=NONE BOLT-
TOL=0.00000000000000 DESCRIPT=,
'NONE' SECTION=2 PRINT=DEFAULT SAVE=DEFAULT
TBIRTH=0.00000000000000,
    TDEATH=0.00000000000000 SPOINT=4
BOLTFORC=0.00000000000000,
    BOLTNCUR=0 TMC-MATE=1 BOLT-NUM=0 BOLT-
LOA=0.00000000000000,
    WARP=NO

****************************************************
****************************************************
******************** MESHING ********************
****************************************************
****************************************************

***************** MESH DENSITY ******************

SUBDIVIDE MODEL MODE=LENGTH
SIZE=0.200000000000000 NDIV=1,
    PROGRESS=GEOMETRIC MINCUR=1

GLINE NODES=2 AUXPOINT=1001 NCOINCID=ALL
NCTOLERA=1.00000000000000E-05,
    SUBSTRUC=0 GROUP=1 MIDNODES=CURVED
XO=0.00000000000000,
    YO=0.00000000000000 ZO=0.00000000000000
XYZOSYST=SKEW
@CLEAR
201
TO
207
250
TO
269
@

***************** MESH GROUPING *****************

GLINE NODES=2 AUXPOINT=1001 NCOINCID=ALL
NCTOLERA=1.00000000000000E-05,
    SUBSTRUC=0 GROUP=2 MIDNODES=CURVED
XO=0.00000000000000,
    YO=0.00000000000000 ZO=0.00000000000000
XYZOSYST=SKEW
@CLEAR
2
TO
21
52
TO
71
@

GLINE NODES=2 AUXPOINT=1001 NCOINCID=ALL
NCTOLERA=1.00000000000000E-05,
    SUBSTRUC=0 GROUP=3 MIDNODES=CURVED
XO=0.00000000000000,
    YO=0.00000000000000 ZO=0.00000000000000
XYZOSYST=SKEW
210
TO
229
@
```

```
GLINE NODES=2 AUXPOINT=1001 NCOINCID=ALL
NCTOLERA=1.00000000000000E-05,
    SUBSTRUC=0 GROUP=4 MIDNODES=CURVED
XO=0.00000000000000,
    YO=0.00000000000000 ZO=0.0000000000000
XYZOSYST=SKEW
@CLEAR
1
51
@


*********************************************
*********************************************
************** BOUNDARY CONDITIONS **************
*********************************************
*********************************************

FIXITY NAME=ROLLER
@CLEAR
 'Z-TRANSLATION'
 'OVALIZATION'
@

FIXITY NAME=XSYMM
@CLEAR
 'Y-TRANSLATION'
 'X-ROTATION'
 'OVALIZATION'
@

FIXITY NAME=YSYMM
@CLEAR
 'X-TRANSLATION'
 'Y-ROTATION'
 'OVALIZATION'
@

FIXITY NAME=ORIGO
@CLEAR
 'X-TRANSLATION'
 'Z-TRANSLATION'
 'Y-ROTATION'
 'OVALIZATION'
@
```

```
FIXITY NAME=XYSYMM
@CLEAR
 'X-TRANSLATION'
 'Y-TRANSLATION'
 'X-ROTATION'
 'Y-ROTATION'
 'OVALIZATION'
@

FIXBOUNDARY POINTS FIXITY=ALL
@CLEAR
2  'ROLLER'
TO
21 'ROLLER'

152 'XSYMM'
TO
171 'XSYMM'

201 'YSYMM'
TO
206 'YSYMM'
101 'YSYMM'

1   'ORIGO'
151 'XYSYMM'
@

*********************************************
*********************************************
***************** LOAD APPLICATION *****************
*********************************************
*********************************************
LOAD FORCE NAME=1 MAGNITUD=12500.00 FX=0.00,
FY=0.00 FZ=-1.00

APPLY-LOAD BODY=0
@CLEAR
1 'FORCE' 1  'POINT' 101 0 1 0.00 0 -1 0 0 0  'NO', 0.00 0.00 1 0
'MID'
2 'FORCE' 1  'POINT' 102 0 1 0.00 0 -1 0 0 0  'NO', 0.00 0.00 1 0
'MID'
3 'FORCE' 1  'POINT' 151 0 1 0.00 0 -1 0 0 0  'NO', 0.00 0.00 1 0
'MID'
4 'FORCE' 1  'POINT' 152 0 1 0.00 0 -1 0 0 0  'NO', 0.00 0.00 1 0
'MID'
@

*********************** END *************************
```

J.2 Cumulative plastic rotation – Cantilever slab

```
DATABASE NEW SAVE=NO PROMPT=NO
FEPROGRAM ADINA
CONTROL FILEVERSION=V89

*********************************************
*********************************************
******************** GEOMETRY ********************
*********************************************
*********************************************

COORDINATES POINT SYSTEM=0
@CLEAR

******************** NODES ********************

*** Line L5
```

1	0	0	0	0
2	0.2	0	0	0
3	0.4	0	0	0
4	0.6	0	0	0
5	0.8	0	0	0
6	1	0	0	0
7	1.2	0	0	0
8	1.4	0	0	0
9	1.6	0	0	0
10	1.8	0	0	0
11	2	0	0	0
12	2.2	0	0	0
13	2.4	0	0	0
14	2.6	0	0	0
15	2.8	0	0	0
16	3	0	0	0
17	3.2	0	0	0
18	3.4	0	0	0
19	3.6	0	0	0
20	3.8	0	0	0
21	4	0	0	0
22	4.2	0	0	0
23	4.4	0	0	0
24	4.6	0	0	0
25	4.8	0	0	0
26	5.0	0	0	0
27	5.2	0	0	0
28	5.4	0	0	0
29	5.6	0	0	0
30	5.8	0	0	0
31	6.0	0	0	0
32	6.2	0	0	0
33	6.4	0	0	0
34	6.6	0	0	0
35	6.8	0	0	0
36	7.0	0	0	0
37	7.2	0	0	0
38	7.4	0	0	0
39	7.6	0	0	0
40	7.8	0	0	0
41	8.0	0	0	0
42	8.2	0	0	0
43	8.4	0	0	0
44	8.6	0	0	0
45	8.8	0	0	0
46	9.0	0	0	0

47	9.2	0	0	0
48	9.4	0	0	0
49	9.6	0	0	0
50	9.8	0	0	0
51	10.0	0	0	0
52	10.2	0	0	0
53	10.4	0	0	0
54	10.6	0	0	0
55	10.8	0	0	0
56	11.0	0	0	0
57	11.2	0	0	0
58	11.4	0	0	0
59	11.6	0	0	0
60	11.8	0	0	0
61	12.0	0	0	0

*** Free edge, x=12

62	12.0	0.2	0	0
63	12.0	0.4	0	0
64	12.0	0.6	0	0
65	12.0	0.8	0	0
66	12.0	1.0	0	0
67	12.0	1.2	0	0
68	12.0	1.4	0	0
69	12.0	1.6	0	0

*** Line L3

70	11.8	1.6	0	0
71	11.6	1.6	0	0
72	11.4	1.6	0	0
73	11.2	1.6	0	0
74	11.0	1.6	0	0
75	10.8	1.6	0	0
76	10.6	1.6	0	0
77	10.4	1.6	0	0
78	10.2	1.6	0	0
79	10.0	1.6	0	0
80	9.8	1.6	0	0
81	9.6	1.6	0	0
82	9.4	1.6	0	0
83	9.2	1.6	0	0
84	9.0	1.6	0	0
85	8.8	1.6	0	0
86	8.6	1.6	0	0
87	8.4	1.6	0	0
88	8.2	1.6	0	0
89	8.0	1.6	0	0
90	7.8	1.6	0	0
91	7.6	1.6	0	0
92	7.4	1.6	0	0
93	7.2	1.6	0	0
94	7.0	1.6	0	0
95	6.8	1.6	0	0
96	6.6	1.6	0	0
97	6.4	1.6	0	0
98	6.2	1.6	0	0
99	6.0	1.6	0	0
100	5.8	1.6	0	0
101	5.6	1.6	0	0
102	5.4	1.6	0	0
103	5.2	1.6	0	0
104	5.0	1.6	0	0
105	4.8	1.6	0	0
106	4.6	1.6	0	0
107	4.4	1.6	0	0
108	4.2	1.6	0	0
109	4	1.6	0	0
110	3.8	1.6	0	0
111	3.6	1.6	0	0
112	3.4	1.6	0	0
113	3.2	1.6	0	0
114	3	1.6	0	0
115	2.8	1.6	0	0
116	2.6	1.6	0	0
117	2.4	1.6	0	0
118	2.2	1.6	0	0
119	2	1.6	0	0
120	1.8	1.6	0	0
121	1.6	1.6	0	0
122	1.4	1.6	0	0
123	1.2	1.6	0	0
124	1	1.6	0	0
125	0.8	1.6	0	0
126	0.6	1.6	0	0
127	0.4	1.6	0	0
128	0.2	1.6	0	0

129	0	1.6	0	0

*** Free edge, x=0

130	0.0	1.4	0	0
131	0.0	1.2	0	0
132	0.0	1.0	0	0
133	0.0	0.8	0	0
134	0.0	0.6	0	0
135	0.0	0.4	0	0
136	0.0	0.2	0	0

*** Line for finer mesh at the fixed support

200	0.2	0.2	0	0
201	0.4	0.2	0	0
202	0.6	0.2	0	0
203	0.8	0.2	0	0
204	1	0.2	0	0
205	1.2	0.2	0	0
206	1.4	0.2	0	0
207	1.6	0.2	0	0
208	1.8	0.2	0	0
209	2	0.2	0	0
210	2.2	0.2	0	0
211	2.4	0.2	0	0
212	2.6	0.2	0	0
213	2.8	0.2	0	0
214	3	0.2	0	0
215	3.2	0.2	0	0
216	3.4	0.2	0	0
217	3.6	0.2	0	0
218	3.8	0.2	0	0
219	4	0.2	0	0
220	4.2	0.2	0	0
221	4.4	0.2	0	0
222	4.6	0.2	0	0
223	4.8	0.2	0	0
224	5.0	0.2	0	0
225	5.2	0.2	0	0
226	5.4	0.2	0	0
227	5.6	0.2	0	0
228	5.8	0.2	0	0
229	6.0	0.2	0	0
230	6.2	0.2	0	0
231	6.4	0.2	0	0
232	6.6	0.2	0	0
233	6.8	0.2	0	0
234	7.0	0.2	0	0
235	7.2	0.2	0	0
236	7.4	0.2	0	0
237	7.6	0.2	0	0
238	7.8	0.2	0	0
239	8.0	0.2	0	0
240	8.2	0.2	0	0
241	8.4	0.2	0	0
242	8.6	0.2	0	0
243	8.8	0.2	0	0
244	9.0	0.2	0	0
245	9.2	0.2	0	0
246	9.4	0.2	0	0
247	9.6	0.2	0	0
248	9.8	0.2	0	0
249	10.0	0.2	0	0
250	10.2	0.2	0	0
251	10.4	0.2	0	0
252	10.6	0.2	0	0
253	10.8	0.2	0	0
254	11.0	0.2	0	0
255	11.2	0.2	0	0
256	11.4	0.2	0	0
257	11.6	0.2	0	0
258	11.8	0.2	0	0

*** AUX point

1000	12.2	1.8	0	0

*********************** LINES ***********************

*** Lines as boundaries

LINE STRAIGHT NAME=1	P1=1	P2=61
LINE STRAIGHT NAME=2	P1=61	P2=62
LINE STRAIGHT NAME=3	P1=129	P2=69
LINE STRAIGHT NAME=4	P1=1	P2=136
LINE STRAIGHT NAME=501	P1=62	P2=69
LINE STRAIGHT NAME=502	P1=136	P2=129

```
*** Lines in y-direction                                    LINE STRAIGHT NAME=124    P1=224    P2=104
LINE STRAIGHT NAME=5      P1=2     P2=200                    LINE STRAIGHT NAME=125    P1=225    P2=103
LINE STRAIGHT NAME=6      P1=3     P2=201                    LINE STRAIGHT NAME=126    P1=226    P2=102
LINE STRAIGHT NAME=7      P1=4     P2=202                    LINE STRAIGHT NAME=127    P1=227    P2=101
LINE STRAIGHT NAME=8      P1=5     P2=203                    LINE STRAIGHT NAME=128    P1=228    P2=100
LINE STRAIGHT NAME=9      P1=6     P2=204                    LINE STRAIGHT NAME=129    P1=229    P2=99
LINE STRAIGHT NAME=10     P1=7     P2=205                    LINE STRAIGHT NAME=130    P1=230    P2=98
LINE STRAIGHT NAME=11     P1=8     P2=206                    LINE STRAIGHT NAME=131    P1=231    P2=97
LINE STRAIGHT NAME=12     P1=9     P2=207                    LINE STRAIGHT NAME=132    P1=232    P2=96
LINE STRAIGHT NAME=13     P1=10    P2=208                    LINE STRAIGHT NAME=133    P1=233    P2=95
LINE STRAIGHT NAME=14     P1=11    P2=209                    LINE STRAIGHT NAME=134    P1=234    P2=94
LINE STRAIGHT NAME=15     P1=12    P2=210                    LINE STRAIGHT NAME=135    P1=235    P2=93
LINE STRAIGHT NAME=16     P1=13    P2=211                    LINE STRAIGHT NAME=136    P1=236    P2=92
LINE STRAIGHT NAME=17     P1=14    P2=212                    LINE STRAIGHT NAME=137    P1=237    P2=91
LINE STRAIGHT NAME=18     P1=15    P2=213                    LINE STRAIGHT NAME=138    P1=238    P2=90
LINE STRAIGHT NAME=19     P1=16    P2=214                    LINE STRAIGHT NAME=139    P1=239    P2=89
LINE STRAIGHT NAME=20     P1=17    P2=215                    LINE STRAIGHT NAME=140    P1=240    P2=88
LINE STRAIGHT NAME=21     P1=18    P2=216                    LINE STRAIGHT NAME=141    P1=241    P2=87
LINE STRAIGHT NAME=22     P1=19    P2=217                    LINE STRAIGHT NAME=142    P1=242    P2=86
LINE STRAIGHT NAME=23     P1=20    P2=218                    LINE STRAIGHT NAME=143    P1=243    P2=85
LINE STRAIGHT NAME=24     P1=21    P2=219                    LINE STRAIGHT NAME=144    P1=244    P2=84
LINE STRAIGHT NAME=25     P1=22    P2=220                    LINE STRAIGHT NAME=145    P1=245    P2=83
LINE STRAIGHT NAME=26     P1=23    P2=221                    LINE STRAIGHT NAME=146    P1=246    P2=82
LINE STRAIGHT NAME=27     P1=24    P2=222                    LINE STRAIGHT NAME=147    P1=247    P2=81
LINE STRAIGHT NAME=28     P1=25    P2=223                    LINE STRAIGHT NAME=148    P1=248    P2=80
LINE STRAIGHT NAME=29     P1=26    P2=224                    LINE STRAIGHT NAME=149    P1=249    P2=79
LINE STRAIGHT NAME=30     P1=27    P2=225                    LINE STRAIGHT NAME=150    P1=250    P2=78
LINE STRAIGHT NAME=31     P1=28    P2=226                    LINE STRAIGHT NAME=151    P1=251    P2=77
LINE STRAIGHT NAME=32     P1=29    P2=227                    LINE STRAIGHT NAME=152    P1=252    P2=76
LINE STRAIGHT NAME=33     P1=30    P2=228                    LINE STRAIGHT NAME=153    P1=253    P2=75
LINE STRAIGHT NAME=34     P1=31    P2=229                    LINE STRAIGHT NAME=154    P1=254    P2=74
LINE STRAIGHT NAME=35     P1=32    P2=230                    LINE STRAIGHT NAME=155    P1=255    P2=73
LINE STRAIGHT NAME=36     P1=33    P2=231                    LINE STRAIGHT NAME=156    P1=256    P2=72
LINE STRAIGHT NAME=37     P1=34    P2=232                    LINE STRAIGHT NAME=157    P1=257    P2=71
LINE STRAIGHT NAME=38     P1=35    P2=233                    LINE STRAIGHT NAME=158    P1=258    P2=70
LINE STRAIGHT NAME=39     P1=36    P2=234
LINE STRAIGHT NAME=40     P1=37    P2=235
LINE STRAIGHT NAME=41     P1=38    P2=236                    *** Lines in x-direction
LINE STRAIGHT NAME=42     P1=39    P2=237                    LINE STRAIGHT NAME=200    P1=136    P2=62
LINE STRAIGHT NAME=43     P1=40    P2=238                    LINE STRAIGHT NAME=201    P1=135    P2=63
LINE STRAIGHT NAME=44     P1=41    P2=239                    LINE STRAIGHT NAME=202    P1=134    P2=64
LINE STRAIGHT NAME=45     P1=42    P2=240                    LINE STRAIGHT NAME=203    P1=133    P2=65
LINE STRAIGHT NAME=46     P1=43    P2=241                    LINE STRAIGHT NAME=204    P1=132    P2=66
LINE STRAIGHT NAME=47     P1=44    P2=242                    LINE STRAIGHT NAME=205    P1=131    P2=67
LINE STRAIGHT NAME=48     P1=45    P2=243                    LINE STRAIGHT NAME=206    P1=130    P2=68
LINE STRAIGHT NAME=49     P1=46    P2=244
LINE STRAIGHT NAME=50     P1=47    P2=245                    ****************************************************
LINE STRAIGHT NAME=51     P1=48    P2=246                    ****************************************************
LINE STRAIGHT NAME=52     P1=49    P2=247                    ********* MOMENT-CURVATURE RELATIONS **********
LINE STRAIGHT NAME=53     P1=50    P2=248                    ****************************************************
LINE STRAIGHT NAME=54     P1=51    P2=249                    ****************************************************
LINE STRAIGHT NAME=55     P1=52    P2=250
LINE STRAIGHT NAME=56     P1=53    P2=251
LINE STRAIGHT NAME=57     P1=54    P2=252                    ****************** GENERAL DATA ******************
LINE STRAIGHT NAME=58     P1=55    P2=253
LINE STRAIGHT NAME=59     P1=56    P2=254                    *** Axial force and axial strain
LINE STRAIGHT NAME=60     P1=57    P2=255                    FORCE-STRAIN NAME=100
LINE STRAIGHT NAME=61     P1=58    P2=256                    @CLEAR
LINE STRAIGHT NAME=62     P1=59    P2=257                    -0.003      -160000
LINE STRAIGHT NAME=63     P1=60    P2=258                    -0.001      -160000
                                                            0           0
*** Lines for finer mesh                                    0.001       160000
LINE STRAIGHT NAME=100    P1=200   P2=128                    0.003       160000
LINE STRAIGHT NAME=101    P1=201   P2=127                    @
LINE STRAIGHT NAME=102    P1=202   P2=126
LINE STRAIGHT NAME=103    P1=203   P2=125                    *** Twist moment, symmetry line
LINE STRAIGHT NAME=104    P1=204   P2=124                    TWIST-MOMENT NAME=100
LINE STRAIGHT NAME=105    P1=205   P2=123                    @CLEAR
LINE STRAIGHT NAME=106    P1=206   P2=122                    -21.185     -1000000
LINE STRAIGHT NAME=107    P1=207   P2=121                    -0.21184    -10000
LINE STRAIGHT NAME=108    P1=208   P2=120                    0           0
LINE STRAIGHT NAME=109    P1=209   P2=119                    0.21184     10000
LINE STRAIGHT NAME=110    P1=210   P2=118                    21.185      1000000
LINE STRAIGHT NAME=111    P1=211   P2=117                    @
LINE STRAIGHT NAME=112    P1=212   P2=116
LINE STRAIGHT NAME=113    P1=213   P2=115                    MOMENT-TWIST NAME=100
LINE STRAIGHT NAME=114    P1=214   P2=114                    @CLEAR
LINE STRAIGHT NAME=115    P1=215   P2=113                    -1E6        100
LINE STRAIGHT NAME=116    P1=216   P2=112                    0           100
LINE STRAIGHT NAME=117    P1=217   P2=111                    1E6         100
LINE STRAIGHT NAME=118    P1=218   P2=110                    @
LINE STRAIGHT NAME=119    P1=219   P2=109
LINE STRAIGHT NAME=120    P1=220   P2=108
LINE STRAIGHT NAME=121    P1=221   P2=107
LINE STRAIGHT NAME=122    P1=222   P2=106
LINE STRAIGHT NAME=123    P1=223   P2=105
```

```
*** Twist moment                                      *** GROUP 4: Used for beam along Y-axis in symmetry line
TWIST-MOMENT NAME=200                                 CURVATURE-MO NAME=4
@CLEAR                                                @CLEAR
-4.305          -1000000                              -10                    -6246
-0.04304        -10000                                -0.01699               -6246
0               0                                     0                      0
0.04304         10000                                 0.01699                6246
4.305           1000000                               10                     6246
@                                                     @

MOMENT-TWIST NAME=200                                 MOMENT-CURVA NAME=4
@CLEAR                                                @CLEAR
-1E6            200                                   -1E6           4
0              200                                    0             4
1E6            200                                    1E6           4
@                                                     @

*** Bending moment, T-direction                       *** GROUP 5: Used for beam along y-axis at the support
CURVATURE-MO NAME=300                                 CURVATURE-MO NAME=5
@CLEAR                                                @CLEAR
-10.0000        -20000                                -2                     -12491
-0.02159        -20000                                -0.01699               -12491
0               0                                     0                      0
0.02159         20000                                 0.01699                12491
10.0000         20000                                 2                      12491
@                                                     @

MOMENT-CURVA NAME=300                                 MOMENT-CURVA NAME=5
@CLEAR                                                @CLEAR
-1E6            300                                   -1E6           5
0              300                                    0             5
1E6            300                                    1E6           5
@                                                     @

********* BENDING MOMENT IN S-DIRECTION **********     *********** MOMENT-CURVATURE GROUPS ************

*** GROUP 1: Used for beams in X-direction            RIGIDITY-MOM PLASTIC-MULTILINEAR NAME=1
CURVATURE-MO NAME=1                                    HARDENIN=ISOTROPIC,
@CLEAR                                                   BETA=0 FORCE-AX=100 MOMENT-R=200 MOMENT-S=1,
-10                    -12491                             MOMENT-T=300 AXIAL-CY=1 BENDING-=1,
-0.01699               -12491                            TORSION-=1 DENSITY=0,
0                      0                                 MASS-ARE=0 MASS-RIN=0,
0.01699                12491                             MASS-SIN=0 MASS-TIN=0,
10                     12491                             ACURVE-T=UNSYMMETRIC TCURVE-
@                                                     T=UNSYMMETRIC BCURVE-T=UNSYMMETRIC,
                                                        ALPHA=0
MOMENT-CURVA NAME=1
@CLEAR                                                RIGIDITY-MOM PLASTIC-MULTILINEAR NAME=2
-1E6            1                                     HARDENIN=ISOTROPIC,
0              1                                        BETA=0 FORCE-AX=100 MOMENT-R=200 MOMENT-S=2,
1E6            1                                        MOMENT-T=300 AXIAL-CY=1 BENDING-=1,
@                                                       TORSION-=1 DENSITY=0,
                                                        MASS-ARE=0 MASS-RIN=0,
*** GROUP 2: Used for beams in Y-direction              MASS-SIN=0 MASS-TIN=0,
CURVATURE-MO NAME=2                                      ACURVE-T=UNSYMMETRIC TCURVE-
@CLEAR                                                T=UNSYMMETRIC BCURVE-T=UNSYMMETRIC,
-10                    -12491                            ALPHA=0
-0.01699               -12491
0                      0                              RIGIDITY-MOM PLASTIC-MULTILINEAR NAME=3
0.01699                12491                          HARDENIN=ISOTROPIC,
10                     12491                            BETA=0 FORCE-AX=100 MOMENT-R=100 MOMENT-S=3,
@                                                       MOMENT-T=300 AXIAL-CY=1 BENDING-=1,
                                                        TORSION-=1 DENSITY=0,
MOMENT-CURVA NAME=2                                      MASS-ARE=0 MASS-RIN=0,
@CLEAR                                                   MASS-SIN=0 MASS-TIN=0,
-1E6            2                                        ACURVE-T=UNSYMMETRIC TCURVE-
0              2                                      T=UNSYMMETRIC BCURVE-T=UNSYMMETRIC,
1E6             2                                        ALPHA=0
@
                                                     RIGIDITY-MOM PLASTIC-MULTILINEAR NAME=4
*** GROUP 3: Used for beam along X-axis in symmetry line  HARDENIN=ISOTROPIC,
CURVATURE-MO NAME=3                                      BETA=0 FORCE-AX=100 MOMENT-R=100 MOMENT-S=4,
@CLEAR                                                   MOMENT-T=300 AXIAL-CY=1 BENDING-=1,
-10                    -6246                             TORSION-=1 DENSITY=0,
-0.01699               -6246                             MASS-ARE=0 MASS-RIN=0,
0                      0                                 MASS-SIN=0 MASS-TIN=0,
0.01699                6246                              ACURVE-T=UNSYMMETRIC TCURVE-
10                     6246                           T=UNSYMMETRIC BCURVE-T=UNSYMMETRIC,
@                                                       ALPHA=0

MOMENT-CURVA NAME=3
@CLEAR
-1E6            3
0              3
1E6            3
@
```

RIGIDITY-MOM PLASTIC-MULTILINEAR NAME=5
HARDENIN=ISOTROPIC,
    BETA=0 FORCE-AX=100 MOMENT-R=200 MOMENT-S=5,
    MOMENT-T=300 AXIAL-CY=1 BENDING-=1,
    TORSION-=1 DENSITY=0,
    MASS-ARE=0 MASS-RIN=0,
    MASS-SIN=0 MASS-TIN=0,
    ACURVE-T=UNSYMMETRIC TCURVE-
T=UNSYMMETRIC BCURVE-T=UNSYMMETRIC,
    ALPHA=0

**************** ELEMENT GROUPS ******************

*** X-AXIS
EGROUP BEAM NAME=1 SUBTYPE=THREE-D
DISPLACE=DEFAULT MATERIAL=1 RINT=5,
    SINT=7 TINT=DEFAULT RESULTS=FORCES
INITIALS=NONE CMASS=DEFAULT,
    RIGIDEND=NONE MOMENT-C=YES RIGIDITY=1
MULTIPLY=1000000.00000000,
    RUPTURE=ADINA OPTION=NONE BOLT-
TOL=0.00000000000000 DESCRIPT=,
'NONE' SECTION=1 PRINT=DEFAULT SAVE=DEFAULT
TBIRTH=0.00000000000000,
    TDEATH=0.00000000000000 SPOINT=4
BOLTFORC=0.00000000000000,
    BOLTNCUR=0 TMC-MATE=1 BOLT-NUM=0 BOLT-
LOA=0.00000000000000,
    WARP=NO

*** Y-AXIS
EGROUP BEAM NAME=2 SUBTYPE=THREE-D
DISPLACE=DEFAULT MATERIAL=2 RINT=5,
    SINT=7 TINT=DEFAULT RESULTS=FORCES
INITIALS=NONE CMASS=DEFAULT,
    RIGIDEND=NONE MOMENT-C=YES RIGIDITY=2
MULTIPLY=1000000.00000000,
    RUPTURE=ADINA OPTION=NONE BOLT-
TOL=0.00000000000000 DESCRIPT=,
'NONE' SECTION=2 PRINT=DEFAULT SAVE=DEFAULT
TBIRTH=0.00000000000000,
    TDEATH=0.00000000000000 SPOINT=4
BOLTFORC=0.00000000000000,
    BOLTNCUR=0 TMC-MATE=1 BOLT-NUM=0 BOLT-
LOA=0.00000000000000,
    WARP=NO

*** X-AXIS SYMMETRY LINE
EGROUP BEAM NAME=3 SUBTYPE=THREE-D
DISPLACE=DEFAULT MATERIAL=2 RINT=5,
    SINT=7 TINT=DEFAULT RESULTS=FORCES
INITIALS=NONE CMASS=DEFAULT,
    RIGIDEND=NONE MOMENT-C=YES RIGIDITY=3
MULTIPLY=1000000.00000000,
    RUPTURE=ADINA OPTION=NONE BOLT-
TOL=0.00000000000000 DESCRIPT=,
'NONE' SECTION=2 PRINT=DEFAULT SAVE=DEFAULT
TBIRTH=0.00000000000000,
    TDEATH=0.00000000000000 SPOINT=4
BOLTFORC=0.00000000000000,
    BOLTNCUR=0 TMC-MATE=1 BOLT-NUM=0 BOLT-
LOA=0.00000000000000,
    WARP=NO

*** Y-AXIS, SYMMETRY LINE
EGROUP BEAM NAME=4 SUBTYPE=THREE-D
DISPLACE=DEFAULT MATERIAL=2 RINT=5,
    SINT=7 TINT=DEFAULT RESULTS=FORCES
INITIALS=NONE CMASS=DEFAULT,
    RIGIDEND=NONE MOMENT-C=YES RIGIDITY=4
MULTIPLY=1000000.00000000,
    RUPTURE=ADINA OPTION=NONE BOLT-
TOL=0.00000000000000 DESCRIPT=,
'NONE' SECTION=2 PRINT=DEFAULT SAVE=DEFAULT
TBIRTH=0.00000000000000,
    TDEATH=0.00000000000000 SPOINT=4
BOLTFORC=0.00000000000000,
    BOLTNCUR=0 TMC-MATE=1 BOLT-NUM=0 BOLT-
LOA=0.00000000000000,
    WARP=NO

*** Y-AXIS, AT SUPPORT
EGROUP BEAM NAME=5 SUBTYPE=THREE-D
DISPLACE=DEFAULT MATERIAL=2 RINT=5,
    SINT=7 TINT=DEFAULT RESULTS=FORCES
INITIALS=NONE CMASS=DEFAULT,
    RIGIDEND=NONE MOMENT-C=YES RIGIDITY=5
MULTIPLY=1000000.00000000,
    RUPTURE=ADINA OPTION=NONE BOLT-
TOL=0.00000000000000 DESCRIPT=,
'NONE' SECTION=2 PRINT=DEFAULT SAVE=DEFAULT
TBIRTH=0.00000000000000,
    TDEATH=0.00000000000000 SPOINT=4
BOLTFORC=0.00000000000000,
    BOLTNCUR=0 TMC-MATE=1 BOLT-NUM=0 BOLT-
LOA=0.00000000000000,
    WARP=NO

****
****
************** BOUNDARY CONDITIONS **************
****
****

FIXITY NAME=P1
@CLEAR
 'X-TRANSLATION'
 'Y-TRANSLATION'
 'Z-TRANSLATION'
 'X-ROTATION'
 'Y-ROTATION'
 'Z-ROTATION'
 'OVALIZATION'
@

FIXBOUNDARY POINTS FIXITY=ALL
@CLEAR
1 'P1'
TO
61 'P1'
@

****
****
********************** MESHING **********************
****
****

******************** MESH DENSITY ******************

SUBDIVIDE MODEL MODE=LENGTH SIZE=0.2 NDIV=1,
    PROGRESS=GEOMETRIC MINCUR=1

SUBDIVIDE LINE NAME=2 MODE=LENGTH SIZE=0.05
@CLEAR
2
4
TO
63
@

******************** MESH GROUPING ****************

*** X-AXIS
GLINE NODES=2 AUXPOINT=1000 NCOINCID=ALL,
    NCTOLERA=1E-05 SUBSTRUC=0 GROUP=1
MIDNODES=CURVED,
    XO=0 YO=0 ZO=0,
    XYZOSYST=SKEW
@CLEAR
200
TO
206
@

*** X-AXIS "SYMMETRY LINE"
GLINE NODES=2 AUXPOINT=1000 NCOINCID=ALL,
    NCTOLERA=1E-05 SUBSTRUC=0 GROUP=3
MIDNODES=CURVED,
    XO=0 YO=0 ZO=0,
    XYZOSYST=SKEW
@CLEAR
1
3
@

```
*** Y-AXIS                                         TIMEFUNCTION NAME=5 IFLIB=1
GLINE NODES=2 AUXPOINT=1000 NCOINCID=ALL,          @CLEAR
    NCTOLERA=1E-05 SUBSTRUC=0 GROUP=2              0          0
MIDNODES=CURVED,                                   40         0
    XO=0 YO=0 ZO=0,                                50         1
    XYZOSYST=SKEW                                  60         0
@CLEAR                                             39010      0
5                                                  @
TO
33                                                 TIMEFUNCTION NAME=6 IFLIB=1
35                                                 @CLEAR
TO                                                 0          0
63                                                 50         0
100                                                60         1
TO                                                 70         0
158                                                39010      0
@                                                  @

*** Y-AXIS, "SYMMETRY LINE"                        TIMEFUNCTION NAME=7 IFLIB=1
GLINE NODES=2 AUXPOINT=1000 NCOINCID=ALL,          @CLEAR
    NCTOLERA=1E-05 SUBSTRUC=0 GROUP=4             0          0
MIDNODES=CURVED,                                   60         0
    XO=0 YO=0 ZO=0,                                70         1
    XYZOSYST=SKEW                                  80         0
@CLEAR                                             39010      0
2                                                  @
4
501                                                TIMEFUNCTION NAME=8 IFLIB=1
502                                                @CLEAR
@                                                  0          0
                                                   70         0
*** Y-AXIS, SUPPORT                                80         1
GLINE NODES=2 AUXPOINT=1000 NCOINCID=ALL,          90         0
    NCTOLERA=1E-05 SUBSTRUC=0 GROUP=5             39010      0
MIDNODES=CURVED,                                   @
    XO=0 YO=0 ZO=0,
    XYZOSYST=SKEW                                  TIMEFUNCTION NAME=9 IFLIB=1
@CLEAR                                             @CLEAR
34                                                 0          0
@                                                  80         0
                                                   90         1
                                                   100        0
****************************************************   39010      0
****************************************************   @
**************** TIMEFUNCTIONS ********************
****************************************************   TIMEFUNCTION NAME=10 IFLIB=1
****************************************************   @CLEAR
                                                   0          0
TIMESTEP NAME=DEFAULT                              90         0
@CLEAR                                             100        1
39010      1                                       110        0
@                                                  39010      0
                                                   @
TIMEFUNCTION NAME=1 IFLIB=1
@CLEAR                                              .
0          0                                        .
0          0                                        .
10         1                                        .
20         0                                        .
39010      0                                        .
@                                                   .
                                                    .
TIMEFUNCTION NAME=2 IFLIB=1                          .
@CLEAR                                               .
0          0                                        .
10         0
20         1                                        TIMEFUNCTION NAME=3740 IFLIB=1
30         0                                        @CLEAR
39010      0                                        0          0
@                                                   38880      0
                                                    38890      1
TIMEFUNCTION NAME=3 IFLIB=1                          38900      0
@CLEAR                                               39010      0
0          0                                        @
20         0
30         1                                        TIMEFUNCTION NAME=3741 IFLIB=1
40         0                                        @CLEAR
39010      0                                        0          0
@                                                   38890      0
                                                    38900      1
TIMEFUNCTION NAME=4 IFLIB=1                          38910      0
@CLEAR                                               39010      0
0          0                                        @
30         0
40         1
50         0
39010      0
```

TIMEFUNCTION NAME=3742 IFLIB=1
@CLEAR
```
0          0
38900      0
38910      1
38920      0
39010      0
@
```

TIMEFUNCTION NAME=3743 IFLIB=1
@CLEAR
```
0          0
38910      0
38920      1
38930      0
39010      0
@
```

TIMEFUNCTION NAME=3744 IFLIB=1
@CLEAR
```
0          0
38920      0
38930      1
38940      0
39010      0
@
```

TIMEFUNCTION NAME=3745 IFLIB=1
@CLEAR
```
0          0
38930      0
38940      1
38950      0
39010      0
@
```

TIMEFUNCTION NAME=3746 IFLIB=1
@CLEAR
```
0          0
38940      0
38950      1
38960      0
39010      0
@
```

TIMEFUNCTION NAME=3747 IFLIB=1
@CLEAR
```
0          0
38950      0
38960      1
38970      0
39010      0
@
```

TIMEFUNCTION NAME=3748 IFLIB=1
@CLEAR
```
0          0
38960      0
38970      1
38980      0
39010      0
@
```

TIMEFUNCTION NAME=3749 IFLIB=1
@CLEAR
```
0          0
38970      0
38980      1
38990      0
39010      0
@
```

TIMEFUNCTION NAME=3750 IFLIB=1
@CLEAR
```
0          0
38980      0
38990      1
39000      0
39010      0
@
```

```
*****************************************************
*****************************************************
***************** LOAD APPLICATION ****************
*****************************************************
*****************************************************
```

LOAD FORCE NAME=1 MAGNITUD=120000 FX=0,
   FY=0 FZ=-1

APPLY-LOAD BODY=0
@CLEAR

```
1    'FORCE' 1 'POINT'  111  0  1  0  0  -1  0  0  0  'NO',
        0  0  1  0  'BOTH'
2    'FORCE' 1 'POINT'  110  0  2  0  0  -1  0  0  0  'NO',
        0  0  1  0  'BOTH'
3    'FORCE' 1 'POINT'  109  0  3  0  0  -1  0  0  0  'NO',
        0  0  1  0  'BOTH'
4    'FORCE' 1 'POINT'  108  0  4  0  0  -1  0  0  0  'NO',
        0  0  1  0  'BOTH'
5    'FORCE' 1 'POINT'  107  0  5  0  0  -1  0  0  0  'NO',
        0  0  1  0  'BOTH'
6    'FORCE' 1 'POINT'  106  0  6  0  0  -1  0  0  0  'NO',
        0  0  1  0  'BOTH'
7    'FORCE' 1 'POINT'  105  0  7  0  0  -1  0  0  0  'NO',
        0  0  1  0  'BOTH'
8    'FORCE' 1 'POINT'  104  0  8  0  0  -1  0  0  0  'NO',
        0  0  1  0  'BOTH'
9    'FORCE' 1 'POINT'  103  0  9  0  0  -1  0  0  0  'NO',
        0  0  1  0  'BOTH'
10    'FORCE' 1 'POINT'  102  0  10  0  0  -1  0  0  0  'NO',
        0  0  1  0  'BOTH'
.
.
.
.
.
.
.
.
.
.
3740    'FORCE' 1 'POINT' 97  0  3740  0  0  -1  0  0  0
'NO', 0  0  1  0  'BOTH'
3741    'FORCE' 1 'POINT' 96  0  3741  0  0  -1  0  0  0
'NO', 0  0  1  0  'BOTH'
3742    'FORCE' 1 'POINT' 95  0  3742  0  0  -1  0  0  0
'NO', 0  0  1  0  'BOTH'
3743    'FORCE' 1 'POINT' 94  0  3743  0  0  -1  0  0  0
'NO', 0  0  1  0  'BOTH'
3744    'FORCE' 1 'POINT' 93  0  3744  0  0  -1  0  0  0
'NO', 0  0  1  0  'BOTH'
3745    'FORCE' 1 'POINT' 92  0  3745  0  0  -1  0  0  0
'NO', 0  0  1  0  'BOTH'
3746    'FORCE' 1 'POINT' 91  0  3746  0  0  -1  0  0  0
'NO', 0  0  1  0  'BOTH'
3747    'FORCE' 1 'POINT' 90  0  3747  0  0  -1  0  0  0
'NO', 0  0  1  0  'BOTH'
3748    'FORCE' 1 'POINT' 89  0  3748  0  0  -1  0  0  0
'NO', 0  0  1  0  'BOTH'
3749    'FORCE' 1 'POINT' 88  0  3749  0  0  -1  0  0  0
'NO', 0  0  1  0  'BOTH'
3750    'FORCE' 1 'POINT' 87  0  3750  0  0  -1  0  0  0
'NO', 0  0  1  0  'BOTH'
```

```
*****************************************************
*****************************************************
********************** ANALYSIS *********************
*****************************************************
*****************************************************
```

```
********************** ANALYSIS *********************
```

MASTER ANALYSIS=STATIC MODEX=EXECUTE
TSTART=0.00000000000000 IDOF=0,
   OVALIZAT=NONE FLUIDPOT=AUTOMATIC
CYCLICPA=1 IPOSIT=STOP,
   REACTION=YES INITIALS=NO FSINTERA=NO
IRINT=DEFAULT CMASS=NO,
   SHELLNDO=AUTOMATIC AUTOMATI=ATS
SOLVER=SPARSE,
   CONTACT-=CONSTRAINT-FUNCTION
TRELEASE=0.0000000000000,
   RESTART-=NO FRACTURE=NO LOAD-CAS=NO LOAD-
PEN=NO SINGULAR=YES,

```
    STIFFNES=0.000100000000000000 MAP-OUTP=NONE
MAP-FORM=NO,
    NODAL-DE=" POROUS-C=NO ADAPTIVE=0 ZOOM-
LAB=1 AXIS-CYC=0,
    PERIODIC=NO VECTOR-S=GEOMETRY EPSI-FIR=NO
STABILIZ=NO,
    STABFACT=1.00000000000000E-10 RESULTS=PORTHOLE
FEFCORR=NO,
    BOLTSTEP=1 EXTEND-S=YES CONVERT-=NO
DEGEN=YES TMC-MODE=NO,
    ENSIGHT-=NO IRSTEPS=1 INITIALT=NO TEMP-INT=NO
ESINTERA=NO,
    OP2GEOM=NO

****************** SAVE RESULTS ******************

PRINT-STEPS SUBSTRUC=0 REUSE=1
@CLEAR
1 1 260 259
2 260 39000 260
@
```

```
NODESAVE-STE ELEMSAVE=NO
@CLEAR
1 1 260 259
2 260 39000 260
@

ELEMSAVE-STE NODESAVE=NO
@CLEAR
1 1 260 259
2 260 39000 260
@

****************** LOGGFILE ********************

CONTROL UNDO=-1 AUTOMREBUILD=NO
FILEECHO OPTION=FILE F=loggfil.ut
FILELOG OPTION=FILE F=loggfil.ut

DATABASE SAVE PERMFILE='1.idb' PROMPT

********************** END ************************
```

CHALMERS, *Civil and Environmental Engineering*, Master's Thesis 2014:73